Electron-electron and electron-phonon interactions in strongly correlated systems

by

Gerardo Sica

A Doctoral Thesis
submitted in partial fulfilment of the requirements for the award of the degree of Doctor of Philosophy of Loughborough University and Università degli Studi di Salerno

February 2013

Supervisors:

Prof. A. S. Alexandrov - Loughborough University
Dr. A. Avella - Università degli Studi di Salerno
Prof. F. Mancini - Università degli Studi di Salerno
Dr. J. H. Samson - Loughborough University

Certificate of Originality

This is to certify that I am responsible for the work submitted in this thesis, that the original work is my own except as specified in acknowledgments or in footnotes, and that neither the thesis nor the original work contained therein has been submitted to this or any other institution for a degree except in accordance with the International Inter-University Collaboration agreement between Loughborough University and Università degli Studi di Salerno.

Gerardo Sica
February 2013

To Prof. Alexander Sergeevitch Alexandrov,
whose dedication to this wonderful job
has been the greatest inspiration
and the most valuable teaching I could ever had.

Acknowledgments

As often happens, the final outcome of a work does not depend only on your efforts, on your dedication or on your self-abnegation, but it also related for most of its part to context and external factors which might or might not put you in a position to do your best and work properly step by step on your daily goals.

This work is the final outcome of a three-year Ph.D. course in Physics, spent for one half in Salerno, and for the other half in Loughborough, but more precisely is the final outcome of an invaluable and unrepeatable period in which I found myself in contact with an incredible number of people, each of them carrying its own teaching, its own experience, its own way to look differently the same thing. Each of them contributing to my formation, as a person more than as a scientist. This work would have never been possible without even one of these little contributions, therefore I do need, I really need to thank all the people who took part in this.

Among all these people, I would like to thank first all my supervisors, Prof. Sasha Alexandrov, Prof. Ferdinando Mancini and Dr. John Samson for being able to teach me, more that their knowledge, their dedication and love to this wonderful job. In the last three years their commitment has been the most powerful inspiration and guide. A special thank goes to Dr. Adolfo Avella and Dr. Evgeny Plekhanov for their unceasing and patience support to my research activity.

I can not avoid to acknowledge the Physics Department of Loughborough University for the hospitality, and all the guys who contributed to make me fell at home during my stay abroad. I also acknowledge all my colleagues and friends in Salerno, with whom I shared joys and concerns in these last three years.

Last, but definitely not least, I sincerely and warmly thank Chiara and all my family for being the essential part of my life during all this period. For supporting me in all the circumstances. For believing in me even when I doubted about myself. For teaching me that, whatever I do and wherever I will be, I will always have their unconditional love and support.

Abstract

In this work we investigate some aspects of the physics of strongly correlated systems by taking into account both electron-electron and electron-phonon interactions as basic mechanisms for reproducing electronic correlations in real materials.

The relevance of the electron-electron interactions is discussed in the first part of this thesis in the framework of a self-consistent theoretical approach, named Composite Operator Method (COM), which accounts for the relevant quasi-particle excitations in terms of a set of composite operators that appear as a result of the modification imposed by the interactions on the canonical electronic fields. We show that the COM allows the calculation of all the relevant Green's and correlation functions in terms of a number of unknown internal parameters to be determined self-consistently. Therefore, depending on the balance between unknown parameters and self-consistent equations, exact and approximate solutions can be obtained. By way of example, we discuss the application of the COM to the extended t-U-J-h model in the atomic limit, and to the two-dimensional single-band Hubbard model. In the former case, we show that the COM provides the exact solution of the model in one dimension. We study the effects of electronic correlations as responsible for the formation of a plethora of different charge and/or spin orderings. We report the phase diagram of the model, as well as a detailed analysis of both zero and finite temperature single-particle and thermodynamic properties. As far as the single-band Hubbard model is concerned, we illustrate an approximated self-consistent scheme based on the choice of a two-field basis. We report a detailed analysis of many unconventional features that arise in single-particle properties, thermodynamics and system's response functions. We emphasize that the accuracy of the COM in describing the effects of electronic correlations strongly relies on the choice of the basis, paving the way for possible multi-pole extensions to the two-field theory. To this purpose, we also study a three-field approach to the single-band Hubbard model, showing a significant step forward in the agreements with numerical data with respect to the two-pole results.

The role of the electron-phonon interaction in the physics of strongly correlated systems is discussed in the second part of this thesis. We show that in highly polarizable lattices the competition between unscreened Coulomb and Fröhlich interactions results in a short-range polaronic exchange term J_p that favours the formation of local and light pairs of bosonic nature, named bipolarons, which condense with a critical temperature well in excess of hundred kelvins. These findings, discussed in

the framework of the so-called polaronic t-J_p model, are further investigated in the presence of a finite on-site potential $\tilde{U}$, coming from the competition between on-site Coulomb and Fröhlich interactions. We discuss the role of $\tilde{U}$ as the driving parameter for a small-to-large bipolaron transition, providing a possible explanation of the BEC-BCS crossover in terms of the properties of the bipolaronic ground state. Finally, we show that a hard-core bipolarons gas, studied as a charged Bose-Fermi mixture, allows for the description of many non Fermi liquid behaviours, allowing also for a microscopic explanation of pseudogap features in terms of a thermal-induced recombination of polarons and bipolarons, without any assumption on preexisting order or broken symmetries.

Contents

List of Figures

List of Tables

Part I

Electron-electron interaction in strongly correlated systems

Chapter 1

Introduction to basic models for correlated systems

In the last decades a large interest arose in the study of transition metal oxides and rare-earths as promising testing grounds for the observation of unconventional properties and anomalous features, often referred to as "non-Fermi-liquid behaviours" in contrast with simple metal behaviours well-described by the Fermi-liquid theory. In these systems, there are several pieces of evidence of coexistence of different competing orders characterized by strong spatial correlations as well as pronounced on-site quantum fluctuations or magnetic behaviours, which led to the conviction that unconventional phenomena, among which we recall the metal-insulator transition, high-temperature superconductivity, colossal magneto-resistance, Kondo effect, quantum phase transitions, can only emerge as macroscopic manifestations of strong microscopic correlations.

On this ground, due to the presence of a strong interplay among a variety of different degrees of freedom (e.g. charge, spin, lattice vibrations) to be, in principle, all accounted on equal footing, any theoretical effort with the aim of describing unconventional features in terms of ab-initio models will be unfeasible. Hence, in the last years a number of different "approximated" models have been proposed, whose applicability can only be considered in particular limits or referred to particular materials. With no claim of being exhaustive, hereafter we will shortly introduce few of them, namely the Hubbard model [1] and its reduction the t-J model [2], the Kondo lattice model [3] and the periodic Anderson model [4], as the basic models for strongly correlated systems accounting for all relevant charge and spin correlations in a large class of materials. We neglect any coupling with lattice degrees of freedoms which will be discussed in the second part of this thesis. At this point it is worth clarifying that it is beyond the scope of this Chapter to undertake a thorough analysis of the aforementioned models. Interested readers can find comprehensive reviews in Ref. [5], Ref.[6] and Ref.[7] for Hubbard, Kondo and Anderson models, respectively.

It is instructive to start from the pioneristic work by Hubbard [1], in which an approximate s-wave description of $3d$-electrons was proposed to describe strong electronic correlations in transition metals. In the presence of an electrostatic Coulomb

interaction among charged carriers one can write the following Hamiltonian as the minimal model for the description of correlated electrons in a lattice:

$$\begin{aligned} H &= \sum_{\boldsymbol{i},\boldsymbol{j};\sigma} t_{\boldsymbol{ij}} \left(c^{\dagger}_{\boldsymbol{i},\sigma} c_{\boldsymbol{j},\sigma} + h.c. \right) + \frac{1}{2} \sum_{\boldsymbol{i},\boldsymbol{j},\boldsymbol{l},\boldsymbol{m}} \sum_{\sigma,\sigma'} \langle \boldsymbol{i},\boldsymbol{j}| \frac{1}{r} |\boldsymbol{l},\boldsymbol{m}\rangle \, c^{\dagger}_{\boldsymbol{i},\sigma} c^{\dagger}_{\boldsymbol{j},\sigma} c_{\boldsymbol{m},\sigma'} c_{\boldsymbol{l},\sigma} \\ &\quad - \sum_{\boldsymbol{i},\boldsymbol{j},\boldsymbol{l},\boldsymbol{m}} \sum_{\sigma} \left(2 \langle \boldsymbol{i},\boldsymbol{j}| \frac{1}{r} |\boldsymbol{l},\boldsymbol{m}\rangle - \langle \boldsymbol{i},\boldsymbol{j}| \frac{1}{r} |\boldsymbol{m},\boldsymbol{l}\rangle \right) \nu_{\boldsymbol{jm}} c^{\dagger}_{\boldsymbol{i},\sigma} c_{\boldsymbol{l},\sigma} \, . \end{aligned} \tag{1.1}$$

Here $\boldsymbol{i}$, $\boldsymbol{j}$, $\boldsymbol{l}$, $\boldsymbol{m}$ are lattice vectors, $\sigma, \sigma' = (\uparrow, \downarrow)$ are spin variables, $c^{\dagger}_{\boldsymbol{i},\sigma}/c_{\boldsymbol{i},\sigma}$ is the operator which creates/annihilates a carrier with spin σ on site $\boldsymbol{i}$,

$$t_{\boldsymbol{ij}} = \frac{1}{N} \sum_{\boldsymbol{k}} \varepsilon_{\boldsymbol{k}} \exp(i\boldsymbol{k} \cdot (\boldsymbol{i} - \boldsymbol{j})) \, , \tag{1.2}$$

is the hopping integral formulated in terms of the non-interacting (Hartree-Fock) band-energy dispersion $\varepsilon(\boldsymbol{k})$, N is the number of sites in the lattice,

$$\nu_{\boldsymbol{ij}} = \frac{1}{N} \sum_{\boldsymbol{k}} \nu_{\boldsymbol{k}} \exp(i\boldsymbol{k} \cdot (\boldsymbol{i} - \boldsymbol{j})) \, , \tag{1.3}$$

where $\nu_{\boldsymbol{k}}$ is the assumed occupation number of the band states in the Hartree-Fock calculation, and:

$$\langle \boldsymbol{i},\boldsymbol{j}| \frac{1}{r} |\boldsymbol{l},\boldsymbol{m}\rangle = e^2 \int d\boldsymbol{x} \int d\boldsymbol{x}' \frac{\phi^*(\boldsymbol{x} - \boldsymbol{i}) \phi(\boldsymbol{x} - \boldsymbol{l}) \phi^*(\boldsymbol{x}' - \boldsymbol{j}) \phi(\boldsymbol{x}' - \boldsymbol{m})}{|\boldsymbol{x} - \boldsymbol{x}'|} \, , \tag{1.4}$$

where $\phi(\boldsymbol{x}) = N^{-\frac{1}{2}} \sum_{\boldsymbol{k}} \psi_{\boldsymbol{k}}(\boldsymbol{x})$ is the Wannier representation of the Bloch functions $\psi_{\boldsymbol{k}}$. Hence in the Hamiltonian (1.1) the first term is responsible for the mobility of the carriers, the second one parametrizes the electrostatic Coulomb interaction. The last term subtracts the potential energy of the electrons which is already taken into account in the Hartree-Fock dispersion $\varepsilon(\boldsymbol{k})$, avoiding double counting. Under the assumption of almost localized states with orbital radius small compared with the inter-atomic spacing, the leading contribution to the integrals (1.4) will be given by the on-site terms $U \equiv \langle \boldsymbol{i},\boldsymbol{i}| \frac{1}{r} |\boldsymbol{i},\boldsymbol{i}\rangle$. Therefore by neglecting all other contributions in (1.1) we obtain:

$$H = \sum_{\boldsymbol{i},\boldsymbol{j};\sigma} t_{\boldsymbol{ij}} \left(c^{\dagger}_{\boldsymbol{i},\sigma} c_{\boldsymbol{j},\sigma} + h.c. \right) + U \sum_{\boldsymbol{i};\sigma} n_{\boldsymbol{i},\sigma} n_{\boldsymbol{i},\bar{\sigma}} - U \sum_{\boldsymbol{i},\sigma} \nu_{\boldsymbol{ii}} n_{\boldsymbol{i},\sigma} \, , \tag{1.5}$$

where $\bar{\sigma}$ is the spin variable opposite to σ ($\bar{\sigma} = \uparrow$ if $\sigma = \downarrow$ and vice versa), $n_{\boldsymbol{i},\sigma} = c^{\dagger}_{\boldsymbol{i},\sigma} c_{\boldsymbol{i},\sigma}$ and $\nu_{\boldsymbol{ii}} = N^{-1} \sum_{\boldsymbol{k}} \nu_{\boldsymbol{k}} = n/2$, where n is the electron density per site. Hence the last term in the above equation can be dropped since it reduces to a constant contribution and we obtain the so-called Hubbard model (HM):

$$H_{HM} = \sum_{\boldsymbol{i},\boldsymbol{j};\sigma} t_{\boldsymbol{ij}} \left(c^{\dagger}_{\boldsymbol{i},\sigma} c_{\boldsymbol{j},\sigma} + h.c. \right) + U \sum_{\boldsymbol{i};\sigma} n_{\boldsymbol{i},\sigma} n_{\boldsymbol{i},\bar{\sigma}} \, . \tag{1.6}$$

The above Hamiltonian can be seen as a minimal model which aims to describe strongly correlations in solids. In particular, Eq.1.6 describes the propagation of strongly correlated electrons in the lattice, where both charge and spin correlations arise from the competition between the two different energy scales t_{ij} and U. Skipping the trivial non-interacting ($t_{ij}/U \gg 1$) limit, in the regime in which $t_{ij} \approx U$, electrons tend to gain energy by hopping from a site to another, trying to avoid the formation of local pairs which is unfavoured by the presence of $U > 0$. Hence the hopping of one electron from a site to another will be not only related to the properties of the electron itself, but also on the electronic density on the final site of the hopping process. In particular, the occupation of a site will cost $-t$, $-t+U$ in energy, depending on whether the final site is occupied or not, or can be even negated according to the Pauli exclusion principle. This behaviour is more clearly visible in the strong coupling regime ($t_{ij}/U \ll 1$) where the hopping from a site to another will only occur if there are no other electrons in the final site. In this case the HM reduces to the well-known t-J Hamiltonian [2]:

$$H_{tJ} = \sum_{\boldsymbol{i},\boldsymbol{j};\sigma} t_{\boldsymbol{ij}} \left[(1 - n_{\boldsymbol{i},\bar{\sigma}})\, c^{\dagger}_{\boldsymbol{i},\sigma} c_{\boldsymbol{j},\sigma}\, (1 - n_{\boldsymbol{j},\bar{\sigma}}) + h.c. \right] + J_{\boldsymbol{ij}} \sum_{\boldsymbol{i};\sigma} \overrightarrow{S}_{\boldsymbol{i}} \cdot \overrightarrow{S}_{\boldsymbol{j}} \,, \tag{1.7}$$

where, in order to maximize the hopping, an antiferromagnetic spin-order arises favoured by the presence of an exchange coupling J_{ij} which is related to hopping amplitude and strength of the on-site Coulomb potential as:

$$J_{\boldsymbol{ij}} = 4t^2_{\boldsymbol{ij}}/U > 0 \,. \tag{1.8}$$

In particular, at half-filling the itinerant nature of the model is completely suppressed and one recovers the antiferromagnetic Heisenberg Hamiltonian:

$$H_{Heis} = \sum_{\boldsymbol{i},\boldsymbol{j}} J_{\boldsymbol{ij}} \overrightarrow{S}_{\boldsymbol{i}} \cdot \overrightarrow{S}_{\boldsymbol{j}} \,, \tag{1.9}$$

which describes magnetic properties of localized but correlated electrons in terms of spin operators only, where in both Eq.1.7 and Eq.1.9 $\overrightarrow{S}_{\boldsymbol{i}}$ is the electronic spin operators defined as $\overrightarrow{S}_{\boldsymbol{i}} = \frac{1}{2} \sum_{\alpha\beta} c^{\dagger}_{\boldsymbol{i};\alpha} \boldsymbol{\sigma}_{\alpha\beta} c_{\boldsymbol{i};\beta}$, where $\boldsymbol{\sigma} = (\sigma_1, \sigma_2, \sigma_3)$ is the vector whose components are given by the three Pauli matrices:

$$\sigma_1 \equiv \begin{pmatrix} 0 & 1 \\ 1 & 0 \end{pmatrix} \,,\; \sigma_2 \equiv \begin{pmatrix} 0 & -i \\ i & 0 \end{pmatrix} \,,\; \sigma_3 \equiv \begin{pmatrix} 1 & 0 \\ 0 & -1 \end{pmatrix} \,. \tag{1.10}$$

On the basis of the above analysis, one can conclude that in the framework of the HM (1.6) spin degrees of freedom become relevant in the regime in which, due to interactions, the mobility of all the carriers is strongly compromised in favour of localized behaviours. However, many compounds (e.g. transition metal oxides and rare earths) are characterized by the coexistence of both localized and itinerant behaviours, whose competition can only be hardly estimated in the framework of the Hubbard model. This observation led to the formulation of the so-called Kondo

lattice model (KLM) [3]:

$$H_{KLM} = \sum_{\boldsymbol{i},\boldsymbol{j};\sigma} t_{\boldsymbol{ij}} \left(c^{\dagger}_{\boldsymbol{i},\sigma} c_{\boldsymbol{j},\sigma} + h.c. \right) + \frac{J_K}{2} \sum_{\boldsymbol{i};\alpha,\beta} \left(\overrightarrow{S}_{\boldsymbol{i}} \cdot \overrightarrow{\sigma}_{\alpha\beta} \right) c^{\dagger}_{\boldsymbol{i},\alpha} c_{\boldsymbol{i},\beta} \ , \tag{1.11}$$

which includes the presence of localized atomic moments $\overrightarrow{S}$, coupled with the spins $\overrightarrow{\sigma}$ of the conduction electrons via an on-site exchange interaction parametrized by J_K. It is worth noting that in the above Hamiltonian neither conduction nor localized spins interact among themselves. All the interactions are only accounted via an exchange coupling mechanism which, differently from the one that arises from the HM in the strong coupling regime (1.8), refers to the interaction among conduction electrons and localized momenta (which belong to the inner atomic shells or to magnetic impurities) rather than to interactions among conduction electrons with themselves. Hence the Kondo exchange coupling constant J_K has a completely different nature with respect to J. These subtle but crucial differences make the Kondo lattice model able to reproduce the properties of many materials whose description in terms of Hubbard or t-J models is inapplicable. In the limit $J_K/t \gg 1$, the exchange interaction localizes the conduction electrons resulting in the formation of fully localized singlet ($J > 0$) or triplet ($J < 0$) states. On the contrary, in the more interesting case in which $J_K/t \lessapprox 1$, both itinerant and localized behaviours are present, whose competition has been considered at the basis of a number of interesting phenomena among which Kondo effect, metal-insulator transition, giant magneto-resistance, transport and magnetic properties of many materials such as heavy-fermions, rare-earths, manganites.

Hence, starting from the Hamiltonian (1.11), a further step forward for the description of strongly correlated systems can be done by including in the Kondo physics the effects of the on-site (Coulomb) interaction, as well as the possibility to have an hybridization between conduction and localized electrons in place of the local Kondo exchange mechanism. By doing this, we obtain the so-called periodic Anderson model (PAM) [4]:

$$\begin{aligned} H_{PAM} \ = \ & \sum_{\boldsymbol{i},\boldsymbol{j};\sigma} t_{\boldsymbol{ij}} \left(c^{\dagger}_{\boldsymbol{i},\sigma} c_{\boldsymbol{j},\sigma} + h.c. \right) + \varepsilon_l \sum_{\boldsymbol{i};\sigma} n^l_{\boldsymbol{i},\sigma} + U \sum_{\boldsymbol{i};\sigma} n^l_{\boldsymbol{i},\sigma} n^l_{\boldsymbol{i},\bar{\sigma}} \\ & + \sum_{\boldsymbol{i},\boldsymbol{j};\sigma} V_{\boldsymbol{ij}} \left(c^{\dagger}_{\boldsymbol{i},\sigma} l_{\boldsymbol{j},\sigma} + l^{\dagger}_{\boldsymbol{j},\sigma} c_{\boldsymbol{i},\sigma} \right) \ , \end{aligned} \tag{1.12}$$

where $c_{\boldsymbol{i},\sigma}/l_{\boldsymbol{i},\sigma}$ and $c^{\dagger}_{\boldsymbol{i},\sigma}/l^{\dagger}_{\boldsymbol{i},\sigma}$ are the canonical fermionic operators which annihilate and create an itinerant/localized electron with spin σ on site $\boldsymbol{i}$, $n^l_{\boldsymbol{i},\sigma} = l^{\dagger}_{\boldsymbol{i},\sigma} l_{\boldsymbol{i},\sigma}$ and ε_l are density per spin and band-energy of localized electrons, respectively, $V_{\boldsymbol{ij}}$ is the hybridization parameter. The PAM represents a basic model for the description of heavy fermions, whose properties are given by the interactions among itinerant d-electrons and localized f-electrons. Despite its simple and intuitive form, it represents one of the most difficult model to deal with and, due to its complexity, few exact results are known, mostly related to particular limits [8, 9] or special cases in which symmetry properties are relevant [10]. Generally, starting from the Hamiltonian (1.12), simplified models are considered in which, for example, only the on-site

contribution to the hybridization is taken into account or only one localized electron, looked as a magnetic impurity, is considered. In particular, it is worth noting that, in the highly localized electron limit, the Hamiltonian (1.12) recovers the physics of the KLM (1.11) which, similarly to as the t-J model comes from the Hubbard one, can be derived from (1.12) following a Schrieffer-Wolf transformation [11]. This property immediately follows from the consideration that, when electrons are strongly localized (e.g. $U \gg 1$), they can hop into the impurity band and then hop back again in order to gain kinetic energy. This process leads to the antiferromagnetic exchange interaction J_K between a local impurity spin and the conduction electron spin at the impurity site which, similarly to (1.8), reads as:

$$J_K = \frac{4V^2}{U} \,, \tag{1.13}$$

and accounts for the same physics already described for the KLM.

It is worth noting that the apparent simplicity of the aforementioned Hubbard (1.6), t-J (1.7), Kondo lattice (1.11) and periodic Anderson (1.12) models, hides a very complex physics whose investigation, currently one of most challenging topics in condensed matter physics, is continually pursued through an increasing number of analytical and numerical approaches. Analytic treatments often require oversimplifications or are based on uncontrolled assumptions which make extremely difficult to understand if a given prediction represents a real feature of the model rather than an artifact of the approximations used. Numerical techniques, in turn, are by their nature restricted by the size of the system which defines the computational efforts required. Hence it becomes evident that analytical and numerical approaches can only be considered as complementary to each other and any new analytical or numerical method could contribute to a better understanding of the model under investigation, giving an invaluable insight of the physics described by it.

Within this context, we present in this part of the thesis an analytical theoretical scheme, named Composite Operator Method (COM), which in the last years has been successfully employed for the study of several models and materials among which: p-d [12], t-J [13], t-t'-U [14], t-U-V [15], Hubbard [16], Kondo [17], Anderson [18], Cuprates [19]. The basic theoretical framework of the model is reported in Chapter 2. It is shown that, differently from many analytical methods, the COM is based on the choice of a proper set of so-called composite fields which are aimed to describe all the relevant stable quasi-particle excitations generated by the interactions rather then bare electrons. Well-consolidated techniques and results, such as Wick theorem, standard Green's function approach, diagrammatic expansion, do not apply in the case of composite fields, therefore a proper Green's function formalism, illustrated in Sec.2.1, needs to be formulated. As shown in Sec.2.3, the aforementioned formalism allows to the calculation of all the relevant Green's functions in terms of a number of unknown internal parameters which can be determined self-consistently by means of symmetry relations or algebraic constraints. Hence, when the number of internal parameters equals the number of self-consistent constraints, depending on the properties of the selected basis of composite fields, the COM can provide both an exact or an approximated solution in the whole range of the model parameters and without any assumption of their strength. Two applications of the

COM are discussed.

In Chapter 3 we introduce the COM as a powerful method for the investigation of a large class of exactly solvable systems and illustrate the exact solution of the one-dimensional t-U-J-h model in the narrow-band limit [20]. We report in Sec.3.1.3 and Sec.3.1.4 zero and finite temperature results, respectively, including a comprehensive analysis of the phase diagram and a detailed study of single particle properties, thermodynamics and system's response functions.

In Chapter 4 we use the COM to obtain an approximated solution of the two-dimensional single-band HM. In particular, two different approximations schemes, namely the polar approximation and the self-consistent Born approximation, are discussed in Sec.4.1-4.2 and Sec.4.3, respectively. We show that the COM is perfectly able to reproduce a variety of unconventional features induced by strong interactions. We also report a detailed comparison of the results of our approximations against different numerical methods, showing a good agreement in all the range of the model parameters.

In Chapter 5 we discuss possible developments and improvements of the approximated theoretical framework illustrated in Chapter 4. In particular we show that it is possible to obtain a better agreement with numerical data by increasing the number of composite fields of the basis. This procedure allows the COM to describe virtual energy scales of the model, however it also introduces a number of unknown parameters in the self-consistent scheme to be determined via further approximations. Finally, we report in Chapter 6 open issues and possible directions.

Chapter 2

The Composite Operator Method

In the last decades many efforts were made to understand strongly correlated electronic systems, largely considered as one of the most puzzling playgrounds for the observation of unconventional features which break down the standard Fermi liquid behaviors observed in normal metals. As it is well known, in these systems strong interactions modify the properties of the particles at a macroscopic level, resulting in the formation of new quasi-particles, different from bare electrons, whose properties are entirely determined by dynamics, strength and nature of the interactions, geometry of the lattice. As a simple example, let us consider the atomic Hamiltonian:

$$\mathcal{H} = -\mu \sum_{\sigma} \varphi_{\sigma}^{\dagger}\varphi_{\sigma} + U\varphi_{\uparrow}^{\dagger}\varphi_{\downarrow}^{\dagger}\varphi_{\downarrow}\varphi_{\uparrow} \,, \tag{2.1}$$

where $\varphi_{\sigma}/\varphi_{\sigma}^{\dagger}$ denotes the Heisenberg representation of the annihilation/creation operators of a bare electron with spin $\sigma \in \{\uparrow,\downarrow\}$, which satisfy the canonical anti-commutation rules (below and after we consider $\hbar = 1$):

$$\begin{cases} \{\varphi_{\sigma}, \varphi_{\rho}\} = \{\varphi_{\sigma}^{\dagger}, \varphi_{\rho}^{\dagger}\} = 0 \\ \{\varphi_{\sigma}, \varphi_{\rho}^{\dagger}\} = \delta_{\sigma\rho} \end{cases} . \tag{2.2}$$

It is immediate to see that the model Hamiltonian (2.1) is exactly solvable in terms of the operators:

$$\xi_{\sigma} \equiv \varphi_{\sigma}\varphi_{\bar{\sigma}}\varphi_{\bar{\sigma}}^{\dagger} = \varphi_{\sigma}\left(1 - \varphi_{\bar{\sigma}}^{\dagger}\varphi_{\bar{\sigma}}\right) \,, \tag{2.3}$$

$$\eta_{\sigma} \equiv \varphi_{\sigma}\varphi_{\bar{\sigma}}^{\dagger}\varphi_{\bar{\sigma}} \,, \tag{2.4}$$

where $\bar{\sigma} = \downarrow$ and $\bar{\sigma} = \uparrow$ for $\sigma = \uparrow$ and $\sigma = \downarrow$, respectively. In fact, by nothing that $\varphi_{\sigma} = \xi_{\sigma} + \eta_{\sigma}$ it is possible to rewrite Eq.2.1 as:

$$\mathcal{H} = -\mu \sum_{\sigma} \xi_{\sigma}^{\dagger}\xi_{\sigma} - \left(\mu - \frac{1}{2}U\right) \sum_{\sigma} \eta_{\sigma}^{\dagger}\eta_{\sigma} \,, \tag{2.5}$$

from which it follows that ξ_σ and η_σ are eigenoperators of $\mathcal{H}$ with energy $E_\xi = -\mu$ and $E_\eta = -(\mu - U)$, respectively:

$$\begin{cases} i\partial_t \xi_\sigma = [\xi_\sigma, \mathcal{H}] = -\mu \xi_\sigma \\ i\partial_t \eta_\sigma = [\eta_\sigma, \mathcal{H}] = -(\mu - U)\,\eta_\sigma \end{cases} . \tag{2.6}$$

Hence, it is immediate to realize that, because of the presence of a trivial interaction term, the properties of bare electrons described by the field φ_σ are no more observed and new stable quasi-particles excitations appear, described by the fields ξ_σ and η_σ, which are responsible for the transitions $|0\rangle \leftrightarrow |\sigma\rangle$, and $|\sigma\rangle \leftrightarrow |\uparrow\downarrow\rangle$, respectively. Consistently, $E_\xi - E_\eta = U$, therefore the two fields ξ_σ and η_σ are completely degenerate in the absence of interaction, recovering the free-electron picture with $E_\xi = E_\eta = -\mu$ as one would expect for the non-interacting case.

On the basis of this evidence, it clearly follows that an analysis in terms of elementary fields (e.g. bare electronic fields) might be inadequate for systems dominated by strong interactions. Also a perturbative treatment will fail since there are no obvious small parameters allowing for a perturbative expansion. Hence, as done before for the trivial atomic model (2.1), a possible alternative procedure consists in reformulating the model Hamiltonian in terms of new fields, called *"composite fields"*, which describe the stable quasi-particle excitations that arise as a result of the interaction. As noticed before, the convenience of this approach lies in the fact that, once all the possible stable excitations have been found, one might in principle exactly solve the problem since the starting Hamiltonian will have a diagonal representation in terms of the new composite fields (see Eq.2.5). However, one should also emphasize that, because of the competition between different energy scales and orders, even for very simple and widely studied models (e.g. the Hubbard model) the identification of composite fields coming from all the possible stable quasi-particle excitations is not an easy task to deal with. Their identification is complicated by the fact that, as follows from the trivial atomic case (2.1), composite operators (Eq.2.3 and Eq.2.4) can be expressed in terms of an arbitrary complicated product of standard electronic fields. Therefore in general they are neither Fermi nor Bose operators, since they do not satisfy canonical (anti)commutation rules and properties. They can only be recognized as fermionic or bosonic operators according to the number, odd or even, of the constituting original electronic fields. For instance, the fields ξ_σ and η_σ, defined by Eq.2.3 and Eq.2.4, respectively, can be recognized as fermionic fields and their algebra is more conveniently described by considering the following anticommutators:

$$\left\{\xi_\sigma, \eta_\rho^\dagger\right\} = \left\{\eta_\sigma, \xi_\rho^\dagger\right\} = 0 \,, \tag{2.7}$$

$$\left\{\xi_\sigma, \xi_\rho^\dagger\right\} = \delta_{\rho\sigma}\left(1 - \varphi_{\bar{\sigma}}^\dagger \varphi_{\bar{\sigma}}\right) \,, \tag{2.8}$$

$$\left\{\eta_\sigma, \eta_\rho^\dagger\right\} = \delta_{\rho\sigma}\varphi_{\bar{\sigma}}^\dagger \varphi_{\bar{\sigma}} \,. \tag{2.9}$$

From the above relations it is worth noting that, different from the case of standard electronic fields, the anticommutators of the composite fields ξ_σ and η_σ are not c-number but operators themselves of bosonic nature satisfying the following

commutation rules:

$$\left[\varphi_\sigma^\dagger \varphi_\sigma, \xi_\rho\right] = -\delta_{\sigma\rho}\xi_\sigma \ , \tag{2.10}$$

$$\left[\varphi_\sigma^\dagger \varphi_\sigma, \eta_\rho\right] = -\delta_{\sigma\rho}\eta_\sigma \ . \tag{2.11}$$

which are different from the canonical ones. Hence the algebra of these composite fields is not closed. As it will discussed in more detail in Sec.2.1, this has a tremendous impact on many aspects and requires a completely revised theoretical framework since most of well-consolidated techniques and results, such as Wick theorem, standard Green's function approach, diagrammatic expansion, do not apply in the case of composite fields.

2.1 Green's functions formalism for composite operators

Let us consider a quantum system of N_e interacting electrons in the Wannier representation, residing on a N-site Bravais lattice of volume V and described by the following Hamiltonian:

$$\mathcal{H} = \mathcal{H}\left[\varphi_\sigma(i)\right] \ . \tag{2.12}$$

Here the notation $\mathcal{H}\left[\varphi_\sigma(i)\right]$ denotes a generic combination of electronic fields $\varphi_\sigma^{(\dagger)}(i) \equiv \varphi_\sigma^{(\dagger)}(\boldsymbol{i}, t)$, related to the annihilation (creation) of a bare Wannier-electron with spin σ at time t on the site labeled by the lattice vector $\boldsymbol{i}$. Hereafter the Heisenberg representation will be used, so that the index i will account for both spatial, $\boldsymbol{i}$ and time, t coordinates as $i \equiv (\boldsymbol{i}, t)$. Any physical property of the system can be connected to the expectation value of a specific operator $A \equiv A[\varphi(i)]$ which, for fixed value of volume and temperature, can be computed in the grand canonical ensemble as:

$$\langle A \rangle = \frac{\mathrm{Tr}\left[e^{-\beta\left(\mathcal{H}-\mu\hat{N}\right)}A\right]}{\mathrm{Tr}\left[e^{-\beta\left(\mathcal{H}-\mu\hat{N}\right)}\right]} = \frac{1}{\mathcal{Z}}\mathrm{Tr}\left[e^{-\beta\left(\mathcal{H}-\mu\hat{N}\right)}A\right] \ , \tag{2.13}$$

where the trace implies a sum over a complete set of states in the Hilbert space. Here $\mathcal{Z} = \mathrm{Tr}\left[e^{-\beta\left(\mathcal{H}-\mu\hat{N}\right)}\right]$ is the partition function, $\beta = 1/k_B T$, $\hat{N}$ is the total number operator:

$$\hat{N} = \sum_{i,\sigma} \varphi_\sigma^\dagger(i)\varphi_\sigma(i) \ , \tag{2.14}$$

while μ is the chemical potential which is fixed according to the constraint $N_e = \left\langle \hat{N} \right\rangle$. For practical purposes it is convenient to define a new Hamiltonian which includes the chemical potential as:

$$H \equiv \mathcal{H}\left[\varphi_\sigma(i)\right] - \mu \sum_{i,\sigma} \varphi_\sigma^\dagger(i)\varphi_\sigma(i) \ , \tag{2.15}$$

so that:

$$\langle A \rangle = \frac{\mathrm{Tr}\left[e^{-\beta H} A\right]}{\mathrm{Tr}\left[e^{-\beta H}\right]} = \frac{1}{\mathcal{Z}} \mathrm{Tr}\left[e^{-\beta H} A\right] \ . \tag{2.16}$$

In order to calculate $\langle A \rangle$, one of the possibilities is to evaluate it by means of the equation of motion formalism which accounts for the calculation of the time derivative of the field $\varphi(i)$ in terms of the commutator $[\varphi(i), \mathcal{H}]$. However, with the understanding that the original electronic fields $\varphi(i)$ are not a good basis in the presence of strong interactions, let us introduce the following set of n composite fields:

$$\psi(i) = \begin{pmatrix} \psi_1(i) \\ \vdots \\ \psi_n(i) \end{pmatrix} \ . \tag{2.17}$$

Up to now, we do not specify the nature, fermionic or bosonic, of the set $\{\psi_n(i)\}$ since both the possibilities are allowed and useful to analyze different properties of the system. In particular, single particle properties are described in terms of fermionic propagators whose calculation, as it will be clear later, requires a fermionic base. On the contrary, response functions such as charge and spin susceptibilities, which are expressed in terms of bosonic propagators, require a bosonic base. Hereafter we will refer to fermionic and bosonic cases as *fermionic sector* and *bosonic sector*, respectively. For the fermionic sector, the following spinorial notation will be used:

$$\psi_m(i) = \begin{pmatrix} \psi_{m,\uparrow} \\ \psi_{m,\downarrow} \end{pmatrix} \ , \ \psi^\dagger_m(i) = \begin{pmatrix} \psi^\dagger_{m,\uparrow} & \psi^\dagger_{m,\downarrow} \end{pmatrix} \ . \tag{2.18}$$

The dynamic of these operators is given by the Heisenberg equation:

$$i\partial_t \psi(i) = [\psi(i), \mathcal{H}] \equiv J(i) \ , \tag{2.19}$$

where $J(i)$, called *"current"* of the basis $\psi(i)$, is a n-component column vector which contains the commutator of each field of the basis with the model Hamiltonian. It is worth noting that is always possible to write the current $J(i)$ as the sum of a contribution proportional to the basis, and a contribution orthogonal to the latter, so that:

$$J(\boldsymbol{i}, t) = \sum_{\boldsymbol{m}} \epsilon(\boldsymbol{i}, \boldsymbol{m}) \psi(\boldsymbol{m}, t) + \delta J(\boldsymbol{i}, t) \ . \tag{2.20}$$

Recalling that the (anti)commutation relation $[A, B]_\eta \equiv AB + \eta BA$ (meaning that $\eta = 1$ for fermions and $\eta = -1$ for bosons) is nothing but the projection of A over B, the requirement of orthogonality implies that:

$$\left\langle \left[\delta J(\boldsymbol{i}, t), \psi^\dagger(\boldsymbol{j}, t)\right]_\eta \right\rangle = 0 \ , \tag{2.21}$$

therefore the linear coefficient ϵ can be derived from the equation:

$$\left\langle \left[J(\boldsymbol{i}, t), \psi^\dagger(\boldsymbol{j}, t)\right]_\eta \right\rangle = \sum_{\boldsymbol{m}} \epsilon(\boldsymbol{i}, \boldsymbol{m}) \left\langle \left[\psi(\boldsymbol{m}, t), \psi^\dagger(\boldsymbol{j}, t)\right]_\eta \right\rangle \ , \tag{2.22}$$

which can be expressed in the following compact form in the Fourier space:

$$m(\boldsymbol{k}) = \epsilon(\boldsymbol{k}) I(\boldsymbol{k}) \tag{2.23}$$

once we define the *normalization matrix*:

$$I(\boldsymbol{i},\boldsymbol{j}) \equiv \left\langle \left[\psi(\boldsymbol{i},t), \psi^\dagger(\boldsymbol{j},t)\right]_\eta \right\rangle = \frac{1}{N}\sum_{\boldsymbol{k}} e^{i\boldsymbol{k}\cdot(\boldsymbol{i}-\boldsymbol{j})} I(\boldsymbol{k}) \ , \tag{2.24}$$

and the *m-matrix*:

$$m(\boldsymbol{i},\boldsymbol{j}) \equiv \left\langle \left[J(\boldsymbol{i},t), \psi^\dagger(\boldsymbol{j},t)\right]_\eta \right\rangle = \frac{1}{N}\sum_{\boldsymbol{k}} e^{i\boldsymbol{k}\cdot(\boldsymbol{i}-\boldsymbol{j})} m(\boldsymbol{k}) \ . \tag{2.25}$$

Unless differently specified, here and after the sum over $\boldsymbol{k}$ will always account for all the possible momenta in the first Brillouin zone. At this point it is important to recall that, because of its definition in terms of composite fields, the normalization matrix $I(\boldsymbol{i},\boldsymbol{j})$ is far from being a trivial identity matrix. Its eigenvalues represent the spectral weight of each field of the basis, allowing for the description of crossover phenomena characterized by a gradual shift of the weight from a field to another which occurs by tuning the intensity of the interaction.

We can now define the generic two-time Green's function:

$$G^Q(i,j) \equiv \left\langle Q\left[\psi(i)\psi^\dagger(j)\right]\right\rangle \ , \tag{2.26}$$

with $Q \in \{C, A, R\}$ for causal, advanced and retarded Green's functions:

$$\begin{aligned} G^C(i,j) &= \left\langle C\left[\psi(i)\psi^\dagger(j)\right]\right\rangle = \theta(t_i - t_j)\left\langle \psi(i)\psi^\dagger(j)\right\rangle & (2.27)\\ &\quad -\eta\theta(t_j - t_i)\left\langle \psi^\dagger(j)\psi(i)\right\rangle \ , & (2.28)\\ G^{R,A}(i,j) &= \left\langle R,A\left[\psi(i)\psi^\dagger(j)\right]\right\rangle = \pm\theta(\pm(t_i - t_j))\left\langle \left[\psi(i),\psi^\dagger(j)\right]_\eta\right\rangle \ . & (2.29) \end{aligned}$$

We recall that in the relations above the temperature dependency is fully contained in the statistical averages $\langle \dots \rangle$ calculated in the grand canonical ensemble (see Eq.2.16). By means of the Heisenberg equation of motion and using the decomposition (2.20) for the current $J(i)$, it is immediate to see that the generic Green's function $G^Q(i,j)$ satisfies the equation:

$$\Lambda(\partial_i) G^Q(i,j) \Lambda^\dagger(\overleftarrow{\partial_j}) = \Lambda(\partial_i) G_0^Q(i,j) \Lambda^\dagger(\overleftarrow{\partial_i}) + \left\langle Q\left[\delta J(i)\delta J^\dagger(j)\right]\right\rangle \ . \tag{2.30}$$

Here $\Lambda(\overleftarrow{\partial_i})$ is a differential operator, which acts to the matrix on its left, defined as:

$$\Lambda(\overleftarrow{\partial_i}) = i\frac{\partial}{\partial t_i} - \epsilon(-i\boldsymbol{\nabla}) \ , \tag{2.31}$$

where, for a generic function $f(x)$, we have:

$$\epsilon(-i\boldsymbol{\nabla}) f(x) = \sum_{\boldsymbol{k}} e^{i\boldsymbol{k}\cdot\boldsymbol{x}} \epsilon(\boldsymbol{k}) f(\boldsymbol{k}) \ . \tag{2.32}$$

The propagator $G_0^Q(i,j)$ is defined by the equation:

$$\Lambda(\partial_i)G_0^Q(i,j) = i\delta\left(t_i - t_j\right) I\left(\boldsymbol{i},\boldsymbol{j}\right) \ . \tag{2.33}$$

Hence, by introducing the Fourier transform:

$$G^Q(i,j) = \frac{1}{N}\sum_{\boldsymbol{k}} \frac{i}{2\pi}\int_{-\infty}^{\infty} d\omega e^{i\boldsymbol{k}\cdot(\boldsymbol{i}-\boldsymbol{j})-i\omega(t_i-t_j)} G^Q(\boldsymbol{k},\omega) \ , \tag{2.34}$$

Eq.2.30 reads as:

$$G^Q(\boldsymbol{k},\omega) = G_0^Q(\boldsymbol{k},\omega) + G_0^Q(\boldsymbol{k},\omega)\Sigma^{Q*}(\boldsymbol{k},\omega)G_0^Q(\boldsymbol{k},\omega) \ , \tag{2.35}$$

where $\Sigma^{Q*}(\boldsymbol{k},\omega)$, called *self-energy*, has the following expression:

$$\Sigma^{Q*}(\boldsymbol{k},\omega) = I^{-1}(\boldsymbol{k})B^Q(\boldsymbol{k},\omega)I^{-1}(\boldsymbol{k}) \ , \tag{2.36}$$

with:

$$B^Q(\boldsymbol{k},\omega) \equiv F.T.\left\langle Q\left[\delta J(i)\delta J^\dagger(j)\right]\right\rangle \ . \tag{2.37}$$

We can also introduce the *irreducible self-energy* $\Sigma^Q(\boldsymbol{k},\omega)$, defined as:

$$\Sigma^Q(\boldsymbol{k},\omega)G^Q(\boldsymbol{k},\omega) = I(\boldsymbol{k})\Sigma^{Q*}(\boldsymbol{k},\omega)G_0^Q(\boldsymbol{k},\omega) \ , \tag{2.38}$$

and use the above relation to rewrite the complete Green's function in terms of the following Dyson-like equation:

$$G^Q(\boldsymbol{k},\omega) = G_0^Q(\boldsymbol{k},\omega) + G_0^Q(\boldsymbol{k},\omega)I^{-1}(\boldsymbol{k})\Sigma^Q(\boldsymbol{k},\omega)G^Q(\boldsymbol{k},\omega) \ , \tag{2.39}$$

which can be formally solved obtaining:

$$G^Q(\boldsymbol{k},\omega) = \frac{I(\boldsymbol{k})}{\omega - \epsilon(\boldsymbol{k}) - \Sigma^Q(\boldsymbol{k},\omega)} \ . \tag{2.40}$$

At this point it is crucial to note that, although formally similar, there is a strict difference between $G^Q(\boldsymbol{k},\omega)$ and the solution of the standard Dyson equation that can be formulated in terms of canonical operators $\varphi(i)$. Unlike in the standard Green's function formalism, $\epsilon(\boldsymbol{k})$ in Eq.2.40 contains part of the interactions since it describes the energy dispersion of composite fields $\psi(i)$ rather than the bare non-interacting dispersion of free-electrons. Furthermore, the normalization matrix $I(\boldsymbol{k})$, which accounts for the weight of the composite fields, is different from the standard identity matrix which appears in the canonical Green's function formalism. Finally, the quantity $G_0^Q(\boldsymbol{k},\omega)$ does not represents a trivial non-interacting propagator since it still contains all the relevant interactions due to its formulation in terms of a basis of composite fields. Because of this, as it will be clear later, unlike in the standard Green's function formalism its calculation represents a hard task to deal with.

2.2 Bosonic and fermionic correlators in the pole-approximation

As follows from Eq.2.39, in the framework of the Green's function formalism for composite operators any (causal, retarded, advanced) two-time Green's function $G^Q(i,j)$ can be completely determined in terms of the "free" propagator $G_0^Q(i,j)$ and the self-energy $\Sigma^Q(\boldsymbol{k},\omega)$, once that a proper basis of composite fields $\{\psi_n(i)\}$ has been selected. We recall that for any choice of $\psi(i)$ we have: $i\partial_t\psi(i) = J(i)$, with $J(\boldsymbol{i},t) = \sum_{\boldsymbol{m}} \epsilon(\boldsymbol{i},\boldsymbol{m})\psi(\boldsymbol{m},t) + \delta J(\boldsymbol{i},t)$ according to Eq.2.39. Hence, if the fields $\{\psi_n(i)\}$ are eigenoperators of the total Hamiltonian, one immediately obtains $\delta J(\boldsymbol{i},t) = 0$, leading to a linear expression for $J(i)$ in terms of the fields of the basis. Consistently, $\Sigma^Q(\boldsymbol{k},\omega) = 0$ as follows from Eq.2.38 and one can solve the problem Hamiltonian by calculating all the relevant two-time correlators in terms of the free propagator only. However, in almost all the relevant cases, an infinite set of composite operators is required in order to take into account all the possible low-energy and virtual processes. Therefore one might simply choose a reasonable number of components for the basic set and then use another approximated method to evaluate the residual dynamical corrections. For example, the fields $\{\psi_n(i)\}$ can be chosen in order to minimize $\delta J(\boldsymbol{i},t)$, so that $\delta J(\boldsymbol{i},t) \approx 0$ compared with the linear contribution. This approximation allows for the calculation of the two-time Green's function $G^Q_{\delta J\approx 0}(i,j)$ in terms of the free-propagator $G_0^Q(i,j)$, however the full propagator $G^Q(i,j)$ still depends on $\delta J(\boldsymbol{i},t)$, therefore all the formalism is only developed with the intention of using the propagators $G^Q_{\delta J\approx 0}(i,j)$ as a basis to set up a perturbative scheme of calculations on the ground of the Dyson equation (2.39).

A slightly different approach consists in completely neglecting the residual operator $\delta J(\boldsymbol{i},t)$ under the assumption that the choice of the extended operatorial basis is such that all the relevant self-energy corrections are included in the free propagator $G_0^Q(i,j)$. Following this approach, called *pole approximation*, one can simply neglect the residual dynamical part of the self-energy which, consistently with the choice of the basis, is believed to have a small total weight. Therefore the full equation of motion for a n-component basis of composite fields reads as:

$$i\partial_t\psi_m(\boldsymbol{i},t) = \sum_{\boldsymbol{j}}\sum_{l=1}^{n} \epsilon_{ml}(\boldsymbol{i},\boldsymbol{j})\psi_l(\boldsymbol{j},t) \;, \tag{2.41}$$

with the energy matrix $\epsilon(\boldsymbol{i},\boldsymbol{j})$ defined by Eq.2.23. Hence one immediately obtains:

$$[\omega - \epsilon(\boldsymbol{k})]\, G^{Q(\eta)}(\boldsymbol{k},\omega) = I^{(\eta)}(\boldsymbol{k}) \;, \tag{2.42}$$

where the dependence on the parameter η, which accounts for the fermionic ($\eta = 1$) or bosonic ($\eta = -1$) nature of the composite fields of the basis, has been explicitly introduced. To solve the above equation one can diagonalize the energy matrix:

$$\sum_{q=1}^{n} \epsilon_{pq}(\boldsymbol{k})\xi_q^{(l)}(\boldsymbol{k}) = \omega_l(\boldsymbol{k})\xi_p^{(l)}(\boldsymbol{k}) \;,\; l \in [1,n] \;, \tag{2.43}$$

where $\xi^{(l)}(\boldsymbol{k})$ and $\omega_l(\boldsymbol{k})$ are eigenvectors and eigenvalues of $\epsilon(\boldsymbol{k})$, and then construct the $n \times n$ transformation matrix $\Omega(\boldsymbol{k})$, whose columns are composed by the eigenvectors $\xi^{(l)}(\boldsymbol{k})$: $\Omega_{pl}(\boldsymbol{k}) = \xi_p^{(l)}(\boldsymbol{k})$, so that:

$$\sum_{b,c=1}^{n} \Omega_{lb}^{-1}(\boldsymbol{k})\epsilon_{bc}(\boldsymbol{k})\Omega_{cd}(\boldsymbol{k}) = \delta_{ld}\omega_l(\boldsymbol{k}) \ , \ l,d \in [1,n] \ . \tag{2.44}$$

By means of this transformation it is possible to rewrite Eq.2.42 under the form:

$$\sum_{c=1}^{n} \left[\omega - \omega_l(\boldsymbol{k})\right] \Omega_{al}(\boldsymbol{k})\Omega_{lc}^{-1}(\boldsymbol{k})G_{cb}^{Q(\eta)}(\boldsymbol{k},\omega) = \sigma_{ab}^{(l)}(\boldsymbol{k}) \ , \ a,b \in [1,n] \ , \tag{2.45}$$

where the *spectral density matrix* $\sigma^{(l)}(\boldsymbol{k})$ is defined as:

$$\sigma_{ab}^{(l)}(\boldsymbol{k}) = \sum_{c=1}^{n} \Omega_{al}(\boldsymbol{k})\Omega_{lc}^{-1}(\boldsymbol{k})I_{cb}(\boldsymbol{k}) \ , \ a,b \in [1,n] \ . \tag{2.46}$$

Finally, we can express a generic two-time Green's function as:

$$G^{Q(\eta)}(\boldsymbol{k},\omega) = \sum_{l=1}^{n} \left\{ \mathcal{P}\left(\frac{\sigma^{(l,\eta)}(\boldsymbol{k})}{\omega - \omega_l(\boldsymbol{k})}\right) - i\pi\delta\left[\omega - \omega_l(\boldsymbol{k})\right] g^{(l,\eta)Q}(\boldsymbol{k}) \right\} \ , \tag{2.47}$$

where the principal value $\mathcal{P}$ includes all the contributions for $\omega \neq \omega_l$ while the contribution for $\omega = \omega_l$ is accounted by the Dirac distribution function $\delta\left[\omega - \omega_l(\boldsymbol{k})\right]$. We can note that while the spectral density matrix $\sigma^{(l)}(\boldsymbol{k})$ is completely determined as a function of energy $\epsilon(\boldsymbol{k})$ and normalization $I(\boldsymbol{k})$ matrices, the matrix $g^{(l,\eta)Q}(\boldsymbol{k})$ depends on the specific: causal (C), retarded (R), advanced (A) nature of the Green's function. In particular, for retarded and advanced Green's functions we have:

$$g^{(l,\eta)R}(\boldsymbol{k}) = -g^{(l,\eta)A}(\boldsymbol{k}) = \sigma^{(l,\eta)}(\boldsymbol{k}) \ , \tag{2.48}$$

and:

$$G^{R,A(\eta)}(\boldsymbol{k},\omega) = \sum_{l=1}^{n} \sigma^{(l,\eta)}(\boldsymbol{k}) \left\{ \mathcal{P}\left(\frac{1}{\omega - \omega_l(\boldsymbol{k})}\right) \mp i\pi\delta\left[\omega - \omega_l(\boldsymbol{k})\right] \right\} \ . \tag{2.49}$$

For the causal (C) Green's function instead, we recall that it can be written as:

$$G^{C(\eta)}(i,j) = \frac{1}{2}\left(G^{R(\eta)}(i,j) + G^{A(\eta)}(i,j) + C_{\psi\psi^\dagger}(i,j) + C_{\psi^\dagger\psi}(i,j)\right) \ , \tag{2.50}$$

where the correlators $C_{\psi\psi^\dagger}(i,j)$ and $C_{\psi^\dagger\psi}(i,j)$ are defined in terms of the unknown momentum-dependent Fourier components $c_{\psi\psi^\dagger}^{(i)}(\boldsymbol{k})$ and $c_{\psi^\dagger\psi}^{(l)}(\boldsymbol{k})$ as follows:

$$C_{\psi\psi^\dagger}(\boldsymbol{k},\omega) \ \equiv \ F.T.\left\langle \psi(i)\psi^\dagger(j)\right\rangle = \sum_{l=1}^{n} \delta\left[\omega - \omega_l(\boldsymbol{k})\right] c_{\psi\psi^\dagger}^{(l)}(\boldsymbol{k}) \ , \tag{2.51}$$

$$C_{\psi^\dagger\psi}(\boldsymbol{k},\omega) \equiv F.T.\left\langle\psi^\dagger(i)\psi(j)\right\rangle = \sum_{l=1}^{n}\delta\left[\omega-\omega_l(\boldsymbol{k})\right]c^{(l)}_{\psi^\dagger\psi}(\boldsymbol{k})\ . \tag{2.52}$$

From a trivial application of the Kubo-Martin-Schwinger (KMS) relation:

$$\langle A(t)B(t')\rangle = \langle B(t')A(t+i\beta)\rangle\ , \tag{2.53}$$

where $A(t)$ and $B(t)$ are generic Heisenberg operators at time t, it immediately follows that:

$$C_{\psi^\dagger\psi}(\boldsymbol{k},\omega) = e^{-\beta\omega}C_{\psi\psi^\dagger}(\boldsymbol{k},\omega)\ , \tag{2.54}$$

meaning that there is only one independent Fourier component: $c^{(l)}_{\psi\psi^\dagger}(\boldsymbol{k})$, which can be determined together with $g^{(l,\eta)C}(\boldsymbol{k})$ by solving the following system of two coupled equations:

$$\begin{cases}\sum_{l=1}^{n}\delta\left(\omega-\omega_l\right)\left[g^{(l,\eta)C}(\boldsymbol{k})-\frac{1}{2\pi}\left(1-\eta e^{-\beta\omega}\right)c^{(l)}_{\psi\psi^\dagger}(\boldsymbol{k})\right]=0\\ \sum_{l=1}^{n}\delta\left(\omega-\omega_l\right)\left[\sigma^{(l,\eta)}(\boldsymbol{k})-\frac{1}{2\pi}\left(1+\eta e^{-\beta\omega}\right)c^{(l)}_{\psi\psi^\dagger}(\boldsymbol{k})\right]=0\end{cases}\ . \tag{2.55}$$

The solution of the above set of coupled equations is remarkably different according to the value of the parameter η. Hence a separate analysis is required for the fermionic ($\eta=1$) and the bosonic ($\eta=-1$) case.

2.2.1 Fermionic sector

In the case of a fermionic basis of composite fields, although commutative and anti-commutative algebra are both possible, it is convenient to choose $\eta=1$. Then the solution of Eq.2.55 is:

$$c^{(l)}(\boldsymbol{k}) = \pi\left[1+\tanh\left(\frac{\beta\omega_l(\boldsymbol{k})}{2}\right)\right]\sigma^{(l,+1)}(\boldsymbol{k})\ , \tag{2.56}$$

$$g^{(l,+1)C}(\boldsymbol{k}) = \tanh\left(\frac{\beta\omega_l(\boldsymbol{k})}{2}\right)\sigma^{(l,+1)}(\boldsymbol{k})\ , \tag{2.57}$$

which gives the following expression for Green's and correlation functions:

$$G^{R,A,(+1)}(\boldsymbol{k},\omega) = \sum_{l=1}^{n}\frac{\sigma^{(l,+1)}(\boldsymbol{k})}{\omega-\omega_l(\boldsymbol{k})\pm i\delta}\ , \tag{2.58}$$

$$G^{C(+1)}(\boldsymbol{k},\omega) = \sum_{l=1}^{n}\sigma^{(l,+1)}(\boldsymbol{k})\left[\frac{1-f_F\left[\omega_l(\boldsymbol{k})\right]}{\omega-\omega_l(\boldsymbol{k})+i\delta}+\frac{f_F\left[\omega_l(\boldsymbol{k})\right]}{\omega-\omega_l(\boldsymbol{k})-i\delta}\right]\ , \tag{2.59}$$

$$C_{\psi\psi^\dagger}(\boldsymbol{k},\omega) = \pi\sum_{l=1}^{n}\delta\left[\omega-\omega_l(\boldsymbol{k})\right]\left[1+\tanh\left(\frac{\beta\omega_l(\boldsymbol{k})}{2}\right)\right]\sigma^{(l,+1)}(\boldsymbol{k})\ , \tag{2.60}$$

$$C_{\psi^\dagger\psi}(\boldsymbol{k},\omega) = \pi\sum_{l=1}^{n}\delta\left[\omega-\omega_l(\boldsymbol{k})\right]\left[1-\tanh\left(\frac{\beta\omega_l(\boldsymbol{k})}{2}\right)\right]\sigma^{(l,+1)}(\boldsymbol{k})\ , \tag{2.61}$$

where $f_F(\omega)$ is the Fermi-Dirac distribution function:

$$f_F(\omega) = \frac{1}{e^{\beta\omega}+1} \ . \tag{2.62}$$

In particular, recalling that:

$$\mathrm{Re}\left[G^{R,A(+1)}(\boldsymbol{k},\omega)\right] = \mp\frac{1}{\pi}\mathcal{P}\int_{-\infty}^{\infty}\frac{d\omega'}{\omega-\omega'}\mathrm{Im}\left[G^{R,A(+1)}(\boldsymbol{k},\omega)\right] \ , \tag{2.63}$$

$$\mathrm{Re}\left[G^{C(+1)}(\boldsymbol{k},\omega)\right] = -\frac{1}{\pi}\mathcal{P}\int_{-\infty}^{\infty}\frac{d\omega'}{\omega-\omega'}\coth\left(\frac{\beta\omega}{2}\right)\mathrm{Im}\left[G^{C(+1)}(\boldsymbol{k},\omega)\right] \tag{2.64}$$

we also immediately obtain the following spectral representations for the Green's functions:

$$G^{R,A(+1)}(\boldsymbol{k},\omega) = \int_{-\infty}^{\infty}d\omega'\frac{\rho^{(+1)}(\boldsymbol{k},\omega)}{\omega-\omega'\pm i\delta} \ , \tag{2.65}$$

$$G^{C(+1)}(\boldsymbol{k},\omega) = \int_{-\infty}^{\infty}d\omega'\rho^{(+1)}(\boldsymbol{k},\omega)\left[\frac{1-f_F(\omega')}{\omega-\omega'\pm i\delta}+\frac{f_F(\omega')}{\omega-\omega'-i\delta}\right] \ , \tag{2.66}$$

where $\rho^{(+1)}(\boldsymbol{k},\omega)$ is the fermionic spectral function defined as:

$$\rho^{(+1)}(\boldsymbol{k},\omega) = \sum_{l=1}^{n}\delta\left[\omega-\omega_l(\boldsymbol{k})\right]\sigma^{(l,+1)}(\boldsymbol{k}) = \mp\frac{1}{\pi}\mathrm{Im}\left[G^{R,A(+1)}(\boldsymbol{k},\omega)\right] \ . \tag{2.67}$$

At this point it is crucial to underline that, in the framework of the Green's function formalism for composite fields developed so far, the correct calculation of any causal Green's function in the fermionic sector can only be done in terms of the retarded/advanced ones as:

$$\mathrm{Re}\left[G^{C(+1)}(\boldsymbol{k},\omega)\right] = \mathrm{Re}\left[G^{R,A(+1)}(\boldsymbol{k},\omega)\right] \ , \tag{2.68}$$

$$\mathrm{Im}\left[G^{C(+1)}(\boldsymbol{k},\omega)\right] = \pm\tanh\left(\frac{\beta\omega}{2}\right)\mathrm{Im}\left[G^{R,A(+1)}(\boldsymbol{k},\omega)\right] \ , \tag{2.69}$$

$$C_{\psi\psi^\dagger}(\boldsymbol{k},\omega) = \mp\left[1+\tanh\left(\frac{\beta\omega}{2}\right)\right]\mathrm{Im}\left[G^{R,A(+1)}(\boldsymbol{k},\omega)\right] \ , \tag{2.70}$$

since the opposite procedure leads to inconsistencies and wrong results. For example, it is immediate to see that the retarded Green's function, calculated as the imaginary part of the causal one (2.59), vanishes at $\omega = 0$. According to Eq.2.58, this would imply that all the weights of the retarded Green's function are zero on the Fermi surface (we recall that the energies are shifted by the chemical potential therefore the locus where $\omega = 0$ defines the Fermi surface), which is obviously not true.

2.2.2 Bosonic sector

For a bosonic set of composite operators, although commutative and anti-commutative algebra are both possible, it is convenient to choose $\eta = -1$. Furthermore, for any

given momentum $\boldsymbol{k}$ it is also convenient to consider two different subspaces $A(\boldsymbol{k})$, $B(\boldsymbol{k})$ such as:

$$\begin{cases} \omega_l(\boldsymbol{k}) = 0 & \text{for } l \in A(\boldsymbol{k}) \subseteq N = \{1, \ldots, n\} \\ \omega_l(\boldsymbol{k}) \neq 0 & \text{for } l \in B(\boldsymbol{k}) = N - A(\boldsymbol{k}) \end{cases} . \tag{2.71}$$

For $l \in B(\boldsymbol{k})$, then for non vanishing values of $\omega_l(\boldsymbol{k})$, the solution of Eq.2.55 is:

$$c^{(l)}(\boldsymbol{k}) = \pi \left[1 + \coth\left(\frac{\beta\omega_l(\boldsymbol{k})}{2} \right) \right] \sigma^{(l,-1)}(\boldsymbol{k}) , \tag{2.72}$$

$$g^{(l,-1)C}(\boldsymbol{k}) = \coth\left(\frac{\beta\omega_l(\boldsymbol{k})}{2} \right) \sigma^{(l,-1)}(\boldsymbol{k}) . \tag{2.73}$$

For all $l \in A(\boldsymbol{k})$ instead, the second of the two equations in (2.55) depends no longer on $c^{(l)}_{\psi\psi^\dagger}(\boldsymbol{k})$ and we come out with one equation and two parameters to be fixed. However, by defining the $\Gamma(\boldsymbol{k})$ function as:

$$\Gamma(\boldsymbol{k}) = \frac{1}{2\pi} \sum_{l \in A(\boldsymbol{k})} c^{(l)}_{\psi\psi^\dagger}(\boldsymbol{k}) = \frac{1}{2} \sum_{l \in A(\boldsymbol{k})} g^{(l,-1)C}(\boldsymbol{k}) , \tag{2.74}$$

it is immediate to see that in the limit for $\omega \to 0$ the second equation in (2.55) gives:

$$\lim_{\omega \to 0} \left[\left(1 - e^{\beta\omega} \right) C_{\psi\psi^\dagger}(\boldsymbol{k}, \omega) \right] = 2\pi\delta(\omega) \sum_{l \in A(\boldsymbol{k})} \sigma^{(l,-1)}(\boldsymbol{k}) . \tag{2.75}$$

We can now distinguish two cases. If $\sum_{l \in A(\boldsymbol{k})} \sigma^{(l,-1)}(\boldsymbol{k}) = 0$ we have:

$$\sum_{l=1}^{n} \delta\left[\omega - \omega_l(\boldsymbol{k}) \right] c^{(l,-1)}_{\psi\psi^\dagger}(\boldsymbol{k}) = 2\pi\delta(\omega)\Gamma(\boldsymbol{k}) + 2\pi \sum_{l \in B(\boldsymbol{k})} \delta\left[\omega - \omega_l(\boldsymbol{k}) \right] \tag{2.76}$$

$$\frac{e^{\beta\omega_l(\boldsymbol{k})}}{e^{\beta\omega_l(\boldsymbol{k})} - 1} \sigma^{(l,-1)}(\boldsymbol{k}) , \tag{2.77}$$

$$\sum_{l=1}^{n} \delta\left[\omega - \omega_l(\boldsymbol{k}) \right] c^{(l,-1)}_{\psi^\dagger\psi}(\boldsymbol{k}) = 2\pi\delta(\omega)\Gamma(\boldsymbol{k}) + 2\pi \sum_{l \in B(\boldsymbol{k})} \delta\left[\omega - \omega_l(\boldsymbol{k}) \right] \tag{2.78}$$

$$\frac{1}{e^{\beta\omega_l(\boldsymbol{k})} - 1} \sigma^{(l,-1)}(\boldsymbol{k}) , \tag{2.79}$$

and:

$$C_{\psi\psi^\dagger}(\boldsymbol{k}, 0) = C_{\psi^\dagger\psi}(\boldsymbol{k}, 0) . \tag{2.80}$$

On the contrary, if $\sum_{l \in A(\boldsymbol{k})} \sigma^{(l,-1)}(\boldsymbol{k}) \neq 0$, $C_{\psi\psi^\dagger}(\boldsymbol{k}, \omega)$ must have a singularity of the type $1/\omega$ in order to satisfy Eq.2.75 in the limit for $\omega \to 0$. Then:

$$\sum_{l=1}^{n} \delta\left[\omega - \omega_l(\boldsymbol{k}) \right] c^{(l,-1)}_{\psi\psi^\dagger}(\boldsymbol{k}) = 2\pi\delta(\omega)\Gamma(\boldsymbol{k}) + 2\pi \sum_{l=1}^{n} \delta\left[\omega - \omega_l(\boldsymbol{k}) \right] \tag{2.81}$$

$$\frac{e^{\beta\omega_l(\boldsymbol{k})}}{e^{\beta\omega_l(\boldsymbol{k})} - 1} \sigma^{(l,-1)}(\boldsymbol{k}) , \tag{2.82}$$

$$\sum_{l=1}^{n} \delta\left[\omega - \omega_l(\boldsymbol{k})\right] c_{\psi^\dagger\psi}^{(l,-1)}(\boldsymbol{k}) = 2\pi\delta(\omega)\Gamma(\boldsymbol{k}) + 2\pi \sum_{l=1}^{n} \delta\left[\omega - \omega_l(\boldsymbol{k})\right] \quad (2.83)$$

$$\frac{1}{e^{\beta\omega_l(\boldsymbol{k})} - 1} \sigma^{(l,-1)}(\boldsymbol{k}) \ , \quad (2.84)$$

and:

$$C_{\psi\psi^\dagger}(\boldsymbol{k}, 0) - C_{\psi^\dagger\psi}(\boldsymbol{k}, 0) = \sum_{l \in A(\boldsymbol{k})} \sigma^{(l,-1)}(\boldsymbol{k}). \quad (2.85)$$

From the above relations it is clear that in the case in which $\sum_{l\in A(\boldsymbol{k})} \sigma^{(l,-1)}(\boldsymbol{k}) \neq 0$ the Fourier coefficients $c_{\psi\psi^\dagger}^{(l,-1)}(\boldsymbol{k})$ and $c_{\psi^\dagger\psi}^{(l,-1)}(\boldsymbol{k})$ diverge as $[\beta\omega_l(\boldsymbol{k})]^{-1}$. However, since correlation functions in direct space must be finite, at finite temperature this is admissible only in the thermodynamic limit and if the dispersion relation $\omega_l(\boldsymbol{k})$ is such that the divergence in momentum space is integrable and the corresponding correlation function in real space remains finite. For finite systems and for infinite systems where the divergence is not integrable we must have $\sum_{l\in A(\boldsymbol{k})} \sigma^{(l,-1)}(\boldsymbol{k}) = 0$ since finite values of the aforementioned quantity are generally related to the presence of long-range orders.

On this basis, under the condition that $\sum_{l\in A(\boldsymbol{k})} \sigma^{(l,-1)}(\boldsymbol{k}) = 0$ as required for finite systems at $T \neq 0$, we obtain:

$$G^{R,A,(-1)}(\boldsymbol{k}, \omega) = \sum_{l=1}^{n} \frac{\sigma^{(l,-1)}(\boldsymbol{k})}{\omega - \omega_l(\boldsymbol{k}) \pm i\delta} \ , \quad (2.86)$$

$$G^{C(-1)}(\boldsymbol{k}, \omega) = \Gamma(\boldsymbol{k}) \left[\frac{1}{\omega + i\delta} - \frac{1}{\omega - i\delta}\right] + \sum_{l\in B(\boldsymbol{k})} \sigma^{(l,-1)}(\boldsymbol{k}) \left[\frac{1 + f_B\left[\omega_l(\boldsymbol{k})\right]}{\omega - \omega_l(\boldsymbol{k}) + i\delta} - \frac{f_B\left[\omega_l(\boldsymbol{k})\right]}{\omega - \omega_l(\boldsymbol{k}) - i\delta}\right] \quad (2.87)$$

$$C_{\psi\psi^\dagger}(\boldsymbol{k}, \omega) = 2\pi\Gamma(\boldsymbol{k})\delta(\omega) + \pi \sum_{l\in B(\boldsymbol{k})} \delta\left[\omega - \omega_l(\boldsymbol{k})\right] \left[1 + \coth\left(\frac{\beta\omega_l(\boldsymbol{k})}{2}\right)\right] \sigma^{(l,-1)}(\boldsymbol{k}) \ , \quad (2.88)$$

$$C_{\psi^\dagger\psi}(\boldsymbol{k}, \omega) = 2\pi\Gamma(\boldsymbol{k})\delta(\omega) - \pi \sum_{l\in B(\boldsymbol{k})} \delta\left[\omega - \omega_l(\boldsymbol{k})\right] \left[1 - \coth\left(\frac{\beta\omega_l(\boldsymbol{k})}{2}\right)\right] \sigma^{(l,-1)}(\boldsymbol{k}) \ , \quad (2.89)$$

where $f_B(\omega)$ is the Bose distribution function:

$$f_B(\omega) = \frac{1}{e^{\beta\omega} - 1} \ . \quad (2.90)$$

We note that:

$$\mathrm{Re}\left[G^{R,A(-1)}(\boldsymbol{k}, \omega)\right] = \mp\frac{1}{\pi}\mathcal{P}\int_{-\infty}^{\infty} \frac{d\omega'}{\omega - \omega'} \mathrm{Im}\left[G^{R,A(-1)}(\boldsymbol{k}, \omega)\right] \ , \quad (2.91)$$

$$\mathrm{Re}\left[G^{C(-1)}(\boldsymbol{k},\omega)\right] = -\frac{1}{\pi}\mathcal{P}\int_{-\infty}^{\infty}\frac{d\omega'}{\omega-\omega'}\tanh\left(\frac{\beta\omega}{2}\right)\mathrm{Im}\left[G^{C(-1)}(\boldsymbol{k},\omega)\right] \quad (2.92)$$

Also in the bosonic case, it is possible to introduce the following spectral function:

$$\rho^{(-1)}(\boldsymbol{k},\omega) = \sum_{l=1}^{n}\delta\left[\omega-\omega_l(\boldsymbol{k})\right]\sigma^{(l,-1)}(\boldsymbol{k}) = \mp\frac{1}{\pi}\mathrm{Im}\left[G^{R,A(-1)}(\boldsymbol{k},\omega)\right] \ . \quad (2.93)$$

However, the $\Gamma(\boldsymbol{k})$ function does not appear in $\rho^{(-1)}(\boldsymbol{k},\omega)$, therefore a spectral representation can only be established for the bosonic retarded/advanced Green's function:

$$G^{R,A(+1)}(\boldsymbol{k},\omega) = \int_{-\infty}^{\infty}d\omega'\frac{\rho^{(-1)}(\boldsymbol{k},\omega)}{\omega-\omega'\pm i\delta} \ . \quad (2.94)$$

The spectral representation for the bosonic causal Green's function exists only when $\Gamma(\boldsymbol{k})=0$:

$$G^{C(-1)}(\boldsymbol{k},\omega) = \int_{-\infty}^{\infty}d\omega'\rho^{(-1)}(\boldsymbol{k},\omega)\left[\frac{1-f_B(\omega')}{\omega-\omega'\pm i\delta}+\frac{f_B(\omega')}{\omega-\omega'-i\delta}\right] \ . \quad (2.95)$$

At this point it is worth emphasizing that, contrarily to the procedure described for the fermionic case, in the bosonic sector the calculation of any retarded/advanced Green's function can only be accounted in terms of the causal ones by means of the following relations:

$$\mathrm{Re}\left[G^{R,A(-1)}(\boldsymbol{k},\omega)\right] = \mathrm{Re}\left[G^{C(-1)}(\boldsymbol{k},\omega)\right] \ , \quad (2.96)$$

$$\mathrm{Im}\left[G^{R,A(-1)}(\boldsymbol{k},\omega)\right] = \pm\tanh\left(\frac{\beta\omega}{2}\right)\mathrm{Im}\left[G^{C(-1)}(\boldsymbol{k},\omega)\right] \ , \quad (2.97)$$

$$C_{\psi\psi^\dagger}(\boldsymbol{k},\omega) = -\left[1+\tanh\left(\frac{\beta\omega}{2}\right)\right]\mathrm{Im}\left[G^{C(-1)}(\boldsymbol{k},\omega)\right] \ . \quad (2.98)$$

The opposite procedure, in fact, is responsible for the loss of information about the $\Gamma(\boldsymbol{k})$ function, whose contribution becomes proportional to $\tan(\omega)\delta(\omega)$.

2.3 Self-consistent scheme

As illustrated in the previous Section, for any given (bosonic or fermionic) set of composite fields it is always possible to set up a proper Green's function formalism which importantly, different from the canonical one, contains part of the interactions in the so-called "free" propagators. Hence, still preserving part of the interactions, in the framework of the pole approximation discussed in Sec.2.2 one can estimate the full Green's function by simply neglecting any additional contribution coming from interactions not accounted in the "free" propagators. Alternatively, unlike in the bare perturbation theory which miserably fails in the strong coupling regime, one might construct a proper composite basis in order to minimize the residual contribution coming from the interactions, allowing for a reliable perturbative calculation of the

full propagators in terms of the "free" ones.

Regardless the particular procedure, a number of problems arise. In particular one can immediately realise that the theoretical framework developed so far only allows for the calculation of any Green's or correlation function that can be expressed in terms of the composite fields of the basis. Hence, if the algebra is not-closed, higher order fields (meaning that they do not belong to the starting basis) appear as unknown parameters in the normalization matrix (2.24), in the equations of motion and then in the m-matrix (2.25), requiring auxiliary constraints to be fixed. To this purpose, in the last decades several approximations among which arbitrary ansatzs, decoupling schemes, use of truncated equations of motion, have been considered in the context of different approaches: Hubbard-I [1] and Hubbard-III [21] approximations, Roth's method [22], Mori truncation [23], Fulde [24] and Plakida [25] projection methods, spectral density approach [26]. However, as shown in Chapter 4 in the context of the Hubbard model, some of these procedures, due to uncontrolled approximations, led to a series of erroneous results characterized by the violation of several sum rules and particle-hole symmetry, the absence of a Mott transition, local quantities in strong disagreement with respect to numerical simulations [27]. All these issues are mainly related to the fact that fixing the external parameters corresponds in putting some constraints on the representation where the Green's functions are realized. As the determination of this representation is not arbitrary, it is clear that there should be no freedom in fixing these quantities which, in principle, must assume values compatible with the dynamics and the algebraic properties of the fields of the basis.

On the basis of these considerations, different from all the other methods developed so far, in the framework of the COM we fix the unknown parameters in terms of a number of self-consistent relations among correlation and Green's functions, called *"Pauli constraints"* (PC) and *"Ward-Takahashi identities"* (WTIs) , which originate from operatorial properties dictated by the algebra of the chosen basis and the symmetries of the model, respectively. These relations, valid at microscopic level, are in principle not satisfied at macroscopic level when expectations values are considered. An example of PC is given by the operatorial relation $\xi(i)\eta(i) = 0$, which is satisfied by the composite fields $\xi(i)$ and $\eta(i)$ defined in Eq.2.3 and Eq.2.4, respectively, in terms of the bare electronic fields. An example of WTI is given by the constraint $\langle A(\boldsymbol{i})\rangle = \langle A(\boldsymbol{j} \neq \boldsymbol{i})\rangle$, which holds in the case of translational invariant systems, or by the relation $\langle A_\uparrow(i)B_\downarrow(j)\rangle = \langle A_\downarrow(i)B_\uparrow(j)\rangle$ which holds for rotational invariant system in the spin-space. Hence, recalling that:

$$\left\langle \psi(i)\psi^\dagger(i)\right\rangle = \frac{1}{N}\sum_{\boldsymbol{k}}\frac{1}{2\pi}\int_{-\infty}^{+\infty} d\omega C_{\psi\psi^\dagger}(\boldsymbol{k},\omega)\ . \tag{2.99}$$

one can easily implement both PCs and WTIs as a set of self-consistent equations in terms of the unknown parameters, allowing for a full consistent calculation of Green's and correlation functions without any ad-hoc or uncontrolled ansatz on the Green's function representation. Then, on the basis of the aforementioned considerations, it is immediate to realise that the presence of unknown parameters, to be fixed self-consistently, does not represent a proper limit for the theory. On the contrary,

it signals the necessity to fix the Green's function representation according to the particular algebra and symmetries under consideration, allowing for the exploration of a plethora of possible different solutions for the model Hamiltonian within an unitary theoretical approach.

Chapter 3

Composite Operator Method for a class of exactly solvable models

As stressed in the previous Chapter, a promising way for the investigation of highly interacting systems consists in reformulate the model Hamiltonian in terms of a set of so-called "composite fields", which appear as the final result of the modifications imposed by the interactions on the original particles. These fields contain from the very beginning the effects of the correlations and, in principle, allow for the exact solution of the model if one succeeds in finding a set of composite operators which completely describes all the possible quasi-particle excitations originated by the interactions. Although the basic theoretical framework is well understood (see Sec.2.1), complications arise from the fact that, in many physical cases, a full description of quasi-particle excitations requires a large or infinite number of composite operators. This issue, which makes the problem analytically unsolvable even for very simple and well-studied models, paves the way to a number of approximated methods among which perturbative approaches or polar approximations.

However, there also exists a large class of fermionic systems, such as finite systems [28, 29], bulk systems with interacting localized electrons [30, 31, 32], Ising-like systems [33, 34, 35, 36], for which a finite number of composite operators suffice to completely describe the properties of the model Hamiltonian [37]. This means that the equations of motion for the composite fields of the basis close, allowing for the exact solution of the model for any dimension in terms of a finite number of parameters, to be self-consistently determined (see. Sec.2.3). As an illustration, we present in this Chapter the exact solution of the t-U-J-h model in the atomic limit, obtained by including an exchange interaction J and an external magnetic field h to the standard t-U Hubbard Hamiltonian [1]. In Sec.3.1.1 we briefly introduce the model and define the theoretical background in the framework of the Composite Operator Method. We show that the COM allows for the exact solution of the model in one dimension, providing a deep insight in the physics of a large class of insulating compounds characterized by charge and spin orderings. The zero temperature phase diagram of the model with a comprehensive characterization of each phase is reported in Sec. 3.1.3. Finite temperature results, including a detailed

study of entropy and system's response functions such as specific heat, charge and spin susceptibilities, is reported in Sec. 3.1.4. Most of the aforementioned results are described in more detail in Ref.[20].

3.1 Hubbard model with magnetic interactions

In the last twenty years, several experimental evidence led to the conviction that single-band Hubbard [1] and t-J models [2] are not sufficient to catch all the relevant features due to strong electronic correlations in a large class of real materials. In fact, although they have been successful in reproducing a plethora of different anomalous phenomena among which magnetic orders [38, 39, 40, 41], Metal Insulator Transition (MIT) [42], Spin Density Waves (SDW) [43] and High-Temperature Superconductivity (HTSC) [44, 45, 46], their application to a large class of compounds is still controversial. The Mott-Hubbard theory, in its simplest formulation, leads to a band gap of the order U ($\sim$ 7-10eV in oxides) which is difficult to justify for charge-transfer insulators such as Co, Ni and Cu. Furthermore, it is also difficult to understand the metallicity of many sulfides among which NiS, CuS and CoS which would require a strong reduction of the on-site interaction U to 1-2eV [47].

Hence, in order to recover the aforementioned physics and with the aim of describing strong interactions between electrons with each other and with other degrees of freedoms (such as lattice vibrations, light), several extensions of the bare Hubbard Hamiltonian have been proposed resulting in the introduction of the so-called Extended Hubbard Models (EHMs). Among these, in the recent years an increasing interest arose in the study of the extended t-U-J model as the minimal model able to reproduce the exchange correlations, widely believed to be the basis of the paring mechanism in Cuprates [48, 49, 50, 51, 52]. Different from Hubbard and t-J models, in the t-U-J Hamiltonian the exchange coupling J is not related to the Hubbard U as $J \approx 4t^2/U$, allowing finite exchange correlations even in the presence of strong on-site couplings. Furthermore, contrarily to the t-J model, an independent treatment of J does not necessarily require the $U \to \infty$ limit in which charge fluctuations are heavily suppressed.

The t-U-J model has been extensively analyzed in 1D and 2D respectively. In the 2D case the t-U-J Hamiltonian has been used as the minimal model capable to describe the charge-transfer nature of Cuprates. In particular, several studies have been done to understand the influence of on-site Coulomb repulsion and spin-spin exchange on superconductivity [53, 54].

Motivated by the discovery of close proximity of magnetic and superconducting ordering in $(TMTSF)_2X$ family of quasi one-dimensional Bechgaard salts [55], analytical and numerical studies on the extended t-U-J model have also been performed in the one-dimensional case. At half-filling, the ground-state phase diagram of the 1D t-U-J model has been intensively studied for both ferro and anti-ferro magnetic couplings in the weak-coupling limit in which $U, J \ll t$. By means of the bosonization procedure, it has been pointed out that, in the presence of ferromagnetic interactions, the system is dominated by superconducting and spin-density-wave instabilities even in the presence of moderate values of the on-site Hubbard interaction [51]. On the contrary, in the presence of an anti-ferromagnetic exchange,

bosonization and transfer-matrix renormalization group methods showed that at half-filling the ground state of the system is a Mott insulator characterized by spontaneous dimerization for $U \ll J$. A transition to a gapless spin liquid phase occurs at $U_c \approx J/2$ [56]. The 1D t-U-J model at $n = 1$ has also been studied with the inclusion of an easy-plane anisotropy in the exchange interaction in order to investigate the coexistence of triplet superconductivity and ferromagnetism in a class of quasi-one-dimensional materials. It has been shown that, in the large bandwidth limit, magnetic correlations are enhanced by the presence of a repulsive Coulomb potential U and a transverse spin-exchange interaction between electrons on nearest-neighbor (NN) sites. Therefore the coexistence of antiferromagnetism and triplet superconductivity is no longer observed except for small values of the Coulomb interaction [57]. Recently it has been also shown that in the weak-coupling limit and for $n = 1$, in the presence of an isotropic anti-ferromagnetic exchange, CDW and bond SDW phases are suppressed and the ground state exhibits an insulating behavior characterized by SDW and bond CDW phases [58].

Because of the complexity of the model, in spite of numerous attempts, there are no exact solutions for the t-U-J Hamiltonian. Within this context we show that the Composite Operators Method, different from other analytical approaches whose applicability is restricted to half-filling or to the weak coupling regime, allows for the exact solution of the one-dimensional t-U-J model in the atomic limit, obtained from the well-known Hubbard model [1] by including an Ising-like spin-spin interaction, parameterized by J, and an external magnetic field h. The resulting t-U-J-h Hamiltonian reads as follows:

$$H = \sum_{\boldsymbol{i},\boldsymbol{j}} \left(t_{\boldsymbol{ij}} - \mu\delta_{\boldsymbol{ij}}\right) c^{\dagger}(i)c(j) + U\sum_{\boldsymbol{i}} n_{\uparrow}(i)n_{\downarrow}(i) + \frac{1}{2}\sum_{\boldsymbol{i}\neq\boldsymbol{j}} J_{ij}n_3(i)n_3(j) - h\sum_{\boldsymbol{i}} n_3(i)\ , \tag{3.1}$$

where $c(i)$ and $c^{\dagger}(i)$ are annihilation and creation operators of electrons in the spinorial notation:

$$c(i) = \begin{pmatrix} c_{\uparrow} \\ c_{\downarrow} \end{pmatrix}\ ,\ c^{\dagger}(i) = \begin{pmatrix} c^{\dagger}_{\uparrow} & c^{\dagger}_{\downarrow} \end{pmatrix}\ . \tag{3.2}$$

satisfying canonical anti-commutation relations . Hereafter the spinorial notation will be used for all fermionic operators. The Heisenberg picture is assumed [$i = (\boldsymbol{i}, t)$], $\boldsymbol{i}$ is a vector of the lattice; $t_{\boldsymbol{i},\boldsymbol{j}}$ denotes the transfer integral and describes hopping between different sites; μ is the chemical potential. $n_{\rho}(i) = c^{\dagger}_{\rho}(i)c_{\rho}(i)$ is the number density operator of electrons at the site $\boldsymbol{i}$ with spin $\rho \in \{\uparrow, \downarrow\}$. The intensity of the local Coulomb interaction is parametrized by U; $n_3(i) = n_{\uparrow}(i) - n_{\downarrow}(i)$ is the third component of the spin density operator; $J_{\boldsymbol{i},\boldsymbol{j}}$ is the exchange inter-site interaction; h represents the strength of the external magnetic field. In this work we restrict our analysis to the narrow-band limit (i.e. $t_{\boldsymbol{ij}} = 0$) and consider only first neighbour interactions by taking $J_{\boldsymbol{i},\boldsymbol{j}} = -2dJ\alpha_{\boldsymbol{i},\boldsymbol{j}}$, where d is the dimensionality of the system and $\alpha_{\boldsymbol{i},\boldsymbol{j}}$ is the projection operator on the nearest neighbour sites. For a d-dimensional cubic Bravais lattice of lattice constant a, the Fourier transform of $\alpha_{\boldsymbol{i},\boldsymbol{j}}$ is $F.T.\left[\alpha_{\boldsymbol{i},\boldsymbol{j}}\right] = \frac{1}{d}\sum_{n=1}^{d}\cos(k_n a)$. Then, the Hamiltonian (3.1) can be written

under the form:

$$H = \sum_{\boldsymbol{i}} \left[-\mu n(i) + UD(i) - hn_3(i) - dJn_3(i)n_3^{\alpha}(i) \right] \ , \tag{3.3}$$

where $n(i) = c^{\dagger}(i)c(i)$ is the total density operator and $D(i) = n_{\uparrow}(i)n_{\downarrow}(i) = \frac{1}{2}n(i)[n(i) - 1]$ the double occupancy operator. Hereafter, for a generic operator $\Phi(i)$ we use the following notation: $\Phi^{\alpha}(i) \equiv \sum_{\boldsymbol{j}} \alpha_{\boldsymbol{ij}} \Phi(\boldsymbol{j}, t)$. We note that (3.3) is invariant under the transformation: $(h \to -h \ , \ n_{\uparrow} \to n_{\downarrow})$. Also, under the particle-hole transformation, the chemical potential scales as $\mu(2 - n) = U - \mu(n)$.

3.1.1 Composite fields and Green's function formalism

According to the standard procedure described in Chapter 3, the first step in the framework of the COM consists in the choice of a proper basis of composite fields which can be determined by taking into account the properties of the system which are aimed to be described. To this end, it is instructive to introduce the following classes of composite fields:

$$\psi_p^{(\xi)}(i) = \xi(i) \left[n_3^{\alpha}(i) \right]^{p-1} \ , \tag{3.4}$$

$$\psi_p^{(\eta)}(i) = \eta(i) \left[n_3^{\alpha}(i) \right]^{p-1} \ , \tag{3.5}$$

which are well-defined for all $p \geqslant 1$, where $\xi(i) = [1 - n(i)]c(i)$ and $\eta(i) = n(i)c(i)$ are the Hubbard operators responsible for the transitions $|0\rangle_i \leftrightarrow |\rho\rangle_i$ at the site $\boldsymbol{i}$, and $|\rho\rangle_i \leftrightarrow |\uparrow\downarrow\rangle_i$, respectively. By simple anticommutations, it is immediate to see that the the equation of motion for a generic field $\psi_p^{(\xi,\eta)}(i)$ only involves the higher order field $\psi_{p+1}^{(\xi,\eta)}(i)$ according to the relations:

$$i\partial_t \psi_p^{(\xi)}(i) = \left[\psi_p^{(\xi)}, H \right] = -\left(\mu + h\sigma_3 \right) \psi_p^{(\xi)}(i) - 2J\sigma_3 \psi_{p+1}^{(\xi)}(i) \ , \tag{3.6}$$

$$i\partial_t \psi_p^{(\eta)}(i) = \left[\psi_p^{(\eta)}, H \right] = -\left(\mu - U + h\sigma_3 \right) \psi_p^{(\eta)}(i) - 2J\sigma_3 \psi_{p+1}^{(\eta)}(i) \ , \tag{3.7}$$

where σ_3 is the third Pauli matrix. Hence one might simply think to build up a closed basis (meaning that the equations of motion for the fields of the basis close) by including all the possible fields $\psi_p^{(\xi,\eta)}(i)$, with $p \geqslant 1$. As follows from the equations of motion of $\psi_p^{(\xi,\eta)}(i)$, this basis will only formally solve the problem Hamiltonian since, in principle, an infinite number of fields are required. However, one might note that, on the basis of the algebraic relations:

$$\begin{array}{lll} D^p(i) = D(i) & , & [n_3(i)]^{2p} = n(i) - 2D(i) \\ n^p = n(i) + (2^p - 2)\, D(i) & , & [n_3(i)]^{2p+1} = n_3(i) \\ n^p(i)D(i) = 2^p D(i) & , & D(i)n_3(i) = 0 \ , \end{array} \tag{3.8}$$

the following recursion formulas can be established for the field $[n_3^\alpha(i)]^p$ for any $p \geqslant 1$:

$$[n_3^\alpha(i)]^{2p-1} = \sum_{m=1}^{2d} A_m^{(p)} [n_3^\alpha(i)]^{2m-1} , \tag{3.9}$$

$$[n_3^\alpha(i)]^{2p} = \sum_{m=1}^{2d} A_m^{(p)} [n_3^\alpha(i)]^{2m} , \tag{3.10}$$

where $A_m^{(p)}$ are rational numbers, satisfying the sum rule $\sum_{m=1}^{4d} A_m^{(p)} = 1$, with $A_m^{(p)} = \delta_{pm}$ for $1 \leqslant p \leqslant m$. For $p > m$ the expressions of the coefficients $A_m^{(p)}$ depend on the coordination number $z = 2d$ and are reported in Appendix A.1. Hence, because of algebraic relations and from Eqs.3.9-3.10, it is immediate to realize that a finite number of composite fields suffice to determine a closed basis $\psi(i)$ allowing for the exact solution of the model in *any dimension*. In particular, for a given dimension d with coordination number $z = 2d$ we have:

$$\psi(i) = \begin{pmatrix} \psi_\uparrow^{(\xi)}(i) \\ \psi_\uparrow^{(\eta)}(i) \\ \psi_\downarrow^{(\xi)}(i) \\ \psi_\downarrow^{(\eta)}(i) \end{pmatrix} , \tag{3.11}$$

where $\psi_\rho^{(\xi,\eta)}(i)$ are multiplet operators of rank $2z+1$ defined as:

$$\psi_\rho^{(\xi)}(i) = \begin{pmatrix} \xi_\rho(i) \\ \xi_\rho(i)\,[n_3^\alpha(i)] \\ \xi_\rho(i)\,[n_3^\alpha(i)]^2 \\ \vdots \\ \xi_\rho(i)\,[n_3^\alpha(i)]^{2z+1} \end{pmatrix} , \psi_\rho^{(\eta)}(i) = \begin{pmatrix} \eta_\rho(i) \\ \eta_\rho(i)\,[n_3^\alpha(i)] \\ \eta_\rho(i)\,[n_3^\alpha(i)]^2 \\ \vdots \\ \eta_\rho(i)\,[n_3^\alpha(i)]^{2z+1} \end{pmatrix} . \tag{3.12}$$

These fields satisfy the equation of motion:

$$i\partial_t \psi_\rho^{(\xi)}(i) = \left[\psi_\rho^{(\xi)}, H\right] = \varepsilon_\rho^{(\xi)} \psi_p^{(\xi)}(i) , \tag{3.13}$$

$$i\partial_t \psi_\rho^{(\eta)}(i) = \left[\psi_\rho^{(\eta)}, H\right] = \varepsilon_\rho^{(\eta)} \psi_p^{(\eta)}(i) , \tag{3.14}$$

where $\varepsilon_\rho^{(\xi)}$ and $\varepsilon_\rho^{(\eta)}$ are the energy matrices which can be calculated by means of the equations of motion (3.6)-(3.7) and the recursion rules (3.9)-(3.10), whose eigenvalues, $E_\rho^{(\xi,n)}$ and $E_\rho^{(\eta,n)}$, with $1 \leqslant n \leqslant 4d+1$, determine the quasi-particle excitation spectrum. Explicit expressions of $\varepsilon_\rho^{(\xi,n)}$ and $E_\rho^{(\xi,n)}$ for the one-dimensional case with $d = 1$ and $z = 2$ are given in Appendix A.2.

Following the procedure described in Sec.(2.1), the knowledge of a complete set of eigenoperators and eigenvalues of the Hamiltonian allows for the exact expression of retarded Green's functions and correlation functions in terms of the spectral density

matrices $\sigma^{(\xi,\eta)}$:

$$G_{\rho}^{(s)}(\omega) = \sum_{n=1}^{2z+1} \frac{\sigma_{\rho}^{(s,n)}}{\omega - E_{\rho}^{(s,n)} + i\delta} , \tag{3.15}$$

$$C_{\rho}^{(s)}(\omega) = \pi \sum_{n=1}^{2z+1} \sigma_{\rho}^{(s,n)} \left[1 + \tanh\left(\frac{E_{\rho}^{(s,n)}}{2k_B T} \right) \right] \delta\left(\omega - E_{\rho}^{(s,n)} \right) , \tag{3.16}$$

where in the above relations $s \in \{\xi, \eta\}$, and the generic ab matrix element of $\sigma^{(\xi,\eta)}$:

$$\sigma_{\rho;ab}^{(s,n)} = \Omega_{\rho,an}^{(s)} \sum_{c=1}^{2z+1} \left[\Omega_{\rho;nc}^{(s)} \right]^{-1} I_{\rho;cb}^{(s)} , \tag{3.17}$$

is defined in terms of the normalization matrix:

$$I_{\rho}^{(s)} = \left\langle \left\{ \psi_{\rho}^{(s)}(\boldsymbol{i}, t), \psi_{\rho}^{(s)\dagger}(\boldsymbol{i}, t) \right\} \right\rangle , \tag{3.18}$$

and the matrix $\Omega_{\rho}^{(s)}$, whose columns contain the eigenvectors of the energy matrices $\varepsilon_{\rho}^{(s)}$. Expressions for $I_{\rho}^{(s)}$ and $\Omega_{\rho}^{(s)}$ in the one-dimensional case are reported in Appendix A.2. It can be noted that while the energy matrices are completely determined in terms of the parameters of the model (see Eq.A.18 and Eq. A.19 in Appendix A.2), because of the algebraic relations (3.9)-(3.10) the matrix elements $I_{\rho;ab}^{(s)}$ can be expressed in terms of the elements of the first row: $I_{\rho;1p}^{(s)}$, with $1 \leqslant p \leqslant 2z+1$, reported below:

$$I_{\rho;1p}^{(\xi)} = \kappa^{(p)} - \lambda_{\bar{\rho}}^{(p)} , \tag{3.19}$$

$$I_{\rho;1p}^{(\eta)} = \lambda_{\bar{\rho}}^{(p)} , \tag{3.20}$$

where $\kappa^{(p)} = \left\langle [n_3^{\alpha}(i)]^{p-1} \right\rangle$ and $\lambda^{(p)} = \left\langle n_{\rho}(i) \, [n_3^{\alpha}(i)]^{p-1} \right\rangle$ are unknown correlators. Hence, the exact solution of the model for a given dimension d depends, apart from the external parameters U, J, h, $n \equiv \langle n(i) \rangle$, also on the aforementioned $2(2z+1)$ correlators (the factor two accounts for spin degeneracy) which, together with the chemical potential μ, play the role of external parameters to be determined self-consistently.

3.1.2 A self-consistent scheme for the one-dimensional case

Let us consider a one-dimensional chain ($d = 1$, $z = 2d = 2$). For such a system the previous analysis shows that the exact solution of the model Hamiltonian (3.3) requires the calculation of six unknown parameters: $\kappa^{(p)}$, $\lambda_{\rho}^{(p)}$ (we recall that although $1 \leqslant p \leqslant 5$, the number of independent correlators is reduced six thanks to algebraic relations, Eqs.3.9-3.10). To this purpose, let us focus our analysis on an arbitrary site of the chain, say $\boldsymbol{i}$, and split the Hamiltonian (3.3) as $H \equiv H_0^{(i)} + H_I^{(i)}$, where $H_I^{(i)}$ connects the site $\boldsymbol{i}$ with its nearest neighbours:

$$H_I^{(i)} = -2J n_3(i) n_3^{\alpha}(i) , \tag{3.21}$$

while $H_0^{(i)}$ accounts for all the remaining interactions including the central site $\boldsymbol{i}$, and therefore, because of the presence of NN interactions only, describes a system where the original lattice has been split in two non-interacting sub-lattices. Hence, by noting that $H_0^{(i)}$ and $H_I^{(i)}$ commute and by defining the $H_0^{(i)}$-representation as the representation in which the statistical average of a generic operator $O(i)$ is accounted in terms of $H_0^{(i)}$ only:

$$\langle O(i)\rangle_0 = \frac{\left\langle O e^{-\beta H_0(i)}\right\rangle}{\left\langle e^{-\beta H_0(i)}\right\rangle} \ , \tag{3.22}$$

we can easily express the full statistical average of any operator $O(i)$ as:

$$\langle O(i)\rangle = \frac{\left\langle O e^{-\beta H_I(i)}\right\rangle_0}{\left\langle e^{-\beta H_I(i)}\right\rangle_0} \ , \tag{3.23}$$

where, by construction, all the correlators in the $H_0^{(i)}$-representation which relate two sites, say $\boldsymbol{i}$ and $\boldsymbol{j}$, belonging to different sub-lattices can be factorized as follows:

$$\langle a(i)b(j)\rangle_0 = \langle a(i)\rangle_0 \langle b(j)\rangle_0 \ . \tag{3.24}$$

As shown in detail in Appendix A.3, following this approach all the relevant statistical averages can be expressed in terms of six unknown parameters:

$$\begin{array}{lll} G_1 \equiv \langle n(i)\rangle_0 & , & X_1 \equiv \langle n^\alpha(i)\rangle_0 \\ G_2 \equiv \langle n_3(i)\rangle_0 & , & X_2 \equiv \langle n_3^\alpha(i)\rangle_0 \\ G_3 \equiv \langle D(i)\rangle_0 & , & X_3 \equiv \langle D^\alpha(i)\rangle_0 \end{array} \tag{3.25}$$

Thanks to algebraic relations, G_1, G_2, G_3 can be calculated analytically in terms of the external parameters and the chemical potential (see Eqs.A.36-A.38 in Appendix A.3) while the remaining three parameters can be fixed according to the following three self-consistent equations:

$$\begin{cases} \langle n(i)\rangle = \langle n^\alpha(i)\rangle \\ \langle n_3(i)\rangle = \langle n_3^\alpha(i)\rangle \\ \langle D(i)\rangle = \langle D^\alpha(i)\rangle \end{cases} \ . \tag{3.26}$$

which hold under the assumption of an homogeneous system and can be written in terms of the internal parameters as reported in EqA.46. Finally, the chemical potential μ is fixed self-consistently by requiring $\langle n(i)\rangle = n$, where n is the total particle density, which gives:

$$n = 2\left(1 - C^{(\xi)}_{\rho;1,1} - C^{(\eta)}_{\rho;1,1}\right) \ , \tag{3.27}$$

and can be expressed in terms of the external parameters as reported in Eq.A.47.

Once that all the internal parameters are known, all single particle properties and correlation functions, among which the chemical potential μ, the internal energy per site E:

$$E = U\langle D(i)\rangle - J\langle n_3(i) n_3^\alpha(i)\rangle - 2hm \ . \tag{3.28}$$

the magnetization $m = \langle n_3(i) \rangle$, can be calculated in terms of G_n and X_n, with $1 \leqslant n \leqslant 3$ (analytical expressions are reported in Appendix A.3). This allows for the calculations of all the relevant response functions, such as specific heat C, charge χ_c and spin χ_s susceptibilities, defined as follows:

$$C = \frac{dE}{dT} \ , \ \chi_c = T\frac{\partial n}{\partial \mu} \ , \ \chi_s = \frac{\partial m}{\partial h} \ . \tag{3.29}$$

Furthermore, by noting that the cross GFs $\left\langle R\left[\psi^{(\xi)}(\boldsymbol{i},t)\psi^{(\eta)\dagger}(\boldsymbol{i},t')\right]\right\rangle$ vanish, it is also possible to calculate the electronic density of states (DOS) for spin ρ as:

$$\begin{aligned} N_\rho(\omega) &= \left(-\frac{1}{\pi}\right) Im\left[G^{(\xi)}_{\rho,11}(\omega) + G^{(\eta)}_{\rho,11}(\omega)\right] = \\ &= \sum_{n=1}^{4d+1}\left[\sigma^{(\xi,n)}_{\rho,11}\delta\left(\omega - E^{(\xi)}_n\right) + \sigma^{(\eta,n)}_{\rho,11}\delta\left(\omega - E^{(\eta)}_n\right)\right] \ . \end{aligned} \tag{3.30}$$

3.1.3 Results in the zero-temperature limit

The zero temperature limit plays a crucial role in the characterization of low-dimensional systems. It represents not only the region in which quantum phase transitions take place, but also the regime in which strongly correlations are greatly enhanced. For one-dimensional systems, according to Mermin and Wagner theorem [59], the presence of long-range orders is merely confined to the $T = 0$ case. Therefore, in the framework of the U-J-h model, this limit is studied with the aim of characterize all the possible phases that appear by varying the external model parameters n, U, J, h. To this purpose, we choose $|J| = 1$ to fix the energy scale and analyze both ferro ($J = 1$) and anti-ferro ($J = -1$) inter-site magnetic couplings by solving numerically the self-consistent equations (3.26), (3.27). Furthermore, because of particle-hole symmetry, we also restrict our analysis to $0 \leqslant n \leqslant 1$.

3.1.3.1 Ferromagnetic inter-site coupling

In the case of ferromagnetic coupling ($J = 1$), the inter-site exchange and the magnetic field are not in a competition since both of them tend to polarize the spins. The only competitive energy scale is U, which tends to create doubly occupied sites, destroying the ferromagnetic ordering. Hence we notice the presence of only two different phases, Fig.(3.1), characterized by the presence or the absence of ferromagnetic long-range order:

NM-phase. This phase, called "non-magnetic" (NM) phase, is observed for $U < U_c$ where $U_c = -2(J + h)$ and for $0 \leq n \leq 2$. As one would expect, it originates when the attractive local U potential prevails on both the magnetic field and the ferromagnetic coupling, resulting in a configuration in which all the sites are doubly occupied. As a result, because of the lack of a pair-pair interaction term in the Hamiltonian (3.3), the system is completely non-interacting at any filling. The on-site potential U is the only energy scale in all the relevant single particle properties and correlation functions which are the squares of the corresponding one-site ones:

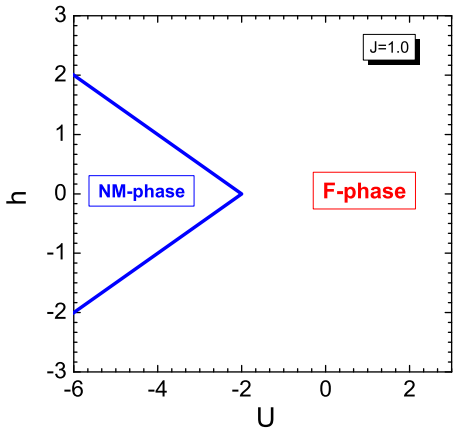

Figure 3.1: Phase diagrams in the U-h plane for $J = 1$ and $0 \leqslant n \leqslant 1$ at $T = 0$.

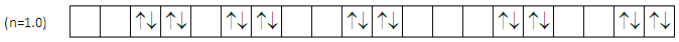

Figure 3.2: One of the possible spin and charge configurations for the NM-phase at $T = 0$, $J = 1$. $\uparrow$and $\downarrow$ represent the two possible spin states.

$$\begin{array}{ll} \mu = U/2 & \langle n(i)n^{\alpha}(i)\rangle = n^2 \\ \langle D(i)\rangle = n/2 & \langle n_3(i)n_3^{\alpha}(i)\rangle = 0 \\ \langle m(i)\rangle = 0 & \langle D(i)D^{\alpha}(i)\rangle = (n/2)^2 \end{array} \quad , \ \forall\ 0 \leq n \leq 2\ . \tag{3.31}$$

Recalling (3.28), it is immediate to see that the internal energy per site has the value $E_{NM} = nU/2$. A typical configuration occurring in this phase is a mixture of doubly occupied and empty sites and is shown in Fig. 3.2.

F-phase. This phase, called "ferromagnetic" (F) phase, is observed for $U > U_c$ and for $0 \leq n \leq 2$. It is characterized by a dominant ferromagnetic order and finite values of magnetization and spin-spin correlation functions. In the region $0 \leq n \leq 1$ the double occupancy is zero and all the spins are polarized. In this regime of filling the on-site potential U does not play any role and all the single particle properties and correlation functions depend on J and h as:

$$\begin{array}{ll} \mu = -J - h & \langle n(i)n^{\alpha}(i)\rangle = n \\ \langle D(i)\rangle = 0 & \langle n_3(i)n_3^{\alpha}(i)\rangle = n \\ \langle m(i)\rangle = n/2 & \langle D(i)D^{\alpha}(i)\rangle = 0 \end{array} \quad , 0 \leq n \leq 1\ . \tag{3.32}$$

At $n = 1$ the chemical potential exhibits a discontinuity and jumps at the value $\mu = U/2$. For $n > 1$ instead we have $\mu = J + h + U$, in agreement with the particle-hole scaling law $\mu(2 - n) = U - \mu(n)$. The double occupancy increases linearly with n; correspondingly, the magnetization and the spin-spin correlation function $\langle n_3(i)n_3^{\alpha}(i)\rangle$ decrease:

$$\begin{array}{ll} \mu = J + h + U & \langle n(i)n^{\alpha}(i)\rangle = 3n - 2 \\ \langle D(i)\rangle = n - 1 & \langle n_3(i)n_3^{\alpha}(i)\rangle = 2 - n \\ \langle m(i)\rangle = 1 - n/2 & \langle D(i)D^{\alpha}(i)\rangle = n - 1 \end{array} \quad , 1 \leq n \leq 2\ . \tag{3.33}$$

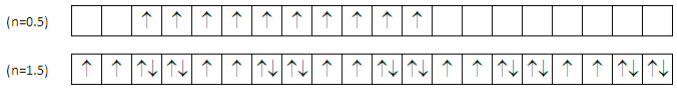

Figure 3.3: Some of the possible spin and charge configurations for the F-phase at $T = 0$, $J = 1$.

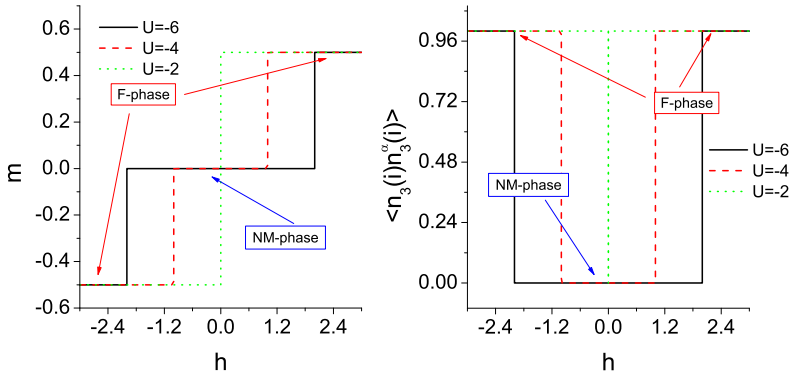

Figure 3.4: Signature of NM-F phase transition in magnetization (left) and spin-spin correlation function (right) plotted as functions of the magnetic field h, for different values of U at $n = 1$ and $J = 1$.

The internal energy (3.28) has the value:

$$E_F = \begin{cases} -n(J+h) & , \ 0 \leq n \leq 1 \\ U(n-1) - (2-n)(J+h) & , \ 1 \leq n \leq 2 \end{cases} . \tag{3.34}$$

A typical configuration occurring in this phase is shown in Fig. 3.3 for the cases $n < 1$ and $n > 1$. We see that:

$$E_F - E_{NM} = \begin{cases} -n\left(J + h + \frac{U}{2}\right) & , \ 0 \leq n \leq 1 \\ -(2-n)\left(J + h + \frac{U}{2}\right) & , \ 1 \leq n \leq 2 \end{cases} , \tag{3.35}$$

therefore, regardless of the specific value of the filling n, there is a critical value of the local potential $U_c = -2(J + h)$ which separates the two phases.

In Fig. 3.4 we report some signatures of the NM-F phase transition occurring in magnetization and spin-spin correlation function.

It is immediate to see that for $U < -2$, there is a phase transition from the NM state to the F phase at $h = h_c = -J - U/2$. According to (3.31), both magnetization and spin-spin correlation functions are zero for $h < h_c$. Vice versa, when $h > h_c$, $\langle m(i) \rangle$ and $\langle n_3(i) n_3^{\alpha}(i) \rangle$ assume finite values according to (3.32)-(3.33). For $U \geq -2$ instead, there is no phase transition: the system is always in the F phase. In particular, even in the absence of magnetic field, there is a magnetic order induced by J signaled by finite spin-spin correlations.

3.1.3.2 Antiferromagnetic inter-site coupling

Contrarily to the ferromagnetic case, for $J = -1$ all the energy scales are in competition since each of them favours a different magnetic order. The on-site potential U, favouring double occupancy, suppresses any magnetic order; J and h favour antiferromagnetic and ferromagnetic orders, respectively. Due to such a competition among different energy scales, we notice a very reach phase diagram, reported in Fig. 3.5. In the regions $0 \leq n \leq 0.5$ and $1.5 \leq n \leq 2$ the phase diagram does not depend on n; as shown in Figs. 3.5*a* and 3.5*b*, we observe three different phases which join at the 3-critical point P_1=$\{U = -2, h = 1\}$. In the region $0.5 \leq n \leq 1.5$ the phase diagram depends on n and is characterized by four different phases and two tricritical points: P_1 and P_2. In Figs. 3.5*c* and 3.5*d* we report the phase diagram for $n = 1$. Contrarily to what happens for P_1 , the position of P_2 depends on the filling, as shown in Fig. 3.7. We can also note that, changing the filling, P_1 and P_2 never coincide and remain always well separated each other. A detailed description of all the observed phases is reported below:

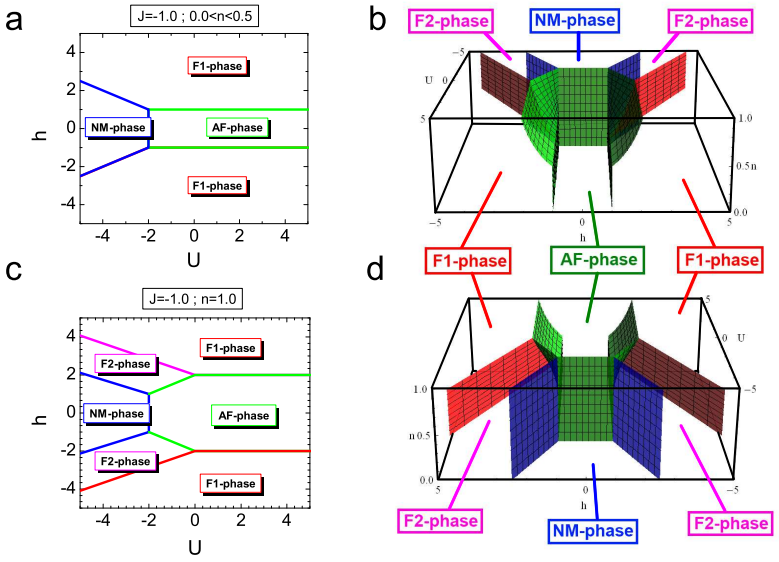

Figure 3.5: 2D and 3D phase diagrams for $J = -1.0$ at $T = 0$.

NM-phase. Regardless on the particular sign ($J = 1$, $J = -1$) of the magnetic inter-site interaction, a "non-magnetic" (NM) phase is observed when the local on-site interaction U dominates with respect to all the other energy scales. As already pointed out for the $J = 1$ case, this phase is characterized by all doubly occupied sites, Fig. 3.2, and all the relevant single particle properties and correlation functions are the squares of the corresponding one-site ones (3.31).

AF-phase. For $U > -2J$ and for low values of the magnetic field h an antiferromagnetic (AF) order is observed in the entire region of filling. This phase is realized in the range in which J is dominant with respect to all the other energy scales, meaning that U is positive or not negative enough to induce a significant double occupancy and h is not sufficient to completely polarize the spins. Hence, this phase is characterized by the absence of magnetization and double occupancy and by negative spin-spin correlations:

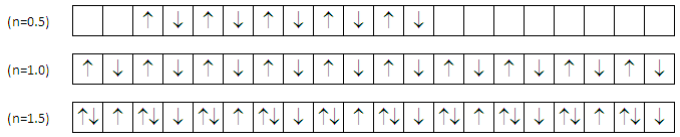

Figure 3.6: Some of the possible spin and charge configurations for the AF-phase at $T = 0$, $J = -1$.

$$\mu = \begin{cases} J & 0 \leq n < 1 \\ U/2 & n = 1 \\ U - J & 1 < n \leq 2 \end{cases} \tag{3.36}$$

$$\langle m(i) \rangle = 0 \quad \forall \quad 0 \leq n \leq 2 \tag{3.37}$$

$$\langle D(i) \rangle = \begin{cases} 0 & 0 \leq n \leq 1 \\ n - 1 & 1 \leq n \leq 2 \end{cases} \tag{3.38}$$

$$\langle n(i) n^{\alpha}(i) \rangle = \begin{cases} n & 0 \leq n \leq 1 \\ 3n - 2 & 1 \leq n \leq 2 \end{cases} \tag{3.39}$$

$$\langle n_3(i) n_3^{\alpha}(i) \rangle = \begin{cases} -n & 0 \leq n \leq 1 \\ n - 2 & 1 \leq n \leq 2 \end{cases} \tag{3.40}$$

$$\langle D(i) D^{\alpha}(i) \rangle = \begin{cases} 0 & 0 \leq n \leq 1 \\ n - 1 & 1 \leq n \leq 2 \end{cases} \tag{3.41}$$

$$E_{AF} = \begin{cases} Jn & 0 \leq n \leq 1 \\ U(n-1) - J(n-2) & 1 \leq n \leq 2 \end{cases} . \tag{3.42}$$

A typical configuration occurring in this phase is shown in Fig. 3.6 for the cases $n = 0.5$, $n = 1$ and $n = 1.5$.

F1-phase. When the external magnetic field is strong enough to dominate with respect to J, a ferromagnetic behavior (F1) is observed despite of the presence of an anti-ferromagnetic coupling. In this phase, the effect of the magnetic field induces a full spin polarization and the magnetization reaches its saturation value. Due to the presence of an anti-ferromagnetic coupling, contrarily to what has been said for the F-phase, nearest-neighbor spin-spin and charge-charge correlation functions remain zero until we reach quarter filling. At $n = 0.5$ a charge order state is observed characterized by a checkerboard structure.

$$\mu = \begin{cases} h & 0 \leq n < 0.5 \\ h - 2J & 0 < n < 1.0 \\ U/2 & n = 1 \\ -h + 2J + U & 1 < n < 1.5 \\ -h + U & 1.5 < n < 2 \end{cases} \tag{3.43}$$

$$\langle m(i)\rangle = \begin{cases} n/2 & 0 \le n \le 1 \\ 1 - n/2 & 1 \le n \le 2 \end{cases} \tag{3.44}$$

$$\langle D(i)\rangle = \begin{cases} 0 & 0 \le n \le 1 \\ n - 1 & 1 \le n \le 2 \end{cases} \tag{3.45}$$

$$\langle n(i)n^{\alpha}(i)\rangle = \begin{cases} 0 & 0 \le n \le 0.5 \\ 2n - 1 & 0.5 \le n \le 1.5 \\ 4(n-1) & 1.5 \le n \le 2 \end{cases} \tag{3.46}$$

$$\langle n_3(i)n_3^{\alpha}(i)\rangle = \begin{cases} 0 & 0 \le n \le 0.5 \\ 2n - 1 & 0.5 \le n \le 1 \\ 3 - 2n & 1 \le n \le 1.5 \\ 0 & 1.5 \le n \le 2 \end{cases} \tag{3.47}$$

$$\langle D(i)D^{\alpha}(i)\rangle = \begin{cases} 0 & 0 \le n \le 1.5 \\ 2n - 3 & 1.5 \le n \le 2 \end{cases} \tag{3.48}$$

$$E_{F1} = \begin{cases} -nh & 0 \le n \le 0.5 \\ -J(2n-1) - nh & 0.5 \le n \le 1 \\ U(n-1) - J(3-2n) - h(2-n) & 1 \le n \le 1.5 \\ U(n-1) - h(2-n) & 1.5 \le n \le 2 \end{cases} . \tag{3.49}$$

For $0.5 < n < 1.5$ instead, as reported in Fig. 3.8, the spin-spin correlation function becomes finite; $\langle n_3(i)n_3^{\alpha}(i)\rangle$ increases with n up to half-filling, then decreases and vanishes for $n \ge 1.5$. For $0.5 < n \le 1.0$, we have no double occupancy and the sites are singly occupied by electrons with aligned spins. Exactly at half-filling, all the sites are singly occupied, all the spins are aligned and the magnetization assumes its maximum value. For $1.0 \le n < 1.5$, the double occupancy becomes finite but the nearest-neighbor correlation function $\langle D(i)D^{\alpha}(i)\rangle$ is always zero; exactly at $n = 1.5$ we observe another checkerboard structure with a pattern composed of alternating singly and doubly occupied sites. For $n \ge 1.5$, $\langle D(i)\rangle$ and $\langle D(i)D^{\alpha}(i)\rangle$ increase up to the maximum value, while the magnetization goes to zero as we approach $n = 2$.

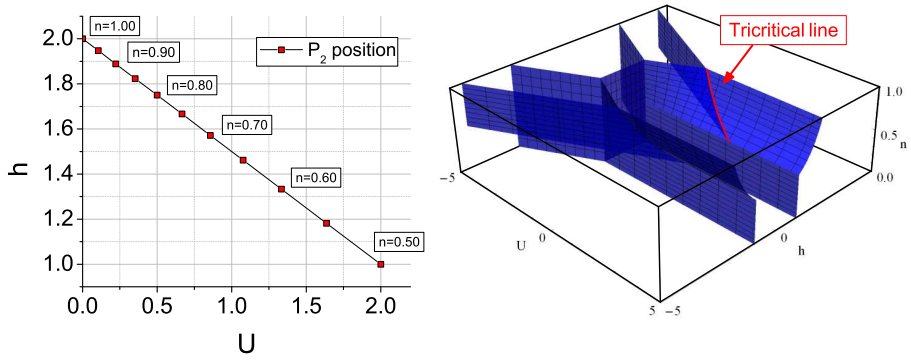

Figure 3.7: Position of P_2 3-critical point in the h-U plane (left) and in the 3D phase diagram (right).

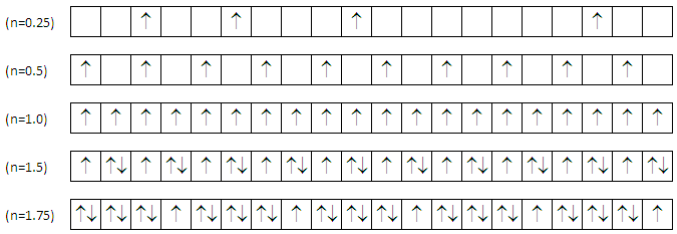

Figure 3.8: Some of the possible spin and charge configurations for the F1-phase at $T = 0$, $J = -1$.

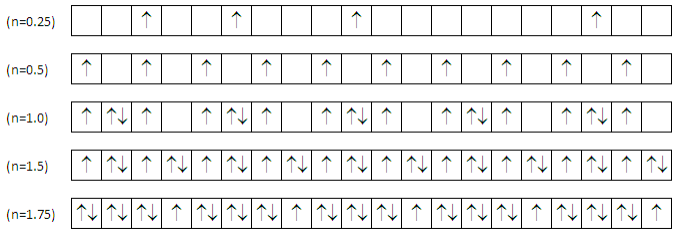

Figure 3.9: Some of the possible spin and charge configurations for the F2-phase at $T = 0$, $J = -1$.

F2-phase. As shown in Fig. 3.5, in the range in which h and J are comparable, for $U < 0$ and for $0.5 < n < 1.5$ we observe an anomalous ferromagnetic phase (F2) induced by the competition between the magnetic field and the antiferromagnetic inter-site coupling. This phase is characterized by no nearest neighbor spin-spin correlations and a constant magnetization.

$$\begin{array}{ll} \mu = U/2 & \langle n(i)n^{\alpha}(i)\rangle = 2n-1 \\ \langle D(i)\rangle = n/2 - 1/4 & \langle n_3(i)n_3^{\alpha}(i)\rangle = 0 \\ \langle m(i)\rangle = 1/4 & \langle D(i)D^{\alpha}(i)\rangle = 0 \\ E_{F2} = U\left(\frac{n}{2} - \frac{1}{4}\right) - \frac{h}{2} & \end{array} \quad . \tag{3.50}$$

As shown in Fig. 3.9, in this phase both $\langle D(i)\rangle$ and $\langle n(i)n^{\alpha}(i)\rangle$ are finite while $\langle n_3(i)n_3^{\alpha}(i)\rangle$ remains zero. At $n = 0.5$ doubly occupied sites appear in between two singly occupied ones; by increasing n, the number of doubly occupied sites increases, while the number of singly occupied sites remains constant. This explains why the magnetization does not change. Exactly at $n = 1$, we observe a particular pattern in which one or more unity cells, composed by two sites singly occupied with aligned spins and one site doubly occupied in between, appear all along the chain separated by empty sites. In Fig. 3.10 we report some signatures of NM-F1-F2 and AF-F1-F2 phase transitions occurring in magnetization and spin-spin correlation function.

As shown in Fig. 3.10, for $U \leq -2$, changing h we cross three different phases: NM, F1 and F2. In that range (solid curves) the magnetization assumes three different values: 0 in the NM-phase, 1/4 in the F2-phase and $n/2$ in the F1-phase. The spin-spin correlation functions jumps from zero (in NM and F2 phases) to one (in the F1-phase). For $-2 \leq U \leq 0$ (dashed curves) instead, NM-phase is replaced by AF-phase and spin-spin correlation function becomes negative when $|h| \leq 1.5$. Finally, for positive values of U (solid curves) F2-phase is not observed:

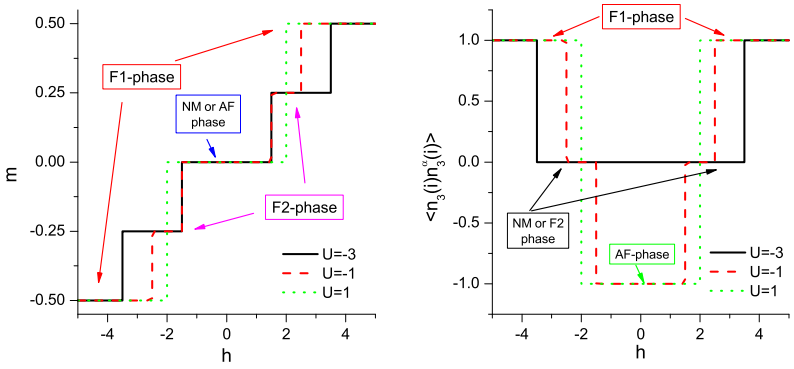

Figure 3.10: Signatures of phase transition in magnetization (left) and spin-spin correlation function (right) plotted as functions of the magnetic field h, for different values of U at $n = 1$ and $J = -1$.

the magnetization jumps from zero (AF-phase) to $n/2$ (F1-phase) while the spin-spin correlation function goes from negative (AF-phase) to positive (F1-phase) values.

3.1.3.3 Charge and spin excitations

The presence of different phases and long-range orders at $T \to 0$ can also be predicted by looking at charge and spin excitations in the response functions such as charge and spin susceptibilities. As shown in the previous Subsection, in each phase at $T = 0$ all single particle properties and correlation functions depend only on n but not on the other model parameters U, J, h. Therefore in all the phases the value of charge and spin susceptibilities is expected to depend only on n, with divergences or discontinuities localized at the phase boundaries where small variations of the model parameters can imply the transition from a charge/spin ordering to another. In particular, one might immediately note that, as long as we remain in the same phase, the magnetization does not depend on h (see Eqs.3.31-3.50) therefore $\chi_s(T = 0) = 0$ for any value of U, J and h with the exception of the phase boundaries where jumps in the magnetization might occur crossing two phases characterized by different magnetic orders (see Fig.3.4 and Fig.3.10). For the charge susceptibility we have instead:

Phase	$\lim_{T\to 0} \chi_c$	
NM	$n(2-n)$	$0 \leqslant n \leqslant 1$
F,AF	∞	$0 < n < 1$
	0	$n = 0$, or, $n = 1$
F1	$n(n-1)(2n-1)$	$0 \leqslant n \leqslant 0.5$
F2	$2n(2-n) - 3/2$	$0.5 \leqslant n \leqslant 1$

(3.51)

Hence, the zero temperature behaviours of charge/spin susceptibilities can be easily advocated as a powerful tool for the investigation of different charge and/or spin orderings since, as reported in Fig.3.11 and Fig.3.12, they clearly reproduce the boundaries of the phase diagram for both $J = 1$ and $J = -1$.

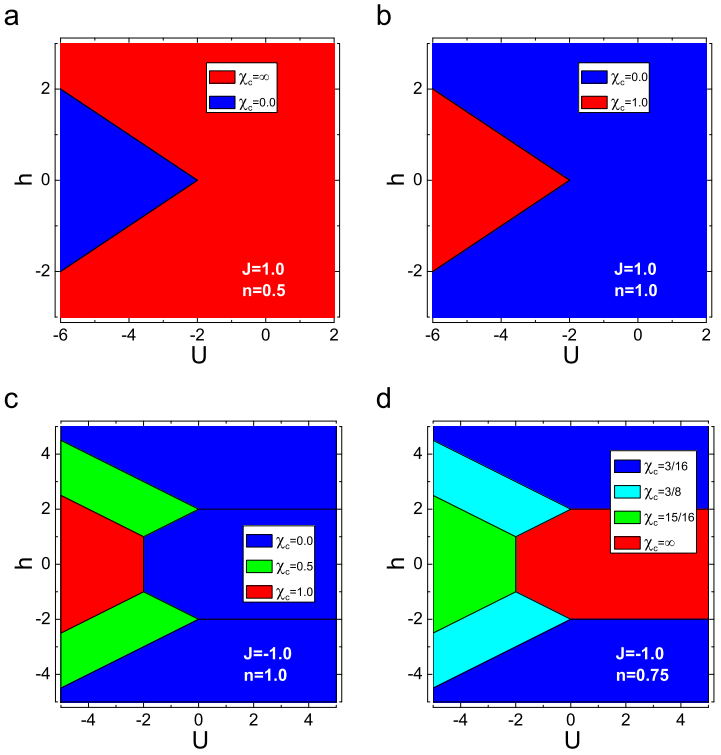

Figure 3.11: Contour-plot of the charge susceptibility at $T = 0.001$ as a function of the external magnetic field h and the local Coulomb potential U for: (a) $J = 1$, $n = 0.5$; (b) $J = 1$, $n = 1$; (c) $J = -1$, $n = 0.75$; (d) $J = -1$, $n = 1$.

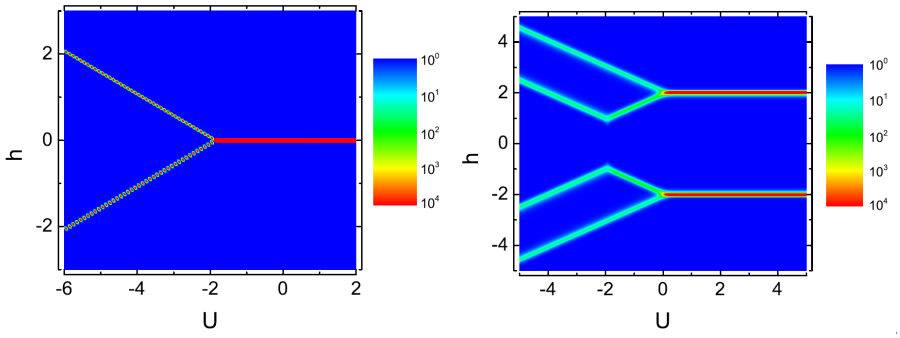

Figure 3.12: Contour-plot of spin susceptibility in the limit of zero temperature ($T = 0.001$) at $n = 1$ as a function of the external magnetic field h and local Coulomb potential U for $J = 1$ (left) and $J = -1$ (right).

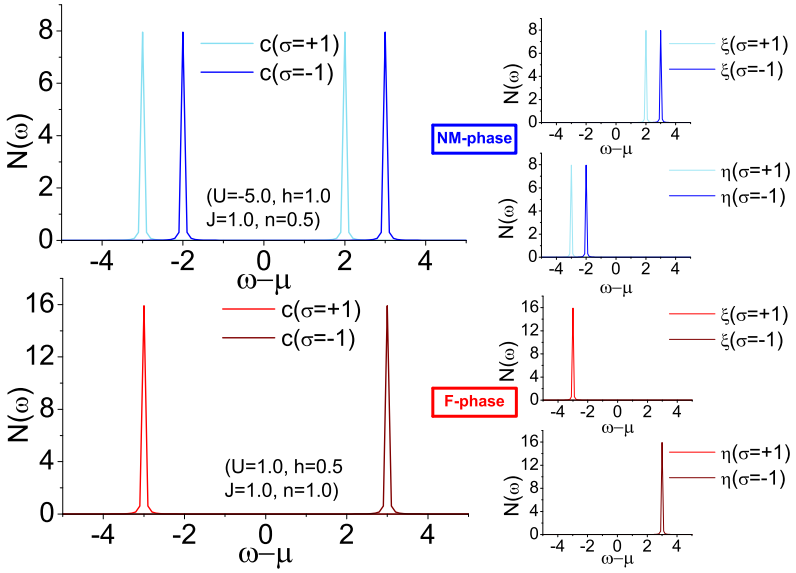

Figure 3.13: Density of states in the limit of zero temperature for the NM and F phases ($J = 1$) . We report the total density of states ($c(i) = \xi(i) + \eta(i)$) contributions for both spin up ($\sigma = +1$) and spin down ($\sigma = -1$). The contributions due only to $\xi(i)$ and $\eta(i)$ fields are also reported in the insets.

3.1.3.4 Density of states

To complete the zero temperature analysis, we report in this Subsection the results obtained for the density of states in the limit of zero temperature. As shown in Eq.3.30, the density of states is expressed as a superposition of several delta functions, each of them centered at the energy levels $E_n^{(a)}$ and weighted by the spectral functions $\rho^{(a,n)}$. In the limit of zero temperature, most of the weights vanish and only few energies, corresponding to the ground state and first excited states, give a contribution. We report in Fig.3.13 and Fig.3.14 the density of states calculated for each phase that appears in the $J = 1$ and $J = -1$ phase diagrams at half-filling and $T = 0.001$.

In the case of a ferromagnetic inter-site coupling, as shown in Fig.3.2, the NM-phase at $n = 1$ is characterized by the presence of either doubly occupied or empty sites. Accordingly, low-lying excitations correspond to configurations with singly occupied sites with spins aligned along h resulting in the presence of a single peak in the DOS, Fig.3.13, induced by $\xi_\uparrow(i)$. On the contrary, the F-phase at $n = 1$ is characterized by all singly occupied sites with spins pointing towards h. Hence low-lying excited states are characterized by a finite double occupancy, resulting in a single peak above the Fermi level induced by $\eta_\downarrow$ as shown in Fig.3.13.

The same considerations can also be done in the case of an antiferromagnetic inter-site coupling (see Fig.3.14) so that the nature of the peaks around the Fermi level can be easily predicted by observing the zero-temperature configuration of each phase. It is worth noting that, only in the F2-phase, both the contributions by ξ and η are allowed thanks to the fact that any F2-configuration comprises either polarized spins or double occupancies (Fig.3.9).

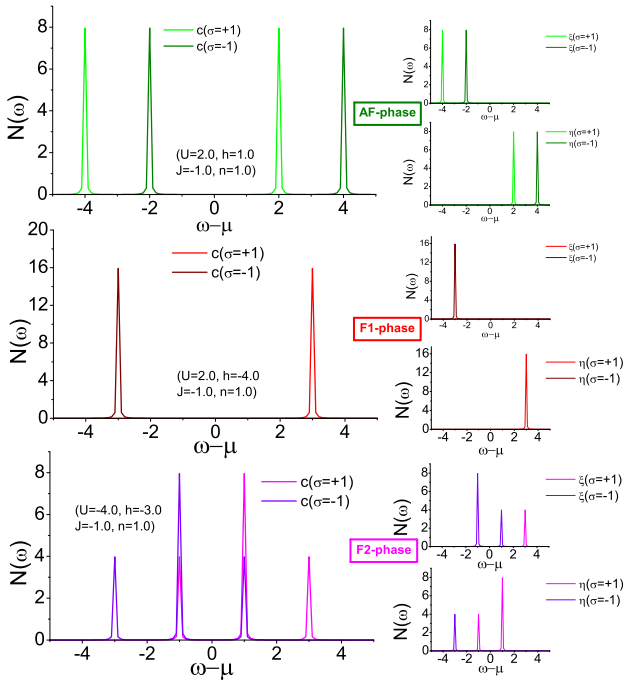

Figure 3.14: Density of states in the limit of zero temperature for the AF, F1 and F2 phases ($J = -1$). We report the contributions for both spin up ($\sigma = +1$) and spin down ($\sigma = -1$). In the insets the contributions due to $\xi(i)$ and $\eta(i)$ fields are reported.

Our analysis of the density of states also allows to get some insight about the energy gap Δ that separates the ground state from the first excited one. It can be seen that, as long as the system remains in the same phase, a finite gap exists as signaled by the presence of several peaks in the DOS which are far from each other. On the contrary, moving from a phase to another, the gap between the peaks corresponding to ground and first excited states closes as one approaches the phase boundaries. These results are also confirmed by the calculation of the specific heat in the zero temperature limit, Fig.3.15, which shows low-temperature peaks corresponding to quasi-particle excitations in the proximity of the phase boundaries.

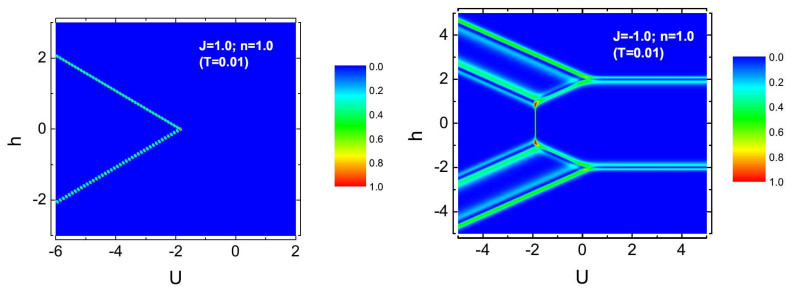

Figure 3.15: Contour-plot of the specific heat at low temperature at half filling for $J = 1$ (left) and $J = -1$ (right) as a function of the external magnetic field h and local Coulomb potential U.

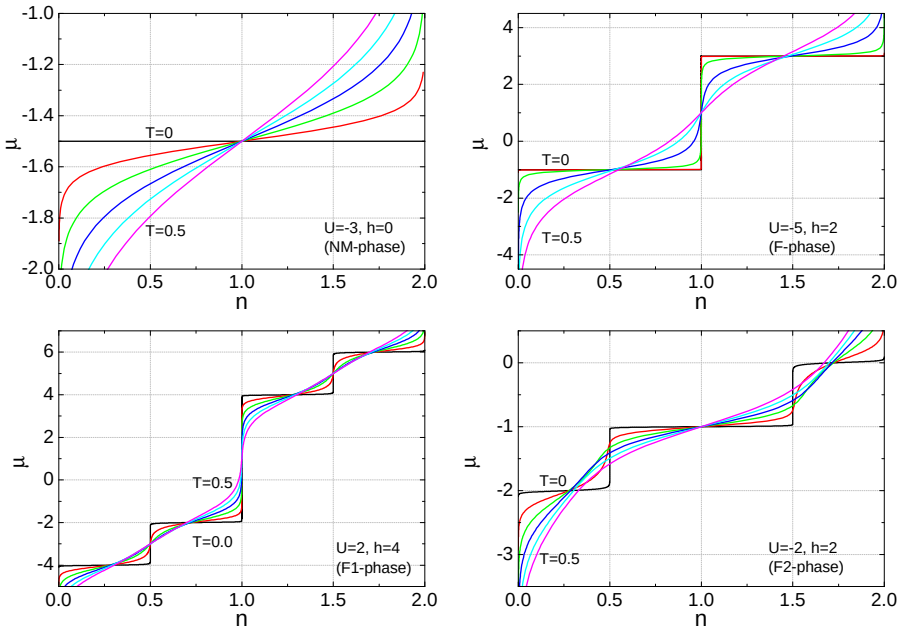

Figure 3.16: Chemical potential plotted as a function of the filling for different temperatures. Different values of h and U are related to NM (top, left), F (top, right), F1 (bottom, right) and F2 (bottom, left) phases..

3.1.4 Response functions at finite temperature

In order to provide a comprehensive study of the model Hamiltonian (3.3), we report in this Subsection some results obtained in the finite temperature regime. According to Mermin and Wagner theorem [59], there is no long-range order at any finite temperature in 1D and therefore the concept of "phase" is meaningless. However, to better identify the parameter space under investigation, in this Subsection we maintain the reference to the $T = 0$ phases described before, in the sense that we label each set of parameter (n, U, h, J) according to the corresponding phase observed at zero temperature. For the sake of brevity, we will restrict our discussion to entropy, specific heat, charge and spin susceptibilities. A more detailed analysis on finite temperature results, including the temperature dependencies of all single particle properties, can be found in Ref.[20].

3.1.4.1 Chemical potential and charge susceptibility

As follows from Eq.3.29, the thermal behaviour of the charge susceptibility strongly depends on the $\mu(n)$ dependence. As shown in Fig.3.16, the chemical potential μ is a step function at $T = 0$, characterized by sharp jumps at commensurate fillings which correspond to the critical values of filling at which a particular order appears or disappears.

In the F-phase, for example, the jump in the $\mu(n, T = 0)$ dependence is localized at $n = 1$ when the add of a particle in the system induces a finite double occupancy, breaking the ferromagnetic order. When this happens, the charge susceptibility can be either constant or it can diverge depending on how the derivative $\partial n/\partial\mu$ changes with temperature.

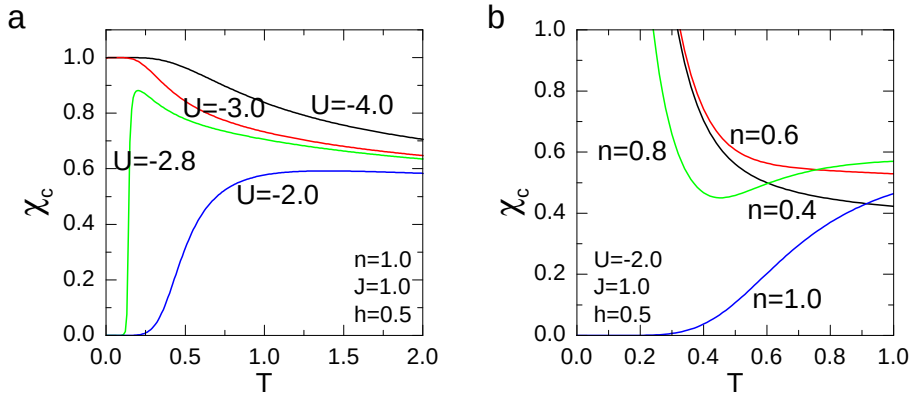

Figure 3.17: The charge susceptibility as a function of temperature at $J = 1$, $h = 0.5$ for: $n = 1$, $-4 \leqslant U \leqslant -2$ (left panel) and $U = -2$ and $0.4 \leqslant n \leqslant 1$ (right panel).

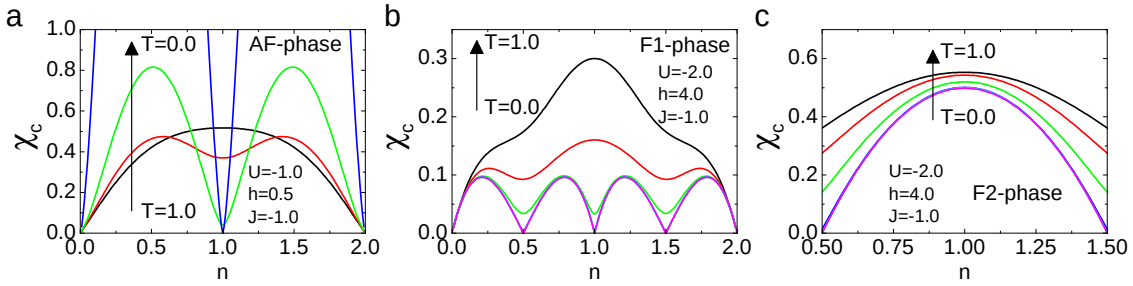

Figure 3.18: The charge susceptibility as a function of the filling and different temperatures for AF-phase (left panel) and F1 (central panel) and F2 phases (right panel).

In particular, for $J = 1$ (Fig.3.17) we note that $\chi_c(T = 0)$ diverges for any $n \neq 1$, corresponding to plateau regions in the $\mu(n)$ dependence, and then rapidly decreases with increasing T. Also, at $n = 1$ $\chi_c(T = 0)$ has a discontinuity, going from $\chi_c(n = 1) = 0$ in the NM-phase to $\chi_c(n = 1) = 1$ the F-phase. The temperature has the only effect to make this discontinuity less and less pronounced. Similar considerations can also be done for the anti-ferromagnetic case ($J = -1$) in which, as reported in Fig.3.18, it can be immediately seen that $\chi_c(T \approx 0) = 0$ in the presence of charge and/or spin orderings also signaled by sharp jumps in the $\mu(n, T \approx 0)$ dependence (see Fig.3.16).

This trend disappears with increasing temperature. In particular, it is worth noting that in the limit of high-temperatures, regardless of the particular phase or sign of the inter-site magnetic coupling, the charge susceptibility tends to a constant value which depends only on n:

$$\lim_{T\to\infty} \chi_c(n, T) = \frac{n}{2}(2 - n) \; . \tag{3.52}$$

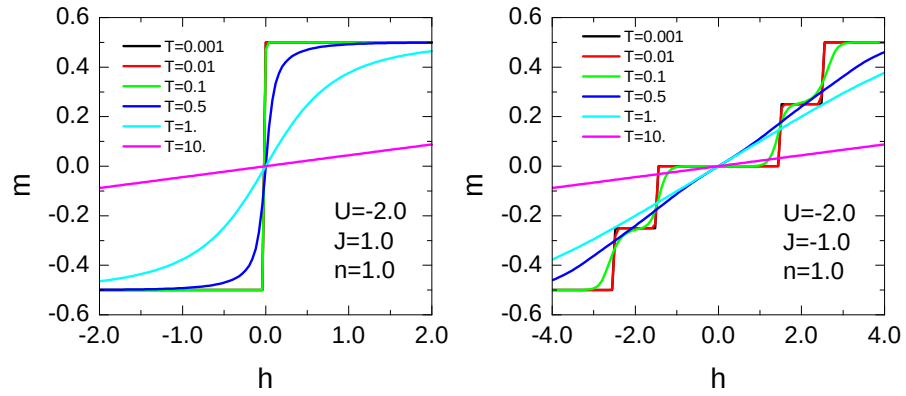

Figure 3.19: Magnetization m versus field h at different temperatures for both ferromagnetic ($J = 1$) and anti-ferromagnetic ($J = -1$) couplings.

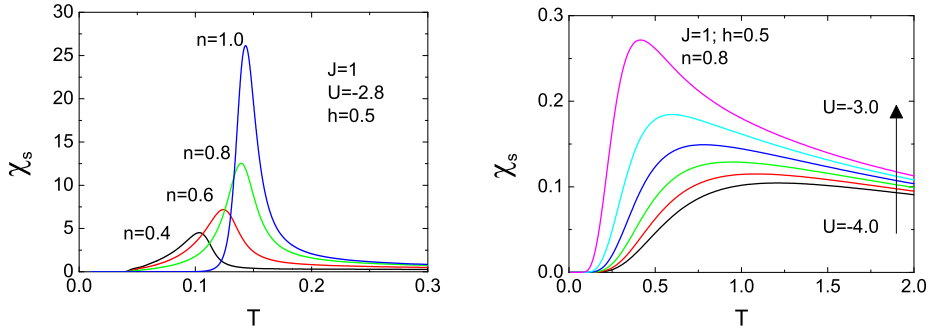

Figure 3.20: The spin susceptibility χ_s as a function of T for $J = 1$, $h = 0.5$; left panel: $n = 0.8$ and various values of U; right panel $U = -2.8$ and various values of n.

3.1.4.2 Magnetization and spin susceptibility

Different from charge susceptibility, as follows from Eq.3.29 χ_s only implicitly depends on temperature via the magnetization $m(h)$. As already pointed out before, in the low-temperature limit χ_s is expected to be always zero, except near the phase boundaries where small variation of h induce jumps in the magnetization. Regardless the particular phase, as shown in Fig.3.19 the magnetization is a continuous function of h at any finite temperature with sharp jumps, localized at the boundaries of the phases with different magnetic orders, which become more and more pronounced as the $T \to 0$ limit is approached.

Consistently, as shown in Fig. 3.20, for $J = 1$ the spin susceptibility is characterized by a low-temperature peak which moves to $T = 0$ as we approach the NM/F phase boundaries. The jump in the magnetization, passing from the NM to the F phase, is proportional to the filling since $m(T \approx 0) = 0$ in the NM-phase while $m(T \approx 0) = n/2$ in the F-phase. Therefore the intensity of the low-temperature peak increases with increasing n. Exactly at $T = 0$, the magnetization jumps from $m = 0$ in the NM phase to $m = n/2$ in the F-phase, leading to a divergence in $\chi_s(T)$ exactly a the phase boundaries which signals the presence of different spin orderings.

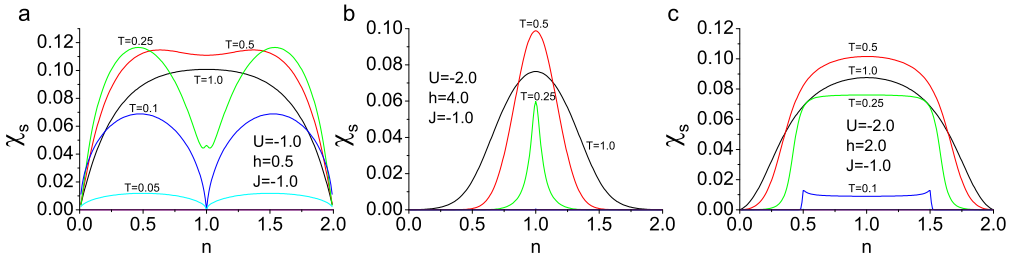

Figure 3.21: The spin susceptibility as a function of the filling and different temperatures for AF-phase (panel a), F1-phase (panel b) and F1 ($0 \leqslant n \leqslant 1/2$, $3/2 \leqslant n \leqslant 2$) - F2 ($1/2 \leqslant n \leqslant 3/2$) phases (panel c).

Similar considerations can also be done in the case of an anti-ferromagnetic coupling ($J = -1$). As shown in Fig. 3.21, although $\chi_s(T \approx 0) = 0$ in each phase, we can distinguish different temperature dependencies according to the particular choice of the external parameters.

Thermal fluctuations have the only effect to decrease the modulus of the magnetization leading to $m(T \to \infty) = 0$ and $\chi_s(T \to \infty) = 0$ as one would expect. However, one can note that, independently on the sign of the spin exchange J, in the limit of high-temperatures the spin susceptibility follows the Curie law with a coefficient which only depends on n:

$$\lim_{T\to\infty} \chi_s = n(2-n)/4T \ . \tag{3.53}$$

Therefore, joining together Eq.3.52 and Eq.3.53 we immediately have:

$$\lim_{T\to\infty} \frac{\chi_s}{\chi_c} = \frac{1}{2T} \ , \tag{3.54}$$

in which the factor two is due to the spin multiplicity.

3.1.4.3 Entropy

The study of the entropy as a function of filling n and temperature T, $S \equiv S(n,T)$, plays a crucial role in the characterization and in the identification of possible ordered phases in which $S(n,T)$ is expected to be zero in the thermodynamic limit. We recall that the entropy can be calculated as a function of the chemical potential as:

$$S(T,n) = -\int_0^n \frac{\partial\mu(T,n')}{\partial T} dn' \ . \tag{3.55}$$

Following the above equation, we report in Fig. 3.22 and Fig.3.23 filling and temperature dependencies of the entropy for both $J = 1$ and $J = -1$ cases.

Regardless the particular phase, for any $T \neq 0$ and due to the absence of any long-range order, the system can be described as a highly degenerate superposition of an increasing number of different configurations. Consistently, the entropy remains finite for any value of the filling. In contrast, at low temperatures the entropy decreases rapidly at those values of n associated with charge and/or spin orderings. At these points, in fact, the state of the system can be uniquely described by a finite

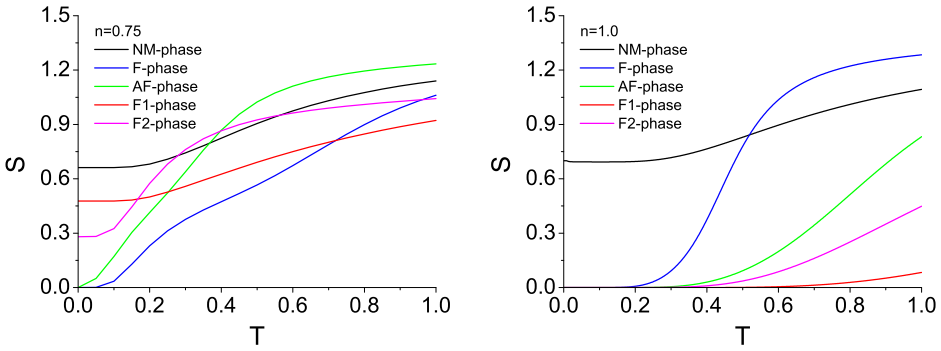

Figure 3.22: Temperature dependence of the entropy plotted for different values of the external parameters corresponding to different phases at $T = 0$.

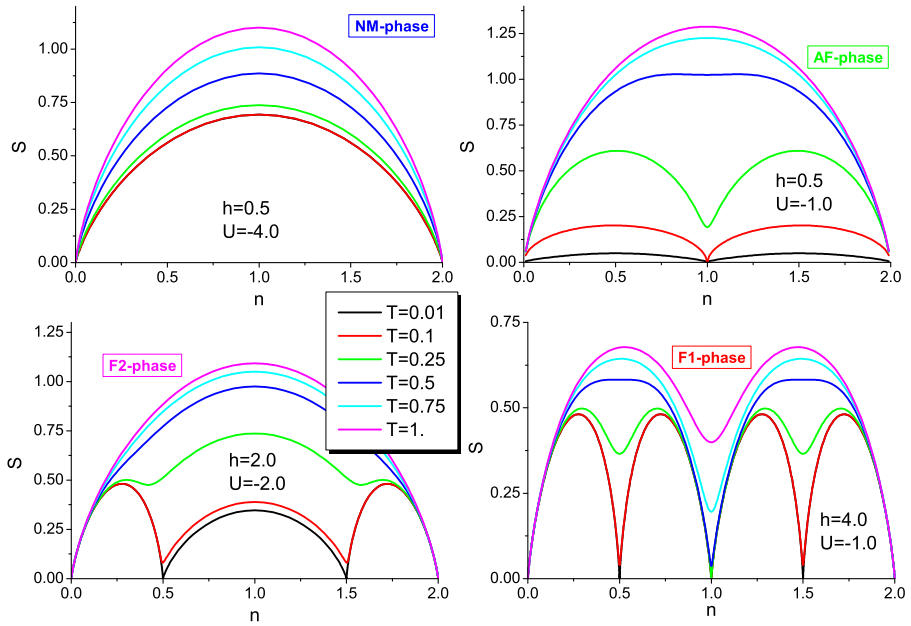

Figure 3.23: Entropy as a function of the filling for different temperatures and four sets of the external parameters U and h corresponding to NM (top-left), AF (top-right), F1 (bottom-right) and F2 (bottom-left) phases observed at $J = -1$ and $T = 0$.

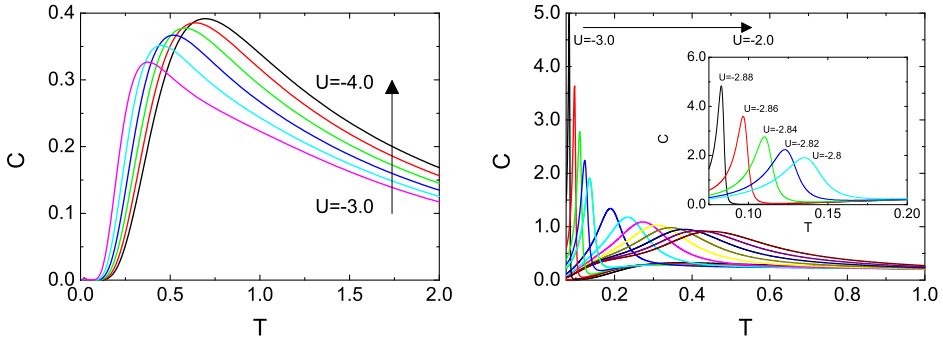

Figure 3.24: Specific heat as a function of temperature for $J = 1$, $h = 0.5$, $n = 0.8$, $-4 \leqslant U \leqslant -3$ (left panel) and $-3 \leqslant U \leqslant -2$ (right panel).

number of configurations (see Figs.3.2, 3.3, 3.6, 3.8, 3.9 for NM, F, AF, F1 and F2 phases, respectively) whose contribution to the entropy is expected to vanish in the thermodynamic limit. At $n = 1$, this happens for the NM phase only. On the contrary, away from half-filling, all the phases have a finite ground state degeneracy with the exception of F and AF phases.

3.1.4.4 Specific heat

It is well-known that specific heat can exhibits a very rich structure in the proximity of phase transitions. In particular, recalling that long-range orders can only appear at zero temperature, in addition to the standard high-temperature peaks due to Schottky anomaly, we expect to find low-temperature peaks in the correspondence of the boundaries of the $T = 0$ phase diagrams shown in Fig.3.1 and Fig.3.5. We report below a detailed analysis of specific heat features for each phase.

In the NM phase, thermal excitations are responsible for transitions to configurations where some sites are singly occupied. This process, which requires high temperature in order to break doubly occupied sites, is signaled by the presence of a high-temperature peak in the left panel of Fig.3.24. As shown in Fig.3.25, the position of this peak, T_2, and its intensity, h_2, decrease by increasing U. In particular, we note that T_2 decreases with almost a linear law.

For the F phase instead, as shown in the right panel of Fig.3.24, C exhibits low (T_1) and high (T_2) temperature peaks, associated to transitions involving the ground state and the low-lying excited states. Approaching the phase boundaries, the ground and the first excited states become quasi degenerate. Hence a temperature of the order of the gap between these two states will be sufficient to induce thermal excitations, resulting in the presence of a low-temperature peak that moves towards $T = 0$. On the contrary, position and intensities of high-temperature excitations, responsible for a second lower and broadened peak, remain almost unchanged. In fact, as shown in Fig. 3.25, the intensity h_2 of the higher temperature peak remains almost constant when U varies. Contrarily, h_1 rapidly increases as U approaches U_c and diverges in the limit $U \to U_c$. This occurs since the degeneracy of the first excited state (belonging to the NM-phase) is infinite in the thermodynamic limit with respect to the degeneracy of the ground state (F-phase).

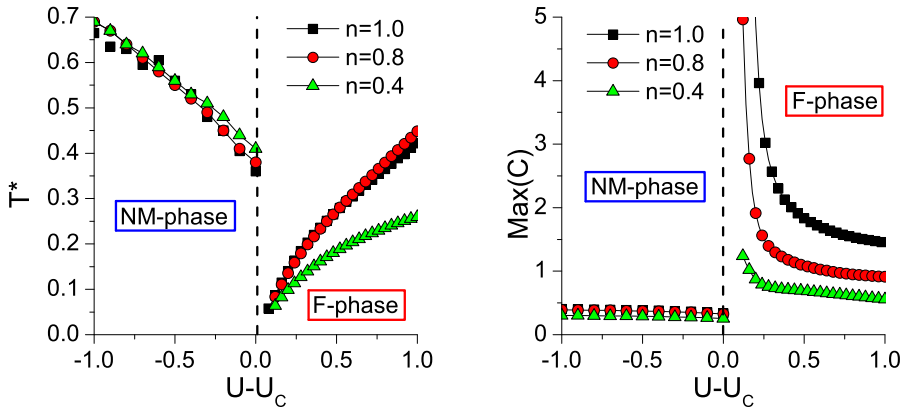

Figure 3.25: Positions (T_1 in F-phase and T_2 in NM-phase) and intensities (h_1 in F-phase and h_2 in NM-phase) where the specific heat has maximas as functions of U for $J = 1$, $h = 0.5$, and different values of the filling.

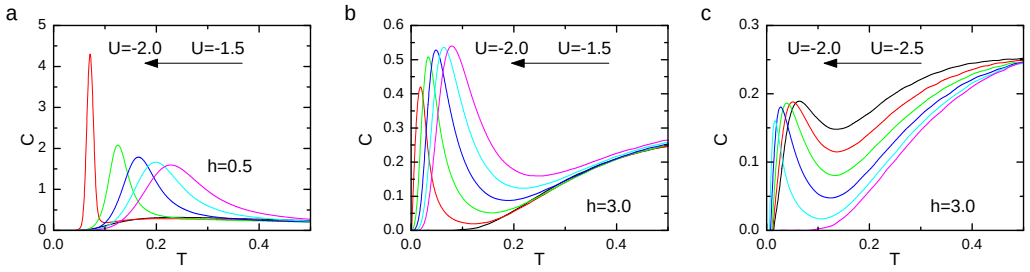

Figure 3.26: Specific heat as a function of temperature at $J = -1$ for AF (left panel), F1 (central panel) and F2 (right panel) phases at $n = 1.0$.

Most of the features observed in the F-phase persist for $J = -1$ in the AF-phase. As shown in Fig.3.26a, the specific heat exhibits a low-temperature peak whose height (dispersion) increases (decreases) as one approaches the phase boundary. As reported in Fig.3.6, the AF-configuration at $n = 1$ is composed exclusively of singly-occupied sites. Therefore, the low-lying features correspond to transitions from the ground states to some excited states with finite D or $m \neq 0$. On the contrary, F1 and F2 phases are characterized by both low and high temperatures peaks whose heights remain quite constant when the phase boundaries are approached. While the position of the former remains roughly constant, the latter moves towards $T = 0$.

We report in Fig.3.27 a detailed analysis of position and height of the low temperature peaks in the specific heat for all possible phase transition occurring at $J = -1$. As already pointed out, the position T^* of low temperature peaks is a linear function of the temperature while, contrarily to what has been observed for the $J = 1$ case, the height remains constant. Furthermore, it is worth noting that, at the transition point, there is a jump in the height of the low temperature peak which can be traced back to the degeneracy ratio between the ground and the first excited states. As reported in Fig.3.28, this last finding, that represents a common fingerprint for all the phase transitions analyzed so far, is not observed at the tri-critical points where the first and the second excited states become degenerate with respect to the ground one.

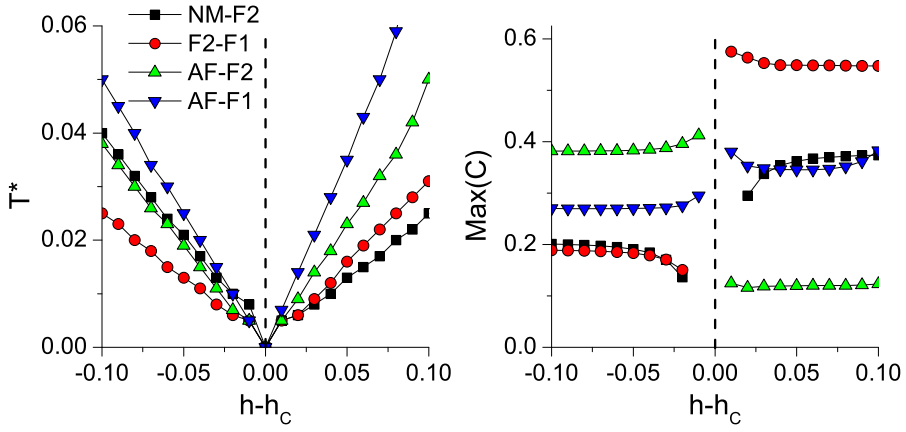

Figure 3.27: Low-temperature features of the specific heat at different transition lines for $J = -1$. The maximum of the specific heat (right panel) and its position T^* (left panel) are reported as a function of $h - h_c$ where h_c is the critical value of the external magnetic field h at the phase transition point.

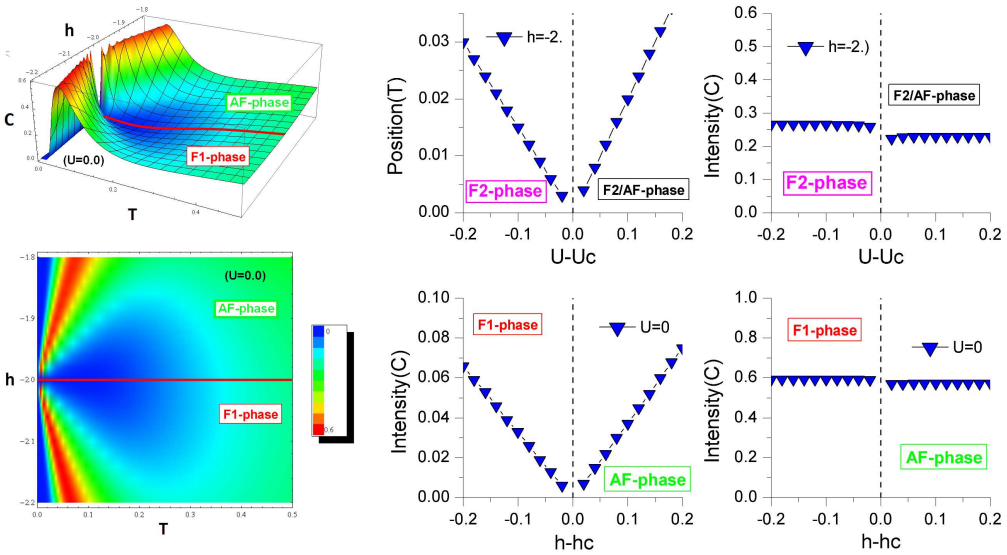

Figure 3.28: Low temperature specific heat features at P_2 tricritical point for $n = 1$ and $J = -1$. Contour-plot and 3Dplot on the left report specific heat at as a function of h and T for $U = 0$. The four plots on the right report position and intensity of low temperature peaks moving to the phase transition point fixing h and changing U (top) and vice versa (bottom).

Chapter 4

A two-field approach to the single-band Hubbard model

As illustrated in detail in Chapter 2, the Composite Operator Method (COM) provides an full-consistent analytical framework for the description of highly interacting systems in the strong coupling regime where many other theoretical approaches, among which perturbative expansions, arbitrary ansatzs, decoupling schemes, fail. The power of this method lies in recognizing that the properties of strongly correlated systems can be more conveniently described in terms of a set of composite fields which accounts for new quasi-particles whose properties, differently from bare electron ones, are entirely determined by dynamics, strength and nature of the interactions. The application of this method to a particular model Hamiltonian can lead to an exact or an approximated solution, depending on the possibility to find a closed set of composite fields which completely describes all quasi-particle excitations.

In general, as reported in Chapter 3 for the case of the t-U-J-h Hamiltonian in the atomic limit, the COM allows for the exact solution of a large class of systems whose properties can be entirely described by a finite number of composite fields. However, in many other cases the choice of a finite set of composite fields is not enough to describe all the possible quasi-particle excitations of the system. This results in the presence of higher order fields in the equation of motion of the basis whose contributions, in the Green's function formalism, can be estimated in terms of self-energy corrections (see Sec.2.1). When this happens, one can simply choose a reasonable number of components for the basic set and then use an approximated method to evaluate the residual dynamical corrections. According to this procedure, in this Chapter we consider a two-field basis and illustrate two approximated schemes and their application to the single-band Hubbard model [1]. In particular, in Section 4.1 we consider a pure two-pole approach, according to which the dynamical part of the self-energy is completely neglected under the assumption that the choice of the extended two-field basis is such that all the relevant self-energy corrections are already included in the free propagator. Finally, the calculation of self-energy corrections is discussed in Section 4.3 where a possible self-consistent scheme is proposed in the framework of the so-called self-consistent Born approximation.

4.1 Two-pole approximation: fermionic sector

As a starting point, let us introduce the following two-field basis:

$$\psi(i) = \left(\begin{array}{c} \xi(i) \\ \eta(i) \end{array} \right) , \tag{4.1}$$

given by the fermionic composite fields $\xi_\sigma(i) \equiv (1-n_{\bar\sigma}(i))c_\sigma(i)$ and $\eta(i) = n_{\bar\sigma}(i)c_\sigma(i)$. According to the notation adopted in the previous Chapters, hereafter for each fermionic operator $\Phi(i)$ the spinorial notation will be used (see Appendix B.1):

$$\Phi(i) = \left(\begin{array}{c} \Phi_\uparrow(i) \\ \Phi_\downarrow(i) \end{array} \right) , \; \Phi^\dagger(i) = \left(\begin{array}{cc} \Phi^\dagger_\uparrow(i) & \Phi^\dagger_\downarrow(i) \end{array} \right) . \tag{4.2}$$

where, consistently with the Heisenberg picture, we have $\Phi(i) \equiv \Phi(\boldsymbol{i}, t)$. $\sigma = (\uparrow, \downarrow)$ ($\bar\sigma = (\downarrow, \uparrow)$) are spin variables, $c_\sigma(i)/c^\dagger_\sigma(i)$ are the canonical annihilation/creation operators of an electron on site $\boldsymbol{i}$ at time t with spin σ, $n_\sigma(i) = c^\dagger_\sigma(i)c_\sigma(i)$ is the electronic particle density per spin. Furthermore, we also use the following notation: $\Phi^\alpha(i) \equiv \sum_{\boldsymbol{j}} \alpha_{\boldsymbol{ij}}\Phi(\boldsymbol{j}, t)$ to express a non-local operator which acts on all the nearest neighbours of site $\boldsymbol{i}$. For a d-dimensional cubic Bravais lattice with lattice constant a and coordination number z we have:

$$\Phi^\alpha(\boldsymbol{i}, t) \equiv \frac{1}{z}\sum_{n=1}^{z} \Phi(\boldsymbol{i}_n, t) , \tag{4.3}$$

where $\boldsymbol{i}_n = \boldsymbol{i} + a\hat{\boldsymbol{e}}_n$ and $\hat{\boldsymbol{e}}_n$ is the n^{th} primitive unitary vector of the lattice with $1 \leqslant n \leqslant d$. Hence the Fourier transform of $\alpha_{\boldsymbol{i},\boldsymbol{j}}$ is $F.T.[\alpha_{\boldsymbol{i},\boldsymbol{j}}] = \frac{1}{d}\sum_{n=1}^{d}\cos(k_n a)$. According to this notation the Hubbard Hamiltonian [1] reads as:

$$H = \sum_{\boldsymbol{i},\boldsymbol{j}} \left(-2dt\alpha_{\boldsymbol{ij}} - \mu\delta_{\boldsymbol{ij}}\right) c^\dagger(i)c(j) + U\sum_{\boldsymbol{i}} n_\uparrow(i)n_\downarrow(i) , \tag{4.4}$$

where μ is the chemical potential, U parametrized the strength of the on-site Coulomb interaction and $t_{\boldsymbol{ij}}$ is the hopping amplitude which has been supposed to be uniform and restricted to nearest-neighbour sites only with $t_{\boldsymbol{ij}} = -2dt\alpha_{\boldsymbol{ij}}$.

As reported in detail in Appendix B.3, the basis $\psi(i)$ satisfies the following equation of motion:

$$i\partial_t\psi(i) = [\psi(i), H] = \left(\begin{array}{c} -\mu\xi(i) - 2dt\left[c^\alpha(i) + \pi(i)\right] \\ (U-\mu)\,\eta(i) + 2dt\pi(i) \end{array} \right) , \tag{4.5}$$

where $\pi(i)$ is a higher order field defined as:

$$\pi(i) = \frac{1}{2}\sigma^\mu n_\mu(i)c^\alpha(i) + c(i)c^{\alpha\dagger}(i)c(i) = \tag{4.6}$$

$$= \left(\begin{array}{c} -c^\dagger_\downarrow(i)c_\downarrow(i)c^\alpha_\downarrow(i) + c^\dagger_\downarrow(i)c_\uparrow(i)c^\alpha_\downarrow(i) - c_\uparrow(i)c_\downarrow(i)c^{\alpha\dagger}_\downarrow(i) \\ -c^\dagger_\uparrow(i)c_\downarrow(i)c^\alpha_\uparrow(i) + c^\dagger_\uparrow(i)c_\uparrow(i)c^\alpha_\downarrow(i) - c_\downarrow(i)c_\uparrow(i)c^{\alpha\dagger}_\uparrow(i) \end{array} \right) , \tag{4.7}$$

$n_\mu(i) = c^\dagger(i)\sigma_\mu c(i)$ is the charge ($\mu = 0$) and spin ($\mu = 1,2,3$) density operator with $\sigma_\mu = (\sigma_0, \boldsymbol{\sigma})$, being σ_0 the 2×2 identity matrix and $\boldsymbol{\sigma}$ the Pauli matrices (see Appendix B.1.2).

In the framework of the pole-approximation, we linearize the equation of motion (4.5) as:

$$i\partial_t \psi(\boldsymbol{i}, t) = \sum_{\boldsymbol{j}} \varepsilon(\boldsymbol{i}, \boldsymbol{j})\psi(\boldsymbol{j}, t) \; , \tag{4.8}$$

where $\varepsilon(\boldsymbol{i}, \boldsymbol{j})$ is the energy matrix which, as follows from Eq.2.23, can be calculated in terms of normalization $I(\boldsymbol{i}, \boldsymbol{j})$ (2.24) and $m(\boldsymbol{i}, \boldsymbol{j})$ (2.25) matrices as:

$$\varepsilon(\boldsymbol{i}, \boldsymbol{j}) = \sum_{\boldsymbol{j}} m(\boldsymbol{i}, \boldsymbol{j}) I^{-1}(\boldsymbol{i}, \boldsymbol{j}) \; . \tag{4.9}$$

This procedure allows us to calculate the linearized equations of motion for the fields of the basis in terms of simple anticommutators. On the basis of the results reported in Appendix B, in the case of an homogeneous and paramagnetic system straightforward but lengthy calculations give:

$$I(\boldsymbol{k}) = \begin{pmatrix} I_{11} & 0 \\ 0 & I_{12} \end{pmatrix} \; , \tag{4.10}$$

$$m(\boldsymbol{k}) = \begin{pmatrix} m_{11}(\boldsymbol{k}) & m_{12}(\boldsymbol{k}) \\ m_{12}(\boldsymbol{k}) & m_{22}(\boldsymbol{k}) \end{pmatrix} \; , \tag{4.11}$$

with:

$$I_{11} = 1 - \frac{n}{2} \; , \; I_{22} = \frac{n}{2} \; , \tag{4.12}$$

and:

$$m_{11}(\boldsymbol{k}) = -\mu \left(1 - \frac{n}{2}\right) - 2dt \left[\Delta + \alpha(\boldsymbol{k}) \left(1 - n + p\right)\right] \tag{4.13}$$

$$m_{12}(\boldsymbol{k}) = 2dt \left[\Delta + \alpha(\boldsymbol{k}) \left(p - \frac{n}{2}\right)\right] \tag{4.14}$$

$$m_{22}(\boldsymbol{k}) = \frac{n}{2} \left(U - \mu\right) - 2dt \left[\Delta + \alpha(\boldsymbol{k}) p\right] \tag{4.15}$$

where n, p and Δ are unknown correlators defined as:

$$n \equiv \langle n(i) \rangle \; , \tag{4.16}$$

$$p \equiv \frac{1}{4} \left\langle n_\mu^\alpha(i) n_\mu(i) \right\rangle - \left\langle \left[c_\uparrow(i) c_\downarrow(i)\right]^\alpha c_\downarrow^\dagger(i) c_\uparrow^\dagger(i) \right\rangle \; , \tag{4.17}$$

$$\Delta \equiv \left\langle \xi^\alpha(i) \xi^\dagger(i) \right\rangle - \left\langle \eta^\alpha(i) \eta^\dagger(i) \right\rangle \; , \tag{4.18}$$

The knowledge of $I(\boldsymbol{i}, \boldsymbol{j})$ and $m(\boldsymbol{i}, \boldsymbol{j})$, then the knowledge of the energy matrix $\varepsilon(\boldsymbol{i}, \boldsymbol{j})$, also allows to obtain an analytical expression of the energy spectra $E_n(\boldsymbol{k})$:

$$E_{\xi,\eta}(\boldsymbol{k}) = R(\boldsymbol{k}) \pm Q(\boldsymbol{k}) \; , \tag{4.19}$$

where:

$$R(\boldsymbol{k}) \equiv -\mu - 2dt\alpha(\boldsymbol{k}) + \frac{U}{2} - \frac{m_{12}(\boldsymbol{k})}{2I_{11}I_{22}} , \tag{4.20}$$

$$Q(\boldsymbol{k}) \equiv \frac{1}{2}\sqrt{g^2(\boldsymbol{k}) + \frac{4m_{12}^2(\boldsymbol{k})}{I_{11}I_{22}}} , \tag{4.21}$$

$$g(\boldsymbol{k}) \equiv \frac{1-n}{I_{11}I_{22}} m_{12}(\boldsymbol{k}) - U , \tag{4.22}$$

and the spectral density matrices (2.46):

$$\sigma^{(\xi)}(\boldsymbol{k}) = \begin{pmatrix} \sigma_{11}^{(\xi)}(\boldsymbol{k}) & \sigma_{12}^{(\xi)}(\boldsymbol{k}) \\ \sigma_{12}^{(\xi)}(\boldsymbol{k}) & \sigma_{22}^{(\xi)}(\boldsymbol{k}) \end{pmatrix} , \; \sigma^{(\eta)}(\boldsymbol{k}) = \begin{pmatrix} \sigma_{11}^{(\eta)}(\boldsymbol{k}) & \sigma_{12}^{(\eta)}(\boldsymbol{k}) \\ \sigma_{12}^{(\eta)}(\boldsymbol{k}) & \sigma_{22}^{(\eta)}(\boldsymbol{k}) \end{pmatrix} , \tag{4.23}$$

with:

$$\begin{array}{ll} \sigma_{11}^{(\xi)}(\boldsymbol{k}) = \frac{I_{11}}{2}\left[1 + \frac{g(\boldsymbol{k})}{2Q(\boldsymbol{k})}\right] & \sigma_{11}^{(\eta)}(\boldsymbol{k}) = \frac{I_{11}}{2}\left[1 - \frac{g(\boldsymbol{k})}{2Q(\boldsymbol{k})}\right] , \\ \sigma_{12}^{(\xi)}(\boldsymbol{k}) = \frac{m_{12}(\boldsymbol{k})}{2Q(\boldsymbol{k})} & \sigma_{12}^{(\eta)}(\boldsymbol{k}) = -\frac{m_{12}(\boldsymbol{k})}{2Q(\boldsymbol{k})} , \\ \sigma_{22}^{(\xi)}(\boldsymbol{k}) = \frac{I_{22}}{2}\left[1 - \frac{g(\boldsymbol{k})}{2Q(\boldsymbol{k})}\right] & \sigma_{22}^{(\eta)}(\boldsymbol{k}) = \frac{I_{22}}{2}\left[1 + \frac{g(\boldsymbol{k})}{2Q(\boldsymbol{k})}\right] . \end{array} \tag{4.24}$$

which allow us to write a generic correlator $C_{ab}^{\alpha^n}(i,j) = \left\langle \psi_a^{\alpha^n}(i)\psi_b^\dagger(j) \right\rangle$ as:

$$C_{ab}^{\alpha^n}(i,j) = \frac{a^d}{(2\pi)^d} \sum_{s=(\xi,\eta)} \int_{\Omega_B} d^d k e^{i\boldsymbol{k}\cdot(\boldsymbol{R}_i - \boldsymbol{R}_j) - iE_s(\boldsymbol{k})(t_i - t_j)} \alpha^n(\boldsymbol{k}) \left[1 - f_F\left(E_n(\boldsymbol{k})\right)\right] \sigma^{(s)}(\boldsymbol{k}) , \tag{4.25}$$

where Ω_B denotes the volume of the first d-dimensional Brillouin zone and α^n denotes the convolution of n nearest-neighbor projectors:

$$\Phi^{\alpha^n}(i) \equiv \sum_{\boldsymbol{i}_1,\ldots,\boldsymbol{i}_{n-1}} \alpha_{\boldsymbol{i}\boldsymbol{i}_1}\alpha_{\boldsymbol{i}_1\boldsymbol{i}_2}\ldots\alpha_{\boldsymbol{i}_{n-3}\boldsymbol{i}_{n-2}}\alpha_{\boldsymbol{i}_{n-2}\boldsymbol{i}_{n-1}}\Phi(\boldsymbol{i}_{n-1},t) . \tag{4.26}$$

Hence it is worth noting that Δ and n can be easily calculated self-consistently since they can be expressed in terms the time-independent correlators $C_{ab}^{\alpha^n} \equiv C_{ab}^{\alpha^n}(i,i)$. In particular, since in any physical system one can vary the particle concentration rather than the chemical potential, we consider the particle density n as an external parameter and calculate μ self-consistently according to the relation:

$$n = 2\left(1 - C_{11} - C_{22}\right) . \tag{4.27}$$

For Δ instead, following its definition (4.18), we have:

$$\Delta = C_{11}^{\alpha} - C_{22}^{\alpha} . \tag{4.28}$$

We are left with one unknown parameter, p, that different from n and Δ, deserves a different treatment since it is defined in terms of fields which do not belong to the chosen basis (4.1). However, from the basic algebra of the composite fields $\xi(i)$ and

$\eta(i)$ one can immediately note that the Pauli exclusion principle requires that:

$$\xi_\sigma(i)\eta^\dagger_\sigma(i) = c_\sigma(i)\left[n_{\bar\sigma}(i) - n^2_{\bar\sigma}(i)\right] c^\dagger_\sigma(i) = 0\ . \tag{4.29}$$

Therefore, the physical constraint given by the Pauli principle, which is self-included in the algebra of the composite fields, requires the following relation to be satisfied:

$$C_{12} = \left\langle \xi(i)\eta^\dagger(i)\right\rangle = 0\ , \tag{4.30}$$

which can be read as an additional self-consistent equation for the last unknown parameter p, providing a full-consistent calculation scheme which is valid for any dimension d. At this point, it becomes evident that, as already discussed in Sec.2.3, the presence of unknown parameters to be fixed self-consistently does not represent a proper limit for the theory. On the contrary, it reflects the necessity to fix the Green's function representation according to the particular algebra and symmetries under consideration. As it will be shown in the next Section, because of the self-consistency, the violation of the Pauli constraint $C_{12} = 0$ does not affect only the estimation of p but reflects in unphysical behaviors and severe limitations to the applicability of the whole calculation scheme.

4.1.1 Single-particle properties and thermodynamics

Let us discuss some results obtained within the two-pole approximation scheme for the two-dimensional Hubbard model in the paramagnetic phase. Due to the high non-linearity of the self-consistent equations (4.27), (4.28), and (4.30), although different solutions are expected, only two coexisting solutions, corresponding to significantly different physical behaviours, are admitted. Hereafter we label these solutions as COM1 and COM2. COM1 represents a pure paramagnetic solution while COM2 is more suitable to describe strong magnetic correlations. Due to this, COM1 is in good agreement with numerical data for many physical quantities in the whole range of filling except in the neighbourhood of half-filling at low-temperature where strong antiferromagnetic correlations are established. In this regime, COM2 is better suited showing a remarked tendency of the system towards an antiferromagnetic phase transition. In a certain sense, COM1 and COM2 represent two different physical behaviors whose nature can be conceived in terms of the competition between different orders observed in real materials. Hence a full-consistent description of real materials can only be found in terms of a proper combination of the two solutions, which has already been proved to be capable of giving a relevant interpretation of many experimental evidence of non-conventional behaviours for a large class of strongly correlated systems [16, 59].

With no claim of being exhaustive (interested readers can found detailed and comprehensive reviews in Ref.[16] and Ref.[59]) we report in this Section some of the results obtained in the framework of the COM, compared with numeric data from finite-temperature Lanczos method (FTLM) and quantum Monte Carlo method (qMC). In particular, we also report a comparison with the so-called Hubbard-I [1] and Roth [22] approximations which correspond to different choices for the self-consistent equations (4.27), (4.28) and (4.30). Without going into the details of

these last two approaches (for a detailed description we refer to the original works [1, 22]), we just recall that the Hubbard-I approximation [1] determines both Δ and p by means of a simple decoupling procedure which leads to:

$$\Delta = 0 \ , \ p = \frac{n^2}{4} \ . \tag{4.31}$$

Following the Roth approximation, instead, Δ is fixed self-consistently as in Eq.4.28 but p is calculated by projecting with respect to the two field basis (4.1) (for details see Appendix B.4) which gives:

$$p = I_{22}^2 - \frac{2-\theta}{I_{11}\left(1-\theta^2\right)}\left[C_{cc}^{\alpha}C_{c\xi}^{\alpha} + C_{c\eta}^{\alpha}\left(\frac{C_{c\eta}^{\alpha}}{I_{22}} - C_{cc}^{\alpha}\right)\right] - \frac{C_{c\eta}^{\alpha}C_{c\xi}^{\alpha}}{I_{11}I_{22}\left(1-\theta\right)} \ , \tag{4.32}$$

where:

$$\theta \equiv \frac{I_{22} - C_{22}^{\alpha} - I_{22}^2}{I_{11}I_{22}} \ , \tag{4.33}$$

$$C_{c\psi}^{\alpha^n} \equiv \left\langle c^{\alpha^n}(i)\psi^{\dagger}(i)\right\rangle = C_{1\psi}^{\alpha^n} + C_{2\psi}^{\alpha^n} \ , \tag{4.34}$$

$$C_{cc}^{\alpha^n} \equiv C_{c\xi}^{\alpha^n} + C_{c\eta}^{\alpha^n} \ . \tag{4.35}$$

As shown in Fig.4.1 both these approximations violate the algebraic constraint $C_{12} = 0$ given by the Pauli exclusion principle which is satisfied only at $n = 0$ and $n = 1$ for any finite U, and for all values of the filling in the limit for $U \to \infty$. Furthermore, as shown in Fig.4.2, both Hubbard-I and Roth solutions violate the particle-hole relations:

$$\mu(2-n) = U - \mu(n) \ , \tag{4.36}$$

$$\Delta(2-n) = -\Delta(n) \ , \tag{4.37}$$

$$p(2-n) = p(n) + 1 - n \ , \tag{4.38}$$

which are automatically satisfied in the framework of the COM.

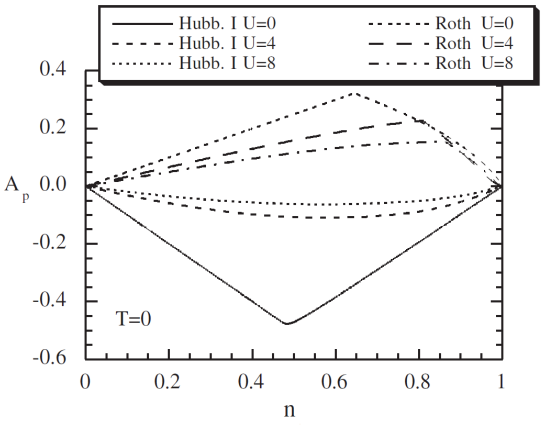

Figure 4.1: Pauli amplitude $A_p = C_{12}/C_{22}$ versus filling n at $T = 0$, plotted for different value of the on-site Coulomb interaction U and different approximations. Figure reprinted from Ref.[16].

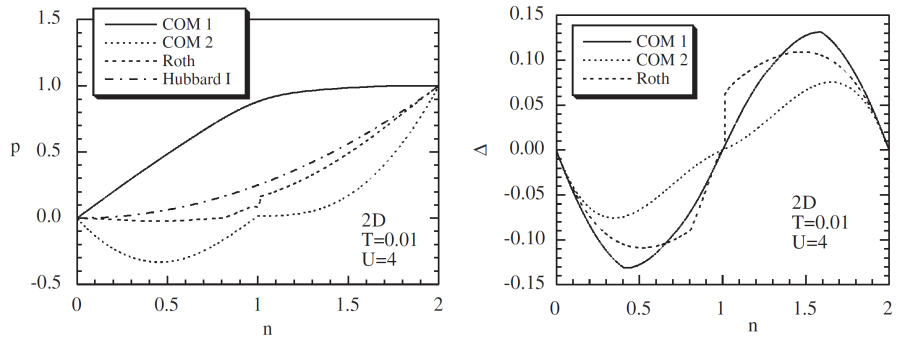

Figure 4.2: Evidence of particle-hole violation for Δ and p calculated in Hubbard-I and Roth approximations for $T = 0.01$ and $U = 4$. In the panel above we label with COM1 and COM2 the two possible solutions of the self-consistent equations (4.27), (4.28) and (4.30). Figure reprinted from Ref.[16].

As it will be better clarified in the rest of this Section, this last findings have a non negligible effect on many properties. In particular in the framework of the Roth approximation, as reported in Fig.(4.3), we emphasize the unphysical behavior of the chemical potential for small U and $0.8 < n < 1.0$. In this regime, a strong violation of the Pauli exclusion principle (see Fig.(4.1)) reflects in an anomalous behavior of the chemical potential which decreases with increasing n, signaling a thermodynamic instability (i.e. negative compressibility). As shown in the top right panel of Fig.4.3, this feature disappears in the strong coupling regime when the algebraic constraint $C_{12} = 0$ and the particle-hole symmetry are recovered. On the contrary, the Hubbard-I approximation is not affected by any thermodynamic instability, but it clearly shows a strong violation of the particle-hole symmetry at $n = 1$ (from Eq.(4.36) we should have $\mu(n = 1) = U/2$).

Another relevant drawback of Hubbard-I and Roth approximations with respect to the COM is found in the squared local magnetic moment S^2, defined as:

$$S^2(n, T, t, U) \equiv \frac{3}{4N} \sum_{\boldsymbol{i}} \left\langle [n_\uparrow(i) - n_\downarrow(i)]^2 \right\rangle \ . \tag{4.39}$$

In the paramagnetic case, meaning that $\langle n_\uparrow(i) \rangle = \langle n_\downarrow(i) \rangle$, by expanding the product in square brackets and thanks to the algebraic relation $[n_\sigma(i)]^2 = n_\sigma(i)$, S^2 can be straightforwardly expressed in terms of filling n and double occupancy D as:

$$S^2(n, T, t, U) = \frac{3}{4} (n - 2D) \ , \tag{4.40}$$

where n is fixed as an external parameter (hence μ is fixed self-consistently according to Eq.4.27), and D is calculated in terms of the correlators (4.25) as:

$$D(n, T, t, U) = \frac{1}{N} \sum_{\boldsymbol{i}} \langle n_\uparrow(i) n_\downarrow(i) \rangle = \frac{n}{2} - \left\langle \eta(i) \eta^\dagger(i) \right\rangle = \frac{n}{2} - C_{22} \ . \tag{4.41}$$

As reported in Fig.4.4, both Hubbard-I and Roth approximations show a relevant discrepancy with respect to numerical data in the low-temperature regime where the effect of quantum fluctuations and correlations is strongly enhanced. On the

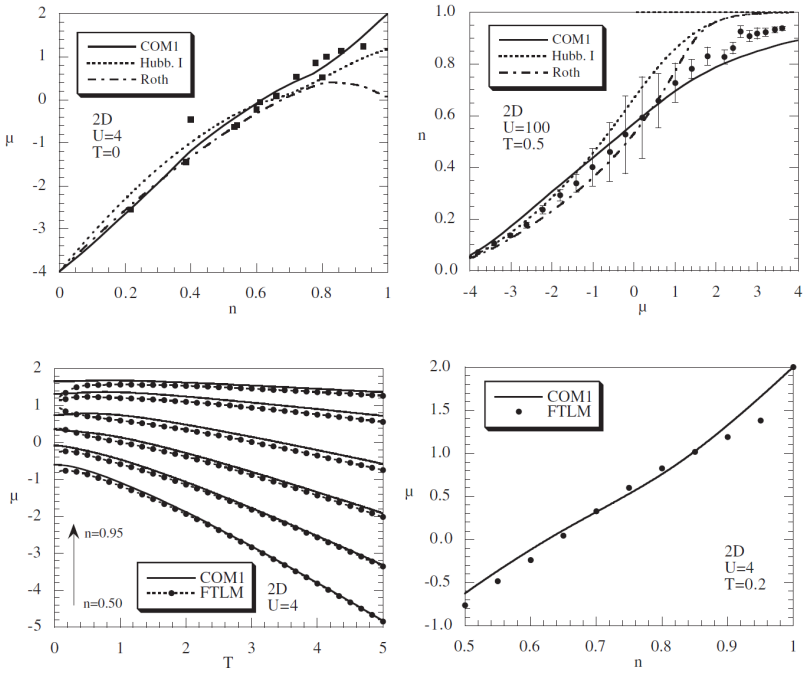

Figure 4.3: Temperature and doping dependence of the chemical potential for different values of temperature T and strength of the on-site Coulomb interaction U. Symbols correspond to numerical data from Refs.[60, 61, 62, 63, 64]. Figure reprinted from Ref.[16].

contrary, the COM qualitatively reproduces the data in the whole range of temperature and approaches Roth and Hubbard-I curves in the limit for $T \to \infty$ as one would expect.

Finally, to complete our analysis we report below few results on the thermodynamic properties, namely the internal energy $E(n,T,t,U)$ and the entropy $S(n,T,t,U)$. We recall that the internal energy E, calculated as the average of the Hamiltonian (4.4), can be expressed as:

$$\begin{aligned} E(n,T,t,U) &= \langle H \rangle = -\mu n + 2dt\,(C^{\alpha}_{11} + 2C^{\alpha}_{12} + C^{\alpha}_{22}) + UD = \\ &= -2\mu\,(1 - C_{11} - C_{22}) + 2dt\,(C^{\alpha}_{11} + 2C^{\alpha}_{12} + C^{\alpha}_{22}) \\ &\quad + U\left(\frac{n}{2} - C_{22}\right)\,, \end{aligned} \tag{4.42}$$

where in the last step we have used Eq.4.27 and Eq.4.41 to express the electronic density n and the double occupancy D, respectively, in terms of correlation functions $C^{\alpha^n}_{ab}$ (4.25). The entropy can be expressed in terms of the chemical potential as:

$$S(n,T,t,U) = -\int_0^n \frac{\partial\mu(\tilde{n},T,t,U)}{\partial T} d\tilde{n}\,. \tag{4.43}$$

As far as the internal energy is concerned, as reported in Fig.4.5, the comparison between COM and qMC data shows a good agreement in the whole range of temperature, strength of the on-site Coulomb potential and filling with only small discrepancies. In particular, as reported in the central panel of Fig.4.5, these dis-

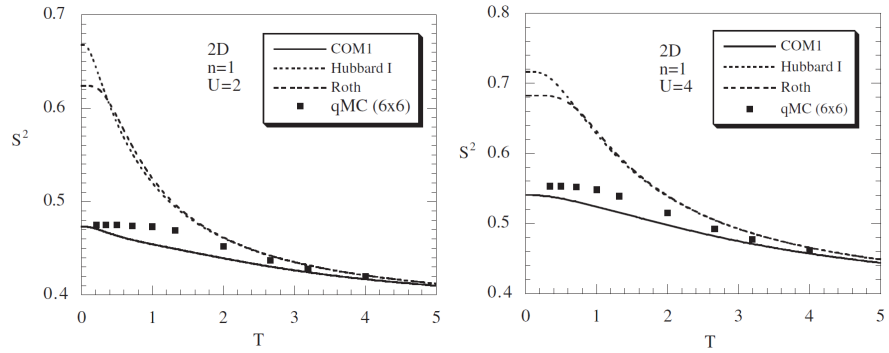

Figure 4.4: Squared local magnetic moment S^2 versus temperature T at $n = 1$ and for different values of the on-site Coulomb interaction U. Symbols correspond to qMC data from Ref.[65]. Figure reprinted from Ref.[16].

crepancies do not depend on U and therefore they seem likely to be due to finite size effects in the numerical simulations. A good agreement is also achieved in the calculation of the entropy whose doping and temperature dependencies are reported in Fig.4.6, compared to FTLM data. In particular, in the case of the entropy we note that a remarkable discrepancy only occurs near half-filling at low temperatures when antiferromagnetic correlations become relevant and COM1, which we recall to be a paramagnetic solution, is no more able to reproduce the physics of the system. As one would expect, for temperature high enough to destroy antiferromagnetic fluctuations, we recover a good agreement with numerical data in the whole range of filling.

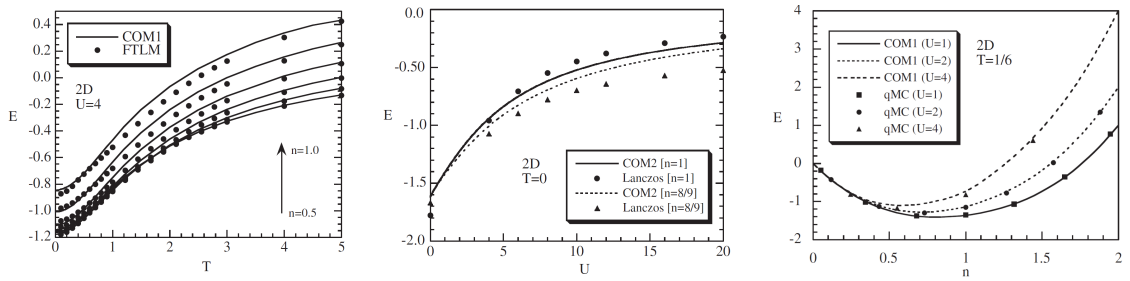

Figure 4.5: Internal energy E versus temperature T (left panel), strength of the on-site Coulomb potential U (central panel) and filling n (right panel). Symbols correspond to FTLM [66, 67] and qMC [68] data. Figure reprinted from Ref.[16].

4.2 Two-pole approximation: bosonic sector

To complete our analysis on the two-pole solution of the single-band Hubbard model we include in this Section a detailed calculation of some system's response functions, namely charge and spin susceptibilities and correlation functions. In the framework of the linear response theory, both charge ($\mu = 0$) and spin ($\mu = \{1, 2, 3\}$) suscepti-

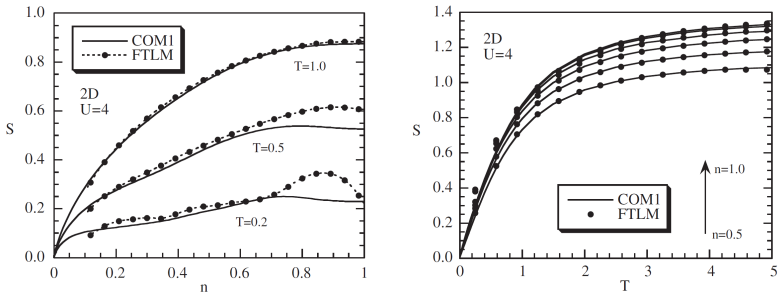

Figure 4.6: Entropy S versus filling n for different temperatures (left panel) and versus temperature T for different values of the filling at $U = 4$. Symbols correspond to FTLM data from Ref.[66]. Figure reprinted from Ref.[16].

bilities can be calculated in terms of the following bosonic propagator:

$$\chi_\mu(\boldsymbol{k}, \omega) = -F.T. \langle \mathcal{R} \left[n_\mu(i) n_\mu(j) \right] \rangle \ , \tag{4.44}$$

Hence, with the aim of calculating all the relevant response functions, two possible approaches can be pursued. One can express the bosonic Green's functions in terms of fermionic propagators (4.25) which can be calculated following the self-consistent scheme developed in the previous Section. This approach is called *"one loop"* approximation. Alternatively, one can introduce a bosonic basis, complementary to the fermionic one (4.1), and then calculate all the relevant bosonic correlators by linearizing the corresponding equations of motion. It is worth noting that these two approaches, in principle completely equivalent, lead to significantly different outcomes if the selected bases are not closed due to different approximations involved in the truncation of the hierarchy of the equations of motion. For the sake of brevity, in this Section we will restrict our analysis to the second method only, and report in Appendix B.4 a detailed calculation of charge-charge, spin-spin and pair-pair correlators in the framework of the so-called one-loop approximation.

As already specified before, there is no general prescription on the choice of the composite fields of the basis. One might simply think to start from the equation of motion of the basic field $n_\mu(i)$ which contains both charge $\mu = 0$ and spin $\mu = \{1, 2, 3\}$ densities. As follows from simple commutations, we obtain:

$$i\partial_t n_\mu(i) = [n_\mu(i), H] = -2dt\rho_\mu(i) \ , \tag{4.45}$$

where:

$$\rho_\mu(i) \equiv c^\dagger(i)\sigma_\mu c^\alpha(i) - c^{\alpha\dagger}(i)\sigma_\mu c(i) \ . \tag{4.46}$$

Then, based on the hierarchy of the equation of motions, we can define the following bosonic basis:

$$N^{(\mu)}(i) = \begin{pmatrix} n_\mu(i) \\ \rho_\mu(i) \end{pmatrix} \ . \tag{4.47}$$

This choice assures that the first four bosonic moments have the correct functional form [69] and, more important, it guarantees the equation of motion of the field $n_\mu(i)$ to be accounted exactly. Hence any approximation due to linearization will

only affects the equation of motion of $\rho_\mu(i)$:

$$i\partial_t \rho_\mu(i) = -2dt l_\mu(i) + U\kappa_\mu(i) \; , \tag{4.48}$$

in which $\kappa_\mu(i)$ and $l_\mu(i)$ appear as higher order fields defined as:

$$\begin{aligned} \kappa_\mu(i) &= c^\dagger(i)\sigma_\mu\eta^\alpha(i) - \eta^\dagger(i)\sigma_\mu c^\alpha(i) + \eta^{\alpha\dagger}(i)\sigma_\mu c(i) - c^{\alpha\dagger}(i)\sigma_\mu\eta(i) \; , & (4.49)\\ l_\mu(i) &= c^\dagger(i)\sigma_\mu c^{\alpha^2}(i) + c^{\alpha^2\dagger}(i)\sigma_\mu c(i) - 2c^{\alpha\dagger}(i)\sigma_\mu c^\alpha(i) \; . & (4.50) \end{aligned}$$

In the framework of the two-pole approximation, by following the same procedure used for the fermionic basis (4.1), we linearize the equation of motion of $N^{(\mu)}(i)$ as:

$$i\partial_t N^{(\mu)}(i) = \sum_{\boldsymbol{j}} \varepsilon^{(\mu)}(\boldsymbol{i},\boldsymbol{j}) N^{(\mu)}(\boldsymbol{j},t) \; , \tag{4.51}$$

where the bosonic energy matrix $\varepsilon^{(\mu)}(\mathbf{i},\mathbf{j})$ can be calculated in terms of normalization $I^{(\mu)}(\mathbf{i},\mathbf{j})$ and $m^{(\mu)}(\mathbf{i},\mathbf{j})$ matrices:

$$\begin{aligned} I^{(\mu)}(\mathbf{i},\mathbf{j}) &\equiv \left\langle \left[N^{(\mu)}(\boldsymbol{i},t), N^{(\mu)\dagger}(\boldsymbol{j},t) \right] \right\rangle \; , & (4.52)\\ m^{(\mu)}(\mathbf{i},\mathbf{j}) &\equiv \left\langle \left[i\partial_t N^{(\mu)}(\boldsymbol{i},t), N^{(\mu)\dagger}(\boldsymbol{j},t) \right] \right\rangle \; . & (4.53) \end{aligned}$$

In the case of a paramagnetic and homogeneous system the two matrices $I^{(\mu)}(\mathbf{i},\mathbf{j})$ and $m^{(\mu)}(\mathbf{i},\mathbf{j})$ have the following form in momentum space [70]:

$$I^{(\mu)}(\mathbf{k}) = \begin{pmatrix} 0 & I_{12}^{(\mu)}(\mathbf{k}) \\ I_{12}^{(\mu)}(\mathbf{k}) & 0 \end{pmatrix} \; , \; m^{(\mu)}(\mathbf{k}) = \begin{pmatrix} m_{11}^{(\mu)}(\mathbf{k}) & 0 \\ 0 & m_{22}^{(\mu)}(\mathbf{k}) \end{pmatrix} \; , \tag{4.54}$$

where:

$$\begin{aligned} I_{12}^{(\mu)}(\mathbf{k}) &= 4\left(1-\alpha(\boldsymbol{k})\right) C_{cc}^{\alpha} \; , & (4.55)\\ m_{11}^{(\mu)}(\mathbf{k}) &= -2dt I_{12}^{(\mu)}(\boldsymbol{k}) \; , & (4.56)\\ m_{22}^{(\mu)}(\mathbf{k}) &= -2dt I_{l_\mu\rho_\mu}(\boldsymbol{k}) + U I_{\kappa_\mu\rho_\mu}(\boldsymbol{k}) \; , & (4.57) \end{aligned}$$

and:

$$\begin{aligned} C_{cc}^{\alpha} &= F.T.\left\langle c^\alpha(i) c^\dagger(i) \right\rangle \; , & (4.58)\\ I_{l_\mu\rho_\mu}(\boldsymbol{k}) &= F.T.\left\langle \left[l_\mu(\boldsymbol{i},t), \rho_\mu^\dagger(\boldsymbol{j},t) \right] \right\rangle \; , & (4.59)\\ I_{\kappa_\mu\rho_\mu}(\boldsymbol{k}) &= F.T.\left\langle \left[\kappa_\mu(\boldsymbol{i},t), \rho_\mu^\dagger(\boldsymbol{j},t) \right] \right\rangle \; , & (4.60) \end{aligned}$$

can be calculated self-consistently by means of algebraic relations and symmetry requirements. Hence the energy matrix can be expressed as:

$$\varepsilon^{(\mu)}(\mathbf{k}) = \begin{pmatrix} 0 & \varepsilon_{12}^{(\mu)}(\mathbf{k}) \\ \varepsilon_{21}^{(\mu)}(\mathbf{k}) & 0 \end{pmatrix} \; , \; \begin{cases} \varepsilon_{12}^{(\mu)}(\mathbf{k}) = -2dt \\ \varepsilon_{21}^{(\mu)}(\mathbf{k}) = m_{22}^{(\mu)}(\mathbf{k}) / I_{12}^{(\mu)}(\mathbf{k}) \end{cases} \; , \tag{4.61}$$

whose eigenvalues are given by:

$$\omega_n^{(\mu)}(\boldsymbol{k}) = (-1)^n \sqrt{\varepsilon_{12}^{(\mu)}(\mathbf{k})\varepsilon_{21}^{(\mu)}(\mathbf{k})} \; . \tag{4.62}$$

The knowledge of the bosonic energy spectra allows us to write the bosonic Green's functions (see Section 2.2.2) as:

$$G^{(\mu)}(\boldsymbol{k}.\omega) = \Gamma^{(\mu)}(\boldsymbol{k}) \left[\frac{1}{\omega + i\delta} - \frac{1}{\omega - i\delta} \right] \tag{4.63}$$

$$+ \sum_{n=1}^{2} \sigma^{(n,\mu)}(\boldsymbol{k}) \left[\frac{1 + f_B(\omega)}{\omega - \omega_n^{(\mu)}(\boldsymbol{k}) + i\delta} - \frac{f_B(\omega)}{\omega - \omega_n^{(\mu)}(\boldsymbol{k}) - i\delta} \right] , \tag{4.64}$$

where $f_B(\omega) = [e^{\beta\omega} - 1]^{-1}$ is the Bose-Einstein distribution function, $\Gamma^{(\mu)}(\boldsymbol{k})$ is the zero frequency function (2.74) and:

$$\sigma^{(n,\mu)}(\boldsymbol{k}) = \frac{I_{12}^{(\mu)}(\mathbf{k})}{2} \begin{pmatrix} \frac{\varepsilon_{12}^{(\mu)}(\mathbf{k})}{\omega_n^{(\mu)}(\boldsymbol{k})} & 1 \\ 1 & \frac{\varepsilon_{21}^{(\mu)}(\mathbf{k})}{\omega_n^{(\mu)}(\boldsymbol{k})} \end{pmatrix} \; . \tag{4.65}$$

By recalling the general relation between advanced and retarded Green's functions (2.96) we finally obtain the following expression for charge ($\mu = 0$) and spin ($\mu \neq 0$) susceptibility:

$$\chi_\mu(\boldsymbol{k}, \omega) = -F.T. \langle \mathcal{R} \left[n_\mu(i) n_\mu(j) \right] \rangle = - \sum_{n=1}^{2} \frac{\sigma^{(n,\mu)}(\boldsymbol{k})}{\omega - \omega_n^{(\mu)}(\boldsymbol{k}) + i\delta} \; , \tag{4.66}$$

which gives:

$$N(\boldsymbol{k}) = \left(\frac{2\pi}{a} \right)^d n^2 \delta^{(d)}(\boldsymbol{k}) - 4dtC_{cc}^{\alpha} \frac{1 - \alpha(\boldsymbol{k})}{\omega^{(0)}(\boldsymbol{k})} \coth \left(\frac{\beta\omega^{(0)}(\boldsymbol{k})}{2} \right) \; , \tag{4.67}$$

$$S(\boldsymbol{k}) = -4dtC_{cc}^{\alpha} \frac{1 - \alpha(\boldsymbol{k})}{\omega^{(3)}(\boldsymbol{k})} \coth \left(\frac{\beta\omega^{(3)}(\boldsymbol{k})}{2} \right) \; , \tag{4.68}$$

for the charge $N(\boldsymbol{k})$ and the spin $S(\boldsymbol{k})$ correlation functions. From the results obtained so far it is immediate to note that, differently from the canonical Green's function formalism, in the framework of the Composite Operator Method a careful treatment of the zero-frequency function $\Gamma^{(\mu)}(\boldsymbol{k})$ is required. In fact, although $\Gamma^{(\mu)}(\boldsymbol{k})$ does not appear in the retarded propagators which determine all the system's response functions, it is directly involved in the calculation of the causal propagators (i.e. correlation functions) which take part in the self-consistent scheme via Pauli constraints and Ward-Takahashi identities. In general, different procedures can be applied for the calculation of $\Gamma^{(\mu)}(\boldsymbol{k})$ but, due to the lack of any prescription, the effect of a particular choice can only be tested by an a posteriori comparison with numerical data. As a first attempt, as done for example for charge (4.67) and spin (4.68) correlation functions , $\Gamma^{(\mu)}(\boldsymbol{k})$ can be fixed by assuming the ergodicity of the

system which gives:

$$\Gamma_{11}^{(\mu)}(\boldsymbol{k}) = \delta_{\mu 0} \left(\frac{2\pi}{a}\right)^d n^2 \delta^{(d)}(\boldsymbol{k}) \; . \tag{4.69}$$

This particular assumption, which is not true in general, is widely justified by a good agreement with numerical data. However, one has to remember that many physical quantities are not ergodic. In these cases different methods have to be used. In particular, $\Gamma^{(\mu)}(\boldsymbol{k})$ can be fixed in the framework of a self-consistent scheme by means of Pauli constraints, or symmetry requirements. Alternatively, by introducing a new bosonic sector: the pair sector (see Appendix B.4.3), as reported in Ref.[71].

4.2.1 Charge and spin correlation functions

Results obtained for charge and spin correlation functions are reported in Fig.4.7 and in Fig.4.8, respectively. As already pointed out before, the ergodicity assumption $\Gamma_{11}^{(\mu)}(\boldsymbol{k}) = \delta_{\mu 0} \left(\frac{2\pi}{a}\right)^d n^2 \delta^{(d)}(\boldsymbol{k})$ results in an excellent agreement with numerical data. In particular, it is worth noting that the COM is able to catch the double-peak structure of $N(\boldsymbol{k})$, with a great enhancement near (π, π) which signals strong charge correlations and the presence of a weak charge ordering. The consistency of the COM is further confirmed by the results obtained for the spin correlation function which show an excellent agreement with numerical (left and central panels in Fig.4.8) and experimental (right panel in Fig.4.8) data. As already discussed before, small discrepancy with respect to numerical data can only be found in high-filling and low-temperature regime where the paramagnetic solution is not able to reproduce strong antiferromagnetic fluctuations in numerical data. However, numerical analysis suffers from finite size effects when the antiferromagnetic correlation length becomes comparable with the size of the cluster [75]. Therefore this last issue does not affect the validity of the approximation that, despite the paramagnetic assumption, is still able to catch the effects of antiferromagnetic fluctuations as clearly shown in the right panel of Fig.4.8 where both position and intensity of the main antiferromagnetic peak at (π, π) are perfectly reproduced.

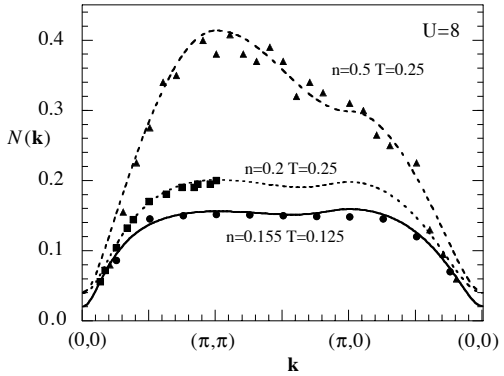

Figure 4.7: Charge correlation function $N(\boldsymbol{k})$ versus momentum $\boldsymbol{k}$ for $U = 8$ and different values of temperature T and filling n. Symbols correspond to qMC data from Ref.[72]. Figure reprinted from Ref.[59].

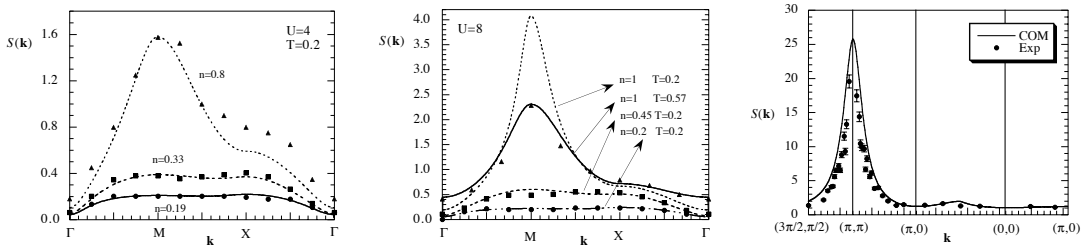

Figure 4.8: Spin correlation function $S(\boldsymbol{k})$ versus momentum $\boldsymbol{k}$ ($\Gamma = (0,0)$, $M = (\pi,\pi)$, $X = (\pi,0)$) for different values of the strength of the on-site Coulomb potential U, temperature T and filling n. Symbols in the left and central panels correspond to qMC data from Ref.[73]. Symbols in the right panel correspond to high-resolution neutron scattering data from Ref.[74]. Figure reprinted from Ref.[59].

4.3 Self-energy corrections to the two-pole approximation

Consistently with the pole-approximation, in the calculation scheme developed so far the residual part of the self-energy was completely neglected under the assumption that all the relevant self-energy corrections were indirectly taken into account in the "free" Green's functions because of the composite nature of the operators of the basis (see Sec.2.2). This assumption, recalling the Green's function formalism illustrated in Section 2.1, allows us to skip the calculation of the high order retarded propagator $B^R(\boldsymbol{k},\omega)$ defined as:

$$B^R(\boldsymbol{k},\omega) \equiv F.T. \left\langle R\left[\delta J(i)\delta J^\dagger(j)\right]\right\rangle \ , \tag{4.70}$$

where $\delta J(i)$ represents the contribution to the current orthogonal with respect to the two-pole basis $\psi(i)$ (see Eq.2.20):

$$i\partial_t \psi(i) = [\psi(i), \mathcal{H}] \equiv J(i) = \sum_{\boldsymbol{m}} \epsilon(\boldsymbol{i},\boldsymbol{m})\psi(\boldsymbol{m},t) + \delta J(\boldsymbol{i},t) \ . \tag{4.71}$$

In almost all the cases the calculation of $B^R(\boldsymbol{k},\omega)$ can not be accounted in the framework of the self-consistent polar scheme since it requires the knowledge of propagators of the type:

$$\mathcal{C}^R(\boldsymbol{k},\omega) = F.T \left\langle R\left[B(i)F(i)F^\dagger(j)B(j)\right]\right\rangle \ , \tag{4.72}$$

where $F(i)$ and $B(i)$ represent non-local fermionic and bosonic operators, respectively. We note that the above propagator can not be calculated self-consistently since it is defined as the average of non-local operators while the fields of the basis are local. Its dependency on both momentum and frequency does not allow to fix it in terms of PCs or WTIs, therefore further approximations necessarily need to be considered. In particular, in the framework of the so-called *"Non-Crossing Approximation"* (NCA) one can assume that fermionic and bosonic modes propagates

independently, allowing for the following factorization of the causal propagator:

$$\mathcal{C}^C(i,j) = \left\langle T\left[B(i)F(i)F^\dagger(j)B(j)\right]\right\rangle \approx f^C(i,j)b^C(i,j)\ . \tag{4.73}$$

where $f^C(\boldsymbol{k},\omega)$ and $b^C(\boldsymbol{k},\omega)$ are the following two-time fermionic and bosonic propagators:

$$\begin{cases} f^C(\boldsymbol{k},\omega) \equiv F.T\left\langle T\left[F(i)F^\dagger(j)\right]\right\rangle \\ b^C(\boldsymbol{k},\omega) \equiv F.T\left\langle T\left[B(i)B(j)\right]\right\rangle \end{cases}\ , \tag{4.74}$$

which can be calculated self-consistently in the polar approximation. Then one can use the spectral representations (2.66) and (2.95) to recover the retarded propagators:

$$f^C(\boldsymbol{k},\omega) = -\frac{1}{\pi}\int_{-\infty}^{+\infty} d\omega' \left[\frac{1-f_F\left(\beta\omega'\right)}{\omega-\omega'+i\delta} + \frac{f_F\left(\beta\omega'\right)}{\omega-\omega'-i\delta}\right] \mathrm{Im}\left[f^R(\boldsymbol{k},\omega')\right] \tag{4.75}$$

$$b^C(\boldsymbol{k},\omega) = -\frac{1}{\pi}\int_{-\infty}^{+\infty} d\omega' \left[\frac{1-f_B\left(\beta\omega'\right)}{\omega-\omega'+i\delta} + \frac{f_B\left(\beta\omega'\right)}{\omega-\omega'-i\delta}\right] \mathrm{Im}\left[b^R(\boldsymbol{k},\omega')\right] \tag{4.76}$$

Therefore, recalling that:

$$\mathcal{C}^R(\boldsymbol{k},\omega) = -\frac{1}{\pi}\int_{-\infty}^{+\infty} \frac{d\omega'}{\omega-\omega'+i\epsilon}\coth\left(\frac{\beta\omega'}{2}\right)\mathrm{Im}\left[\mathcal{C}^C(\boldsymbol{k},\omega)\right]\ , \tag{4.77}$$

one immediately obtains:

$$\begin{aligned}\mathcal{C}^R(\boldsymbol{k},\omega) = \frac{1}{\pi}\int_{-\infty}^{+\infty} \frac{d\omega'}{\omega-\omega'+i\delta\,(2\pi)^{d+1}}\int_{\Omega_B} d^dp \int_{-\infty}^{+\infty} d\Omega \mathrm{Im}\left[f^R(\boldsymbol{p},\Omega)\right] \\ \mathrm{Im}\left[b^R(\boldsymbol{k}-\boldsymbol{p},\omega'-\Omega)\right]\left[\tanh\left(\frac{\beta\Omega}{2}\right)+\coth\left(\frac{\beta\left(\omega'-\Omega\right)}{2}\right)\right]\end{aligned} \tag{4.78}$$

Let us now apply the NCA to calculate self-energy corrections in the framework of the two-pole approximation. Starting from the basis of composite fields defined in Eq.4.1, by neglecting the pair term $c(i)c^{\alpha\dagger}(i)c(i)$ in the equations of motion of $\xi(i)$ and $\eta(i)$ (see Eq.4.5), one obtains

$$J(\boldsymbol{i},t) = \sum_{\boldsymbol{j}} a(\boldsymbol{i},\boldsymbol{j})\psi(\boldsymbol{j},t)\ , \tag{4.79}$$

where:

$$a(\boldsymbol{i},\boldsymbol{j}) = \begin{pmatrix} -\mu\delta_{\boldsymbol{ij}} - 2dt\alpha_{\boldsymbol{ij}} - dt\alpha_{\boldsymbol{ij}}\sigma^\mu n_\mu(i) & -2dt\alpha_{\boldsymbol{ij}} - dt\alpha_{\boldsymbol{ij}}\sigma^\mu n_\mu(i) \\ dt\alpha_{\boldsymbol{ij}}\sigma^\mu n_\mu(i) & \left(U-\mu\right)\delta_{\boldsymbol{ij}} + dt\alpha_{\boldsymbol{ij}}\sigma^\mu n_\mu(i) \end{pmatrix}\ . \tag{4.80}$$

However, according to Eq.2.38, the calculation of the self-energy only requires the irreducible part of the propagator $B^R(\boldsymbol{k},\omega)$ which can be calculated in terms of the fluctuation of $a(\boldsymbol{i},\boldsymbol{j})$ with respect to its mean value as:

$$\delta J(\boldsymbol{i},t) \approx \sum_{\boldsymbol{j}} \left[a(\boldsymbol{i},\boldsymbol{j}) - \langle a(\boldsymbol{i},\boldsymbol{j})\rangle\right]\psi(j,t)\ , \tag{4.81}$$

which gives:

$$B^R_{irr}(\boldsymbol{k},\omega) = d^2t^2 \left\langle R\left[\sigma^\mu \delta n_\mu(i) c^\alpha(i) c^{\alpha\dagger}(j) \delta n_\nu(j) \sigma^\nu\right]\right\rangle \begin{pmatrix} 1 & -1 \\ -1 & 1 \end{pmatrix} , \tag{4.82}$$

where $\delta n_\mu(i) \equiv n_\mu(i) - \langle n_\mu(i)\rangle$. Hence, according to Eq.2.36 we obtain:

$$\Sigma(\boldsymbol{k},\omega) = d^2t^2 F(\boldsymbol{k},\omega) \begin{pmatrix} I_{11}^{-2} & -I_{11}^{-1} I_{22}^{-1} \\ -I_{11}^{-1} I_{22}^{-1} & I_{22}^{-2} \end{pmatrix} , \tag{4.83}$$

where $F(\boldsymbol{k},\omega) \equiv F.T.\left[F(i,j)\right]$ is the Fourier transform of the high-order retarded propagator $F(i,j)$ defined as:

$$F(i,j) \equiv \left\langle R\left[\sigma^\mu \delta n_\mu(i) c^\alpha(i) c^{\alpha\dagger}(j) \delta n_\nu(j) \sigma^\nu\right]\right\rangle . \tag{4.84}$$

In the framework of the NCA the above quantity can be factorized as:

$$F(i,j) \approx \langle \delta n_\mu(i) \delta n_\mu(j)\rangle \left\langle c^\alpha(i) c^{\alpha\dagger}(j)\right\rangle . \tag{4.85}$$

By means of the spectral theorem, fermionic and bosonic contributions in the above equation can be expressed as:

$$\begin{aligned} \left\langle c^\alpha(i) c^{\alpha\dagger}(j)\right\rangle &= -\frac{a^d}{(2\pi)^{d+1}} \int_{\Omega_B} d^dk \int_{-\infty}^{+\infty} d\omega e^{i\boldsymbol{k}\cdot(\boldsymbol{i}-\boldsymbol{j}) - i\omega(t_i - t_j)} \alpha^2(\boldsymbol{k}) \\ &\quad \left[1 + \tanh\left(\frac{\beta\omega}{2}\right)\right] \mathrm{Im}\left[G_{cc}(\boldsymbol{k},\omega)\right] , \end{aligned} \tag{4.86}$$

$$\begin{aligned} \langle \delta n_\mu(i) \delta n_\mu(j)\rangle &= -\frac{a^d}{(2\pi)^{d+1}} \int_{\Omega_B} d^dk \int_{-\infty}^{+\infty} d\omega e^{i\boldsymbol{k}\cdot(\boldsymbol{i}-\boldsymbol{j}) - i\omega(t_i - t_j)} \\ &\quad \left[1 + \coth\left(\frac{\beta\omega}{2}\right)\right] \mathrm{Im}\left[\chi(\boldsymbol{k},\omega)\right] , \end{aligned} \tag{4.87}$$

were, following the relation $c(i) = \xi(i) + \eta(i)$, we have defined:

$$G_{cc}(\boldsymbol{k},\omega) = G_{11}(\boldsymbol{k},\omega) + 2G_{12}(\boldsymbol{k},\omega) + G_{22}(\boldsymbol{k},\omega) . \tag{4.88}$$

We recall that the retarded correlators of fermionic, $G(\boldsymbol{k},\omega)$, and bosonic, $\chi(\boldsymbol{k},\omega)$, nature can be calculated by means of the two-pole self-consistent schemes developed in Sec.4.1 and Sec.4.2. Then, by substituting the in the expression of $F(\boldsymbol{k},\omega)$ we obtain:

$$\begin{aligned} F(\boldsymbol{k},\omega) &= \frac{a^d}{(2\pi)^{d+2}} \int_{\Omega_B} d^dp \int_{-\infty}^{+\infty} d\Omega \int_{-\infty}^{+\infty} d\omega' \mathrm{Im}\left[\chi(\boldsymbol{k}-\boldsymbol{p},\omega'-\Omega)\right] \\ &\quad \mathrm{Im}\left[G_{cc}(\boldsymbol{p},\Omega)\right] \left[1 + \tanh\left(\frac{\beta\Omega}{2}\right)\right] \left[1 + \coth\left(\frac{\beta(\omega'-\Omega)}{2}\right)\right] \end{aligned} \tag{4.89}$$

The correlator $F(\boldsymbol{k},\omega)$ can also be expressed in terms of spectral density matrices $\sigma(\boldsymbol{k})$, fermionic $E_n(\boldsymbol{k})$ and bosonic $\omega_m^{(\mu)}$ energy spectra. In fact, from Eq.2.58 and

Eq.4.66 we have:

$$F(\boldsymbol{k},\omega) = \frac{a^d}{(2\pi)^{d+2}} \sum_{\mu=0}^{3} \sum_{m=1}^{2} \sum_{a,b=1}^{2} \sum_{n=1}^{2} \int_{\Omega_B} d^d p \alpha^2(\boldsymbol{p}) \left[\frac{\sigma_{ab}^{(n)}(\boldsymbol{p}) \sigma_{11}(\boldsymbol{k}-\boldsymbol{p})}{\omega - E_n(\boldsymbol{p}) - \omega_m^{(\mu)}(\boldsymbol{k}-\boldsymbol{p}) + i\delta} \right] \left[\tanh\left(\frac{E_n(\boldsymbol{p})}{2k_BT}\right) + \coth\left(\frac{\omega_m^{(\mu)}(\boldsymbol{k}-\boldsymbol{p})}{2k_BT}\right) \right] , \tag{4.90}$$

which, as follows from Eq.4.83, represents the dynamical part of the self-energy calculated at the first order in the NCA. In fact, as better emphasized in Eq.4.89, $F(\boldsymbol{k},\omega)$ depends on the complete Green's functions which in turn depend on $\Sigma(\boldsymbol{k},\omega)$:

$$G(\boldsymbol{k},\omega) = \frac{I(\boldsymbol{k})}{\omega - \epsilon(\boldsymbol{k}) - \Sigma(\boldsymbol{k},\omega)} . \tag{4.91}$$

Therefore Eq.4.90 defines nothing but the first step of a self-consistent procedure which is required for the calculation of self-energy corrections. The whole self-consistent scheme, illustrated in Fig.4.9, can be described as follows.

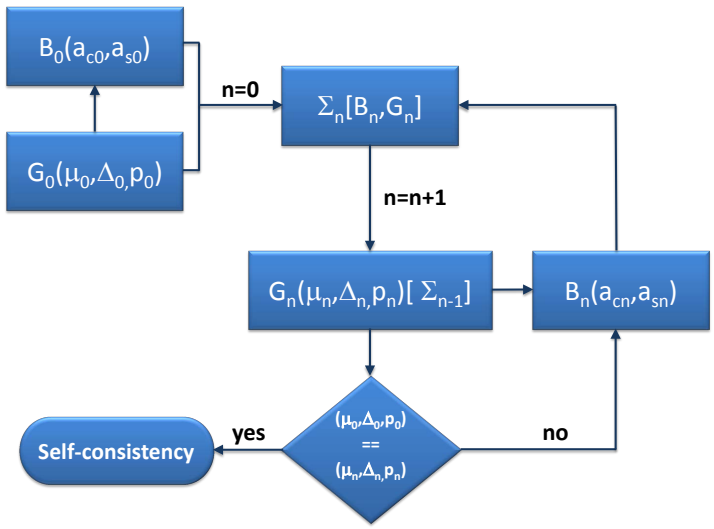

Figure 4.9: Self Consistent Born Approximation scheme for the calculation of the fermionic full propagator G in terms of charge-charge and spin-spin two-pole propagators B and residual self-energy Σ.

At the first iteration we just neglect self-energy corrections and calculate all the retarded Green's functions and correlations functions following the two-pole self-consistent scheme illustrated in Sec.4.1 with:

$$G(\boldsymbol{k},\omega) = G^{(0)}(\boldsymbol{k},\omega) = \frac{I(\boldsymbol{k})}{\omega - \epsilon(\boldsymbol{k})} = \sum_{n=1}^{2} \frac{\sigma^{(n)}(\boldsymbol{k})}{\omega - E_n(\boldsymbol{k}) + i\delta} . \tag{4.92}$$

This allows us to calculate the fermionic energy spectra $E_n(\boldsymbol{k})$ (4.19) and the spectral density matrices $\sigma^{(n)}(\boldsymbol{k})$ (4.23). Then bosonic energies $\omega_n^{(\mu)}(\boldsymbol{k})$ (4.62) and bosonic

correlators (4.66) can be calculated in terms of the fermionic ones (see Sec.4.2). The knowledge of fermionic and bosonic energy spectra and spectral density matrices allows us to calculate first order self-energy corrections, $\Sigma^{(1)}(\boldsymbol{k},\omega)$, according to Eq.4.83, with $F(\boldsymbol{k},\omega)$ given by Eq.4.90. Hence $\Sigma^{(1)}(\boldsymbol{k},\omega)$ can be used to estimate the complete Green's functions (4.91):

$$G^{(1)}(\boldsymbol{k},\omega) = \frac{I(\boldsymbol{k})}{\omega - \epsilon^{(1)}(\boldsymbol{k}) - \Sigma^{(0)}(\boldsymbol{k},\omega)} \ , \tag{4.93}$$

which, in turn, can be inserted in the two-pole self-consistent scheme for the calculation of first order energy spectra and spectral functions. Then the whole procedure can be repeated recursively, allowing to calculate self-energy corrections to Green's functions up to a generic n^{th}-order as:

$$G^{(n)}(\boldsymbol{k},\omega) = \frac{I(\boldsymbol{k})}{\omega - \epsilon^{(n)}(\boldsymbol{k}) - \Sigma^{(n-1)}(\boldsymbol{k},\omega)} \ , \tag{4.94}$$

where $\epsilon^{(n)}(\boldsymbol{k})$ is the fermionic energy matrix which includes self-energy correction up to the $(n-1)^{th}$-order. The self-consistent procedure stops when the variation of the self-consistent parameters μ, p, Δ within two consecutive steps satisfies the required accuracy, meaning that no further steps in the self-consistent procedure need to be evaluated.

The relevance of the calculation scheme described so far resides in providing a full microscopic description of the self-energy, accounted in terms of the convolution of electronic propagators, charge, spin and pair susceptibilities (Eq.4.83 and Eq.4.89). Then, different from other numerical and analytical approaches in which these quantities, as well as filling and correlation lengths, suffer from finite size effects or can only be accounted phenomenologically, within the COM all the relevant fermionic and bosonic propagators are determined microscopically in the framework of the two-pole approximation, providing a more reliable treatment of non-local correlations and unconventional effects due to strong interactions.

4.3.1 Spectral functions and momentum distribution functions in the NCA

Let us discuss some results obtained in the framework of the NCA for the two-dimensional Hubbard model (4.4). For the sake of brevity, in this Subsection we restrict our analysis to spectral functions $A(\boldsymbol{k})$, momentum distribution functions $n(\boldsymbol{k})$ and density of states per spin $N(\omega)$ (a more detailed analysis can be found in Ref.[76]). We recall that $A(\boldsymbol{k},\omega)$ is proportional to the imaginary part of the full fermionic Green's function :

$$A(\boldsymbol{k},\omega) \equiv -\frac{1}{\pi}\mathrm{Im}\left[G_{cc}(\boldsymbol{k},\omega)\right] \ , \tag{4.95}$$

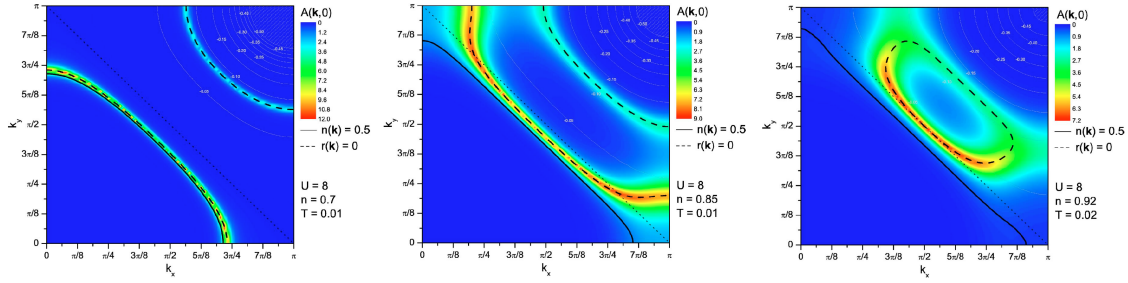

Figure 4.10: Spectral function at the chemical potential $A(\boldsymbol{k}, \omega = 0)$ as a function of the momentum $\boldsymbol{k}$ at $U = 8$ and for different values of filling n and temperature T. Solid lines correspond to the Fermi surface observed for an ordinary Fermi-liquid. Dashed lines are a guide to the eye. Figure reprinted from Ref.[76].

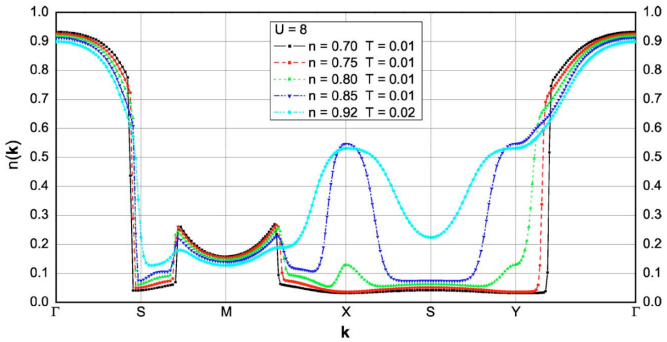

Figure 4.11: Momentum distribution function $n(\boldsymbol{k})$ along the principal directions of the first Brillouin zone ($\Gamma = (0,0)$, $S = (\pi/2, \pi/2)$, $M = (\pi, \pi)$, $X = (\pi, 0)$, $Y = (0, \pi)$) for $U = 8$ and different values of filling n and temperature T. Figure reprinted from Ref.[76].

with $G_{cc}(\boldsymbol{k}, \omega)$ defined in (4.88). Momentum distribution $n(\boldsymbol{k})$ and density of states per spin $N(\omega)$ can be defined in terms of the spectral functions as:

$$n(\boldsymbol{k}) \;=\; \int_{-\infty}^{+\infty} d\omega f_F(\omega) A(\boldsymbol{k}, \omega) \;,\; N(\omega) = \int_{\Omega_B} d^2k A(\boldsymbol{k}, \omega) \;, \tag{4.96}$$

where Ω_B is the volume of the first Brillouin zone and $f_F(\omega)$ is the Fermi-Dirac distribution function. Let us first concentrate our analysis on the Fermi surface which can be obtained by plotting the value of the spectral functions at the Fermi level: $A(\boldsymbol{k}, \omega = 0)$. As shown in Fig.4.83, self-energy corrections enhance non-Fermi-liquid behaviours at high doping ($n \approx 1$) as signaled by the presence of a strong discrepancy between $A(\boldsymbol{k}, \omega = 0)$ in the NCA and the large Fermi surface of a normal metal (solid lines in Fig.4.83) obtained as the locus in which $n(\boldsymbol{k}) = 0.5$. In particular, by increasing the filling there is a change in the topology of the Fermi surface which becomes small and closed at low doping. Finally, in the proximity of half-filling (right panel of Fig.4.83) the Fermi surface becomes ill-defined, meaning that it does not enclose a well-defined region in the momentum space, leading to

the formation of hole-pockets almost centered at $(\pi/2, \pi/2)$ as observed in ARPES experiments [77]. Unconventional (non-Fermi-liquid) behaviours are also observed in momentum distribution function, $n(\boldsymbol{k})$, and density of states $N(\omega)$. As reported in Fig.4.11, the sharp jump at $n(\boldsymbol{k}) = 0.5$, which is a prerogative of the Fermi-liquid theory, rapidly disappears with increasing filling and $n(\boldsymbol{k})$ acquires a finite slope at that level which signals the presence of non-Fermi-liquid excitations.

Summarizing, we have shown that the COM, in the framework of the NCA, is perfectly able to reproduce non-Fermi liquid behaviours in the 2D Hubbard model. Furthermore, different from other models proposed so far, it also provides a full microscopic treatment of self-energy corrections which are responsible for unconventional features in spectral function and momentum distribution function which are in a qualitative agreement with ARPES experiments.

Chapter 5

Beyond the two-field description: a three-pole approach to the single-band Hubbard model

As widely discussed in Chapter 2, the main advantage of the COM in describing strongly correlated systems with respect to other analytical techniques (e.g. canonical Green's function formalism, standard perturbation theory) lays in the choice of a proper basis of composite fields which, differently from the canonical electronic operators, describe stable quasi-particle excitations in the systems rather than bare electrons. Based on the choice of these fields, a proper Green's function formalism has been developed (see Sec. 2.1) which allows to calculate all the relevant two-time fermionic and bosonic correlators as functions of a number of internal parameters which can be determined self-consistently by means of symmetry requirements and algebraic constraints (see Sec. 2.3). As shown in Chapter 4, in the framework of the single band Hubbard model (4.4), a simple two-field basis suffices to catch most of the relevant unconventional features due to strong interactions. In particular, in the case discussed in Chapter 4 we chose as fields of the basis the so-called Hubbard operators $\xi(i)$ and $\eta(i)$ (4.1) which describe quasi-particle excitations separated by the characteristic the energy scale of U, where U parametrizes the the intensity of the on-site Coulomb potential. However, U is not the only energy scale contained in the model. As it is well-known, in the strong coupling regime ($U \gg t$) and in the proximity of half-filling ($n \approx 1$) electrons start to singly occupy all the available sites establishing strong antiferromagnetic correlations which favour nearest-neighbour hopping processes. In this regime the energy scale of U becomes too high to be relevant at low-temperatures and the physics of the Hubbard model is mainly dictated by the exchange interaction $J = 4t^2/U > 0$ which, at low-temperatures, appears as the relevant energy scale driving antiferromagnetic correlations. This finding paves the way for a possible extension of the two-field approach, voted to the inclusion of additional fermionic fields to the well consolidated two-field basis (4.1) with the aim of describing quasi-particle excitations related to the energy scale of J, rather than U. The importance of this point is further bolstered by the clear observation of

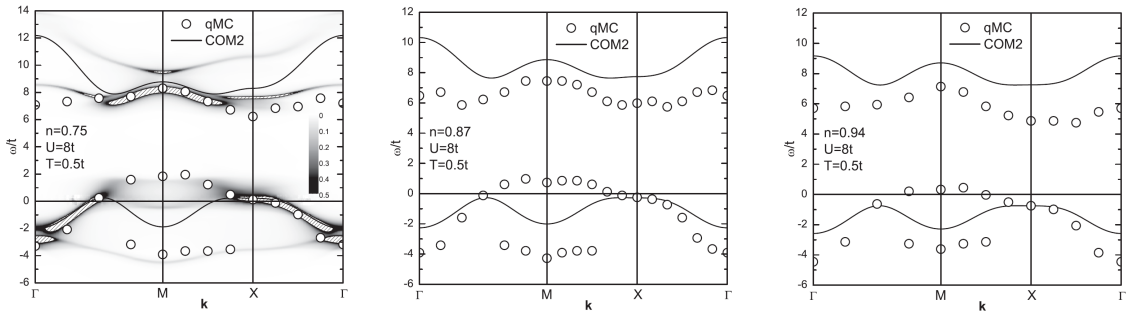

Figure 5.1: Energy dispersion along the principal directions of the first Brillouin zone ($\Gamma = (0,0)$, $M = (\pi,\pi)$, $X = (\pi,0)$) for different values of filling n, at $T/t = 0.5$ and $U/t = 8$. Dashed areas in the left panel correspond to the spectral functions calculated with the non-crossing approximation (see Sec. 4.3). Circles correspond to qMC data from Ref. [78]. Figure reprinted from Ref.[16].

multiple low-energy bands in qMC simulations near half-filling and for high values of U [78]. In this regime, as shown in Fig.5.1, the two-pole approach fails since, as clearly follows from NCA data (see Sec. 4.3) reported in the left panel of Fig.5.1, an operatorial basis constituted by at least three or four composite fields needs to be considered in order to get a significant agreement with numerics.

Based on the aforementioned motivations, we report in the following Sections a detailed analysis of a three-pole approach to the single-band Hubbard model. The self-consistent scheme, containing a detailed discussion on the choice of the fields of the basis, is reported in Section 5.1. We show that the inclusion of a third field to the two-pole basis (4.1) results in additional Pauli constraints, but also in a remarkable increase of the number of unknown parameters to be fixed. Hence, differently from the two-pole approach, due to the unbalanced number of unknown parameters with respect to the number of self-consistent equations, the use of proper and well-consolidated approximated methods becomes of crucial importance not only for the purpose of closing the self-consistent scheme, but especially for obtaining a reliable picture of the physics which is aimed to be described. Based on this last point and with the aim of testing the calculation scheme proposed in Section 5.1, results obtained in the framework of the three-pole approximation are discussed in Section 5.2 in comparison with quantum Monte Carlo (qMC), Dynamical Cluster Approximation (DCA) and Lanczos data. We report a detailed analysis on band structure, filling and U dependencies of chemical potential and double occupancy, showing a better agreement with numerical data with respect to the two-pole solution described in Chapter 4.

5.1 Self-consistent scheme

In considering the possibility to formulate a three-pole or a four-pole approach to the single-band Hubbard model, a first issue arises from the choice of the basis. As discussed in the previous Chapters, the accuracy of the COM in describing correlated systems strongly relies on this choice and therefore one needs to carefully assess a

proper way to extend the operatorial basis in order to include the particular scales of energy which are aimed to be described. To this purpose, one can in principle consider the possibility to extend the two pole basis (4.1) by adding one by one all the higher order fields which appear in the equations of motion of the Hubbard operators $\xi(i)$ and $\eta(i)$. This procedure is at the basis of the exact solutions found for a large class of exactly solvable systems (see Chapter 3), furthermore it has also the main advantage of preserving the spectral moments [69]. Then, on the basis of the aforementioned considerations, recalling the equations of motion of the Hubbard operators (see Appendix B.3):

$$i\partial_t \xi(i) = -\mu\xi(i) - 2dt\left[c^{\alpha}(i) + \pi(i)\right] , \tag{5.1}$$

$$i\partial_t \eta(i) = (U-\mu)\,\eta(i) + 2dt\pi(i) , \tag{5.2}$$

the most natural choice for the third field of the basis falls on $\pi(i)$, which is defined in spinorial notation as:

$$\pi(i) = \frac{1}{2}\sigma^{\mu} n_{\mu}(i) c^{\alpha}(i) + c(i)c^{\alpha\dagger}(i)c(i) . \tag{5.3}$$

or, alternatively, as the sum of its charge $\pi_c(i)$, spin $\pi_s(i)$ and pairs $\pi_p(i)$ components as:

$$\pi(i) \equiv \pi_c(i) + \pi_s(i) + \pi_p(i) , \begin{cases} \pi_c(i) = -\frac{1}{2} n(i) c^{\alpha}(i) \\ \pi_s(i) = \frac{1}{2}\sigma_k n_k(i) c^{\alpha}(i) \\ \pi_p(i) = c(i)c^{\alpha\dagger}(i)c(i) \end{cases} , \; 1 \leqslant k \leqslant 3 . \tag{5.4}$$

Thus a possible three-pole basis coming from the hierarchy of the equations of motion is the following:

$$\psi(i) = \begin{pmatrix} \xi(i) \\ \eta(i) \\ \pi(i) \end{pmatrix} . \tag{5.5}$$

It is worth noting that the inclusion of $\pi(i)$ does not close the equations of motion of $\psi(i)$. In fact, simple but lengthy calculations give:

$$i\partial_t \pi(i) = -\mu\pi(i) + 2dt\left[\rho(i) - \theta(i)\right] + U\eta_s(i) , \tag{5.6}$$

where $\rho(i)$, $\theta(i)$ and $\eta_s(i)$ are higher order fields defined as:

$$\eta_s(i) = \frac{1}{2}\sigma^{\mu} n_{\mu}(i)\eta^{\alpha}(i) + c(i)\xi^{\alpha\dagger}(i)c(i) , \tag{5.7}$$

$$\rho(i) = \frac{1}{2}\sigma^{\mu}\left[c^{\alpha\dagger}(i)\sigma_{\mu}c(i) - c^{\dagger}(i)\sigma_{\mu}c^{\alpha}(i)\right] c^{\alpha}(i) , \tag{5.8}$$

$$\theta(i) = c^{\alpha}(i)c^{\alpha\dagger}(i)c(i) + c(i)c^{\alpha\dagger}(i)c^{\alpha}(i) - c(i)c^{\alpha^2\dagger}(i)c(i) + \frac{1}{2}\sigma^{\mu} n_{\mu}(i) c^{\alpha^2}(i) , \tag{5.9}$$

whose contribution, as reported in Chapter 2, has to be accounted in the calculation of the $m(\boldsymbol{k})$ matrix (2.25). At this point, due to the complicated analytical expressions of the fields (5.7)-(5.9), with the aim of reducing analytical efforts it is useful

to consider as a first approximations the following restriction to three-pole basis:

$$\psi(i) = \begin{pmatrix} \xi(i) \\ \eta(i) \\ c_s(i) \end{pmatrix} , \tag{5.10}$$

in which, with respect to Eq.5.5, the field $\pi(i)$ has been substituted by $c_s(i)$, where:

$$c_s(i) = \sigma_k n_k(i) c^{\alpha}(i) . \tag{5.11}$$

The physical meaning of this approximation immediately follows by a simple comparison with Eq.5.3, from which it is immediate to note that the field $c_s(i)$ is nothing but the spin component of the starting filed $\pi(i)$ which is supposed to provide the leading contribution in the description of the dynamical energy scales which arise in the high-filling and low-temperature regime. The equation of motion for the third field can be written as:

$$i\partial_t c_s(i) = -\mu c_s(i) + 4t\left(\kappa_s(i) - \rho_s(i)\right) + U\eta_s(i) , \tag{5.12}$$

where now the higher order fields $\bar{\eta}_s(i)$, $\kappa_s(i)$ and $\rho_s(i)$ read as:

$$\bar{\eta}_s(i) = \sigma_k n_k(i)\eta^{\alpha}(i) , \tag{5.13}$$

$$\kappa_s(i) = \sigma_k c^{\alpha\dagger}(i)\sigma_k c(i) c^{\alpha}(i) - \sigma_k c^{\dagger}(i)\sigma_k c^{\alpha}(i) c^{\alpha}(i) , \tag{5.14}$$

$$\rho_s(i) = \sigma_k n_k(i) c^{\alpha^2}(i) . \tag{5.15}$$

In the polar approximation (see Sec.2.2) we linearize the equations of motion as:

$$i\partial_t \psi_m(\boldsymbol{i}, t) = \sum_{\boldsymbol{j}} \sum_{l=1}^{3} \epsilon_{ml}(\boldsymbol{i}, \boldsymbol{j}) \psi_l(\boldsymbol{j}, t) , \tag{5.16}$$

where, according to Eq.2.23, the energy matrix $\epsilon(\boldsymbol{i}, \boldsymbol{j})$ can be calculated in terms of $I(\boldsymbol{i}, \boldsymbol{j})$ and $m(\boldsymbol{i}, \boldsymbol{j})$ matrices (defined in Eq.2.24 and Eq.2.25, respectively). In particular, for the chosen three-field basis (5.10) we obtain:

$$I(\boldsymbol{k}) = \begin{pmatrix} I_{11}(\boldsymbol{k}) & 0 & I_{13}(\boldsymbol{k}) \\ 0 & I_{22}(\boldsymbol{k}) & I_{23}(\boldsymbol{k}) \\ I_{13}(\boldsymbol{k}) & I_{23}(\boldsymbol{k}) & I_{33}(\boldsymbol{k}) \end{pmatrix} , m(\boldsymbol{k}) = \begin{pmatrix} m_{11}(\boldsymbol{k}) & m_{12}(\boldsymbol{k}) & m_{13}(\boldsymbol{k}) \\ m_{12}(\boldsymbol{k}) & m_{22}(\boldsymbol{k}) & m_{23}(\boldsymbol{k}) \\ m_{13}(\boldsymbol{k}) & m_{23}(\boldsymbol{k}) & m_{33}(\boldsymbol{k}) \end{pmatrix} . \tag{5.17}$$

where, for a paramagnetic and homogeneous system, the elements of the first two lines and columns can be written in terms of the three self-consistent parameters μ, p and Δ as:

$$I_{11}(\boldsymbol{k}) \equiv I_{11} = 1 - \frac{n}{2} \quad , \quad I_{22}(\boldsymbol{k}) \equiv I_{22} = \frac{n}{2} , \tag{5.18}$$

$$m_{11}(\boldsymbol{k}) = -\mu I_{11} - 4t\left[\Delta + (p + 1 - n)\,\alpha(\boldsymbol{k})\right] , \tag{5.19}$$

$$m_{12}(\boldsymbol{k}) = 4t\left[\Delta + (p - I_{22})\,\alpha(\boldsymbol{k})\right] , \tag{5.20}$$

$$m_{22}(\boldsymbol{k}) = (U - \mu)\, I_{22} - 4t\left[\Delta + p\alpha(\boldsymbol{k})\right] , \tag{5.21}$$

where t is the hopping integral, μ is the chemical potential, n is the particle density and $\alpha(\boldsymbol{k})$ is the Fourier transform of the nearest-neighbour projector (B.7). Taking all the terms up to the first order in $\alpha(\boldsymbol{k})$, the elements of the remaining rows and columns can be expressed as:

$$I_{13}(\boldsymbol{k}) = 3C^{\alpha}_{\xi c} + \frac{3}{2}\chi^{\alpha}_{s}\alpha(\boldsymbol{k}) \ , \tag{5.22}$$

$$I_{23}(\boldsymbol{k}) = 3C^{\alpha}_{\eta c} - \frac{3}{2}\chi^{\alpha}_{s}\alpha(\boldsymbol{k}) \ , \tag{5.23}$$

$$I_{33}(\boldsymbol{k}) = I^{(0)}_{33} + \alpha(\boldsymbol{k})I^{(\alpha)}_{33} \ , \ \begin{cases} I^{(0)}_{33} = & 4C^{\alpha}_{cc_s} + \frac{3}{2}C^{\delta}_{\eta\eta} \\ I^{(\alpha)}_{33} = & -3\left(2f_s - \frac{1}{4}C^{\alpha}_{cc}\right) \end{cases} \ , \tag{5.24}$$

according with the notation $C^{(\kappa)}_{\Phi_1\Phi_2} \equiv \left\langle \Phi^{\kappa}_1(i)\Phi^{\dagger}_2(i) \right\rangle$, being $\kappa \in \{\delta, \alpha, \beta, \eta, \lambda, \mu\}$ a generic projector (see Appendix B.1.1), where χ^{α}_s is the nearest-neighbour spin-spin correlation function:

$$\chi^{\alpha}_{s} \equiv \frac{1}{3}\left\langle n_k(i)n^{\alpha}_k(i) \right\rangle \ , \tag{5.25}$$

and f_s is the following three-site correlator:

$$f_s \equiv \frac{1}{3}\left\langle \sigma_k n^{\alpha}_k(i)c(i)c^{\alpha\dagger}(i) \right\rangle \ . \tag{5.26}$$

From the knowledge of the elements of the normalization matrix, a straightforward calculation of the $m(\boldsymbol{i},\boldsymbol{j})$-matrix gives:

$$\begin{aligned} m_{13}(\boldsymbol{i},\boldsymbol{j}) &= \left\langle \left\{ i\partial_t c_s(\boldsymbol{i}), \xi^{\dagger}(\boldsymbol{j}) \right\} \right\rangle = \left\langle \left\{ i\partial_t \xi(\boldsymbol{i}), c^{\dagger}_s(\boldsymbol{j}) \right\} \right\rangle = \\ &= \left\langle \left\{ -\mu\xi(\boldsymbol{i}) - 2dt\left(c^{\alpha}(\boldsymbol{i}) + \pi(\boldsymbol{i})\right), c^{\dagger}_s(\boldsymbol{j}) \right\} \right\rangle = \\ &= \left\langle \left\{ -\mu\xi(\boldsymbol{i}) - 2dt\left(c^{\alpha}(\boldsymbol{i}) + \bar{\pi}(\boldsymbol{i}) + \frac{1}{2}c_s(\boldsymbol{i})\right), c^{\dagger}_s(\boldsymbol{j}) \right\} \right\rangle = \\ &= -\left(\mu + 2dt\alpha_{\boldsymbol{ij}}\right) I_{13}(\boldsymbol{i},\boldsymbol{j}) - 2dt\alpha_{\boldsymbol{ij}} I_{23}(\boldsymbol{i},\boldsymbol{j}) - dtI_{33}(\boldsymbol{i},\boldsymbol{j}) \\ &\quad -2dtI_{\bar{\pi},c_s}(\boldsymbol{i},\boldsymbol{j}) \ , \end{aligned} \tag{5.27}$$

$$\begin{aligned} m_{23}(\boldsymbol{i},\boldsymbol{j}) &= \left\langle \left\{ i\partial_t c_s(\boldsymbol{i}), \eta^{\dagger}(\boldsymbol{j}) \right\} \right\rangle = \left\langle \left\{ i\partial_t \eta(\boldsymbol{i}), c^{\dagger}_s(\boldsymbol{j}) \right\} \right\rangle = \\ &= \left\langle \left\{ \left(U-\mu\right)\eta(\boldsymbol{i}) + 2dt\pi(\boldsymbol{i}), c^{\dagger}_s(\boldsymbol{j}) \right\} \right\rangle = \\ &= \left\langle \left\{ \left(U-\mu\right)\eta(\boldsymbol{i}) + 2dt\left(\bar{\pi}(\boldsymbol{i}) + \frac{1}{2}c_s(\boldsymbol{i})\right), c^{\dagger}_s(\boldsymbol{j}) \right\} \right\rangle = \\ &= \left(U-\mu\right) I_{23} + dtI_{33}(\boldsymbol{i},\boldsymbol{j}) + 2dtI_{\bar{\pi},c_s}(\boldsymbol{i},\boldsymbol{j}) \ , \end{aligned} \tag{5.28}$$

$$\begin{aligned} m_{33}(\boldsymbol{i},\boldsymbol{j}) &= -\mu I_{33}(\boldsymbol{i},\boldsymbol{j}) + 2dtI_{\kappa_s\rho_s,c^{\dagger}_s}(\boldsymbol{i},\boldsymbol{j}) + UI_{\bar{\eta}_s,c^{\dagger}_s}(\boldsymbol{i},\boldsymbol{j}) = \\ &= -\mu I_{33}(\boldsymbol{i},\boldsymbol{j}) + 2dtI_{\kappa_s\rho_s,c^{\dagger}_s}(\boldsymbol{i},\boldsymbol{j}) + U\left(I_{33}(\boldsymbol{i},\boldsymbol{j}) - I_{\bar{\xi}_s,c^{\dagger}_s}(\boldsymbol{i},\boldsymbol{j})\right) = \\ &= \left(U-\mu\right) I_{33}(\boldsymbol{i},\boldsymbol{j}) + \left(2dtI_{\kappa_s\rho_s,c^{\dagger}_s}(\boldsymbol{i},\boldsymbol{j}) - UI_{\bar{\xi}_s,c^{\dagger}_s}(\boldsymbol{i},\boldsymbol{j})\right) \ , \end{aligned} \tag{5.29}$$

where $I_{\bar{\pi},c_s}(\boldsymbol{i},\boldsymbol{j})$, $I_{\bar{\xi}_s c^{\dagger}_s}(\boldsymbol{i},\boldsymbol{j})$ and $I_{\kappa_s\rho_s,c^{\dagger}_s}(\boldsymbol{i},\boldsymbol{j})$ are defined in terms of the higher order fields (5.13)-(5.15) that appear in the equation of motion of $c_s(i)$ which, consistently with the choice of truncating all the terms up to the first order in $\alpha(\boldsymbol{k})$, can be

written as the sum of their local (0) and nearest-neighbour (α) components as:

$$I_{\bar{\pi},c_s}(\boldsymbol{i},\boldsymbol{j}) = \left\langle \left\{ \pi(\boldsymbol{i}) - \frac{1}{2} c_s(\boldsymbol{i}), c_s^\dagger(\boldsymbol{j}) \right\} \right\rangle \equiv \delta_{\boldsymbol{ij}} I^{(0)}_{\bar{\pi},c_s} + \alpha_{\boldsymbol{ij}} I^{(\alpha)}_{\bar{\pi},c_s} \,, \tag{5.30}$$

$$I_{\bar{\xi}_s,c_s^\dagger}(\boldsymbol{i},\boldsymbol{j}) = \left\langle \left\{ c_s(\boldsymbol{i}) - \bar{\eta}_s(\boldsymbol{i}), c_s^\dagger(\boldsymbol{j}) \right\} \right\rangle \equiv \delta_{\boldsymbol{ij}} I^{(0)}_{\bar{\xi}_s,c_s^\dagger} + \alpha_{\boldsymbol{ij}} I^{(\alpha)}_{\bar{\xi}_s,c_s^\dagger} \,, \tag{5.31}$$

$$I_{\kappa_s\rho_s,c_s^\dagger}(\boldsymbol{i},\boldsymbol{j}) = \left\langle \left\{ \kappa_s(\boldsymbol{i}) - \rho_s(\boldsymbol{i}), c_s^\dagger(\boldsymbol{j}) \right\} \right\rangle \equiv \delta_{\boldsymbol{ij}} I^{(0)}_{\kappa_s\rho_s,c_s^\dagger} + \alpha_{\boldsymbol{ij}} I^{(\alpha)}_{\kappa_s\rho_s,c_s^\dagger} \,. \tag{5.32}$$

With the exception of $I^{(0)}_{\bar{\pi},c_s}$ for which analytical calculations immediately give:

$$I^{(0)}_{\bar{\pi},c_s} = 0 \,, \tag{5.33}$$

the calculation of the remaining quantities can be meaningless as well as cumbersome since, due to the very complicated operatorial expressions of the fields involved, it will introduce additional unknown parameters which, in turn, need to be fixed by means of auxiliary approximated methods. At this point it is worth emphasizing that, although it is always possible to use approximate methods to estimate unknown correlators (we report in Appendix C approximated expressions for f_s obtained within two different techniques , namely the decoupling and the projection), a large use of these approaches might induce uncontrolled approximations whose effects on the self-consistent scheme, then on the final results, could be hard to estimate by a posteriori analysis. In this context, Pauli constraints offer the only reliable way to fix unknown correlators as they allow the system to adjust its internal parameters in order to satisfy algebraic relations or symmetry requirements which are valid for any coupling and any value of the external parameters.

It goes without saying that, on the basis of the aforementioned considerations, any extension to the number of possible self-consistent equations will provide an invaluable contribution to the build of a proper self-consistent scheme. To this purpose, by exploiting all the possible algebraic constraints and contraction rules among the fields of the basis, we note the following operatorial relations:

$$c(i)c_s^\dagger(i) = 3\xi(i)c^\dagger(i) \,, \tag{5.34}$$

$$\eta(i)c_s^\dagger(i) = 0 \,, \tag{5.35}$$

whose averages give:

$$C^\delta_{\xi c_s} \equiv \left\langle \xi(i)c_s^\dagger(i) \right\rangle = 3\left\langle \xi^\alpha(i)c^\dagger(i) \right\rangle = 3C^\alpha_{\xi c} \,, \tag{5.36}$$

$$C^\delta_{\eta c_s} \equiv \left\langle \eta(i)c_s^\dagger(i) \right\rangle = 0 \,. \tag{5.37}$$

Hence, including the above relation to the ones already discussed in the framework of the two-pole approach (4.27), (4.28), (4.30), we come up with the following set of five self-consistent equations:

$$n = 2\left(1 - C_{\xi\xi} - C^\delta_{\eta\eta}\right) \,, \tag{5.38}$$

$$\Delta = C^\alpha_{\xi\xi} - C^\alpha_{\eta\eta} \,, \tag{5.39}$$

$$C^\delta_{\xi\eta} = 0 \,, \tag{5.40}$$

$$C^{\delta}_{\xi c_s} = 3C^{\alpha}_{\xi c} \,, \tag{5.41}$$

$$C^{\delta}_{\eta c_s} = 0 \,. \tag{5.42}$$

and ten (μ, p, Δ, f_s, χ^{α}_s, $I^{(\alpha)}_{\bar{\pi},c_s}$, $I^{(0)}_{\bar{\xi}_s,c^{\dagger}_s}$, $I^{(\alpha)}_{\bar{\xi}_s,c^{\dagger}_s}$, $I^{(0)}_{\kappa_s\rho_s,c^{\dagger}_s}$, $I^{(\alpha)}_{\kappa_s\rho_s,c^{\dagger}_s}$) unknown parameters to be fixed. However we note that both $I_{\bar{\xi}_s,c^{\dagger}_s}(\boldsymbol{i},\boldsymbol{j})$ and $I_{\kappa_s\rho_s,c^{\dagger}_s}(\boldsymbol{i},\boldsymbol{j})$ only appear in the expression of $m_{33}(\boldsymbol{i},\boldsymbol{j})$ and therefore, in order to minimize the number of unknown correlators, it is convenient to parametrize $m_{33}(\boldsymbol{i},\boldsymbol{j})$ as:

$$m_{33}(\boldsymbol{i},\boldsymbol{j}) = (U-\mu)\, I_{33}(\boldsymbol{i},\boldsymbol{j}) + \bar{m}^{(0)}_{33}\delta_{\boldsymbol{ij}} + \bar{m}^{(\alpha)}_{33}\alpha_{\boldsymbol{ij}} \,, \tag{5.43}$$

which allows us to reduce from four to two the number of unknowns correlators in $m_{33}(\boldsymbol{i},\boldsymbol{j})$, where now $\bar{m}^{(0)}_{33}$ and $\bar{m}^{(\alpha)}_{33}$ accounts, respectively, for the complementary local and $\alpha_{\boldsymbol{ij}}$ contributions of $m_{33}(\boldsymbol{i},\boldsymbol{j})$ with respect to $I_{33}(\boldsymbol{i},\boldsymbol{j})$. Furthermore, we also recall that the p, the self-consistent parameter appearing in the two-pole self-consistent scheme, can be written as the sum of nearest-neighbour charge-charge χ^{α}_0, spin-spin χ^{α}_s and pair-pair χ^{α}_p correlation functions as:

$$p = \frac{1}{4}\left(\chi^{\alpha}_0 + 3\chi^{\alpha}_s\right) - \chi^{\alpha}_p \,, \tag{5.44}$$

where:

$$\chi^{\alpha}_p \equiv \left\langle \left[c_{\uparrow}(i)c_{\downarrow}(i)\right]^{\alpha} c^{\dagger}_{\downarrow}(i)c^{\dagger}_{\uparrow}(i)\right\rangle \,. \tag{5.45}$$

Then, unlikely in the two-pole approximation, because of the presence of χ^{α}_s in both $I(\boldsymbol{i},\boldsymbol{j})$ and $m(\boldsymbol{i},\boldsymbol{j})$ matrices, it is convenient to use Eq.5.44 in order to schematize all the unknown quantities as a set of six fermionic parameters: μ, Δ, f_s, $I^{(\alpha)}_{\bar{\pi},c_s}$, $\bar{m}^{(0)}_{33}$, $\bar{m}^{(\alpha)}_{33}$, and three bosonic correlation functions: χ^{α}_0, χ^{α}_s, χ^{α}_p. At this point we recall that, as already discussed in Chapter 4 for the case of a two-pole approach to the single band Hubbard model, a number of well-consolidated techniques are available for the calculation of charge-charge, χ^{α}_0, spin-spin, χ^{α}_s, and pair-pair, χ^{α}_p, correlation functions (for example they can be estimated by opening the bosonic sector, see Section 2.2.2, or by means of the one-loop approximation, see Appendix B.4). Therefore, without opening the bosonic sector, we can safely fix χ^{α}_0, χ^{α}_s and χ^{α}_p with the corresponding values obtained in the framework of the one-loop approximation and then use the Pauli constraints to determine the remaining fermionic correlators. In particular, we note that μ, Δ, $I^{(\alpha)}_{\bar{\pi},c_s}$, $\bar{m}^{(0)}_{33}$, $\bar{m}^{(\alpha)}_{33}$ must necessarily be fixed self-consistently since, the first two, are intimately related to Eq.5.38 and Eq.5.39, respectively, while the remaining ones are completely unknown in their analytical form. Then, starting from the initial set of ten unknown parameters and given the overall decision to fix χ^{α}_0, χ^{α}_s and χ^{α}_p consistently with the one-loop approximation, we are left with only f_s to be determined in order to close the self-consistent scheme. In particular, hereafter we use the projection method described in Appendix C to fix f_s which gives :

$$f_s \;\approx\; \frac{1}{2d}C^{\alpha}_{c\xi} + \frac{2d-1}{2d}\left[\frac{1}{2}\chi^{\alpha}_s\left(\frac{C^{\alpha}_{c\xi}}{I_{11}} - \frac{C^{\alpha}_{c\eta}}{I_{22}}\right)\right]$$

Correlator	Approximated expression
f_s	$\frac{1}{2d}C^{\alpha}_{c\xi} + \frac{2d-1}{2d}\left[\frac{1}{2}\chi^{\alpha}_{s}\left(\frac{C^{\alpha}_{c\xi}}{I_{11}} - \frac{C^{\alpha}_{c\eta}}{I_{22}}\right)\right]$ $+\frac{C^{\alpha}_{c\xi}}{I_{11}}\left(C^{\alpha^2}_{c\xi} - \frac{1}{2d}C^{\delta}_{c\xi}\right) + \frac{C^{\alpha}_{c\eta}}{I_{22}}\left(C^{\alpha^2}_{c\eta} - \frac{1}{2d}C^{\delta}_{c\eta}\right)$
χ^{α}_{0}	$n^2 - 2I_{11}\left(C^{\alpha}_{c\eta}\right)^2 / C^{\delta}_{\eta\eta} - 2I_{22}\left(C^{\alpha}_{c\xi}\right)^2 / C^{\delta}_{\eta\eta}$
χ^{κ}_{s}	$-2I_{11}\left(C^{\kappa}_{c\eta}\right)^2 / \left(2I_{11}I_{22} - C^{\delta}_{\eta\eta}\right) - 2I_{22}\left(C^{\kappa}_{c\xi}\right)^2 / \left(2I_{11}I_{22} - C^{\delta}_{\eta\eta}\right)$
χ^{α}_{p}	$C^{\alpha}_{c\xi}C^{\alpha}_{\eta c}/C^{\delta}_{\eta\eta}$

Table 5.1: Approximated expressions for all the internal parameters of the three-pole calculation scheme for the single-band Hubbard model. Here f_s is calculated by means of the projection method described in Appendix C, χ^{α}_{0}, χ^{α}_{s} and χ^{α}_{p} are fixed in the framework of the one-loop approximation.

$$+\frac{C^{\alpha}_{c\xi}}{I_{11}}\left(C^{\alpha^2}_{c\xi} - \frac{1}{2d}C^{\delta}_{c\xi}\right) + \frac{C^{\alpha}_{c\eta}}{I_{22}}\left(C^{\alpha^2}_{c\eta} - \frac{1}{2d}C^{\delta}_{c\eta}\right) \ . \tag{5.46}$$

Then, summarizing, in the framework of the self-consistent scheme developed in this Section, $I(\boldsymbol{k})$ and $m(\boldsymbol{k})$ read as:

$$I(\boldsymbol{k}) = \begin{pmatrix} I_{11}(\boldsymbol{k}) & 0 & I_{13}(\boldsymbol{k}) \\ 0 & I_{22}(\boldsymbol{k}) & I_{23}(\boldsymbol{k}) \\ I_{13}(\boldsymbol{k}) & I_{23}(\boldsymbol{k}) & I_{33}(\boldsymbol{k}) \end{pmatrix} , m(\boldsymbol{k}) = \begin{pmatrix} m_{11}(\boldsymbol{k}) & m_{12}(\boldsymbol{k}) & m_{13}(\boldsymbol{k}) \\ m_{12}(\boldsymbol{k}) & m_{22}(\boldsymbol{k}) & m_{23}(\boldsymbol{k}) \\ m_{13}(\boldsymbol{k}) & m_{23}(\boldsymbol{k}) & m_{33}(\boldsymbol{k}) \end{pmatrix} . \tag{5.47}$$

with:

$$\begin{cases} I_{11}(\boldsymbol{k}) = 1 - \frac{n}{2} \ , \\ I_{22}(\boldsymbol{k}) = \frac{n}{2} \\ I_{13}(\boldsymbol{k}) = 3C^{\alpha}_{\xi c} + \frac{3}{2}\chi^{\alpha}_{s}\alpha(\boldsymbol{k}) \ , \\ I_{23}(\boldsymbol{k}) = 3C^{\alpha}_{\eta c} - \frac{3}{2}\chi^{\alpha}_{s}\alpha(\boldsymbol{k}) \ , \\ I_{33}(\boldsymbol{k}) = 4C^{\alpha}_{cc_s} + \frac{3}{2}C_{\eta\eta} - 3\alpha(\boldsymbol{k})\left(2f_s - \frac{1}{4}C^{\alpha}_{cc}\right) \ , \end{cases} \tag{5.48}$$

and:

$$\begin{cases} m_{11}(\boldsymbol{k}) = -\mu I_{11}(\boldsymbol{k}) - 4t\left[\Delta + \left(\frac{1}{4}\left(\chi^{\alpha}_{0} + 3\chi^{\alpha}_{s}\right) - \chi^{\alpha}_{p} + 1 - n\right)\alpha(\boldsymbol{k})\right] \ , \\ m_{12}(\boldsymbol{k}) = 4t\left[\Delta + \left(\frac{1}{4}\left(\chi^{\alpha}_{0} + 3\chi^{\alpha}_{s}\right) - \chi^{\alpha}_{p} - I_{22}(\boldsymbol{k})\right)\alpha(\boldsymbol{k})\right] \ , \\ m_{22}(\boldsymbol{k}) = \left(U - \mu\right) I_{22}(\boldsymbol{k}) - 4t\left[\Delta + \frac{1}{4}\left(\chi^{\alpha}_{0} + 3\chi^{\alpha}_{s}\right) - \chi^{\alpha}_{p}\alpha(\boldsymbol{k})\right] \ , \\ m_{13}(\boldsymbol{k}) = -\left(\mu + 2dt\alpha(\boldsymbol{k})\right) I_{13}(\boldsymbol{k}) - 2dt\alpha(\boldsymbol{k})I_{23}(\boldsymbol{k}) - dtI_{33}(\boldsymbol{k}) - 2dtI_{\bar{\pi}(i),c_s}(\boldsymbol{k}) \ , \\ m_{23}(\boldsymbol{k}) = \left(U - \mu\right) I_{23}(\boldsymbol{k}) + dtI_{33}(\boldsymbol{k}) + 2dtI_{\bar{\pi}(i),c_s}(\boldsymbol{k}) \ , \\ m_{33}(\boldsymbol{k}) = \left(U - \mu\right) I_{33}(\boldsymbol{k}) + \bar{m}^{(0)}_{33} + \bar{m}^{(\alpha)}_{33}\alpha(\boldsymbol{k}) \ . \end{cases} \tag{5.49}$$

In the above relations χ^{α}_{0}, χ^{α}_{s} and χ^{α}_{p} are calculated in the framework of the one-loop approximation, μ, Δ, $I^{(\alpha)}_{\bar{\pi},c_s}$, $\bar{m}^{(0)}_{33}$, $\bar{m}^{(\alpha)}_{33}$ are fixed via Pauli constraints (5.38)-(5.42) while f_s is fixed by means of the projection method (see Appendix C). Analytical expressions of all the parameters involved in the self-consistent scheme are reported in Tab.5.1.

With the aim of testing the accuracy of the three-pole solution proposed for

the single-band Hubbard model, we report in the next Section our study on energy dispersion, filling and U dependencies of chemical potential and double occupancy obtained in the framework of the self-consistent scheme developed above. We compare our results with qMC, DCA and Lanczos data, showing an excellent agreement in a wide range of filling and strength of the on site potential, which definitely allows to consider the three-pole solution as a step forward with respect to the the two-pole approximation.

5.2 Results and comparisons: double occupancy, chemical potential and energy dispersion

Filling, temperature and U dependencies of chemical potential and double occupancy represent a severe testing ground for many theories aiming the description of strongly correlated systems. It is well known in fact that how the aforementioned quantities depend on the internal parameters of a given model is intimately related to the nature and the strength of the interactions taken into account, and therefore to the competition between different orderings or instabilities in the system. In this regards, one of the most relevant achievements of the two-pole theory consists in a quantitative fit of quantum Monte Carlo (qMC) and Dynamical Cluster Approximation (DCA) data for the $D(n)$ and the $\mu(n)$ dependencies, in the whole range of filling $0 \leqslant n \leqslant 1$, at low values of the on-site Coulomb potential (e.g. $U = 1$ and $U = 2$)[16]. However with increasing ratio U/t (e.g. for $U/t = 4$), as clearly follows from Fig.5.2, although the two-pole solution maintains a good agreement with numerics for $\mu(n)$ and $D(n)$ at low fillings, with increasing filling a quantitative description of $D(n)$ and $\mu(n)$ dependencies can only be found in terms of a crossover between the two possible two-pole solutions, $p < 0$ and $p > 0$, which has been argued to take place in the range of n in which antiferromagnetic correlations dominates with respect to the paramagnetic behaviour (see discussion in Section 4.1).

We immediately note that this issue is completely overcome in the three-pole approximation which, as follows from Fig.5.3, dynamically reproduces the crossover from negative to positive values of p going from $n = 0$ to $n = 1$. In particular, by comparing the values of charge, spin and pair fluctuations (Fig.5.4) it is also immediate to note that the crossover region is localized in the regime in which spin fluctuations become dominant with respect to charge and pair ones for $U/t \gg 1$, consistently with what has been argued in the two-pole approach. Last but not least, unlike the two-pole solutions, the value of p calculated in the framework of the three-pole approach remains confined to physical values in the whole range of filling.

A further check of the three-pole solution has been done by comparing the $D(U)$ dependence with qMC and Lanczos data. As follows from the left panel of Fig.5.5, results obtained in the three-pole approximation are qualitatively and quantitatively in agreement with numerics, reproducing the correct trend of the double occupancy in a large range of U/t . In particular, as follows from the right panel of Fig.5.5, by increasing the ratio U/t we also notice a strong suppression of all charge and pair

fluctuations. On the contrary, strong antiferromagnetic fluctuations persist in the $U/t \gg 1$ limit and further bolster the choice of the $c_s(i)$ as the leading contribution of the original third field $\pi(i)$ in the strong coupling regime.

Let us now analyze the band structure resulting from the energy distribution of single-particle excitations in $\boldsymbol{k}$-space. As one would expect from a polar approximation, in the framework of a three-pole approach we have three bands, each of them related to one of the composite fields of the chosen basis (5.10). In particular, as immediately follows from Fig.5.6 and Fig.5.7, the contributions coming from $\xi(i)$ and $\eta(i)$ are shifted by U with respect to each other, while the one related to the third field $c_s(i)$, not sensitive to U, remains centered at the value of the chemical potential. By simple comparison with the two-pole results, Fig.5.1, it is immediate to note that the presence of the third band at $\omega = \mu$ has a crucial effect on the dispersions of $\xi(i)$ and $\eta(i)$ which, unlike in the two-pole approximations (Fig.5.1), are both characterized by a maximum in the $M = (\pi, \pi)$ point and a minimum in $\Gamma = (0, 0)$ point. This last feature, which indeed improves the agreement with qMC data with respect to the two-pole approach, allows for a qualitatively description of numerical results in terms of a superposition of three quasi-particle dispersions, rather than in terms of a single band only, characterized by an evident transfer of weight among the three bands as signaled by the strong $\boldsymbol{k}$ and ω dependencies of the intensity $\mathcal{I}(\boldsymbol{k}, \omega)$, calculated in terms of energy dispersions $E_n(\boldsymbol{k})$ and corresponding spectral density matrices $\sigma^{(n)}_{ab}(\boldsymbol{k})$ as:

$$\mathcal{I}(\boldsymbol{k}, \omega) = \sum_{n=1}^{3} L(\omega, E_n(\boldsymbol{k}), \Gamma) \left(\sigma^{(n)}_{11}(\boldsymbol{k}) + 2\sigma^{(n)}_{12}(\boldsymbol{k}) + \sigma^{(n)}_{22}(\boldsymbol{k}) \right) , \tag{5.50}$$

being $L(\omega, \omega_0, \Gamma)$ the Lorentzian distribution function with center at $\omega = \omega_0$ and dispersion Γ:

$$L(\omega, \omega_0, \Gamma) = \frac{1}{\pi} \frac{\Gamma/2}{(\omega - \omega_0)^2 + (\Gamma/2)^2} . \tag{5.51}$$

To better emphasize this point, we report separately in Fig.5.7 for the case $T/t = 0.5$, $U/t = 8$ and $n = 0.94$ illustrated in Fig.5.6, the energy dispersions and the corresponding spectral density matrices where, for the only sake of clarity, we have labeled with $E(c_s)$, $E(\xi)$, $E(\eta)$ the central, the lower and the upper band, respectively, and with $\sigma(c_s)$, $\sigma(\xi)$, $\sigma(\eta)$ the corresponding weights. By analyzing the momentum dependence of all the quantities we note that while the weight of the central band, given by $\sigma(c_s)$, remains always far from zero, the spectral density of the upper band, $\sigma(\eta)$, is strongly suppressed near (π, π), in advantage of the ones related to the lower, $\sigma(\xi)$, and the central, $\sigma(c_s)$, bands, whose intensities increase in the region of the $\boldsymbol{k}$-space where the corresponding energy dispersions approach the maxima of the upper and the central qMC bands, respectively, at (π, π).

Then, by looking at all the results described so far, we can conclude that the three-pole solution undoubtedly represents a step forward with respect to the two-pole approach, providing a noticeable agreement in filling and U dependencies of chemical potential and double occupancy (Fig.5.2) with respect to different numerical methods. Some discrepancies still persist in the momentum-dependent quantities

(e.g. energy dispersions) especially in the region near (π, π) where the role played by antiferromagnetic correlations is expected to be relevant (Fig.5.6). These correlations, given the overall assumption of a uniform and paramagnetic phase, can be only partially accounted in the framework of the three-pole approach described so far (see Fig.5.4), leading to the possibility to qualitatively but not quantitatively reproduce numerical data. In this regards, as already discussed at the beginning of this Chapter, a four pole approach could be essential and worthwhile to be investigated in order to significantly improve the agreement.

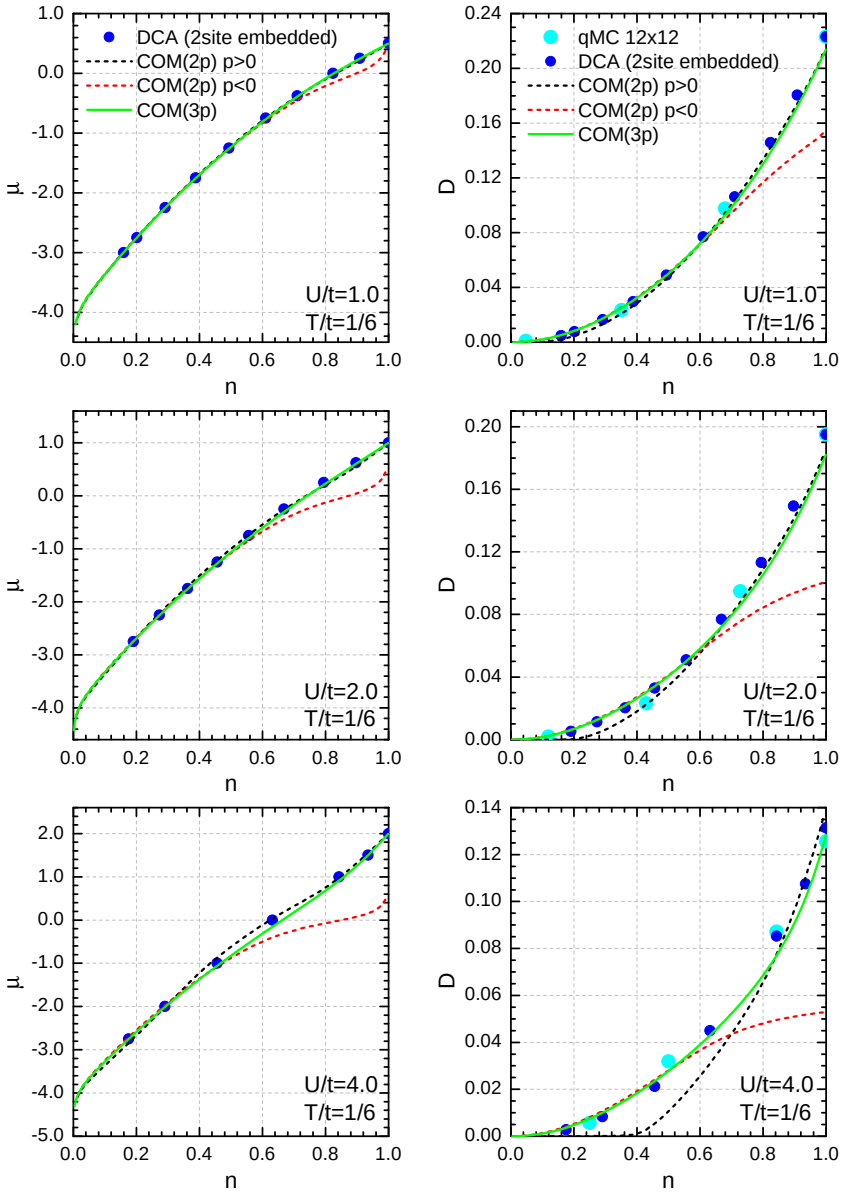

Figure 5.2: Filling dependence of chemical potential μ (left column), and double occupancy D (right column) for $T/t = 1/6$ and $U/t = 1.0$ (top line), $U/t = 2.0$ (central line) and $U/t = 4.0$ (bottom line). Black and red dashed lines denotes the two possible solutions with $p > 0$ and $p < 0$, respectively (see discussion in Section 4.1), the solid green line represents the solution in the three-pole approximation. Symbols refer to qMC [68] (cyan circles) and DCA [79] (blue circles) data.

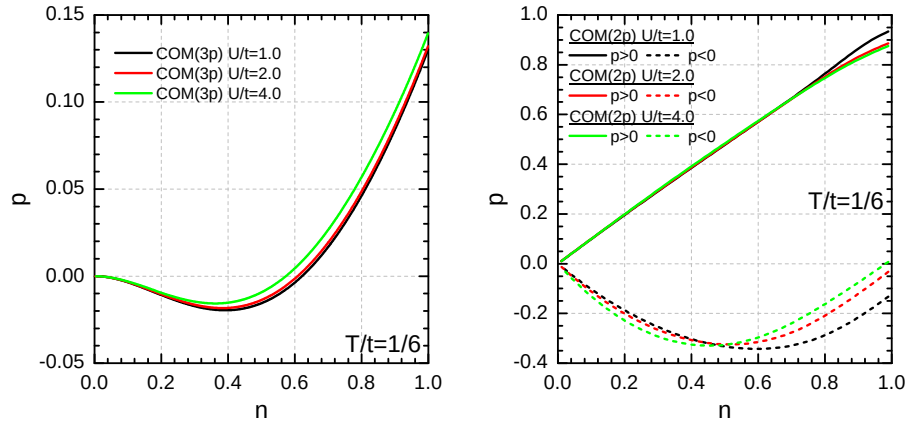

Figure 5.3: Filling dependence of p (Eq.5.44) for $T/t = 1/6$ and $U/t = 1.0$ (black lines), $U/t = 2.0$ (red lines) and $U/t = 4.0$ (green lines). Left and right panels report the data obtained in the framework of the three-pole and the two-pole approximations, respectively.

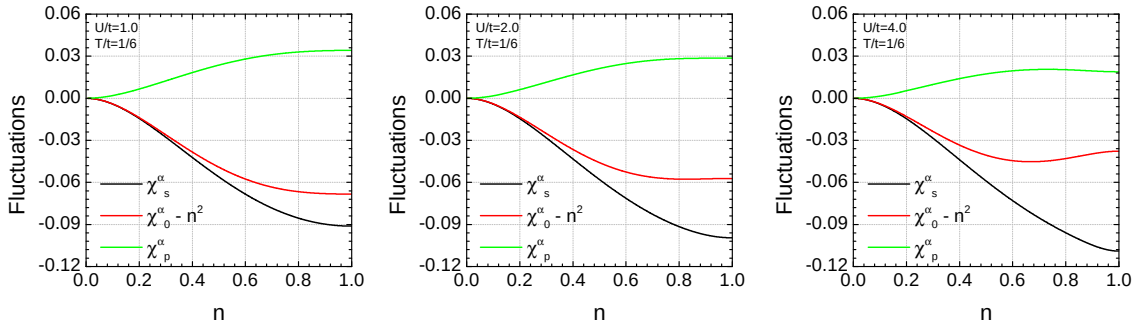

Figure 5.4: Filling dependence of spin (black lines), charge (red lines) and pair (green lines) fluctuations for $T/t = 1/6$ and $U/t = 1.0$ (left panel), $U/t = 2.0$ (central panel) and $U/t = 4.0$ (right panel).

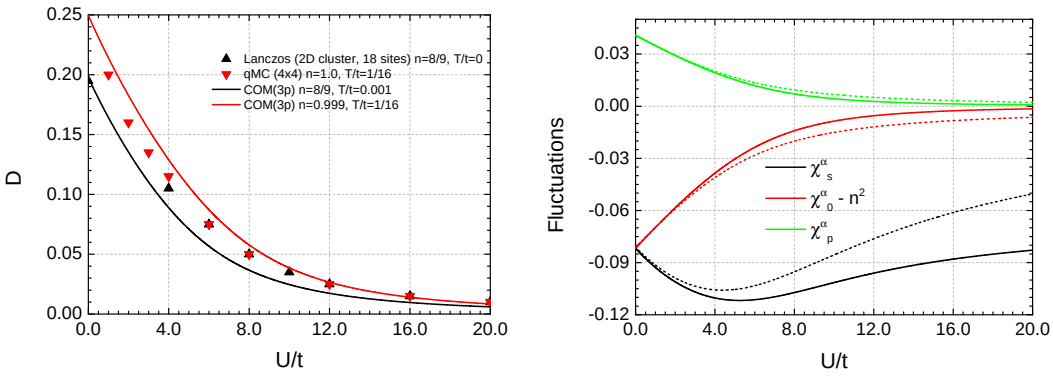

Figure 5.5: Left panel: comparison between three-pole results (solid lines), qMC [75] and Lanczos [80] data (symbols) in the $D(U/t)$ dependence for different values of filling and temperature. Right panel: three-pole results for charge, spin and pair fluctuations versus U/t plotted for $n = 8/9$, $T = 0.001$ (solid lines) and $n = 0.999$, $T = 1/16$ (dashed lines).

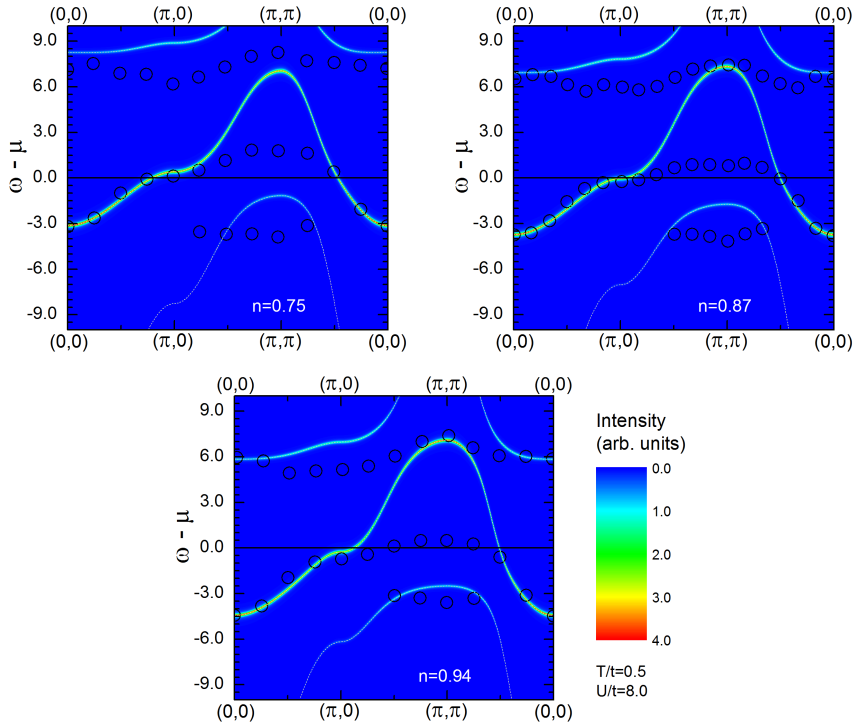

Figure 5.6: Energy dispersions along the principal directions of the first Brillouin zone. Data obtained in the three-pole approach are compared with qMC data [78] (open circles) for $T/t = 0.5$, $U/t = 8.0$ and different values of the filling. Dashed lines correspond to the bare energy dispersions $E(\boldsymbol{k})$ as reported in the left panel of Fig.5.7.

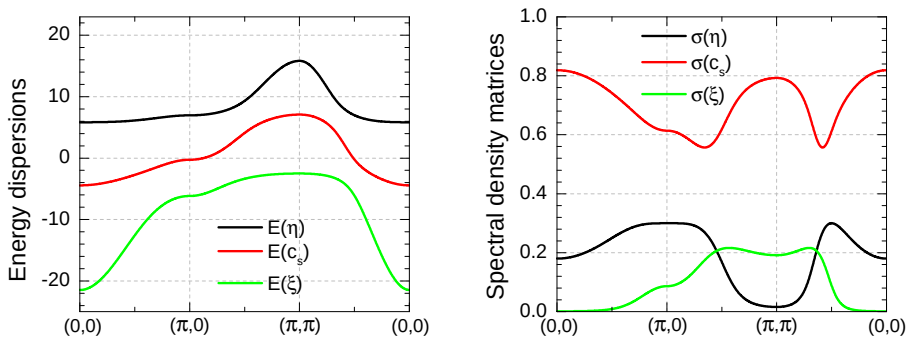

Figure 5.7: Energy dispersions (left panel) and corresponding spectral density matrices (right panel) along the principal directions of the first Brillouin zone for $U/t = 8.0$, $T/t = 0.5$ and $n = 0.94$. Different colors correspond to the contributions related to fields $\xi(i)$ (green), $\eta(i)$ (black) and $c_s(i)$ (red).

Chapter 6

Open issues and possible directions

As shown in the previous Chapters, the Composite Operator Method represents a powerful and full-consistent analytical tool for the investigation of strongly correlated electronic systems. As already said before, beyond its application to extended U-J-h and single band Hubbard models discussed in Chapter 3 and Chapter 4, respectively, in the last fifteen years it has been also successfully employed for the study of several other models and materials among which: p-d [12], t-J [13], t-t'-U [14], t-U-V [15], Kondo [17], Anderson [18], Cuprates [19]. The main advantage of the COM resides in the use of the so-called composite fields as building blocks for the construction of a proper Green's function formalism as illustrated in Sec.2.1. These fields, differently from the canonical electronic operators, are generated by the interactions and describe stable quasi-particle excitations in the systems rather than bare electrons. Hence, within the resulting Green's function formalism the effects of the interactions are contained not only in the self-energy corrections, but also in the "free" propagators. The calculation of both these quantities represents a hard task to deal with and, as shown in Chapter 4, can only be done in terms of a number of internal parameters to be determined self-consistently by means of symmetry requirements and algebraic constraints (see Sec.2.3). In this context a crucial role is played by the choice of the composite basis.

As pointed out in Chapter 4, in the case of the single-band Hubbard model a simple two-field basis, of either bosonic or fermionic nature, suffice to describe most of the relevant effects induced by strong correlations. However, due to the presence of multiple energy scales in the model Hamiltonian, a full-consistent description of all single-particle properties requires an extension to, at least, a three-field or a four-field basis. As discussed in Chapter 5, this procedure, which from one side introduces non-trivial complications due to the presence of a high number of internal parameters to be determined, from the other side allows to get a noticeable agreement with different numerical methods, providing a remarkable steps forward with respect to the two-pole approach. Some discrepancies still persist in the momentum-dependent quantities (e.g. energy dispersions, Fig.5.6) especially in the region near (π, π) where the role played by antiferromagnetic correlations is expected to be relevant at large U. These correlations, given the overall assumption of an uniform and

paramagnetic phase, can be only partially accounted in the framework of the three-pole approach described (see Fig.5.4), leading to the possibility to qualitatively but not quantitatively reproduce numerical data. In this regards, a four pole approach could be essential and worthwhile to investigate in order to significantly improve the agreement.

Then it is clear that, starting from the well-assessed and widely studied two-pole solution, a lot can still be done concerning possible three-pole and four-pole extensions of the theory, aiming to a better description of correlations and multiple energy scales in the strong coupling regime. In particular, as far as the three-pole approximation is concerned, it would be of great interest to estimate possible corrections to the calculation scheme described in Chapter 4 by considering $\pi(i)$, rather than its spin part $c_s(i)$, as a third field of the basis. Alternatively, on the basis of the same motivations which led to the splitting of the canonical electronic field $c(i)$ in its two components $\xi(i)$ and $\eta(i)$, it would be even more promising, yet fascinating, to investigate a four-pole solution in which the third field $\pi(i)$ appears divided in two auxiliaries components whose contributions in the energy spectra, similarly to the ones that arise from $\xi(i)$ and $\eta(i)$, are expected to separate among each other with increasing U. It is worth emphasizing that, beyond the relevance of the agreement with numerical data, this last suggestion could pave the way for a theory which, differently form many others, not only remains applicable in the whole range of filling, temperature and strength of the on-site potential U, but also dynamically takes into account both the energy scales of U and J in the crossover from the weak to the strong coupling regime. These proposals, whose realization would represent a significant step forward in the development of the method, are currently under investigation. In addition, is still under investigation the possibility to apply the COM to a large class of exactly solvable systems, among which spin systems and extended Hubbard models, with the aim of providing the exact solutions in two dimensions.

Bibliography

[1] J. Hubbard, Proc. R. Soc. Lond. A **276**, 238 (1963).

[2] J. E. Hirsch, Phys. Rev. Lett. **54**, 1317 (1985).

[3] S. Doniach, Physica B **91**, 231 (1977).

[4] P. W. Anderson, Phys. Rev. **124**, 41 (1961).

[5] Hal Tasaki, J. Phys.: Condens. Matter **10**, 4353 (1998).

[6] H. Tsunetsugu, M. Sigrist, and K. Ueda, Rev. Mod. Phys. **69**, 809 (1997); M. Gulacsi, Adv. Phys. **53**, 769 (2004).

[7] P. Fulde, J. Keller, and G. Zwicknagl, *"Solid State Physics: Advances in Research and Applications"*, edited by H. Ehrenreich and D. Turnbell (Academic Press, San Diego, 1988), Vol. 41, pp. 1-150 ; P. Fazekas, *"Lecture Notes on Electron Correlation and Magnetism"* (World Scientific, Singapore 1999); A. C. Hewson, *"The Kondo Problem to Heavy Fermions"* (Cambridge University Press, Cambridge, 1993).

[8] Z. Gulácsi, and D. Vollhardt, Phys. Rev. B **72**, 075130 (2005); Phys. Rev. Lett. **91**, 186401 (2003).

[9] P. Gurin, and Z. Gulácsi, Phys. Rev. B **64**, 045118 (2001).

[10] C. Noce, Phys. Rep. **431**, 173 (2006).

[11] J. R. Schrieffer, and P. A. Wolff , Phys. Rev. **149**, 491-492 (1966).

[12] A. Avella, F. Mancini, F. P. Mancini, E. Plekhanov, J. Phys. Chem. Solids **72**, 384 (2011).

[13] A. Avella, S. Feng, and F. Mancini, Physica B, **312-313**, 537 (2002).

[14] A. Avella, F. Mancini, and D. Villani, Phys. Lett. A, **240**, 235 (1998); A. Avella, F. Mancini, D. Villani and H. Matsumoto, Eur. Phys. J. B, **20**, 303 (2001); A. Avella, and F. Mancini, Physica C, **408-410**, 284 (2004).

[15] A. Avella, and F. Mancini, Eur. Phys. J. B, **41**, 149 (2004); J. Phys. Chem. Solids **67**, 142 (2006).

[16] F. Mancini, and A. Avella, Adv. Phys. **53**, 537 (2004).

[17] D. Villani, E. Lange, A. Avella, and G. Kotliar, Phys. Rev. Lett. **85**, 804 (2000).

[18] A. Avella, F. Mancini, and R. Hayn, Eur. Phys. J. B **37**, 465 (2004).

[19] A. Avella, F. Mancini, and D. Villani, Solid State Comm. **108**, 723 (1998); A. Avella, and F. Mancini, Eur. Phys. J. B **32**, 27 (2003); A. Avella, and F. Mancini, Phys. Rev. B **75**, 134518 (2007).

[20] F. Mancini, E. Plakhanov, and G. Sica, arXiv:1211.6551.

[21] J. Hubbard, Proc. R. Soc. Lond. A **281**, 401 (1964).

[22] L. M. Roth, Phys. Rev., **184**, 451 (1969); Phys. Rev., **186**, 428 (1969).

[23] H. Mori, Prog. Theor. Phys. **33**, 423 (1965).

[24] P. Fulde, *"Electron Correlations in Molecules and Solids"*, 3rd edn (Berlin: Springer 1995).

[25] N. M. Plakida, Physica C **282-287**, 1737 (1997).

[26] O. K. Kalashnikov, and E. S. Fradkin, Sov. Phys. JEPT, **28**, 317 (1969).

[27] A. Avella, F. Mancini, D. Villani, L. Siurakshina, and V. Y. Yushankhai, Int. J. Mod. phys. B, **12**, 81 (1998).

[28] F. Mancini, and A. Avella, Eur. Phys. J. B, **36**, 37 (2003).

[29] A. Avella, and F. Mancini, Eur. Phys. J. B, **36**, 445 (2003).

[30] F. Mancini, Europhys. Lett. **70**, 485 (2005).

[31] F. Mancini, and F. P. Mancini, Phys. Rev. E **77**, 061120 (2008).

[32] F. Mancini, and F. P. Mancini, Euro. Phys. J. B **73**, 581 (2010).

[33] F. Mancini, Euro. Phys. J. B **45**, 497 (2005).

[34] F. Mancini, and A. Naddeo, Phys. Rev. E **74**, 061108 (2006).

[35] A. Avella, and F. Mancini, Euro. Phys. J. B **50**, 527 (2006).

[36] F. Mancini, and F. P. Mancini, Condens. Matter Phys. **11**, 543 (2008).

[37] F. Mancini, Condensed Matter Physics, Vol. **9**, 393 (2006).

[38] S. Miyashita, Prog. Theor. Phys. **120**, 785 (2008).

[39] H. Tasaki, Eur. Phys. J. B **64**, 365 (2008).

[40] M. Fleck, A. I. Lichtenstein and E. Pavarini, Phys. Rev. Lett. **84**, 4962 (2000).

[41] H. Schweitzer and G. Czycholl, Z. Phys. B **83**, 93 (1991).

[42] S. Pankov and V. Dobrosavljevic, Phys. Rev. B **77**, 085104 (2008).

[43] H. J. Schulz, Phys. Rev. Lett. **64**, 1445 (1990).

[44] K. Y. Yang, C. T. Shih, C. P. Chou, S. M. Huang, T. K. Lee, T. Xiang and F. C. Zhang, Phys. Rev. B **73**, 224513 (2006).

[45] C. P. Chou, T. K. Lee and C. M. Ho, Phys. Rev. B **74**, 092503 (2006).

[46] V. F. Mitrovic, M. H. Julien, C. de Vaulx, M. Horvatic, C. Berthier, T. Suzuki and K. Yamada, Phys. Rev. B **78**, 014504 (2008).

[47] J. Zaanen, G. A. Sawatzky, and J.W. Allen, Phys. Rev. Lett. **55**, 418 (1985).

[48] E. Dagotto, J. Riera, and D.J. Scalapino, Phys. Rev. B **45**, 5744 (1992).

[49] T.M. Rice, M. Troyer, and H. Tsunetsugu, J. Phys. Chem. Solids **56**, 1663 (1995).

[50] R. Arita, K. Kuroki, H. Aoki, and M. Fabrizio, Phys. Rev. B **57**, 10324 (1998).

[51] G. I. Japaridze, and E. Muller-Hartmann, Phys. Rev. B **61**, 9019 (2000).

[52] S. Daul, D. J. Scalapino, and S. R. White, Phys. Rev. Lett. **84**, 4188-4191 (2000).

[53] R. B. Laughlin, arXiv:cond-mat/0209269v1 (2002); Phil. Mag. **86**, 1165 (2006).

[54] F. C. Zhang, Phys. Rev. Lett. **90**, 207002 (2003).

[55] D. Jérome, A. Mazaud, M. Ribault and K. Bechgaard, J. Physique - Lettres **41**, L-95 - L-98 (1980).

[56] J. Dai, X. Feng, T. Xiang and Y. Yu, Phys. Rev. B **70**, 064518 (2004).

[57] C. Dziurzik, G.I. Japaridze, A. Schadschneider and J. Zittartz, EPJ B **37**, 453 (2004).

[58] H. Ding and Y. Wang, Modern Physics Letters B, Volume **24**, Issue 28, pp. 2769 - 2783 (2010).

[59] A. Avella and F. Mancini, in "Strongly Correlated Systems: Theoretical Methods", edited by A. Avella and F. Mancini (Springer Berlin Heidelberg, 2012), vol. 171 of Springer Series in Solid-State Sciences, pp. 103-141.

[60] D. Duffy, and A. Moreo, Phys. Rev. B **52**, 15607 (1995).

[61] N. Furukawa, and M. Imada, Physica B, **186-188**, 931 (1993).

[62] E. Dagotto, A. Moreo, F. Ortolani, D. Poilblanc, and J. Riera. Phys. Rev. B, **45**, 10741 (1992).

[63] N. Furukawa, and M. Imada, J. Phys. Soc. Jpn., **61**, 3331 (1992).

[64] X. Y. Zhang, E. Abrahams, and G. Kotliar, Phys. Rev. Lett., **66**, 1236 (1991)

[65] J. E. Hirsch, Phys. Rev. B, **31**, 4403 (1985).

[66] J. Bonča, and P. Prelovšek, Phys. Rev. B, **67**, 085103 (2003).

[67] F. Becca, A. Parola, and S. Sorella, Phys. Rev. B, **61**, 16287 (2000).

[68] A. Moreo, D. J. Scalapino, R. L. Sugar, S. R. White, and N. E. Bickers, Phys. Rev. B, **41**, 2313 (1990).

[69] F. Mancini, Physics Letters A, **249**, 231 (1998).

[70] S. Marra, F. Mancini, A. M. Allega, and H. Matsumoto, Physica C, **235**, 2253 (1994).

[71] A. Avella, and F. Mancini, Physica C, **408**, 287 (2004).

[72] Y. C. Chen, A. Moreo, F. Ortolani, E. Dagotto, T. K. Lee, Phys. Rev. B **50**, 655 (1994).

[73] Y. M. Vilk, L. Chen, A. M. S. Tremblay, Phys. Rev. B **49**, 13267 (1994).

[74] R. Coldea, S. Hayden, G. Aeppli, T. Perring, C. Frost, T. Mason, S. W. Cheong, Z. Fisk, Phys. Rev. Lett. **86**, 5377 (2001).

[75] S. R. White, D. J. Scalapino, R. L. Sugar, E. Y. Loh, J. E. Gubernatis, R. T. Scalettar, Phys. Rev. B **40**, 506 (1989).

[76] A. Avella, and F. Mancini, Phys. Rev. B, **75**, 134518 (2007).

[77] A. Damascelli, Z. Hussain, and Z.-X. Shen, Rev. Mod. Phys. **75**, 473 (2003).

[78] N. Bulut, D. J. Scalapino, and S. R. White, Phys. Rev. B, **50**, 7215 (1994).

[79] Private communication, G. Sangiovanni.

[80] F. Becca, A. Parola, and S. Sorella, Phys. Rev. B, **61**, 16287 (2000).

Part II

Electron-phonon interaction in strongly correlated systems

Chapter 7

Introduction to polaron and bipolaron theory

In the last years, after the discovery of high-temperature superconductivity, a new interest arose in the study of polaron and bipolaron theory as a full-consistent alternative to other possible scenarios proposed to explain not only superconducting features, but also non-Fermi liquid behaviors observed in the normal state of a large class of superconducting materials. Polaron and bipolaron theory, originated from electron-phonon coupling, has its roots in 1933 when the concept of "polaron" was first introduced by Landau [1] as the result of the interaction between a single carrier (electron or hole) with the self-induced polarization field in a semiconductor or ionic crystal. The standard Hamiltonian which describes this interaction was first derived by Fröhlich [2] :

$$\mathcal{H}_{el-ph} = \frac{1}{\sqrt{2N}} \sum_{\boldsymbol{k},\boldsymbol{q}} \sum_{n,n',\nu,\sigma} \left(V_{nn'}(\boldsymbol{q},\boldsymbol{k},\nu)\omega_{\boldsymbol{q}\nu} c^{\dagger}_{n,\sigma}(\boldsymbol{k}) c_{n,\sigma}(\boldsymbol{k}-\boldsymbol{q}) d_{\nu}(\boldsymbol{q}) + H.c. \right) , \quad (7.1)$$

where $\boldsymbol{q}$ and $\boldsymbol{k}$ are phononic and electronic momenta, ν and n are phonon mode and electronic band indices, respectively, σ is the spin of the carrier. The operators $c^{\dagger}_{n,\sigma}(\boldsymbol{k})/c_{n,\sigma}(\boldsymbol{k})$ create/annihilate a carrier with momentum $\boldsymbol{k}$ and spin σ on the n^{th}-band; similarly the operators $d^{\dagger}_{\nu}(\boldsymbol{q})/d_{\nu}(\boldsymbol{q})$ create/annihilate a phonon with momentum $\boldsymbol{q}$ on the ν^{th} mode. Finally, $V(\boldsymbol{q},\boldsymbol{k},\nu)$ is the dimensionless matrix which parametrizes the Fourier transform of the electron-phonon interaction (EPI):

$$V_{nn',\sigma}(\boldsymbol{q},\boldsymbol{k},\nu) = -\frac{N}{\sqrt{M}\omega^{3/2}_{\boldsymbol{q}\nu}} \int d^d r \left(\boldsymbol{e}_{\boldsymbol{q}\nu} \cdot \nabla v(\boldsymbol{r}) \right) \psi^{*}_{n,\sigma}(\boldsymbol{r},\boldsymbol{k}) \psi_{n',\sigma}(\boldsymbol{r},\boldsymbol{k}-\boldsymbol{q}) , \quad (7.2)$$

where $\boldsymbol{e}_{\boldsymbol{q}\nu}$ is the unit polarization vector of the phonon mode ν while $v(\boldsymbol{r})$ parametrizes the interaction among two charged carriers at distance $\boldsymbol{r}$. Although Eq.7.1 represents the most general expression for the EPI, for the sake of simplicity hereafter we will restrict our analysis to a single-band picture in which the EPI matrix only depends on the transferred momentum $V_{nn',\sigma}(\boldsymbol{q},\boldsymbol{k},\nu) \equiv V(\boldsymbol{q})$ allowing for the following

simple form for the EPI:

$$\mathcal{H}_{el-ph} = \sum_{\boldsymbol{q},\boldsymbol{m}} \omega_{\boldsymbol{q}} n_i \left[u_{\boldsymbol{m}}(\boldsymbol{q}) d_{\boldsymbol{q}} + H.c. \right] \ , \tag{7.3}$$

where the Wannier representation has been used, with $n_{\boldsymbol{m}} = \sum_\sigma c^\dagger_\sigma(\boldsymbol{m}) c_\sigma(\boldsymbol{m})$ and:

$$u_{\boldsymbol{m}}(\boldsymbol{q}) = \frac{1}{\sqrt{2N}} V(\boldsymbol{q}) e^{i\boldsymbol{q}\cdot\boldsymbol{m}} \ . \tag{7.4}$$

The Hamiltonian (7.1) allows for different descriptions of the polaronic state according to the values of the characteristic phonon frequencies. With no claim of being exhaustive (for a comprehensive review see Refs.[3, 4, 5, 6]), we just recall that if the phonon frequencies $\omega_{\boldsymbol{q}}$ are sufficiently low, the deformation induced in the crystal affects many lattice sites resulting in the presence of a "large" or "continuum" polarons. Vice versa, when the polaron binding energy is larger than the electronic half-bandwidth, the deformation of the lattice is confined to few lattice sites resulting in the so-called "small" or "lattice" polaron regime.

The large polaron regime has been extensively studied in both strong and weak coupling regimes showing that large polarons almost behave as free electrons moving in the lattice with a moderate mass renormalization. In the strong coupling regime a strong coupling expansion in terms of the Fröhlich coupling constant α gives the following value for polaron ground-state energy E_0 and polaron effective mass m^* [7]:

$$\frac{E_0}{\hbar\omega_0} = -0.108513\alpha^2 - 2.836 \ , \tag{7.5}$$

$$\frac{m^*}{m_e} = 1 + 0.0227019\alpha^4 \ , \tag{7.6}$$

where m_e is the bare band-mass of the carrier while α is defined in terms of static, ε_0 and dynamic, ε_∞ dielectric constants as:

$$\alpha = \frac{e^2}{\hbar c} \sqrt{\frac{m_e c^2}{2\hbar\omega_0}} \left(\frac{1}{\varepsilon_\infty} - \frac{1}{\varepsilon_0} \right) \ . \tag{7.7}$$

In the weak coupling regime the same quantities calculated weak-coupling expansion read as [8, 9]:

$$\frac{E_0}{\hbar\omega_0} = -\alpha - 0.0159196220\alpha^2 - 0.000806070048\alpha^3 + o(\alpha^4) \ , \tag{7.8}$$

$$\frac{m^*}{m_e} = 1 + \frac{\alpha}{6} + 0.02362763\alpha^2 + o(\alpha^3) \ . \tag{7.9}$$

The opposite behavior comes in the play under the assumption, supported by experimental evidence in oxides, that the self-induced polarization field could be mostly confined in a region with dimensions comparable to the lattice spacing . In this regime, which is realized when the polaron binding energy is larger than the

electronic half-bandwidth, strong and short range interactions localize carriers with a strong mass renormalization, resulting in the formation of small polarons. The time in which the carrier is localized on a single lattice site is larger compared with the relaxation time of the lattice, allowing for a localized description of the polaron dynamics in the real space, rather than in the momentum space. Hence, polaron properties such as ground state energy and effective mass are strongly dependent on the particular lattice geometry. However, a common fingerprint of the small bipolaron regime can be found in the polaron mobility. As suggested by Lang and Firsov [10], polaron hopping processes can only be induced by thermal excitations since the jump of a carrier from a site to another induces a shift in the lattice deformation. In particular, for $k_BT > \hbar\omega_0/4$ the typical occupation time Δt related to the presence of a carrier on a site, satisfies the relation: $t_0 \ll \Delta t \ll t_p$ where:

$$t_0 \sim \frac{\hbar}{\sqrt{\Delta_T k_B T}} , \tag{7.10}$$

$$t_p \sim \frac{\hbar}{W} , \tag{7.11}$$

being W the polaron bandwidth and Δ_T the thermal activation energy for hopping given by 1/2 the polaron binding energy . Hence, in the small-polaron picture, the polaron mobility μ strongly depends on temperature according to the following relation [10, 11]:

$$\mu = \frac{ea^2\omega_0}{6k_BT} e^{-\frac{\Delta_T}{k_BT}} , \tag{7.12}$$

which holds for $T > \theta_D/2$, where θ_D is the Debye temperature, e is the charge of the carrier and a is the lattice constant.

Because of their nature, small and large polarons interact with each other via a renormalized coupling which comes out from the competition between the Coulomb repulsion and an effective attraction of phononic nature . Different from the standard electrostatic repulsion, two carriers of same charge in a ionic lattice might attract each other in order to minimize the self-induced deformation. The resulting long-range interaction, which is attractive at short distance, at large distances is found to be weak end repulsive [12] since, although $\varepsilon_0 \gg 1$, Fröhlich EPI can only reduce the electrostatic repulsion without overscreen it. Importantly, this last findings holds even in the case of multi-polaron systems where Fröhlich EPI in remains unscreened, independently on the polaron density, since polarons are too slow to screen high-frequency optical phonons [13, 14]. Hence when the electron-phonon contribution is dominant with respect to the Coulomb one, a bound state of two polarons, called "bipolaron", might arise. The properties of this bound state depend on the polaronic regime, so that is is possible to have two large polarons bound in a "large bipolaron" (also called "Fröhlich bipolaron") as well as two small polarons paired in a small and tightly bound "small bipolaron" (also called "Holstein bipolaron").

Large bipolarons have been intensively studied in the continuous limit [15, 16]. It has been shown that the bipolaron energy depends on the intensity of the Coulomb

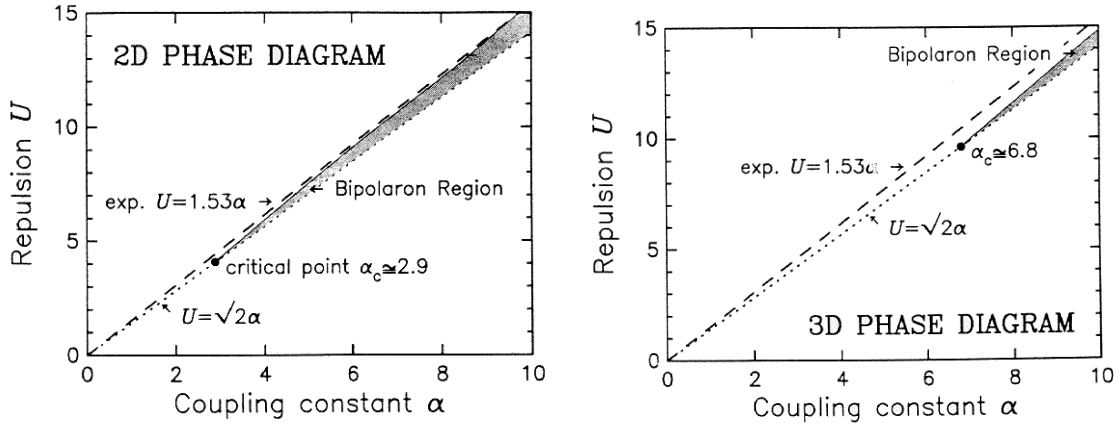

Figure 7.1: The stability region for bipolaron formation in 2D (left panel) and in 3D (right panel). The dotted line $U = \sqrt{2}\alpha$ separates the physical region ($U \geq \sqrt{2}\alpha$) from the non-physical ($U \leq \sqrt{2}\alpha$). The shaded area is the stability region in physical space. The dashed (dotted) "characteristic line" $U = 1.537\alpha$ ($U = 1.526\alpha$) is determined by $U = \sqrt{2}\alpha/(1-\varepsilon_\infty/\varepsilon_0)$ with the experimental values (from Ref. [19]) $\varepsilon_\infty = 4$ and $\varepsilon_0 = 50$ for La_2CuO_4 ($\varepsilon_\infty = 4.7$ and $\varepsilon_0 = 64.7$ for $YBa_2Cu_3O_7$ calculated using the experimental data in Refs.[20, 21]). The critical points $\alpha_c = 6.8$ for 3D and $\alpha_c = 2.9$ for 2D are represented as full dots. Reproduced from Refs.[17, 18].

repulsion, parametrized by the dimensionless parameter U:

$$U = \frac{\sqrt{2}\alpha}{1 - \varepsilon_\infty/\varepsilon_0} \,, \tag{7.13}$$

with $U \geq \sqrt{2}\alpha$ since $\varepsilon_0 \gg \varepsilon_\infty$ in ionic crystals, α is defined in Eq.7.7. The stability of the bipolaronic state, as follows from the constraint $E_b \leq 2E_p$ (E_b and E_p are bipolaron and single polaron energies), has also been studied in two and three dimensions [17, 18], resulting in the phase diagrams reported in Fig.7.1 which show a substantial increase in the bipolaron stability in 2D with respect to the 3D case.

Due to the very narrow-band, the small bipolaron regime has been mostly studied in the framework of the so-called Holstein-Hubbard model (HHM):

$$\mathcal{H}_{HHM} = \sum_{i,j} \left(-t_{ij} c_i^\dagger c_j + \frac{1}{2} V_{ij}^C c_i^\dagger c_j^\dagger c_j c_i \right) + \sum_{\boldsymbol{q},\nu} \omega_{\boldsymbol{q}\nu} \left(d_{\boldsymbol{q}\nu}^\dagger d_{\boldsymbol{q}\nu} + \frac{1}{2} \right) + \mathcal{H}_{el-ph} \,, \tag{7.14}$$

where $\mathcal{H}_{el-ph}$ is the electron-phonon interaction described in Eq.7.3, $V^C(\boldsymbol{m}-\boldsymbol{n}) = e^2/\varepsilon_0 \, |\boldsymbol{m}-\boldsymbol{n}|$ parametrizes the potential, $\omega_{\boldsymbol{q}\nu}$ is the phonon frequency of a phonon in the ν^{th} mode with momentum $\boldsymbol{q}$ and t_{ij} is the hopping term, which is a perturbation under the assumption that the energy of two small polarons is much larger than the polaron bandwidth [22, 23]. It has been shown that on-site bipolarons, which are stable under the condition $U < 2E_p$, are the ground state of the HHM in the non-dispersive limit [23, 24, 25, 26, 27]. In this limit the bipolaron binding energy $\Delta = 2E_p - U$ is much larger than the bandwidth, hence in the ground state all polarons are

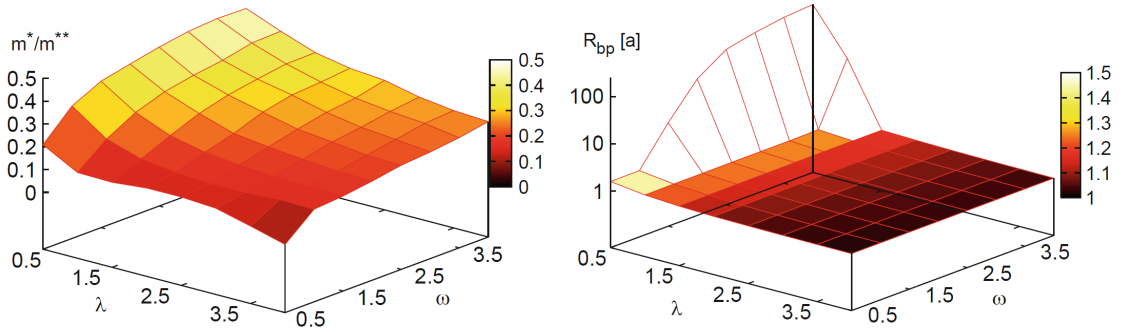

Figure 7.2: Polaron to bipolaron mass ratio (left panel) and bipolaron radius in units of the lattice constant a (right panel) on a staggered ladder for a range of $\bar{\omega} = \omega_0/T(a)$ and λ showing mobile small bipolarons in the adiabatic regime $\bar{\omega} = 0.5$ for coupling λ up to 2.5. Reproduced from Ref.[29].

paired, with an effective bipolaron-bipolaron and bipolaron-polaron repulsion which originates from the Pauli exclusion principle (two or more bipolarons, as well as three or more polarons, can not occupy the same site). Bipolaronic configurations have also been studied in the presence of a finite hopping by considering t_{ij} as a coherent bipolaron hopping integral and projecting the HHM Hamiltonian in a subspace characterized by all bipolaronic states with no unpaired polarons [23].

Beyond the narrow-band limit, bipolaron formation and stability have also been studied in the framework of the so-called Fröhlich-Coulomb model [28] which, under the assumption of dispersionless phonon modes of frequency ω_0, accounts for finite-range Coulomb repulsion $V^C(\boldsymbol{m}-\boldsymbol{n}) = e^2/\varepsilon_0\,|\boldsymbol{m}-\boldsymbol{n}|$ and long-range Fröhlich EPI as:

$$\begin{aligned}\mathcal{H}_{FCM} \;=\; & \sum_{\boldsymbol{m}\neq\boldsymbol{n}'} T(\boldsymbol{n}-\boldsymbol{n}')c^\dagger_{\boldsymbol{n}}c_{\boldsymbol{n}'} + \frac{1}{2}\sum_{\boldsymbol{m}\neq\boldsymbol{n}} V^C(\boldsymbol{m}-\boldsymbol{n})c^\dagger_{\boldsymbol{n}}c_{\boldsymbol{n}}c^\dagger_{\boldsymbol{n}'}c_{\boldsymbol{n}'} \\ & +\omega_0 \sum_{\boldsymbol{m}\neq\boldsymbol{n}} g(\boldsymbol{m}-\boldsymbol{n})\,(\boldsymbol{e}_{\boldsymbol{m}}\cdot\boldsymbol{u}_{\boldsymbol{m}-\boldsymbol{n}})\,n_{\boldsymbol{n}}\left(d^\dagger_{\boldsymbol{m}}+d_{\boldsymbol{m}}\right) \\ & +\omega_0 \sum_{\boldsymbol{m}}\left(d^\dagger_{\boldsymbol{m}}d_{\boldsymbol{m}}+\frac{1}{2}\right)\;, \end{aligned} \tag{7.15}$$

where $\boldsymbol{e}_{\boldsymbol{m}}$ is the polarization vector at site $\boldsymbol{m}$, $\boldsymbol{u}_{\boldsymbol{m}-\boldsymbol{n}} = (\boldsymbol{m}-\boldsymbol{n})/\,|\boldsymbol{m}-\boldsymbol{n}|$ is the unit vector pointing from $\boldsymbol{m}$ to $\boldsymbol{n}$, $g(\boldsymbol{m}-\boldsymbol{n})$ is a dimensionless parameter. The FCM has been studied in the whole range of parameters and for different 2D and 3D geometries [29, 30, 31, 32, 33] by means of the Continuous-time quantum Monte Carlo (CT-QMC) technique for bipolarons [29]. By considering Coulomb repulsion up to nearest-neighbour, bipolaron formation has been found in a wide range of electron-phonon couplings and phonon frequencies. As follows from Fig.7.2, bipolarons are small and perfectly mobile since the bipolaron to polaron mass ratio $2 \leq m^{**}/m^{*} \leq 4$ and the bipolaron radius $R_{bp} \approx a$ (a is the lattice constant) going from the weak $\lambda \ll 1$ to the strong $\lambda \leq 2.5$ coupling regime.

In all the aforementioned models, bipolaron formation has been widely advocated as one of the possible mechanisms at the basis of high-T$_c$ superconductivity

and non-Fermi liquid behaviors observed in a large class of compounds. Local and tightly bound pairs, such as small and perfectly mobile bipolarons, are good candidate for a Bose-Einstein condensation (BEC) which has already been argued to provide a very high critical temperature (see Sec.10.2). However, a correct description of all bipolarons features requires unscreened Fröhlich and Coulomb to be taken into account, which makes the problem more and more complicated to deal with. Because of this, for many years the formation of small bipolarons has been mostly considered in a class of non-retarded models, e.g. negative-U models, which can only phenomenologically account of real unscreened Coulomb and electron-phonon interactions. These models, although able to reproduce the formation of tightly bound polarons pairs in real space, are not able to recover the crossover to the standard BCS regime of large and weakly interacting Cooper pairs, which has been argued to be one of the key-features for polaron and bipolaron theory of superconductivity.

Within this context, we derive in this part of the thesis the results obtained in the framework of the polaronic $t-J_p$ [34, 35] and $t-J_p-\tilde{U}$ [36, 37] models which, proposed as alternative models for high-temperature superconductors, for the first time account for unscreened long-range electron-electron (Coulomb) and electron-phonon (Fröhlich) interactions on microscopic grounds. In Chapter 8 we introduce a microscopic Hamiltonian for the description of high-polarizable ionic lattices, based on unscreened electron-electron (Coulomb) and electron-phonon (Fröhlich) interactions. We show that, without any assumption on their range and relative magnitude, long-range Coulomb and Fröhlich interaction almost negate each other giving rise to an effective model in which electronic and phononic degrees of freedom are both contained in a rescaled hopping operator. The aforementioned model is studied in Sec.8.1 and Sec.8.2 in the weak and strong coupling regimes, respectively. It is shown that, by applying the BCS-Eliashberg formalism in the weak coupling regime, the model allows a phase transition to a superconducting phase with a critical temperature $T_c \approx 20K$. This superconducting phase is characterized by Cooper pairs which are preserved, even in the presence of a strong electron-electron coupling, thanks to the "Tolmachev-Morel-Anderson" logarithm which rescales the Coulomb potential. In the strong coupling regime, due to non-negligible of multi-phonon vertex corrections and finite bandwidths effects, the model Hamiltonian is studied within a perturbative approach, by averaging the rescaled hopping operator with respect to the phonon vacuum and considering the remaining part as a perturbation. Within this scheme, it is shown that the application of a Schrieffer-Wolf transformation leads to the so-called polaronic $t-J_p$ model. Here t_{ij} is the renormalized polaron hopping integral, which describes the motion of strongly inter-correlated fermions, also accounting for their interaction with the lattice. $J_p > t$ is the the residual polaron-multi-phonon exchange interaction which has a twofold effect: is responsible for the formation of small and perfectly mobile pairs of polarons called bipolarons and, unlike in the standard $t-J$ model, also protects the ground state from clustering giving rise to an effective pair-pair repulsion.

Numerical and analytical results on the ground state of the polaronic $t-J_p$ model are reported in Chapter 9 for different lattice geometries. The static limit is analyzed in Sec.9.1. It is shown that, in the extreme strong coupling regime in which $t \ll J_p$, the ground state is a spin singlet made up by pairs of nearest-neighbor

bipolarons separated by at least one empty site, with an effective pair-pair repulsion proportional to J_p. Further results beyond the static limit are reported in Sec.9.2. It is shown that, in the regime in which the bipolaron radius is small compared to the system size, the hopping has the only effect to coherently propagate the pairs in the lattice. Therefore, without the loss of generality, analytical and numerical results have been obtained by solving the two-particle problem and then projecting the Hamiltonian on the repulsive Bose gas of small inter-site bipolarons. A complete characterization of the ground state configurations has been given in terms of energy dispersion, effective mass, bipolaron radius in the framework of the so-called Singlet-Subspace-Projection (SSP) method which has been applied to characterize singlet and triplet states of one and two dimensional systems.

Finally, in Chapter 10 we analyze the effect of an on-site coupling $\tilde{U}$ on the ground state configurations of the polaronic $t - J_p$ model. It is shown that the inclusion of $\tilde{U}$, which results in the formulation of the so-called polaronic $t - J_p - \tilde{U}$ model, has a twofold effect since, by limiting the double occupancy, it also reduces the polaronic exchange $J_p \equiv J_p(\tilde{U})$. The role of $\tilde{U}$ has been argued to be at the basis of the small-to-large bipolaron transition, which is studied in Sec.10.1. It is shown that, for both one and two dimensional geometries and finite values of $\tilde{U}$, a critical value of the ratio $t/J_p(\tilde{U})$ exists above which pairs of polarons become unbound. Signatures of the small-to-large bipolaron transition are reported in bipolaron radius and effective mass. On the light of the small-to-large bipolaron transition, the polaronic $t-J_p(\tilde{U})-\tilde{U}$ and its connections with high-temperature superconductivity are studied in Sec.10.2. It is shown that the $t-J_p(\tilde{U})-\tilde{U}$ Hamiltonian accounts for a phase transition to a superconducting state characterized by a critical temperature well in excess of 100K. The on-site interaction $\tilde{U}$, by suppressing the exchange interaction J_p, reduces the critical temperature driving the system to a BEC/BCS crossover in which the condensation energy of pairs of polarons, no more tightly bound in the real space, appears in the form of Cooper pairs in the momentum space with a lower critical temperature. Finally, in Sec.10.3 is discussed the applicability of the model to Cuprate superconductors. It is shown that, without any ad-hoc assumption on preexisting orders or broken symmetries in the normal state of the model, the polaronic t-J_p-$\tilde{U}$ Hamiltonian is able to reproduce pseudogap features in density of states, spin susceptibility and electric conductivity in terms of a thermal-induced recombination of bipolarons and unpaired polarons, studied as a charged and ideal Fermi-Bose mixture. Open issues and possible directions are reported in Chapter 11.

Chapter 8

Microscopic Hamiltonian for high-polarizable lattices

Theoretical efforts in calculating the properties of strongly correlated real materials are often related to the formulation of new microscopic models, which account for strong electron-electron correlations as well as interactions of electrons with other degrees of freedoms (such as lattice vibrations, light). In particular, it is widely believed that the competition between electron-electron and electron-phonon interactions could be at the basis of most of the relevant features of strongly correlated systems. Therefore, as a first step in the derivation of a first-principle Hamiltonian, one might simply consider that charged carriers interact among themselves but also with ion vibrations via the so-called "electron-electron" (Coulomb) and "electron-phonon" (Fröhlich) interactions. These interactions couple together electronic and ionic degrees of freedom resulting in the following microscopic Hamiltonian:

$$
\begin{aligned}
H = \quad & \underbrace{-\sum_{i,j}\left(T_{ij}\delta_{ss'}+\mu\delta_{ij}\right)\hat{c}_i^{\dagger}\hat{c}_j}_{H_{kin}} \quad + \quad \underbrace{\frac{1}{2}\sum_{\boldsymbol{m}\neq\boldsymbol{n}}\sum_{s,s'}\frac{e^2}{\epsilon_\infty|\boldsymbol{m}-\boldsymbol{n}|}\hat{n}_{\boldsymbol{m},s}\hat{n}_{\boldsymbol{n},s'}}_{H_{el-el}} \quad + \\
& + \underbrace{\sum_{\boldsymbol{q},i}\hbar\omega_0\hat{n}_i\left[u(\boldsymbol{m},\boldsymbol{q})\hat{d}_q+H.c.\right]}_{H_{el-ph}} \quad + \quad \underbrace{\sum_{\boldsymbol{q}}\hbar\omega_0\left(\hat{d}_{\boldsymbol{q}}^{\dagger}\hat{d}_{\boldsymbol{q}}+\frac{1}{2}\right)}_{H_{ph}},
\end{aligned}
\tag{8.1}
$$

where H_{kin} is the kinetic term, H_{ph} contains the pure phononic contribution while H_{el-el} and H_{el-ph} represent *unscreened* Coulomb and Fröhlich interactions, respectively, which operate on the same scale without any ad hoc assumption on their range and relative magnitude. Here $T_{ij} \equiv T(\boldsymbol{m}-\boldsymbol{n})$ is the bare hopping integral related to the overlap of two single-particle Wannier orbitals centered at sites $\boldsymbol{m}$ and $\boldsymbol{n}$, μ is the chemical potential, $i=(\boldsymbol{m},s)$ and $j=(\boldsymbol{n},s')$ include both site $(\boldsymbol{m},\boldsymbol{n})$ and spin (s,s') states. The operator $\hat{c}_i/\hat{c}_i^{\dagger}$ annihilates/creates an electron on site

$\boldsymbol{m}$ with spin s, the operator $\hat{d}_{\boldsymbol{q}}/\hat{d}^{\dagger}_{\boldsymbol{q}}$ annihilates/creates a phonon with momentum $\boldsymbol{q}$. The operator $\hat{n}_i \equiv \hat{n}_{\boldsymbol{m},s}{=}\hat{c}^{\dagger}_{\boldsymbol{m},s}\hat{c}_{\boldsymbol{m},s}$ represents the electronic density, $u(\boldsymbol{m},\boldsymbol{q})$ is defined as:

$$u(\boldsymbol{m},\boldsymbol{q}) \;=\; \frac{\gamma(\boldsymbol{q})}{\sqrt{2N}} e^{i\boldsymbol{q}\cdot\boldsymbol{m}} \;, \tag{8.2}$$

where $\gamma(\boldsymbol{q})$ is the following dimensionless parameter:

$$\gamma(\boldsymbol{q}) \equiv \sqrt{\frac{4\pi e^2}{\kappa\Omega\hbar\omega_0 q^2}} \;, \tag{8.3}$$

in which Ω is the volume of the unit cell, N is the number of unit cells in the crystal, ω_0 is the optical phonon frequency and κ is a universal parameter defined in terms of the high-frequency, ε_∞ and the static, ε_0 dielectric constants:

$$\kappa \equiv \frac{\epsilon_\infty \epsilon_0}{\epsilon_0 - \epsilon_\infty} \;. \tag{8.4}$$

A frequently employed transformation in polaron theory is the one that displays ions to the new equilibrium positions depending on the electron coordinates. This transformation, called Lang-Firsov (LF) transformation [10], is defined in terms of the following unitary operator:

$$U \equiv e^{S} \;, \tag{8.5}$$

with:

$$S \equiv -\sum_{\boldsymbol{q},i} \hat{n}_i \left[u(\boldsymbol{m},\boldsymbol{q}) d_q - H.c.\right] \;. \tag{8.6}$$

It is worth noting that $S^{\dagger} = -S$. As shown in detail in the Appendix E, following the unitary transformation (8.5), the operators in the Hamiltonian (8.1) read as (hereafter we denote with a tilde the transformed quantities with respect to U: $\tilde{O} \equiv U^{\dagger} O U$):

$$\begin{aligned}
&\tilde{c}_i = \exp\left[\sum_{\boldsymbol{q}} \left(u(\boldsymbol{m},\boldsymbol{q})\hat{d}_q - H.c.\right)\right] \hat{c}_i \equiv \hat{X}_i \hat{c}_i \\
&\tilde{d}_q = \hat{d}_q - \sum_i \hat{n}_i u^*(\boldsymbol{m},\boldsymbol{q}) \\
&\tilde{d^{\dagger}_q} = \hat{d}^{\dagger}_q - \sum_i \hat{n}_i u(\boldsymbol{m},\boldsymbol{q}) \\
&\tilde{n}_i = \hat{n}_i \\
&\tilde{n_i d_q} = \hat{n}_i \hat{d}_q - \hat{n}_i \sum_j \hat{n}_j u^*(\boldsymbol{n},\boldsymbol{q}) \\
&\tilde{n_i d^{\dagger}_q} = \hat{n}_i \hat{d}^{\dagger}_q - \hat{n}_i \sum_j \hat{n}_j u(\boldsymbol{n},\boldsymbol{q}) \\
&\tilde{d^{\dagger}_q d_q} = \hat{d}^{\dagger}_q \hat{d}_q - \sum_i \left[\hat{d}^{\dagger}_q \hat{n}_i u^*(\boldsymbol{m},\boldsymbol{q}) + \hat{d}_q \hat{n}_i u(\boldsymbol{m},\boldsymbol{q})\right]
\end{aligned} \tag{8.7}$$

therefore, by substituting in Eq.8.1 we obtain:

$$\tilde{H} = -\sum_{i,j} \left[\hat{\sigma}_{ij}\delta_{ss'} + \tilde{\mu}\delta_{ij}\right] \hat{c}_i^\dagger \hat{c}_j + \frac{1}{2}\sum_{\boldsymbol{m}\neq\boldsymbol{n}}\sum_{s,s'} \frac{e^2}{|\boldsymbol{m}-\boldsymbol{n}|}\left(\frac{1}{\epsilon_\infty} - \frac{1}{\kappa}\right)\hat{n}_{\boldsymbol{m},s}\hat{n}_{\boldsymbol{n},s'} + H_{ph}\ . \tag{8.8}$$

As follows from the above equation, the LF-transformation allows to write the atomic Hamiltonian (8.1) in a very simplified form in which the electron-phonon interaction has been included in the renormalized hopping operator:

$$\hat{\sigma}_{ij} \equiv T_{ij}\hat{X}_i^\dagger \hat{X}_j\ , \tag{8.9}$$

where:

$$\hat{X}_i \equiv \exp\left[\sum_{\boldsymbol{q}}\left(u(\boldsymbol{m},\boldsymbol{q})\hat{d}_q - u^*(\boldsymbol{m},\boldsymbol{q})\hat{d}_q^\dagger\right)\right]\ , \tag{8.10}$$

and the chemical potential is shifted by the polaron energy E_p:

$$\begin{cases} \tilde{\mu} \equiv \mu + E_p \\ E_p \equiv \frac{2\pi e^2}{\kappa}\int_{BZ}\frac{d^3q}{(2\pi)^3}\frac{1}{q^2} \end{cases}\ . \tag{8.11}$$

At this point, recalling the definition (8.4), it is immediate to note that in highly polarizable lattices with $\epsilon_0 \to \infty$, $\kappa \to \epsilon_\infty$. Hence Eq.8.8 reads as:

$$\tilde{H}_{HPL} = -\sum_{i,j}\left(\hat{\sigma}_{ij}\delta_{ss'} + \tilde{\mu}\delta_{ij}\right)\hat{c}_i^\dagger\hat{c}_j + H_{ph}\ . \tag{8.12}$$

Given the overall constraint $\kappa \to \epsilon_\infty$, the above Hamiltonian is exact and still contains all the relevant information about electron-electron and electron-phonon interactions since it follows from the application of the unitary LF-transformation (8.5) on the microscopic Hamiltonian (8.1). In particular one might note that, although the interaction term in (8.8) disappears, phononic degrees of freedom are still contained in the hopping operator $\hat{\sigma}_{ij}$ which is not just a mere renormalization of the bare hopping integral T_{ij} in (8.1). Its functional dependence on $\hat{X}_i$, given in Eq.8.9, accounts for all the possible multi-phonon transitions, making the Hamiltonian (8.12) a difficult and challenging task to deal with.

In the following Sections, the Hamiltonian (8.12), and its connection with high-temperature superconductivity, will be analyzed. Weak ($\lambda \lessapprox 0.5$) and strong ($\lambda \gtrapprox 0.5$) coupling regimes are analyzed in Section 8.1 and Section 8.2, respectively. Here $\lambda = 2E_p\mathcal{N}(0)$ is the electron-phonon coupling constant defined as a function of polaron level shift E_p (8.11) and density of state at the Fermi level $\mathcal{N}(0)$. We show that in both the limits the model allows a phase transition to a superconducting state characterized by bound states of two polarons with different values of the critical temperature.

8.1 Weak coupling regime

As it is well known, due to the presence of a quantum (exchange) interaction between two polarons, a two-particle bound state exists even in the weak-coupling regime, $\lambda \lessapprox 0.5$, and it is characterized by weakly coupled polarons which pair together at large distances forming the so-called large bipolaronic state [6]. These weakly coupled large pairs overlap in dense systems, so that their many-particle ground state is a BCS-like superconductor with Cooper pairs. In this case we have not only $\lambda \lessapprox 0.5$ but also a small number of phonons dressing the carrier resulting in $E_p/\hbar\omega_0 \ll 1$. In this limit we can expand $\hat{X}_i$ from Eq.8.10 in powers of $\gamma(\boldsymbol{q})$ keeping just single-phonon transitions therefore, from Eq.8.3 and Eq.8.10 we have:

$$\begin{aligned} \hat{X}_i &\equiv \exp\left[\sum_{\boldsymbol{q}} \frac{\gamma(\boldsymbol{q})}{\sqrt{2N}}\left(e^{i\boldsymbol{q}\cdot\boldsymbol{m}}\hat{d}_q - e^{-i\boldsymbol{q}\cdot\boldsymbol{m}}\hat{d}_q^\dagger\right)\right] = \\ &= 1 + \sum_{\boldsymbol{q}} \frac{\gamma(\boldsymbol{q})}{\sqrt{2N}}\left(e^{i\boldsymbol{q}\cdot\boldsymbol{m}}\hat{d}_q - e^{-i\boldsymbol{q}\cdot\boldsymbol{m}}\hat{d}_q^\dagger\right) + o\left(|\gamma(\boldsymbol{q})|^2\right) \ . \end{aligned} \tag{8.13}$$

According to this, the renormalized hopping parameter can be written as:

$$\begin{aligned} \hat{\sigma}_{ij} &\equiv T_{ij}\hat{X}_i^\dagger\hat{X}_j = T_{ij}\left[1 + \sum_{\boldsymbol{q}} \frac{\gamma(\boldsymbol{q})}{\sqrt{2N}}\left(e^{-i\boldsymbol{q}\cdot\boldsymbol{m}}\hat{d}_{\boldsymbol{q}}^\dagger - e^{i\boldsymbol{q}\cdot\boldsymbol{m}}\hat{d}_{\boldsymbol{q}}\right)\right] \\ &\quad \left[1 + \sum_{\boldsymbol{q'}} \frac{\gamma(\boldsymbol{q'})}{\sqrt{2N}}\left(e^{i\boldsymbol{q'}\cdot\boldsymbol{n}}\hat{d}_{\boldsymbol{q'}} - e^{-i\boldsymbol{q'}\cdot\boldsymbol{n}}\hat{d}_{\boldsymbol{q'}}^\dagger\right)\right] + o\left(|\gamma(\boldsymbol{q})|^2\right) = \\ &= T_{ij} + T_{ij}\sum_{\boldsymbol{q}} \frac{\gamma(\boldsymbol{q})}{\sqrt{2N}}\left[\left(e^{i\boldsymbol{q}\cdot\boldsymbol{n}} - e^{i\boldsymbol{q}\cdot\boldsymbol{m}}\right)\hat{d}_{\boldsymbol{q}} - \left(e^{-i\boldsymbol{q}\cdot\boldsymbol{n}} - e^{-i\boldsymbol{q}\cdot\boldsymbol{m}}\right)\hat{d}_{\boldsymbol{q}}^\dagger\right] + o\left(|\gamma(\boldsymbol{q})|^2\right) = \\ &\equiv \hat{\sigma}_{ij}^{(0)} + \hat{\sigma}_{ij}^{(1)} + o\left(|\gamma(\boldsymbol{q})|^2\right) \ , \end{aligned}$$

so, by substituting in (8.12), we obtain:

$$\tilde{H}_{HPL} = -\sum_{i,j}\left[\left(\hat{\sigma}_{ij}^{(0)} + \hat{\sigma}_{ij}^{(1)}\right)\delta_{ss'} + \tilde{\mu}\delta_{ij}\right]\hat{c}_i^\dagger\hat{c}_j + H_{ph} \ , \tag{8.14}$$

in which $\hat{\sigma}_{ij}^{(0)}$ and $\hat{\sigma}_{ij}^{(1)}$ represent the the zero and the first order in $\gamma(\boldsymbol{q})$ of the renormalized hopping integral $\hat{\sigma}_{ij}$:

$$\begin{cases} \hat{\sigma}_{ij}^{(0)} & \equiv T_{ij} \\ \hat{\sigma}_{ij}^{(1)} & \equiv T_{ij}\sum_{\boldsymbol{q}} \frac{\gamma(\boldsymbol{q})}{\sqrt{2N}}\left[\left(e^{i\boldsymbol{q}\cdot\boldsymbol{n}} - e^{i\boldsymbol{q}\cdot\boldsymbol{m}}\right)\hat{d}_{\boldsymbol{q}} - \left(e^{-i\boldsymbol{q}\cdot\boldsymbol{n}} - e^{-i\boldsymbol{q}\cdot\boldsymbol{m}}\right)\hat{d}_{\boldsymbol{q}}^\dagger\right] \end{cases} . \tag{8.15}$$

It is useful to write this Hamiltonian in the momentum space. Taking into account only the term proportional to $\hat{\sigma}_{ij}^{(0)}$ we get:

$$-\sum_{ij}\hat{\sigma}_{ij}^{(0)}\hat{c}_i^\dagger\hat{c}_j\delta_{s,s'} = -\sum_{ij}T_{ij}\hat{c}_i^\dagger\hat{c}_j\delta_{s,s'} = -\sum_{\boldsymbol{m},\boldsymbol{n},s}T(\boldsymbol{m}-\boldsymbol{n})\hat{c}_s^\dagger(\boldsymbol{m})\hat{c}_s(\boldsymbol{n}) =$$

$$= -\sum_{\boldsymbol{m},\boldsymbol{n},s} T(\boldsymbol{m}-\boldsymbol{n}) \sum_{k} e^{-i\boldsymbol{k}\cdot\boldsymbol{m}} \hat{c}^{\dagger}_{k,s} \sum_{k'} e^{i\boldsymbol{k'}\cdot\boldsymbol{n}} \hat{c}_{k',s} \ . \tag{8.16}$$

By introducing the vector $\boldsymbol{a} \equiv \boldsymbol{m} - \boldsymbol{n}$ the previous relation reads as:

$$\begin{aligned} -\sum_{ij} T_{ij} \hat{c}^{\dagger}_{i} \hat{c}_{j} \delta_{s,s'} &= -\sum_{\boldsymbol{a},s} \sum_{\boldsymbol{k},\boldsymbol{k'}} T(\boldsymbol{a}) \left(\sum_{\boldsymbol{m}} e^{-i\boldsymbol{m}\cdot(\boldsymbol{k}-\boldsymbol{k'})} \right) e^{-i\boldsymbol{k'}\cdot\boldsymbol{a}} \hat{c}^{\dagger}_{\boldsymbol{k},s} \hat{c}_{\boldsymbol{k'},s} = \\ &= -\sum_{\boldsymbol{a},s} \sum_{\boldsymbol{k},\boldsymbol{k'}} T(\boldsymbol{a}) \delta\left(\boldsymbol{k}-\boldsymbol{k'}\right) e^{-i\boldsymbol{k'}\cdot\boldsymbol{a}} \hat{c}^{\dagger}_{\boldsymbol{k},s} \hat{c}_{\boldsymbol{k'},s} = \\ &= \sum_{\boldsymbol{k},s} \left(-\sum_{\boldsymbol{a}} T(\boldsymbol{a}) e^{-i\boldsymbol{k}\cdot\boldsymbol{a}} \right) \hat{c}^{\dagger}_{\boldsymbol{k},s} \hat{c}_{\boldsymbol{k},s} \equiv \sum_{\boldsymbol{k},s} E_{\boldsymbol{k}} \hat{c}^{\dagger}_{\boldsymbol{k},s} \hat{c}_{\boldsymbol{k},s} \ , \end{aligned} \tag{8.17}$$

where we have defined:

$$E_{\boldsymbol{k}} \equiv -\sum_{\boldsymbol{a}} T(\boldsymbol{a}) e^{-i\boldsymbol{k}\cdot\boldsymbol{a}} \ . \tag{8.18}$$

For the term proportional to $\hat{\sigma}^{(1)}_{ij}$ we get instead:

$$\begin{aligned} -\sum_{ij} \hat{\sigma}^{(1)}_{ij} \hat{c}^{\dagger}_{i} \hat{c}_{j} \delta_{s,s'} &= -\sum_{ij} \sum_{\boldsymbol{q}} T_{ij} \frac{\gamma(\boldsymbol{q})}{\sqrt{2N}} \Big[\left(e^{i\boldsymbol{q}\cdot\boldsymbol{n}} - e^{i\boldsymbol{q}\cdot\boldsymbol{m}} \right) \hat{d}_{\boldsymbol{q}} \\ &\qquad - \left(e^{-i\boldsymbol{q}\cdot\boldsymbol{n}} - e^{-i\boldsymbol{q}\cdot\boldsymbol{m}} \right) \hat{d}^{\dagger}_{\boldsymbol{q}} \Big] \hat{c}^{\dagger}_{i} \hat{c}_{j} \delta_{s,s'} = \\ &= -\sum_{\boldsymbol{m},\boldsymbol{n},s} \sum_{\boldsymbol{k},\boldsymbol{k'},\boldsymbol{q}} T(\boldsymbol{m}-\boldsymbol{n}) \frac{\gamma(\boldsymbol{q})}{\sqrt{2N}} \Big[\left(e^{i\boldsymbol{q}\cdot\boldsymbol{n}} - e^{i\boldsymbol{q}\cdot\boldsymbol{m}} \right) \hat{d}_{\boldsymbol{q}} \\ &\qquad - \left(e^{-i\boldsymbol{q}\cdot\boldsymbol{n}} - e^{-i\boldsymbol{q}\cdot\boldsymbol{m}} \right) \hat{d}^{\dagger}_{\boldsymbol{q}} \Big] e^{-i\boldsymbol{k}\cdot\boldsymbol{m}} e^{i\boldsymbol{k'}\cdot\boldsymbol{n}} \hat{c}^{\dagger}_{\boldsymbol{k},s} \hat{c}_{\boldsymbol{k'},s} \ . \end{aligned}$$

By putting $\boldsymbol{q} \to -\boldsymbol{q}$ we have[1]:

$$\begin{aligned} -\sum_{ij} \hat{\sigma}^{(1)}_{ij} \hat{c}^{\dagger}_{i} \hat{c}_{j} \delta_{s,s'} &= -\sum_{\boldsymbol{m},\boldsymbol{n},s} \sum_{\boldsymbol{k},\boldsymbol{k'},\boldsymbol{q}} T(\boldsymbol{m}-\boldsymbol{n}) \frac{\gamma(\boldsymbol{q})}{\sqrt{2N}} \left(e^{i\boldsymbol{q}\cdot\boldsymbol{n}} - e^{i\boldsymbol{q}\cdot\boldsymbol{m}} \right) e^{-i\boldsymbol{k}\cdot\boldsymbol{m}} e^{i\boldsymbol{k'}\cdot\boldsymbol{n}} \\ &\qquad \left[\hat{d}_{\boldsymbol{q}} - \hat{d}^{\dagger}_{-\boldsymbol{q}} \right] \hat{c}^{\dagger}_{\boldsymbol{k},s} \hat{c}_{\boldsymbol{k'},s} = \\ &= -\sum_{\boldsymbol{m},\boldsymbol{n},s} \sum_{\boldsymbol{k},\boldsymbol{k'},\boldsymbol{q}} T(\boldsymbol{m}-\boldsymbol{n}) \frac{\gamma(\boldsymbol{q})}{\sqrt{2N}} \left(e^{i(\boldsymbol{q}+\boldsymbol{k'})\cdot\boldsymbol{n}} e^{-i\boldsymbol{k}\cdot\boldsymbol{m}} - e^{i(\boldsymbol{q}-\boldsymbol{k})\cdot\boldsymbol{m}} e^{i\boldsymbol{k'}\cdot\boldsymbol{n}} \right) \\ &\qquad \left[\hat{d}_{\boldsymbol{q}} - \hat{d}^{\dagger}_{-\boldsymbol{q}} \right] \hat{c}^{\dagger}_{\boldsymbol{k},s} \hat{c}_{\boldsymbol{k'},s} \ . \end{aligned}$$

[1] We recall that γ is an even function of $\boldsymbol{q}$ so that $\gamma(\boldsymbol{q}) = \gamma(-\boldsymbol{q})$

Once again, by defining the vector $\boldsymbol{a} \equiv \boldsymbol{m} - \boldsymbol{n}$ we get:

$$
\begin{aligned}
-\sum_{ij} \hat{\sigma}_{ij}^{(1)} \hat{c}_i^\dagger \hat{c}_j \delta_{s,s'} &= -\sum_{\boldsymbol{m},\boldsymbol{a},s} \sum_{\boldsymbol{k},\boldsymbol{k'},\boldsymbol{q}} T(\boldsymbol{a}) \frac{\gamma(\boldsymbol{q})}{\sqrt{2N}} \left(e^{i(\boldsymbol{q}+\boldsymbol{k'}-\boldsymbol{k})\cdot\boldsymbol{m}} e^{-i(\boldsymbol{q}+\boldsymbol{k'})\cdot\boldsymbol{a}} - e^{i(\boldsymbol{q}-\boldsymbol{k}+\boldsymbol{k'})\cdot\boldsymbol{m}} e^{-i\boldsymbol{k'}\cdot\boldsymbol{a}} \right) \\
&\quad \cdot \left[\hat{d}_{\boldsymbol{q}} - \hat{d}_{-\boldsymbol{q}}^\dagger \right] \hat{c}_{\boldsymbol{k},s}^\dagger \hat{c}_{\boldsymbol{k'},s} = \\
&= \sum_{\boldsymbol{k},\boldsymbol{k'},\boldsymbol{q},s} \frac{\gamma(\boldsymbol{q})}{\sqrt{2N}} \left[\sum_{\boldsymbol{m}} e^{i(\boldsymbol{q}+\boldsymbol{k'}-\boldsymbol{k})\cdot\boldsymbol{m}} \right] \left[E_{\boldsymbol{q}+\boldsymbol{k'}} - E_{\boldsymbol{k'}} \right] \left[\hat{d}_{\boldsymbol{q}} - \hat{d}_{-\boldsymbol{q}}^\dagger \right] \hat{c}_{\boldsymbol{k},s}^\dagger \hat{c}_{\boldsymbol{k'},s} = \\
&= \sum_{\boldsymbol{k},\boldsymbol{k'},\boldsymbol{q},s} \frac{\gamma(\boldsymbol{q})}{\sqrt{2N}} \delta\left(\boldsymbol{q}+\boldsymbol{k'}-\boldsymbol{k}\right) \left[E_{\boldsymbol{q}+\boldsymbol{k'}} - E_{\boldsymbol{k'}} \right] \left[\hat{d}_{\boldsymbol{q}} - \hat{d}_{-\boldsymbol{q}}^\dagger \right] \hat{c}_{\boldsymbol{k},s}^\dagger \hat{c}_{\boldsymbol{k'},s} = \\
&= \sum_{\boldsymbol{k},\boldsymbol{q},s} \frac{\gamma(\boldsymbol{q})}{\sqrt{2N}} \left[E_{\boldsymbol{k}} - E_{\boldsymbol{k}-\boldsymbol{q}} \right] \left[\hat{d}_{\boldsymbol{q}} - \hat{d}_{-\boldsymbol{q}}^\dagger \right] \hat{c}_{\boldsymbol{k},s}^\dagger \hat{c}_{\boldsymbol{k}-\boldsymbol{q},s} \ .
\end{aligned}
$$

Finally, by putting $\boldsymbol{k} \to \boldsymbol{k} + \boldsymbol{q}$ we obtain:

$$
\begin{aligned}
-\sum_{ij} \hat{\sigma}_{ij}^{(1)} \hat{c}_i^\dagger \hat{c}_j \delta_{s,s'} &= \sum_{\boldsymbol{k},\boldsymbol{q},s} \frac{\gamma(\boldsymbol{q})}{\sqrt{2N}} \left(E_{\boldsymbol{k}+\boldsymbol{q}} - E_{\boldsymbol{k}} \right) \left(\hat{d}_{\boldsymbol{q}} - \hat{d}_{-\boldsymbol{q}}^\dagger \right) \hat{c}_{\boldsymbol{k}+\boldsymbol{q},s}^\dagger \hat{c}_{\boldsymbol{k},s} = \\
&\equiv \sum_{\boldsymbol{k},\boldsymbol{q},s} \tilde{M}(\boldsymbol{k},\boldsymbol{q}) \hat{c}_{\boldsymbol{k}+\boldsymbol{q},s}^\dagger \hat{c}_{\boldsymbol{k},s} \left(\hat{d}_{\boldsymbol{q}} - \hat{d}_{-\boldsymbol{q}}^\dagger \right) \ , \qquad (8.19)
\end{aligned}
$$

where we have defined:

$$
\tilde{M}(\boldsymbol{k},\boldsymbol{q}) \equiv \frac{\gamma(\boldsymbol{q})}{\sqrt{2N}} \left(E_{\boldsymbol{k}+\boldsymbol{q}} - E_{\boldsymbol{k}} \right) \ . \qquad (8.20)
$$

Joining together the contributions (8.17) and (8.19), the transformed Hamiltonian in highly polarizable lattices (8.12) reads as:

$$
\tilde{H}_{HPL}^{WC} = \sum_{\boldsymbol{k},s} \xi_{\boldsymbol{k}} \hat{c}_{\boldsymbol{k},s}^\dagger \hat{c}_{\boldsymbol{k},s} + \sum_{\boldsymbol{k},\boldsymbol{q},s} \tilde{M}(\boldsymbol{k},\boldsymbol{q}) \hat{c}_{\boldsymbol{k}+\boldsymbol{q},s}^\dagger \hat{c}_{\boldsymbol{k},s} \left(\hat{d}_{\boldsymbol{q}} - \hat{d}_{-\boldsymbol{q}}^\dagger \right) + H_{ph} \ , \qquad (8.21)
$$

Applying the BCS-Eliashberg formalism [40] yields the master equation for the superconducting order parameter $\Delta(\Omega_n, \boldsymbol{k})$:

$$
\Delta(\Omega_n, \boldsymbol{k}) = k_B T \sum_{\boldsymbol{k'},\Omega_{n'}} \frac{\tilde{M}(\boldsymbol{k},\boldsymbol{k}-\boldsymbol{k'})^2 D(\Omega_n - \Omega_{n'}) \Delta(\Omega_{n'}, \boldsymbol{k'})}{\Omega_{n'}^2 + \xi_{\boldsymbol{k'}}^2 + \left| \Delta(\Omega_{n'}, \boldsymbol{k'}) \right|^2} \ , \qquad (8.22)
$$

where $D(\Omega_n - \Omega_{n'})$ is the phonon propagator:

$$
D(\Omega_n - \Omega_{n'}) \equiv -\frac{\hbar\omega_0}{\left(\Omega_n - \Omega_{n'}\right)^2 + \hbar^2\omega_0^2} \ , \qquad (8.23)
$$

and Ω_n are the Matsubara frequencies:

$$
\Omega_n = \pi k_B T (2n+1) \ . \qquad (8.24)
$$

Depending on the particular shape of the band dispersion, equation (8.22) allows for different symmetries of the order parameter since the electron-phonon interaction is not local [39]. Here we confine our analysis to a simple estimate of the superconducting critical temperature T_c by assuming a k-independent gap function: $\Delta(\Omega_{n'}, \boldsymbol{k'}) \approx \Delta(\Omega_{n'})$. Factorizing the kernel of (8.22) on the "mass shell", we have $E(\boldsymbol{k'}) - E(\boldsymbol{k}) = \Omega_{n'} - \Omega_n$. Due to this no k' dependence appears except into $\xi^2_{\boldsymbol{k'}}$ so we can transform the sum over $\boldsymbol{k'}$ into an integral with respect to ξ and obtain:

$$\Delta(\Omega_n) = k_B T \sum_{\omega_{n'}} K(\Omega_n - \Omega_{n'}) \Delta(\Omega_{n'}) \int_{-\infty}^{+\infty} \frac{d\xi}{\Omega^2_{n'} + \xi^2 + |\Delta(\Omega_{n'})|^2} \, , \tag{8.25}$$

in which, hereafter, we denote with $K(\Omega_n - \Omega_{n'})$ the kernel of the equation. At $T = T_c$ we can neglect second and higher powers of the order parameter: $|\Delta(\Omega_{n'})|^2_{T=T_c} \approx 0$ so, by integrating over ξ, we get:

$$\Delta(\Omega_n) = \pi k_B T_c \sum_{\Omega_{n'}} K(\Omega_n - \Omega_{n'}) \frac{\Delta(\Omega_{n'})}{|\Omega_{n'}|} \, . \tag{8.26}$$

Let us now adopt the BCS-like approximation for the kernel:

$$K(\Omega_n - \Omega_{n'}) \approx \lambda \Theta\left(\hbar\omega_0 - |\Omega_n|\right) \Theta\left(\hbar\omega_0 - |\Omega_{n'}|\right) - \mu_c \Theta\left(2\hbar\omega_C - |\Omega_n|\right) \Theta\left(2\hbar\omega_C - |\Omega_{n'}|\right) \, , \tag{8.27}$$

where $\hbar\omega_C$ is the Coulomb frequency which defines the electronic cut-off frequency given by the constraint $\pi k_B T_c \ll \hbar\omega_0 \ll \hbar\omega_C$. Here λ is the electron-phonon interaction constant of the BCS-Eliashberg theory while μ_c parametrizes the Coulomb interaction and can be expressed in terms of the Fourier component of the Coulomb potential V_c and the electronic density of states $N(\varepsilon)$ as follows:

$$\mu_c \equiv V_c N(E_F) \, . \tag{8.28}$$

Because of the constraint $\pi k_B T_c \ll \hbar\omega_0 \ll \hbar\omega_C$ we can replace the summation over all the Matsubara frequencies by the integral:

$$\pi k_B T_c \sum_{\Omega_{n'}} \approx \int_{\pi k_B T_c}^{\infty} d\omega' \, , \tag{8.29}$$

and obtain:

$$\begin{aligned} \Delta(\omega) \;\; = \;\; & \int_{\pi k_B T_c}^{\infty} \frac{\Delta(\omega')}{|\omega'|} \Big[\lambda \Theta\left(\hbar\omega_0 - |\omega'|\right) \Theta\left(\hbar\omega_0 - |\omega'|\right) \\ & - \mu_c \Theta\left(2\hbar\omega_C - |\omega'|\right) \Theta\left(2\hbar\omega_C - |\omega'|\right) \Big] d\omega' \, . \end{aligned} \tag{8.30}$$

This equation allows solutions of the form:

$$\Delta(\omega) = \Delta_1 \Theta\left(\hbar\omega_0 - |\omega|\right) + \Delta_2 \Theta\left(2\hbar\omega_C - |\omega|\right) \Theta\left(|\omega| - \hbar\omega_0\right) \, , \tag{8.31}$$

in which Δ_1 and Δ_2 are the two constant values that the order parameter assumes

for $|\omega| < \hbar\omega_0$ and $\hbar\omega_0 \leq |\omega| \leq 2\hbar\omega_C$, respectively. By substituting equation (8.31) into (8.30) and integrating with respect to ω' we have:

$$\begin{aligned}
\Delta_1 &= (\lambda - \mu_c) \int_{\pi k_B T_c}^{\hbar\omega_0} d\omega' \frac{\Delta_1}{\omega'} - \mu_c \int_{\hbar\omega_0}^{2\hbar\omega_C} d\omega' \frac{\Delta_2}{\omega'} = \\
&= \Delta_1 (\lambda - \mu_c) \ln\left(\frac{\hbar\omega_0}{\pi k_B T_c}\right) - \Delta_1 \mu_c \ln\left(\frac{\hbar\omega_0}{\pi k_B T_c}\right) - \Delta_2 \mu_c \ln\left(\frac{2\hbar\omega_C}{\hbar\omega_0}\right) , \\
\Delta_2 &= -\mu_c \int_{\pi k_B T_c}^{\hbar\omega_0} d\omega' \frac{\Delta_1}{\omega'} - \mu_c \int_{\hbar\omega_0}^{2\hbar\omega_C} d\omega' \frac{\Delta_2}{\omega'} = \\
&= -\Delta_1 \mu_c \ln\left(\frac{\hbar\omega_0}{\pi k_B T_c}\right) - \Delta_2 \mu_c \ln\left(\frac{2\hbar\omega_C}{\hbar\omega_0}\right) .
\end{aligned}$$

Collecting together these two results we get a set of two coupled linear equations with respect to the two variables Δ_1 and Δ_2:

$$\begin{cases} \Delta_1 \left[1 - (\lambda - \mu_c) \ln\left(\frac{\hbar\omega_0}{\pi k_B T_c}\right)\right] + \Delta_2 \left[\mu_c \ln\left(\frac{2\omega_C}{\omega_0}\right)\right] = 0 \\ \Delta_1 \left[\mu_c \ln\left(\frac{\hbar\omega_0}{\pi k_B T_c}\right)\right] + \Delta_2 \left[1 + \mu_c \ln\left(\frac{2\omega_C}{\omega_0}\right)\right] = 0 \end{cases} , \tag{8.32}$$

that admits a non trivial solution only if:

$$\left[1 - (\lambda - \mu_c) \ln\left(\frac{\hbar\omega_0}{\pi k_B T_c}\right)\right] [1 + \mu_c L] - \mu_c^2 L \ln\left(\frac{\hbar\omega_0}{\pi k_B T_c}\right) = 0 ,$$

in which, for the sake of simplicity, we have labeled L the "Tolmachev-Morel-Anderson" logarithm:

$$L \equiv \ln\left(\frac{2\omega_C}{\omega_0}\right) . \tag{8.33}$$

This equation can be used for a simple estimation of T_c in fact, by solving with respect to T_c, we have:

$$\ln\left(\frac{\hbar\omega_0}{\pi k_B T_c}\right) = \frac{1 + \mu_c L}{\lambda (1 + \mu_c L) - \mu_c} , \tag{8.34}$$

that gives:

$$k_B T_c = \frac{\hbar\omega_0}{\pi} \exp\left(-\frac{1}{\lambda - \mu_c^*}\right) , \tag{8.35}$$

where μ_c^* is the Coulomb pseudo-potential defined as:

$$\mu_c^* \equiv \frac{\mu_c}{1 + \mu_c L} = \frac{\mu_c}{1 + \mu_c \ln(2\omega_C/\omega_0)} . \tag{8.36}$$

This remarkable result, which explains why, at least for conventional superconductors, a weak electron-phonon interaction can drive superconductivity rather than the strong Coulomb repulsion, simply represents the macroscopic manifestation of the retarded nature of the electron-phonon interaction. The electron-phonon interaction, in fact, acts well after two electrons meet each other and such a time delay

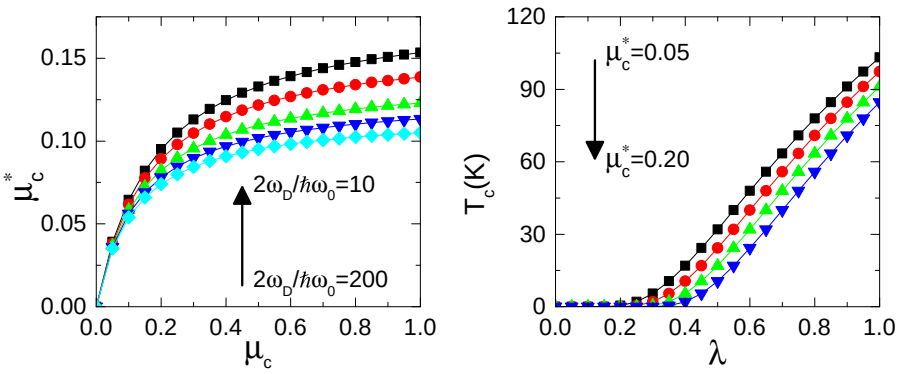

Figure 8.1: Left panel: Coulomb pseudo-potential versus μ_c from from Eq.8.36 for different values of the ratio $2\omega_C/\hbar\omega_0$. Right panel: weak coupling estimate of the superconductive critical temperature (Eq.8.35) versus λ for different values of the Coulomb pseudo-potential μ_c^*.

is sufficient for two electrons to be separated by a relative distance at which the Coulomb repulsion is small [38]. Hence, Cooper pairs are preserved even for large values of μ_c since its contribution is strongly suppressed by $\ln^{-1}(2\omega_C/\hbar\omega_0)$.

Importantly, one might immediately note that, as reported in Fig.8.1, with the typical values $\lambda = 0.5$, $\mu_c^* = 0.14$ and with the Debye energy $\hbar\omega_C = 400K$, one immediately obtains from Eq.8.35 $T_c \approx 20K$ which correctly describes simple metals and alloys but is clearly too low to be consistent with experimental data for high-temperature superconductors. A higher critical temperature requires larger values of λ which are in contrast with the standard formulation of the Migdal-Eliashberg theory whose applicability is restricted in the region for $\lambda < 1$[41, 40].

8.2 Strong coupling regime: the polaronic $t - J_p$ Hamiltonian

In the case of two-dimensional systems, by approximating the density of states per spin at the Fermi level as $\mathcal{N}(0) \approx ma^2/2\pi\hbar^2$, one immediately obtains $E_p \sim eV$ [42] which put $\lambda = 2E_p\mathcal{N}(0) \gtrapprox 0.5$ for a large class of compounds. Actually $E_p/\hbar\omega_0 \gg 1$ in oxides and some other polar lattices, with the characteristic (oxygen) optical phonon energy $\hbar\omega_0 \lesssim 80meV$. In this regime finite bandwidth [43, 44] and multi-phonon vertex [45, 46] corrections are essential in the expansion of the hopping operator $\hat{\sigma}_{ij}$ therefore, in order to deal with this challenging problem, one might think to single out the coherent hopping term in (8.12) by averaging $\hat{\sigma}_{ij}$ with respect to the phonon vacuum and considering the remaining part as perturbation. Following this procedure, Eq.8.12 reads:

$$\tilde{H}_{HPL} = H_0 + H_{p-ph} \ , \tag{8.37}$$

where:

$$H_0 \equiv -\sum_{i,j} \left(\langle\hat{\sigma}_{ij}\rangle \, \delta_{s,s'} + \tilde{\mu}\delta_{ij}\right) c_i^\dagger c_j + H_{ph} \ , \tag{8.38}$$

describes free phonons and polarons coherently propagating in a narrow band and:

$$H_{p-ph} = \sum_{i,j} \left(\langle \hat{\sigma}_{ij} \rangle - \hat{\sigma}_{ij} \right) \delta_{ss'} c_i^\dagger c_j \ , \tag{8.39}$$

is the residual multipolaron interaction, which is a perturbation at large λ.

In order to calculate the average of the renormalized hopping operator let us recall the result (D.15). In the limit in which $0 \approx k_B T \ll \hbar\omega_0$, the Bose-Einstein distribution function n_ω does not contribute ($n_\omega \approx 0$) and we obtain:

$$\langle \hat{X}_i^\dagger \hat{X}_j \rangle \ = \ \prod_q \exp \left\{ -\frac{\gamma(q)^2}{2N} \left[1 - \cos\left(\boldsymbol{q} \cdot (\boldsymbol{m} - \boldsymbol{n}) \right) - i \sin\left(\boldsymbol{q} \cdot (\boldsymbol{m} - \boldsymbol{n}) \right) \right] \right\} \ .$$

If the lattice has an inversion symmetry, the above relation has to be invariant under the transformation $\boldsymbol{q} \to -\boldsymbol{q}$. Hence, recalling that $\gamma(\boldsymbol{q}) = \gamma(-\boldsymbol{q})$ from (8.3), the term proportional to the sine function cancels by parity and we get:

$$\langle \hat{X}_i^\dagger \hat{X}_j \rangle \ = \ \prod_q \exp \left\{ -\frac{\gamma(q)^2}{2N} \left[1 - \cos\left(\boldsymbol{q} \cdot (\boldsymbol{m} - \boldsymbol{n}) \right) \right] \right\} \ .$$

Recalling the expression of the renormalized hopping parameter (8.9), we can now define:

$$\langle \hat{\sigma}_{ij} \rangle \equiv t_{ij} = T\left(\boldsymbol{m} - \boldsymbol{n} \right) \exp\left[-g^2\left(\boldsymbol{m} - \boldsymbol{n} \right) \right] \ , \tag{8.40}$$

where:

$$g^2(\boldsymbol{m}) = \frac{1}{2N} \sum_q \gamma(q)^2 \left[1 - \cos\left(\boldsymbol{q} \cdot \boldsymbol{m} \right) \right] \ . \tag{8.41}$$

The average of H_{ph} with respect to the phonon vacuum gives no contribution, therefore the whole averaged unperturbed Hamiltonian reads as:

$$\mathcal{H}_0 \equiv \langle 0 | \, H_0 \, | 0 \rangle = -\sum_{i,j} \left(t_{ij} \delta_{s,s'} + \tilde{\mu} \delta_{ij} \right) c_i^\dagger c_j \ . \tag{8.42}$$

Let us now focus our analysis on the perturbation H_{p-ph} making a perturbative expansion and projecting each term with respect to to the phonon vacuum. It can be seen that H_{p-ph} has no diagonal matrix elements with respect to phonon occupation number. Hence the first order in the perturbation expansion can be removed by means of a standard Schrieffer-Wolf canonical transformation [47] $\mathcal{H} = e^{S_2} H_{HPL} e^{-S_2}$. According to the Baker-Hausdorff formula we have:

$$\begin{aligned} \mathcal{H} \ \equiv \ & e^{S_2} \tilde{H}_{HPL} e^{-S_2} = \tilde{H}_{HPL} + \left[S_2, \tilde{H}_{HPL} \right] + \frac{1}{2} \left[S_2, \left[S_2, \tilde{H}_{HPL} \right] \right] \\ & + \frac{1}{3!} \left[S_2, \left[S_2, \left[S_2, \tilde{H}_{HPL} \right] \right] \right] + \dots \ , \end{aligned} \tag{8.43}$$

so, recalling that $\tilde{H}_{HPL} = H_0 + H_{p-ph}$ we get:

$$\mathcal{H} = H_0 + H_{p-ph} + [S_2, H_0] + [S_2, H_{p-ph}] + \frac{1}{2}[S_2, [S_2, H_0]] + \frac{1}{2}[S_2, [S_2, H_{p-ph}]] + \dots \ . \tag{8.44}$$

From the previous relation it is immediate to note that, by choosing S_2 such that:

$$H_{p-ph} + [S_2, H_0] = 0 \ , \tag{8.45}$$

we succeed in eliminating the contribution at the first order in the perturbative expansion. In this case S_2 reads as :

$$(S_2)_{nn'} = \sum_{i,j} \frac{\langle n' | \left(\hat{\sigma}_{ij} - t_{ij}\right) c_i^\dagger c_j | n \rangle}{E_{n'} - E_n} \ , \tag{8.46}$$

where E_n, $E_{n'}$ and $|n\rangle$, $|n'\rangle$ are the energy levels and the eigenstates of H_0, respectively. Neglecting all the terms up to the second order we obtain:

$$\mathcal{H} \ \approx \ \mathcal{H}_0 + \mathcal{H}_{(II)} \ , \tag{8.47}$$

where $\mathcal{H}_{(II)}$ contains the projection of the second order term in the perturbation expansion with respect to the phonon vacuum:

$$\mathcal{H}_{(II)} \equiv -\frac{1}{2} \sum_{i \neq j, i' \neq j'} \sum_{m \neq 0} \frac{\langle 0 | \left(t_{ij} - \hat{\sigma}_{ij}\right) c_i^\dagger c_j \, | m \rangle \, \langle m | \left(t_{ij} - \hat{\sigma}_{ij}\right) c_{i'}^\dagger c_{j'} \, | 0 \rangle}{E_m - E_n} \ . \tag{8.48}$$

in which the intermediate states $|m\rangle$ are referred to a generic configuration characterized by any number of phonons. Recalling that t_{ij} is a constant defined by the average of the renormalized hopping parameter $\hat{\sigma}_{ij}$ with respect to the phonon vacuum, due to the orthogonality of the basis we have:

$$\begin{cases} \langle 0 | t_{ij} | m \rangle = t_{ij} \langle 0 | m \rangle = 0 \\ \langle m | t_{ij} | 0 \rangle = t_{ij} \langle m | 0 \rangle = 0 \end{cases} \ , \tag{8.49}$$

therefore the previous expression reads as:

$$\mathcal{H}_{(II)} = \sum_{i \neq j, i' \neq j'} \sum_{m} c_i^\dagger c_j c_{i'}^\dagger c_{j'} T_{ij} T_{i'j'} \frac{\langle 0 | \, X_i^\dagger X_j \, | m \rangle \, \langle m | \, X_{i'}^\dagger X_{j'} \, | 0 \rangle}{E_m - E_0} \ . \tag{8.50}$$

We can also note that, in the strong-coupling regime, the polaron Fermi energy is small compared with the phonon energy:

$$\frac{1}{E_m - E_0} \approx \frac{1}{\hbar\omega_0 \sum_{\boldsymbol{q}} n_{\boldsymbol{q}}} = i \int_0^\infty dt e^{it\hbar\omega_0 \sum_{\boldsymbol{q}} n_{\boldsymbol{q}}^{(m)}} \ , \tag{8.51}$$

and $\mathcal{H}_{(II)}$ can be written as:

$$\mathcal{H}_{(II)} = i \sum_{i \neq j, i' \neq j'} c_i^\dagger c_j c_{i'}^\dagger c_{j'} T_{ij} T_{i'j'} \int_0^{+\infty} \langle\langle X_i^\dagger(t) X_j(t) X_{i'}^\dagger X_{j'} \rangle\rangle dt \ , \tag{8.52}$$

where $X_i^\dagger(t)$ and $X_j(t)$ represent the standard multi-phonon operators (8.10) in the Heisenberg representation: $X_i(t) = e^{\frac{i}{\hbar}\mathcal{H}t} X_i e^{-\frac{i}{\hbar}\mathcal{H}t}$. Hereafter we put:

$$\begin{aligned} X_i(t) &= \exp\left[\sum_{\boldsymbol{q}} \left(u(\boldsymbol{m}, \boldsymbol{q}) \hat{d}_q e^{i\omega_0 t} - u^*(\boldsymbol{m}, \boldsymbol{q}) \hat{d}_q^\dagger e^{-i\omega_0 t} \right)\right] = \\ &\equiv \exp\left[\sum_{\boldsymbol{q}} \left(u_{\boldsymbol{q}}(\boldsymbol{m}, t) \hat{d}_q - u_{\boldsymbol{q}}^*(\boldsymbol{m}, t) \hat{d}_q^\dagger \right)\right] \ . \end{aligned} \tag{8.53}$$

For $k_B T \ll 1$, analytical calculations reported in Appendix D.1 show that:

$$\langle\langle X_i^\dagger(t) X_j(t) X_{i'}^\dagger X_{j'} \rangle\rangle = e^{-g^2(\boldsymbol{m}-\boldsymbol{n})} e^{-g^2(\boldsymbol{m'}-\boldsymbol{n'})} e^{f(\boldsymbol{m},\boldsymbol{n};\boldsymbol{m'},\boldsymbol{n'}) e^{-i\hbar\omega_0 t}} \ , \tag{8.54}$$

where:

$$\begin{aligned} f(\boldsymbol{m}, \boldsymbol{n}; \boldsymbol{m'}, \boldsymbol{n'}) \ \equiv \ & \sum_{\boldsymbol{q}} \frac{\gamma^2(\boldsymbol{q})}{2N} \left[\cos\left(\boldsymbol{q} \cdot (\boldsymbol{m} - \boldsymbol{n'})\right) + \cos\left(\boldsymbol{q} \cdot (\boldsymbol{n} - \boldsymbol{m'})\right) + \right. \\ & \left. - \cos\left(\boldsymbol{q} \cdot (\boldsymbol{m} - \boldsymbol{m'})\right) - \cos\left(\boldsymbol{q} \cdot (\boldsymbol{n} - \boldsymbol{n'})\right) \right] \ . \end{aligned} \tag{8.55}$$

Substituting in the previous equation and recalling that $t_{ij} \equiv T_{ij} e^{-g^2(m-n)}$ we obtain:

$$\mathcal{H}_{(II)} = i \sum_{i \neq j, i' \neq j'} c_i^\dagger c_j c_{i'}^\dagger c_{j'} t_{ij} t_{i'j'} \int_0^{+\infty} e^{f(\boldsymbol{m},\boldsymbol{n};\boldsymbol{m'},\boldsymbol{n'}) e^{-i\hbar\omega_0 t}} dt \ . \tag{8.56}$$

It can be seen that [48]:

$$\int_0^\infty \exp\left\{-a e^{nx}\right\} dx = -\frac{1}{n} Ei(-a) \ , \tag{8.57}$$

where $Ei(x)$ is the exponential integral function which, for finite and non-zero values of x, is defined as:

$$Ei(x) = \int_{-\infty}^{x} \frac{e^y}{y} dy = c + \ln\left(|x|\right) + \sum_{k=1}^{\infty} \frac{x^k}{k! k} \tag{8.58}$$

and c is the Euler constant:

$$c \equiv \lim_{n \to \infty} \left(1 + \frac{1}{2} + \cdots + \frac{1}{n} - \ln(n) \right) \approx 0.57721566490 \ . \tag{8.59}$$

In our case $a = -f(\boldsymbol{m},\boldsymbol{n};\boldsymbol{m'},\boldsymbol{n'})$ and $n = -i\hbar\omega_0$ so:

$$\mathcal{H}_{(II)} = \sum_{i\neq j, i'\neq j'} c_i^\dagger c_j c_{i'}^\dagger c_{j'} \frac{t_{ij}t_{i'j'}}{\hbar\omega_0} E_i(f(\boldsymbol{m},\boldsymbol{n};\boldsymbol{m'},\boldsymbol{n'})) \; . \tag{8.60}$$

Collecting together the zero and the second order terms, projected onto the phonon vacuum, we finally obtain:

$$\mathcal{H}_{HPL}^{SC} = -\sum_{i,j} \left(t_{ij}\delta_{s,s'} + \tilde{\mu}\delta_{ij}\right) c_i^\dagger c_j - \sum_{\boldsymbol{m}\neq\boldsymbol{n}} \sum_{s,s'} V_{\boldsymbol{mn}}^{\boldsymbol{m'n'}} c_s^\dagger(\boldsymbol{m}) c_s(\boldsymbol{n}) c_{s'}^\dagger(\boldsymbol{m'}) c_{s'}(\boldsymbol{n'}) \; , \tag{8.61}$$

where:

$$V_{\boldsymbol{mn}}^{\boldsymbol{m'n'}} \equiv \frac{t_{ij}t_{i'j'}}{\hbar\omega_0} E_i(f(\boldsymbol{m},\boldsymbol{n};\boldsymbol{m'},\boldsymbol{n'})) \; . \tag{8.62}$$

Starting from the above relation, one can immediately note that all matrix elements of the polaron-polaron interaction (8.62) are small compared with the polaron kinetic energy except the contribution: $J_p(\boldsymbol{m}-\boldsymbol{n}) \equiv V_{\boldsymbol{mn}}^{\boldsymbol{nm}}$ such that $f(\boldsymbol{m},\boldsymbol{n};\boldsymbol{m'},\boldsymbol{n'}) = 2g^2(\boldsymbol{m}-\boldsymbol{n})$. Hence, using $E_i(y) \approx e^y/y$ (for large y) one obtains the following substantial exchange interaction:

$$J_p(\boldsymbol{m}-\boldsymbol{n}) = \frac{t_{ij}t_{i'j'}}{\hbar\omega_0} \frac{e^{2g^2(\boldsymbol{m}-\boldsymbol{n})}}{2g^2(\boldsymbol{m}-\boldsymbol{n})} = \frac{T^2(\boldsymbol{m}-\boldsymbol{n})}{2\hbar\omega_0 g^2(\boldsymbol{m}-\boldsymbol{n})} \; , \tag{8.63}$$

that is much larger than the polaron hopping integral in the strong coupling limit:

$$\frac{t_{ij}}{J_p(\boldsymbol{m}-\boldsymbol{n})} \propto \frac{2\hbar\omega_0 g^2(\boldsymbol{m}-\boldsymbol{n})}{T^2(\boldsymbol{m}-\boldsymbol{n})} T(\boldsymbol{m}-\boldsymbol{n}) e^{-g^2(\boldsymbol{m}-\boldsymbol{n})} = \frac{2\hbar\omega_0 g^2(\boldsymbol{m}-\boldsymbol{n})}{T(\boldsymbol{m}-\boldsymbol{n})} e^{-g^2(\boldsymbol{m}-\boldsymbol{n})} \ll 1 \; . \tag{8.64}$$

It can be also seen that, in the case in which $\boldsymbol{n'} = \boldsymbol{m}$ and $\boldsymbol{m'} = \boldsymbol{n}$, the operatorial part of the interaction term can be written as:

$$c_s^\dagger(\boldsymbol{m}) c_s(\boldsymbol{n}) c_{s'}^\dagger(\boldsymbol{n}) c_{s'}(\boldsymbol{m}) \;\; = \;\; 2\delta_{\boldsymbol{m},\boldsymbol{n}} c_s^\dagger(\boldsymbol{m}) c_s(\boldsymbol{m}) - c_s^\dagger(\boldsymbol{m}) c_{s'}(\boldsymbol{m}) c_{s'}^\dagger(\boldsymbol{n}) c_s(\boldsymbol{n}) \tag{8.65}$$

The first term further renormalizes the chemical potential. Making the sum over all spin and lattice indices, we obtain:

$$\tilde{\tilde{\mu}} \equiv \tilde{\mu} + 2\sum_{\boldsymbol{m}} J_p(\boldsymbol{m}) \; . \tag{8.66}$$

The remaining term, as shown in detail in Appendix D.2, can be written in the following form:

$$\sum_{\boldsymbol{m}\neq\boldsymbol{n}} \sum_{s,s'} J_p(\boldsymbol{m}-\boldsymbol{n}) c_s^\dagger(\boldsymbol{m}) c_{s'}(\boldsymbol{m}) c_{s'}^\dagger(\boldsymbol{n}) c_s(\boldsymbol{n}) = 2\sum_{\boldsymbol{m}\neq\boldsymbol{n}} J_p(\boldsymbol{m}-\boldsymbol{n}) \left(\overrightarrow{S}_{\boldsymbol{m}} \cdot \overrightarrow{S}_{\boldsymbol{n}} + \frac{1}{4}\hat{n}_{\boldsymbol{m}}\hat{n}_{\boldsymbol{n}} \right) \; , \tag{8.67}$$

where $\overrightarrow{S}_{\boldsymbol{i}}$ is the spin-1/2 operator defined in terms of the Pauli matrices $\overrightarrow{\tau}$ as:

$$\overrightarrow{S}_{\boldsymbol{i}} \equiv \sum_{s,s'} c_s^{\dagger}(\boldsymbol{i}) \left(\overrightarrow{\tau}\right)_{s,s'} c_{s'}(\boldsymbol{i}) \ , \tag{8.68}$$

while $\hat{n}_{\boldsymbol{i}}$ is the standard density operator: $\hat{n}_{\boldsymbol{i}} = \sum_s c_s^{\dagger}(\boldsymbol{i}) c_s(\boldsymbol{i})$. Joining together all the contributions we finally arrive with the polaronic "t-J_p" Hamiltonian:

$$\mathcal{H} = -\sum_{i,j} \left(t_{ij}\delta_{s,s'} + \tilde{\tilde{\mu}}\delta_{ij}\right) c_i^{\dagger} c_j + 2 \sum_{\boldsymbol{m}\neq\boldsymbol{n}} J_p(\boldsymbol{m}-\boldsymbol{n}) \left(\overrightarrow{S}_{\boldsymbol{m}} \cdot \overrightarrow{S}_{\boldsymbol{n}} + \frac{1}{4}\hat{n}_{\boldsymbol{m}}\hat{n}_{\boldsymbol{n}}\right) \ . \tag{8.69}$$

It is worth noting that there is a striking difference between this polaronic t-J_p Hamiltonian and the familiar t-J model derived from the repulsive Hubbard-U model in the limit $U \gg t$ omitting the so-called three-site hoppings and EPI [49]. In the polaronic t-J_p Hamiltonian the bare hopping integral T_{ij}, as appears in Eq.8.1, is renormalized by the strong EPI which results in the polaronic band narrowing factor $\exp(-g^2)$ reported in Eq.8.40. Hence, unlike in the $t-J$ model, the kinetic term in Eq.8.69 describes the motion of strongly inter-correlated fermions in the presence of *unscreened* long-range Coulomb and electron-phonon interactions. The momentum-dependence of the phononic degrees of freedoms is intrinsically contained in t_{ij} via g^2 , leading to a substantial reduction of the polaronic band narrowing factor $\exp(-g^2)$ if the $\boldsymbol{q}$-dependence of γ is neglected. This feature, that would eliminate any possibility of high temperature superconductivity and even metallicity for small Holstein polarons, leads to the formation of small and perfectly mobile pairs of polarons in the case of the long-range (Fröhlich) EPI, as confirmed by recent Quantum Monte-Carlo studies [30, 31, 29, 32, 33]. Furthermore, the exchange interaction J_p, of pure phononic origin, is not merely related to spin-flip hoppings as in the standard $t-J$ model. As it will be shown later in Chapter 9, J_p describes the spin exchange of carriers doped into polar insulators as, for instance, oxygen holes in the Cuprates, rather than antiferromagnetic correlations of copper spins in the parent insulator (which are well described by the conventional J). Therefore J_p is responsible for the formation of two-particle bound states and, importantly, can be determined through the real material parameters ($J_p > 0$) as a function of the bare hopping integral T_{ij} which can be measured using first principle density functional theory in a parent polar insulator [50]. It is also worth noting that, due to a complete compensation between long-range Coulomb and Fröhlich interactions, there is no constraint on the double on-site occupancy even in the strong coupling regime. Therefore, while the $t-J$ model acts on a projected Hilbert space with no on-site double occupancy, the polaronic $t-J_p$ model accounts for finite double occupancy, acting on a non-projected Hilbert space with four single-particle states per sites. Finally, the different sign (plus instead of minus) of the density-density term in Eq.(8.69) with respect to the standard $t-J$ model results in an effective repulsion between pairs which protects the ground state from clustering allowing for the presence of small and perfectly mobile pairs even at large J_p.

Chapter 9

Analytical and numerical results on the polaronic $t - J_p$ model

Despite its very simple form, the polaronic $t - J_p$ Hamiltonian (8.69) represents a difficult task to deal with. To better understand the physics underneath this model, in this Chapter we report a detailed discussion of analytical and numerical results obtained for fixed number of particles and different geometries. Most of the following results are also discussed in Ref.[35].

The rest of this Chapter is organized as follows. A detailed analysis of the ground state configurations in the static limit (i.e. $t/J_p \ll 1$) is reported in Section 9.1 for different lattice geometries. We analyze the role of the polaronic exchange coupling J_p as responsible for the bipolaron formation but also for the bipolaron-bipolaron repulsion which prevents the bipolaronic ground state from clustering. The role of the hopping is discussed in Section 9.2. We show that in the dilute regime, meaning that the number of polarons is much less than the number of sites, the ground-state properties of the t-J_p model can be derived by looking to a two-particle problem and then projecting the model Hamiltonian on a repulsive Bose gas of small inter-site bipolarons. To this purpose, we introduce in Subsecs.9.2.1-9.2.3 the so-called Singlet Subspace Projection (SSP) method and report a detailed analysis on the bipolaronic ground state configurations for both one and two dimensional lattice geometries.

Here and after, in order to account the short range nature of $J_p(\boldsymbol{m} - \boldsymbol{n})$, only nearest-neighbour interactions will be taken into account. Furthermore, we will restrict our analysis to translational invariant systems characterized by a constant lattice spacing $\boldsymbol{a}$, neglecting any site dependence on the hopping parameter ($t_{ij} = t$) and exchange interaction ($J_p(\boldsymbol{m} - \boldsymbol{n}) = J_p > 0$). The following relation will also be used:

$$\overrightarrow{S}_{\boldsymbol{n}} \cdot \overrightarrow{S}_{\boldsymbol{m}} = S^z_{\boldsymbol{n}} S^z_{\boldsymbol{m}} + \frac{1}{2}\left(S^+_{\boldsymbol{n}} S^-_{\boldsymbol{m}} + S^-_{\boldsymbol{n}} S^+_{\boldsymbol{m}}\right) \ , \tag{9.1}$$

where $S^{\pm}_{\boldsymbol{n}}$ and $S^z_{\boldsymbol{n}}$ represent the raising/lowering operators and the third component

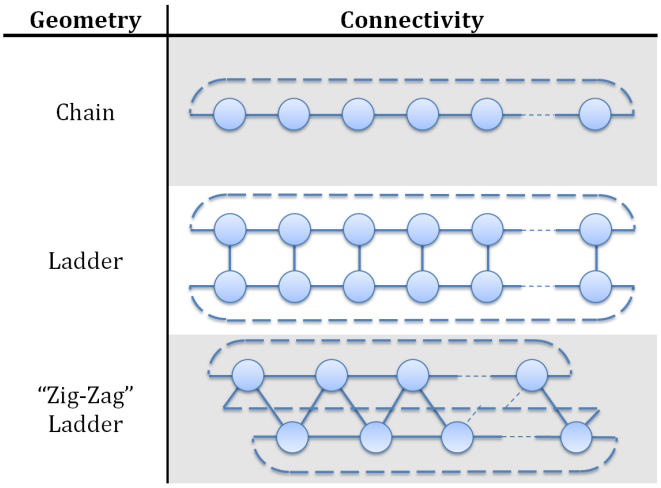

Figure 9.1: Connectivities for three possible geometries. Nearest neighbour interaction channels have been represented by solid lines while dashed ones denote nearest neighbour interaction channels provided by periodic boundary conditions.

of the spin angular momentum, respectively. Hence, Eq.8.69 reads as:

$$\begin{aligned}\mathcal{H} \;=\; & -\sum_{\boldsymbol{m},s}\left[t\sum_{n=1}^{z} c^{\dagger}_{\boldsymbol{m},s}c_{\boldsymbol{m}+\boldsymbol{a}_n,s}+\tilde{\tilde{\mu}}n_{\boldsymbol{m},s}\right]+2J_p\sum_{\boldsymbol{m}}\sum_{n=1}^{z}\left[\frac{1}{2}\left(S^z_{\boldsymbol{m}}S^z_{\boldsymbol{m}+\boldsymbol{a}_n}+S^z_{\boldsymbol{m}}S^z_{\boldsymbol{m}-\boldsymbol{a}_n}\right)\right. \\ & +\frac{1}{4}\left(S^+_{\boldsymbol{m}}S^-_{\boldsymbol{m}+\boldsymbol{a}_n}+S^+_{\boldsymbol{m}}S^-_{\boldsymbol{m}-\boldsymbol{a}_n}+S^-_{\boldsymbol{m}}S^+_{\boldsymbol{m}+\boldsymbol{a}_n}+S^-_{\boldsymbol{m}}S^+_{\boldsymbol{m}-\boldsymbol{a}_n}\right) \\ & \left.+\frac{1}{8}\sum_{s,s'}\left(n_{\boldsymbol{m},s}n_{\boldsymbol{m}+\boldsymbol{a}_n,s'}+n_{\boldsymbol{m},s}n_{\boldsymbol{m}-\boldsymbol{a}_n,s'}\right)\right], \end{aligned} \tag{9.2}$$

where $\boldsymbol{m}$ is a generic site of the lattice and $\boldsymbol{a}_n$ is the lattice vector that connects the site $\boldsymbol{m}$ with its n^{th} nearest neighbour. The sum over n takes into account all the possible z nearest-neighbour sites, being z the coordination number related to the particular lattice geometry. Hereafter we will focus our attention on three different geometries: chain, ladder and zig-zag ladder for which we have:

$$\{\boldsymbol{a}_n\}_{n\in\{1,z\}}=\begin{cases}\{-a,a\} & chain\\ \{-2a,-a,a,2a\} & zig-zag\ ladder\\ \{(-a,0),(0,-a),(a,0),(0,a)\} & ladder\end{cases}. \tag{9.3}$$

Periodic boundary conditions will also be used. The connectivity of each geometry is reported in Fig.9.1.

9.1 Static configurations in the low-density limit

In order to have a comprehensive overview of the physics described by the $t-J_p$ model, it is instructive to start with a systematic study of the $t=0$ case in the low-density limit in which the number of sites N_s is larger than the number of particles

N_p. In this limit, which corresponds to an extreme strong-coupling regime with $J_p(\boldsymbol{m} - \boldsymbol{n}) \gg t$, the hopping is negated by a strong exchange interaction, then the Hamiltonian (8.69) reads as:

$$\mathcal{H} = -\sum_{\boldsymbol{m},s} \mu c^{\dagger}_{\boldsymbol{m},s} c_{\boldsymbol{m},s} + 2 \sum_{\boldsymbol{m} \neq \boldsymbol{n}} J_p(\boldsymbol{m} - \boldsymbol{n}) \left(\overrightarrow{S}_{\boldsymbol{m}} \cdot \overrightarrow{S}_{\boldsymbol{n}} + \frac{1}{4} \sum_{s,s'} \hat{n}_{\boldsymbol{m},s} \hat{n}_{\boldsymbol{n},s'} \right) . \quad (9.4)$$

In the above equation the contribution coming from the chemical potential only shifts the energy according to the total number of particles and the polaronic $t - J_p$ Hamiltonian simply reduces to a combination of density-density and Heisenberg spin-spin interactions. Hence, by considering the total spin angular momentum S and one of its components as good quantum numbers, the dimension of the Hilbert space for a generic N_s-site lattice will be $(2N_s)!/[(2N_s - N_p)!N_p!]$. However, because of the presence of a repulsive density-density interaction term, for $N_p \ll N_s$ almost all states comprise non-interacting configurations made up by all unbound polarons with $E = 0$. According to this, a simple analysis restricted to a small number of particles $N_p = (1, 2, 3, 4)$ will suffice to estimate the ground state properties in the dilute limit since there are enough symmetries in the model to reduce the problem to the diagonalization of a finite-dimensional matrix for any value of N_s. We briefly sketch below the calculations for a two, three and four particle problem in a one-dimensional geometry.

Two-particle problem Let us define a minimal set $\mathcal{C}$ of possible configurations. Because of the presence of only the exchange interaction J_p we have:

$$\mathcal{C} = \{ |0, \ldots, 0, \uparrow, \uparrow, 0, \ldots, 0\rangle , |0, \ldots, 0, \uparrow, \downarrow, 0, \ldots, 0\rangle , |0, \ldots, 0, \uparrow, 0, \downarrow, 0, \ldots, 0\rangle \} , \quad (9.5)$$

where we have listed the two possible types of spin interactions and a non-interacting configuration. By applying the Hamiltonian (9.4) to this set of configurations we can define the Fock space $\mathcal{F}$ as:

$$\begin{aligned} \mathcal{F} \;=\; & \big\{ |0, \ldots, 0, \uparrow, \uparrow, 0, \ldots, 0\rangle , |0, \ldots, 0, \uparrow, \downarrow, 0, \ldots, 0\rangle , |0, \ldots, 0, \downarrow, \uparrow, 0, \ldots, 0\rangle , \\ & |0, \ldots, 0, \uparrow, 0, \downarrow, 0, \ldots, 0\rangle \big\} , \end{aligned} \quad (9.6)$$

and then construct the matrix representation of Hamiltonian:

$$\mathcal{H}^{(\mathcal{F})}_{ij} \equiv \langle \mathcal{F}_i | \, \mathcal{H} \, | \mathcal{F}_j \rangle , \quad (9.7)$$

where $\mathcal{F}_i$ is the i^{th} component of $\mathcal{F}$. In this simple case we have a 4×4 matrix from which we get the following representation for the ground state:

$$|\psi_0\rangle = \frac{1}{\sqrt{2}} \left[|0, \ldots, 0, \uparrow, \downarrow, 0, \ldots, 0\rangle - |0, \ldots, 0, \downarrow, \uparrow, 0, \ldots, 0\rangle \right] . \quad (9.8)$$

The energy associated to this configuration is: $E_0 = -J_p - 2\mu$. We conclude that, due to J_p, the low energy state is a two-particle singlet state characterized by polarons on nearest neighbour sites.

Three-particle problem On the basis of the results obtained for the two-particle problem, the $\mathcal{C}$-space for three particles will be the following:

$$\mathcal{C} = \{|0,\ldots,0,\uparrow,\downarrow,\uparrow,0,\ldots,0\rangle\,,|0,\ldots,0,\uparrow,\downarrow,0,\uparrow,0,\ldots,0\rangle\}\ , \tag{9.9}$$

where we have neglected the contributions coming from the non-interacting states since we are only interested in the ground state configuration. By applying the Hamiltonian (9.4) to this set of configurations we obtain the following Fock space:

$$\begin{aligned}\mathcal{F} \;=\; & \{|0,\ldots,0,\uparrow,\downarrow,\uparrow,0,\ldots,0\rangle\,,|0,\ldots,0,\downarrow,\uparrow,\uparrow,0,\ldots,0\rangle\,,|0,\ldots,0,\uparrow,\uparrow,\downarrow,0,\ldots,0\rangle\,,\\ & |0,\ldots,0,\uparrow,\downarrow,0,\uparrow,0,\ldots,0\rangle\,,|0,\ldots,0,\downarrow,\uparrow,0,\uparrow,0,\ldots,0\rangle\}\ .\end{aligned} \tag{9.10}$$

then, by diagonalizing the matrix representation (9.7) in the $\mathcal{F}$ space we find the following degenerate ground states:

$$\begin{cases}\left|\psi_0^{(1)}\right\rangle = & \sqrt{\frac{1}{2}}\left[|0,\ldots,0,\uparrow,\downarrow,0,\ldots,0\uparrow,0\ldots,0\rangle - |0,\ldots,0,\downarrow,\uparrow,0,\ldots,0\uparrow,0\ldots,0\rangle\right]\\ \left|\psi_0^{(2)}\right\rangle = & \sqrt{\frac{1}{3}}\big[|0,\ldots,0,\downarrow,\uparrow,\uparrow,0,\ldots,0\rangle + |0,\ldots,0,\uparrow,\uparrow,\downarrow,0,\ldots,0\rangle\\ & \quad -\sqrt{2}\,|0,\ldots,0,\uparrow,\downarrow,\uparrow,0,\ldots,0\rangle\ .\end{cases} \tag{9.11}$$

The corresponding energy is $E_0 = -J_p - 3\mu$.

Four-particle problem From the studies done in the previous section we can easily write down the $\mathcal{C}$-space for a four-particle system as:

$$\begin{aligned}\mathcal{C} \;=\; & \{|0,\ldots,0,\uparrow,\downarrow,\uparrow,\downarrow,0,\ldots,0\rangle\,,|0,\ldots,0,\uparrow,\uparrow,\downarrow,\downarrow,0,\ldots,0\rangle\,,\\ & |0,\ldots,0,\uparrow,0,\ldots,0\downarrow,\uparrow,\downarrow,0,\ldots,0\rangle\,,\\ & |0,\ldots,0,\uparrow,\downarrow,0,\ldots,0,\uparrow,\downarrow,0,\ldots,0\rangle\}\ .\end{aligned} \tag{9.12}$$

The resulting Fock space $\mathcal{F}$ is the following:

$$\begin{aligned}\mathcal{F} \;=\; & \{|0,\ldots,0,\uparrow,\downarrow,\uparrow,\downarrow,0,\ldots,0\rangle\,,|0,\ldots,0,\downarrow,\uparrow,\uparrow,\downarrow,0,\ldots,0\rangle\,,|0,\ldots,0,\uparrow,\downarrow,\downarrow,\uparrow,0,\ldots,0\rangle\,,\\ & |0,\ldots,0,\uparrow,\uparrow,\downarrow,\downarrow,\ldots,0\rangle\,,|0,\ldots,0,\downarrow,\uparrow,0,\ldots,0,\uparrow,\downarrow,0,\ldots,0\rangle\,,\\ & |0,\ldots,0,\uparrow,\downarrow,0,\ldots,0,\downarrow,\uparrow,0,\ldots,0\rangle\,,|0,\ldots0,\uparrow,\downarrow,0,\ldots,0,\uparrow,\downarrow,0,\ldots,0\rangle\,,\\ & |0,\ldots0,\downarrow,\uparrow,0,\ldots,0,\downarrow,\uparrow,0,\ldots,0\rangle\,,|0,\ldots,0,\uparrow,\downarrow,\uparrow,0,\ldots,0\rangle\,,\\ & |0,\ldots,0,\uparrow,0,\downarrow,\uparrow,\uparrow,0,\ldots,0\rangle\,,|0,\ldots,0,\uparrow,0,\uparrow,\uparrow,\downarrow,0,\ldots,0\rangle\}\ .\end{aligned} \tag{9.13}$$

Hence, by diagonalizing the matrix representation of the static Hamiltonian with respect to $\mathcal{F}$ space we find the following representation for the ground state:

$$\begin{aligned}|\psi_0\rangle \;=\; & \frac{1}{4}\big[|0,\ldots,0,\uparrow,\downarrow,0,\ldots,0,\downarrow,\uparrow,0,\ldots,0\rangle - |0,\ldots0,\uparrow,\downarrow,0,\ldots,0,\uparrow,\downarrow,0,\ldots,0\rangle\\ & + |0,\ldots,0,\downarrow,\uparrow,0,\ldots,0,\uparrow,\downarrow,0,\ldots,0\rangle\\ & - |0,\ldots0,\downarrow,\uparrow,0,\ldots,0,\downarrow,\uparrow,0,\ldots,0\rangle\big]\ .\end{aligned} \tag{9.14}$$

The corresponding energy is $E_0 = -2J_p - 4\mu$.

Summarizing, following the above procedure, which can be straightforwardly generalized to all the geometries listed in Fig.9.1, we immediately find that the static ground state configuration for a two-particle problem is a bipolaronic spin-singlet, made up by two polarons on nearest neighbour (NN) sites. The ground state energy is $E = -J_p - 2\mu$ and its degeneracy $\nu = N_s - 1$. The first excited state includes all the non-interacting configurations with $E = -2\mu$ and $\nu = 2N_s^2 - 3N_s + 4$, characterized by two polarons separated by at least one empty site. Finally, the higher energy levels are given by the NN spin-triplet state, with $E = J_p - 2\mu$ and $\nu = 2(N - 1)$. For $N_p = 3$ the ground state is characterized by a complete degeneracy between the anti-ferromagnetic cluster of three polarons on NN sites and the three-particle configurations characterized by an isolated polaron separated from a NN dimer by at least one empty site. For both the configurations we have $E = -J_p - 3\mu$ since spin-spin and density-density interaction terms compensate each others. Therefore, as long as $t = 0$, there is no gain for the system in preserving the bipolaron configuration. The opposite conclusion can be drawn for $N_p = 4$. In this case in fact the presence of a density-density interaction leads to the formation of two isolated bipolarons. This configuration, with $E = -2J_p - 4\mu$, is lower in energy with respect to the NN four-particle singlet that represents the first excited state with $E = -\sqrt{3}J_p - 4\mu$. A straightforward comparison between the ground and the first excited state energies allows us to estimate the effective static repulsion among pairs as:

$$E_r^{t=0} = \left(2 - \sqrt{3}\right) J_p \, . \tag{9.15}$$

At this stage it is worth emphasizing that the static bipolaron repulsion energy is nothing but the macroscopic manifestation of the pure quantum nature of the spin-spin interaction. In fact, because of the presence of the Heisenberg exchange coupling in (9.4), polarons on nearest neighbour sites have not only to align their spins in opposite directions. They also have to arrange their spins in a global antisymmetric wave function in order to minimize their energy. Hence it becomes immediately clear that, because of the anti-symmetrization, a clustered state with all polarons on NN sites will have a higher energy with respect to the dimerized one since it will be composed by a linear combination of spin configurations among which, at least one of them, will have aligned NN spins, as reported below for the simple case of a four-particle system:

$$\begin{aligned} |\psi_0\rangle &= A_1 \Big[|\uparrow,\downarrow,0,\ldots,0,\downarrow,\uparrow\rangle - |\uparrow,\downarrow,0,\ldots,0,\uparrow,\downarrow\rangle \\ &\quad + |\downarrow,\uparrow,0,\ldots,0,\uparrow,\downarrow\rangle - |\downarrow,\uparrow,0,\ldots,0,\downarrow,\uparrow\rangle \Big] \, , \end{aligned} \tag{9.16}$$

$$\begin{aligned} |\psi_0\rangle &= B_1 \, |0,\ldots,0\downarrow,\downarrow,\uparrow,\uparrow,0,\ldots,0\rangle + B_2 \, |0,\ldots,0,\downarrow,\uparrow,\downarrow,\uparrow,0,\ldots,0\rangle \\ &\quad + B_3 \, |0,\ldots,0,\downarrow,\uparrow,\uparrow,\downarrow,0,\ldots,0\rangle - B_3 \, |0,\downarrow,\uparrow,\uparrow,\downarrow,0\rangle \\ &\quad - B_2 \, |0,\uparrow,\downarrow,\uparrow,\downarrow,0\rangle - B_1 \, |0,\uparrow\uparrow,,\downarrow,\downarrow,0\rangle \ . \end{aligned} \tag{9.17}$$

Because of this, $E_r^{t=0}$ does not simply rescale linearly with the number of particles as shown in Fig.(9.2).

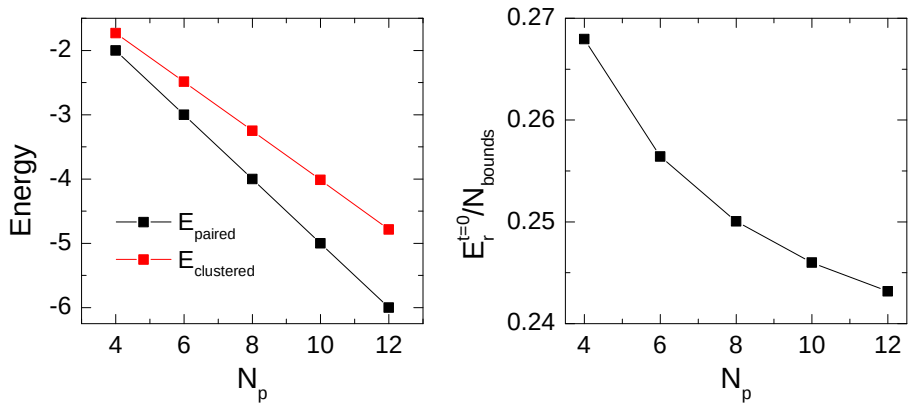

Figure 9.2: Left panel: ground state energy for a complete clustered (all polarons on NN sites) and a complete dimerized (pairs of polarons separated by at least one empty site) 1D static system versus number of particles. Right panel: the resulting 1D static repulsion energy rescaled with respect to the number of bounds: $E_r^{t=0} = (E_{cluster} - E_{paired})/(N_p/2 - 1)$.

9.2 Beyond the static limit: the role of the hopping

In the previous Section we have pointed out that, in the static and dilute limits, the ground state of the polaronic $t-J_p$ model is a bipolaronic configuration characterized by pairs of NN polarons, separated by at least one empty site. We have shown that the exchange interaction J_p is responsible for the pairing, but it also originates a static repulsion among pairs (9.15) which protect the ground state from clustering. Hence, it is immediate to realize that in the dilute limit and for $t < J_p$, as long as the bipolaron size d remains small compared to the dimension N of the system, the hopping will have the only effect to coherently propagate the static configurations. It follows that, beyond any approximation, the ground state properties of the $t - J_p$ model in the dilute limit can be straightforwardly derived from the analysis of a two-particle system without the loss of generality. The critical value of the filling, n_c which breaks down the dilute limit regime, will depend on the bipolaron size according to the relation $n_c \approx N/d$. On the basis of these considerations, we report in this Section a complete characterization of the ground state features of the $t - J_p$ Hamiltonian in the dilute limit by comparing analytical and numerical results obtained by solving the two-particle problem and then projecting the Hamiltonian on the repulsive Bose gas of small inter-site bipolarons.

9.2.1 Singlet-subspace projection (SSP) method

Let us consider the simple two-particle case. From the results showed in Sec.9.1 we know that the ground state configuration of the polaronic t-J_p Hamiltonian is a spin singlet at $t = 0$. To take into account this symmetry, it is useful to define a symmetry-adapted singlet basis, representing the internal structure of a singlet in terms of the spacing d between the two particle and the position of the centre-of-mass

in the k-space:

$$|d, \boldsymbol{k}\rangle = \frac{1}{\sqrt{N}} \sum_{m,s} A_s e^{i\left(m+\frac{d}{2}\right)\boldsymbol{k}\cdot\boldsymbol{a}} c_s^\dagger(m) c_{\bar{s}}^\dagger(m+d) \, |0\rangle \ , \ A_s = \begin{cases} \left(\frac{1}{\sqrt{2}}, -\frac{1}{\sqrt{2}}\right) & , d > 0 \\ \left(\frac{1}{2}, -\frac{1}{2}\right) & , d = 0 \end{cases} , \tag{9.18}$$

where $|0\rangle$ is the vacuum and N is the number of sites in an infinite system. It is worth noting that for $d = 0$ the chosen basis includes all the possible configurations with a doubly occupied site:

$$\begin{aligned} |0, \boldsymbol{k}\rangle &= \frac{1}{\sqrt{N}} \sum_m e^{im\boldsymbol{k}\cdot\boldsymbol{a}} c_\uparrow^\dagger(m) c_\downarrow^\dagger(m) \, |0\rangle = \frac{1}{\sqrt{N}} \Big(|\uparrow\downarrow, 0, \dots\rangle + \\ &= + e^{i\boldsymbol{k}\cdot\boldsymbol{a}} \, |0, \uparrow\downarrow, 0, \dots\rangle + e^{2i\boldsymbol{k}\cdot\boldsymbol{a}} \, |0, 0, \uparrow\downarrow, 0, \dots\rangle + \dots \Big) , \end{aligned} \tag{9.19}$$

while $|d, \boldsymbol{k}\rangle$, with $d > 0$, describes all the possible configurations in which two polarons are separated by d empty sites:

$$\begin{aligned} |1, \boldsymbol{k}\rangle &= \frac{1}{\sqrt{N}} \sum_m e^{i\left(m+\frac{1}{2}\right)\boldsymbol{k}\cdot\boldsymbol{a}} \frac{1}{\sqrt{2}} \Big(c_\uparrow^\dagger(m) c_\downarrow^\dagger(m+a) - c_\downarrow^\dagger(m) c_\uparrow^\dagger(m+a) \Big) |0\rangle = \\ &= \frac{1}{\sqrt{N}} \Bigg(\frac{1}{\sqrt{2}} e^{i\frac{\boldsymbol{k}\cdot\boldsymbol{a}}{2}} \left(|\uparrow, 0, \downarrow, 0, \dots\rangle - |\downarrow, 0, \uparrow, 0, \dots\rangle \right) \\ &\quad + \frac{1}{\sqrt{2}} e^{\frac{3}{2}i\boldsymbol{k}\cdot\boldsymbol{a}} \left(|0, \uparrow, 0, \downarrow, 0, \dots\rangle - |0, \downarrow, 0, \uparrow, 0, \dots\rangle \right) + \dots \Bigg) , \end{aligned} \tag{9.20}$$

$$\begin{aligned} |2, \boldsymbol{k}\rangle &= \frac{1}{\sqrt{N}} \sum_m e^{i(m+1)\boldsymbol{k}\cdot\boldsymbol{a}} \frac{1}{\sqrt{2}} \Big(c_\uparrow^\dagger(m) c_\downarrow^\dagger(m+2a) - c_\downarrow^\dagger(m) c_\uparrow^\dagger(m+2a) \Big) |0\rangle = \\ &= \frac{1}{\sqrt{N}} \Bigg(\frac{1}{\sqrt{2}} e^{i\boldsymbol{k}\cdot\boldsymbol{a}} \left(|\uparrow, 0, 0, \downarrow, 0, \dots\rangle - |\downarrow, 0, 0, \uparrow, 0, \dots\rangle \right) \\ &\quad + \frac{1}{\sqrt{2}} e^{2i\boldsymbol{k}\cdot\boldsymbol{a}} \left(|0, \uparrow, 0, 0, \downarrow, 0, \dots\rangle - |0, \downarrow, 0, 0, \uparrow, 0, \dots\rangle \right) + \dots \Bigg) . \end{aligned} \tag{9.21}$$

At this point, we can easily calculate the the matrix representation of the $t - J_p$ Hamiltonian with respect to the $|d, \boldsymbol{k}\rangle$ basis. To this purpose, it is useful to rewrite the Hamiltonian (8.69) as:

$$\mathcal{H}_{t-J_p} \equiv \mathcal{H}_t + \mathcal{H}_{J_p} \ , \ \begin{cases} \mathcal{H}_t \equiv -t \sum_{\boldsymbol{i},\boldsymbol{j},\sigma} c_{\boldsymbol{i},\sigma}^\dagger c_{\boldsymbol{j},\sigma} \\ \mathcal{H}_{J_p} \equiv -\tilde{\tilde{\mu}} \sum_{\boldsymbol{i},\sigma} c_{\boldsymbol{i},\sigma}^\dagger c_{\boldsymbol{i},\sigma} + 2J_p \sum_{\boldsymbol{m}\neq\boldsymbol{n}} \left(\overrightarrow{S}_{\boldsymbol{m}} \cdot \overrightarrow{S}_{\boldsymbol{n}} + \frac{1}{4} \hat{n}_{\boldsymbol{m}} \hat{n}_{\boldsymbol{n}} \right) \end{cases} , \tag{9.22}$$

in which we have neglected any spatial dependence in hopping and exchange amplitudes. It is immediate to note that the exchange term $\mathcal{H}_{J_p}$ has a diagonal represen-

tation with respect to (9.18). In particular by means of the following relation:

$$\begin{aligned}\left(\overrightarrow{S}_{tot}\right)^2 &= s(s+1) = 0 = \left(\overrightarrow{S}_{\boldsymbol{i}} + \overrightarrow{S}_{\boldsymbol{j}}\right)^2 = \\ &= \left(\overrightarrow{S}_{\boldsymbol{i}}\right)^2 + \left(\overrightarrow{S}_{\boldsymbol{j}}\right)^2 + 2\overrightarrow{S}_{\boldsymbol{i}} \cdot \overrightarrow{S}_{\boldsymbol{j}} \ , \end{aligned} \tag{9.23}$$

where $\left(\overrightarrow{S}_{\boldsymbol{i},\boldsymbol{j}}\right)^2 = \frac{1}{2}\left(\frac{1}{2}+1\right) = \frac{3}{4}$, we have $\overrightarrow{S}_{\boldsymbol{i}} \cdot \overrightarrow{S}_{\boldsymbol{j}} = -3/4$ and $\overrightarrow{S}_{\boldsymbol{i}} \cdot \overrightarrow{S}_{\boldsymbol{j}} = 1/4$ for singlet ($s = 0$) and triplet ($s = 1$) states, respectively. Therefore, by adding the diagonal contribution coming from the density-density interaction term, we finally obtain:

$$\langle d_1, \boldsymbol{k}| \mathcal{H}_{J_p} |d_2, \boldsymbol{k}'\rangle = -J_p \delta_{d_1,d_2} \delta_{d_1,1} \ . \tag{9.24}$$

Let us now focus our attention to the hopping term. It is immediate to see that $\mathcal{H}_t$ has a non-diagonal representation in the chosen basis since it couples states with different values of d depending on the range of the allowed hopping processes. Then, for a fixed geometry in the presence of any finite-range interaction, the ground state properties of the polaronic t-J_p model can be easily obtained by diagonalizing an infinite-dimensional sparse matrix given by the Singlet-Subspace Projection (SSP) of $\mathcal{H}_{t-J_p}$. Hereafter we will restrict the hopping processes and the range of all the interactions to NN sites and report below detailed calculations for chain, zig-zag ladder geometries. In the following Subsections, we also report the generalization of the SSP method to the spin-triplet case and 2D geometries.

Chain In the case of a one-dimensional chain the hopping operator will couple a $d > 1$ dimer to a superposition of $d \pm 1$ while the doubly occupied states ($d = 0$) will be connected with the nearest neighbour singlet ($d = 1$) only. For the $d \geq 1$ case we have:

$$\begin{aligned}\mathcal{H}_t |d,k\rangle &= -t \sum_{i,\sigma} \sum_{m,s} A_s e^{ika(m+d/2)} \left(c^\dagger_\sigma(i+1)c_\sigma(i) + c^\dagger_\sigma(i-1)c_\sigma(i)\right) c^\dagger_s(m) c^\dagger_{\bar{s}}(m+d) |0\rangle = \\ &= -t \sum_{i,\sigma} \sum_{m,s} A_s e^{ika(m+d/2)} \Bigg(c^\dagger_\sigma(i+1)c_\sigma(i)c^\dagger_s(m)c^\dagger_{\bar{s}}(m+d) \\ &\qquad + c^\dagger_\sigma(i-1)c_\sigma(i)c^\dagger_s(m)c^\dagger_{\bar{s}}(m+d)\Bigg) |0\rangle = \\ &= -t \sum_{i,\sigma} \sum_{m,s} A_s e^{ika(m+d/2)} \delta_{\boldsymbol{im}} \delta_{s\sigma} \Big(c^\dagger_\sigma(i+1)c^\dagger_{\bar{s}}(m+d) \\ &\qquad + c^\dagger_\sigma(i-1)c^\dagger_{\bar{s}}(m+d)\Big) |0\rangle = \\ &= -t \sum_{m,s} A_s e^{ika(m+d/2)} \Bigg[c^\dagger_s(m+1)c^\dagger_{\bar{s}}(m+d) \\ &\qquad + c^\dagger_s(m-1)c^\dagger_{\bar{s}}(m+d)\Bigg] |0\rangle = \end{aligned}$$

$$
\begin{aligned}
&= -t \sum_{m,s} A_s e^{ika(m+\frac{d+1}{2})} c_s^\dagger(m) c_{\bar{s}}^\dagger(m+d+1) \left(e^{-ika/2} + e^{ika/2}\right) |0\rangle \\
&\quad -t \sum_{m,s} A_s e^{ika(m+\frac{d-1}{2})} c_s^\dagger(m) c_{\bar{s}}^\dagger(m+d-1) \left(e^{-ika/2} + e^{ika/2}\right) |0\rangle = \\
&= -2t \cos\left(\frac{ka}{2}\right) \left(|d+1,k\rangle + |d-1,k\rangle\right) \ . \qquad (9.25)
\end{aligned}
$$

For the $d = 1$ and $d = 0$ cases instead we obtain:

$$
\begin{aligned}
\mathcal{H}_t |1,k\rangle &= -t \sum_{i,\sigma} \sum_{m,s} A_s e^{ika(m+1/2)} \left(c_\sigma^\dagger(i+1) c_\sigma(i) + c_\sigma^\dagger(i-1) c_\sigma(i)\right) c_s^\dagger(m) c_{\bar{s}}^\dagger(m+1) |0\rangle = \\
&= -t \sum_{i,\sigma} \sum_{m,s} A_s e^{ika(m+1/2)} \Big(c_\sigma^\dagger(i+1) c_\sigma(i) c_s^\dagger(m) c_{\bar{s}}^\dagger(m+1) \\
&\qquad + c_\sigma^\dagger(i-1) c_\sigma(i) c_s^\dagger(m) c_{\bar{s}}^\dagger(m+1)\Big) |0\rangle = \\
&= -t \sum_{m,s} A_s e^{ikam} \left[e^{ika/2} \left(e^{-ika} + 1\right)\right] c_s^\dagger(m) c_{\bar{s}}^\dagger(m) |0\rangle \\
&\quad -t \sum_{m,s} A_s e^{ika(m+2)} \left[e^{-ika/2} \left(1 + e^{ika}\right)\right] c_s^\dagger(m) c_{\bar{s}}^\dagger(m+2) |0\rangle = \\
&= -\frac{t}{\sqrt{2}} \sum_{m,s} e^{ikam} \left[2\cos\left(\frac{ka}{2}\right)\right] \left[c_\uparrow^\dagger(m) c_\downarrow^\dagger(m) - c_\downarrow^\dagger(m) c_\uparrow^\dagger(m)\right] |0\rangle \\
&\quad -2t \cos\left(\frac{ka}{2}\right) \sum_{m,s} A_s e^{ika(m+2)} c_s^\dagger(m) c_{\bar{s}}^\dagger(m+2) |0\rangle = \\
&= -2t \cos\left(\frac{ka}{2}\right) \left[|2,k\rangle + \sqrt{2} |0,k\rangle\right] \ . \qquad (9.26)
\end{aligned}
$$

$$
\begin{aligned}
\mathcal{H}_t |0,k\rangle &= -t \sum_{i,\sigma} \sum_{m} e^{ikam} \left(c_\sigma^\dagger(i+1) c_\sigma^\dagger(i) + c_\sigma^\dagger(i-1) c_\sigma^\dagger(i)\right) c_\uparrow^\dagger(m) c_\downarrow^\dagger(m) |0\rangle = \\
&= -t \sum_{m} e^{ikam} \Big(c_\uparrow^\dagger(m+1) c_\downarrow^\dagger(m) - c_\downarrow^\dagger(m+1) c_\uparrow^\dagger(m) \\
&\qquad + c_\uparrow^\dagger(m-1) c_\downarrow^\dagger(m) - c_\downarrow^\dagger(m-1) c_\rho^\dagger(m)\Big) |0\rangle = \\
&= -\sqrt{2}t \sum_{m} \frac{1}{\sqrt{2}} e^{ika(m+1/2)} \left[e^{-ika/2} \left(1 + e^{ika}\right)\right] \Big(c_\uparrow^\dagger(m) c_\downarrow^\dagger(m+1) \\
&\qquad - c_\downarrow^\dagger(m) c_\uparrow^\dagger(m+1)\Big) |0\rangle = \\
&= -2\sqrt{2}t \cos\left(\frac{ka}{2}\right) |1,k\rangle \ . \qquad (9.27)
\end{aligned}
$$

This allows us to write the following tri-diagonal representation for $t - J_p$ Hamiltonian in the singlet subspace:

$$\langle d_i, k| \mathcal{H}_{t-J_p} |d_j, k\rangle = \begin{pmatrix} 0 & -\sqrt{2}\epsilon_k & 0 & \dots & 0 \\ -\sqrt{2}\epsilon_k & -J_p & -\epsilon_k & 0 & \dots \\ 0 & -\epsilon_k & 0 & -\epsilon_k & \ddots \\ 0 & 0 & -\epsilon_k & 0 & \ddots \\ \vdots & \vdots & \ddots & \ddots & \ddots \end{pmatrix} , \ \epsilon_k = 2t \cos\left(\frac{ka}{2}\right) . \tag{9.28}$$

It is well known that the wave function of a bound state must decay exponentially at some rate in the region where the potential vanishes. On the basis of this consideration we can look for a solution of the kind:

$$\begin{pmatrix} 0 & -\sqrt{2}\epsilon_k & 0 & \dots & 0 \\ -\sqrt{2}\epsilon_k & -J_p & -\epsilon_k & 0 & \dots \\ 0 & -\epsilon_k & 0 & -\epsilon_k & \ddots \\ 0 & 0 & -\epsilon_k & 0 & \ddots \\ \vdots & \vdots & \ddots & \ddots & \ddots \end{pmatrix} \begin{pmatrix} d \\ 1 \\ e^{-\alpha} \\ e^{-2\alpha} \\ \vdots \end{pmatrix} = E(k) \begin{pmatrix} d \\ 1 \\ e^{-\alpha} \\ e^{-2\alpha} \\ \vdots \end{pmatrix} , \tag{9.29}$$

where $E(k)$ is the ground-state dispersion and d is the amplitude of on-site pairs. The above eigenequation reduces to three coupled equations:

$$\begin{cases} -\sqrt{2}\epsilon_k = E(k)d \\ -\sqrt{2}\epsilon_k d - J_p - \epsilon_k e^{-\alpha} = E(k) \\ -\epsilon_k \left(e^{-\alpha} + e^{\alpha}\right) = E(k) \end{cases} , \tag{9.30}$$

where it is immediate to note that there is no way of stopping singlets from having weight on an on-site pair (except when $k = \pi/a$). Elimination of d and $E(k)$ and a little manipulation gives the following cubic for e^{α}:

$$\epsilon_k e^{3\alpha} - J_p e^{2\alpha} - \epsilon_k e^{\alpha} - J_p = 0 . \tag{9.31}$$

According to the results showed by Valiente et al. [52], a potential of range ρ leads to a $(2\rho + 1)^{th}$ order polynomial for the decay rate. In our case it is possible to see that the above cubic has only one positive root, meaning there is only one bound state that persists for all $J_p > 0$.

In the $t \ll J_p$ limit, by Taylor expansion, one finds :

$$e^{\alpha} = \frac{J_p}{\epsilon_k} + \frac{2\epsilon_k}{J_p} + \dots = \tag{9.32}$$

$$E(k) = -J_p - \frac{3\epsilon_k^2}{J_p} + \dots = -J_p - \frac{12t^2}{J_p} \cos^2\left(\frac{ka}{2}\right) + O\left(t^4\right) . \tag{9.33}$$

$$d = \frac{2\sqrt{2}t}{J_p} \cos\left(\frac{ka}{2}\right) , \tag{9.34}$$

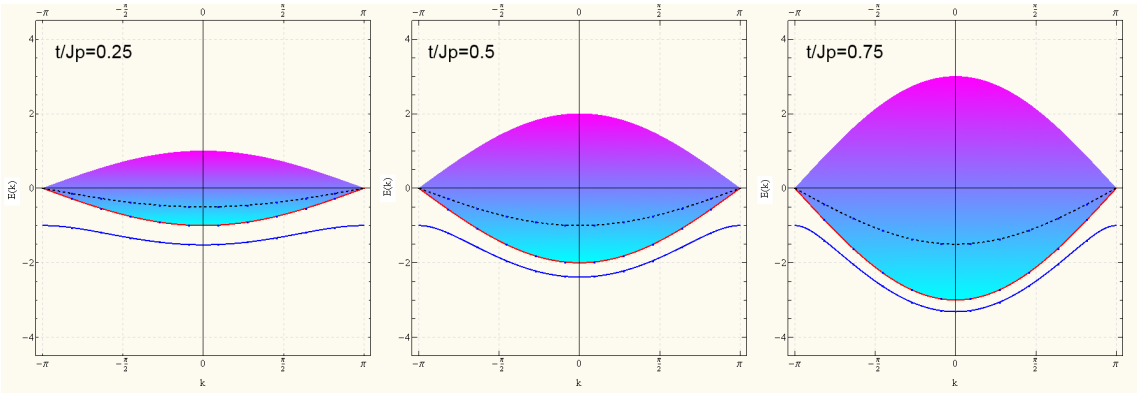

Figure 9.3: Energy dispersion for bipolaron (blue line), single polaron (dashed line) and two unpaired polarons (red lines) in a chain for different values of t/J_p. Filled areas correspond to all the possible scattering states.

In particular, from the ground state dispersion $E(k)$ one can immediately obtain the bipolaron effective mass m^{**} according to the relation:

$$m^{**} \equiv \hbar^2 / \left. \frac{\partial^2 E_0(k)}{\partial k^2} \right|_{k=k_{min}} , \tag{9.35}$$

which gives:

$$m^{**}_C|_{t \ll J_p} = \frac{\hbar^2 J_p}{6a^2 t^2} . \tag{9.36}$$

The basis (9.18) is complete, so we can also get the scattering states by taking $\alpha = iqa$. The resulting dispersion $E(k, q)$ reads as:

$$\begin{aligned} E(k,q) &= -2\epsilon_k \cos(qa) = -4t \cos\left(\frac{ka}{2}\right) \cos(qa) = \\ &= -2t \left[\cos\left(qa + \frac{ka}{2}\right) + \cos\left(qa - \frac{ka}{2}\right) \right] , \end{aligned} \tag{9.37}$$

that is the sum of two free polaron bands once we transform back from relative and centre-of-mass coordinates. The results obtained by solving the cubic equation (9.31), reported in Fig.9.3, show in fact that the bipolaron dispersion (blue line) lies below the dispersion of two unpaired polarons (red line) and the single polaron dispersion (dashed line). Importantly, as one would expect [53, 54], the unpaired polarons dispersion lies at the bottom of a continuum which originates from all the possible scattering states (9.37) with $q \in \{-\pi, \pi\}$.

Zig-zag ladder In the case of a zig-zag ladder, the application of the SSP method requires the zig-zag ladder to be mapped into a chain. It is well known that the zig-zag ladder configuration with lattice spacing a, in the presence of nearest neighbour (NN) interactions, can be mapped into a chain with lattice spacing $a/2$ and next NN interactions (see Fig.9.4).

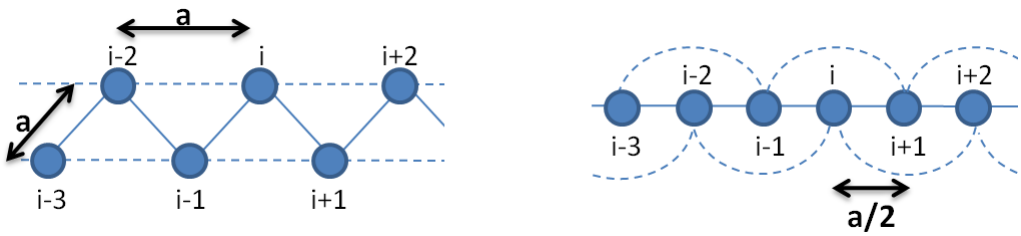

Figure 9.4: Mapping between zig-zag ladder and chain.

According with this mapping, the exchange part of the $t-J_p$ Hamiltonian gives:

$$\langle d_1, \boldsymbol{k}| \mathcal{H}_{J_p} |d_2, \boldsymbol{k}'\rangle = -J_p \delta_{d_1,d_2} \left(\delta_{d_1,1} + \delta_{d_1,2}\right) \ , \tag{9.38}$$

while the hopping part, related to the states with $d > 2$ gives:

$$\begin{aligned}
\mathcal{H}_t |d,k\rangle &= \frac{-t}{\sqrt{N}} \sum_j e^{i\frac{k}{2}(j+d/2)a} \sum_{i,\sigma,s} A_s \Big(c^\dagger_\sigma(i+2)c_\sigma(i) + c^\dagger_\sigma(i+1)c_\sigma(i) \\
&\quad + c^\dagger_\sigma(i-1)c_\sigma(i) + c^\dagger_\sigma(i-2)c_\sigma(i) \Big) c^\dagger_s(j) c^\dagger_{\bar{s}}(j+m) |0\rangle = \\
&= \frac{-t}{\sqrt{N}} \sum_{j,\rho} A_s \Big[c^\dagger_s(j) c^\dagger_{\bar{s}}(j+m-2) \left(e^{-ika+ika/2} + e^{ika}\right) e^{ik(j+(d-2)/2)a/2} + \\
&\quad + c^\dagger_s(j) c^\dagger_{\bar{s}}(j+m-1) \left(e^{-ika/2+ika/4} + e^{ika/2}\right) e^{ik(j+(d-1)/2)a/2} + \\
&\quad + c^\dagger_s(j) c^\dagger_{\bar{s}}(j+m+1) \left(e^{ika/2-ika/4} + e^{-ika/2}\right) e^{ik(j+(d+1)/2)a/2} + \\
&\quad + c^\dagger_s(j) c^\dagger_{\bar{s}}(j+m+2) \left(e^{ika-ika/2} + e^{-ika/2}\right) e^{ik(j+(d+2)/2)a/2} \Big] |0\rangle = \\
&= -2t \Bigg[\cos\left(\frac{ka}{2}\right) \left(|d+2,k\rangle + |d-2,k\rangle\right) \\
&\quad + \cos\left(\frac{ka}{4}\right) \left(|d+1,k\rangle + |d-1,k\rangle\right) \Bigg] \ ,
\end{aligned} \tag{9.39}$$

which accounts for two different k-dispersions related to the two different hopping (NN and next NN) processes. For $d < 2$ instead, by taking into account the contribution coming from doubly occupied sites, we have:

$$\begin{aligned}
\mathcal{H}_t |0,k\rangle &= \frac{-t}{\sqrt{N}} \sum_j e^{ikja/2} \sum_{i,\sigma} \Big(c^\dagger_\sigma(i+2)c_\sigma(i) + c^\dagger_\sigma(i+1)c_\sigma(i) \\
&\quad + c^\dagger_\sigma(i-1)c_\sigma(i) + c^\dagger_\sigma(i-2)c_\sigma(i) \Big) c^\dagger_\uparrow(j) c^\dagger_\downarrow(j) |0\rangle = \\
&= -\frac{t}{\sqrt{N}} \sum_j \Big[c^\dagger_\uparrow(j+2)c^\dagger_\downarrow(j) - c^\dagger_\downarrow(j+2)c^\dagger_\uparrow(j) + \\
&\quad + c^\dagger_\uparrow(j+1)c^\dagger_\downarrow(j) - c^\dagger_\downarrow(j+1)c^\dagger_\uparrow(j) + c^\dagger_\uparrow(j-1)c^\dagger_\downarrow(j) - c^\dagger_\downarrow(j-1)c^\dagger_\uparrow(j) \\
&\quad + c^\dagger_\uparrow(j-2)c^\dagger_\downarrow(j) - c^\dagger_\downarrow(j-2)c^\dagger_\uparrow(j) \Big] |0\rangle =
\end{aligned}$$

$$
\begin{aligned}
&= -\frac{\sqrt{2}t}{\sqrt{2N}}\sum_j\Bigg[e^{ik(j+1)a/2}\left(c^\dagger_\uparrow(j+2)c^\dagger_\downarrow(j)-c^\dagger_\downarrow(j+2)c^\dagger_\uparrow(j)\right)\\
&\qquad\left(e^{-ika/2}+e^{ika-ika/2}\right)\Bigg]|0\rangle+\\
&\quad -\frac{\sqrt{2}t}{\sqrt{2N}}\sum_j\Bigg[e^{ik(j+1/2)a/2}\left(c^\dagger_\uparrow(j+1)c^\dagger_\downarrow(j)-c^\dagger_\downarrow(j+1)c^\dagger_\uparrow(j)\right)\\
&\qquad\left(e^{-ika/4}+e^{ika/2-ika/4}\right)\Bigg]|0\rangle=\\
&= -2\sqrt{2}\left[\cos\left(\frac{ka}{2}\right)|2,k\rangle+\cos\left(\frac{ka}{4}\right)|1,k\rangle\right]\,, \qquad (9.40)
\end{aligned}
$$

$$
\begin{aligned}
\mathcal{H}_t|1,k\rangle &= \frac{-t}{\sqrt{N}}\sum_j e^{i\frac{k}{2}(j+m/2)a}\sum_{i,\sigma,s}A_s\Big(c^\dagger_\sigma(i+2)c_\sigma(i)+c^\dagger_\sigma(i+1)c_\sigma(i)\\
&\qquad +c^\dagger_\sigma(i-1)c_\sigma(i)+c^\dagger_\sigma(i-2)c_\sigma(i)\Big)c^\dagger_s(j)c^\dagger_{\bar{s}}(j+1)|0\rangle=\\
&= -\frac{t}{\sqrt{N}}\sum_{j,s}A_s\Big[e^{ik(j-1/2)a/2}c^\dagger_s(j)c^\dagger_{\bar{s}}(j-1)\left(e^{-ika+ika/2}+e^{ika/2}\right)+\\
&\qquad +e^{ik(j+1)a/2}c^\dagger_s(j)c^\dagger_{\bar{s}}(j+2)\left(e^{ika/2-ika/4}+e^{-ika/4}\right)+\\
&\qquad +e^{ik(j+3/2)a/2}c^\dagger_s(j)c^\dagger_{\bar{s}}(j+3)\left(e^{ika-ika/2}+e^{-ika/2}\right)\Big]+\\
&\quad -\frac{\sqrt{2}t}{\sqrt{N}}\sum_j e^{ikja/2}\left[c^\dagger_\uparrow(j)c^\dagger_\downarrow(j)\left(e^{-ika/2+ika/4}+e^{ika/4}\right)\right]=\\
&= -2t\Bigg[\cos\left(\frac{ka}{2}\right)|3,k\rangle+\cos\left(\frac{ka}{4}\right)|2,k\rangle\\
&\qquad +\cos\left(\frac{ka}{2}\right)|-1,k\rangle+\sqrt{2}\cos\left(\frac{ka}{4}\right)|0,k\rangle\Bigg]=\\
&= -2t\Bigg[\cos\left(\frac{ka}{2}\right)|3,k\rangle+\cos\left(\frac{ka}{4}\right)|2,k\rangle\\
&\qquad +\cos\left(\frac{ka}{2}\right)|1,k\rangle+\sqrt{2}\cos\left(\frac{ka}{4}\right)|0,k\rangle\Bigg]\,, \qquad (9.41)
\end{aligned}
$$

where in the last step, because of translational invariance, we put $|-1,k\rangle=|1,k\rangle$. It is worth noting that, contrarily to what happens for a 1D-chain, for the zig-zag ladder the hopping operator has a non zero element on the diagonal. We are left with the last contribution which has $d=2$. Following the same procedure we obtain:

$$
\begin{aligned}
\mathcal{H}_t|2,k\rangle &= \frac{-t}{\sqrt{N}}\sum_j e^{i\frac{k}{2}(j+m/2)a}\sum_{i,\sigma,s}A_s\Bigg(c^\dagger_\sigma(i+2)c_\sigma(i)+c^\dagger_\sigma(i+1)c_\sigma(i)
\end{aligned}
$$

$$+c_\sigma^\dagger(i-1)c_\sigma(i)+c_\sigma^\dagger(i-2)c_\sigma(i)\Big)c_s^\dagger(j)c_{\bar{s}}^\dagger(j+2)\,|0\rangle =$$

$$= -2t\Bigg[\cos\left(\frac{ka}{2}\right)|4,k\rangle+\cos\left(\frac{ka}{4}\right)|3,k\rangle$$

$$+\cos\left(\frac{ka}{4}\right)|1,k\rangle+\sqrt{2}\cos\left(\frac{ka}{2}\right)|0,k\rangle\Bigg]\ . \tag{9.42}$$

Finally, collecting together all the results we can write the following matrix representation for the $t-J_p$ Hamiltonian:

$$\langle d_i,k|\,\mathcal{H}_{t-J_p}\,|d_j,k\rangle = \begin{pmatrix} 0 & -\sqrt{2}\epsilon_k^{(1)} & -\sqrt{2}\epsilon_k^{(2)} & 0 & 0 & \dots \\ -\sqrt{2}\epsilon_k^{(1)} & -J_p+\epsilon_k^{(2)} & -\epsilon_k^{(1)} & \epsilon_k^{(2)} & 0 & \dots \\ -\sqrt{2}\epsilon_k^{(2)} & -\epsilon_k^{(1)} & -J_p & -\epsilon_k^{(1)} & \epsilon_k^{(2)} & \ddots \\ 0 & -\epsilon_k^{(2)} & -\epsilon_k^{(1)} & 0 & -\epsilon_k^{(1)} & \ddots \\ 0 & 0 & -\epsilon_k^{(2)} & -\epsilon_k^{(1)} & 0 & \ddots \\ \vdots & \vdots & \ddots & \ddots & \ddots & \ddots \end{pmatrix}\ , \tag{9.43}$$

with

$$\epsilon_k^{(1)} = 2t\cos\left(\frac{ka}{4}\right)\ ,\ \epsilon_k^{(2)} = 2t\cos\left(\frac{ka}{2}\right)\ . \tag{9.44}$$

As one would expect, the above results reduce to the ones obtained in the case of a 1D-chain for $\epsilon_k^{(2)} \to 0$ and $k \to k/2$. The complete ground-state dispersion, reported in Fig.9.5, can be found by diagonalizing the matrix representation (9.43). Analytical results can only be obtained in the limit for $t \ll J_p$ in which the bipolaron dispersion can be written as:

$$E_s(k) = -J_p - t\left[\cos\left(\frac{ka}{2}\right)+\sqrt{1+4\cos^4\left(\frac{ka}{4}\right)}\right]+O\left(t^2\right)\ . \tag{9.45}$$

It is worth noting that, as one would expect, $E_s(k)$ exhibits a linear-t dependence with respect to the one-dimensional dispersion (9.45) since, for this particular geometry, a single hopping is sufficient for the coherent propagation of the inter-site bipolaron through the lattice.

According to Eq.9.35, the above ground state dispersion leads to the following bipolaron effective mass m^{**}:

$$m^{**}_{ZZL}|_{t\ll J_p} = \frac{20\hbar^2}{\left(5+2\sqrt{5}\right)a^2 t}\ . \tag{9.46}$$

A straightforward comparison with the results obtained in the case of a one-dimensional chain gives:

$$\left.\frac{m^{**}}{m^*}\right|_{t\ll J_p} = \begin{cases} J_p/3t & \text{chain} \\ 50-20\sqrt{5} & \text{zig-zag ladder} \end{cases}\ , \tag{9.47}$$

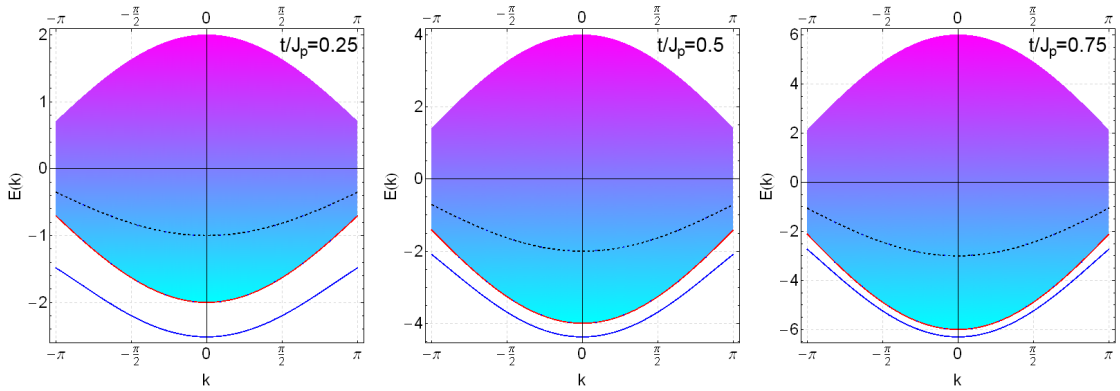

Figure 9.5: Energy dispersion for bipolaron (blue line), single polaron (dashed line) and two unpaired polarons (red lines) in a zig-zag ladder for different values of t/J_p. Filled areas correspond to all the possible scattering states.

where m^* is the single polaron mass:

$$m^* = \begin{cases} \hbar^2/2a^2t & \text{chain} \\ 2\hbar^2/5a^2t & \text{zig-zag ladder} \end{cases} . \tag{9.48}$$

As reported in the right panel of Fig.9.6, the linear-t dependence in the zig-zag ladder dispersion (9.45) leads to a constant ratio m^{**}/m^* for $t \ll J_p$, which is strongly reduced if one takes into account the full bipolaron dispersion by diagonalizing numerically $\mathcal{H}_{t-J_p}$ from Eq.9.43. Importantly, by comparing Fig.9.6 and Fig.9.7 it is immediate to realize that, regardless of the particular geometry, there is a finite probability to find NN bipolarons in the same range in which $m^{**} \approx 2m^*$, signaling the presence of small and super-light pairs of polarons which propagate coherently in the lattice. This evidence is further bolstered by the finding of a very small bipolaron radius r, calculated as the inverse of the decay length α. In fact, as reported in Fig.9.6, we have $d < 2a$ in the whole range $0 \leq t/J_p \leq 1$ with $d < a$ in the region for $t \ll J_p$ where the double occupancy plays a non-negligible role.

9.2.2 Generalization to the triplet case

It is worth noting that, with very small changes, the basis reported in Eq.9.18 can be easily generalized to the case of a spin-triplet configuration by defining :

$$|d, \boldsymbol{k}\rangle_{s=1} = \frac{1}{\sqrt{2N}} \sum_{m,\rho} e^{i\left(m+\frac{d}{2}\right)\boldsymbol{k}\cdot\boldsymbol{a}} c^\dagger_\rho(m) c^\dagger_\rho(m+d) \, |0\rangle \ . \tag{9.49}$$

Unlike in the singlet case, according to the notation reported in Eq.9.22 the exchange Hamiltonian $\mathcal{H}_{J_p}$ gives:

$$\langle d_1, \boldsymbol{k}| \, \mathcal{H}_{J_p} \, |d_2, \boldsymbol{k}'\rangle_{s=1} = J_p \delta_{d_1,d_2} \ . \tag{9.50}$$

On the contrary, regardless the particular geometry, the hopping part does not care about the spin symmetry and therefore we have the same hopping contributions

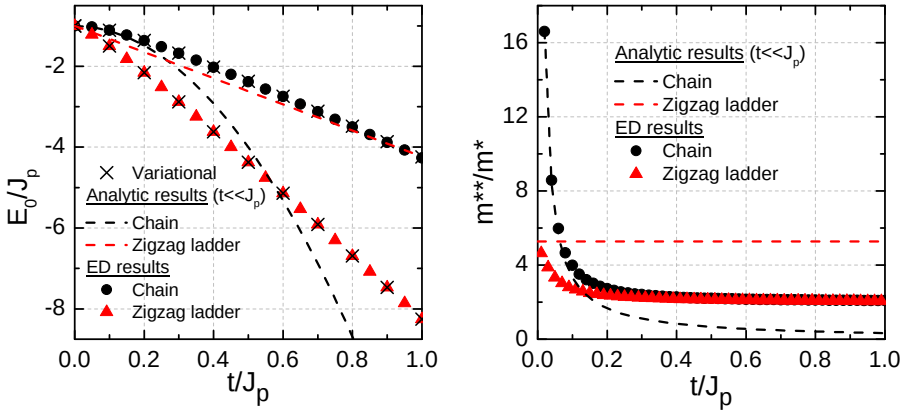

Figure 9.6: Left panel: bipolaron dispersion in the ground state of the polaronic $t - J_p$ model as a function of the ratio t/J_p. Right panel: ratio of bipolaron to polaron effective mass. Data obtained by exact diagonalization of $\mathcal{H}_{tJ_p}$ (symbols) from (9.28) and (9.43) have been compared with analytical results (dashed lines) in the $t \ll J_p$ limit (Eq.9.33 and Eq.9.43) and variational results (crosses, left panel only) obtained with the method developed in Ref.[55].

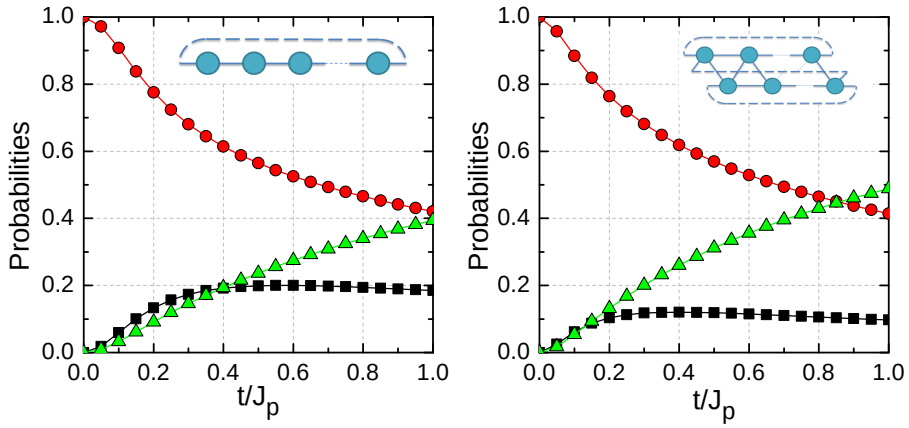

Figure 9.7: Probability of finding two polarons on the nearest-neighbour sites (circles), on more distant sites (triangles) and on the same site (squares) in the ground state of the polaronic $t - J_p$ Hamiltonian for chain (left panel) and zigzag ladder (right panel).

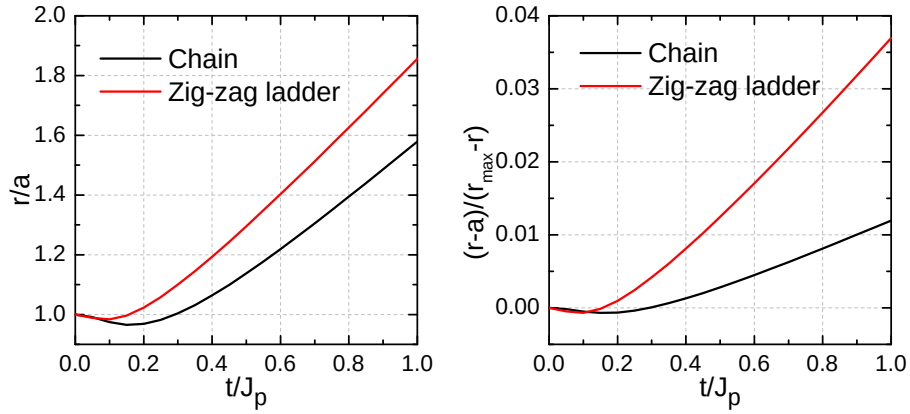

Figure 9.8: Averaged distance r between two polarons (left panel) and the corresponding rescaled value (right panel) plotted versus the ratio t/J_p for a 100-site chain and zig-zag ladder. Here a is the lattice constant and r_{max} is the maximum distance that can be reached according to the dimension of the lattice with periodic boundary conditions: $r_{max} = Na/2$ for a N-site chain, and $r = a\sqrt{(N/2-1)^2 + 3/4}$ for a N-site zig-zag ladder.

for chain and zig-zag ladder already described in Sec.9.2. The only difference with respect to the singlet case lays in the complete absence of any transition to doubly occupied states which are negated by symmetrization and Pauli exclusion principle. Hence the matrix representation of the polaronic $t-J_p$ Hamiltonian in the projected two-particle triplet subspace can be easily obtained by removing the first column and the first row of the singlet-subspace projection. Therefore, from Eq.9.37 and Eq.9.43 we obtain:

$$\langle d_i, k| \mathcal{H}_{t-J_p} |d_j, k\rangle_{s=1} = \begin{pmatrix} J_p & -\epsilon_k & 0 & \dots \\ -\epsilon_k & 0 & -\epsilon_k & \ddots \\ 0 & -\epsilon_k & 0 & \ddots \\ \vdots & \ddots & \ddots & \ddots \end{pmatrix} , \ \epsilon_k = 2t\cos\left(\frac{ka}{2}\right) , \quad (9.51)$$

for a 1D-chain, while for the zig-zag ladder we have:

$$\langle d_i, k| \mathcal{H}_{t-J_p} |d_j, k\rangle_{s=1} = \begin{pmatrix} J_p + \epsilon_k^{(2)} & -\epsilon_k^{(1)} & \epsilon_k^{(2)} & 0 & \dots \\ -\epsilon_k^{(1)} & J_p & -\epsilon_k^{(1)} & \epsilon_k^{(2)} & \ddots \\ \epsilon_k^{(2)} & -\epsilon_k^{(1)} & 0 & -\epsilon_k^{(1)} & \ddots \\ 0 & 0 & -\epsilon_k^{(1)} & 0 & \ddots \\ \vdots & \vdots & \ddots & \ddots & \ddots \end{pmatrix} , \quad (9.52)$$

with:

$$\begin{cases} \epsilon_k^{(1)} = 2t\cos\left(\frac{ka}{4}\right) \\ \epsilon_k^{(2)} = 2t\cos\left(\frac{ka}{2}\right) \end{cases} . \quad (9.53)$$

Since the triplet state is unbound, we can not calculate analytically the energy dispersion $E(k)$ because we do not have any hint for the ground-state wave function.

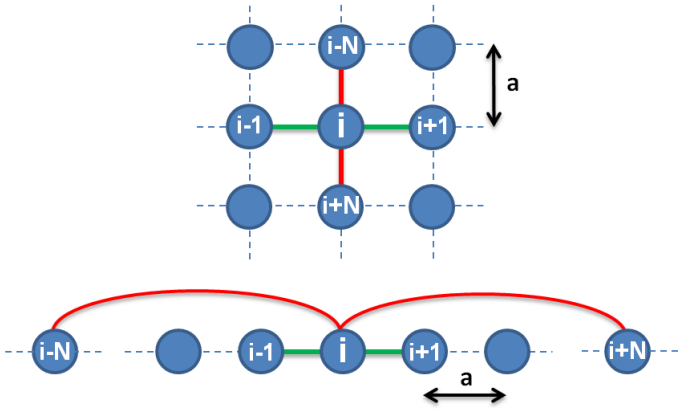

Figure 9.9: (Color online) Square lattice to chain mapping in the case of NN interactions.

However, a complete analysis of the ground state properties can be obtained by exact diagonalization. In particular it can be seen that the ground state energy, calculated as the minimum eigenvalue of the $t - J_p$ matrix representation, converges to a finite value when d exceeds a threshold value d^*, which can be seen as the minimum size of the system above which finite-size effects become negligible. As one would expect, d^* is intrinsically related to the bipolaron size, therefore it increases with increasing ratio t/J_p. However, as long as the ground state configuration is bound, its energy can be always obtained by solving numerically the eigenvalue problem of a finite $d \times d$ matrix, with $(d > d^\star)$, without the loss of generality. For the triplet state instead, which is unbound, we note that as long as the interaction range is finite, two polarons with aligned spins prefer not to sit on nearest neighbour sites in order to minimize their energy. Hence we have a complete degeneracy between the triplet and the unbound ground state configurations, on which basis the triplet ground state energy can be straightforwardly estimated.

9.2.3 Generalization to two-dimensional geometries

Let us consider a generic two-dimensional $N \times N$ lattice. In principle, according to the notation introduced in the previous Sections, the ground state configuration for a 2D geometry can still be described as a superposition of all the possible singlet configurations with distance $\boldsymbol{d}$ between two particle. In this case $\boldsymbol{d}$ will be a vector of components d_x and d_y along the x and the y axes, respectively. At this point we can note that it is always possible to map a two-dimensional $N \times N$ configuration into a one-dimensional chain of N^2 sites by extending the range of all the interactions according to the particular geometry. An example is reported in Fig.9.9 for a square lattice with NN interactions.

By means of this mapping we can use the following generalization of the symmetry-adapted singlet basis introduced in Eq.9.18:

$$|d, \boldsymbol{k}\rangle = \frac{1}{\sqrt{N}} \sum_{\rho,j} \rho E(j, d, \boldsymbol{k}) c^\dagger_\rho(j+d) c_{\bar{\rho}}(j) \, |0\rangle \ , \tag{9.54}$$

where x and y components of the centre-of-mass position (j) and the distance (d) between the two polarons can be easily derived from the one-dimensional parameters j and d as follows:

$$\begin{cases} j_x = Rem\,[j, N] \\ j_y = Mod\,[j, N] \end{cases} , \begin{cases} d_x = Rem\,[d, N] \\ d_y = Mod\,[d, N] \end{cases} , \tag{9.55}$$

where $Mod[x, y]$ and $Rem[x, y]$ give the quotient and the reminder of x/y, respectively. Finally, $E(j, d, \boldsymbol{k})$ is a scalar function that takes into account all the possible translations of the centre-of-mass:

$$E(j, d, \boldsymbol{k}) \equiv e^{i(j_x + d_x/2)k_x a_x} e^{i(j_y + d_y/2)k_y a_y} . \tag{9.56}$$

In this case, the translation $d \to d + n_y N$ in the $1D$ system will correspond, for the $2D$ system, to the increase of the distance between the two electron of n_y unit cells along the y-direction. According to Eq.9.55, if we call d_{x0}, d_{y0}, j_{x0} and j_{y0} the original coordinates of the system, we have:

$$\begin{cases} d_x = Rem[d + n_y N, N] = Rem[d_{x0} + d_{y0}, N] + Rem[n_y N, N] = \\ \quad = Rem[d_{x0} + d_{y0}, N] = d_{x0} \\ d_y = Mod[d + n_y N, N] = Mod[d_{x0} + d_{y0}, N] + Mod[n_y N, N] = \\ \quad = Mod[d_{x0} + d_{y0}, N] + n_y = d_{y0} + n_y \end{cases} . \tag{9.57}$$

Then Eq.9.56 gives the following contribution for the resulting translation of the centre-of-mass: $E(j, d + n_y N, \boldsymbol{k}) = E(j, d + n_y N, \boldsymbol{k}) e^{i n_y k_y a_y/2}$. Similarly, the translation $d \to d + n_x$, with $n_x < N$, will correspond to the increase of the distance between the two electron of n_x unit cells along the x-direction:

$$\begin{cases} d_x = Rem[d + n_x N, N] = Rem[d_{x0} + d_{y0}, N] + Rem[n_x N, N] = \\ \quad = Rem[d_{x0} + d_{y0}, N] + n_x = d_{x0} + n_x \\ d_y = Mod[d + n_x N, N] = Mod[d_{x0} + d_{y0}, N] + Mod[n_x N, N] = \\ \quad = Mod[d_{x0} + d_{y0}, N] = d_{y0} \end{cases} , \tag{9.58}$$

with the following translation for the centre-of-mass: $E(j, d + n_y N, \boldsymbol{k}) = E(j, d + n_x N, \boldsymbol{k}) e^{i n_x k_x a_x/2}$. We report in Fig.9.10 the matrix-plot of the singlet-subspace projection with respect to the basis (9.54) obtained for the $t - J_p$ Hamiltonian in the case of square and a triangular lattices.

Regardless of the particular geometry, as already discussed for the 1D case, the ground state energy, calculated as the minimum eigenvalue of the $t - J_p$ matrix representation, converges to a finite value after that a critical dimension d^* has been achieved. Then the ground state dispersion can be calculated by solving numerically the eigenvalue problem of a $d \times d$ sparse matrix, with $d > d^*$, without the loss of generality. Moreover, following the prescription outlined in the previous Section, the spin-triplet dispersion can be also obtained by taking $J_p \to -J_p$ on the diagonal and removing the first row and the first column. Singlet and triplet energy dispersions are reported in Fig.9.11 in the case of a square lattice.

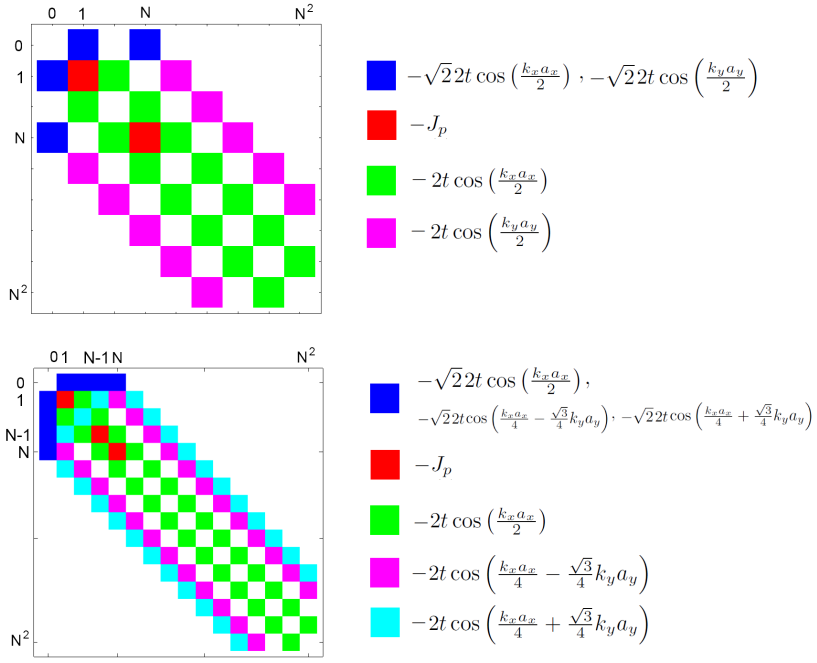

Figure 9.10: (Color online) Matrix-plot for the $N^2 \times N^2$ matrix representation of the $t - J_p$ Hamiltonian in the singlet subspace for a square lattice (upper panel) and a triangular lattice (lower panel).

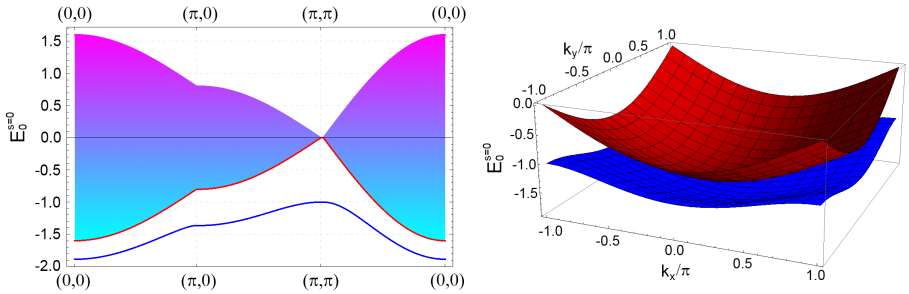

Figure 9.11: (Color online) Energy dispersion for bipolaron (blue line, blue surface in the 3D plot), single polaron (dashed line) and two unpaired polarons (red lines, red surface in the 3D plot) for a square lattice at $t/J_p = 0.2$. All the possible scattering states are represented by the filled area. Filling colors from cyan to magenta correspond to different values of the scattering vector $\boldsymbol{q}$ from $(0, 0)$ to (π, π).

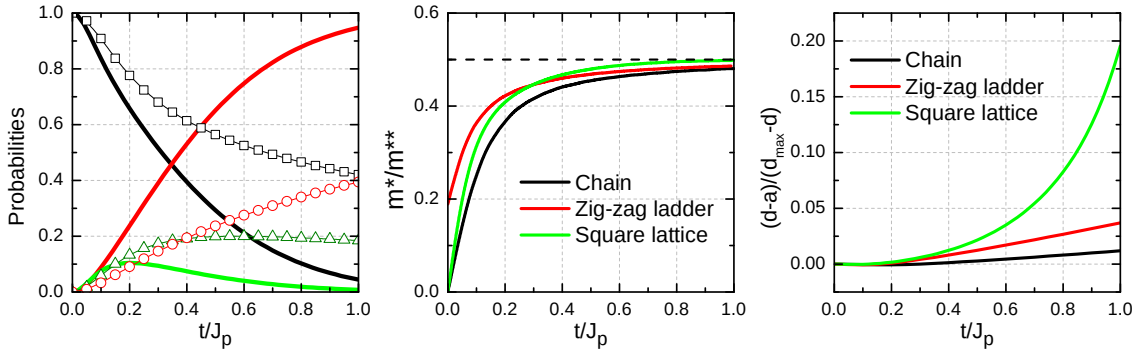

Figure 9.12: Left panel: probability of finding two polarons on the nearest-neighbour sites (black curves), on more distant sites (red curves) and on the same site (green curves) in the ground state of the polaronic $t - J_p$ Hamiltonian for a 2D square lattice versus t/J_p for chain (symbols) and square lattice (solid lines). Central panel: single polaron to bipolaron mass ratio for chain, zig-zag ladder and square lattice (m^* = for the 2D square lattice) versus t/J_p. Right panel: rescaled bipolaron radius versus t/J_p for different geometries ($d_{max} = aN/\sqrt{2}$ for a $N \times N$ square lattice).

A straightforward comparison between 1D and 2D results on NN bipolaron density, bipolaron effective mass and bipolaron radius, reported in Fig.9.12, show that the probability to find NN and on-site bipolarons is strongly suppressed in the case of a square lattice, leading to a strong enhancement of the probability to find large bipolarons. This feature is also reflected in the calculation of bipolaron effective mass m^{**} and bipolaron radius d. In fact, as shown in central and right panels of Fig.9.12, $m^{**} \approx 2m^*$ and, coherently, the rescaled bipolaron size increases in the range in which $t \approx J_p$.

Square lattice: detailed calculations

As reported in Fig.9.9, the square lattice can be mapped into a $1D$ chain with hopping and exchange interaction restricted to nearest neighbours and to N-distant sites, reproducing the interaction along x and y axis, respectively. By means of (9.22), it is immediate to see that the exchange contribution reads as:

$$\langle d_1, \boldsymbol{k}| \mathcal{H}_{J_p} |d_2, \boldsymbol{k}'\rangle = -J_p \delta_{d_1,d_2} \left(\delta_{d_1,1} + \delta_{d_1,N}\right) \ , . \tag{9.59}$$

For the hopping part instead, for any distance $d \neq \{0, 1, N\}$, we have:

$$\begin{aligned}
\mathcal{H}_t |d, \boldsymbol{k}\rangle &= \frac{-t}{\sqrt{N}} \sum_{\rho,j} \sum_{i\sigma} \rho E(j, d, \boldsymbol{k}) \Big[c^\dagger_\sigma(i+N) c_\sigma(i) + c^\dagger_\sigma(i-N) c_\sigma(i) \\
&\quad + c^\dagger_\sigma(i+1) c_\sigma(i) + c^\dagger_\sigma(i-1) c_\sigma(i) \Big] c^\dagger_\rho(j+d) c_{\bar\rho}(j) |0\rangle = \\
&= \frac{-t}{\sqrt{N}} \sum_{\rho,j} \rho E(j, d, \boldsymbol{k}) \Big[c^\dagger_\rho(j+d+N) c^\dagger_{\bar\rho}(j) + c^\dagger_\rho(j+d-N) c^\dagger_{\bar\rho}(j) \\
&\quad + c^\dagger_\rho(j+d+1) c^\dagger_{\bar\rho}(j) + c^\dagger_\rho(j+d-1) c^\dagger_{\bar\rho}(j) +
\end{aligned}$$

$$
\begin{aligned}
&+c^\dagger_\rho(j+d)c^\dagger_{\bar\rho}(j+N)+c^\dagger_\rho(j+d)c^\dagger_{\bar\rho}(j-N)\\
&+c^\dagger_\rho(j+d)c^\dagger_{\bar\rho}(j+1)+c^\dagger_\rho(j+d)c^\dagger_{\bar\rho}(j-1)\Big]|0\rangle =\\
=\;& \frac{-t}{\sqrt{N}}\sum_{\rho,j}\Big[c^\dagger_\rho(j+d+N)c_{\bar\rho}(j)E(j,d+N,\boldsymbol{k})e^{-ik_ya_y/2}\left[1+e^{ik_ya_y}\right]+\\
&+c^\dagger_\rho(j+d-N)c_{\bar\rho}(j)E(j,d-N,\boldsymbol{k})e^{ik_ya_y/2}\left[1+e^{-ik_ya_y}\right]+\\
&+c^\dagger_\rho(j+d+1)c_{\bar\rho}(j)E(j,d+1,\boldsymbol{k})e^{-ik_xa_x/2}\left[1+e^{ik_xa_x}\right]+\\
&+c^\dagger_\rho(j+d-1)c_{\bar\rho}(j)E(j,d-1,\boldsymbol{k})e^{ik_xa_x/2}\left[1+e^{-ik_xa_x}\right]\Big]|0\rangle =\\
=\;& -2t\Bigg[\cos\left(\frac{k_xa_x}{2}\right)\left(|d+1,\boldsymbol{k}\rangle+|d-1,\boldsymbol{k}\rangle\right)\\
&+\cos\left(\frac{k_ya_y}{2}\right)\left(|d+N,\boldsymbol{k}\rangle+||d-N|,\boldsymbol{k}\rangle\right)\Bigg], \qquad (9.60)
\end{aligned}
$$

while for the $d=0,1,N$ cases, in which configurations with doubly occupied sites are involved, we have:

$$
\begin{aligned}
\mathcal{H}_t|0,\boldsymbol{k}\rangle =\;& \frac{-t}{\sqrt{N}}\sum_{i,j,\sigma}e^{ij(k_xa_x+k_ya_y)}\Big[c^\dagger_\sigma(i+N)c_\sigma(i)+c^\dagger_\sigma(i-N)c_\sigma(i)+\\
&c^\dagger_\sigma(i+1)c_\sigma(i)+c^\dagger_\sigma(i-1)c_\sigma(i)\Big]c^\dagger_\uparrow(j)c_\downarrow(j)|0\rangle =\\
=\;& \frac{-t}{\sqrt{N}}\sum_j e^{ij(k_xa_x+k_ya_y)}\Big[c^\dagger_\uparrow(j+N)c^\dagger_\downarrow(j)-c^\dagger_\downarrow(j+N)c^\dagger_\uparrow(j)\\
&+c^\dagger_\uparrow(j-N)c^\dagger_\downarrow(j)-c^\dagger_\downarrow(j-N)c^\dagger_\uparrow(j)\\
&+c^\dagger_\uparrow(j+1)c^\dagger_\downarrow(j)-c^\dagger_\downarrow(j+1)c^\dagger_\uparrow(j)\\
&+c^\dagger_\uparrow(j-1)c^\dagger_\downarrow(j)-c^\dagger_\downarrow(j-1)c^\dagger_\uparrow(j)\Big]|0\rangle =\\
=\;& \frac{-\sqrt{2}t}{\sqrt{N}}\sum_{\rho,j}\Big[\rho c^\dagger_\rho(j+N)c_{\bar\rho}(j)E(j,N,\boldsymbol{k})e^{-ik_ya_y/2}\left[1+e^{ik_ya_y}\right]+\\
&+c^\dagger_\rho(j+1)c_{\bar\rho}(j)E(j,d-1,\boldsymbol{k})e^{-ik_xa_x/2}\left[1+e^{ik_xa_x}\right]\Big]|0\rangle =\\
=\;& -2\sqrt{2}t\left[\cos\left(\frac{k_xa_x}{2}\right)|1,\boldsymbol{k}\rangle+\cos\left(\frac{k_ya_y}{2}\right)|N,\boldsymbol{k}\rangle\right], \qquad (9.61)
\end{aligned}
$$

$$
\begin{aligned}
\mathcal{H}_t|1,\boldsymbol{k}\rangle =\;& \frac{-t}{\sqrt{N}}\sum_{\rho,j}\sum_{i\sigma}\rho E(j,1,\boldsymbol{k})\Big[c^\dagger_\sigma(i+N)c_\sigma(i)+c^\dagger_\sigma(i-N)c_\sigma(i)\\
&+c^\dagger_\sigma(i+1)c_\sigma(i)+c^\dagger_\sigma(i-1)c_\sigma(i)\Big]c^\dagger_\rho(j+1)c_{\bar\rho}(j)|0\rangle =\\
=\;& \frac{-t}{\sqrt{N}}\sum_{\rho,j}\rho E(j,1,\boldsymbol{k})\Big[c^\dagger_\rho(j+1+N)c^\dagger_{\bar\rho}(j)+c^\dagger_\rho(j+1-N)c^\dagger_{\bar\rho}(j)\\
&+c^\dagger_\rho(j+2)c^\dagger_{\bar\rho}(j)+c^\dagger_\rho(j)c^\dagger_{\bar\rho}(j)+c^\dagger_\rho(j+1)c^\dagger_{\bar\rho}(j+N)
\end{aligned}
$$

$$
\begin{aligned}
&+c^\dagger_\rho(j+1)c^\dagger_{\bar\rho}(j-N)+c^\dagger_\rho(j+1)c^\dagger_{\bar\rho}(j+1)+c^\dagger_\rho(j-1)c^\dagger_{\bar\rho}(j+1)\Big]|0\rangle = \\
= \;& \frac{-t}{\sqrt{N}}\sum_{\rho,j}\Big[c^\dagger_\rho(j+N+1)c_{\bar\rho}(j)E(j,N+1,\boldsymbol{k})e^{-ik_ya_y/2}\left[1+e^{ik_ya_y}\right]+ \\
&+c^\dagger_\rho(j+1-N)c_{\bar\rho}(j)E(j,1-N,\boldsymbol{k})e^{ik_ya_y/2}\left[1+e^{-ik_ya_y}\right]+ \\
&+c^\dagger_\rho(j+2)c_{\bar\rho}(j)E(j,2,\boldsymbol{k})e^{-ik_xa_x/2}\left[1+e^{ik_xa_x}\right]\Big]|0\rangle + \\
&\frac{-\sqrt{2}t}{\sqrt{N}}\sum_j c^\dagger_\rho(j)c_{\bar\rho}(j)e^{ik_xa_x/2}\left[1+e^{-ik_xa_x}\right]|0\rangle = \\
= \;& -2t\Bigg[\cos\left(\frac{k_xa_x}{2}\right)|2,\boldsymbol{k}\rangle+\cos\left(\frac{k_ya_y}{2}\right)|N+1,\boldsymbol{k}\rangle \\
&+\cos\left(\frac{k_ya_y}{2}\right)|N-1,\boldsymbol{k}\rangle+\sqrt{2}\cos\left(\frac{k_xa_x}{2}\right)|0,\boldsymbol{k}\rangle\Bigg], \qquad (9.62)
\end{aligned}
$$

$$
\begin{aligned}
\mathcal{H}_t|N,\boldsymbol{k}\rangle \;=\; & \frac{-t}{\sqrt{N}}\sum_{\rho,j}\sum_{i\sigma}\rho E(j,N,\boldsymbol{k})\Big[c^\dagger_\sigma(i+N)c_\sigma(i)+c^\dagger_\sigma(i-N)c_\sigma(i) \\
&+c^\dagger_\sigma(i+1)c_\sigma(i)+c^\dagger_\sigma(i-1)c_\sigma(i)\Big]c^\dagger_\rho(j+N)c_{\bar\rho}(j)|0\rangle = \\
= \;& \frac{-t}{\sqrt{N}}\sum_{\rho,j}\rho E(j,N,\boldsymbol{k})\Big[c^\dagger_\rho(j+2N)c^\dagger_{\bar\rho}(j)+c^\dagger_\rho(j)c^\dagger_{\bar\rho}(j)+ \\
&c^\dagger_\rho(j+N+1)c^\dagger_{\bar\rho}(j)+c^\dagger_\rho(j+N-1)c^\dagger_{\bar\rho}(j)+c^\dagger_\rho(j+N)c^\dagger_{\bar\rho}(j+N) \\
&+c^\dagger_\rho(j+N)c^\dagger_{\bar\rho}(j-N)+c^\dagger_\rho(j+N)c^\dagger_{\bar\rho}(j+1)+c^\dagger_\rho(j+N)c^\dagger_{\bar\rho}(j-1)\Big]|0\rangle = \\
= \;& \frac{-t}{\sqrt{N}}\sum_{\rho,j}\Big[c^\dagger_\rho(j+2N)c_{\bar\rho}(j)E(j,2N,\boldsymbol{k})e^{-ik_ya_y/2}\left[1+e^{ik_ya_y}\right]+ \\
&+c^\dagger_\rho(j+N+1)c_{\bar\rho}(j)E(j,N+1,\boldsymbol{k})e^{-ik_xa_x/2}\left[1+e^{ik_xa_x}\right]+ \\
&+c^\dagger_\rho(j+N-1)c_{\bar\rho}(j)E(j,N-1,\boldsymbol{k})e^{ik_xa_x/2}\left[1+e^{-ik_xa_x}\right]\Big]|0\rangle + \\
&\frac{-\sqrt{2}t}{\sqrt{N}}\sum_j c^\dagger_\rho(j)c_{\bar\rho}(j)e^{ik_ya_y/2}\left[1+e^{-ik_ya_y}\right]|0\rangle = \\
= \;& -2t\Bigg[\cos\left(\frac{k_xa_x}{2}\right)|N+1,\boldsymbol{k}\rangle+\cos\left(\frac{k_xa_x}{2}\right)|N-1,\boldsymbol{k}\rangle \\
&+\cos\left(\frac{k_ya_y}{2}\right)|d+N,\boldsymbol{k}\rangle+\sqrt{2}\cos\left(\frac{k_ya_y}{2}\right)|0,\boldsymbol{k}\rangle\Bigg]. \qquad (9.63)
\end{aligned}
$$

Then, the matrix representation of $\mathcal{H}_{t-J_p}$ for a $N\times N$ square lattice can be immediately obtained by adding together all the contributions according to the relation $\langle d_1,\boldsymbol{k}|\,\mathcal{H}_{t-J_p}\,|d_2,\boldsymbol{k}\rangle$. A schematic representation is reported in Fig.9.10. Similarly to the triplet case, we do not have an analytical relation for the ground state dispersion in the $N\to\infty$ limit. However, numerical calculations show that the ground state energy, calculated as the minimum eigenvalue of the $t-J_p$ matrix representation,

converges to a finite value after a critical dimension $d^\star$ has been achieved. It follows that the ground state energy can be obtained by solving numerically the eigenvalue problem of a $d \times d$ matrix, with $(d > d^\star)$, without the loss of generality.

Chapter 10

$t - J_p$ and $t - J_p - \tilde{U}$ models

As shown in detail in Sec.8.2, in highly polarizable ionic lattices, bare *long-range* Coulomb and Fröhlich interactions almost negate each other giving rise to a new physics described by the polaronic t-J_p Hamiltonian [34]

$$\mathcal{H} = -\sum_{i,j} \left(t_{ij}\delta_{s,s'} + \tilde{\tilde{\mu}}\delta_{ij} \right) c_i^\dagger c_j + 2 \sum_{\boldsymbol{m}\neq\boldsymbol{n}} J_p(\boldsymbol{m}-\boldsymbol{n}) \left(\overrightarrow{S}_{\boldsymbol{m}} \cdot \overrightarrow{S}_{\boldsymbol{n}} + \frac{1}{4}\hat{n}_{\boldsymbol{m}}\hat{n}_{\boldsymbol{n}} \right) \ , \quad (10.1)$$

where t_{ij} is the renormalized hopping integral given in Eq.(8.40), $\tilde{\tilde{\mu}}$ is the rescaled chemical potential (8.66) and $J_p(\boldsymbol{m}-\boldsymbol{n})$ is the exchange interaction between polarons on different sites, coming from a residual polaron-multiphonon interactions (8.63). Here $i = (\boldsymbol{m}, s)$ and $j = (\boldsymbol{n}, s')$ include both site $(\boldsymbol{m}, \boldsymbol{n})$ and spin (s, s') states, while the sum over $\boldsymbol{m} \neq \boldsymbol{n}$ counts each pair once only. $\boldsymbol{S}_{\boldsymbol{m}} = (1/2)\sum_{\sigma\sigma'} c^\dagger_{\boldsymbol{m}\sigma} \overrightarrow{\tau}_{\sigma\sigma'} c_{\boldsymbol{m}\sigma'}$ is the spin-(1/2) operator ($\overrightarrow{\tau}$ are the Pauli matrices), $n_{\boldsymbol{m}} = n_{\boldsymbol{m}\uparrow} + n_{\boldsymbol{m}\downarrow}$, and $n_{\boldsymbol{m}\sigma} = c^\dagger_{\boldsymbol{m}\sigma} c_{\boldsymbol{m}\sigma}$ are the site occupation operators.

It is worth noting that, given the overall constraint $\varepsilon_0 \gg \varepsilon_\infty$ on static ε_0 and dynamic ε_∞ dielectric constants, which follows under the assumption of high-polarizable lattices, the t-J_p model is exact since the Schrieffer-Wolf transformation adopted in the derivation of the model (see Sec.8.2) is accurate for intermediate and strong electron-phonon couplings with $\lambda \geqslant 1/\sqrt{2}z$. Here λ parametrizes the strength of the electron-phonon coupling and z is the lattice coordination number. The residual inter-site interactions, not accounted in (10.1), are small compared to the exchange interaction J_p if $\varepsilon_0 \gg \varepsilon_\infty$. However the on-site contribution, which has been initially neglected in the bare microscopic Hamiltonian (8.1) from which the model is derived, could be relevant if the size of the Wannier orbitals is small compared to the lattice constant. This contribution reflects in the presence of an additional on-site coupling $\tilde{U}$, with $\tilde{U} > 0$, given by the competition between on-site Coulomb and electron-phonon interactions. Different from the bare Hubbard-U, $\tilde{U}$ can only be as large as few hundred meV since for almost all the relevant compounds the bare U (e.g. the bare Hubbard-U on the oxygen orbitals in a rigid Cuprate lattice) is of the same order of magnitude of the on-site Fröhlich interaction (from 1eV

to2eV approximately [42]). Regardless of its value, it can be seen that by including an on-site Hubbard-$\tilde{U}$ contribution in the microscopic Hamiltonian (8.1) and performing Lang-Firsov and Schrieffer-Wolf transformations (see Chapter 8), one also obtains the following expression for the exchange interaction:

$$J_p(\boldsymbol{m}-\boldsymbol{n}) \rightarrow J_p(\boldsymbol{m}-\boldsymbol{n},\tilde{U}) \equiv \frac{t^2}{\hbar\omega_0}\sum_{k=1}^{\infty}\frac{\left(2g^2(\boldsymbol{m}-\boldsymbol{n})\right)^k}{k!\left(k+\tilde{U}/\hbar\omega_0\right)}\,, \tag{10.2}$$

where g^2 the dimensionless parameter defined in Eq.8.41 and ω_0 is the electron-phonon frequency. Hence it is immediate to realize that the role of $\tilde{U}$ in the physics described by the polaronic t-J_p model goes much more beyond the mere addition of an on-site contribution in the model Hamiltonian (10.1). $\tilde{U}$ also rescales the polaronic exchange coupling J_p, whose reduction with respect to $J_p(\boldsymbol{m}-\boldsymbol{n},\tilde{U}=0)$, shown in Fig.10.1, can be substantial for $\tilde{U}/\hbar\omega_0 > 2g^2$. This follows from the fact

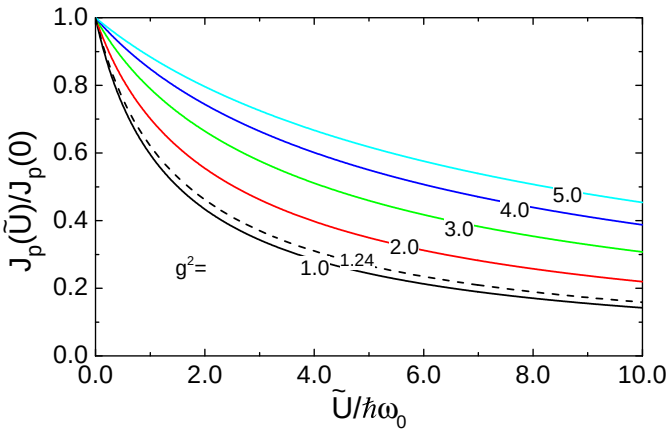

Figure 10.1: Reduction of the inter-site exchange attraction $J_p(\tilde{U})/J_p(0)$ by the on-site residual polaron-polaron repulsion $\tilde{U}/\hbar\omega_0$ for different values of the polaron exponent g^2.

that, as sketched in Fig.10.2, the exchange process is mediated by an intermediate doubly occupied state with energy $\tilde{U}$ with respect to the initial state. Therefore, although there is no potential barrier between two polarons on nearest neighbor sites induced by lattice deformation, the gap between the initial and the intermediate state could be so high as to almost suppress the exchange mechanism, as one would expect.

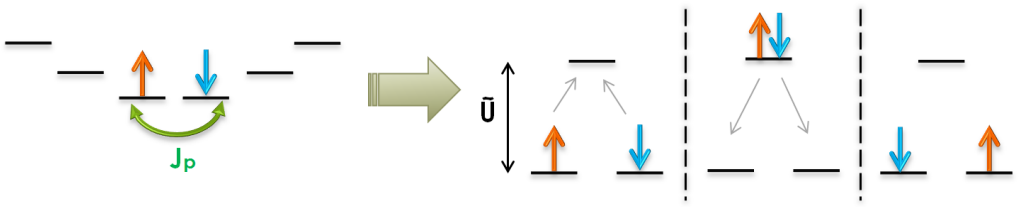

Figure 10.2: Exchange transfer of two polarons with opposite spins between nearest-neighbor sites with no potential barrier induced by lattice deformation.

Hence, by taking into account the twofold effect of the on-site interaction $\tilde{U}$, we come up with the so-called extended polaronic t-J_p-$\tilde{U}$ Hamiltonian:

$$\begin{aligned}\mathcal{H} &= -\sum_{i,j}\left(t_{ij}\delta_{s,s'}+\tilde{\tilde{\mu}}\delta_{ij}\right)c_i^{\dagger}c_j+2\sum_{\boldsymbol{m}\neq\boldsymbol{n}}J_p(\boldsymbol{m}-\boldsymbol{n},\tilde{U})\Bigg(\overrightarrow{S}_{\boldsymbol{m}}\cdot\overrightarrow{S}_{\boldsymbol{n}} \\ &\quad +\frac{1}{4}\hat{n}_{\boldsymbol{m}}\hat{n}_{\boldsymbol{n}}\Bigg)+\tilde{U}\sum_{\boldsymbol{m}}\hat{n}_{\boldsymbol{m},\uparrow}\hat{n}_{\boldsymbol{n},\downarrow}\,, \end{aligned} \tag{10.3}$$

which has been argued to describe most of the relevant feature of superconducting and normal states of a large class of compounds among which Cuprates [36, 37]. In particular, it has been shown that, like in the t-J_p model, the ground state of the polaronic t-J_p-$\tilde{U}$ Hamiltonian accounts for the formation of small and super-light pairs of polarons which condense with a critical temperature well in excess of 100K. The effective on-site term $\tilde{U}$, limiting the double occupancy, reduces the inter-site polaron exchange J_p resulting in a transition from small-to-large bipolarons at some critical value of $\tilde{U}$ [36]. Furthermore, the study of thermal-induced recombination of polarons and bipolarons as a charged Bose-Fermi mixture showed that the model is also able to describe pseudogap features in the underdoped normal state of Cuprate superconductors [37]. All the aforementioned topics will be discussed in detail in the following Sections.

In Sec.10.1 we analyze the effect of $\tilde{U}$ on the ground state bipolaronic configuration. We show that the on-site interaction $\tilde{U}$ drives the system to a small-to-large bipolaron transition and eventually destroys the bipolaronic ground state when the ratio $t/J_p(\tilde{U})$ exceeds a critical value. We derive the phase diagram of the model in the case of 1D and 2D geometries. In Sec.10.2 we provide an explanation for high temperature superconductivity in terms of Bose-Einstein condensation (BEC) of small and light pairs of polarons with a critical temperature well in excess of 100K. We show that the small-to-large bipolaron transition induced by $\tilde{U}$ accounts for the BEC/BCS crossover which reconciles the polaron and bipolaron theory of superconductivity with the observation of a large Fermi surface in the underdoped regime of high-temperature superconductors. In Sec.10.3 we discuss the applicability of the model to Cuprates. We show that, without any ad-hoc assumption on preexisting orders or broken symmetries in the normal state of the model, the polaronic t-J_p-$\tilde{U}$ Hamiltonian is able to describe pseudogap features in density of states, spin susceptibility and electric conductivity in terms of a thermal-induced recombination of bipolarons and unpaired polarons.

10.1 Small to large bipolaron transition

It is immediate to see that, as long as $J_p(\tilde{U})$ is finite, which is always true for all the physical values of $\tilde{U}$ and g^2 (Fig.10.1), the presence of any finite on-site interaction does not change the properties of the static ground state configurations obtained in Sec.9.1 for the $\tilde{U}=0$ case. In fact, by neglecting the polaronic hopping t, we immediately find that in the NN approximation the ground and the higher energy states are still bipolaronic spin-singlet and spin-triplet. Configurations with all polarons

separated by at least one empty site constitute the zero-energy states while the ones with doubly occupied sites appear with higher energies since $\tilde{U} > 0$. Hence, as one would expect, the presence of a finite on-site interaction will only affect the ground state configurations with $t \neq 0$ in which double occupied states might arise from the overlap of polarons induced by the hopping. To better characterize the ground state configuration with finite t, hereafter we adopt the strong coupling approach already described Sec.9.2 for the $\tilde{U} = 0$ case solving first a two-particle problem and then projecting the Hamiltonian on the repulsive Bose gas of small inter-site bipolarons. Hence, for any lattice geometry, the ground state energy dispersion $E(\boldsymbol{k})$ can be determined by solving the Schrödinger equation $\mathcal{H}_{S=0}\psi = E(\boldsymbol{k})\psi$ where $\mathcal{H}_{S=0}$ is the projection of the Hamiltonian (10.3) in the singlet subspace and ψ is the system wave function. Hereafter we will restrict our analysis to 1D chain and 2D square lattice geometries only. For these two cases, we report in Fig.10.3 the projection of the t-J_p-$\tilde{U}$ Hamiltonian (10.3) obtained according to the procedure reported in Sec.10.3 for the one-dimensional chain, and to its generalization to the two-dimensional case reported in Sec.9.2.3.

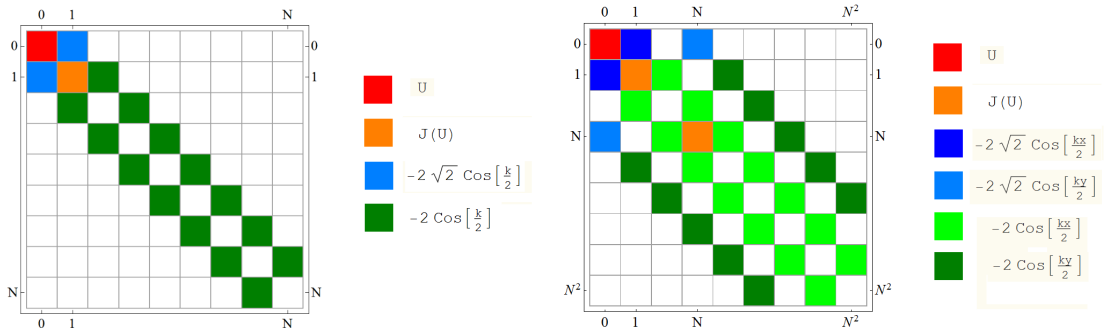

Figure 10.3: Matrix-plot of the $t-J_p(U)$ Hamiltonian in the singlet subspace for a N-site chain (left) and a $N^2 \times N^2$ square lattice (right).

In the presence of a bound state, the ground state dispersion $E(k)$ can be found by imposing a wave solution that is exponentially decaying at some rate in the region where the potential vanishes. In particular for the one-dimensional chain we have:

$$\begin{pmatrix} \tilde{U} & -\sqrt{2}\epsilon_k & 0 & \dots & 0 \\ -\sqrt{2}\epsilon_k & -J_p(\tilde{U}) & -\epsilon_k & 0 & \dots \\ 0 & -\epsilon_k & 0 & -\epsilon_k & \ddots \\ 0 & 0 & -\epsilon_k & 0 & \ddots \\ \vdots & \vdots & \ddots & \ddots & \ddots \end{pmatrix} \begin{pmatrix} d \\ 1 \\ e^{-\alpha} \\ e^{-2\alpha} \\ \vdots \end{pmatrix} = E(k) \begin{pmatrix} d \\ 1 \\ e^{-\alpha} \\ e^{-2\alpha} \\ \vdots \end{pmatrix}, \qquad (10.4)$$

where $\epsilon_k = 2t\cos(ka/2)$, d is the amplitude of on-site pairs and α is the decay rate of the ground state wave function. The three unknowns d, $E(k)$ and α can be determined from the following system of three coupled equations:

$$\begin{cases} d\tilde{U} - \sqrt{2}\epsilon_k = E(k)d \\ -\sqrt{2}\epsilon_k d - J_p(\tilde{U}) - \epsilon_k e^{-\alpha} = E(k) \\ -\epsilon_k\left(e^{-\alpha} + e^{\alpha}\right) = E(k) \end{cases}, \qquad (10.5)$$

resulting in a cubic for the decay rate e^{α}:

$$\epsilon_k^2 e^{3\alpha} + \epsilon_k \left(\tilde{U} - J_p(\tilde{U})\right) e^{2\alpha} - \left(\epsilon_k^2 + \tilde{U} J_p(\tilde{U})\right) e^{\alpha} - \epsilon_k J_p(\tilde{U}) = 0 \,, \tag{10.6}$$

that reduces to the one reported in Sec.9.2.1, Eq.9.31, for $\tilde{U} = 0$. In particular it is worth noting that from the first equation in (10.5) one can readily obtain:

$$d = \frac{\sqrt{2}\epsilon_k}{\tilde{U} - E(k)} \,, \tag{10.7}$$

hence, as one would expect, $d \to 0$ for $\tilde{U} \gg 1$. Substituting into the last two equations, we have:

$$\begin{cases} e^{\alpha} = J_p^{\infty}/\epsilon_k = J_p^{\infty}/2t\cos(ka/2) \\ E(k) = -J_p^{\infty} - \frac{4t^2}{J_p^{\infty}}\cos^2(ka/2) \end{cases} \,, \tag{10.8}$$

where $J_p^{\infty} = J_p(\tilde{U} \to \infty)$, and the bipolaron to polaron ratio for the effective mass $m^{**}/m^{*} = J_p^{\infty}/t$. It is important to recall that Eq.(10.6) and Eq.(10.8) hold only as long as we have a bound state.

The same procedure can also be applied for a $N \times N$ square lattice. In this case, according with the notation reported in Sec.9.2.3, the wave function ψ_{SL} can be represented as the following N^2-element matrix:

$$\psi_{SL} = \begin{pmatrix} d & a & e^{-\alpha} & e^{-2\alpha} & \dots \\ a & e^{-\alpha} & e^{-2\alpha} & e^{-3\alpha} & \dots \\ e^{-\alpha} & e^{-2\alpha} & e^{-3\alpha} & e^{-4\alpha} & \dots \\ e^{-2\alpha} & e^{-3\alpha} & e^{-4\alpha} & e^{-5\alpha} & \dots \\ \vdots & \vdots & \vdots & \vdots & \ddots \end{pmatrix} \,. \tag{10.9}$$

in which the i^{th} row contains the wave function components from $(N(i-1)+1)^{th}$ to $(iN)^{th}$ with open boundary conditions. Here d and a are the amplitudes of on-site and nearest-neighbor pairs, α is the uniform decay rate along both x and y directions. Contrarily to the one-dimensional case, in which the exponential decaying wave function represents the solution of the Schrödinger equation (10.4), Eq.10.9 is not a solution of Schrödinger's equation, except at $\alpha = 0$, because of the presence of a discontinuity in the gradient of the wave function at $x = 0$ and $y = 0$. However, it represents a good approximation in the strongly localized regime ($\alpha \gg 1$) when the bipolaron size is much smaller than the size of the system and the errors on the coordinate axes will be exponentially small in α. Hence, by applying the Hamiltonian $\mathcal{H}_{S=0}$ (Fig.10.3) to ψ_{SL} it is immediate to obtain the following set of coupled equations:

$$E(k_x, k_y)d = \tilde{U}d - \sqrt{2}a\left(\epsilon_{k_x} + \epsilon_{k_y}\right) \,, \tag{10.10}$$

$$2E(k_x, k_y)a = 2J_p(\tilde{U})a - \left(\epsilon_{k_x} + \epsilon_{k_y}\right)\left(a + 2e^{-\alpha} + \sqrt{2}d\right) \,, \tag{10.11}$$

$$3E(k_x, k_y)e^{-\alpha} = -\left(\epsilon_{k_x} + \epsilon_{k_y}\right)\left(2a + e^{-\alpha} + 3e^{-2\alpha}\right) \,, \tag{10.12}$$

$$4E(k_x,k_y)e^{-2\alpha} = -\left(\epsilon_{k_x}+\epsilon_{k_y}\right)\left(3e^{-\alpha}+e^{-2\alpha}+4e^{-3\alpha}\right)\ , \tag{10.13}$$

which, in the limit for $\alpha \ll 1$, allows us to determine d, a and the energy dispersion $E(k_x,k_y)$ as a function of the decay rate α as follows:

$$d = \frac{\sqrt{2}a\left(\epsilon_{k_x}+\epsilon_{k_y}\right)}{U-E(k_x,k_y)}\ , \tag{10.14}$$

$$a = \frac{1}{8}\left(9-e^{-\alpha}\right)\ , \tag{10.15}$$

$$E(k_x,k_y) = -\frac{1}{4}\left(\epsilon_{k_x}+\epsilon_{k_y}\right)\left(3e^{-\alpha}+e^{-2\alpha}+4e^{-3\alpha}\right)\ . \tag{10.16}$$

Finally, the decay rate can be determined self-consistently according to the following equation:

$$2E(k_x,k_y)a + 2J_p(\tilde{U}) + \left(\epsilon_{k_x}+\epsilon_{k_y}\right) = 0\ . \tag{10.17}$$

For $\tilde{U}=0$ rigorous results show that in one and two dimensions the presence of any attractive interaction results in a bound ground state that persists for any values of the hopping. However, in the presence of a sufficiently high on-site interaction, the bound state can be destroyed when the ratio $t/J_p(\tilde{U})$ exceeds a critical value. Such a critical value can be determined by solving the Schrödinger equation for $\mathcal{H}_{S=0}$ with $\alpha=0$ in the system wave function. Then, for the ground state ($k=0$) of a 1D-chain, according to Eq.10.5, we have:

$$\begin{cases} E_0 d = d\tilde{U} - \sqrt{2}\epsilon_0 \\ E_0 = -\sqrt{2}\epsilon_0 d - J_p(\tilde{U}) - \epsilon_0 \\ E_0 = -2\epsilon_0 \end{cases}\ , \tag{10.18}$$

where $\epsilon_0 \equiv \epsilon(k=0) = 2t$ and $E_0 \equiv E(k=0)$. From the system above one can readily obtain $E_0 = -4t$, $d = 2\sqrt{2}t/(\tilde{U}+8t)$ and the following critical value for the hopping integral:

$$t_c^{1D} = \frac{\tilde{U}J_p(\tilde{U})}{2\tilde{U}-4J_p(\tilde{U})}\ . \tag{10.19}$$

Because of the constraint $t \leq J_p(\tilde{U})$, one also gets $\tilde{U} \geq 4J_p(\tilde{U})$ that can be read as a self-consistent equation that allow us to determine the critical value of the on-site interaction required to have a phase transition to an unbound state.

Similar considerations can be done for the 2D square lattice. By solving the Schrödinger equation $\mathcal{H}_{S=0}\psi_{SL} = E(\boldsymbol{k})\psi_{SL}$ with $\alpha=0$ in Eq.10.9 we get the following system of coupled equations:

$$\begin{cases} E_0 d = d\tilde{U} - 2\sqrt{2}\epsilon_0 \\ E_0 = -\left(3+\sqrt{2}d\right)\epsilon_0 - J_p(\tilde{U}) \\ E_0 = -4\epsilon_0 \end{cases}\ , \tag{10.20}$$

The solution of the system gives $E_0 = -8t$, $d = 4\sqrt{2}t/(\tilde{U}+8t)$ and the following

critical values for the hopping integral:

$$t_c^{2D} = \frac{\tilde{U} J_p(\tilde{U})}{2\tilde{U} - 8J_p(\tilde{U})} \,, \tag{10.21}$$

allowing for a phase transition to an unbound state in the physical regime $t \leq J_p(\tilde{U})$ only for $\tilde{U} \geq 8J_p(\tilde{U})$. The resulting phase diagram for both chain and square lattice geometries is reported in Fig.10.4.

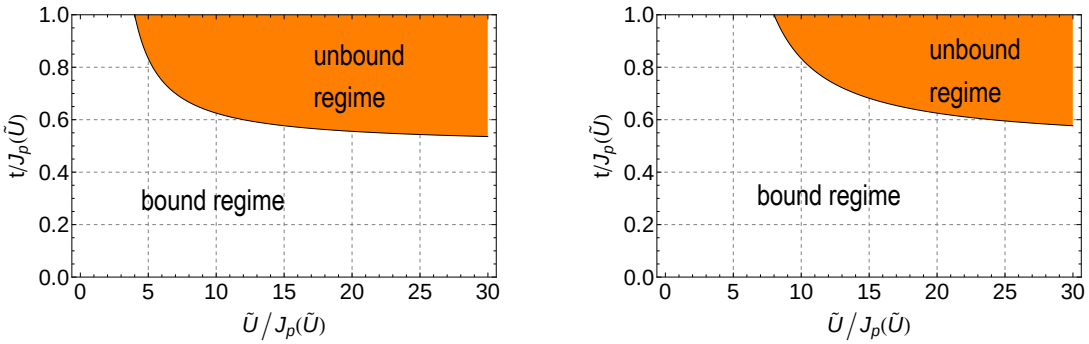

Figure 10.4: Ground state phase diagram of the polaronic $t - J_p - \tilde{U}$ model for a chain (left panel) and a square lattice (right panel).

Signatures of the crossover from a small to a large bipolaron configuration also appear in the NN bipolaron density and in the bipolaron radius r whose calculation, for the sake of brevity, is reported in Figs.10.5-10.7 for the only case of a square lattice geometry. As shown in Fig.10.5, consistently to the analytical results obtained so far, the bipolaron size increases approaching the critical line defined by Eq.10.21. Importantly, as shown in the right panel of Fig.10.5, in the region with $t > t_c^{2D}$ the bipolaron size increases linearly with the dimension of the system signaling the presence of an unbound state.We can also note the presence of an almost linear $r(N)$ dependence for $t \lesssim t_c^{2D}$. In this region, although we do not have an unbound state, the bipolaron size is comparable to the dimension of the system signaling the presence of a large, but still bound, bipolaronic ground state. This state is also characterized by the vanishing of the probability P_{bp} to find nearest-neighbor bipolaron in the ground state of the model. As reported in the left panel of Fig.10.6 in fact, P_{bp} becomes zero well before the critical value t_c^{2D} signaling the crossover from a small to a large bipolaronic ground state in the proximity of the unbound region. According to the conditions: $P_{bp} = 0$ and $r/a \approx N$ we obtain the phase diagram reported in Fig.10.7.

In conclusion we can infer that, although the small bipolaronic configuration persists for any values of the hopping at $\tilde{U} = 0$, for finite values of the hopping up to a critical value t_c, the inclusion of an on-site interaction leads to the crossover from a small to a large bipolaronic configuration characterized by $P_{bp} = 0$ and a bipolaron radius comparable with the dimension of the system. Finally, for further increasing t ($t > t_c$) the system undergoes a phase transition to an unbound state characterized by a bipolaron radius that increases linearly with the dimension of the system.

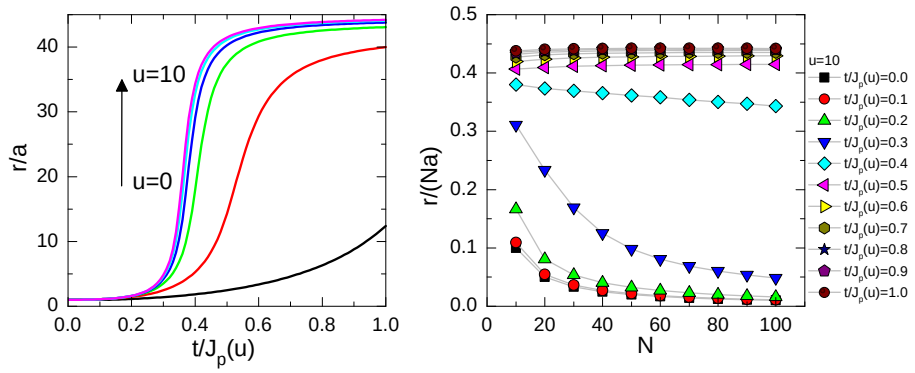

Figure 10.5: Left panel: bipolaron radius, r versus $t/J_p(u)$ for a 100×100 square lattice and different values of the dimensionless parameter $u = \tilde{U}/\hbar\omega_0$. Right panel: bipolaron radius, r to system size, Na ratio versus N for a $N \times N$ square lattice and different values of the ratio $t/J_p(u)$ at $u = 10$. Here a is the lattice constant, $g^2 = 1.24$.

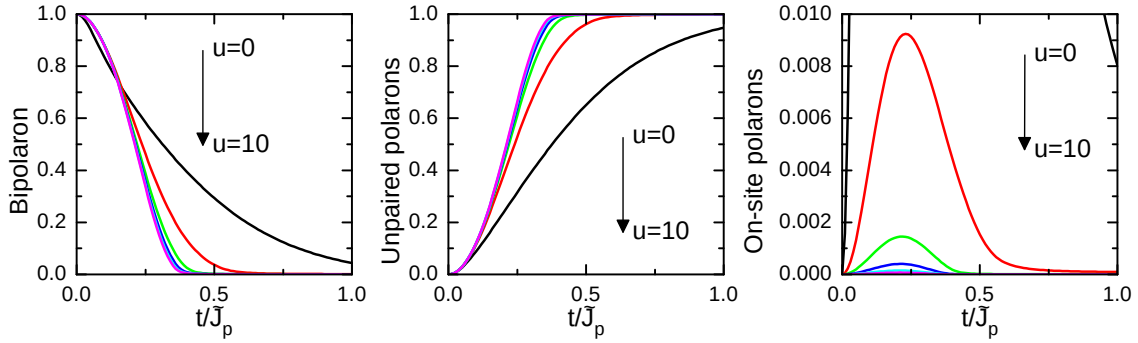

Figure 10.6: Probability to find NN bipolarons, unpaired polarons and on-site polarons in the ground state of the $t-J_p(u)$ model as a function of the ratio $t/J_p(u)$ for different values of the dimensionless parameter $u = \tilde{U}/\hbar\omega_0$ with $g^2 = 1.24$.

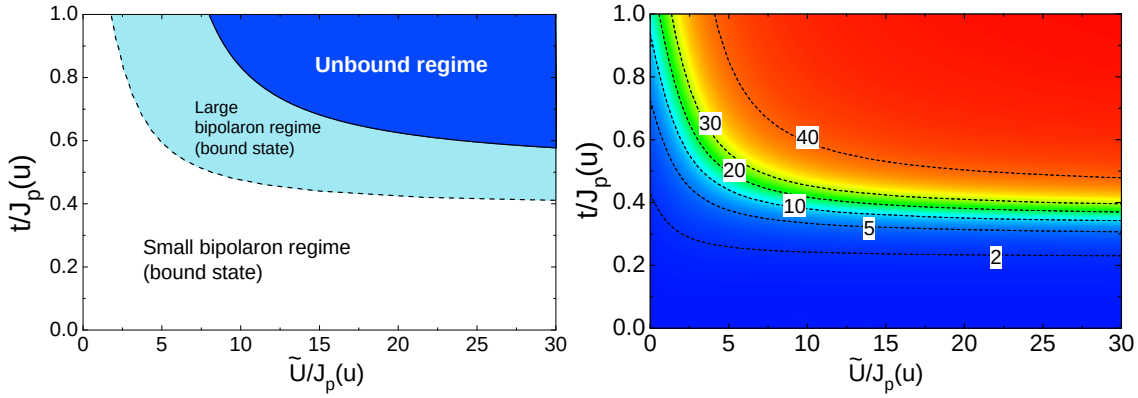

Figure 10.7: Left panel: ground state phase diagram of the polaronic $t-J_p(u)$ model for a square lattice including the crossover regime (light blue area) corresponding to a large but still bound bipolaronic state. Right panel: contour-plot of the bipolaron radius r/a (a is the lattice constant) for a 100×100 square lattice. Numbers represent the value of the ratio r/a along the lines. Here $g^2 = 1.24$ and $u = \tilde{U}/\hbar\omega_0$.

10.2 Superconducting phase transition in the dilute bipolaron limit

Growing evidence of non Fermi-liquid and non-BCS behaviors in normal and superconducting states, respectively, lead to the conviction that most of the high-temperature superconductors, among which Cuprates [12], are neither BCS nor BEC superfluids but they are in a crossover region from one to another [56], [57]. The standard BEC theory, applied to a charged and uniform 3D gas of local pairs, has already been shown to provide a very high-T_c with a simple expression for the critical temperature [58]:

$$T_c^{BEC} \propto \frac{2\pi\hbar^2}{k_B m^{**}} \left(\frac{n_b}{\zeta(3/2)} \right)^{2/3} \approx 2.9 \times 10^{-11} \frac{m_e}{m^{**}} n_b^{2/3} \mathrm{cm}^2 K \ , \tag{10.22}$$

Here m_e is the bare electron mass, n_b and m^{**} are density and effective mass of bosons, respectively and $\zeta(3/2)$ is the Riemann zeta function. It is immediate to see that the above equation gives $T_c^{BEC} \approx 300K$ if one considers the typical bipolaron effective mass $m^{**} \approx 10 m_e$ and $n_b \approx 10^{21} \mathrm{cm}^{-3}$. However, despite the very high critical temperature, the BEC theory itself it is not sufficient to explain some other well-known experimental findings among which small/large Fermi surfaces and d-wave pairing. In fact, the bosonic ground-state band, which describes quasi-particle excitations, always lays below the chemical potential, resulting in the complete lack of any Fermi surface. Furthermore, bosonic pairs, tightly bound in the real space, have no internal structure in the momentum space which makes difficult to justify a d-wave symmetry for the gap function. It is immediate to see that these and many other issues, which do not occur in the standard theory of superconductivity (BCS and its extensions), can be immediately fixed if one admits a crossover from a BEC to a BCS-like regime of weakly interacting fermions. However, although several theories have been proposed so far, there is no general consensus on the main mechanism that should drive this phenomenon.

In the framework of the bipolaron theory developed here and in the previous Chapter, we report in this Section the calculation of the superconducting critical temperature in the BEC regime of the 2D polaronic t-J_p-$\tilde{U}$ model, providing a possible explanation of the BEC-BCS crossover in terms of the properties of the bipolaronic ground state. As shown in Sec.10.1 (Fig.9.12 and Fig.10.5), the ground state of the polaronic t-J_p-$\tilde{U}$ model describes very small and perfectly mobile carriers, which coherently propagate in the lattice, in a wide range of model parameters (see the phase diagram in Fig.10.7). These pairs, which are tightly bound in the real space rather than in the momentum space, represent good candidates for the BEC regime. In particular, in the dilute limit with a small number of bipolarons compared to the dimension of the system, pairs of polarons do not see each other allowing for a description of the superconducting state as a weakly interacting, charged and hard-core bipolaron gas. According to Mermin and Wagner theorem [59], there is no superconducting phase transition, meaning that the critical temperature T_c is strictly zero, in any two-dimensional system since there is no continuous symmetry breaking. However, the possibility of a non-zero T_c phase transition can still exist

via the Berezinsky-Kosterlitz-Thouless (BKT) mechanism [62]. For two-dimensional Bose gases, even if Bose-Einstein condensation does not occur in the ideal case [60], [61], a phase transition to a superfluid state is expected in the interacting case [62]. In particular, it has been shown [63] that in the very dilute limit in which:

$$\ln\left(\ln\left(\frac{1}{\gamma}\right)\right) \gg 1 \ , \ \gamma \equiv n_b a^2 \ , \tag{10.23}$$

where n_b is the boson density per unit area and a is proportional to the range of the hard-core boson interaction, the critical temperature at which this phase transition occurs is:

$$T_c^{BKT} = \frac{2\pi\hbar^2 n_b}{k_B m^{**} \ln\left(\ln\left(1/n_b r^2\right)\right)} \ , \tag{10.24}$$

which provides a good estimation for the superconducting critical temperature T_c since $(T_c - T_c^{BKT})/T_c \approx 1/\ln(\ln(1/n_b)) \ll 1$ in the dilute limit. In our case $r \approx a$ and m^{**} is the bipolaron mass. From (10.24), since the effective mass is inversely proportional to t, one may conclude that the BKT critical temperature will increase as the hopping increases. On the other hand, our numerical results obtained by exact diagonalization showed that, despite of the particular geometry, the probability to have small (nearest-neighbor) bipolarons decreases as the hopping increases and goes to zero after that a critical value has been reached (see Fig.(9.12)). It follows that, in a more reliable picture, Eq.10.24 has to be properly weighted by the probability $P_{bp}(t/J_p)$ to find NN bipolarons in the ground state configuration leading to the following expression for the renormalized critical temperature:

$$T_c^*(t/J_p(\tilde{U}), n_b) \equiv P_{bp}(t/J_p(\tilde{U}))T_c^{BKT}(n_b) \ . \tag{10.25}$$

Here $P_{bp}(t/J_p)$ should be read as a bipolaron density, meaning that for $P_{bp}(t/J_p) \to 0$ there are no nearest-neighbors bipolarons and therefore the hard-core boson picture can be no longer justified. Coherently, as emphasized in Fig.10.8, results obtained from the application of Eq.10.25 with the bipolaron effective mass calculated in the case of a square lattice geometry (see bottom left panel in Fig.9.12), show that the renormalized critical temperature $T_c^*(n_b)$ has a maximum in the correspondence of the small-polaron regimes, then gradually decreases with increasing ratio t/J_p.

It is worth noting that in the small bipolaron regime, despite the very low density limit, the polaronic $t - J_p - \tilde{U}$ Hamiltonian is perfectly able to reproduce critical temperatures well in excess of hundred kelvin. In particular, in the case of Cuprate superconductors, with the polaron shift in the range $0.5\text{eV} \leqslant E_p \leqslant 1.0\text{eV}$ and the bipolaron binding energy $0.3\text{eV} \leqslant J_p(\tilde{U}=0) \leqslant 1.0\text{eV}$ [34] one gets the realistic value of the bare hopping integral $0.2\text{eV} \leqslant T(a) \leqslant 0.4\text{eV}$ that gives $0.05 \leqslant t/J_p \leqslant 0.27$ and the critical temperature $40\text{K} \leqslant T_c \leqslant 125\text{K}$ at $n_b = 0.05$ in the physical range $6 \leqslant \tilde{U}/\hbar\omega_0 \leqslant 10$. Furthermore, at this point it is also important to recall that Eq.10.25 intrinsically depends on the ion mass M via the polaronic hopping t since it is defined as $t \sim \exp(-E_p/\hbar\omega_0)$ where E_p is the polaron energy level shift and ω_0 is the well-known phonon frequency which depends on the ion-mass as $\omega_0 \propto \sqrt{M}$.

At sufficiently low density, BEC should not depend on whether bipolarons are nearest neighbor or next nearest neighbor, so long as they are bound and the bipo-

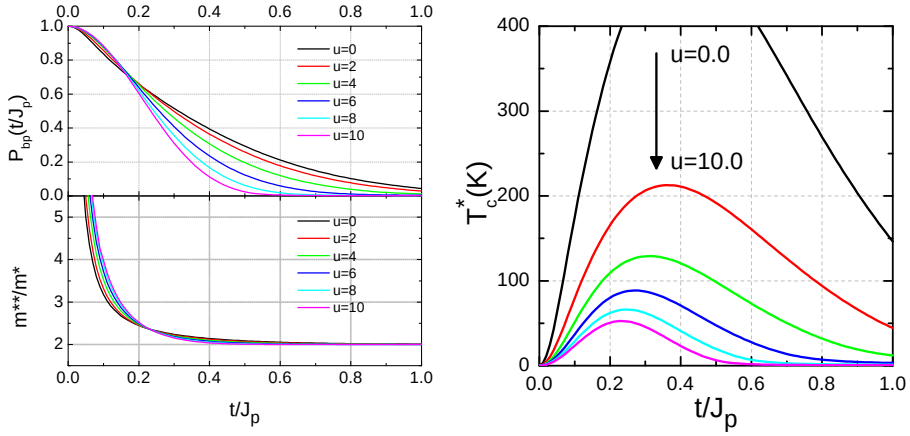

Figure 10.8: Left panel: probability to find NN bipolarons (top) and bipolaron effective mass to single polaron effective mass ratio versus $t/J_p(\tilde{U})$ for different values of $u = \tilde{U}/\hbar\omega_0$. Right panel: renormalized superconducting critical temperature T_c^* from Eq.10.25 as a function of the ratio $t/J_p(\tilde{U})$ for different values of $u = \tilde{U}/\hbar\omega_0$. Here $g^2 = 1.24$, $\hbar\omega_0 = 0.08$eV and $n_b = 0.05$.

laron spacing is much greater than the typical polaron separation. However, as shown in Fig.10.7, the polaronic $t - J_p - \tilde{U}$ model also admits the presence of a large bipolaronic ground state in a particular range of the model parameters. In this region the ground state configuration is characterized by pairs of polarons separated by a distance which is proportional to the dimension of the system, leading to a significant pair-pair overlap even in the low density limit. Hence, pair condensation appears in the form of the Cooper pairs in the momentum space with a lower critical temperature, rather than in real space, providing a reliable picture for the BEC-BCS crossover [23, 70]. Consistently to this picture, the critical temperature $T_c^*(t, n_b)$, plotted in Fig.10.8, should read as representative of the BEC contribution only, with a lower-temperature tail (see Sec.8.1, Fig.8.1) that, in principle, could be added if one considers the BCS contribution.

10.3 Pseudogap signatures in a boson-fermion mixture of polarons and bipolarons

In the last few years the presence of unconventional non-Fermi liquid behaviors in the normal state of high temperature superconductors has been widely advocated as one of the key-features to be addressed in order to better understand the origin of the high-T_c superconducting mechanism. In particular, in underdoped Cuprates, one of the main signature of a non-Fermi liquid behavior is given by the presence of an energy gap, at temperatures well above T_c, apparently unrelated to the superconducting gap and so called "pseudogap" (PG). Although several theories have been proposed so far and several experimental techniques, among which angle resolved photoemission spectroscopy (ARPES), Raman and neutron scattering, nuclear magnetic relaxation (NMR), have been employed to better characterize the properties of the PG regime (for a review see Refs.[71, 72, 73, 74]), a comprehensive and widely

accepted view is still missing. Historically, the main interpretation of PG features has been given in terms of pre-formed Cooper pairs [75, 76] and strong suppression of low-energy antiferromagnetic fluctuations [77, 78, 79]. These pictures, initially supported by NMR observations of an anomalous depression in the temperature dependence of the Knight shift for underdoped samples of YBCO [80], were called into question due to a later interpretation of NMR data as a consequence of a depression in the electron density of states (DOS). The presence of this depression, which can be in principle induced by any instability such as stripes, charge/spin density waves, polaron formation, lead to the conclusion that PG features might not necessarily imply spin-singlet formation. Moreover, strong evidence of particle-hole symmetry breaking in the pseudogap state of Bi2201 shed doubts about the possibility to consider the PG as a precursor of a Cooper pairing superconducting gap in the normal state [81]. Hence, a plethora of other different theories were proposed in which PG might emerge due to SU(2) rotation [82], coexistence of charge and spin density waves [83], inhomogeneous charge distributions [84, 85]. So far, polaron and bipolaron theory, supported by earlier and more recent ARPES experiments [86], was only able to give a phenomenological explanation of pseudogap features in terms of the bipolaron binding energy [87].

Within this context, we report in this Section our study of the pseudogap regime in the framework of the polaronic t-J_p-$\tilde{U}$ model, which has already been proved to admit a phase transition to a superconducting state, characterized by weakly interacting and charged hard-core bipolarons, with a critical temperature well in excess of hundred kelvin (see Sec.10.2 and Ref.[36]). We will show that the hard-core bipolarons gas, studied as a charged Bose-Fermi mixture, is responsible for a non-Fermi liquid behavior of the normal state, characterized by pseudogap signatures in spin susceptibility, specific heat and tunneling conductance. These signatures allow for a microscopical explanation of the pseudogap regime in terms of a thermal-induced recombination of polarons and bipolarons, without any assumption on pre-existing order or broken symmetries in the normal state of the model [37].

10.3.1 Bose-Fermi description

Let us consider an ideal gas of N polarons in a N_s-site high polarizable ionic lattice in the presence of a static and uniform magnetic field h. It has been pointed out that for such a system the competition between bare long-range Coulomb and electron-phonon interactions results in the presence of a short range spin-exchange coupling that is responsible for the formation of bound pairs of polarons, called bipolarons, described by a bosonic band. Unpaired polarons left are described by a polaronic (fermionic) band. In the dilute limit ($N/N_s \ll 1$) analytical and numerical results show that, in the absence of any magnetic field, the bipolaronic configuration represents the ground state for 1D and 2D geometries while polaronic states are accessible by thermal excitations. Then, for a fixed value of doping $x = N/N_s$, as long as the interactions between bipolarons and polarons are negligible, the system described above can be considered as an ideal (non-interacting) Bose-Fermi mixture

of N_b bipolarons (bosons) and N_p unpaired polarons (fermions) with:

$$x = 2n_b + n_p \ , \tag{10.26}$$

where $n_{b,p} = N_{b,p}/N$ is the bipolaron/unpaired polarons density.

With the aim of describing the thermodynamic of the Fermi-Bose gas at equilibrium, it is useful to introduce the thermodynamic potential $\Omega(n_b, n_p, T, h)$ of the mixture, defined as a function of temperature T and chemical potential μ, for fixed values of entropy S and total particle density n, as follows:

$$d\Omega = -SdT - nd\mu \ . \tag{10.27}$$

We recall that in the dilute limit all the thermodynamic quantities enjoy the additivity property. Hence $\Omega(n_b, n_p, T, h)$ can be expressed in terms of bipolarons $\Omega_b(n_b, T, h)$ and unpaired polarons $\Omega_p(n_p, T, h)$ potentials:

$$\Omega(n_b, n_p, T, h) = \Omega_b(n_b, T, h) + \Omega_p(n_p, T, h) \ , \tag{10.28}$$

where $\mu_{p,b}$ is the unpaired polaron / bipolaron chemical potential and:

$$\Omega_{p,b}(n_{p,b}, T, h) = \mp k_B T \sum_s \int_{-\infty}^{+\infty} d\epsilon \mathcal{N}_{p,b}^{(s)}(\epsilon) \ln\left(1 \pm \exp\left[\left(\mu_{p,b} - \epsilon\right)/k_B T\right]\right) \ , \tag{10.29}$$

Here the sum over s takes into account all the possible spin states and $\mathcal{N}_{b,p}^{(s)}(\epsilon, h)$ is the density of spin-polarized states in the bipolaron/unpaired polaron band, respectively. The chemical potential of unpaired polarons and bipolarons can be calculated as a function of the chemical potential μ of the mixture by means of the detailed equilibrium principle associated to the phonon induced bipolaron - unpaired polarons transition. In this transition a bipolaron with energy E decays into two unpaired polarons with energy ϵ and ϵ' via the absorption of a phonon with energy $\hbar\omega$. On the other side, two unpaired polarons with energy ϵ and ϵ' can emit a phonon with energy $\hbar\omega$ and collapse in a bipolaronic state. At the equilibrium, the number of possible bipolaron to polaron transitions is equal to the number of possible polaron to bipolaron transitions and we have:

$$f_b(E)\mathcal{N}_{ph}(\omega)\left(1 - f_p(\epsilon)\right)\left(1 - f_p(\epsilon')\right) = f_p(\epsilon)f_p(\epsilon')\left(\mathcal{N}_{ph}(\omega) + 1\right)\left(1 + f_b(E)\right) \ , \tag{10.30}$$

where:

$$f_{p,b}(\mu_{p,b}, T, \epsilon) = \frac{1}{\exp\left(\frac{\epsilon - \mu_{p,b}}{k_B T}\right) \pm 1} \ , \ \mathcal{N}_{ph}(\omega) = \frac{1}{\exp\left(\frac{\hbar\omega}{k_B T}\right) - 1} \ , \tag{10.31}$$

Solving Eq.10.30 with respect to μ_p one readily obtains:

$$\mu_p = \frac{1}{2}\left(\epsilon + \epsilon' - \hbar\omega - E + \mu_b\right) \ , \tag{10.32}$$

then, by requiring the conservation of the total energy: $\epsilon + \epsilon' = E + \hbar\omega$, we have:

$$\mu_b = 2\mu_p \ . \tag{10.33}$$

Therefore, recalling that:

$$\begin{aligned} n_{p,b}(T) &= -\frac{\partial \Omega_{p,b}(n_{p,b}, T)}{\partial \mu_{p,b}} = & (10.34)\\ &= \pm k_B T \sum_s \int_{-\infty}^{+\infty} d\epsilon \mathcal{N}_{p,b}^{(s)}(\epsilon) \frac{\partial}{\partial \mu_{p,b}} \ln\left(1 \pm e^{\frac{\mu_{p,b}(T)-\epsilon}{k_B T}}\right) = & (10.35)\\ &= \sum_s \int_{-\infty}^{+\infty} d\epsilon \mathcal{N}_{p,b}(\epsilon) f_{p,b}(\mu_{p,b}, \epsilon, T) & (10.36) \end{aligned}$$

for a fixed value of the doping x, the chemical potential can be calculated self-consistently according to Eq.10.26 that gives:

$$x = 2\sum_s \int_{-\infty}^{+\infty} d\epsilon f_b(2\mu, \epsilon, T)\mathcal{N}_b(\epsilon) + \sum_s \int_{-\infty}^{+\infty} d\epsilon f_p(\mu, \epsilon, T)\mathcal{N}_p(\epsilon) \tag{10.37}$$

It is important to note that, although the density of states $\mathcal{N}_{p,b}^{(s)}(\epsilon)$ is well-known to be temperature independent for non-interacting systems, it implicitly depends on the intensity h of the applied magnetic field and on all the model parameters (t, J_p, $\tilde{U}$) via the energy dispersion $\epsilon \equiv \epsilon(t/J_p, \tilde{U}, h)$. Hereafter, for the sake of brevity, we will omit t/J_p, $\tilde{U}$ and x dependencies, therefore $\Omega_{p,b} \equiv \Omega_{p,b}(T, h)$. The knowledge of the thermodynamic potential $\Omega(T, h)$ allows to the calculation of some response functions such as entropy $S(T, h)$, specific heat $C_V(T, h)$, total spin-momentum (magnetization) $m(T, h)$, charge $\chi_c(T, h)$ and spin $\chi_s(T, h)$ susceptibilities, where:

$$S(T,h) = -\left.\frac{\partial \Omega}{\partial T}(T,h)\right|_{\mu=const.} \tag{10.38}$$

$$C_V(T,h) = T\left.\frac{\partial S}{\partial T}(T,h)\right|_{V,n=const.} \tag{10.39}$$

$$m(T,h) = -\left.\frac{\partial}{\partial h}\Omega(T,h)\right|_{V,n=const.} \tag{10.40}$$

$$\chi_s(T,h) = \left.\frac{\partial}{\partial h}m(T,h)\right|_{V,n=const.} \tag{10.41}$$

$$\chi_c(T,h) = T\left.\frac{\partial}{\partial \mu}n(T,h)\right|_{V,n=const.} \tag{10.42}$$

Analytical expressions of the above quantities are reported in Appendix F.

10.3.2 Pseudogap signatures in density of states, specific heat and spin susceptibility

As explained at the beginning of this Chapter, pseudogap features can emerge in several physical quantities such as density of states, specific heat and spin susceptibility [71, 72, 73, 74]. Density of states, as well as specific heat, is expected to decrease in a particular range of energy due to the lack of excited states within the pseudogap. Similarly, spin susceptibility is also expected to decrease in the limit for $T \to 0$, providing a precursor signal of singlet pair formation. In order to characterize all these features in the framework of the polaronic t-J_p-$\tilde{U}$ model (10.3), it is convenient to introduce the "occupation density of states" (ODOS), $\rho(\omega, T)$, by weighting the standard temperature-independent DOS $\mathcal{N}_{p,b}(\omega)$ with the Fermi-Dirac and the Bose-Einstein distribution functions:

$$\rho(\omega, T) \equiv f_b(\omega, T)\mathcal{N}_b(\omega) + 2f_p(\omega, T)\mathcal{N}_p(\epsilon) \ , \tag{10.43}$$

with $f_{b,p}(\omega, T) = \left[\exp\left(\left(\omega - \mu_{p,b}\right)/k_B T\right) \mp 1\right]^{-1}$ and:

$$\mathcal{N}_{b,p}(\omega) = \frac{a}{2\pi}\int_{-\pi/a}^{\pi/a} d\boldsymbol{k}\delta\left[\omega - E_{b,p}(\boldsymbol{k})\right] \ . \tag{10.44}$$

Here, according to the Bose-Fermi mixture description, we shall restrict our analysis to an effective two-band model with the bipolaronic two-particle (bosonic) band, labeled by the index b, which described the properties of the bipolaron gas, and the single-particle (fermionic) polaron band, labeled by the index p, which describes the gas of unpaired polarons. Hence, $E_{b,p}(\boldsymbol{k})$ is the (bi)polaron dispersion with polaron μ_p and bipolaron μ_b chemical potentials fixed in terms of the chemical potential μ of the whole mixture according to the detailed equilibrium principle (10.30) which gives: $\mu_p = \mu_b/2 = \mu$. At this point it is convenient to introduce the following potential shift to the model Hamiltonian:

$$\mathcal{H} \to \mathcal{H} - \frac{1}{2}E_0\sum_{\boldsymbol{m}} n_{\boldsymbol{m}} \ , \tag{10.45}$$

where E_0 is the bipolaron ground state energy which depends on the model parameters (e.g. $E_0 = -J_p(\tilde{U})$ at $t/J_p(\tilde{U}) = 0$). It goes without saying that the shift (10.45) has no effect on the physics described by the model. However, it has the good property of shifting the zero of bipolaron and unpaired polaron energies providing a more intuitive picture in which all energy eigenstates of the shifted Hamiltonian are non-negative (see Fig.10.9). To this purpose, we note that two different shifts, namely $E_0^{(b)} = E_0$ and $E_0^{(p)} = E_0/2$, are applied for bipolaron and unpaired polaron bands, respectively.

As already pointed out in Chapter 9, bipolarons repel each other and also repel single polarons leading to dimerized low-energy configurations with no pair-pair interactions in the dilute limit. Hence, it is immediate to see in the static limit ($t = 0$) the total DOS will be given by the superposition of two contributions corresponding to the singlet bipolaron ground state and the unpaired polaron states, with a single

charge/spin gap $\Delta_c = \Delta_s = J_p(\tilde{U})/2$. By increasing the ratio $t/J_p(\tilde{U})$, as shown in Fig.10.9, the two peaks become broadened and the gap closes. Importantly, it is worth noting that while $\Delta_c = 0$ for any $t \neq 0$ because of gapless intra-band excitations in the bipolaronic (bosonic) band, the spin gap Δ_s remains finite as long as there is no overlap between bipolaron and unpaired polaron contributions and the unpaired polaron band remains unoccupied.

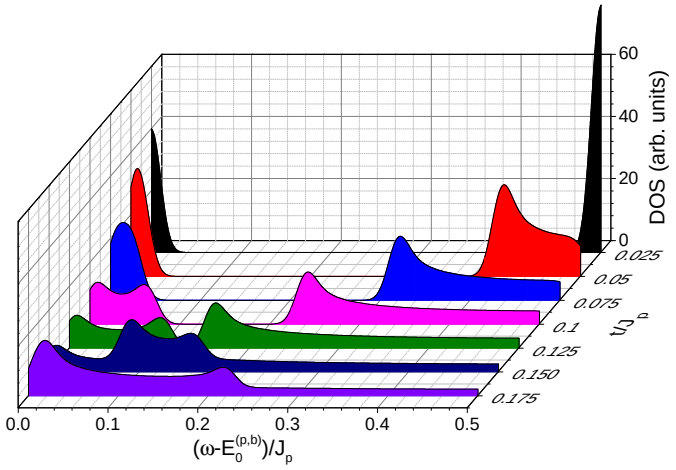

Figure 10.9: Density of states versus energy, for different values of the ratio $t/J_p(\tilde{U})$ for a one-dimensional chain. Left and right peaks represent bipolaron and unpaired polaron contributions, respectively. Here $E_0^{(b,p)}$ are the energy shifts applied to bipolarons and unpaired polaron bands, respectively, with $E_0^b = 2E_0^p = E_0$ being E_0 the bipolaron ground state energy.

As follows from Eq.10.43, the occupation depends on temperature via the Fermi-Dirac and the Bose-Einstein distributions. Hence, as far as the temperature is low enough with respect to $J_p(\tilde{U})$, only the bottom of the bipolaron band will be occupied leading to a pure bosonic singlet state. With increasing T, when the temperature becomes comparable with the bipolaron binding energy, thermal excitations break bipolarons inducing a finite population of the the polaronic (fermionic) band. Hence, pseudogap features appear as a result of the competition between bipolaron and unpaired polaron contributions. In fact, as reported in Fig.10.10, in a narrow range of the ratio t/J_p, the ODOS exhibits a strong depression for $\omega - E_0^{(b,p)} \ll J_p(\tilde{U})$. In this regime the occupation of the upper edge of the bipolaron band is strongly suppressed in order to favor the creation of unpaired polarons at the lower edge of the polaronic band. As one would expect, this suppression in the ODOS, which persists for $T \gg T_c$, becomes less and less pronounced with increasing T when the population of the states within the pseudogap becomes favored by thermal excitations. Hence, a characteristic pseudogap temperature T^* exists above which the pseudogap is suppressed.

As follows from Eq.10.43, except for few simple cases, the ODOS $\rho(\omega)$ can only be calculated numerically since the energy dispersion in the DOS $\mathcal{N}_{p,b}^{(s)}(\epsilon)$ is, in principle, not known in its analytical form. The same issue also affects the calculation of the thermodynamic quantities (10.38)-(10.42) which depend on $\mathcal{N}_{p,b}^{(s)}(\epsilon)$ via the thermodynamic potential Ω. Although a plethora of different techniques accounts

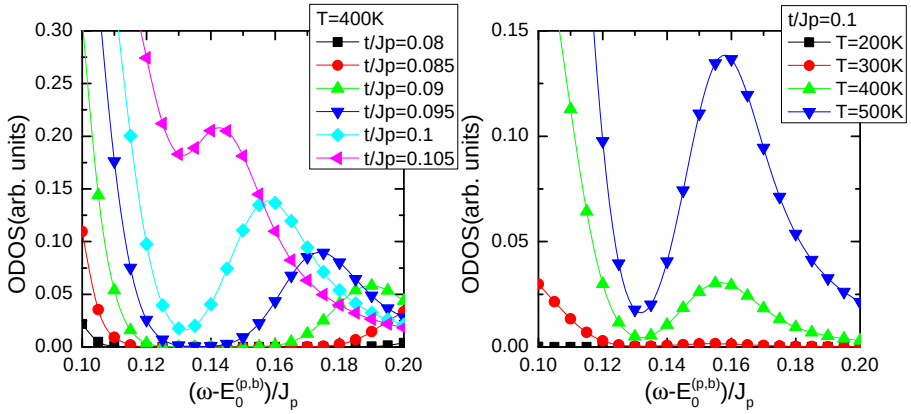

Figure 10.10: Signatures of pseudogap opening in the ODOS for different values of polaron hopping (left panel) and temperature (right panel) calculated for the chain with a Gaussian broadening $\delta = 0.01 J_p$, modeling a disorder effect in the δ function in Eq.10.44. Here $E_0^{(b,p)}$ are the energy shifts applied to bipolarons and unpaired polaron bands, respectively, with $E_0^b = 2E_0^p = E_0$ being E_0 the bipolaron ground state energy..

for the calculation of bipolaron and unpaired polaron dispersions, among which the SSP method described in Sec.(9.2), in many cases non conventional behaviors in DOS and thermodynamic quantities do not depend on the particular shape of the ODOS but on main features such as intensity and bandwidths of polaron and bipolaron contributions. In this regard, with the only purpose of describing qualitatively the thermodynamic properties of a Bose-Fermi mixture of bipolarons and unpaired polarons, we can adopt the following approximation (see Fig.(F.1)):

$$\begin{cases} \mathcal{N}_p(\epsilon) = A_p \Theta\left(\epsilon - \Delta\right) \Theta\left(\Delta + 2w_p - \epsilon\right) \\ \mathcal{N}_b(\epsilon) = A_b \Theta\left(\epsilon\right) \Theta\left(2w_b - \epsilon\right) \end{cases} , \tag{10.46}$$

which holds once that the potential shift (10.45) has been applied in order to set the bipolaronic ground state level as the zero of the energy scale. Here $A_{p,b}$ and $w_{p,b}$ are intensity and half-bandwidth of polaron and bipolaron terms, while Δ it the gap between the bottom of the bipolaron band and the bottom of the unpaired polaron band. In a square lattice with nearest-neighbor couplings there are only two possible bonds per site which are doubly degenerate because of spin symmetry. Thus the rectangular DOS (10.46) needs to satisfy the constraint $\int \mathcal{N}_{p,b}(\epsilon) d\epsilon = 2$, leading to $A_{p,b} = 1/w_{p,b}$. At this point it is crucial to note that all the parameters in (10.46) are strongly related to the model parameters t, $J_p(\tilde{U})$ and $\tilde{U}$ as shown in Fig.10.11. In particular, the unpaired (non-interacting) polaron bandwidth immediately follows from the kinetic term in (10.3) with $w_p = 8t$ while the bipolaron dispersion can be calculated numerically in the framework of the SSP method and gives $w_b \propto t^2/J_p(\tilde{U})$ for $t \ll J_p(\tilde{U})$ (see Sec.(9.2)). Importantly, the gap Δ corresponding to the binding energy per polaron is close to $J_p(\tilde{U})/2$ for $t/J_p(\tilde{U}) \ll 1$. Then, as shown in Fig.10.11, it rapidly decreases with increasing ratio $t/J_p(\tilde{U})$ until vanishing when the bottom of the unpaired polaron band approaches the bipolaron ground state energy.

As shown in detail in Appendix F, the approximation (F.31) allows to obtain

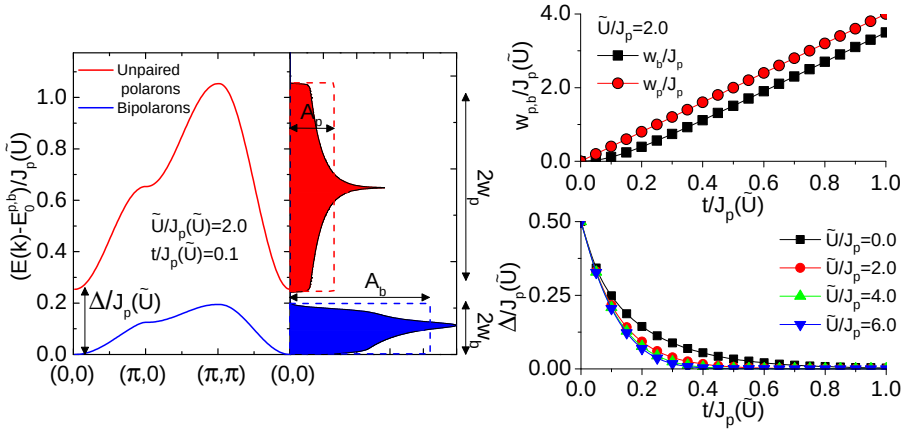

Figure 10.11: Left panel: bipolaron (bottom) and unpaired polaron (top) bands with the corresponding DOS: $\mathcal{N}_{p,b}(E)$ (filled area) for $\tilde{U} = J_p(\tilde{U}) = 2.0$ and $t = J_p(\tilde{U}) = 0.1$. Here $E_0^b = 2E_0^p = E_0$ are energy shifts coming from (10.45), where E_0 is the two-particle ground state energy. Dashed lines on the DOS represent the resulting Heaviside-theta approximation (10.46). Right panels: DOS parameters versus $t = J_p(\tilde{U})$ for different values of the ratio $\tilde{U} = J_p(\tilde{U})$.

analytical expressions for all the relevant physical properties in terms of the model parameters. In particular, for bipolaron and unpaired polaron densities we have:

$$n_b(T) = -1 + \frac{k_B T}{w_b} \ln \left[\frac{\sinh\left(\frac{w_b - \mu}{k_B T}\right)}{\sinh\left(-\frac{\mu}{k_B T}\right)} \right] , \tag{10.47}$$

$$n_p(T) = 1 - \frac{k_B T}{w_p} \ln \left[\frac{\sinh\left(\frac{w_b - \mu}{k_B T}\right)}{\sinh\left(-\frac{\mu}{k_B T}\right)} \right] , \tag{10.48}$$

from which the chemical potential $\mu(T)$ of the whole mixture can be calculated self-consistently for any given particle number x according to the relation $x = 2n_b(T) + n_p(T)$. As reported in Fig.(10.12), consistently with analytical and numerical results on the ground state configuration reported in this Chapter, the ground state ($T = 0$) configuration can be described as a pure bipolaron gas with $n_b = x/2$ and $n_p = 0$. The unpaired polaron density remains zero as long as $k_B T \ll \Delta$ then, as one would expect, it increases with increasing T when thermal excitations start to destroy pairs. Consistently, the bipolaron density decreases with the temperature keeping fixed the total particle density x.

Importantly, we can define a crossover temperature T^* at which half of the bipolarons are dissociated and the charge is equally distributed between polarons and bipolarons: $n_b(T^*) = 2n_p(T^*)$. As reported in Fig.(10.13), we note that the ratio $\Delta/k_B T^*$ varies linearly with $\ln(1/x)$ in a wide range of doping, with $k_B T^* = 2\Delta/\ln((4/x-1)^2/(1+8/x))$ in the limit for $w_{p,b}/\Delta \to 0$, in agreement with the exact analytical calculations done in the narrow band limit reported in the Appendix F.3.2, Eq.F.59.

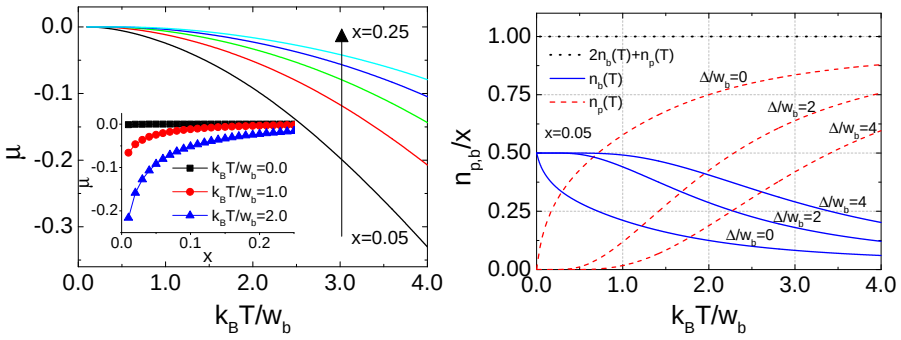

Figure 10.12: Left panel: chemical potential μ versus temperature for different values of the doping x. The $\mu(x)$ dependence is shown in the inset. Right panel: relative bipolaron (solid)/unpaired polaron (dashed) density versus temperature for different values of the gap . The dotted line represents the total particle density $x = 2n_b + n_p$.

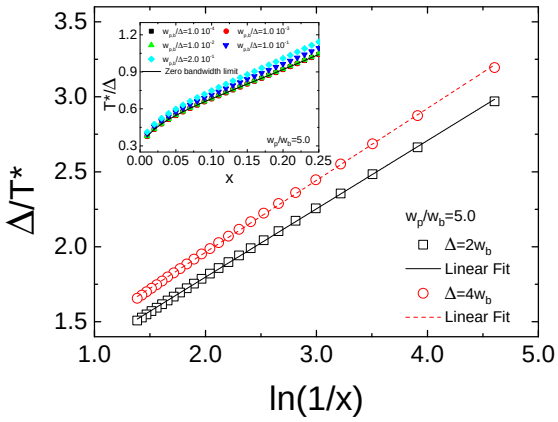

Figure 10.13: Linear dependence of the ratio Δ/T^* with respect to $ln(1/x)$ for different value of the gap Δ. In the inset the doping dependence of T^*/Δ (symbols) is compared with the exact analytical dependence (line) obtained in the zero-bandwidth limit. Here T^* is the crossover temperature at which $n_b(T^*) = 2n_p(T^*)$.

The thermal induced recombination of polarons and bipolarons also results in a number of anomalous features in specific heat $C(T)$ and spin susceptibility $\chi_s(T,h)$, where h is the intensity of a static and uniform external magnetic field. As shown in detail in Appendix F.3, in the framework of the Bose-Fermi mixture description and with the Heaviside-Theta approximation for the DOS given in Eq.10.46, $C(T)$ and $\chi_s(T,h)$ read as:

$$\chi_s(T,h) = \frac{\mu_B^2}{2k_BT}\int_{-\infty}^{\infty} d\epsilon \mathcal{N}_p(\epsilon)\frac{1+\cosh\left[\frac{\epsilon-\mu_p}{k_BT}\right]\cosh\left[\frac{\mu_B h}{k_BT}\right]}{\left(\cosh\left[\frac{\epsilon-\mu_p}{k_BT}\right]+\cosh\left[\frac{\mu_B h}{k_BT}\right]\right)^2}\,, \tag{10.49}$$

$$C(T) = k_BT\sum_{k=b,p} A_k\left[k_BI_k^{(2)}(x)+\frac{d\mu_n}{dT}I_k^{(1)}(x)\right]_{x_k^{in}}^{x_k^{fin}}\,, \tag{10.50}$$

where μ_B is the Bohr magneton and:

$$\begin{cases} x_b^{in} = -\frac{\mu_b}{k_BT} \\ x_b^{fin} = \frac{2w_b-\mu_b}{k_BT} \end{cases}, \begin{cases} x_p^{in} = \frac{\Delta-\mu_p}{k_BT} \\ x_p^{fin} = \frac{\Delta+2w_p-\mu_p}{k_BT} \end{cases}, \tag{10.51}$$

while $I_{p,b}^{(n)}(x) \equiv \int dx \frac{x^n e^x}{(e^x\pm1)^2}$ is expressed in terms of the poly-logarithm function $Li_s(z)=\sum_{k=1}^{\infty} z^k/k^s$ as:

$$I_{p,b}^{(n)}(x) = \begin{cases} \frac{xe^x}{1\pm e^x} \mp \ln\left(1\pm e^x\right) & ,\ n=1 \\ x\left(\frac{xe^x}{1\pm e^x} \mp 2\ln\left(1\pm e^x\right)\right) \mp Li_2\left(\mp e^x\right) & ,\ n=2 \end{cases}. \tag{10.52}$$

As shown in Fig.10.14, the specific heat is characterized by a superposition of two main low-temperature features corresponding to intra-band and bipolaron to unpaired polarons excitations. For $\Delta = 0$ bipolaron and unpaired polaron bands are completely overlapped (see Fig.10.11) with a single peak in the specific heat coefficient $\gamma(T) = C(T)/T$ leading to $\gamma(T) \propto 1/T$. On the contrary, the presence of a finite pseudogap Δ results in a non monotonic $\gamma(T)$ dependence, characterized by a strong suppression for $k_BT \approx w_b$ when thermal excitations start to break bipolarons making unfavorable the population of the upper part of the bipolaron band with respect to the lower part of the polaronic band. As one would expect, this feature also depends on doping x. With increasing x, in fact, the chemical potential approaches to zero (see Fig.(10.12)), therefore the thermal weight induced by Fermi-Dirac and Bose-Einstein distribution functions to the states with energy $E \approx \Delta$ also increases. Hence the population of the states in the pseudogap, negated by the condition $\Delta - \mu \ll k_BT$ which is true for $x \ll 1$, becomes as relevant as x increases ($\mu \to 0$) resulting in the close of the pseudogap when a particular doping is reached. Consistently, the depression in the specific heat at small dopings, which signals the lack of occupied states with energy $E \approx \Delta$, rapidly disappears with increasing x as clearly follows from Fig.10.14.

Pseudogap features also emerge in the magnetic response of the system to a perturbation induced by a static and uniform magnetic field of intensity h. In fact, as shown in Fig.10.15, the spin susceptibility $\chi_s(T,h)$ immediately drops to zero in

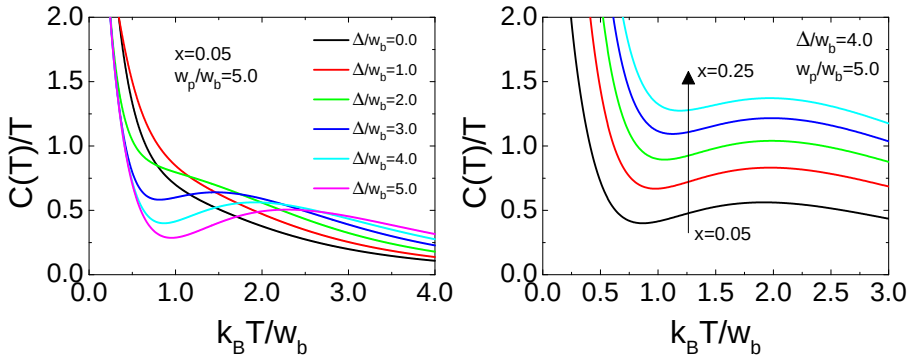

Figure 10.14: Specific heat coefficient $\gamma(T) = C(T)/T$ versus temperature plotted for different values of gap Δ (left panel) and doping x (right panel). Here $w_{b,p}$ is the half-bandwidth of the bipolaron/unpaired polaron band.

the low temperature regime for any $\Delta \neq 0$ and $\mu_B h \lessapprox \Delta$ when the population of the bipolaron (spin-singlet) band becomes dominant. Consistently with the results plotted in Fig.10.12, with increasing temperature $n_b(T) \approx n_p(T)$ and $\chi_s(T)$ naturally recovers the standard Curie behavior $\chi_s(T, h = 0) \propto 1/T$ which is also present in the absence of pseudogap. For $\mu_B h > \Delta$, instead, the magnetic field induces a finite magnetization in the system resulting in a singlet to triplet phase transition at $\mu_B h = \Delta$ which is signaled by a discontinuity in the spin susceptibility at $T = 0$.

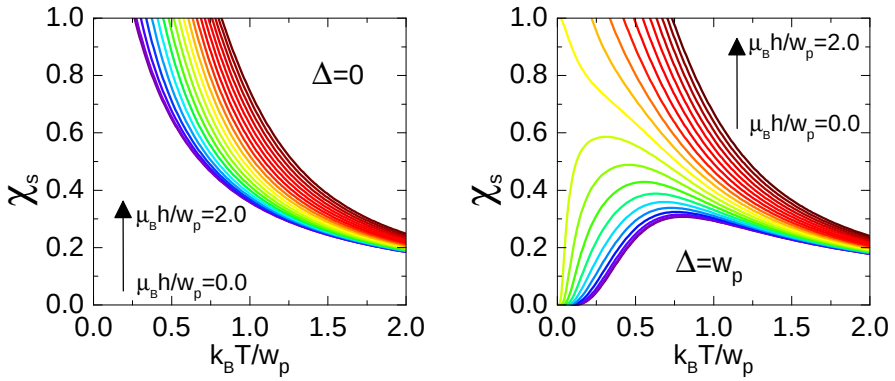

Figure 10.15: Spin susceptibility $\chi_s(T, h)$ versus temperature plotted for different values of the external magnetic field h. Here Δ is the gap between bipolaron and unpaired polaron bands, w_p is the half-bandwidth of the polaronic band (see Fig.10.11).

10.4 Tunneling conductance

To complete our survey on pseudogap features in the the polaronic t-$J_p(\tilde{U})$-$\tilde{U}$ model, let us discuss the tunneling conductance in a normal metal - bipolaronic superconductor (NS) junction. Measurements of the low temperature tunneling current have been advocated as the most powerful tool to investigate the electronic DOS and

reproduce gap and pseudogap features in high-T_c superconductors. As shown in Fig.10.16, these features should result in a depression of the conductance for $T > T_c$ in the zero bias region.

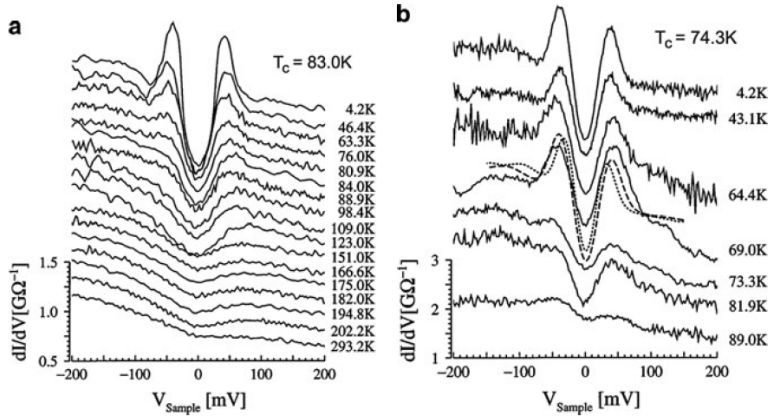

Figure 10.16: Temperature dependence of the tunneling spectra (a) on the UD Bi-2212 ($T_c = 83.0$K) and (b) on the OD Bi-2212 ($T_c = 74.3$K). A gap-like feature at zero bias is seen to persist in the normal state which is direct evidence of a pseudogap in the tunneling conductance. (from Ref.[88]).

From a theoretical point of view, the bias conductivity $\sigma(V)$ depends on the voltage V and on the tunneling current $I_{NS}(V)$ as:

$$\sigma(V) = \frac{dI_{NS}(V)}{dV} \ . \tag{10.53}$$

In order to calculate $I_{NS}(V)$, let us consider a NS junction in which undressed carriers in the normal metal (N) are faced with polarons and bipolarons in the superconducting (S) medium. All the relevant contributions to the tunneling amplitude are given by single-particle tunneling processes between the normal and superconducting states, reported in Fig.10.17. Therefore the NS tunneling Hamiltonian can be written as:

$$H_{NS} = P \sum_{\nu\nu'} p^{\dagger}_{\nu'} c_{\nu} + \frac{B}{\sqrt{N}} \sum_{\nu\nu'\eta'} \left(b^{\dagger}_{\eta'} p_{\nu'} c_{\nu} + H.c. \right) \ . \tag{10.54}$$

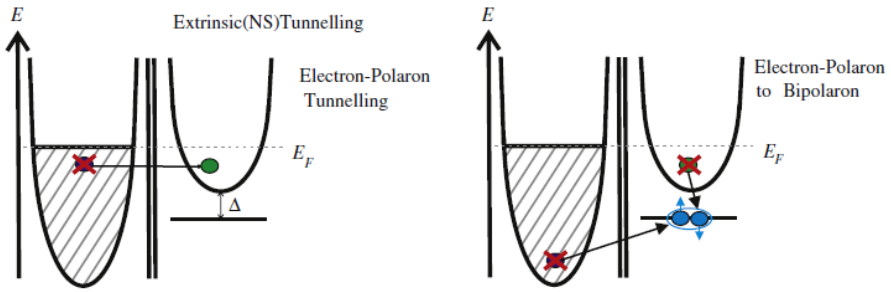

Figure 10.17: Cartoon demonstrating the two possible single-particle tunneling scenarios. Left panel: the annihilation of an electron in the normal-metal with the creation of a polaron in the polaronic band. Right panel: the annihilation of an electron in the metal and the annihilation of a polaron in the superconductor with the creation of a composed boson (from Ref.[89]).

Here the $c_\nu^{(\dagger)}$ describes the annihilation (creation) of a single carrier in the state ν of the metallic tip, $p_{\nu'}^{(\dagger)}/b_\eta^{(\dagger)}$ describe the annihilation (creation) of a single polaron/bipolaron in the state ν'/η in the superconducting side, N is the number of lattice cells. P and B are tunneling matrix elements respectively with and without the involvement of a bipolaron (generally $B \geq P$ [89]). Hence, the tunneling current I_{NS} circulating in the junction, induced by the application of an external potential V, can be expressed as:

$$I_{NS}(V) = e\left(W_{N\to S} - W_{S\to N}\right) \ , \tag{10.55}$$

where $W_{X\to Y}$ represents the tunneling probability of transition, per unit time, from the X to the Y side of the junction. According to Fermi's golden rule, the transition from a state ψ_{in} with energy E_{in} to a state ψ_{fin} with energy E_{fin} is given by:

$$W_{in\to fin} = \frac{2\pi}{\hbar}\left|\langle\psi_{in}|\, H_{NS}\, |\psi_{fin}\rangle\right|^2 \delta\left(E_{fin} - E_{in}\right) \ , \tag{10.56}$$

then we have:

$$\begin{aligned} W_{N\to S} &= \frac{2\pi}{\hbar}\Bigg\{|P|^2 \int_{-\infty}^{+\infty} d\xi \rho_M(\xi) \int_{-\infty}^{+\infty} d\xi' \rho_p(\xi') F(\xi)\left[1 - f_F(\xi')\right]\delta\left(\xi - \xi' + eV\right) \\ &\quad + |B|^2 \int_{-\infty}^{+\infty} d\xi \rho_M(\xi) \int_{-\infty}^{+\infty} d\xi' \rho_p(\xi') \\ &\quad \int_{-\infty}^{+\infty} d\eta \rho_b(\eta)\left(1 + f_B(\eta)\right) f_F(\xi') F(\xi) \delta\left(\eta - \xi - \xi' - eV\right)\Bigg\} = \\ &= \frac{2\pi}{\hbar}\Bigg\{|P|^2 \int_{-\infty}^{+\infty} d\xi' \rho_M(\xi' - eV)\rho_p(\xi') F(\xi' - eV)\left[1 - f_F(\xi')\right] \\ &\quad + |B|^2 \int_{-\infty}^{+\infty} d\eta \int_{-\infty}^{+\infty} d\xi' \rho_M(\xi' - eV)\rho_p(\xi')\rho_b(\eta) \end{aligned}$$

$$\left.(1+f_B(\eta))\,f_F(\xi')F(\xi)\right\}, \tag{10.57}$$

$$\begin{aligned}
W_{S\to N} &= \frac{2\pi}{\hbar}\Bigg\{|P|^2\int_{-\infty}^{+\infty}d\xi\rho_M(\xi)\int_{-\infty}^{+\infty}d\xi'\rho_p(\xi')f_F(\xi')\left[1-F(\xi)\right]\delta\left(\xi-\xi'+eV\right)\\
&\quad+|B|^2\int_{-\infty}^{+\infty}d\xi\rho_M(\xi)\int_{-\infty}^{+\infty}d\xi'\rho_p(\xi')\\
&\quad\int_{-\infty}^{+\infty}d\eta\rho_b(\eta)f_B(\eta)\left(1-f_F(\xi')\right)\left(1-F(\xi)\right)\delta\left(\eta-\xi-\xi'-eV\right)\Bigg\}=\\
&= \frac{2\pi}{\hbar}\Bigg\{|P|^2\int_{-\infty}^{+\infty}d\xi'\rho_M(\xi'-eV)\rho_p(\xi')f_F(\xi')\left[1-F(\xi'-eV)\right]\\
&\quad+|B|^2\int_{-\infty}^{+\infty}d\eta\int_{-\infty}^{+\infty}d\xi'\rho_M(\eta-\xi'-eV)\rho_p(\xi')\rho_b(\eta)f_B(\eta)\\
&\quad\left(1-f_F(\xi')\right)\left(1-F(\eta-\xi'-eV)\right)\Bigg\}.
\end{aligned} \tag{10.58}$$

Here $\rho_M(\xi)$, $\rho_p(\xi')$, $\rho_b(\eta)$ and $F(\xi)=\left[\exp\left(\xi/k_BT\right)+1\right]^{-1}$, $f_F(\xi')=\left[\exp\left(\xi'/k_BT\right)+1\right]^{-1}$, $f_B(\eta)=\left[\exp\left(\eta/k_BT\right)-1\right]^{-1}$ represent the DOS, and the corresponding distribution function, associated to normal metal, bipolaronic band and polaronic band, respectively. Hence, $\rho_M(\xi)F(\xi)$, $\rho_p(\xi')f_p(\xi')$ and $\rho_b(\eta)f_B(\eta)$ represent the number of occupied states at a given temperature T with energy $\xi+d\xi$ in the normal metal, $\xi'+d\xi'$ and $\eta+d\eta$ in the polaronic and bipolaronic bands, respectively. By substituting into (10.55) we have:

$$\begin{aligned}
I_{NS}(V) &= \frac{2\pi e}{\hbar}\Bigg\{|P|^2\int_{-\infty}^{+\infty}d\xi'\rho_M(\xi'-eV)\rho_p(\xi')\left[F(\xi'-eV)-f_F(\xi')\right]\\
&\quad+|B|^2\int_{-\infty}^{+\infty}d\eta\int_{-\infty}^{+\infty}d\xi'\rho_M(\eta-\xi'-eV)\rho_p(\xi')\rho_b(\eta)\\
&\qquad F(\eta-\xi'-eV)f_F(\xi')+\\
&\quad-|B|^2\int_{-\infty}^{+\infty}d\eta\int_{-\infty}^{+\infty}d\xi'\rho_M(\eta-\xi'-eV)\rho_p(\xi')\rho_b(\eta)f_B(\eta)\\
&\qquad\left(1-f_F(\xi')-F(\eta-\xi'-eV)\right)\Bigg\}.
\end{aligned} \tag{10.59}$$

Therefore, neglecting the energy dependence of the metallic DOS: $\rho_M(\xi)=A_m$ since near the Fermi energy it is approximately a constant, from Eq.F.31 we can express the tunneling current in terms of the DOS parameters as follows:

$$I_{NS}(V) = \frac{2\pi e}{\hbar}A_mA_p\Bigg\{|P|^2\int_{\Delta}^{\Delta+2w_p}d\xi'\left[F(\xi'-eV)-f_F(\xi')\right]$$

$$+ |B|^2 A_b \int_0^{2w_b} d\eta \int_\Delta^{\Delta+2w_p} d\xi' F(\eta - \xi' - eV) f_F(\xi')$$
$$- |B|^2 A_b \int_0^{2w_b} d\eta \int_\Delta^{\Delta+2w_p} d\xi' f_B(\eta) \Big(1 - f_F(\xi')$$
$$- F(\eta - \xi' - eV) \Big) \Bigg\} . \tag{10.60}$$

Then the bias conductance can be easily calculated by taking the derivative with respect to the bias:

$$\begin{aligned} \sigma_{NS}(V) &= \frac{2\pi e}{\hbar} A_m A_p \Bigg\{ |P|^2 \int_\Delta^{\Delta+2w_p} d\xi' \frac{d}{dV} F(\xi' - eV) \\ &+ |B|^2 A_b \int_0^{2w_b} d\eta \int_\Delta^{\Delta+2w_p} d\xi' \Bigg[f_F(\xi') \frac{dF}{dV}(\eta - \xi' - eV) \\ &+ f_B(\eta) \frac{dF}{dV}(\eta - \xi' - eV) \Bigg] \Bigg\} , \end{aligned} \tag{10.61}$$

and we can immediately identify the contributions coming from "electron-polaron" tunneling $\sigma_p(eV)$ and "electron-polaron to bipolaron" tunneling $\sigma_b(eV)$, respectively:

$$\sigma_p(V) = \frac{2\pi e}{\hbar} |P|^2 A_m A_p \int_\Delta^{\Delta+2w_p} d\xi' \frac{d}{dV} F(\xi' - eV) , \tag{10.62}$$

$$\begin{aligned} \sigma_b(V) &= \frac{2\pi e}{\hbar} |B|^2 A_m A_p A_b \int_0^{2w_b} d\eta \int_\Delta^{\Delta+2w_p} d\xi' \Bigg[f_F(\xi') \frac{dF}{dV}(\eta - \xi' - eV) \\ &+ f_B(\eta) \frac{dF}{dV}(\eta - \xi' - eV) \Bigg] . \end{aligned} \tag{10.63}$$

As reported in Fig.10.18, numerical results obtained from Eq.10.60 in the case of a Heaviside-theta DOS (F.31) confirm a strong depression of $\sigma(V)$ in the zero bias regime for $k_B T \leq \Delta$, where pseudogap features also emerge in specific heat (Fig.10.14) and spin susceptibility (Fig.10.15). Importantly, our data perfectly reproduce the asymmetry between negative and positive bias conductance providing a further confirmation that the van Hove singularity, ignored in our DOS (see Fig.10.11) and not observed in many experiments such as momentum integrated photoemission [90], does not affect transport properties. Hence, pseudogap features in the tunneling conductance, as well as in specific heat (Fig.10.14) and spin susceptibility (Fig.10.15), naturally appear as a consequence of a thermal induced mixture of polarons and bipolarons, without any ad-hoc assumption on pre-existing orders or broken symmetries in the model.

The plausibility of this explanation is also supported by a good agreement between our data and experimental measurements on the doping dependence of the asymmetry coefficient $R(x, T)$, Fig.10.18, defined as a function of doping x and

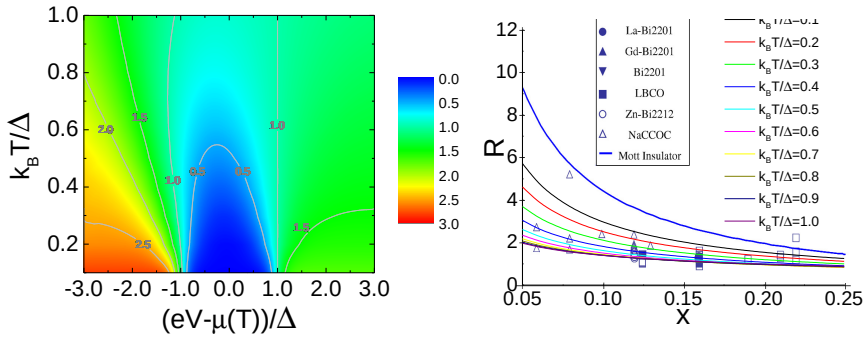

Figure 10.18: Left panel: density plot of the normalized conductivity $\sigma_{NM}(V)/\sigma_{NM}(\Delta)$ in the k_BT/Δ-$(eV-\mu)/\Delta$ plane. Right panel: doping dependence of the asymmetry coefficient $R(x,T)$, Eq.10.64. Numerical results obtained by integrating the normalized conductivity $\sigma(eV)/\sigma(\Delta)$ from 0 to $\pm\Delta$ for different values of the temperature are compared with experimental results in Cuprates (from Ref.[89]).

temperature T as:

$$R(x,T) = \frac{\int_{-\Delta}^{0} \sigma(eV)dV}{\int_{0}^{\Delta} \sigma(eV)dV} = \frac{I_{NS}(-\Delta)}{I_{NS}(\Delta)} \,. \tag{10.64}$$

In fact, as already pointed out before, as long as thermal excitations are not sufficient to break bipolaron pairs ($k_BT \ll \Delta$), the Bose-Fermi mixture can be safely considered as a pure Bose gas with $n_b(T) \approx x/2$ (see Fig.10.12). In this regime, while the polaronic contribution to the tunneling conductance remains almost constant, the bipolaron contribution scales linearly with doping since it is proportional to the bipolaron density $n_b(T)$ as clearly follows from Fig.10.19 and from Eq.10.60 if one neglects the bipolaron energy dispersion in the narrow-band limit.

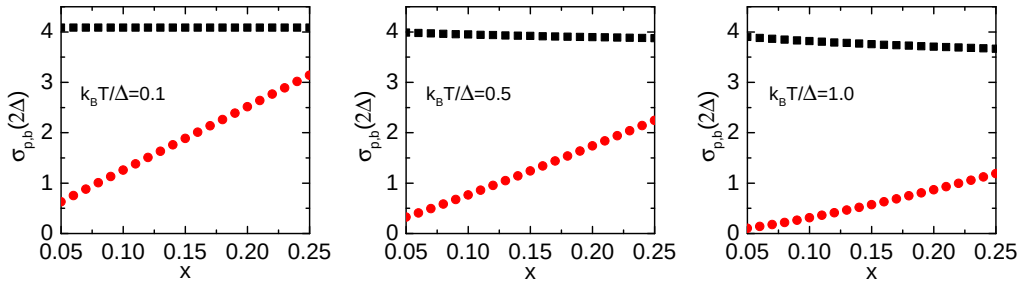

Figure 10.19: Contributions to the tunneling conductance at $eV = \Delta/2$ versus doping and for different values of the temperature. Here $\sigma_{p,b}(\Delta/2)$ represents the two contributions described in Fig.10.17, namely: $\sigma_p(\Delta/2)$ (squares) is induced by the annihilation of an electron in the normal-metal and the creation of a polaron in the polaronic band; $\sigma_b(\Delta/2)$ (circles) is induced by the annihilation of an electron in the metal and the annihilation of a polaron in the superconductor with the creation of a composed boson.

This feature, which persists as long as $n_b(T) \gg n_p(T)$, is strongly suppressed

for $k_B T \gtrapprox \Delta$ when both bipolaron and unpaired polaron bands are populated. Importantly, it is worth noting that numerical data for $R(x, T)$ have been calculated by integrating the rescaled conductivity $\sigma(eV)/\sigma(\Delta)$, therefore do not depend on the particular choice of the tunneling matrix elements B, and P in Eq.10.60. As one would expect, the only relevant quantities are the DOS parameters which are related to the model parameters t, $J_p(\tilde{U})$ and $\tilde{U}$ (see Fig.10.11) since they determine, for a fixed value of the filling, how bipolaron and unpaired polaron densities change with temperature according to Eq.10.47 and Eq.10.48.

Chapter 11

Open issues and possible directions

In the last few years, polaron and bipolaron theory of superconductivity has been widely developed, bolstered by an increasing number of experimental evidence which shed doubts about electron-phonon interaction as an unavoidable ingredient for the explanation of non-conventional behaviors observed in a large class of compounds. In particular, the confirmation that many high-temperature superconductors lie in the very narrow regime in which bipolarons are stable (see Fig.7.1), contributes to a growing understanding that the true origin of high-T_c superconductivity can only be found in a proper combination of *unscreened* Coulomb and Fröhlich electron-phonon interactions. In this regards, the polaronic $t - J_p$ [34, 35] and $t - J_p - \tilde{U}$ [36] models, which account for both Coulomb Fröhlich interactions without any ad hoc assumption on their range or relative strength, lay a microscopic foundation for polaron-bipolaron theory of superconductivity. They provide a full consistent description of the dynamic of polarons and bipolarons into a doped polar insulators as, for instance, oxygen holes in a cuprate lattice. In the low-density limit, the thermal-induced recombination of polarons and bipolarons has been proposed as a possible mechanism responsible for pseudogap features in the normal state of cuprate superconductors. In the same limit, the Bose-Einstein condensation of small and perfectly mobile pairs accounts for a phase transition to a superconducting state with a critical temperature well in excess of hundred kelvin.

Although several analytical and numerical results have been obtained in the dilute limit, only a few can be said in the high-doping regime where the overlap between polarons and bipolarons is expected to play a crucial role in the physics described by the models. With increasing doping, bipolaron configurations are expected to be energetically unfavoured because of bipolaron-bipolaron repulsion. Also, their mobility will be strongly compromised, resulting in the drop of the critical temperature. All these features have been only partially described in the framework of the polaronic $t - J_p - \tilde{U}$. In fact, although a full consistent multi-polaron analysis is still missing, clear signatures of the crossover from a small to a large bipolaronic regime have been found only in the dilute limit. This crossover is characterized by a strong decreasing of the superconducting critical temperature (see Fig.7.1 and Fig.10.8) which also corresponds to the suppression of the gap between the bottom

of polaron and bipolaron bands (see Fig.10.11). Hence, the overlap among pairs has been argued to be responsible for a BEC-BCS crossover which would reconcile the polaron-bipolaron theory with the observation of a d-wave symmetry for the gap function and a small to large Fermi surface transition which occurs moving from half-filling towards the very underdoped regime. These last points, which up to now represent some of the most promising developments of the polaron-bipolaron theory, are currently under investigation via analytic and numerical methods.

Bibliography

[1] L. D. Landau, Phys. Z. Sowjetunion **3**, 664 (1933).

[2] H. Fröhlich, Advances in Physics **3**, 11 (1954).

[3] J. T. Devresee, Encyclopedia of Applied Physics, Vol. **14**, pp. 383-409 (1996).

[4] J.Ranninger, and G. De Filippis, IOS Press Amsterdam (2006) pp 1-25, arXiv:cond-mat/0606665v1.

[5] J. T. Devresee, A. S. Alexandrov, Rep. Prog. Phys. **72**, 066501 (2009).

[6] A. S. Alexandrov, and J. T. Devreese, "Advances in Polaron Physics"*, Springer Series in Solid-State Sciences, Vol. 159. (2010).*

[7] S. J. Miyake, J. Phys. Soc. Japan **43**, 181 (1975).

[8] M. A. Smondyrev, Theor. Math. Phys. **68**, 653 (1986).

[9] O. V. Selyugin, and M. A. Smondyrev, Phys. Stat. Sol. (b) **155**, 155 - 167 (1989).

[10] I. G. Lang and Y. A. Firsov, Zh. Eksp. Teor. Fiz. **43**, 1843 (1962) [Sov. Phys. JETP **16**, 1301 (1962)].

[11] Reik, H. G. , in J. T. Devreese (Ed.), Polarons in Ionic Crystals and Polar Semiconductors, Amsterdam: North-Holland (1972), p. 679 - 714.

[12] A. S. Alexandrov and N. F. Mott, *"Polarons and Bipolarons"* (World Scientific, Singapore, 1995).

[13] A. S. Alexandrov, Phys. Rev. B **46**, 2838 (1992).

[14] A. S. Alexandrov, Phys. Rev. B **61**, 12315 (2000).

[15] M.A. Smondyrev, V.M. Fomin, in *"Polarons and Applications"* (Proceedings in Nonlinear Science), ed. by V.D. Lakhno (JohnWiley & Sons, Chichester, 1994), p. 13.

[16] J.T. Devreese, in Proceedings of the International School of Physics "Enrico Fermi", Course CXXXVI, Varenna, 1997, *"Models and Phenomenology for Conventional and High-Temperature Superconductivity"*, ed. by G. Iadonisi.

[17] G. Verbist, F. M. Peeters, and J. T. Devreese, Solid State Commun. **76**, 1005 (1990).

[18] G. Verbist, F. M. Peeters, and J. T. Devreese, Phys. Rev. B **43**, 2712 (1991).

[19] D. Reagor, E. Ahrens, S.-W. Cheong, A. Migliori, and Z. Fisk, Phys. Rev. Lett. **62**, 2048 (1989).

[20] W. Kress, U. Schröder, J. Prade, A. D. Kulkarni, and F. W. deWette, Phys. Rev. B **38**, 2906 (1988).

[21] L. Genzel, A. Wittlin, M. Bauer, M. Cardona, E. Schönherr and A. Simon, Phys. Rev. B **40**, 2170 (1989).

[22] A. S. Alexandrov, Zh. Fiz. Khim. **57**, 273 (1983); A. S. Alexandrov, Russ. J. Phys. Chem. **57**, 167 (1983).

[23] A. S. Alexandrov, and J. Ranninger, Phys. Rev. B **23**, 1796 (1981); A. S. Alexandrov, and J. Ranninger, Phys. Rev. B 24, 1164 (1981).

[24] G. Beni, P. Pincus, and J. KanamoriPhys. Rev. B **10**, 1896 (1974).

[25] P. W. Anderson, Phys. Rev. Lett. **34**, 953 (1975).

[26] R. A. Street, and N. F. Mott, Phys. Rev. Lett. **35**, 1293 (1975).

[27] S. Aubry, J. Physique (France) IV Colloque C2 **3** 349 (1993); S. Aubry *"Polarons and Bipolarons in High Tc Superconductors and related materials"*, ed. E. K. H. Salje et al (Cambridge: Cambridge University Press, 1995), p 271.

[28] A. S. Alexandrov, and P. E. Kornilovitch, J. Phys. Condens. Matter **14**, 5337 (2002).

[29] J. P. Hague, P. E. Kornilovitch, J. H. Samson, and A. S. Alexandrov Phys. Rev. B **98**, 037002 (2007).

[30] A. S. Alexandrov and P. E. Kornilovitch, Phys. Rev. Lett. **82**, 807 (1999).

[31] J. P. Hague, P. E. Kornilovitch, A. S. Alexandrov, and J. H. Samson, Phys. Rev. B **73**, 054303 (2006).

[32] J. P. Hague, and P. E. Kornilovitch Phys. Rev. B **80**, 054301 (2009).

[33] J. P. Hague, and P. E. Kornilovitch Phys. Rev. B **82**, 094301 (2010).

[34] A. S. Alexandrov, Europhys. Lett. **95**, 27004 (2011).

[35] A. S. Alexandrov, J. H. Samson, and G. Sica, Phys. Rev. B **85**, 104520 (2012).

[36] A. S. Alexandrov, J. H. Samson, and G. Sica Europhys. Lett. **100**, 17011 (2012).

[37] G. Sica, J. H. Samson, and A. S. Alexandrov, Europhys. Lett. **100**, 37005 (2012).

[38] V. V. Tolmachev, *"A new Method in the Theory of Superconductivity"* (1959) ed N. N. Bogoliubov et al. (New York: Consultant Bureau); P. Morel, and P.W. Anderson, Phys. Rev. B **125**, 1263 (1962).

[39] A. S. Alexandrov, Phys. Rev. B **77**, 094502 (2008).

[40] G. M. Eliashberg, Zh. Eksp. Teor. Fiz. **38**, 966 (1960); Zh. Eksp. Teor. Fiz. **39**, 1437 (1960); Sov. Phys. - JEPT **11**, 696 (1960); Sov. Phys. - JEPT **12**, 1000 (1960).

[41] A. B. Migdal, Zh. Eksp. Teor. Fiz. **34**, 1438 (1958); Sov. Phys. - JEPT **7**, 996 (1958).

[42] A. S. Alexandrov, and A. M. Bratkovsky Phys. Rev. Lett. **105**, 226408 (2010), and Phys. Rev. Lett. **84**, 2043-2043 (2000).

[43] A.S. Alexandrov, V.N. Grebenev, E.A. Mazur, Pis'ma Zh. Eksp. Teor. Fiz. **45**, 357 (1987) [JETP Lett. **45**, 455].

[44] F. Dogan, F. Marsiglio, Phys. Rev. B **68**, 165102 (2003).

[45] J. P. Hague, J. Phys. Condens. Matter 15, 2535 (2003).

[46] L. Pietronero, S. Str¨assler, C. Grimaldi, Phys. Rev. B **52**, 10516 (1995).

[47] J. R. Schrieffer, and P. A. Wolff , Phys. Rev. **149**, 491-492 (1966).

[48] I.S. Gradshteyn and I.M. Ryzhik, Table of Integrals, Series, and Products. Elsevier Inc.

[49] J. Spałek, Phys. Rev. B **37**, 533-536 (1988).

[50] T. Bauer, and C. Falter Phys. Rev. B **80**, 094525 (2009).

[51] F. C. Zhang, C. Gros, T. M. Rice, and H. Shiba, Supercond. Sci. Technol. **1**, 36 (1988).

[52] M Valiente, Phys. Rev. A **81**, 042102 (2010).

[53] Rune T. Piil, Nicolai Nygaard, and Klaus Mølmer, Phys. Rev. A **78**, 033611 (2008).

[54] M Valiente and D Petrosyan, J. Phys. B **41**, 161002 (2008).

[55] J. Bonča, S. A. Trugman, and I. Batistić, Phys. Rev. B **60**, 1633 (1999); J. Bonča, T. Katrašnik, and S. A. Trugman, Phys. Rev. Lett. **84**, 3153 (2000).

[56] Y. J. Uemura et al., Phys. Rev. Lett. **66**, 2665-2668 (1991).

[57] Y. J. Uemura, in Polarons and Bipolarons in High-Tc Superconductors and Related Materials, edited by E. K. H. Salje, A. S. Alexandrov, and W. Y. Liang (Cambridge University Press, Cambridge, 1995), p. 453.

[58] C. J. Pethick and H. Smith, *"Bose-Einstein condensation in dilute gases"* (Cambridge University Press, Cambridge, UK, 2002).

[59] N. D. Mermin, and H. Wagner, Phys. Rev. Lett. **17**, 1133-1136 (1966).

[60] J. D. Gunton and M. J. Buckingham, Phys. Rev. **166**, 152-158 (1968).

[61] P. C. Hohenberg, Phys. Rev. **158**, 383-386 (1967).

[62] J. M. Kosterlitz and D. J.Thouless, J. Phys. C **6**, 1181 (1973).

[63] Daniel S. Fisher and P. C. Hohenberg, Phys. Rev. B **37**, 4936-4943 (1988).

[64] V. L. Berezinskii, Zh. Eksp. Teor. Fiz. **61** 1144, (1971) [JETP Lett. **34**, 610 (1972)].

[65] J. M. Kosterlitz, J. Phys. C: Solid State Phys. **7**, 1046 (1974).

[66] P. C. E. Stamp, L. Forro, and C. Ayache, Phys. Rev. B **38**, 2847 (1988).

[67] S. Martin et al. , Phys. Rev. Lett. **62**, 677 (1989).

[68] N. C. Yeh and C. C. Tsuei, Phys. Rev. B **39**, 9708 (1989).

[69] S. N. Artemenko, I. G. Govorova, and Yu. I. Latyshev, Pis'ma Zh. Eksp. Teor. Fiz. **49**, 566 (1989) [JETP Lett. **49**, 654 (1989)].

[70] A. S. Alexandrov, Russ. J. Phys. Chem. 57, 167 (1983).

[71] T. Timusk, and B. Statt, Rep. Prog. Phys. **62**, 61 (1999).

[72] A. Damascelli, Z. Hussain, Z.-X. Shen, Rev. Mod. Phys. **75**, 473 (2003).

[73] M. R. Norman, D. Pines, and C. Kallin, Adv. Phys. **54**, 715 (2005).

[74] N. Plakida, "High-Temperature Cuprate Superconductors", *Springer Series in Solid-State physics, Vol. 166. (2010).*

[75] V. J. Emery, and S. A. Kivelson, Nature **374**, 434 (1995).

[76] V. J. Emery, S. A. Kivelson, and O. Zachar, Phys. Rev. B **56**, 6120 (1997).

[77] D. C. Johnston, Phys. Rev. Lett. **62** 957 (1989).

[78] T. Nakano, M. Oda, C. Manabe, N. Momono, Y. Miura and M. Ido, Phys. Rev. B **49**, 16000 (1994).

[79] N. Curro, Z. Fisk and D. Pines, MRS Bulletin **30**(6) 442 (2005).

[80] W. W. Jr. Warren, R. E. Walstedt, J. F. Brennert, R. J. Cava, R. Tycko, R. F. Bell, and G. Dabbagh, Phys. Rev. Lett. **62**, 1193 (1989).

[81] M. Hashimoto, H.R. He, K. Tanaka, J.P. Testaud, \emph{et al.}, Nat. Phys. **6**, 414 (2010).

[82] X. G. Wen, and P. A. Lee, Phys. Rev. Lett. **76**, 503 (1996).

[83] B. Pradhan, B. K. Raj, and G. C. Rout, Physica C **468**, 2332 (2008).

[84] E. V. L. de Mello, M. T. D. Orlando, J. L. Gonzalez, E. S. Caixeiro, and E. Baggio-Saitovich, Phys. Rev. B **66**, 092504 (2002).

[85] V. J. Emery, S. A. Kivelson, and H. Q. Lin, Phys. Rev. Lett. **64**, 475 (1990).

[86] K.M. Shen, F. Ronning, D.H. Lu, W.S. Lee, N.J.C. Ingle, W. Meevasana, F. Baumberger, A. Damascelli, N.P. Armitage, L.L. Miller, Y. Kohsaka, M. Azuma, M. Takano, H. Takagai and Z.-X. Shen, Phys. Rev. Lett. **93**, 267002 (2004).

[87] A. S. Alexandrov, and D. K. Ray, Phil. Mag. Lett. 63, 295 (1991).

[88] Renner Ch, Revaz B, Genoud J-Y, Kadowaki K and Fischer O, Phys. Rev. Lett. **80**, 149 (1998).

[89] A. S. Alexandrov and J. Beanland, Phys. Rev. Lett. **104**, 026401 (2010), J. Phis.: Condens. Matter **22**, 403202 (2010).

[90] R-H. He, X. J. Zhou, M. Hashimoto et al. New J. Phys. **13**, 013031 (2011).

Part III

Appendices

Appendix A

Detailed calculations for the 1D U-J-h model

We report in this Appendix detailed calculations of single particle properties and two-time correlators for the one-dimensional U-J-h model described in Chapter 3.1.

A.1 $A_m^{(p)}$ coefficients

Exploiting the algebra satisfied by $n(i)$, $n_3(i)$ and $D(i)$ operators it is easy to obtain the following algebraic relations:

$$\begin{array}{ll} n^p(i) = n(i) + a_p D(i) & \\ n(i)n_3(i) = n_3(i) & [n_3(i)]^{2p} = n(i) - 2D(i) \\ D(i)n_3(i) = 0 & [n_3(i)]^{2p+1} = n_3(i) \\ D^p(i) = D(i) & \\ n(i)D(i) = 2D(i) & \end{array} \quad , \tag{A.1}$$

where $a_p = 2^p - 2$ and $p \geqslant 1$. Hence we get:

$$\begin{aligned} [n^\alpha(i)]^p &= \left[\frac{1}{2}\left(n(i-a) + n(i+a)\right)\right]^p = \frac{1}{2^p}\sum_{m=0}^{p}\left(\begin{array}{c} p \\ m \end{array}\right) n^{p-m}(i+a)n^m(i-a) = \\ &= \frac{1}{2^p}n^p(i+a) + \frac{1}{2^p}n^p(i-a) + \frac{1}{2^p}\sum_{m=1}^{p-1}\left(\begin{array}{c} p \\ m \end{array}\right) n^{p-m}(i+a)n^m(i-a) = \\ &= \frac{1}{2^{p-1}}\left[n^\alpha(i) + a_p D^\alpha(i)\right] + \frac{1}{2^p}\sum_{m=1}^{p-1}\left(\begin{array}{c} p \\ m \end{array}\right)\left[n(i+a) + a_{p-m}D(i+a)\right] \\ &\quad \left[n(i-a) + a_m D(i-a)\right] = \\ &= \frac{1}{2^{p-1}}\left[n^\alpha(i) + a_p D^\alpha(i)\right] + \frac{1}{2^p}n(i+a)n(i-a)\sum_{m=1}^{p-1}\left(\begin{array}{c} p \\ m \end{array}\right) + \end{aligned}$$

$$+\frac{1}{2^p}n(i+a)D(i-a)\sum_{m=1}^{p-1}\left(\begin{array}{c} p \\ m \end{array}\right)a_m+\frac{1}{2^p}n(i-a)D(i+a)\sum_{m=1}^{p-1}\left(\begin{array}{c} p \\ m \end{array}\right)a_{p-m}+$$
$$+\frac{1}{2^p}D(i+a)D(i-a)\sum_{m=1}^{p-1}\left(\begin{array}{c} p \\ m \end{array}\right)a_{p-m}a_m \quad .$$

Let us define the following quantities:

$$a_p \equiv \sum_{m=1}^{p-1}\left(\begin{array}{c} p \\ m \end{array}\right) = 2^p - 2 \ ,$$
$$b_p \equiv \sum_{m=1}^{p-1}\left(\begin{array}{c} p \\ m \end{array}\right)a_m = \sum_{m=1}^{p-1}\left(\begin{array}{c} p \\ m \end{array}\right)a_{p-m} = 3\left(1-2^p+3^{p-1}\right) \ ,$$
$$c_p \equiv \sum_{m=1}^{p-1}\left(\begin{array}{c} p \\ m \end{array}\right)a_{p-m}a_m = 4\left(-1-3^p+4^{p-1}\right)+3\cdot 2^{p+1} \ ,$$

then $[n^\alpha(i)]^p$ can be rewritten as:

$$\begin{aligned}[n^\alpha(i)]^p &= \frac{1}{2^{p-1}}n^\alpha(i)+\frac{1}{2^{p-1}}a_p\left[D^\alpha(i)+\frac{1}{2^p}n(i+a)n(i-a)\right] \\ &+\frac{1}{2^p}b_p\left[n(i+a)D(i-a)+n(i-a)D(i+a)\right] \\ &+\frac{1}{2^p}c_pD(i+a)D(i-a) \ . \end{aligned} \tag{A.2}$$

From the above relation we observe that:

$$D^\alpha(i)+\frac{1}{2}n(i+a)n(i-a) = [n^\alpha(i)]^2-\frac{1}{2}n^\alpha(i)$$
$$D(i+a)n(i-a)+D(i-a)n(i+a) = \frac{4}{3}[n^\alpha(i)]^3-2[n^\alpha(i)]^2+\frac{2}{3}n^\alpha(i)$$
$$D(i+a)D(i-a) = \frac{2}{3}[n^\alpha(i)]^4-2[n^\alpha(i)]^3+\frac{11}{6}[n^\alpha(i)]^2-\frac{1}{2}n^\alpha(i)$$

so, substituting in the expression of $[n^\alpha(i)]^p$, we obtain the following recursion formula:

$$\begin{aligned}[n^\alpha(i)]^p &= \frac{1}{2^{p-1}}\left[1-\frac{1}{2}a_p+\frac{1}{3}b_pn^\alpha(i)-\frac{1}{4}c_p\right]n^\alpha(i)+\frac{1}{2^{p-1}}\left[a_p-b_p+\frac{11}{12}c_p\right][n^\alpha(i)]^2+ \\ &+\frac{1}{2^{p-1}}\left[\frac{2}{3}b_p-c_p\right][n^\alpha(i)]^3+\frac{1}{3}\frac{1}{2^{p-1}}c_p[n^\alpha(i)]^4 \ , \end{aligned}$$

that can be also written in the following form:

$$[n^\alpha(i)]^p = \sum_{m=1}^{4}A_m^{(p)}[n^\alpha(i)]^m \quad , \tag{A.3}$$

p	$(z=2)$		$(z=4)$			
	$A_1^{(p)}$	$A_2^{(p)}$	$A_1^{(p)}$	$A_2^{(p)}$	$A_3^{(p)}$	$A_4^{(p)}$
1	1	0	1	0	0	0
2	0	1	0	1	0	0
3	$-1/4$	$5/4$	0	0	1	0
4	$-5/16$	$21/16$	0	0	0	1
5	$-21/64$	$85/64$	$-9/1024$	$205/1024$	$-273/256$	$15/8$
6	$-85/256$	$364/256$	$-135/8192$	$3003/8192$	$-3685/2048$	$627/256$

Table A.1: Values of the coefficients $A_m^{(p)}$ for $p = 1, \ldots, 6$ and $z = 2, 4$.

where:

$$A_1^{(p)} = \frac{1}{2^{p-1}}\left[1 - \frac{1}{2}a_p + \frac{1}{3}b_p n^{\alpha}(i) - \frac{1}{4}c_p\right] = -6 + 2^{3-p} - 2^{p-1} + 2^{3-p}\cdot 3^{p-1}$$

$$A_2^{(p)} = \frac{1}{2^{p-1}}\left[a_p - b_p + \frac{11}{12}c_p\right] = \frac{1}{3\cdot 2^{p+1}}\left[-104 + 57\cdot 2^{p+1} - 56\cdot 3^p + 11\cdot 4^p\right]$$

$$A_3^{(p)} = \frac{1}{2^{p-1}}\left[\frac{2}{3}b_p - c_p\right] = \frac{1}{3\cdot 2^{p-1}}\left[18 - 3\cdot 2^{p+3} + 14\cdot 3^p - 3\cdot 4^p\right]$$

$$A_4^{(p)} = \frac{1}{2^{p-1}}\frac{1}{3}c_p = \frac{1}{3\cdot 2^{p-1}}\left[-4 + 3\cdot 2^{p+1} - 4\cdot 3^p + 4^p\right]$$

It is worth noting that the following property is satisfied:

$$\sum_{m=1}^{4} A_m^{(p)} = 1 \quad . \tag{A.4}$$

In Tab.A.1 we report some values for $z = 2$ and $z = 4$.

A.2 Normalization and energy matrices

Recalling the definition of the normalization matrix:

$$I^{(s)} = \left\langle \left\{ \psi^{(s)}(\boldsymbol{i}, t), \psi^{(s)\dagger}(\boldsymbol{i}, t) \right\} \right\rangle \ , (, s = \xi, \eta) \ , \tag{A.5}$$

it is easy to see that:

$$\begin{aligned}
I_{n,m}^{\sigma\sigma'(\xi)} &= \left\langle \left\{ \psi_n^{\sigma(\xi)}(\boldsymbol{i}, t), \psi_m^{\sigma'(\xi)\dagger}(\boldsymbol{i}, t) \right\} \right\rangle = \left\langle \left\{ \xi_\sigma(i) \left[n_3^{\alpha}(i)\right]^{n-1}, \left[n_3^{\alpha}(i)\right]^{m-1} \xi_{\sigma'}^{\dagger}(i) \right\} \right\rangle = \\
&= \left\langle \left\{ \xi_\sigma(i), \xi_{\sigma'}^{\dagger}(i) \right\} \left[n_3^{\alpha}(i)\right]^{n-1} \left[n_3^{\alpha}(i)\right]^{m-1} \right\rangle = \\
&\quad \delta_{\sigma\sigma'} \left\langle \left(1 - n_{\bar{\sigma}}(i)\right) \left[n_3^{\alpha}(i)\right]^{n-1} \left[n_3^{\alpha}(i)\right]^{m-1} \right\rangle \ , \qquad \text{(A.6)} \\
I_{n,m}^{\sigma\sigma'(\eta)} &= \left\langle \left\{ \psi_n^{\sigma(\eta)}(\boldsymbol{i}, t), \psi_m^{\sigma'(\eta)\dagger}(\boldsymbol{i}, t) \right\} \right\rangle = \left\langle \left\{ \eta_\sigma(i) \left[n_3^{\alpha}(i)\right]^{n-1}, \left[n_3^{\alpha}(i)\right]^{m-1} \eta_{\sigma'}^{\dagger}(i) \right\} \right\rangle =
\end{aligned}$$

$$= \left\langle \left\{ \eta_\sigma(i), \eta^\dagger_{\sigma'}(i) \right\} \left[n^\alpha_3(i) \right]^{n-1} \left[n^\alpha_3(i) \right]^{m-1} \right\rangle = \delta_{\sigma\sigma'} \left\langle n_{\bar\sigma}(i) \left[n^\alpha_3(i) \right]^{n-1} \left[n^\alpha_3(i) \right]^{m-1} \right\rangle \ , \tag{A.7}$$

hence, by means of the recursion formulas (3.9)-(3.10) we obtain:

$$I^{(a)} = \begin{pmatrix} I^{\uparrow\uparrow(a)} & 0 \\ 0 & I^{\downarrow\downarrow(a)} \end{pmatrix} \ , \tag{A.8}$$

where:

$$I^{\uparrow\uparrow(a)} = \begin{pmatrix} I^{(a)}_{1,1} & I^{(a)}_{1,2} & I^{(a)}_{1,3} & I^{(a)}_{1,4} & I^{(a)}_{1,5} \\ I^{(a)}_{1,2} & I^{(a)}_{1,3} & I^{(a)}_{1,4} & I^{(a)}_{1,5} & I^{(a)}_{2,5} \\ I^{(a)}_{1,3} & I^{(a)}_{1,4} & I^{(a)}_{1,5} & I^{(a)}_{2,5} & I^{(a)}_{3,5} \\ I^{(a)}_{1,4} & I^{(a)}_{1,5} & I^{(a)}_{2,5} & I^{(a)}_{3,5} & I^{(a)}_{4,5} \\ I^{(a)}_{1,5} & I^{(a)}_{2,5} & I^{(a)}_{3,5} & I^{(a)}_{4,5} & I^{(a)}_{5,5} \end{pmatrix} \ , \ I^{\downarrow\downarrow(a)} = \begin{pmatrix} I^{(a)}_{6,6} & I^{(a)}_{6,7} & I^{(a)}_{6,8} & I^{(a)}_{6,9} & I^{(a)}_{6,10} \\ I^{(a)}_{6,7} & I^{(a)}_{6,8} & I^{(a)}_{6,9} & I^{(a)}_{6,10} & I^{(a)}_{7,10} \\ I^{(a)}_{6,8} & I^{(a)}_{6,9} & I^{(a)}_{6,10} & I^{(a)}_{7,10} & I^{(a)}_{8,10} \\ I^{(a)}_{6,9} & I^{(a)}_{6,10} & I^{(a)}_{7,10} & I^{(a)}_{8,10} & I^{(a)}_{9,10} \\ I^{(a)}_{6,10} & I^{(a)}_{7,10} & I^{(a)}_{8,10} & I^{(a)}_{9,10} & I^{(a)}_{10,10} \end{pmatrix} . \tag{A.9}$$

It is worth noting that the matrix elements $I^{(s)}_{\sigma;ab}$ can be expressed in terms of the elements of the first row: $I^{(s)}_{\sigma;1p}$ as:

$$\begin{array}{ll} I^{(a)}_{2,5} = -\frac{1}{4} I^{(a)}_{1,2} + \frac{5}{4} I^{(a)}_{1,4} & I^{(a)}_{7,10} = -\frac{1}{4} I^{(a)}_{6,7} + \frac{5}{4} I^{(a)}_{6,9} \\ I^{(a)}_{3,5} = -\frac{1}{4} I^{(a)}_{1,3} + \frac{5}{4} I^{(a)}_{1,5} & I^{(a)}_{8,10} = -\frac{1}{4} I^{(a)}_{6,8} + \frac{5}{4} I^{(a)}_{6,10} \\ I^{(a)}_{4,5} = -\frac{5}{16} I^{(a)}_{1,2} + \frac{21}{16} I^{(a)}_{1,4} & I^{(a)}_{9,10} = -\frac{5}{16} I^{(a)}_{6,7} + \frac{21}{16} I^{(a)}_{6,9} \\ I^{(a)}_{5,5} = -\frac{5}{16} I^{(a)}_{1,3} + \frac{21}{16} I^{(a)}_{1,5} & I^{(a)}_{10,10} = -\frac{5}{16} I^{(a)}_{6,8} + \frac{21}{16} I^{(a)}_{6,10} \end{array} \tag{A.10}$$

while, as reported in detail in Section 3.1.2 for the one-dimensional case, the remaining unknown components: $I^{(a)}_{1,1}$, $I^{(a)}_{1,2}$, $I^{(a)}_{1,3}$, $I^{(a)}_{1,4}$, $I^{(a)}_{1,5}$ and $I^{(a)}_{6,6}$, $I^{(a)}_{6,7}$, $I^{(a)}_{6,8}$, $I^{(a)}_{6,9}$, $I^{(a)}_{6,10}$ can be fixed in terms of the correlators $\kappa^{(p)} \equiv \left\langle [n^\alpha_3(i)]^{p-1} \right\rangle$ and $\lambda^{(p)}_\sigma \equiv \left\langle n_\sigma(i) \left[n^\alpha_3(i) \right]^{p-1} \right\rangle$ according to the following self-consistent equations:

$$\begin{array}{ll} I^{(\xi)}_{1,p} = \kappa^{(p)} - \lambda^{(p)}_\downarrow & \\ I^{(\eta)}_{1,p} = \lambda^{(p)}_\downarrow & 1 \leqslant p \leqslant 5 \end{array} \quad , \quad \begin{array}{ll} I^{(\xi)}_{6,p} = \kappa^{(p-5)} - \lambda^{(p-5)}_\uparrow & \\ I^{(n)}_{6,p} = \lambda^{(p-5)}_\uparrow & 6 \leqslant p \leqslant 10 \ . \end{array} \tag{A.11}$$

where $\kappa^{(p)}$ and $\lambda^{(p)}_\sigma$ can be easily calculated in terms of X_i and G_i as:

$$\kappa^{(1)} = 1 \ , \tag{A.12}$$

$$\lambda^{(1)}_\sigma = \frac{1}{2 \left\langle e^{-\beta H^{(i)}_I} \right\rangle_i} \Big\{ (G_1 + \sigma G_2) + 2a \Big[G_2 + \sigma \left(G_1 - 2G_3 \right) \Big] X_2 \left[1 + b \left(X_1 - 2X_3 \right) \right] + \left(G_1 - 2G_3 + \sigma G_2 \right) \Big[a^2 X_2^2 + + 2b \left(X_1 - 2X_3 \right) + b^2 \left(X_1 - 2X_3 \right)^2 \Big] \Big\} \ , \tag{A.13}$$

$$\kappa^{(2)} = \frac{1}{2 \left\langle e^{-\beta H^{(i)}_I} \right\rangle_i} \Big\{ X_2 + aG_2 \big\{ (1+b) X_2^2 + \left[1 + b \left(X_1 - 2X_3 \right) \right] \left(X_1 - 2X_3 \right) \big\} + \left(G_1 - 2G_3 \right) X_2 \Big[b + \left(a^2 + b + b^2 \right) \left(X_1 - 2X_3 \right) \Big] \Big\} \ , \tag{A.14}$$

$$\lambda_\sigma^{(2)} = \frac{1}{2\left\langle e^{-\beta H_I^{(i)}}\right\rangle_i}\Big\{(G_1+\sigma G_2)X_2 + a\left[G_2+\sigma\left(G_1-2G_3\right)\right]\Big\{\left(1+b\right)X_2^2 + \left[1+b\left(X_1-2X_3\right)\right]\left(X_1-2X_3\right)\Big\} + \left(G_1-2G_3+\sigma G_2\right)\Big[bX_2 + \left(a^2+b+b^2\right)X_2\left(X_1-2X_3\right)\Big]\,, \tag{A.15}$$

$$\kappa^{(3)} = \frac{1}{2\left\langle e^{-\beta H_I^{(i)}}\right\rangle_i}\Big\{X_1-2X_3+X_2^2+G_2\left(f_1+2f_3\right) + \left(G_1-2G_3\right)\left(f_2+f_4\right)\Big\}\,, \tag{A.16}$$

$$\lambda_\sigma^{(3)} = \frac{1}{4\left\langle e^{-\beta H_I^{(i)}}\right\rangle_i}\Big\{\left(G_1+\sigma G_2\right)\left(X_1-2X_3+X_2^2\right)\left[G_2+\sigma\left(G_1-2G_3\right)\right] + \left(f_1+2f_3\right)+\left(G_1-2G_3+\sigma G_2\right)\left(f_2+f_4\right)\Big\}\,. \tag{A.17}$$

We report in Tab.A.2 the analytical expressions of $\kappa^{(p)}$ and $\lambda_\sigma^{(p)}$ obtained for each phase in the limit of zero temperature as a function of the filling.

For the calculation of the energy matrix, in the one-dimensional case with $z=2$, we have:

$$\varepsilon_\sigma^{(\xi)} = \begin{pmatrix} -\mu-\sigma & -2\sigma J & 0 & 0 & 0 \\ 0 & -\mu-\sigma h & -2\sigma J & 0 & 0 \\ 0 & 0 & -\mu-\sigma h & -2\sigma J & 0 \\ 0 & 0 & 0 & -\mu-\sigma h & -2\sigma J \\ 0 & \sigma J/2 & 0 & -5\sigma J/2 & -\mu-\sigma h \end{pmatrix}\,, \tag{A.18}$$

$$\varepsilon_\sigma^{(\eta)} = \varepsilon_\sigma^{(\xi)} + U\cdot\boldsymbol{I}_{5\times5}\,, \tag{A.19}$$

where $\sigma=(\uparrow,\downarrow)$ or $\sigma=(+1,-1)$ and $\boldsymbol{I}_{5\times5}$ is the 5×5 identity matrix. The eigenvalues of these matrices are:

$$E_n^{(\xi,\sigma)} = \begin{pmatrix} -\mu-\sigma \\ -\mu-\sigma h-2\sigma J \\ -\mu-\sigma h-\sigma J \\ -\mu-\sigma h+\sigma J \\ -\mu-\sigma h+2\sigma J \end{pmatrix}\quad,\quad E_n^{(\eta,\sigma)} = \begin{pmatrix} U-\mu-\sigma \\ U-\mu-\sigma h-2\sigma J \\ U-\mu-\sigma h-\sigma J \\ U-\mu-\sigma h+\sigma J \\ U-\mu-\sigma h+2\sigma J \end{pmatrix}\,. \tag{A.20}$$

The eigenvectors define the columns of the $\Omega_\sigma^{(s)}$ matrices, $s=\xi,\eta$, which read as:

$$\Omega_\sigma^{(s)} = \begin{pmatrix} 1 & 1 & 2^4 & 2^4 & 1 \\ 0 & 1 & 2^3 & -2^3 & -1 \\ 0 & 1 & 2^2 & 2^2 & 1 \\ 0 & 1 & 2 & -2 & -1 \\ 0 & 1 & 1 & 1 & 1 \end{pmatrix}\,. \tag{A.21}$$

It is worth noting that the above matrix does not depend on σ and on the particular

$(0 < n < 1)$							
J	Phase	$\kappa^{(1)}$	$\kappa^{(2)} = \kappa^{(4)}$	$\kappa^{(3)} = \kappa^{(5)}$	$\lambda_\sigma^{(1)}$	$\lambda_\sigma^{(2)} = \lambda_\sigma^{(4)}$	$\lambda_\sigma^{(3)} = \lambda_\sigma^{(5)}$
$J > 0$	NM	1	0	0	$\frac{n}{2}$	0	0
	F	1	$\frac{h}{\lvert h\rvert}n$	n	$\frac{n(1+\sigma)}{2}$	$\frac{h(1+\sigma)n}{2\lvert h\rvert}$	$\frac{n(1+\sigma)}{2}$
$J < 0$	NM	1	0	0	$\frac{n}{2}$	0	0
	AF	1	0	n	$\frac{n}{2}$	$-\frac{n}{2}\sigma$	$\frac{n}{2}$
	F1	1	$\frac{h}{\lvert h\rvert}n$	n	$\frac{n(1-\sigma)}{2}$	$\begin{cases} 0 & 0 < n < 0.5 \\ \frac{h(2n-1)(1-\sigma)}{2\lvert h\rvert} & 0.5 < n < 1 \end{cases}$	$\begin{cases} 0 & 0 < n < 0.5 \\ \frac{(2n-1)(1-\sigma)}{2} & 0.5 < n < 1 \end{cases}$
	F2*	1	$\frac{h}{2\lvert h\rvert}$	$\frac{1}{2}$	$\frac{2n-\sigma}{4}$	$\frac{h(n-1/2)}{2\lvert h\rvert}$	$\frac{n-1/2}{2}$

$(1 < n < 2)$							
J	Phase	$\kappa^{(1)}$	$\kappa^{(2)} = \kappa^{(4)}$	$\kappa^{(3)} = \kappa^{(5)}$	$\lambda_\sigma^{(1)}$	$\lambda_\sigma^{(2)} = \lambda_\sigma^{(4)}$	$\lambda_\sigma^{(3)} = \lambda_\sigma^{(5)}$
$J > 0$	NM	1	0	0	$\frac{n}{2}$	0	0
	F	1	$\frac{h(2-n)}{\lvert h\rvert}$	$2-n$	$\frac{n(1-\sigma)}{2}+\sigma$	$\frac{h(1+\sigma)(2-n)}{2\lvert h\rvert}$	$\frac{(1+\sigma)(2-n)}{2}$
$J < 0$	NM	1	0	0	$\frac{n}{2}$	0	0
	AF	1	0	$2-n$	$\frac{n}{2}$	$-\frac{2-n}{2}\sigma$	$\frac{2-n}{2}$
	F1	1	$\frac{h(2-n)}{\lvert h\rvert}$	$2-n$	$\frac{n(1+\sigma)}{2}-\sigma$	$\begin{cases} \frac{h(1-\sigma(3-2n))}{2\lvert h\rvert} & 1 < n < \frac{3}{2} \\ \frac{h(2-n)}{2\lvert h\rvert} & \frac{3}{2} < n < 2 \end{cases}$	$\begin{cases} \frac{1-\sigma(3-2n)}{2} & 1 < n < 1.5 \\ \frac{2-n}{2} & 1.5 < n < 2 \end{cases}$
	F2*	1	$\frac{h}{2\lvert h\rvert}$	$\frac{1}{2}$	$\frac{2n-\sigma}{4}$	$\frac{h(n-1/2)}{2\lvert h\rvert}$	$\frac{n-1/2}{2}$

Table A.2: Values of $\kappa^{(p)}$ and $\lambda_\sigma^{(p)}$ obtained in the limit of zero temperature. *We recall that F2-phase exists only in the range of fillings $0.5 \leq n \leq 1.5$.

choice of $s = \xi,\eta$.

A.3 Two time correlators and self-consistent equations

As explained in detail in Section 3.1.2 for the one-dimensional case, by considering separately all the interactions which involve a single site, say $\boldsymbol{i}$, of the system, one can split a chain into two separate sub-lattices. Hence the correlators involving sites on two different sub-lattices can be factorized and the statistic average of a generic operator $O(i)$ can be written as:

$$\langle O(i)\rangle = \frac{\left\langle O e^{-\beta H_I(i)}\right\rangle_0}{\left\langle e^{-\beta H_I(i)}\right\rangle_0} \,, \tag{A.22}$$

where the average $\langle \dots \rangle_0$ is considered in the so-called H_0-representation since it is accounted in terms of $H_0^{(i)}$ only:

$$\langle O(i)\rangle_0 = \frac{\left\langle O e^{-\beta H_0(i)}\right\rangle}{\left\langle e^{-\beta H_0(i)}\right\rangle} \,, \tag{A.23}$$

By means of these properties and the algebraic relations (3.9) and (3.10) one can easily obtain:

$$\begin{aligned} e^{\beta J n_3(i) n_3(j)} &= 1 + \sum_{m=1}^{\infty} \frac{1}{m!} (\beta J)^m n_3^m(i) n_3^m(j) = \\ &= 1 + a n_3(i) n_3(j) + b\left[n(i) - 2D(i)\right]\left[n(j) - 2D(j)\right] \,, \end{aligned} \tag{A.24}$$

where:

$$\begin{cases} a = \sinh(\beta J) \\ b = \cosh(\beta J) - 1 \end{cases} . \tag{A.25}$$

Then:

$$\begin{aligned} e^{-\beta H_I(i)} &= \exp\left\{2\beta J n_3(i) n_3^{\alpha}(i)\right\} = \exp\left\{\beta J n_3(i)\left[n_3(i+1) + n_3(i-1)\right]\right\} = \\ &= \prod_{p=1}^{2} \exp\left[\beta J n_3(i) n_3(i + (-1)^p)\right] = \\ &= 1 + a n_3(i)\left[n_3(i+1) + n_3(i-1)\right] + b\left[n(i) - 2D(i)\right] \cdot \\ &\quad \cdot \left[n(i+1) - 2D(i+1) + n(i-1) - 2D(i-1)\right] + \\ &\quad + a^2\left[n(i) - 2D(i)\right] n_3(i+1) n_3(i-1) + b^2\left[n(i) - 2D(i)\right] \cdot \\ &\quad \cdot \left[n(i+1) - 2D(i+1)\right]\left[n(i-1) - 2D(i-1)\right] + a b n_3(i) \\ &\quad \left\{n_3(i-1)\left[n(i+1) - 2D(i+1)\right] + n_3(i+1)\left[n(i-1) - 2D(i-1)\right]\right\} \,. \end{aligned}$$

The average of the above quantity gives

$$\left\langle e^{-\beta H_I^{(i)}} \right\rangle = 1 + 2aG_2X_2\left[1 + b\left(X_1 - 2X_3\right)\right] + \left(G_1 - 2G_3\right) \left[a^2X_2^2 + 2b\left(X_1 - 2X_3\right) + b^2\left(X_1 - 2X_3\right)^2\right], \quad \text{(A.26)}$$

where:

$$\begin{array}{lll} G_1 \equiv \langle n(i)\rangle_0 & , & X_1 \equiv \langle n^\alpha(i)\rangle_0 \\ G_2 \equiv \langle n_3(i)\rangle_0 & , & X_2 \equiv \langle n_3^\alpha(i)\rangle_0 \\ G_3 \equiv \langle D(i)\rangle_0 & , & X_3 \equiv \langle D^\alpha(i)\rangle_0 \end{array} . \quad \text{(A.27)}$$

While X_1, X_2 and X_3 can be determined self-consistently (3.26), G_1, G_2 and G_3 can be calculated starting from the retarded Green's functions in the H_0-representation:

$$\begin{cases} G_\sigma^{(\xi,0)}(t-t') = \left\langle R\left[\xi_\sigma(i,t)\xi_\sigma^\dagger(i,t')\right]\right\rangle_0 = \frac{i}{2\pi}\int_{-\infty}^{+\infty} e^{-i\omega(t-t')}G_\sigma^{(\xi,0)}(\omega)d\omega \\ G_\sigma^{(\eta,0)}(t-t') = \left\langle R\left[\eta_\sigma(i,t)\eta_\sigma^\dagger(i,t')\right]\right\rangle_0 = \frac{i}{2\pi}\int_{-\infty}^{+\infty} e^{-i\omega(t-t')}G_\sigma^{(\eta,0)}(\omega)d\omega \end{cases}, \quad \text{(A.28)}$$

It is worth noting that the Hubbard operators satisfy the equations of motion:

$$\begin{cases} i\frac{\partial}{\partial t}\xi(i) = [\xi(i), \mathcal{H}_0(i)] = -\left(\mu + h\sigma_3\right)\xi(i) \\ i\frac{\partial}{\partial t}\eta(i) = [\eta(i), \mathcal{H}_0(i)] = -\left(\mu + h\sigma_3 - U\right)\eta(i) \end{cases}, \quad \text{(A.29)}$$

therefore retarded Green's functions in the H_0-representation read as:

$$\begin{cases} G_\sigma^{(\xi,0)}(\omega) = \frac{1-\langle n_{\bar\sigma}(i)\rangle_0}{\omega+\mu+\sigma h+i\delta} \\ G_\sigma^{(\eta,0)}(\omega) = \frac{\langle n_{\bar\sigma}(i)\rangle_0}{\omega+\mu+\sigma h-U+i\delta} \end{cases} . \quad \text{(A.30)}$$

The knowledge of the retarded Green's functions allows for the calculation of the correlation functions according to the relation:

$$C(\omega) = -\left[1 + \tanh\left(\frac{\beta\omega}{2}\right)\right] Im\left[G(\omega)\right] = -\frac{2}{1+e^{-\beta\omega}} Im\left[G(\omega)\right], \quad \text{(A.31)}$$

which, at equal time, gives:

$$\begin{cases} C_\sigma^{(\xi,0)} = \left\langle \xi_\sigma(i)\xi_\sigma^\dagger(i)\right\rangle_0 = \frac{1-\langle n_{\bar\sigma}(i)\rangle_0}{1+e^{\beta(\mu+\sigma h)}} \\ C_\sigma^{(\eta,0)} = \left\langle \eta_\sigma(i)\eta_\sigma^\dagger(i)\right\rangle_0 = \frac{\langle n_{\bar\sigma}(i)\rangle_0}{1+e^{\beta(\mu+\sigma h-U)}} \end{cases} . \quad \text{(A.32)}$$

Therefore, from the following basic algebraic properties:

$$\begin{cases} \xi_\sigma(i)\xi_\sigma^\dagger(i) + \eta_\sigma\eta_\sigma^\dagger(i) = 1 - n_\sigma(i) \\ \eta_\sigma(i)\eta_\sigma^\dagger(i) = n_{\bar\sigma}(i) - n_\uparrow(i)n_\downarrow(i) \end{cases}, \quad \text{(A.33)}$$

we obtain:

$$\langle n_\uparrow(i)\rangle_0 = \frac{e^{\beta(\mu+2h)} + e^{\beta(2\mu+h-U)}}{e^{\beta h} + e^{\beta\mu} + e^{\beta(\mu+2h)} + e^{\beta(2\mu+h-U)}}, \quad \text{(A.34)}$$

$$\langle n_{\downarrow}(i)\rangle_0 = \frac{e^{\beta\mu} + e^{\beta(2\mu+h-U)}}{e^{\beta h} + e^{\beta\mu} + e^{\beta(\mu+2h)} + e^{\beta(2\mu+h-U)}} , \tag{A.35}$$

and:

$$G_1 \equiv \langle n(i)\rangle_0 = \frac{e^{\beta\mu}\left(1 + e^{2\beta h} + e^{\beta(\mu+h-U)}\right)}{e^{\beta h} + e^{\beta\mu} + e^{\beta(\mu+2h)} + e^{\beta(2\mu+h-U)}} , \tag{A.36}$$

$$G_2 \equiv \langle n_3(i)\rangle_0 = \frac{e^{\beta(\mu+2h)} - e^{\beta\mu}}{e^{\beta h} + e^{\beta\mu} + e^{\beta(\mu+2h)} + e^{\beta(2\mu+h-U)}} , \tag{A.37}$$

$$G_3 \equiv \langle D(i)\rangle_0 = \frac{e^{\beta(2\mu+h-U)}}{e^{\beta h} + e^{\beta\mu} + e^{\beta(\mu+2h)} + e^{\beta(2\mu+h-U)}} . \tag{A.38}$$

Starting from the operatorial expression of $e^{-\beta H_I(i)}$ and by means of the algebraic relations (3.9) and (3.7) one can also easily obtain:

$$\begin{aligned}
\left\langle e^{-\beta\mathcal{H}_I(i)}\right\rangle_0 &= 1 + 2aG_2X_2\left[1 + b\left(X_1 - 2X_3\right)\right] + \left(G_1 - 2G_3\right) \\
&\quad \left[a^2X_2^2 + 2b\left(X_1 - 2X_3\right) + b^2\left(X_1 - 2X_3\right)^2\right] && \text{(A.39)} \\
\left\langle n(i)e^{-\beta\mathcal{H}_I(i)}\right\rangle_0 &= G_1 + 2aG_2X_2\left[1 + b\left(X_1 - 2X_3\right)\right] + \left(G_1 - 2G_3\right) \\
&\quad \left[a^2X_2^2 + 2b\left(X_1 - 2X_3\right) + b^2\left(X_1 - 2X_3\right)^2\right] && \text{(A.40)} \\
\left\langle n(i+1)e^{-\beta\mathcal{H}_I(i)}\right\rangle_0 &= X_1 + aG_2X_2\left[1 + X_1 + 2b\left(X_1 - 2X_3\right)\right] + \left(G_1 - 2G_3\right) \\
&\quad \left[a^2X_2^2 + b\left(1 + X_1\right)\left(X_1 - 2X_3\right) + b^2\left(X_1 - 2X_3\right)^2\right] && \text{(A.41)} \\
\left\langle n_3(i)e^{-\beta\mathcal{H}_I(i)}\right\rangle_0 &= G_2 + 2a\left(G_1 - 2G_3\right)X_2\left[1 + b\left(X_1 - 2X_3\right)\right] \\
&\quad + G_2\left[a^2X_2^2 + 2b\left(X_1 - 2X_3\right) + b^2\left(X_1 - 2X_3\right)^2\right] && \text{(A.42)} \\
\left\langle n_3(i+1)e^{-\beta\mathcal{H}_I(i)}\right\rangle_0 &= X_2 + \left(G_1 - 2G_3\right)X_2\left[b + \left(a^2 + b + b^2\right)\left(X_1 - 2X_3\right)\right] \\
&\quad + aG_2\left[X_2^2\left(1 + b\right) + \left(X_1 - 2X_3\right) + b\left(X_1 - 2X_3\right)^2\right] && \text{(A.43)} \\
\left\langle D(i)e^{-\beta\mathcal{H}_I(i)}\right\rangle_0 &= G_3 && \text{(A.44)} \\
\left\langle D(i+1)e^{-\beta\mathcal{H}_I(i)}\right\rangle_0 &= X_3\left[1 + aG_2X_2 + b\left(G_1 - 2G_3\right)\left(X_1 - 2X_3\right)\right] . && \text{(A.45)}
\end{aligned}$$

Hence, putting Eqs.A.39-A.45 into the constraints (3.26) we get :

$$\begin{cases}
F_1 = & G_1 - X_1 + aG_2X_2(1 - X_1) + b(G_1 - 2G_3)(1 - X_1)(X_1 - 2X_3) = 0 \\
F_2 = & G_2 - X_2 + (G_1 - 2G_3)X_2\left\{2a - b - \left[b + (a-b)^2\right]\left(X_1 - 2X_3\right)\right\} \\
& + G_2\left\{aX_2^2(a - b - 1) + \left(X_1 - 2X_3\right)\left[2b - a + b(b-a)(X_1 - 2X_3)\right]\right\} = 0 \\
F_3 = & G_3 - X_3\left[1 + aG_2X_2 + b(G_1 - 2G_3)(X_1 - 2X_3)\right] = 0
\end{cases} , \tag{A.46}$$

which represents as a set of three self-consistent equations in terms of the parameters X_1, X_2 and X_3. We have also to consider that, once the filling n is fixed, the chemical potential μ has to be fixed according to the relation $n = \langle n(i)\rangle$. This gives a fourth self-consistent equation that, according to (A.39) and (A.40) can be written as follows:

$$\begin{aligned}
F_4 &= G_1 - n + (1-n)2aG_2X_2\left[1 + b(X_1 - 2X_3)\right] + (1-n) \\
&\quad \left(G_1 - 2G_3\right)\left[a^2X_2^2 + 2b\left(X_1 - 2X_3\right) + b^2\left(X_1 - 2X_3\right)^2\right] = 0 . && \text{(A.47)}
\end{aligned}$$

Appendix B

Detailed calculations for the two-pole approximation scheme

In this Appendix are reported some definitions and detailed calculations of useful quantities in the framework of the two-field approach to the Hubbard model illustrated in Chapter 4.

B.1 Spinorial notation and useful quantities

According to the formalism of second quantization, in order to properly define a generic fermionic operator of spin S, $\Phi^{(\dagger)}$, one has to specify both spatial and spin degrees of freedoms according with the notation $\Phi^{(\dagger)} \equiv \Phi^{(\dagger)}_{\sigma}(i)$, where $i = (\boldsymbol{i}, t)$ accounts for both position and time coordinates (the Heisenberg picture is assumed), while $-S \leqslant \sigma \leqslant S$ represents the spin index. Hence, according with this notation, the total particle density $n_{\Phi}(i)$ can be written as:

$$n_{\Phi}(i) = \sum_{\sigma=-S}^{S} \Phi^{\dagger}_{\sigma}(i)\Phi_{\sigma}(i) \, , \tag{B.1}$$

with a sum over all the possible spin states. However, it is immediate to realize that one can get immediately read of any spin index by defining the fermionic operator $\Phi^{(\dagger)}(i)$ as a vector of dimension $2S+1$, whose components are given by all the possible spin states on which the fermionic operator can act:

$$\Phi(i) \equiv \begin{pmatrix} \Phi_{\sigma_1}(i) \\ \Phi_{\sigma_1}(i) \\ \vdots \\ \Phi_{\sigma_{2S+1}}(i) \end{pmatrix} \, , \; \Phi^{\dagger}(i) \equiv \begin{pmatrix} \Phi^{\dagger}_{\sigma_1}(i) & \Phi^{\dagger}_{\sigma_1}(i) & \dots & \Phi^{\dagger}_{\sigma_{2S+1}}(i) \end{pmatrix} \, . \tag{B.2}$$

Hence, according to this notation the total particle density reads as:

$$n_\Phi(i) = \Phi^\dagger(i)\Phi(i) \ , \tag{B.3}$$

where the matrix product of rows and columns is assumed among the two spinors. In general, for two spinors $A(i)$, $B(i)$, the quantity $A^\dagger(i)B(i)$ is assumed to be a scalar, meaning that there is no dependency on any spin index. On the contrary, the quantity $A(i)B^\dagger(i)$ is a 2×2 matrix which includes all the possible combinations of spins. For example, for the trivial case with $S = 1/2$ we have:

$$A^\dagger(i)B(i) = \begin{pmatrix} A^\dagger_\uparrow(i) & A^\dagger_\downarrow(i) \end{pmatrix} \cdot \begin{pmatrix} B_\uparrow(i) \\ B_\downarrow(i) \end{pmatrix} = A^\dagger_\uparrow(i)B_\uparrow(i) + A^\dagger_\downarrow(i)B_\downarrow(i) \ , \tag{B.4}$$

$$A(i)B^\dagger(i) = \begin{pmatrix} A_\uparrow(i) \\ A_\downarrow(i) \end{pmatrix} \cdot \begin{pmatrix} B^\dagger_\uparrow(i) & B^\dagger_\downarrow(i) \end{pmatrix} = \begin{pmatrix} A_\uparrow(i)B^\dagger_\uparrow(i) & A_\uparrow(i)B^\dagger_\downarrow(i) \\ A_\downarrow(i)B^\dagger_\uparrow(i) & A_\downarrow(i)B^\dagger_\downarrow(i) \end{pmatrix} \tag{B.5}$$

We report in the following Subsections the calculation of some useful spinors.

B.1.1 Non local spinors

Starting from a generic spinor $\Phi(i)$, we define the non-local spinor of rank n as:

$$\Phi^{\alpha^n}(i) \equiv \sum_{\boldsymbol{i}_1,\ldots,\boldsymbol{i}_{n-1}} \alpha_{\boldsymbol{i}\boldsymbol{i}_1}\alpha_{\boldsymbol{i}_1\boldsymbol{i}_2}\ldots\alpha_{\boldsymbol{i}_{n-3}\boldsymbol{i}_{n-2}}\alpha_{\boldsymbol{i}_{n-2}\boldsymbol{i}_{n-1}}\Phi(\boldsymbol{i}_{n-1},t) \ , \tag{B.6}$$

where $\alpha_{\boldsymbol{ij}}$ is the operator which projects the site $\boldsymbol{j}$ on the nearest neighbour sites of $\boldsymbol{i}$:

$$\alpha_{\boldsymbol{ij}} = \begin{cases} 1/z & \text{if } |\boldsymbol{i}-\boldsymbol{j}| = |\boldsymbol{a}| \\ 0 & \text{otherwise} \end{cases} \ , \ \alpha(\boldsymbol{k}) = \frac{2}{z}\sum_{n=1}^{z/2}\cos\left(k_n a\right) \ , \tag{B.7}$$

being $\boldsymbol{a}$ the lattice vector and z the coordination number. In particular, for a d-dimensional cubic lattice $z = 2d$, therefore a generic non-local spinor of rank one can be written as:

$$\Phi^\alpha(i) \equiv \frac{1}{2d}\sum_{n=1}^{d}\left(\Phi(\boldsymbol{i}+\hat{\boldsymbol{e}}_n,t) + \Phi(\boldsymbol{i}-\hat{\boldsymbol{e}}_n,t)\right) \ , \tag{B.8}$$

where $\hat{\boldsymbol{e}}_n$ is the n^{th} primitive unitary vector of the lattice with $1 \leqslant n \leqslant d$. Non-local spinors of higher rank can be defined recursively:

$$\begin{aligned} \Phi^{\alpha^2}(i) &\equiv \frac{1}{2d}\sum_{n=1}^{d}\left(\Phi^\alpha(\boldsymbol{i}+\hat{\boldsymbol{e}}_n,t) + \Phi^\alpha(\boldsymbol{i}-\hat{\boldsymbol{e}}_n,t)\right) = \\ &= \frac{1}{(2d)^2}\sum_{n,m=1}^{d}\Big(\Phi(\boldsymbol{i}+\hat{\boldsymbol{e}}_m+\hat{\boldsymbol{e}}_n,t) + \Phi(\boldsymbol{i}+\hat{\boldsymbol{e}}_m-\hat{\boldsymbol{e}}_n,t) \\ &\quad +\Phi(\boldsymbol{i}-\hat{\boldsymbol{e}}_m+\hat{\boldsymbol{e}}_n,t) + \Phi(\boldsymbol{i}-\hat{\boldsymbol{e}}_m-\hat{\boldsymbol{e}}_n,t)\Big) \end{aligned} \tag{B.9}$$

Hence it is immediate to realize that the rank n is merely connected to the maximum distance within which an operator acts. For a one-dimensional cubic lattices we have:

$$\Phi^{\alpha}(i) = \frac{1}{2}\left(\Phi(i+a,t)+\Phi(i-a,t)\right) , \tag{B.10}$$

$$\Phi^{\alpha^2}(i) = \frac{1}{4}\left(\Phi(i+2a,t)+2\Phi(i,t)+\Phi(i-2a,t)\right) , \tag{B.11}$$

$$\vdots$$

similarly, for a two-dimensional cubic lattice we have instead:

$$\Phi^{\alpha}(i) = \frac{1}{2}\Bigg(\Phi(\boldsymbol{i}+\hat{\boldsymbol{e}}_x,t)+\Phi(\boldsymbol{i}+\hat{\boldsymbol{e}}_y,t)+\Phi(\boldsymbol{i}-\hat{\boldsymbol{e}}_x,t)+\Phi(\boldsymbol{i}-\hat{\boldsymbol{e}}_y,t)\Bigg) \tag{B.12}$$

$$\Phi^{\alpha^2}(i) = \frac{1}{4}\Bigg(\Phi(\boldsymbol{i}+2\hat{\boldsymbol{e}}_x,t)+\Phi(\boldsymbol{i},t)+\Phi(\boldsymbol{i}-2\hat{\boldsymbol{e}}_x,t) \tag{B.13}$$

$$+\Phi(\boldsymbol{i}+2\hat{\boldsymbol{e}}_y,t)+\Phi(\boldsymbol{i},t)+\Phi(\boldsymbol{i}-2\hat{\boldsymbol{e}}_y,t) \tag{B.14}$$

$$+\Phi(\boldsymbol{i}+\hat{\boldsymbol{e}}_x+\hat{\boldsymbol{e}}_y,t)+\Phi(\boldsymbol{i}+\hat{\boldsymbol{e}}_x-\hat{\boldsymbol{e}}_y,t) \tag{B.15}$$

$$+\Phi(\boldsymbol{i}-\hat{\boldsymbol{e}}_x-\hat{\boldsymbol{e}}_y,t)+\Phi(\boldsymbol{i}-\hat{\boldsymbol{e}}_x+\hat{\boldsymbol{e}}_y,t)\Bigg) , \tag{B.16}$$

$$\vdots \tag{B.17}$$

All the above relations can be more conveniently written in terms of higher order projectors. For the one-dimensional case we can introduce the second and third neighbour projectors, $\eta(k)$, $\mu(k)$, defined as:

$$\eta(k) \equiv \cos(2ka) \ , \ \mu(k) \equiv \cos(3ka) , \tag{B.18}$$

so that:

$$\alpha^2(k) = \frac{1}{2}\left[1+\eta(k)\right] , \tag{B.19}$$

$$\alpha^3(k) = \frac{1}{4}\left[3\alpha(k)+\mu(k)\right] . \tag{B.20}$$

For the two-dimensional case instead, a generic non-local operator up to rank three can be expressed in terms of the following higher-order projectors :

$$\beta(\boldsymbol{k}) \equiv \frac{1}{2}\left\{\cos\left[a\left(k_x+k_y\right)\right]+\cos\left[a\left(k_x-k_y\right)\right]\right\} , \tag{B.21}$$

$$\eta(\boldsymbol{k}) \equiv \frac{1}{2}\left[\cos\left(2ak_x\right)+\cos\left(2ak_y\right)\right] , \tag{B.22}$$

$$\lambda(\boldsymbol{k}) \equiv \frac{1}{4}\left\{\cos\left[a\left(2k_x+k_y\right)\right]+\cos\left[a\left(k_x+2k_y\right)\right]\right. \tag{B.23}$$

$$\left.+\cos\left[a\left(2k_x-k_y\right)\right]+\cos\left[a\left(k_x-2k_y\right)\right]\right\} , \tag{B.24}$$

$$\mu(\boldsymbol{k}) \equiv \frac{1}{2}\left[\cos\left(3ak_x\right)+\cos\left(3ak_y\right)\right] , \tag{B.25}$$

so that:

$$\alpha^2(\boldsymbol{k}) = \frac{1}{4}\left[1 + 2\beta(\boldsymbol{k}) + \eta(\boldsymbol{k})\right] , \tag{B.26}$$

$$\alpha^3(\boldsymbol{k}) = \frac{1}{16}\left[9\alpha(\boldsymbol{k}) + 6\lambda(\boldsymbol{k}) + \mu(\boldsymbol{k})\right] . \tag{B.27}$$

B.1.2 Spinor $\sigma^\mu n_\mu(i)$

Let us calculate the spinor $\sigma^\mu n_\mu(i)$. We recall that the sum over all the possible values of μ is assumed, so that:

$$\sigma^\mu n_\mu(i) \equiv \sum_{\mu=0}^{3} \sigma^\mu n_\mu(i) \quad , \tag{B.28}$$

where σ_μ is a 4-component vector composed by the 2×2 identity matrix σ_0 and the three Pauli matrices $\boldsymbol{\sigma} \equiv (\sigma_1, \sigma_2, \sigma_3)$:

$$\sigma_\mu \equiv (\sigma_0, \boldsymbol{\sigma}) \quad , \quad \sigma^\mu \equiv (-\sigma_0, \boldsymbol{\sigma}) \quad . \tag{B.29}$$

The bosonic operator $n_\mu(i)$ is defined as follow:

$$n_\mu(i) \equiv c^\dagger(i)\sigma_\mu c(i) \quad , \tag{B.30}$$

therefore, recalling the expressions of the three Pauli matrices:

$$\sigma_1 \equiv \begin{pmatrix} 0 & 1 \\ 1 & 0 \end{pmatrix} , \ \sigma_2 \equiv \begin{pmatrix} 0 & -i \\ i & 0 \end{pmatrix} , \ \sigma_3 \equiv \begin{pmatrix} 1 & 0 \\ 0 & -1 \end{pmatrix} , \tag{B.31}$$

we immediately obtain:

$$n_0(i) = c^\dagger(i)\sigma_0 c(i) = \begin{pmatrix} c_\uparrow^\dagger(i) & c_\downarrow^\dagger(i) \end{pmatrix} \begin{pmatrix} 1 & 0 \\ 0 & 1 \end{pmatrix} \begin{pmatrix} c_\uparrow(i) \\ c_\downarrow(i) \end{pmatrix} = \tag{B.32}$$

$$= \begin{pmatrix} c_\uparrow^\dagger(i) & c_\downarrow^\dagger(i) \end{pmatrix} \begin{pmatrix} c_\uparrow(i) \\ c_\downarrow(i) \end{pmatrix} = c_\uparrow^\dagger(i)c_\uparrow(i) + c_\downarrow^\dagger(i)c_\downarrow(i) , \tag{B.33}$$

$$n_1(i) = c^\dagger(i)\sigma_1 c(i) = \begin{pmatrix} c_\uparrow^\dagger(i) & c_\downarrow^\dagger(i) \end{pmatrix} \begin{pmatrix} 0 & 1 \\ 1 & 0 \end{pmatrix} \begin{pmatrix} c_\uparrow(i) \\ c_\downarrow(i) \end{pmatrix} = \tag{B.34}$$

$$= \begin{pmatrix} c_\uparrow^\dagger(i) & c_\downarrow^\dagger(i) \end{pmatrix} \begin{pmatrix} c_\downarrow(i) \\ c_\uparrow(i) \end{pmatrix} = c_\uparrow^\dagger(i)c_\downarrow(i) + c_\downarrow^\dagger(i)c_\uparrow(i) , \tag{B.35}$$

$$n_2(i) = c^\dagger(i)\sigma_2 c(i) = \begin{pmatrix} c_\uparrow^\dagger(i) & c_\downarrow^\dagger(i) \end{pmatrix} \begin{pmatrix} 0 & -i \\ i & 0 \end{pmatrix} \begin{pmatrix} c_\uparrow(i) \\ c_\downarrow(i) \end{pmatrix} = \tag{B.36}$$

$$= \begin{pmatrix} c_\uparrow^\dagger(i) & c_\downarrow^\dagger(i) \end{pmatrix} \begin{pmatrix} c_\uparrow(i) \\ c_\downarrow(i) \end{pmatrix} = -ic_\uparrow^\dagger(i)c_\downarrow(i) + ic_\downarrow^\dagger(i)c_\uparrow(i) , \tag{B.37}$$

$$n_3(i) = c^\dagger(i)\sigma_3 c(i) = \left(c_\uparrow^\dagger(i) \quad c_\downarrow^\dagger(i)\right)\left(\begin{array}{cc} 1 & 0 \\ 0 & -1 \end{array}\right)\left(\begin{array}{c} c_\uparrow(i) \\ c_\downarrow(i) \end{array}\right) = \tag{B.38}$$

$$= \left(c_\uparrow^\dagger(i) \quad c_\downarrow^\dagger(i)\right)\left(\begin{array}{c} c_\uparrow(i) \\ c_\downarrow(i) \end{array}\right) = c_\uparrow^\dagger(i)c_\uparrow(i) - c_\downarrow^\dagger(i)c_\downarrow(i) \tag{B.39}$$

which give:

$$\sigma^\mu n_\mu(i) = \left(\begin{array}{cc} -1 & 0 \\ 0 & -1 \end{array}\right)\left[c_\uparrow^\dagger(i)c_\uparrow(i) + c_\downarrow^\dagger(i)c_\downarrow(i)\right] \tag{B.40}$$

$$+\left(\begin{array}{cc} 0 & 1 \\ 1 & 0 \end{array}\right)\left[c_\uparrow^\dagger(i)c_\downarrow(i) + c_\downarrow^\dagger(i)c_\uparrow(i)\right] \tag{B.41}$$

$$+\left(\begin{array}{cc} 0 & -i \\ i & 0 \end{array}\right)\left[-ic_\uparrow^\dagger(i)c_\downarrow(i) + ic_\downarrow^\dagger(i)c_\uparrow(i)\right] \tag{B.42}$$

$$+\left(\begin{array}{cc} 1 & 0 \\ 0 & -1 \end{array}\right)\left[c_\uparrow^\dagger(i)c_\uparrow(i) - c_\downarrow^\dagger(i)c_\downarrow(i)\right] . \tag{B.43}$$

Hence, adding together all the contributions we obtain:

$$\sigma^\mu n_\mu(i) = 2\left(\begin{array}{cc} -n_\downarrow(i) & c_\downarrow^\dagger(i)c_\uparrow(i) \\ c_\uparrow^\dagger(i)c_\downarrow(i) & -n_\uparrow(i) \end{array}\right) . \tag{B.44}$$

B.2 Basic anticommutation rules

Starting from the canonical anticommutation rules among fermionic operators:

$$\begin{cases} \{c_\sigma(i), c_{\sigma'}(j)\} = \left\{c_\sigma^\dagger(i), c_{\sigma'}^\dagger(j)\right\} = 0 \\ \left\{c_\sigma(i), c_{\sigma'}^\dagger(j)\right\} = \left\{c_\sigma^\dagger(i), c_{\sigma'}(j)\right\} = \delta_{ij}\delta_{\sigma\sigma'} \end{cases} , \tag{B.45}$$

we derive in this Section the basic anticommutation rules for the composite fields $\xi(i)$ and $\eta(i)$. To this purpose, we recall the following anticommutation rules:

$$\begin{aligned} \{b_1 f_1, b_2 f_2\} &= b_1 f_1 b_2 f_2 + b_2 f_2 b_1 f_1 = \\ &= b_1 f_1 b_2 f_2 - b_1 b_2 f_1 f_2 + b_1 b_2 f_1 f_2 + b_2 f_2 b_1 f_1 - b_2 b_1 f_2 f_1 + b_2 b_1 f_2 f_1 = \\ &= b_1 [f_1, b_2] f_2 + b_1 b_2 f_1 f_2 + b_2 [f_2, b_1] f_1 + b_2 b_1 f_2 f_1 = \\ &= b_1 [f_1, b_2] f_2 + b_2 [f_2, b_1] f_1 + b_1 b_2 f_1 f_2 - b_2 b_1 f_1 f_2 + b_2 b_1 f_1 f_2 + b_2 b_1 f_2 f_1 = \\ &= b_1 [f_1, b_2] f_2 + b_2 [f_2, b_1] f_1 + [b_1, b_2] f_1 f_2 + b_2 b_1 \{f_2, f_1\} \quad , \end{aligned} \tag{B.46}$$

$$\begin{aligned} \{b_1 f_1, f_2 b_2\} &= b_1 f_1 f_2 b_2 + f_2 b_2 b_1 f_1 = \\ &= b_1 (f_1 f_2 + f_2 f_1) b_2 - b_1 f_2 f_1 b_2 + f_2 b_2 b_1 f_1 = \\ &= b_1 \{f_1, f_2\} b_2 - (b_1 f_2 - f_2 b_1) f_1 b_2 - f_2 b_1 f_1 b_2 + f_2 b_2 b_1 f_1 = \\ &= b_1 \{f_1, f_2\} b_2 - [b_1, f_2] f_1 b_2 - f_2 b_1 (f_1 b_2 - b_2 f_1) - f_2 b_1 b_2 f_1 + f_2 b_2 b_1 f_1 = \\ &= b_1 \{f_1, f_2\} b_2 - [b_1, f_2] f_1 b_2 - f_2 b_1 [f_1, b_2] + f_2 [b_2, b_1] f_1 \quad , \end{aligned} \tag{B.47}$$

$\{A(i), B(j)\}$	$\xi(i)$	$\xi^\dagger(i)$	$\eta(i)$	$\eta^\dagger(i)$
$\xi(j)$	0	$\delta_{ij}\left(1+\frac{1}{2}\sigma^\mu n_\mu(i)\right)$	$c(i)c(i)$	0
$\xi^\dagger(j)$	$\delta_{ij}\left(1+\frac{1}{2}\left(\sigma^\mu\right)^T n_\mu(i)\right)$	0	0	$-c^\dagger(i)c^\dagger(i)$
$\eta(j)$	$-c(i)c(i)$	0	0	$-\frac{1}{2}\delta_{ij}\sigma^\mu n_\mu(i)$
$\eta^\dagger(j)$	0	$c^\dagger(i)c^\dagger(i)$	$-\frac{1}{2}\delta_{ij}\left(\sigma^\mu\right)^T n_\mu(i)$	0

Table B.1: Anticommutation rules among composite fields in spinorial notation.

$$\begin{aligned}\{f_1b_1, b_2f_2\} &= f_1b_1b_2f_2 + b_2f_2f_1b_1 = \\ &= f_1\left[b_1, b_2\right]f_2 + f_1b_2b_1f_2 + b_2f_2f_1b_1 = \\ &= f_1\left[b_1, b_2\right]f_2 + \left[f_1, b_2\right]b_1f_2 + b_2f_1b_1f_2 + b_2f_2f_1b_1 = \\ &= f_1\left[b_1, b_2\right]f_2 + \left[f_1, b_2\right]b_1f_2 + b_2f_1\left[b_1, f_2\right] + b_2f_1f_2b_1 + b_2f_2f_1b_1 = \\ &= f_1\left[b_1, b_2\right]f_2 + \left[f_1, b_2\right]b_1f_2 + b_2f_1\left[b_1, f_2\right] + b_2\left\{f_1, f_2\right\}b_1 \quad ,\end{aligned} \tag{B.48}$$

$$\begin{aligned}\{f_1b_1, f_2b_2\} &= f_1b_1f_2b_2 + f_2b_2f_1b_1 = \\ &= f_1\left[b_1, f_2\right]b_2 + f_1f_2b_1b_2 + f_2b_2f_1b_1 = \\ &= f_1\left[b_1, f_2\right]b_2 + \left\{f_1, f_2\right\}b_1b_2 - f_2f_1b_1b_2 + f_2b_2f_1b_1 = \\ &= f_1\left[b_1, f_2\right]b_2 + \left\{f_1, f_2\right\}b_1b_2 - f_2f_1\left[b_1, b_2\right] - f_2f_1b_2b_1 + f_2b_2f_1b_1 = \\ &= f_1\left[b_1, f_2\right]b_2 + \left\{f_1, f_2\right\}b_1b_2 - f_2f_1\left[b_1, b_2\right] - f_2\left[f_1, b_2\right]b_1 - \cancel{f_2b_2f_1b_1} + \cancel{f_2b_2f_1b_1} = \\ &= f_1\left[b_1, f_2\right]b_2 + \left\{f_1, f_2\right\}b_1b_2 - f_2f_1\left[b_1, b_2\right] - f_2\left[f_1, b_2\right]b_1 \quad .\end{aligned} \tag{B.49}$$

which give:

$$\left\{b_1f_1, b_2f_2\right\} = b_1\left[f_1, b_2\right]f_2 + b_2\left[f_2, b_1\right]f_1 + \left[b_1, b_2\right]f_1f_2 + b_2b_1\left\{f_2, f_1\right\} \quad , \tag{B.50}$$

$$\left\{b_1f_1, f_2b_2\right\} = b_1\left\{f_1, f_2\right\}b_2 - \left[b_1, f_2\right]f_1b_2 - f_2b_1\left[f_1, b_2\right] + f_2\left[b_2, b_1\right]f_1 \quad , \tag{B.51}$$

$$\left\{f_1b_1, b_2f_2\right\} = f_1\left[b_1, b_2\right]f_2 + \left[f_1, b_2\right]b_1f_2 + b_2f_1\left[b_1, f_2\right] + b_2\left\{f_1, f_2\right\}b_1 \quad , \tag{B.52}$$

$$\left\{f_1b_1, f_2b_2\right\} = f_1\left[b_1, f_2\right]b_2 + \left\{f_1, f_2\right\}b_1b_2 - f_2f_1\left[b_1, b_2\right] - f_2\left[f_1, b_2\right]b_1 \quad . \tag{B.53}$$

All anticommutation rules are summarized in Tab.B.1.

Calculation of $\{\xi_\sigma(i), \xi_{\sigma'}(j)\}$. The anticommutator $\{\xi_\sigma(i), \xi_{\sigma'}(j)\}$ can be written as follow:

$$\left\{\xi_\sigma(i), \xi_{\sigma'}(j)\right\} = \left\{(1-n_{\bar{\sigma}}(i))c_\sigma(i), (1-n_{\bar{\sigma'}}(j))c_{\sigma'}(j)\right\} \quad . \tag{B.54}$$

This is of the type $\{b_1 f_1, b_2 f_2\}$ so, from (B.50) we have:

$$\begin{aligned}
\{\xi_\sigma(i), \xi_{\sigma'}(j)\} &= (1-n_{\bar\sigma}(i))\,[c_\sigma(i), 1-n_{\bar\sigma'}(j)]\,c_{\sigma'}(j) + (1-n_{\bar\sigma'}(j))\,[c_{\sigma'}(j), 1-n_{\bar\sigma}(i)]\,c_\sigma(i) \\
&\quad + \cancel{[1-n_{\bar\sigma}(i), 1-n_{\bar\sigma'}(j)]\,c_\sigma(i)c_{\sigma'}(j)} + \cancel{(1-n_{\bar\sigma'}(j))(1-n_{\bar\sigma}(i))\,\{c_{\sigma'}(j), c_\sigma(i)\}} = \\
&= -\cancel{(1-n_{\bar\sigma}(i))\,[c_\sigma(i), n_{\bar\sigma'}(j)]\,c_{\sigma'}(j)} - \cancel{(1-n_{\bar\sigma'}(j))\,[c_{\sigma'}(j), n_{\bar\sigma}(i)]\,c_\sigma(i)} = \\
&= -\delta_{ij}\delta_{\sigma\bar\sigma'}\Big[(1-n_{\bar\sigma}(i))c_\sigma(i)c_{\bar\sigma}(i) + (1-n_\sigma(i))c_{\bar\sigma}(i)c_\sigma(i)\Big] = \\
&= -\delta_{ij}\delta_{\sigma\bar\sigma'}\Big[c_\sigma(i)c_{\bar\sigma}(i) - \cancel{n_{\bar\sigma}(i)c_{\bar\sigma}(i)c_{\bar\sigma}(i)} + c_{\bar\sigma}(i)c_\sigma(i) - \cancel{n_\sigma(i)c_{\bar\sigma}(i)c_\sigma(i)}\Big] = \\
&= -\delta_{ij}\delta_{\sigma\bar\sigma'}\Big[c_\sigma(i)c_{\bar\sigma}(i) + c_{\bar\sigma}(i)c_\sigma(i)\Big] = \\
&= -\delta_{ij}\delta_{\sigma\bar\sigma'}\Big[c_\sigma(i)c_{\bar\sigma}(i) - c_\sigma(i)c_{\bar\sigma}(i)\Big] = 0 \quad ,
\end{aligned} \tag{B.55}$$

therefore in spinorial notation we immediately obtain:

$$\{\xi(i), \xi(j)\} = 0 \quad , \tag{B.56}$$

Calculation of $\{\xi_\sigma(i), \xi^\dagger_{\sigma'}(j)\}$. The anticommutator $\Big\{\xi_\sigma(i), \xi^\dagger_{\sigma'}(j)\Big\}$ can be written as follow:

$$\Big\{\xi_\sigma(i), \xi^\dagger_{\sigma'}(j)\Big\} = \Big\{(1-n_{\bar\sigma}(i))c_\sigma(i), c^\dagger_{\sigma'}(j)(1-n_{\bar\sigma'}(j))\Big\} \quad . \tag{B.57}$$

This is of the type $\{b_1 f_1, f_2 b_2\}$ so, from (B.51) we have:

$$\begin{aligned}
\Big\{\xi_\sigma(i), \xi^\dagger_{\sigma'}(j)\Big\} &= (1-n_{\bar\sigma}(i))\,\Big\{c_\sigma(i), c^\dagger_{\sigma'}(j)\Big\}\,(1-n_{\bar\sigma'}(j)) \\
&\quad - \Big[1-n_{\bar\sigma}(i), c^\dagger_{\sigma'}(j)\Big]\,c_\sigma(i)(1-n_{\bar\sigma'}(j)) \\
&\quad - c^\dagger_{\sigma'}(j)(1-n_{\bar\sigma}(i))\,[c_\sigma(i), 1-n_{\bar\sigma'}(j)] \\
&\quad + \cancel{c^\dagger_{\sigma'}(j)\,[1-n_{\bar\sigma'}(j), 1-n_{\bar\sigma}(i)]\,c_\sigma(i)} = \\
&= \cancel{\delta_{ij}\delta_{\sigma\sigma'}\,[1-n_{\bar\sigma}(i)]^2} \\
&\quad + \delta_{ij}\delta_{\bar\sigma\sigma'}\Big[c^\dagger_{\bar\sigma}(i)c_\sigma(i)(1-n_\sigma(i)) + c^\dagger_{\bar\sigma}(i)(1-\cancel{n_{\bar\sigma}(i)})c_\sigma(i)\Big] = \\
&= \delta_{ij}\delta_{\sigma\sigma'}\,[1-n_{\bar\sigma}(i)] + \\
&\quad + \delta_{ij}\delta_{\sigma\bar\sigma'}\Big[c^\dagger_{\bar\sigma}(i)c_\sigma(i) - c^\dagger_{\bar\sigma}(i)c_\sigma(i)n_\sigma(i) + c^\dagger_{\bar\sigma}(i)c_\sigma(i)\Big] = \\
&= \delta_{ij}\delta_{\sigma\sigma'}\,[1-n_{\bar\sigma}(i)] \\
&\quad + \delta_{ij}\delta_{\sigma\bar\sigma'}\Big[2c^\dagger_{\bar\sigma}(i)c_\sigma(i) - c^\dagger_{\bar\sigma}(i)\,(c_\sigma(i) + \cancel{n_\sigma(i)c_\sigma(i)})\Big] = \\
&= \delta_{ij}\delta_{\sigma\sigma'}\,[1-n_{\bar\sigma}(i)] \\
&\quad + \delta_{ij}\delta_{\sigma\bar\sigma'}\Big[2c^\dagger_{\bar\sigma}(i)c_\sigma(i) - \cancel{c^\dagger_{\bar\sigma}(i)c_\sigma(i)}\Big] = \\
&= \delta_{ij}\delta_{\sigma\sigma'}\,[1-n_{\bar\sigma}(i)] + \delta_{ij}\delta_{\sigma\bar\sigma'}c^\dagger_{\bar\sigma}(i)c_\sigma(i) \quad .
\end{aligned} \tag{B.58}$$

Hence we obtain:

$$\left\{\xi_\sigma(i),\xi^\dagger_{\sigma'}(j)\right\} = \delta_{ij}\delta_{\sigma\sigma'}\left[1-n_{\bar\sigma}(i)\right] + \delta_{ij}\delta_{\sigma\bar\sigma'}c^\dagger_{\bar\sigma}(i)c_\sigma(i) \quad , \tag{B.59}$$

which can be written in terms of the composite field $n_\mu(i)$ (see Appendix B.1.2) as:

$$\begin{aligned}\left\{\xi_\sigma(i),\xi^\dagger_{\sigma'}(j)\right\}_{\sigma\sigma'} &= 1+\frac{1}{2}\left[\sigma^\mu n_\mu\right]_{\sigma\sigma'} \\ \left\{\xi_\sigma(i),\xi^\dagger_{\sigma'}(j)\right\}_{\sigma\bar\sigma'} &= \frac{1}{2}\left[\sigma^\mu n_\mu\right]_{\sigma\bar\sigma'}\end{aligned} \quad . \tag{B.60}$$

The above relation allows us to write the anticommutator $\left\{\xi(i),\xi^\dagger(j)\right\}$ in the following spinorial form:

$$\left\{\xi(i),\xi^\dagger(j)\right\} = \delta_{ij}\left[1+\frac{1}{2}\sigma^\mu n_\mu(i)\right] \quad . \tag{B.61}$$

Calculation of $\{\eta_\sigma(i),\eta_{\sigma'}(j)\}$. The anticommutator $\{\eta_\sigma(i),\eta_{\sigma'}(j)\}$ can be written as follow:

$$\{\eta_\sigma(i),\eta_{\sigma'}(j)\} = \{n_{\bar\sigma}(i)c_\sigma(i), n_{\bar\sigma'}(j)c_{\sigma'}(j)\} \quad . \tag{B.62}$$

This is of the type $\{b_1f_1,b_2f_2\}$ so, from (B.50) we obtain:

$$\begin{aligned}\{\eta_\sigma(i),\eta_{\sigma'}(j)\} &= n_{\bar\sigma}(i)\left[c_\sigma(i),n_{\bar\sigma'}(j)\right]c_{\sigma'}(j) + n_{\bar\sigma'}(j)\left[c_{\sigma'}(j),n_{\bar\sigma}(i)\right]c_\sigma(i) + \\ &\quad + \cancel{\left[n_{\bar\sigma}(i),n_{\bar\sigma'}(j)\right]c_\sigma(i)c_{\sigma'}(j)} + \cancel{n_{\bar\sigma'}(j)n_{\bar\sigma}(i)\left\{c_{\sigma'}(j),c_\sigma(i)\right\}} = \\ &= \cancel{\delta_{ij}\delta_{\sigma\bar\sigma'}}\left[n_{\bar\sigma}(i)c_\sigma(i)c_{\bar\sigma}(i) + n_\sigma(i)c_{\bar\sigma}(i)c_\sigma(i)\right] = \\ &= -\delta_{ij}\delta_{\sigma\bar\sigma'}\left[\cancel{n_{\bar\sigma}(i)c_{\bar\sigma}(i)c_\sigma(i)} + \cancel{n_\sigma(i)c_{\bar\sigma}(i)c_{\bar\sigma}(i)}\right] = 0 \quad .\end{aligned} \tag{B.63}$$

therefore in spinorial notation we immediately obtain:

$$\{\eta(i),\eta(j)\} = 0\,. \tag{B.64}$$

Calculation of $\{\eta^\dagger_\sigma(i),\eta_{\sigma'}(j)\}$. The anticommutator $\left\{\eta^\dagger_\sigma(i),\eta_{\sigma'}(j)\right\}$ can be written as follow:

$$\left\{\eta^\dagger_\sigma(i),\eta_{\sigma'}(j)\right\} = \left\{c^\dagger_\sigma(i)n_{\bar\sigma}(i), n_{\bar\sigma'}(j)c_{\sigma'}(j)\right\} \quad . \tag{B.65}$$

This is of the type $\{f_1b_1,b_2f_2\}$ so, from (B.52) we have:

$$\begin{aligned}\left\{\eta^\dagger_\sigma(i),\eta_{\sigma'}(j)\right\} &= n_{\bar\sigma'}(i)\left\{c^\dagger_\sigma(i),c_{\sigma'}(j)\right\}n_{\bar\sigma}(j) + \left[c^\dagger_\sigma(i),n_{\bar\sigma'}(j)\right]n_{\bar\sigma}(i)c_{\sigma'}(j) + \\ &\quad + n_{\bar\sigma'}(j)c^\dagger_\sigma(i)\left[n_{\bar\sigma}(i),c_{\sigma'}(j)\right] + \cancel{c^\dagger_\sigma(i)\left[n_{\bar\sigma}(i),n_{\bar\sigma'}(j)\right]c_{\sigma'}(j)} = \\ &= -\delta_{ij}\delta_{\sigma\bar\sigma'}\left[\cancel{c^\dagger_{\bar\sigma}(i)n_{\bar\sigma}(i)c_{\bar\sigma}(j)} + n_\sigma(i)c^\dagger_\sigma(i)c_{\bar\sigma}(i)\right] + \delta_{ij}\delta_{\sigma\sigma'}n_{\bar\sigma}(i) = \\ &= \delta_{ij}\delta_{\sigma\sigma'}n_{\bar\sigma}(i) - \delta_{ij}\delta_{\sigma\bar\sigma'}n_\sigma(i)c^\dagger_\sigma(i)c_{\bar\sigma}(i)\,.\end{aligned} \tag{B.66}$$

Hence we obtain:

$$\left\{\eta^\dagger_\sigma(i),\eta_{\sigma'}(j)\right\} = \delta_{ij}\delta_{\sigma\sigma'}n_{\bar\sigma}(i) - \delta_{ij}\delta_{\sigma\bar\sigma'}c^\dagger_{\bar\sigma}(i)c_\sigma(i) \quad , \tag{B.67}$$

which can be written in terms of the composite field $n_\mu(i)$ (see Appendix B.1.2) as:

$$\begin{aligned} \left\{\eta^\dagger_\sigma(i), \eta_{\sigma'}(j)\right\}_{\sigma\sigma'} &= -\frac{1}{2}\left[\sigma^\mu n_\mu\right]_{\sigma\sigma'} \\ \left\{\eta^\dagger_\sigma(i), \eta_{\sigma'}(j)\right\}_{\sigma\bar{\sigma}'} &= -\frac{1}{2}\left[\sigma^\mu n_\mu\right]_{\sigma\bar{\sigma}'} \end{aligned} \quad , \tag{B.68}$$

The above relation allows us to write the anticommutator $\left\{\eta^\dagger_\sigma(i), \eta_{\sigma'}(j)\right\}$ in the following spinorial form:

$$\left\{\eta^\dagger(i), \eta(j)\right\} = -\frac{1}{2}\delta_{ij}\sigma^\mu n_\mu(i) \quad . \tag{B.69}$$

Calculation of $\{\xi_\sigma(i), \eta_{\sigma'}(j)\}$. The anticommutator $\{\xi_\sigma(i), \eta_{\sigma'}(j)\}$ can be written as follow:

$$\{\xi_\sigma(i), \eta_{\sigma'}(j)\} = \{n_{\bar{\sigma}}(i)c_\sigma(i), (1 - n_{\bar{\sigma}'}(j))\, c_{\sigma'}(j)\} \quad . \tag{B.70}$$

This is of the type $\{b_1 f_1, b_2 f_2\}$ so, from (B.50) we have:

$$\begin{aligned} \{\xi_\sigma(i), \eta_{\sigma'}(j)\} &= n_{\bar{\sigma}}(i)\left[c_\sigma(i), (1 - n_{\bar{\sigma}'}(j))\right] c_{\sigma'}(j) + (1 - n_{\bar{\sigma}'}(j))\left[c_{\sigma'}(j), n_{\bar{\sigma}}(i)\right] c_\sigma(i) + \\ &\quad + \cancel{\left[n_{\bar{\sigma}}(i), (1 - n_{\bar{\sigma}'}(j))\right] c_\sigma(i)c_{\sigma'}(j)} + \cancel{(1 - n_{\bar{\sigma}'}(j))\, n_{\bar{\sigma}}(i)\left\{c_{\sigma'}(j), c_\sigma(i)\right\}} = \\ &= -\cancel{n_{\bar{\sigma}}(i)\left[c_\sigma(i), n_{\bar{\sigma}'}(j)\right] c_{\sigma'}(j)} + (1 - n_{\bar{\sigma}'}(j))\left[c_{\sigma'}(j), n_{\bar{\sigma}}(i)\right] c_\sigma(i) = \\ &= -\cancel{\delta_{ij}\delta_{\sigma\bar{\sigma}'} n_{\bar{\sigma}}(i)c_\sigma(i)c_{\bar{\sigma}}(i)} + \delta_{ij}\delta_{\sigma'\bar{\sigma}}\left(1 - n_\sigma(i)\right) c_{\bar{\sigma}}(i)c_\sigma(i) = \\ &= \delta_{ij}\delta_{\sigma\bar{\sigma}'}\left[\cancel{n_{\bar{\sigma}}(i)c_{\bar{\sigma}}(i)c_\sigma(i)} + c_{\bar{\sigma}}(i)c_\sigma(i) - \cancel{n_\sigma(i)c_{\bar{\sigma}}(i)c_\sigma(i)}\right] = \\ &= \delta_{ij}\delta_{\sigma\bar{\sigma}'} c_{\bar{\sigma}}(i)c_\sigma(i) \quad . \end{aligned} \tag{B.71}$$

The above relation allows us to write $\{\xi_\sigma(i), \eta_{\sigma'}(j)\}$ in the following spinorial form:

$$\{\xi(i), \eta(j)\} = c(i)c(i) \; . \tag{B.72}$$

Calculation of $\{\xi^\dagger_\sigma(i), \eta_{\sigma'}(j)\}$. The anticommutator $\{\xi^\dagger_\sigma(i), \eta_{\sigma'}(j)\}$ can be written as follow:

$$\left\{\xi^\dagger_\sigma(i), \eta_{\sigma'}(j)\right\} = \left\{c^\dagger_\sigma(i)\left(1 - n_{\bar{\sigma}}(i)\right), n_{\bar{\sigma}'}(j)c_{\sigma'}(j)\right\} \quad . \tag{B.73}$$

This is of the type $\{f_1 b_1, b_2 f_2\}$ so, from (B.52) we have:

$$\begin{aligned}\left\{\xi^\dagger_\sigma(i), \eta_{\sigma'}(j)\right\} &= \cancel{c^\dagger_\sigma(i)\left[(1-n_{\bar\sigma}(i)), n_{\bar\sigma'}(j)\right] c_{\sigma'}(j)} + \\ &+ \left[c^\dagger_\sigma(i), n_{\bar\sigma'}(j)\right](1-n_{\bar\sigma}(i))\, c_{\sigma'}(j) + n_{\bar\sigma'}(j) c^\dagger_\sigma(i)\left[(1-n_{\bar\sigma}(i)), c_{\sigma'}(j)\right] + \\ &+ n_{\bar\sigma'}(j)\left\{c^\dagger_\sigma(i), c_{\sigma'}(j)\right\}(1-n_{\bar\sigma}(i)) = \\ &= \delta_{ij}\delta_{\sigma\bar\sigma'}\left[-c^\dagger_\sigma(i)\left(1-\cancel{n_{\bar\sigma}(i)}\right) c_{\bar\sigma}(i) + n_\sigma(i) c^\dagger_\sigma(i) c_{\bar\sigma}(i)\right] + \\ &+ \cancel{\delta_{ij}\delta_{\sigma\sigma'} n_{\bar\sigma}(1-n_{\bar\sigma}(i))} = \\ &= \delta_{ij}\delta_{\sigma\bar\sigma'}\left[-c^\dagger_\sigma(i) c_{\bar\sigma}(i) + \left(c^\dagger_\sigma(i) + \cancel{c^\dagger_\sigma(i) n_\sigma(i)}\right) c_{\bar\sigma}(i)\right] = \\ &= \delta_{ij}\delta_{\sigma\bar\sigma'}\left[c^\dagger_\sigma(i) c_{\bar\sigma}(i) - c^\dagger_\sigma(i) c_{\bar\sigma}(i)\right] = 0\ .\end{aligned} \tag{B.74}$$

The above relation allows us to write $\left\{\xi^\dagger_\sigma(i), \eta_{\sigma'}(j)\right\}$ in the following spinorial form:

$$\left\{\xi^\dagger(i), \eta(j)\right\} = 0\ . \tag{B.75}$$

Calculation of $\{\xi_\sigma(i), \eta^\dagger_{\sigma'}(j)\}$. In order to calculate the anticommutator $\left\{\xi_\sigma(i), \eta^\dagger_{\sigma'}(j)\right\}$ it is useful to note that:

$$\begin{aligned}\left\{\xi^\dagger_\sigma(i), \eta_{\sigma'}(j)\right\}^\dagger &= \left[\xi^\dagger_\sigma(i)\eta_{\sigma'}(j) + \eta_{\sigma'}(j)\xi^\dagger_\sigma(i)\right]^\dagger = \left[\eta^\dagger_{\sigma'}(j)\xi_\sigma(i) + \xi_\sigma(i)\eta^\dagger_{\sigma'}(j)\right] = \\ &= \left\{\xi_\sigma(i), \eta^\dagger_{\sigma'}(j)\right\}\quad .\end{aligned} \tag{B.76}$$

Then from Eq.B.75 we immediately have:

$$\left\{\xi(i), \eta^\dagger(j)\right\} = 0\ . \tag{B.77}$$

Calculation of $\{\xi^\dagger_\sigma(i), \eta^\dagger_{\sigma'}(j)\}$. In order to calculate the anticommutator $\left\{\xi^\dagger_\sigma(i), \eta^\dagger_{\sigma'}(j)\right\}$ it is useful to note that:

$$\begin{aligned}\left\{\xi_\sigma(i), \eta_{\sigma'}(j)\right\}^\dagger &= \left[\xi_\sigma(i)\eta_{\sigma'}(j) + \eta_{\sigma'}(j)\xi_\sigma(i)\right]^\dagger = \left[\eta^\dagger_{\sigma'}(j)\xi^\dagger_\sigma(i) + \xi^\dagger_\sigma(i)\eta^\dagger_{\sigma'}(j)\right] = \\ &= \left\{\xi^\dagger_\sigma(i), \eta^\dagger_{\sigma'}(j)\right\}\quad .\end{aligned} \tag{B.78}$$

Then from Eq.B.72 we immediately have:

$$\left\{\xi^\dagger(i), \eta^\dagger(j)\right\} = -\delta_{ij} c^\dagger(i) c^\dagger(i)\quad . \tag{B.79}$$

B.3 Equations of motion for composite operators

In this Section we derive the equations of motion for the canonical fermionic $c(i)/c^\dagger(i)$ and bosonic $n(i)$ operators and then for the composite fields $\xi(i)$, $\eta(i)$ and $n_\mu(i)$.

We recall that for a generic field $\Phi(i)$ we have:

$$i\partial_t \psi \Phi(i) = [\Phi(i), H] \ . \tag{B.80}$$

where H represents the model Hamiltonian under investigation. We restrict our analysis to the Hubbard Hamiltonian:

$$H = \sum_{i,j} \left(t_{ij} - \mu\delta_{ij}\right) c^\dagger(i)c(j) + U \sum_i n_\uparrow(i) n_\downarrow(i) \ , \tag{B.81}$$

where, here and after, the spinorial notation is assumed for each fermionic operator.

B.3.1 Equation of motion for $c(i)$

To obtain the equation of motion for the annihilator operator let us calculate the commutation relation between the σ' component of spinor $c(i)$ and the Hubbard operator:

$$\begin{aligned} i\partial_t c_{\sigma'}(i) &= [c_{\sigma'}(i), H] = \\ &= \sum_{lm,\sigma} \left(t_{lm} - \mu\delta_{lm}\right) \left[c_{\sigma'}(i), c^\dagger_\sigma(l)c_\sigma(m)\right] + \frac{U}{2} \sum_{l,\sigma} \left[c_{\sigma'}(i), n_\sigma(l) n_{\bar\sigma}(l)\right] \ . \end{aligned} \tag{B.82}$$

The first commutator can be evaluated by using the following relation:

$$\begin{aligned} [f_1, f_2 f_3] &= f_1 f_2 f_3 - f_2 f_3 f_1 = f_1 f_2 f_3 + f_2 f_1 f_3 - f_2 f_1 f_3 - f_2 f_3 f_1 = \\ &= \{f_1, f_2\} f_3 - f_2 \{f_1, f_3\} \ , \end{aligned} \tag{B.83}$$

so:

$$\begin{aligned} \left[c_{\sigma'}(i), c^\dagger_\sigma(l)c_\sigma(m)\right] &= \left\{c_{\sigma'}(i), c^\dagger_\sigma(l)\right\} c_\sigma(m) - \cancel{c^\dagger_\sigma(l) \left\{c_{\sigma'}(i), c_\sigma(m)\right\}} = \\ &= \delta_{il}\delta_{\sigma\sigma'} c_{\sigma'}(i) \ . \end{aligned} \tag{B.84}$$

For the second commutator we have:

$$\begin{aligned} \left[c_{\sigma'}(i), n_\sigma(l) n_{\bar\sigma}(l)\right] &= n_\sigma(l) \left[c_{\sigma'}(i), n_{\bar\sigma}(l)\right] + \left[c_{\sigma'}(i), n_\sigma(l)\right] n_{\bar\sigma}(l) = & \text{(B.85)} \\ &= \delta_{il}\delta_{\sigma'\bar\sigma} n_\sigma(l) c_{\bar\sigma}(l) + \delta_{il}\delta_{\sigma'\sigma} c_\sigma(l) n_{\bar\sigma}(l) = & \text{(B.86)} \\ &= \delta_{il} \left(\delta_{\sigma'\bar\sigma} n_\sigma(l) c_{\bar\sigma}(l) + \delta_{\sigma'\sigma} c_\sigma(l) n_{\bar\sigma}(l)\right) \ . & \text{(B.87)} \end{aligned}$$

Using the relations obtained before, the equation of motion for the annihilator operator can be written as follow:

$$\begin{aligned} i\partial_t c_{\sigma'}(i) &= \sum_j \left(t_{ij} - \mu\delta_{ij}\right) c_{\sigma'}(i) + \frac{U}{2} \left[2 n_{\bar\sigma'}(i) c_{\sigma'}(i)\right] = \\ &= \sum_j t_{ij} c_{\sigma'}(i) - \mu c_{\sigma'}(i) + U n_{\sigma'}(i) c_{\sigma'}(i) = \\ &= -2dt c^\alpha_{\sigma'}(i) - \mu c_{\sigma'}(i) + U \eta_{\sigma'}(i) \ , \end{aligned} \tag{B.88}$$

so the spinor $c(i)$ satisfies the equation:

$$i\partial_t c(i) = -2dtc^{\alpha}(i) - \mu c(i) + U\eta(i) \; . \tag{B.89}$$

By taking the complex conjugate of the above equation, one immediately obtains:

$$i\partial_t c^{\dagger}(i) = 2dtc^{\alpha\dagger}_{\sigma'}(i) + \mu c^{\dagger}_{\sigma'}(i) - U\eta^{\dagger}_{\sigma'}(i) \; . \tag{B.90}$$

B.3.2 Equation of motion for $n(i)$

Using the properties of derivation operator, the equation of motion for the spinor $n(i)$ can be written in terms of the equation of motion obtained for the spinors $c(i)$ and $c^{\dagger}(i)$ ad follow:

$$i\partial_t n(i) = i\partial_t \left(c^{\dagger}(i)c(i)\right) = \left(i\partial_t c^{\dagger}(i)\right) c(i) + c^{\dagger}(i) \left(i\partial_t c(i)\right) \; . \tag{B.91}$$

Using (B.89) and (B.90) relations we have:

$$\begin{aligned} i\partial_t n(i) = 2dtc^{\alpha\dagger}(i)c(i) + \cancel{\mu c^{\dagger}(i)c(i)} - \cancel{U\eta^{\dagger}(i)c(i)} + \\ - 2dtc^{\dagger}(i)c^{\alpha}(i) - \cancel{\mu c^{\dagger}(i)c(i)} + \cancel{Uc^{\dagger}(i)\eta(i)} \quad , \end{aligned} \tag{B.92}$$

so the spinor $n(i)$ satisfies the relation:

$$i\partial_t n(i) = 2dt \left(c^{\alpha\dagger}(i)c(i) - c^{\dagger}(i)c^{\alpha}(i)\right) \quad . \tag{B.93}$$

B.3.3 Equation of motion for $\xi(i)$

The equation of motion for $\xi(i)$ can be calculated as follow:

$$\begin{aligned} i\partial_t \xi(i) = i\partial_t \left[(1 - n(i))\, c(i)\right] = \left(i\partial_t (1 - n(i))\right) c(i) + (1 - n(i)) \left(i\partial_t c(i)\right) = \\ = - \left(i\partial_t n(i)\right) c(i) + (1 - n(i)) \left(i\partial_t c(i)\right) \quad . \end{aligned} \tag{B.94}$$

Using all the equation of motion obtained before we have:

$$\begin{aligned} i\partial_t \xi(i) &= -2dt \left[c^{\alpha\dagger}(i)c(i) - c^{\dagger}(i)c^{\alpha}(i)\right] c(i) + (1 - n(i)) \left[-2dtc^{\alpha}(i) - \mu c(i) + \cancel{U\eta(i)}\right] = \\ &= -2dt \left[c^{\alpha\dagger}(i)c(i) - c^{\dagger}(i)c^{\alpha}(i)\right] c(i) - 2dt \left(1 - n(i)\right) c^{\alpha}(i) - \mu \left(1 - n(i)\right) c(i) = \\ &= -\mu\xi(i) - 2dt \left[c^{\alpha}(i) - n(i)c^{\alpha}(i) + \left(c^{\alpha\dagger}(i)c(i) - c^{\dagger}(i)c^{\alpha}(i)\right) c(i)\right] \quad , \end{aligned} \tag{B.95}$$

in which the relation $(1 - n(i))\eta(i) = 0$ has been used. Hence, we can define the composite field $\pi(i)$ as:

$$\pi(i) \equiv -n(i)c^{\alpha}(i) + \left(c^{\alpha\dagger}(i)c(i) - c^{\dagger}(i)c^{\alpha}(i)\right) c(i) \; , \tag{B.96}$$

and then obtain:

$$i\partial_t \xi(i) = -\mu\xi(i) - 2dt \left[\xi^{\alpha}(i) + \eta^{\alpha}(i) + \pi(i)\right] \quad . \tag{B.97}$$

B.3.4 Equation of motion for $\eta(i)$

The equation of motion for the spinor $\eta(i)$ can be written as:

$$\begin{aligned} i\partial_t\eta(i) &= i\partial_t\left(n(i)c(i)\right) = \left(i\partial_t n(i)\right)c(i) + n(i)\left(i\partial_t c(i)\right) = \\ &= 2dt\left(c^{\alpha\dagger}(i)c(i) - c^{\dagger}(i)c^{\alpha}(i)\right)c(i) - 2dtn(i)c^{\alpha}(i) + \\ &\quad - \mu n(i)c(i) + Un(i)\eta(i) = \\ &= (U-\mu)\,\eta(i) + 2dt\left[\left(c^{\alpha\dagger}(i)c(i) - c^{\dagger}(i)c^{\alpha}(i)\right)c(i) - n(i)c^{\alpha}(i)\right] \quad . \end{aligned} \tag{B.98}$$

The second part of the last two equation can be written in terms of the field $\pi(i)$:

$$\pi(i) \equiv -n(i)c^{\alpha}(i) + \left(c^{\alpha\dagger}(i)c(i) - c^{\dagger}(i)c^{\alpha}(i)\right)c(i)\ , \tag{B.99}$$

therefore we obtain:

$$i\partial_t\eta(i) = (U-\mu)\,\eta(i) + 2dt\pi(i) \quad . \tag{B.100}$$

B.3.5 Equation of motion for $n_\mu(i)$

The field $n_\mu(i)$ is defined as:

$$n_\mu(i) \equiv c^{\dagger}(i)\sigma_\mu c(i)\ , \tag{B.101}$$

where σ_μ is a 4-component vector composed by the 2×2 identity matrix and the Pauli matrices: $\sigma_\mu \equiv (I_{2\times 2}, \boldsymbol{\sigma})$. Using the equation of motion obtained for the fields $c(i)$ and $c^{\dagger}(i)$, the equation of motion for that spinor can be written as follow:

$$\begin{aligned} i\partial_t n_\mu(i) &= i\partial_t\left(c^{\dagger}(i)\sigma_\mu c(i)\right) = \left(i\partial_t c^{\dagger}(i)\right)\sigma_\mu c(i) + c^{\dagger}(i)\sigma_\mu\left(i\partial_t c(i)\right) = \\ &= 2dtc^{\alpha\dagger}(i)\sigma_\mu c(i) + \cancel{\mu c^{\dagger}(i)\sigma_\mu c(i)} - U\eta^{\dagger}(i)\sigma_\mu c(i) + \\ &\quad + Uc^{\dagger}(i)\sigma_\mu\eta(i) - \cancel{\mu c^{\dagger}(i)\sigma_\mu c(i)} - 2dtc^{\dagger}(i)\sigma_\mu c^{\alpha}(i) \quad . \end{aligned} \tag{B.102}$$

Hence the equation of motion of $n_\mu(i)$ reads as:

$$i\partial_t n_\mu(i) = 2dt\left(c^{\alpha\dagger}(i)\sigma_\mu c(i) - c^{\dagger}(i)\sigma_\mu c^{\alpha}(i)\right) + U\left(c^{\dagger}(i)\sigma_\mu\eta(i) - \eta^{\dagger}(i)\sigma_\mu c(i)\right) \quad . \tag{B.103}$$

It can be easily shown that the term proportional to U is zero. In order to show this let us write the canonical creation and the annihilation operators in terms of $\xi(i)$ and $\eta(i)$:

$$\begin{aligned} c^{\dagger}(i)\sigma_\mu\eta(i) - \eta^{\dagger}(i)\sigma_\mu c(i) &= \left(\xi^{\dagger}(i) + \eta^{\dagger}(i)\right)\sigma_\mu\eta(i) - \eta^{\dagger}(i)\sigma_\mu\left(\xi(i) + \eta(i)\right) = \\ &= \xi^{\dagger}(i)\sigma_\mu\eta(i) + \eta^{\dagger}(i)\sigma_\mu\eta(i) + \\ &\quad - \eta^{\dagger}(i)\sigma_\mu\xi(i) - \eta^{\dagger}(i)\sigma_\mu\eta(i) \quad . \end{aligned} \tag{B.104}$$

Hence recalling that, due to Pauli exclusion principle, $\xi(i)\eta^{\dagger}(i) = \eta(i)\xi^{\dagger}(i) = 0$, it is immediate to note that the crossing terms $\xi^{\dagger}(i)\sigma_\mu\eta(i)$ and $\eta^{\dagger}(i)\sigma_\mu\xi(i)$ in the above

relation are zero and we remain with:

$$c^{\dagger}(i)\sigma_{\mu}\eta(i) - \eta^{\dagger}(i)\sigma_{\mu}c(i) = \eta^{\dagger}(i)\sigma_{\mu}\eta(i) - \eta^{\dagger}(i)\sigma_{\mu}\eta(i) = 0 \quad . \tag{B.105}$$

Considering this, the equation of motion of $n_{\mu}(i)$ is only proportional to the hopping amplitude t and satisfies the following relation:

$$i\partial_t n_{\mu}(i) = 2dt\left(c^{\alpha\dagger}(i)\sigma_{\mu}c(i) - c^{\dagger}(i)\sigma_{\mu}c^{\alpha}(i)\right) \quad . \tag{B.106}$$

B.4 One-loop approximation

In the following sections will be reported in detail the calculation of bosonic correlators in the one-loop approximation.

B.4.1 Density-density and spin-spin correlation functions

By definition, in the framework of the linear response theory, the calculation of system's response functions such as charge and spin susceptibilities (4.44) requires the knowledge of the bosonic correlator $\langle n_{\mu}(i)n_{\mu}(j)\rangle$. To this purpose, let us define the thermal Green's function[1]:

$$L_{\mu}^{\mathcal{Q},ab}(i,l,j) \equiv \left\langle \mathcal{Q}\left[\psi_{\alpha}^{(a)}(i)\,(\sigma_{\mu})_{\alpha\beta}\,\psi_{\beta}^{(b)\dagger}(l)n_{\mu}(j)\right]\right\rangle \ , \tag{B.107}$$

where $\mathcal{Q} = \{\mathcal{A},\mathcal{R},\mathcal{T}\}$ for the advanced, the retarded or the causal component; $a,b = \{1,2\}$ specify the composite field of the basis according with the notation: $\psi_{\sigma}^{(1)}(i) = \xi_{\sigma}(i)$, $\psi_{\sigma}^{(2)}(i) = \eta_{\sigma}(i)$, while $\mu = \{0,k\}$, $k \in \{1,3\}$, selects density-density and spin-spin interaction term, respectively. It is worth noting that:

$$\langle n_{\mu}(i)n_{\mu}(j)\rangle = -\lim_{l\to i^{+}}\sum_{a,b=1}^{2} L_{\mu}^{R,ab}(i,l,j) \ , \tag{B.108}$$

from which we have:

$$\langle n(i)n(j)\rangle = -\lim_{l\to i^{+}}\sum_{a,b=1}^{2} L_{0}^{R,ab}(i,l,j) \ , \tag{B.109}$$

$$\sum_{k=1}^{3}\langle n_k(i)n_k(j)\rangle = -\lim_{l\to i^{+}}\sum_{a,b=1}^{2}\sum_{k=1}^{3} L_{k}^{R,ab}(i,l,j) \ , \tag{B.110}$$

where the retarded correlator $L_{\mu}^{R,ab}(i,l,j)$ has to be calculated starting from the causal Green's function $L_{\mu}^{C,ab}(i,l,j)$, with:

$$L_{\mu}^{R,ab}(i,l,j) = \left\langle \mathcal{R}\left[\psi_{\alpha}^{(a)}(i)\,(\sigma_{\mu})_{\alpha\beta}\,\psi_{\beta}^{(b)\dagger}(l)n_{\mu}(j)\right]\right\rangle \ , \tag{B.111}$$

[1] $L_{\mu}(i,l,j)$ depends on the particular value of $\mu \in \{0,3\}$, then there is no implicit sum over μ on the right side of the equation while the sum over all spin indices α and β is understood.

$$L_{\mu}^{C,ab}(i,l,j) \;=\; \left\langle \mathcal{T}\left[\psi_{\alpha}^{(a)}(i)\,(\sigma_{\mu})_{\alpha\beta}\,\psi_{\beta}^{(b)\dagger}(l)n_{\mu}(j)\right]\right\rangle \,. \tag{B.112}$$

Following the one-loop approximation prescription, the equation of motion for the causal propagator reads as:

$$\begin{aligned}\hat{\Lambda}_{ac}L_{\mu}^{C,cb}(i,l,j) \;&=\; L_{ab}^{\delta J}(i,l,j)+i\delta(t_i-t_l)\left\langle \mathcal{T}\left[(\sigma_{\mu})_{\alpha\beta}\left\{\psi_{\alpha}^{(a)}(i),\psi_{\beta}^{(b)\dagger}(l)\right\}n_{\mu}(j)\right]\right\rangle \\ &\quad +i\delta(t_i-t_j)\left\langle \mathcal{T}\left[\left[\psi_{\alpha}^{(a)}(i),n_{\mu}(j)\right](\sigma_{\mu})_{\alpha\beta}\,\psi_{\beta}^{(b)\dagger}(l)\right]\right\rangle \,,\end{aligned} \tag{B.113}$$

where $\hat{\Lambda}_{ab} \equiv \delta_{ab}i\partial_t - \varepsilon_{ab}(i,j)$, $\varepsilon(i,j)$ is the fermionic energy matrix (4.9) and $L_{ab}^{\delta J}(i,l,j)$ represents the contribution generated by non-linear terms $\delta J(i)$ in the equations of motion of $\psi(i)$. Consistently with the pole approximation, we can neglect $L_{ab}^{\delta J}(i,l,j)$ since we take only the linear terms in the equation of motion of $\psi(i)$. Hence, from the standard algebraic relations among the composite fields of the basis, we get:

$$\hat{\Lambda}_{ac}L_{\mu}^{C,cb}(i,l,j) \;=\; i\delta(t_i-t_l)\delta_{\boldsymbol{il}}\,(\sigma_{\mu})_{\alpha\beta}\left\langle \mathcal{T}\left[N_{\alpha\beta}^{ab}(i)n_{\mu}(j)\right]\right\rangle \tag{B.114}$$

$$+i\delta(t_i-t_j)\delta_{\boldsymbol{ij}}\left\langle \mathcal{T}\left[(\sigma_{\mu})_{\alpha\gamma}\,\psi_{\gamma}^{(a)}(j)\,(\sigma_{\mu})_{\alpha\beta}\,\psi_{\beta}^{(b)\dagger}(l)\right]\right\rangle \tag{B.115}$$

in which we have taken into account that $[\psi(i),n_{\mu}(j)] = \delta_{ij}\sigma_{\mu}\psi(i)$ with:

$$N_{\alpha\beta}(i) = \begin{pmatrix} \delta_{\alpha\beta}+\frac{1}{2}\,(\sigma^{\nu})_{\alpha\beta}\,n_{\nu}(i) & 0 \\ 0 & -\frac{1}{2}\,(\sigma^{\nu})_{\alpha\beta}\,n_{\nu}(i)\end{pmatrix} \,. \tag{B.116}$$

We can now consider that for the causal single-particle propagator we have:

$$\hat{\Lambda}_{ac}G_{cb}^{C}(i,j) = i\delta(t_i-t_j)\delta_{\boldsymbol{ij}}I_{ab} \;\Rightarrow i\delta(t_i-t_j)\delta_{\boldsymbol{ij}} = \hat{\Lambda}_{ac}G_{cb}^{C}(i,j)I_{ba}^{-1} \,, \tag{B.117}$$

then the equation of motion of $L^{C}(i,l,j)$ can be written as:

$$\begin{aligned}\hat{\Lambda}_{ac}\left[L_{\mu}^{C,cb}(i,l,j)\right] \;&=\; \hat{\Lambda}_{ac}\Bigg[G_{cd}^{C}(i,l)I_{de}^{-1}\,(\sigma_{\mu})_{\alpha\beta}\left\langle \mathcal{T}\left[N_{\alpha\beta}^{eb}(i)n_{\mu}(j)\right]\right\rangle \\ &\quad +G_{cd}^{C}(i,j)I_{de}^{-1}\,(\sigma_{\mu})_{\alpha\beta}\,(\sigma_{\mu})_{\alpha\gamma} \\ &\quad \left\langle \mathcal{T}\left[\psi_{\gamma}^{(e)}(j)\psi_{\beta}^{(b)\dagger}(l)\right]\right\rangle\Bigg] \,,\end{aligned} \tag{B.118}$$

from which we get:

$$\begin{aligned}L_{\mu}^{C,ab}(i,l,j) \;&=\; G_{ac}^{C}(i,l)I_{cd}^{-1}\,(\sigma_{\mu})_{\alpha\beta}\left\langle \mathcal{T}\left[N_{\alpha\beta}^{db}(i)n_{\mu}(j)\right]\right\rangle + \\ &\quad +G_{ac}^{C}(i,j)I_{cd}^{-1}\,(\sigma_{\mu})_{\alpha\beta}\,(\sigma_{\mu})_{\alpha\gamma}\left\langle \mathcal{T}\left[\psi_{\gamma}^{(d)}(j)\psi_{\beta}^{(b)\dagger}(l)\right]\right\rangle = \\ &=\; G_{ab}^{C}(i,l)I_{bb}^{-1}\,(\sigma_{\mu})_{\alpha\beta}\left\langle \mathcal{T}\left[N_{\alpha\beta}^{bb}(i)n_{\mu}(j)\right]\right\rangle + \\ &\quad +G_{ac}^{C}(i,j)I_{cc}^{-1}\,(\sigma_{\mu})_{\alpha\beta}\,(\sigma_{\mu})_{\alpha\gamma}\left\langle \mathcal{T}\left[\psi_{\gamma}^{(c)}(j)\psi_{\beta}^{(b)\dagger}(l)\right]\right\rangle \,,\end{aligned} \tag{B.119}$$

where, in the last step, we have contracted all the indices referred to $N(i)$ and $I(i,j)$ because of their diagonal representation. We can now note that, according to the relation $(\sigma_k)_{\alpha\beta}(\sigma_k)_{\gamma\rho} = \delta_{\alpha\rho}\delta_{\beta\gamma} - \delta_{\alpha\beta}\delta_{\gamma\rho}$, we have:

$$(\sigma_\mu)_{\alpha\beta}(\sigma_\mu)_{\alpha\gamma}\left\langle \mathcal{T}\left[\psi_\gamma^{(c)}(j)\psi_\beta^{(b)\dagger}(l)\right]\right\rangle = \left\langle \mathcal{T}\left[\psi_\alpha^{(c)}(j)\psi_\alpha^{(b)\dagger}(l)\right]\right\rangle = 2G_{ab}^C(j,l)\ , \quad \text{(B.120)}$$

then by substituting in the expression of $L_\mu^{C,ab}(i,l,j)$ we obtain:

$$L_\mu^{C,ab}(i,l,j) = G_{ab}^C(i,l)I_{bb}^{-1}(\sigma_\mu)_{\alpha\beta}\left\langle \mathcal{T}\left[N_{\alpha\beta}^{bb}(i)n_\mu(j)\right]\right\rangle + 2G_{ac}^C(i,j)I_{cc}^{-1}G_{ab}^C(j,l)\ ,$$

where the sum over all repeated indices is understood. In the limit $l \to i^+$, taking the sum over a and b we get:

$$\begin{aligned}\sum_{a,b=1}^{2}\lim_{l\to i^+} L_\mu^{C,ab}(i,l,j) &= \sum_{a,b=1}^{2} G_{ab}^C(i,i^+)I_{bb}^{-1}(\sigma_\mu)_{\alpha\beta}\left\langle \mathcal{T}\left[N_{\alpha\beta}^{bb}(i)n_\mu(j)\right]\right\rangle \\ &\quad +2\sum_{a,b=1}^{2} G_{ac}^C(i,j)I_{cc}^{-1}G_{cb}^C(j,i) = \\ &= A_\mu^C(i,j) + B^C(i,j)\ , \end{aligned} \quad \text{(B.121)}$$

with:

$$\begin{cases} A_\mu^C(i,j) \equiv \sum_{a,b=1}^{2} G_{ab}^C(i,i^+)I_{bb}^{-1}(\sigma_\mu)_{\alpha\beta}\left\langle \mathcal{T}\left[N_{\alpha\beta}^{bb}(i)n_\mu(j)\right]\right\rangle \\ B^C(i,j) \equiv 2\sum_{a,b=1}^{2} G_{ac}^C(i,j)I_{cc}^{-1}G_{cb}^C(j,i) \end{cases} . \quad \text{(B.122)}$$

By means of Eq.4.10 and Eq.B.116, recalling that $(\sigma_\mu)_{\alpha\beta}(\sigma^\mu)_{\alpha\beta} = 2(1-2\delta_{\mu 0})$, it is immediate to have:

$$\begin{aligned}(\sigma_\mu)_{\alpha\beta}\left\langle \mathcal{T}\left[N_{\alpha\beta}^{11}(i)n_\mu(j)\right]\right\rangle &= (\sigma_\mu)_{\alpha\beta}\delta_{\alpha\beta}\langle \mathcal{T}[n_\mu(j)]\rangle + \frac{1}{2}(\sigma_\mu)_{\alpha\beta}(\sigma^\nu)_{\alpha\beta} \\ &\quad \langle \mathcal{T}[n_\nu(i)n_\mu(j)]\rangle = \quad \text{(B.123)} \\ &= \delta_{\mu 0}n(\sigma_0)_{\alpha\alpha} + \frac{1}{2}(\sigma_\mu)_{\alpha\beta}(\sigma^\mu)_{\alpha\beta}\langle \mathcal{T}[n_\mu(i)n_\mu(j)]\rangle = \\ &= \delta_{\mu 0}2n + (1-2\delta_{\mu 0})\langle \mathcal{T}[n_\mu(i)n_\mu(j)]\rangle\ , \quad \text{(B.124)}\end{aligned}$$

$$\begin{aligned}(\sigma_\mu)_{\alpha\beta}\left\langle \mathcal{T}\left[N_{\alpha\beta}^{22}(i)n_\mu(j)\right]\right\rangle &= -\frac{1}{2}(\sigma_\mu)_{\alpha\beta}(\sigma^\nu)_{\alpha\beta}\langle \mathcal{T}[n_\nu(i)n_\mu(j)]\rangle = \\ &= -\frac{1}{2}(\sigma_\mu)_{\alpha\beta}(\sigma^\mu)_{\alpha\beta}\langle \mathcal{T}[n_\mu(i)n_\mu(j)]\rangle = \\ &= -(1-2\delta_{\mu 0})\langle \mathcal{T}[n_\mu(i)n_\mu(j)]\rangle\ , \quad \text{(B.125)}\end{aligned}$$

then:

$$\begin{aligned}A_\mu^C(i,j) &= \left[G_{11}^C(i,i^+) + G_{21}^C(i,i^+)\right]I_{11}^{-1}\left[\delta_{\mu 0}2n + (1-2\delta_{\mu 0})\langle \mathcal{T}[n_\mu(i)n_\mu(j)]\rangle\right] \\ &\quad -\left[G_{12}^C(i,i^+) + G_{22}^C(i,i^+)\right]I_{22}^{-1}(1-2\delta_{\mu 0})\langle \mathcal{T}[n_\mu(i)n_\mu(j)]\rangle =\end{aligned}$$

$$
\begin{aligned}
&= 2n\delta_{\mu 0}\left(\frac{G^C_{11}(i,i^+)+G^C_{21}(i,i^+)}{I_{11}}\right)+(1-2\delta_{\mu 0}) \\
&\left[\frac{G^C_{11}(i,i^+)+G^C_{21}(i,i^+)}{I_{11}}-\frac{G^C_{12}(i,i^+)+G^C_{22}(i,i^+)}{I_{22}}\right] \\
&\langle \mathcal{T}\left[n_\mu(i)n_\mu(j)\right]\rangle \ , \qquad \text{(B.126)}
\end{aligned}
$$

$$
\begin{aligned}
B^C(i,j) &= 2\left[\frac{G^C_{11}(i,j)G^C_{11}(j,i)}{I_{11}}+\frac{G^C_{12}(i,j)G^C_{21}(j,i)}{I_{22}}+\frac{G^C_{11}(i,j)G^C_{12}(j,i)}{I_{11}}\right. \\
&+\frac{G^C_{12}(i,j)G^C_{22}(j,i)}{I_{22}}+\frac{G^C_{21}(i,j)G^C_{11}(j,i)}{I_{11}}+\frac{G^C_{22}(i,j)G^C_{21}(j,i)}{I_{22}} \\
&\left.+\frac{G^C_{21}(i,j)G^C_{12}(j,i)}{I_{11}}+\frac{G^C_{22}(i,j)G^C_{22}(j,i)}{I_{22}}\right] . \qquad \text{(B.127)}
\end{aligned}
$$

Then, recalling that:

$$
\begin{cases} G^C(i,j)=\theta(t_i-t_j)\left\langle\psi(i)\psi^\dagger(j)\right\rangle-\eta\theta(t_j-t_i)\left\langle\psi^\dagger(j)\psi(i)\right\rangle \\ G^{R,A}(i,j)=\pm\theta[\pm(t_i-t_j)]\left\langle\left[\psi(i),\psi^\dagger(j)\right]_\eta\right\rangle \end{cases} , \qquad \text{(B.128)}
$$

where $\eta=\pm 1$ for fermions and bosons, respectively, the causal Green's functions $G^C_{ab}(i,i^+)$ can be rewritten according to the following relations:

$$
\begin{array}{lll}
\left\langle\xi^\dagger_\sigma(i)\xi_{\sigma'}(i)\right\rangle=\delta_{\sigma\sigma'}\left(\frac{n}{2}-D\right) & , & \left\langle\xi_\sigma(i)\xi^\dagger_{\sigma'}(i)\right\rangle=\delta_{\sigma\sigma'}\left(1-n+D\right) \\
\left\langle\eta^\dagger_\sigma(i)\eta_{\sigma'}(i)\right\rangle=\delta_{\sigma\sigma'}D & , & \left\langle\eta_\sigma(i)\eta^\dagger_{\sigma'}(i)\right\rangle=\delta_{\sigma\sigma'}\left(\frac{n}{2}-D\right) \\
\left\langle\eta^\dagger_\sigma(i)\xi_{\sigma'}(i)\right\rangle=0 & , & \left\langle\xi_\sigma(i)\eta^\dagger_{\sigma'}(i)\right\rangle=0
\end{array} , \qquad \text{(B.129)}
$$

in order to have:

$$
\begin{cases} A^C_\mu(i,j)= & -\delta_{\mu 0}\frac{2n(n-2D)}{2-n}+(1-2\delta_{\mu 0})\frac{4D-n^2}{n(2-n)}\left\langle\mathcal{T}\left[n_\mu(i)n_\mu(j)\right]\right\rangle \\ B^C(i,j)= & 2\sum_{a,b,c=1}^{2} I^{-1}_{aa}G^C_{ab}(i,j)G^C_{ac}(j,i) \end{cases} . \qquad \text{(B.130)}
$$

Finally, according to Eq.B.109, (B.110) and Eq.B.121, it's immediate to see that:

$$
\begin{aligned}
\left\langle\mathcal{T}\left[n(i)n(j)\right]\right\rangle &= -\left(A^C_0(i,j)+B^C(i,j)\right)= \\
&= n^2-\frac{n(2-n)}{n-2D}\sum_{a,b,c=1}^{2} I^{-1}_{aa}G^C_{ab}(i,j)G^C_{ac}(j,i) \ , \qquad \text{(B.131)}
\end{aligned}
$$

$$
\begin{aligned}
\left\langle\mathcal{T}\left[n_k(i)n_k(j)\right]\right\rangle &= -\left(A^C_k(i,j)+B^C_k(i,j)\right)= \\
&= -\frac{n\,(2-n)}{n+2D-n^2}\sum_{a,b,c=1}^{2} G^C_{ac}(i,j)I^{-1}_{cc}G^C_{cb}(j,i) \ .
\end{aligned}
$$

It is worth noting that both spin-spin and density-density correlation functions can be expressed in terms of a fermionic loop, described by the convolution $G^C_{ab}(i,j)G^C_{cd}(j,i)$.

Then, it is useful to introduce the fermionic correlator:

$$\begin{aligned} Q_{abcd}(i,j) &\equiv G_{ab}(i,j)G_{cd}(j,i) = \\ &= \frac{i\Omega^d}{(2\pi)^{d+1}}\int_{\Omega_B} d^dk \int_{-\infty}^{+\infty} d\omega e^{i\boldsymbol{k}\cdot(\boldsymbol{R}_i-\boldsymbol{R}_j)-i\omega(t_i-t_j)} Q_{abcd}(\boldsymbol{k},\omega) \end{aligned} \quad (B.132)$$

and express the correlation functions in the real space as follows:

$$\langle \mathcal{T}\left[n_\mu(i)n_\mu(j)\right]\rangle = n^2\delta_{\mu 0} - g_\mu \sum_{a,b,c=1}^{2} \frac{Q^C_{abac}(i,j)}{I_{aa}} \ , \ \begin{cases} g_\mu = \frac{n(2-n)}{n-2D} & , \ \mu = 0 \\ g_\mu = \frac{n(2-n)}{n+2D-n^2} & , \ \mu = k \in \{1,2,3\} \end{cases} . \quad (B.133)$$

or, alternatively, in the Fourier space as:

$$\chi_\mu(\boldsymbol{k},\omega) = -\frac{i\,(2\pi)^{d+1}}{a^d} n^2\delta(\omega)\delta(\boldsymbol{k}) - g_\mu \sum_{a,b,c=1}^{2} \frac{Q^C_{abac}(\boldsymbol{k},\omega)}{I_{aa}(\boldsymbol{k})} \ , \quad (B.134)$$

with:

$$\begin{cases} g_\mu = \frac{n(2-n)}{n-2D} & , \ \mu = 0 \\ g_\mu = \frac{n(2-n)}{n+2D-n^2} & , \ \mu = k \in \{1,2,3\} \end{cases} . \quad (B.135)$$

It is also immediate to note that, by taking the sum over all the possible values of μ we get:

$$\begin{aligned} \sum_{\mu=0}^{3} \langle \mathcal{T}\left[n_\mu(i)n_\mu(j)\right]\rangle &= n^2 - (g_0 + 3g_k) \sum_{a,b,c=1}^{2} \frac{Q^C_{abac}(i,j)}{I_{aa}} = \\ &= n^2 - \frac{(2-n)\,(4n-4D-n^2)}{(n-2D)\,(n+2D-n^2)} \\ &\quad \sum_{a,b,c=1}^{2} \frac{Q^C_{abac}(i,j)}{I_{aa}} \ , \end{aligned} \quad (B.136)$$

or:

$$\sum_{\mu=0}^{3} \chi_\mu(\boldsymbol{k},\omega) = -\frac{i\,(2\pi)^{d+1}}{a^d} n^2\delta(\omega)\delta(\boldsymbol{k}) - \frac{(2-n)\,(4n-4D-n^2)}{(n-2D)\,(n+2D-n^2)} \sum_{a,b,c=1}^{2} \frac{Q^C_{abac}(\boldsymbol{k},\omega)}{I_{aa}(\boldsymbol{k})} . \quad (B.137)$$

B.4.2 Fermionic loop $Q_{abcd}(i,j)$

In order to calculate the fermionic loop $Q_{abcd}(i,j) \equiv G_{ab}(i,j)G_{cd}(i,j)$, let us recall that:

$$Q^C_{abcd}(\boldsymbol{k},\omega) = \frac{i\Omega^d}{(2\pi)^{d+1}} \int_{\Omega_B} d^dp \int_{-\infty}^{+\infty} d\omega_0 G^C_{ab}(\boldsymbol{k}+\boldsymbol{p},\omega+\omega_0) G^C_{cd}(\boldsymbol{p},\omega_0) \ . \quad (B.138)$$

Here $G^C(\boldsymbol{k},\omega)$ is the Fourier Transform of the causal Green's function that in the pole approximation reads as:

$$G^C(\boldsymbol{k},\omega) = \sum_{l=1}^{2} \sigma^{(l)}(\boldsymbol{k}) \left[\frac{1 - f_F[E_l(\boldsymbol{k})]}{\omega - E_l(\boldsymbol{k}) + i\delta} + \frac{f_F[E_l(\boldsymbol{k})]}{\omega - E_l(\boldsymbol{k}) - i\delta} \right] , \tag{B.139}$$

$E_l(\boldsymbol{k})$ is the l^{th} eigenvalue of the fermionic energy matrix (4.9) and $\sigma^{(l)}(\boldsymbol{k})$ represents the spectral density matrix that can be computed as:

$$\sigma^{(l)}_{ab}(\boldsymbol{k}) = \sum_{c=1}^{2} \Omega_{al}(\boldsymbol{k}) \Omega^{-1}_{lc}(\boldsymbol{k}) I_{cb}(\boldsymbol{k}) , \tag{B.140}$$

in which $\Omega(\boldsymbol{k})$ is a $n \times n$ matrix whose columns are the eigenvectors of the energy matrix. Because of the pole structure of the causal Green's function, by substituting the expression of $G^C(\boldsymbol{k},\omega)$ in $Q^C_{abcd}(\boldsymbol{k},\omega)$ the integration over ω_0 can be easily done and we get:

$$\begin{aligned} Q^C_{abcd}(\boldsymbol{k},\omega) &= \frac{\Omega^d}{(2\pi)^d} \sum_{i,j=1}^{2} \int_{\Omega_B} d^d p \left\{ \frac{\left(1 - f_F[E_i(\boldsymbol{k}+\boldsymbol{p})]\right) f_F[E_j(\boldsymbol{p})] \sigma^{(i)}_{ab}(\boldsymbol{k}+\boldsymbol{p}) \sigma^{(j)}_{cd}(\boldsymbol{p})}{\omega + E_i(\boldsymbol{k}+\boldsymbol{p}) - E_j(\boldsymbol{p}) - i\delta} + \right. \\ &\left. - \frac{f_F[E_i(\boldsymbol{k}+\boldsymbol{p})] \left(1 - f_F[E_j(\boldsymbol{p})]\right) \sigma^{(i)}_{ab}(\boldsymbol{k}+\boldsymbol{p}) \sigma^{(j)}_{cd}(\boldsymbol{p})}{\omega + E_i(\boldsymbol{k}+\boldsymbol{p}) - E_j(\boldsymbol{p}) + i\delta} \right\} = \end{aligned} \tag{B.141}$$

Recalling the relation between causal and retarded correlation functions:

$$Q^R_{abcd}(\boldsymbol{k},\omega) = - \left[1 + \tanh\left(\frac{\beta\omega}{2} \right) \right] Im\left[Q^c_{abcd}(\boldsymbol{k},\omega) \right] , \tag{B.142}$$

from the previous equation we have:

$$\begin{aligned} Q^C_{abcd}(\boldsymbol{k},\omega) &= - \frac{\Omega^d}{(2\pi)^d} \left[1 + \tanh\left(\frac{\beta\omega}{2} \right) \right] \sum_{i,j=1}^{2} \int_{\Omega_B} d^d p \delta\left(\omega + E_i(\boldsymbol{k}+\boldsymbol{p}) - E_j(\boldsymbol{p}) \right) \\ &\quad \sigma^{(i)}_{ab}(\boldsymbol{k}+\boldsymbol{p}) \sigma^{(j)}_{cd}(\boldsymbol{p}) \Big\{ f_F[E_j(\boldsymbol{p})] + f_F[E_i(\boldsymbol{k}+\boldsymbol{p})] \\ &\quad - 2 f_F[E_i(\boldsymbol{k}+\boldsymbol{p})] f_F[E_j(\boldsymbol{p})] \Big\} . \end{aligned} \tag{B.143}$$

By using the relation:

$$\left\{ \left[1 - f_F(a)\right] f_F(b) + f_F(a) \left[1 - f_F(b)\right] \right\} \left[1 - 2 f_F(b-a)\right] = f_F(a) - f_F(b) , \tag{B.144}$$

we can finally express the retarded part that appears in the Fourier Transform of $\langle \mathcal{T}\left[n_\mu(i) n_\mu(j) \right] \rangle$ correlator reads as:

$$Q^R_{abcd}(\boldsymbol{k},\omega) = \frac{2\pi\Omega^d}{(2\pi)^d} \sum_{i,j=1}^{2} \int_{\Omega_B} d^d p \delta\left(\omega + E_i(\boldsymbol{k}+\boldsymbol{p}) - E_j(\boldsymbol{p}) \right) \left(f_F[E_j(\boldsymbol{p})] - f_F[E_i(\boldsymbol{k}+\boldsymbol{p})] \right)$$

$$f_F[E_j(\boldsymbol{p})]\sigma^{(i)}_{ab}(\boldsymbol{k}+\boldsymbol{p})\sigma^{(j)}_{cd}(\boldsymbol{p}) \ . \tag{B.145}$$

Next, by means of the relations:

$$\begin{cases} f_F[E_i(\boldsymbol{k}+\boldsymbol{p})] = \frac{1}{2}\left[1 - T_i(\boldsymbol{k}+\boldsymbol{p})\right] \\ f_F[E_j(\boldsymbol{p})] = \frac{1}{2}\left[1 - T_j(\boldsymbol{p})\right] \end{cases} , \begin{cases} T_i(\boldsymbol{k}+\boldsymbol{p}) = \tanh\left[\frac{\beta E_i(\boldsymbol{k}+\boldsymbol{p})}{2}\right] \\ T_j(\boldsymbol{p}) = \tanh\left[\frac{\beta E_j(\boldsymbol{p})}{2}\right] \end{cases} , \tag{B.146}$$

we can rewrite the previous equation as follows:

$$\begin{aligned} Q^R_{abcd}(\boldsymbol{k},\omega) &= \frac{\pi\Omega^d}{2(2\pi)^d}\sum_{i,j=1}^{2}\int_{\Omega_B} d^dp\delta\left(\omega + E_i(\boldsymbol{k}+\boldsymbol{p}) - E_j(\boldsymbol{p})\right)\sigma^{(i)}_{ab}(\boldsymbol{k}+\boldsymbol{p})\sigma^{(j)}_{cd}(\boldsymbol{p}) \\ &\quad \left\{\left[1 - T_i(\boldsymbol{k}+\boldsymbol{p})\right]\left[1 - T_j(\boldsymbol{p})\right]\right\} \ . \end{aligned} \tag{B.147}$$

We can also note that, by definition, in the real space we have:

$$Q^R_{abcd}(i,j) = \frac{\Omega^d}{2(2\pi)^{d+1}}\int d^dk e^{i\boldsymbol{k}\cdot(\boldsymbol{R}_i - \boldsymbol{R}_j) - i\omega(t_i - t_j)} Q^R_{abcd}(\boldsymbol{k},\omega) \ , \tag{B.148}$$

then, by means of Eq.B.147, we get:

$$\begin{aligned} Q^R_{abcd}(l,m) &= \frac{\Omega^d}{2(2\pi)^{d+1}}\sum_{n=1}^{2}\int d^dk e^{i\boldsymbol{k}\cdot(\boldsymbol{R}_i - \boldsymbol{R}_j) - iE_n(t_l - t_m)}\sigma^{(n)}_{ab}(\boldsymbol{k})\left[1 - T_n(\boldsymbol{k})\right] = \\ &= \frac{\Omega^d}{2(2\pi)^{d+1}}\sum_{n=1}^{2}\int d^dp e^{i\boldsymbol{p}\cdot(\boldsymbol{R}_l - \boldsymbol{R}_m) - iE_n(t_l - t_m)}\sigma^{(n)}_{cd}(\boldsymbol{p}) \\ &\quad \left[1 + T_n(\boldsymbol{p})\right] \ . \end{aligned} \tag{B.149}$$

We now recall that:

$$\begin{aligned} C_{\alpha\beta}(i,j) &= \left\langle \psi_\alpha(i)\psi^\dagger_\beta(j)\right\rangle = \frac{\Omega^d}{2(2\pi)^d}\sum_{n=1}^{2}\int_{\Omega_b} d^dk\int d\omega e^{i\boldsymbol{k}\cdot(\boldsymbol{R}_i - \boldsymbol{R}_j) - iE_n(t_l - t_m)} \\ &\quad \sigma^{(n)}_{\alpha\beta}(\boldsymbol{k})\left[1 + T_n(\boldsymbol{k})\right] \ , \end{aligned} \tag{B.150}$$

$$\begin{aligned} \hat{C}_{\alpha\beta}(i,j) &= \left\langle \psi^\dagger_\beta(j)\psi_\alpha(i)\right\rangle = \frac{\Omega^d}{2(2\pi)^d}\sum_{n=1}^{2}\int_{\Omega_b} d^dk\int d\omega e^{i\boldsymbol{k}\cdot(\boldsymbol{R}_i - \boldsymbol{R}_j) - iE_n(t_l - t_m)} \\ &\quad \sigma^{(n)}_{\alpha\beta}(\boldsymbol{k})\left[1 - T_n(\boldsymbol{k})\right] \ , \end{aligned} \tag{B.151}$$

then the correlator $Q^R_{abcd}(l,m)$ reads as:

$$Q^R_{abcd}(i,j) = \left\langle \psi^\dagger_b(j)\psi_a(i)\right\rangle\left\langle \psi_c(i)\psi^\dagger_d(j)\right\rangle \ , \tag{B.152}$$

that in the special case of equal time (i.e. $t_i = t_j$) takes the form:

$$\begin{cases} Q_{abcd}(\boldsymbol{i},\boldsymbol{j}) = \left[I_{ab}(\boldsymbol{i},\boldsymbol{j}) - C_{ab}(\boldsymbol{i},\boldsymbol{j})\right]C_{cd}(\boldsymbol{i},\boldsymbol{j}) \\ Q^\alpha_{abcd}(\boldsymbol{i},\boldsymbol{j}) = -C^\alpha_{ab}(\boldsymbol{i},\boldsymbol{j})C^\alpha_{cd}(\boldsymbol{i},\boldsymbol{j}) \end{cases} . \tag{B.153}$$

B.4.3 Pair propagator

Let us now introduce the pair propagator $P(i,j) \equiv \left\langle \mathcal{T}\left[p(i)p^{\dagger}(j)\right]\right\rangle$, with $p(i) = c_{\uparrow}(i)c_{\downarrow}(i)$. With the aim of calculating $P(i,j)$ let us define the basis:

$$\psi(i) = \begin{pmatrix} \xi_{\uparrow}(i) \\ \eta_{\uparrow}(i) \\ \xi_{\downarrow}(i) \\ \eta_{\downarrow}(i) \end{pmatrix} \ , \ I(i,j) \equiv \left\langle \left\{\psi(i), \psi^{\dagger}(j)\right\}\right\rangle = \delta_{ij} \begin{pmatrix} 1-\frac{n}{2} & 0 & 0 & 0 \\ 0 & \frac{n}{2} & 0 & 0 \\ 0 & 0 & 1-\frac{n}{2} & 0 \\ 0 & 0 & 0 & \frac{n}{2} \end{pmatrix} , \tag{B.154}$$

and the correlator:

$$X_a(i,l,j) \equiv \left\langle \mathcal{T}\left[\psi_a(i)c_{\uparrow}(l)p^{\dagger}(j)\right]\right\rangle \ , \ \psi(i) = \begin{pmatrix} \xi_{\uparrow}(i) \\ \eta_{\uparrow}(i) \\ \xi_{\downarrow}(i) \\ \eta_{\downarrow}(i) \end{pmatrix} , \tag{B.155}$$

that allow us to write $P(i,j)$ as:

$$P(i,j) = \lim_{l \to i^{-}} \left[X_3(i,l,j) + X_4(i,l,j)\right] \ . \tag{B.156}$$

The equation of motion for $X(i,l,j)$ gives:

$$\begin{aligned} \Lambda_{ab}X_b(i,l,j) &= i\delta(t_i - t_l)\left\langle \mathcal{T}\left[\left\{\psi_a(i), c_{\uparrow}(l)\right\}p^{\dagger}(j)\right]\right\rangle \\ &\quad + i\delta(t_i - t_l)\left\langle \mathcal{T}\left[c_{\uparrow}(l)\left[\psi_a(i), p^{\dagger}(j)\right]\right]\right\rangle = && \text{(B.157)} \\ &= i\delta(t_i - t_l)\delta_{\boldsymbol{il}}\left\langle \mathcal{T}\left[N_a^{(1)}(i)p^{\dagger}(j)\right]\right\rangle && \text{(B.158)} \\ &\quad + i\delta(t_i - t_l)\delta_{\boldsymbol{ij}}\left\langle \mathcal{T}\left[c_{\uparrow}(l)N_a^{(2)}(j)\right]\right\rangle \ , && \text{(B.159)} \end{aligned}$$

where, recalling that:

$$\begin{cases} \left[c_{\sigma}(i), p^{\dagger}(j)\right] = \delta_{ij}\left(\delta_{\sigma\downarrow}c_{\uparrow}^{\dagger}(i) - \delta_{\sigma\uparrow}c_{\downarrow}^{\dagger}(i)\right) \\ \left[\xi_{\sigma}(i), p^{\dagger}(j)\right] = \delta_{ij}\left(\delta_{\sigma\downarrow}\eta_{\uparrow}^{\dagger}(i) - \delta_{\sigma\uparrow}\eta_{\downarrow}^{\dagger}(j)\right) \\ \left[\eta_{\sigma}(i), p^{\dagger}(j)\right] = \delta_{ij}\left(\delta_{\sigma\downarrow}\xi_{\uparrow}^{\dagger}(i) - \delta_{\sigma\uparrow}\xi_{\downarrow}^{\dagger}(j)\right) \end{cases} , \tag{B.160}$$

$N^{(1)}(i)$ and $N^{(2)}(i)$ are defined as follows:

$$N^{(1)}(i) \equiv \left\{\psi(i), c_{\uparrow}(i)\right\} = \begin{pmatrix} 0 \\ 0 \\ -p(i) \\ p(i) \end{pmatrix} \ , \ N^{(2)}(i) \equiv \left[\psi(i), p^{\dagger}(i)\right] = \begin{pmatrix} -\eta_{\downarrow}^{\dagger}(i) \\ -\xi_{\downarrow}^{\dagger}(i) \\ \eta_{\uparrow}^{\dagger}(i) \\ \xi_{\uparrow}^{\dagger}(i) \end{pmatrix} . \tag{B.161}$$

We can now consider that for the causal single-particle propagator we have:

$$\hat{\Lambda}_{ac}G_{cb}^{C}(i,j) = i\delta(t_i - t_j)\delta_{\boldsymbol{ij}}I_{ab} \ \Rightarrow i\delta(t_i - t_j)\delta_{\boldsymbol{ij}} = \hat{\Lambda}_{ac}G_{cb}^{C}(i,j)I_{ba}^{-1} \ , \tag{B.162}$$

then the equation of motion of $X_a(i,l,j)$ can be written as:

$$\begin{aligned}
\Lambda_{ab}X_b(i,l,j) &= \Lambda_{ab}G^C_{bc}(i,l)I^{-1}_{cd}\left\langle \mathcal{T}\left[N^{(1)}_d(i)p^\dagger(j)\right]\right\rangle \\
&\quad +\Lambda_{ab}G^C_{bc}(i,j)I^{-1}_{cd}\left\langle \mathcal{T}\left[c_\uparrow(l)N^{(2)}_d(j)\right]\right\rangle = \qquad \text{(B.163)}\\
&= \Lambda_{ab}G^C_{bc}(i,l)I^{-1}_{cc}\left\langle \mathcal{T}\left[N^{(1)}_c(i)p^\dagger(j)\right]\right\rangle \qquad \text{(B.164)}\\
&\quad +\Lambda_{ab}G^C_{bc}(i,j)I^{-1}_{cc}\left\langle \mathcal{T}\left[c_\uparrow(l)N^{(2)}_c(j)\right]\right\rangle \qquad \text{(B.165)}
\end{aligned}$$

in which we have taken into account the diagonal form of the normalization matrix. In the limit $l \to i^-$, taking the sum over a, we have:

$$\begin{aligned}
P(i,j) &= \sum_{a=3}^{4}\lim_{l\to i^-} X_a(i,l,j) = \\
&= \left(\frac{G^C_{34}(i,i^-)+G^C_{44}(i,i^-)}{I_{44}} - \frac{G^C_{33}(i,i^-)+G^C_{43}(i,i^-)}{I_{33}}\right)P(i,j) \qquad \text{(B.166)}\\
&\quad +\sum_{a=3}^{4}G^C_{ab}(i,j)I^{-1}_{bb}\left\langle \mathcal{T}\left[c_\uparrow(i^-)N^{(2)}_b(j)\right]\right\rangle = \qquad \text{(B.167)}
\end{aligned}$$

then the pair correlator can be written as follows:

$$P(i,j) = A(i)B(i,j)\ ,\ \begin{cases} A(i) \equiv \frac{I_{33}I_{44}}{I_{33}I_{44}+I_{44}\left[G^C_{33}(i,i^-)+G^C_{43}(i,i^-)\right]-I_{33}\left[G^C_{34}(i,i^-)+G^C_{44}(i,i^-)\right]} \\ B(i,j) \equiv \sum_{a=3}^{4}G^C_{ab}(i,j)I^{-1}_{bb}\left\langle \mathcal{T}\left[c_\uparrow(i^-)N^{(2)}_b(j)\right]\right\rangle \end{cases} . \qquad \text{(B.168)}$$

Recalling that $G^C_{ab}(i,i^-) = \left\langle T\left[\psi_a(i)\psi^\dagger_b(i^-)\right]\right\rangle = \left\langle \psi^\dagger_b(i^-)\psi_a(i)\right\rangle$, the calculation of $A(i)$, according to the following relations:

$$\begin{array}{lll}
\left\langle \xi^\dagger_\sigma(i)\xi_{\sigma'}(i)\right\rangle = \delta_{\sigma\sigma'}\left(\frac{n}{2}-D\right) & , & \left\langle \xi_\sigma(i)\xi^\dagger_{\sigma'}(i)\right\rangle = \delta_{\sigma\sigma'}\left(1-n+D\right) \\
\left\langle \eta^\dagger_\sigma(i)\eta_{\sigma'}(i)\right\rangle = \delta_{\sigma\sigma'}D & , & \left\langle \eta_\sigma(i)\eta^\dagger_{\sigma'}(i)\right\rangle = \delta_{\sigma\sigma'}\left(\frac{n}{2}-D\right) \\
\left\langle \eta^\dagger_\sigma(i)\xi_{\sigma'}(i)\right\rangle = 0 & , & \left\langle \xi_\sigma(i)\eta^\dagger_{\sigma'}(i)\right\rangle = 0
\end{array} \quad , \qquad \text{(B.169)}$$

gives:

$$\begin{aligned}
A(i) &= \frac{I_{33}I_{44}}{I_{33}I_{44}+I_{44}G^C_{33}(i,i^-)-I_{33}G^C_{44}(i,i^-)} = \\
&= \frac{n(2-n)/4}{\frac{n(2-n)}{4}+\frac{n(n-2D)}{4}-\frac{2(2-n)D}{4}} = \frac{n(2-n)}{2(n-2D)}\ . \qquad \text{(B.170)}
\end{aligned}$$

For the $B(i,j)$ contribution we have instead:

$$\begin{aligned}
B(i,j) &= \frac{G^C_{33}(i,j)+G^C_{43}(i,j)}{I_{33}}\left\langle \mathcal{T}\left[c_\uparrow(i^-)\eta^\dagger_\uparrow(i)\right]\right\rangle \\
&\quad +\frac{G^C_{43}(i,j)+G^C_{44}(i,j)}{I_{44}}\left\langle \mathcal{T}\left[c_\uparrow(i^-)\xi^\dagger_\uparrow(i)\right]\right\rangle = \qquad \text{(B.171)}
\end{aligned}$$

$$= \frac{I_{33}+I_{44}}{I_{33}I_{44}}\left(G_{11}^{(C)}(i,j)+G_{21}^{C}(i,j)\right)\left(G_{12}^{(C)}(i,j)+G_{22}^{C}(i,j)\right) =$$
$$= \frac{4}{n(2-n)}\left(G_{11}^{(C)}(i,j)+G_{21}^{C}(i,j)\right)\left(G_{12}^{(C)}(i,j)+G_{22}^{C}(i,j)\right) . \quad \text{(B.172)}$$

Finally, by substituting in the expression of $P(i,j)$ we obtain:

$$P(i,j) = \frac{n(2-n)}{2(n-2D)}\frac{4}{n(2-n)}\left(G_{11}^{C}(i,j)+G_{12}^{C}(i,j)\right)\left(G_{12}^{C}(i,j)+G_{22}^{C}(i,j)\right) =$$
$$= \frac{1}{n/2-D}\sum_{a,b=1}^{2} Q_{1ab2}^{C}(i,j) , \quad \text{(B.173)}$$

where the correlator $Q_{abcd}(i,j) \equiv G_{ab}(i,j)G_{cd}(j,i)$ reproduces the fermionic loop defined in Eq.B.132.

Appendix C

Detailed calculations for the three-pole approximation scheme

We report in this Appendix detailed calculations for the three-pole approximation scheme to the single band Hubbard model described in Chapter 5. In particular, we focus our attention on two approximated techniques, namely the decoupling and the projection methods, as possible tools for the estimation of the internal parameter f_s:

$$f_s = \frac{1}{3} \left\langle \sigma_k n_k^{\alpha}(i) c(i) c^{\alpha\dagger}(i) \right\rangle \ , \tag{C.1}$$

which contains in principle both two-site and three-site correlators. Before applying any approximation, it is worth separating from the above expression all the possible two-site contributions of the type $\left\langle \varphi^{\dagger}_{1,\sigma_1}(i) \varphi^{\kappa}_{2,\sigma_2}(i) \right\rangle$, being κ a generic projector and both $\varphi_{1,\sigma_1}(i)$ and $\varphi_{2,\sigma_2}(i)$ fields of the basis, which, as reported in Chapter 2, can be calculated self-consistently as two-site correlation functions $C^{\kappa}_{\varphi_1\varphi_2}$ and therefore do not need to be approximated. To this purpose, recalling the properties of the nearest neighbour projector $\alpha_{\boldsymbol{ij}}$, we note that the two non-local operators $n_k^{\alpha}(i)$ and $c^{\alpha\dagger}(i)$ can act at distance δ, β or η among each other, always remaining at distance α from the site $\boldsymbol{i}$. Therefore, starting from Eq.C.1, we can rewrite f_s as:

$$f_s = f_s|^{2site} + \frac{2(d-1)}{2d} \, f_s|^{(\beta)} + \frac{1}{2d} \, f_s|^{(\eta)} \ , \tag{C.2}$$

where the $f_s|^{2site}$ is the two-site contribution:

$$f_s|^{2site} \equiv \frac{1}{6d} \, (\sigma_k)_{\uparrow\mu} \left\langle c_{\mu}(i) \left[c^{\dagger}_{\rho}(i) \, (\sigma_k)_{\rho\lambda} \, c_{\lambda}(i) c^{\dagger}_{\uparrow}(i) \right]^{\alpha} \right\rangle \ , \tag{C.3}$$

and:

$$f_s|^{(\kappa)} \equiv \frac{1}{3} \left\langle \sigma_k \overline{n_k^{\alpha(\kappa)}}(i) c(i) c^{\overline{\alpha}\dagger}(i) \right\rangle \ , \ \kappa = (\beta, \eta) \ . \tag{C.4}$$

Here the bar over the projectors reminds that the two operators act at distance α from $\boldsymbol{i}$ but at distance $\kappa = (\beta, \eta)$ among each other. A trivial application the

canonical anticommutation rules gives:

$$
\begin{aligned}
f_s|^{2site} &\equiv \frac{1}{6d}(\sigma_k)_{\uparrow\mu}\left\langle c_\mu(i)\left[c^\dagger_\rho(i)(\sigma_k)_{\rho\lambda}c_\lambda(i)c^\dagger_\uparrow(i)\right]^\alpha\right\rangle = \\
&= \frac{1}{6d}(\sigma_k)_{\uparrow\mu}(\sigma_k)_{\rho\lambda}\left\langle c_\mu(i)\left[\left(\delta_{\rho\lambda}-c_\lambda(i)c^\dagger_\rho(i)\right)c^\dagger_\uparrow(i)\right]^\alpha\right\rangle = \\
&= \frac{1}{6d}(\sigma_k)_{\uparrow\uparrow}(\sigma_k)_{\rho\rho}\left\langle c_\uparrow(i)c^{\alpha\dagger}_\uparrow(i)\right\rangle - \frac{1}{6d}(\sigma_k)_{\uparrow\downarrow}(\sigma_k)_{\downarrow\uparrow}\left\langle c_\downarrow(i)\left[c_\uparrow(i)c^\dagger_\downarrow(i)c^\dagger_\uparrow(i)\right]^\alpha\right\rangle \\
&\quad -\frac{1}{6d}(\sigma_k)_{\uparrow\uparrow}(\sigma_k)_{\downarrow\downarrow}\left\langle c_\uparrow(i)\left[c_\downarrow(i)c^\dagger_\downarrow(i)c^\dagger_\uparrow(i)\right]^\alpha\right\rangle = \\
&= \frac{1}{3d}\left\langle c_\downarrow(i)\xi^{\alpha\dagger}_\downarrow(i)\right\rangle + \frac{1}{6d}\left\langle c_\uparrow(i)\xi^{\alpha\dagger}_\uparrow(i)\right\rangle = \frac{1}{2d}C^\alpha_{c\xi}\,, \qquad \text{(C.5)}
\end{aligned}
$$

therefore we can express f_s as:

$$
f_s = \frac{1}{2d}C^\alpha_{c\xi} + \frac{2(d-1)}{2d}\,f_s|^{(\beta)} + \frac{1}{2d}\,f_s|^{(\eta)}\,, \qquad \text{(C.6)}
$$

where now $f_s|^{(\beta)}$ and $f_s|^{(\eta)}$ represent the three-site contributions of the starting correlators f_s which can only be calculated by means of approximated approaches. We report in the following Sections detailed calculations of the aforementioned quantities obtained by using the decoupling and the projection methods.

C.1 Decoupling method

The approximation named "*decoupling*" (DC) consists in approximating an unknown correlator as the product of all the possible couples of fermionic operators contained in its expression. In doing this, it is convenient to rewrite f_s as follows:

$$
f_s \approx f_s|_{DC} + \left[f_s|^{2site} - f_s|^{2site}_{DC}\right]\,, \qquad \text{(C.7)}
$$

where $f_s|_{DC}$ is the decoupling of the whole correlator f_s (without preserving its two-site component $f_s|^{2site}$) and $f_s|^{2site}_{DC}$ is the approximated expression of its 2-site component only. Then, following the decoupling prescription, for a paramagnetic and homogeneous system we obtain:

$$
\begin{aligned}
f_s|_{DC} &= \frac{1}{3}(\sigma_k)_{\uparrow\mu}\left\langle\left[c^\dagger_\rho(i)(\sigma_k)_{\rho\lambda}c_\lambda(i)\right]^\alpha c_\mu(i)c^{\alpha\dagger}_\uparrow(i)\right\rangle_{DC} = && \text{(C.8)}\\
&= \frac{1}{6}(\sigma_k)_{\gamma\mu}(\sigma_k)_{\rho\lambda}\left\langle c^\dagger_\rho(i)c_\lambda(i)\right\rangle\left\langle c_\mu(i)c^{\alpha\dagger}_\gamma(i)\right\rangle && \text{(C.9)}\\
&\quad -\frac{1}{6}(\sigma_k)_{\gamma\mu}(\sigma_k)_{\rho\lambda}\left\langle c^{\alpha\dagger}_\rho(i)c_\mu(i)\right\rangle\left\langle c^\alpha_\lambda(i)c^{\alpha\dagger}_\gamma(i)\right\rangle = && \text{(C.10)}\\
&= \frac{1}{6}\frac{n}{2}C^\alpha_{cc}(\sigma_k)_{\gamma\gamma}(\sigma_k)_{\lambda\lambda} + \frac{1}{6}(\sigma_k)_{\gamma\rho}(\sigma_k)_{\rho\gamma}C^\alpha_{cc}C^{\alpha^2}_{cc} = && \text{(C.11)}\\
&= C^\alpha_{cc}C^{\alpha^2}_{cc}\,, && \text{(C.12)}
\end{aligned}
$$

and:

$$\begin{aligned} f_s|_{DC}^{2site} &= \frac{1}{6d}\left(\sigma_k\right)_{\uparrow\mu}\left\langle c_\mu(i)\left[c_\rho^\dagger(i)\left(\sigma_k\right)_{\rho\lambda}c_\lambda(i)c_\uparrow^\dagger(i)\right]^\alpha\right\rangle_{DC} = \\ &= \frac{1}{6d}\left(\sigma_k\right)_{\uparrow\rho}\left(\sigma_k\right)_{\rho\uparrow}\left\langle c_\rho(i)c_\rho^{\alpha\dagger}(i)\right\rangle\left\langle c_\uparrow(i)c_\uparrow^\dagger(i)\right\rangle \\ &\quad +\frac{1}{6d}\left(\sigma_k\right)_{\uparrow\uparrow}\left(\sigma_k\right)_{\rho\rho}\left\langle c_\uparrow(i)c_\uparrow^{\alpha\dagger}(i)\right\rangle\left\langle c_\uparrow^\dagger(i)c_\uparrow(i)\right\rangle = \\ &= \frac{1}{2d}\left(1-\frac{n}{2}\right)C_{cc}^\alpha\,, \end{aligned} \tag{C.13}$$

which give:

$$f_s \approx C_{cc}^\alpha C_{cc}^{\alpha^2} + \left[\frac{1}{2d}C_{c\xi}^\alpha - \frac{1}{2d}\left(1-\frac{n}{2}\right)C_{cc}^\alpha\right]. \tag{C.14}$$

C.2 Projection method

With the aim of improving the decoupling approximation scheme, an alternative method to approximate the three-site contributions (C.4) consists in preserving one of the fields of the starting correlators and then projecting the remaining part with respect to the fields of the basis. We recall that the projection of a generic field $\varphi(i)$ with respect to a N-field basis $\{\psi_i(j)\}_N$ reads as:

$$\varphi_\sigma(i) \approx \sum_{l=1}^{N}\sum_{j,\sigma'}\frac{\left\langle\left\{\varphi_\sigma(i),\psi_{l,\sigma'}^\dagger(j)\right\}\right\rangle}{\left\langle\left\{\psi_{l,\sigma}(i),\psi_{l,\sigma'}^\dagger(j)\right\}\right\rangle}\psi_{l,\sigma'}(j)\,, \tag{C.15}$$

where the sum over $l \in \{1, N\}$ runs over all the fields of the basis, σ' includes spin degrees of freedom while j accounts for all the possible distances (e.g. on-site, nearest-neighbour, next nearest neighbour contributions and so on) between operators in the averages.

Following this prescription, with the aim of projecting the three-site correlator f_s it is convenient to introduce the following composite field:

$$\psi_\sigma^\mu(i) \equiv \left(\sigma_\mu\right)_{\sigma\gamma} n_\mu^\alpha(i)c_\gamma(i)\,, \tag{C.16}$$

with no sum over μ in the right hand side, so that:

$$f_s \equiv \frac{1}{3}\sum_{k=1}^{3}\left\langle\psi_\uparrow^k(i)c_\uparrow^{\alpha\dagger}(i)\right\rangle\,. \tag{C.17}$$

Then, by projecting $\psi_\mu(i)$ with respect to the two-pole basis $\{\phi\}_n = \{\xi(i), \eta(i)\}$, recalling that:

$$\{b_1 f_1, f_2\} = b_1\{f_1, f_2\} - [b_1, f_2]\, f_1\,, \tag{C.18}$$

we obtain:

$$\begin{aligned}
\left\langle \left\{ \psi_\gamma^0(i), \xi_\rho^\dagger(j) \right\} \right\rangle &= \left\langle \left\{ n^\alpha(i) c_\gamma(i), \xi_\rho^\dagger(j) \right\} \right\rangle = \\
&= \left\langle n^\alpha(i) \left\{ c_\gamma(i), \xi_\rho^\dagger(j) \right\} \right\rangle - \sum_m \alpha_{im} \left\langle \left[n(m), \xi_\rho^\dagger(j) \right] c_\gamma(i) \right\rangle = \\
&= \delta_{ij} \left\langle n^\alpha(i) \left(\delta_{\gamma\rho} + \frac{1}{2} \left(\sigma^\mu \right)_{\gamma\rho} n_\mu(i) \right) \right\rangle - \alpha_{ij} \left\langle \xi_\rho^\dagger(j) c_\gamma(i) \right\rangle = \\
&= \delta_{\gamma\rho} \left[\delta_{ij} \left(n - \frac{1}{2} \left\langle n^\alpha(i) n(i) \right\rangle \right) + \alpha_{ij} C_{c\xi}^\alpha \right] , \qquad \text{(C.19)}
\end{aligned}$$

$$\begin{aligned}
\left\langle \left\{ \psi_\gamma^0(i), \eta_\rho^\dagger(j) \right\} \right\rangle &= \left\langle \left\{ n^\alpha(i) c_\gamma(i), \eta_\rho^\dagger(j) \right\} \right\rangle = \\
&= \left\langle n^\alpha(i) \left\{ c_\gamma(i), \eta_\rho^\dagger(j) \right\} \right\rangle - \sum_m \alpha_{im} \left\langle \left[n(m), \eta_\rho^\dagger(j) \right] c_\gamma(i) \right\rangle = \\
&= -\delta_{ij} \left\langle n^\alpha(i) \left(\frac{1}{2} \left(\sigma^\mu \right)_{\gamma\rho} n_\mu(i) \right) \right\rangle - \alpha_{ij} \left\langle \eta_\rho^\dagger(j) c_\gamma(i) \right\rangle = \\
&= \delta_{\gamma\rho} \left[\delta_{ij} \frac{1}{2} \left\langle n^\alpha(i) n(i) \right\rangle + \alpha_{ij} C_{c\eta}^\alpha \right] , \qquad \text{(C.20)}
\end{aligned}$$

$$\begin{aligned}
\left\langle \left\{ \psi_\gamma^k(i), \xi_\rho^\dagger(j) \right\} \right\rangle &= \left(\sigma_k \right)_{\gamma\lambda} \left\langle \left\{ n_k^\alpha(i) c_\lambda(i), \xi_\rho^\dagger(j) \right\} \right\rangle = \left(\sigma_k \right)_{\gamma\lambda} \left\langle n_k^\alpha(i) \left\{ c_\lambda(i), \xi_\rho^\dagger(j) \right\} \right\rangle \\
&\quad - \sum_m \alpha_{im} \left(\sigma_k \right)_{\gamma\lambda} \left\langle \left[n_k(m), \xi_\rho^\dagger(j) \right] c_\lambda(i) \right\rangle = \\
&= \delta_{ij} \left(\sigma_k \right)_{\gamma\lambda} \left\langle n_k^\alpha(i) \left(\delta_{\lambda\rho} + \frac{1}{2} \left(\sigma^\mu \right)_{\lambda\rho} n_\mu(i) \right) \right\rangle \\
&\quad - \alpha_{ij} \left(\sigma_k \right)_{\gamma\lambda} \left(\sigma_k \right)_{\sigma\rho} \left\langle \xi_\sigma^\dagger(j) c_\lambda(i) \right\rangle = \\
&= \delta_{\gamma\rho} \left[\delta_{ij} \left(\frac{1}{2} \left\langle n_k^\alpha(i) n_k(i) \right\rangle \right) + \alpha_{ij} C_{c\xi}^\alpha \right] . \qquad \text{(C.21)}
\end{aligned}$$

$$\begin{aligned}
\left\langle \left\{ \psi_\gamma^k(i), \eta_\rho^\dagger(j) \right\} \right\rangle &= \left(\sigma_k \right)_{\gamma\lambda} \left\langle \left\{ n_k^\alpha(i) c_\lambda(i), \eta_\rho^\dagger(j) \right\} \right\rangle = \left(\sigma_k \right)_{\gamma\lambda} \left\langle n_k^\alpha(i) \left\{ c_\lambda(i), \eta_\rho^\dagger(j) \right\} \right\rangle \\
&\quad - \sum_m \alpha_{im} \left(\sigma_k \right)_{\gamma\lambda} \left\langle \left[n_k(m), \eta_\rho^\dagger(j) \right] c_\lambda(i) \right\rangle = \\
&= -\delta_{ij} \left(\sigma_k \right)_{\gamma\lambda} \left\langle n_k^\alpha(i) \left(\frac{1}{2} \left(\sigma^\mu \right)_{\lambda\rho} n_\mu(i) \right) \right\rangle \\
&\quad - \alpha_{ij} \left(\sigma_k \right)_{\gamma\lambda} \left(\sigma_k \right)_{\sigma\rho} \left\langle \eta_\sigma^\dagger(j) c_\lambda(i) \right\rangle = \\
&= \delta_{\gamma\rho} \left[\delta_{ij} \left(-\frac{1}{2} \left\langle n_k^\alpha(i) n_k(i) \right\rangle \right) + \alpha_{ij} C_{c\eta}^\alpha \right] . \qquad \text{(C.22)}
\end{aligned}$$

Hence the projection of $\psi_\sigma^\mu(i)$ reads as:

$$\psi_\uparrow^0(i) \approx \frac{1}{I_{11}} \left[\left(n - \frac{1}{2} \chi_0^\alpha \right) \xi_\uparrow(i) + C_{c\xi}^\alpha \xi_\uparrow^\alpha(i) \right] + \frac{1}{I_{22}} \left[\frac{1}{2} \chi_0^\alpha \eta_\uparrow(i) + C_{c\eta}^\alpha \eta_\uparrow^\alpha(i) \right] \qquad \text{(C.23)}$$

$$\begin{aligned}\psi^k_\uparrow(i) &\approx \frac{1}{I_{11}}\left[\frac{1}{2}\left\langle n^\alpha_k(i)n_k(i)\right\rangle \xi_\uparrow(i) + C^\alpha_{c\xi}\xi^\alpha_\uparrow(i)\right] \\ &+\frac{1}{I_{22}}\left[-\frac{1}{2}\left\langle n^\alpha_k(i)n_k(i)\right\rangle \eta_\uparrow(i) + C^\alpha_{c\eta}\eta^\alpha_\uparrow(i)\right] ,\end{aligned} \tag{C.24}$$

which immediately gives:

$$\begin{aligned}f_s|^{(\kappa)} &\approx \frac{1}{I_{11}}\left[\frac{1}{2}\chi^\alpha_s\left\langle \xi_\uparrow(i)c^{\alpha\dagger}_\uparrow(i)\right\rangle + C^\alpha_{c\xi}\left\langle \overline{\xi^{\alpha(\kappa)}_\uparrow}(i)c^{\alpha\dagger}_\uparrow(i)\right\rangle\right] \\ &+\frac{1}{I_{22}}\left[\frac{1}{2}\chi^\alpha_s\left\langle \xi_\uparrow(i)c^{\alpha\dagger}_\uparrow(i)\right\rangle + C^\alpha_{c\xi}\left\langle \overline{\xi^{\alpha(\kappa)}_\uparrow}(i)c^{\alpha\dagger}_\uparrow(i)\right\rangle\right] = \\ &= \frac{1}{I_{11}}\left[\frac{1}{2}\chi^\alpha_s C^\alpha_{c\xi} + C^\alpha_{c\xi}C^\kappa_{c\xi}\right] + \frac{1}{I_{22}}\left[-\frac{1}{2}\chi^\alpha_s C^\alpha_{c\eta} + C^\alpha_{c\eta}C^\kappa_{c\eta}\right] .\end{aligned} \tag{C.25}$$

Finally, according with Eq.C.6 we obtain:

$$\begin{aligned}f_s &\approx \frac{1}{2d}C^\alpha_{c\xi} + \frac{2d-1}{2d}\left[\frac{1}{2}\chi^\alpha_s\left(\frac{C^\alpha_{c\xi}}{I_{11}} - \frac{C^\alpha_{c\eta}}{I_{22}}\right)\right] \\ &+\frac{2d-1}{2d}\left[\frac{C^\alpha_{c\xi}}{I_{11}}\overline{C^{(\beta\eta)}_{c\xi}} + \frac{C^\alpha_{c\eta}}{I_{22}}\overline{C^{(\beta\eta)}_{c\eta}}\right] ,\end{aligned} \tag{C.26}$$

where we have used the assumption: $C^\beta_{c\psi} \approx C^\eta_{c\psi} \equiv \overline{C^{(\beta\eta)}_{c\psi}}$ for any $\psi \in \{\xi, \eta\}$, where $\overline{C^{(\beta\eta)}_{c\psi}}$ can be easily calculated recalling that:

$$\begin{aligned}C^{\alpha^2}_{c\psi} &= \frac{1}{2d}C^\delta_{c\psi} + \frac{2(d-1)}{2d}C^\beta_{c\psi} + \frac{1}{2d}C^\eta_{c\psi} = \\ &\approx \frac{1}{2d}C^\delta_{c\psi} + \frac{2d-1}{2d}\overline{C^{(\beta\eta)}_{c\psi}} .\end{aligned} \tag{C.27}$$

with $C^\delta_{c\xi} = 1 - n + D$, and $C^\delta_{c\eta} = n/2 - D$. Summarizing, the projections of the three-site correlator f_s reads as:

$$\begin{aligned}f_s &\approx \frac{1}{2d}C^\alpha_{c\xi} + \frac{2d-1}{2d}\left[\frac{1}{2}\chi^\alpha_s\left(\frac{C^\alpha_{c\xi}}{I_{11}} - \frac{C^\alpha_{c\eta}}{I_{22}}\right)\right] \\ &+\frac{C^\alpha_{c\xi}}{I_{11}}\left(C^{\alpha^2}_{c\xi} - \frac{1}{2d}C^\delta_{c\xi}\right) + \frac{C^\alpha_{c\eta}}{I_{22}}\left(C^{\alpha^2}_{c\eta} - \frac{1}{2d}C^\delta_{c\eta}\right) .\end{aligned} \tag{C.28}$$

Appendix D

Operatorial relations among polaronic and spin operators

In this Appendix are reported some useful operatorial relations among X_i and spin operators.

D.1 Relations involving X_i

Let us introduce the quantity:

$$X_i \equiv \exp\left[\sum_{\boldsymbol{q}} \left(u(\boldsymbol{m},\boldsymbol{q})d_q - u^*(\boldsymbol{m},\boldsymbol{q})d_q^\dagger\right)\right] , \tag{D.1}$$

where $u(\boldsymbol{m},\boldsymbol{q})$ is defined by 8.2. By means of the following operatorial identity:

$$e^{\hat{A}+\hat{B}} = a^{\hat{A}} e^{\hat{B}} e^{-\frac{1}{2}\left[\hat{A},\hat{B}\right]} , \tag{D.2}$$

it is straightforward to see that (we recall that $\left[d_q^\dagger, d_p\right] = -\delta_{pq}$ and $\left[d_q^\dagger, d_p^\dagger\right] = [d_q, d_p] = 0$):

$$\begin{aligned}
X_i^\dagger X_j &= \exp\left[\sum_{\boldsymbol{q}} \left(u^*(\boldsymbol{m},\boldsymbol{q})d_q^\dagger - u(\boldsymbol{m},\boldsymbol{q})d_q\right)\right] \exp\left[\sum_{\boldsymbol{q'}} \left(u(\boldsymbol{n},\boldsymbol{q'})d_{q'} - u^*(\boldsymbol{n},\boldsymbol{q'})d_{q'}^\dagger\right)\right] = \\
&= \exp\left[\sum_{\boldsymbol{q}} \left(u^*(\boldsymbol{m},\boldsymbol{q})d_q^\dagger - u(\boldsymbol{m},\boldsymbol{q})d_q + u(\boldsymbol{n},\boldsymbol{q})d_q - u^*(\boldsymbol{n},\boldsymbol{q})d_q^\dagger\right)\right] \cdot \\
&\quad \cdot \exp\left[\frac{1}{2}\sum_{\boldsymbol{q}} \left[u(\boldsymbol{m},\boldsymbol{q})u^*(\boldsymbol{n},\boldsymbol{q}) - u^*(\boldsymbol{m},\boldsymbol{q})u(\boldsymbol{n},\boldsymbol{q})\right]\right] = \\
&= \exp\left[\sum_{\boldsymbol{q}} \left(\alpha_{m,n}^*(\boldsymbol{q})d_q^\dagger - \alpha_{m,n}(\boldsymbol{q})d_q\right)\right]
\end{aligned}$$

$$\exp\left[\frac{1}{2}\sum_{\boldsymbol{q}}\left[u(\boldsymbol{m},\boldsymbol{q})u^*(\boldsymbol{n},\boldsymbol{q})-u^*(\boldsymbol{m},\boldsymbol{q})u(\boldsymbol{n},\boldsymbol{q})\right]\right]\ , \tag{D.3}$$

where α is defined as:

$$\alpha_{m,n}(\boldsymbol{q}) \equiv u(\boldsymbol{m},\boldsymbol{q}) - u(\boldsymbol{n},\boldsymbol{q})\ . \tag{D.4}$$

On the same way, applying again D.2 we get:

$$\begin{aligned} X_i^\dagger X_j &= \exp\left[\sum_{\boldsymbol{q}}\left(\alpha^*_{m,n}(\boldsymbol{q})d_q^\dagger - \alpha_{m,n}(\boldsymbol{q})d_q\right)\right] \\ &\quad \exp\left[\frac{1}{2}\sum_{\boldsymbol{q}}\left[u(\boldsymbol{m},\boldsymbol{q})u^*(\boldsymbol{n},\boldsymbol{q})-u^*(\boldsymbol{m},\boldsymbol{q})u(\boldsymbol{n},\boldsymbol{q})\right]\right] = \\ &= \exp\left[\sum_{\boldsymbol{q}}\alpha^*_{m,n}(\boldsymbol{q})d_q^\dagger\right]\exp\left[-\sum_{\boldsymbol{q}}\alpha_{m,n}(\boldsymbol{q})d_q\right]\exp\left[-\frac{1}{2}\sum_{\boldsymbol{q}}|\alpha_{m,n}(\boldsymbol{q})|^2\right]\cdot \\ &\quad \cdot\exp\left[\frac{1}{2}\sum_{\boldsymbol{q}}\left[u(\boldsymbol{m},\boldsymbol{q})u^*(\boldsymbol{n},\boldsymbol{q})-u^*(\boldsymbol{m},\boldsymbol{q})u(\boldsymbol{n},\boldsymbol{q})\right]\right]\ . \end{aligned} \tag{D.5}$$

D.1.1 $\langle \hat{X}_i^\dagger \hat{X}_j \rangle$ average

It is instructive to calculate the quantum statistical average of $\hat{X}_i^\dagger \hat{X}_j$ operator since it represent the operatorial part of the renormalized hopping parameter and determines the polaron bandwidth. In this case we will overlook constant terms in (D.5) and focus our analysis only on the operatorial part. Quantum statistical averages are calculated by expanding the exponents in the trace as follows:

$$\langle e^{\alpha_q^* d^\dagger} e^{-\alpha_q d}\rangle = \frac{1}{\mathcal{Z}_{ph}}\sum_{N=0}^{\infty}\sum_{n=0}^{N} p^N(-1)^n\frac{|\alpha_q|^{2n}}{(n!)^2}N(N-1)\times\cdots\times(N-n+1)\ , \tag{D.6}$$

where $p \equiv e^{-\omega_q/T}$ and we have dropped phonon and site quantum numbers for transparency. Here the single-mode phonon partition function is:

$$\mathcal{Z}_{ph} \equiv \frac{1}{1-p} = \frac{1}{1-e^{-\omega_q/T}}\ . \tag{D.7}$$

It can be seen [10] that the quantum statistical average can be also written in the form:

$$\langle e^{\alpha_q^* d^\dagger} e^{-\alpha_q d}\rangle = (1-p)\sum_{n=0}^{N}(-1)^n\frac{|\alpha_q|^{2n}}{(n!)^2}p^n\frac{d^n}{dp^n}\sum_{M=0}^{\infty}p^M\ , \tag{D.8}$$

so, recalling that:

$$\sum_{M=0}^{M} p^M = \frac{1}{1-p}\ , \tag{D.9}$$

and differentiating it n-times yields $n!$ in the numerator after which we have:

$$\langle e^{\alpha_q^* d^\dagger} e^{-\alpha_q d} \rangle = \sum_{n=0}^{\infty} (-1)^n \frac{|\alpha_q|^{2n}}{(n!)} p^n = e^{-|\alpha_q|^2 n_\omega} \ , \tag{D.10}$$

where n_ω is the Bose-Einstein distribution function of phonons:

$$n_\omega \equiv \frac{1}{e^{\omega_q/T} - 1} \ . \tag{D.11}$$

Collecting together all the multipliers from equation (D.5) we get:

$$\begin{aligned} \langle \hat{X}_i^\dagger \hat{X}_j \rangle &= \exp\Bigg\{ \frac{1}{2} \sum_{\boldsymbol{q}} \Big[-|\alpha_{m,n}(\boldsymbol{q})|^2 \left(1 + 2n_\omega\right) & \text{(D.12)} \\ &\quad + u(\boldsymbol{m},\boldsymbol{q}) u^*(\boldsymbol{n},\boldsymbol{q}) - u^*(\boldsymbol{m},\boldsymbol{q}) u(\boldsymbol{n},\boldsymbol{q}) \Big] \Bigg\} . & \text{(D.13)} \end{aligned}$$

Recalling the definition of $\alpha_{m,n}(\boldsymbol{q})$ D.4 we get:

$$\begin{aligned} \langle \hat{X}_i^\dagger \hat{X}_j \rangle &= \prod_q \exp\Bigg\{ \frac{1}{2} \Big[\cancel{u^*(\boldsymbol{m},\boldsymbol{q}) u(\boldsymbol{n},\boldsymbol{q})} + 2u(\boldsymbol{m},\boldsymbol{q}) u^*(\boldsymbol{n},\boldsymbol{q}) - \cancel{u^*(\boldsymbol{m},\boldsymbol{q}) u(\boldsymbol{n},\boldsymbol{q})} \\ &\quad - |u(\boldsymbol{m},\boldsymbol{q})|^2 - |u(\boldsymbol{n},\boldsymbol{q})|^2 \Big] - n_\omega \Big[|u(\boldsymbol{m},\boldsymbol{q})|^2 + |u(\boldsymbol{n},\boldsymbol{q})|^2 - u^*(\boldsymbol{m},\boldsymbol{q}) u(\boldsymbol{n},\boldsymbol{q}) \\ &\quad - u(\boldsymbol{m},\boldsymbol{q}) u^*(\boldsymbol{n},\boldsymbol{q}) \Big] \Bigg\} = & \text{(D.14)} \\ &= \prod_q \exp\Bigg\{ -\frac{\gamma(q)^2}{2N} \left[1 - \cos\left(\boldsymbol{q} \cdot (\boldsymbol{m} - \boldsymbol{n})\right) - i \sin\left(\boldsymbol{q} \cdot (\boldsymbol{m} - \boldsymbol{n})\right) \right] - n_\omega \\ &\quad \Big[|u(\boldsymbol{m},\boldsymbol{q})|^2 + |u(\boldsymbol{n},\boldsymbol{q})|^2 - u^*(\boldsymbol{m},\boldsymbol{q}) u(\boldsymbol{n},\boldsymbol{q}) - u(\boldsymbol{m},\boldsymbol{q}) u^*(\boldsymbol{n},\boldsymbol{q}) \Big] \Bigg\} & \text{(D.15)} \end{aligned}$$

D.1.2 $\langle \hat{X}_i^\dagger(t) \hat{X}_j(t) \hat{X}_i^\dagger \hat{X}_j \rangle$ average

In order to calculate $\langle \hat{X}_i^\dagger(t) \hat{X}_j(t) \hat{X}_i^\dagger \hat{X}_j \rangle$ average it is worth noting that $\hat{X}_i(t)$ and $\hat{X}_{i'}(t)$ commute for any $\gamma(\boldsymbol{q}) = \gamma(-\boldsymbol{q})$ so, according to (D.2) we can write:

$$\hat{X}_i(t) \hat{X}_j(t) = \prod_{\boldsymbol{q}} e^{\left[(u_j(\boldsymbol{q},t) - u_i(\boldsymbol{q},t)) d_{\boldsymbol{q}} - H.c. \right]} \ , \tag{D.16}$$

$$\hat{X}_{i'} \hat{X}_{j'} = \prod_{\boldsymbol{q}} e^{\left[\left(u_{j'}(\boldsymbol{q},t) - u_{i'}(\boldsymbol{q},t) \right) d_{\boldsymbol{q}} - H.c. \right]} \ . \tag{D.17}$$

Applying (D.2) again, the product of the two terms can be written as:

$$\hat{X}_i^\dagger(t)\hat{X}_j(t)\hat{X}_i^\dagger\hat{X}_j = \prod_{\boldsymbol{q}} \exp\left(\beta^* d_{\boldsymbol{q}}^\dagger\right)\exp\left(-\beta d_{\boldsymbol{q}}\right)\exp\left(-\frac{1}{2}|\beta|^2\right) \tag{D.18}$$

$$\exp\left[\frac{1}{2}\left[\left(u_j(\boldsymbol{q},t)-u_i(\boldsymbol{q},t)\right)\left(u_{j'}(\boldsymbol{q},t)-u_{i'}(\boldsymbol{q},t)\right)-H.c.\right]\right], \tag{D.19}$$

where:

$$\beta = u_i(\boldsymbol{q},t) - u_j(\boldsymbol{q},t) + u_{i'}(\boldsymbol{q}) - u_{j'}(\boldsymbol{q})\ . \tag{D.20}$$

Now the average can be done by using Eq.(D.15). Furthermore, recalling that $u_i(\boldsymbol{q},t) \equiv \frac{\gamma(\boldsymbol{q})}{\sqrt{2N}} e^{i(\boldsymbol{q}\cdot\boldsymbol{m}+\hbar\omega_0 t)}$ yields:

$$\langle\langle \hat{X}_i^\dagger(t)\hat{X}_j(t)\hat{X}_i^\dagger\hat{X}_j\rangle\rangle = e^{-g^2(\boldsymbol{m}-\boldsymbol{n})}e^{-g^2(\boldsymbol{m'}-\boldsymbol{n'})}\exp\left\{\sum_{\boldsymbol{q}}\frac{\gamma(\boldsymbol{q})^2}{2N}\right.$$

$$\left. F_{\boldsymbol{q}}(\boldsymbol{m},\boldsymbol{n};\boldsymbol{m'},\boldsymbol{n'})\frac{\cosh\left[\omega_{\boldsymbol{q}}\left(\frac{1}{2T}-it\right)\right]}{\sinh\left[\omega_{\boldsymbol{q}}/2T\right]}\right\}, \tag{D.21}$$

where:

$$F_{\boldsymbol{q}}(\boldsymbol{m},\boldsymbol{n};\boldsymbol{m'},\boldsymbol{n'}) \equiv \cos\left(\boldsymbol{q}\cdot(\boldsymbol{m}-\boldsymbol{n'})\right)+\cos\left(\boldsymbol{q}\cdot(\boldsymbol{n}-\boldsymbol{m'})\right) \tag{D.22}$$

$$-\cos\left(\boldsymbol{q}\cdot(\boldsymbol{m}-\boldsymbol{m'})\right)-\cos\left(\boldsymbol{q}\cdot(\boldsymbol{n}-\boldsymbol{n'})\right)\ . \tag{D.23}$$

D.2 Spin-spin and density-density contributions

As explained in Chapter III, identity (8.67) plays a crucial role in the formulation of the $t-J_p$ Hamiltonian. Hereafter we report a detailed demonstration. Starting from the definition of spin 1/2 operator:

$$\overrightarrow{S}_{\boldsymbol{i}} \equiv \frac{1}{2}c_s^\dagger(\boldsymbol{i})\left(\overrightarrow{\tau}\right)_{s,s'}c_{s'}(\boldsymbol{i})\ , \tag{D.24}$$

and recalling the definitions of the Pauli matrices:

$$\tau_x = \begin{pmatrix} 0 & 1 \\ 1 & 0 \end{pmatrix}\ ,\ \tau_y = \begin{pmatrix} 0 & -i \\ i & 0 \end{pmatrix}\ ,\ \tau_z = \begin{pmatrix} 1 & 0 \\ 0 & -1 \end{pmatrix}\ , \tag{D.25}$$

the standard scalar product $\overrightarrow{S}_{\boldsymbol{m}}\cdot\overrightarrow{S}_{\boldsymbol{n}}$ can be written as:

$$\overrightarrow{S}_{\boldsymbol{m}}\cdot\overrightarrow{S}_{\boldsymbol{n}} = \frac{1}{4}\sum_{s,s'}\left[\left(c_s^\dagger(\boldsymbol{m})\begin{pmatrix} 0 & 1 \\ 1 & 0 \end{pmatrix}_{s,s'}c_{s'}(\boldsymbol{m}) + c_s^\dagger(\boldsymbol{m})\begin{pmatrix} 0 & -i \\ i & 0 \end{pmatrix}_{s,s'}c_{s'}(\boldsymbol{m})\right.\right.$$

$$\left.\left. + c_s^\dagger(\boldsymbol{m})\begin{pmatrix} 1 & 0 \\ 0 & -1 \end{pmatrix}_{s,s'}c_{s'}(\boldsymbol{m})\right)\cdot\left(c_s^\dagger(\boldsymbol{n})\begin{pmatrix} 0 & 1 \\ 1 & 0 \end{pmatrix}_{s,s'}c_{s'}(\boldsymbol{n})\right.\right.$$

$$+c_s^\dagger(\boldsymbol{n})\begin{pmatrix} 0 & -i \\ i & 0 \end{pmatrix}_{s,s'} c_{s'}(\boldsymbol{n}) + c_s^\dagger(\boldsymbol{n})\begin{pmatrix} 1 & 0 \\ 0 & -1 \end{pmatrix}_{s,s'} c_{s'}(\boldsymbol{n})\Bigg)\Bigg] \quad \text{(D.26)}$$

where s, s' are spin indices that run over all the possible spin states: $s, s' = \{\uparrow, \downarrow\}$. Making the sum over all the possible values of s and s' yields:

$$\begin{aligned}\overrightarrow{S}_{\boldsymbol{m}} \cdot \overrightarrow{S}_{\boldsymbol{n}} &= \frac{1}{2}\left[c_\uparrow^\dagger(\boldsymbol{m})c_\downarrow(\boldsymbol{m})c_\downarrow^\dagger(\boldsymbol{n})c_\uparrow(\boldsymbol{n}) + c_\downarrow^\dagger(\boldsymbol{m})c_\uparrow(\boldsymbol{m})c_\uparrow^\dagger(\boldsymbol{n})c_\downarrow(\boldsymbol{n})\right] + \\ &+\frac{1}{4}\Big[c_\uparrow^\dagger(\boldsymbol{m})c_\uparrow(\boldsymbol{m})c_\uparrow^\dagger(\boldsymbol{n})c_\uparrow(\boldsymbol{n}) + c_\downarrow^\dagger(\boldsymbol{m})c_\downarrow(\boldsymbol{m})c_\downarrow^\dagger(\boldsymbol{n})c_\downarrow(\boldsymbol{n}) + \\ &\quad -c_\uparrow^\dagger(\boldsymbol{m})c_\uparrow(\boldsymbol{m})c_\downarrow^\dagger(\boldsymbol{n})c_\downarrow(\boldsymbol{n}) - c_\downarrow^\dagger(\boldsymbol{m})c_\downarrow(\boldsymbol{m})c_\uparrow^\dagger(\boldsymbol{n})c_\uparrow(\boldsymbol{n})\Big] \quad \text{(D.27)}\end{aligned}$$

We can write the previous equation as:

$$\begin{aligned}\overrightarrow{S}_{\boldsymbol{m}} \cdot \overrightarrow{S}_{\boldsymbol{n}} &= \frac{1}{2}\Big[c_\uparrow^\dagger(\boldsymbol{m})c_\downarrow(\boldsymbol{m})c_\downarrow^\dagger(\boldsymbol{n})c_\uparrow(\boldsymbol{n}) + c_\downarrow^\dagger(\boldsymbol{m})c_\uparrow(\boldsymbol{m})c_\uparrow^\dagger(\boldsymbol{n})c_\downarrow(\boldsymbol{n}) + \\ &\quad +c_\uparrow^\dagger(\boldsymbol{m})c_\uparrow(\boldsymbol{m})c_\uparrow^\dagger(\boldsymbol{n})c_\uparrow(\boldsymbol{n}) + c_\downarrow^\dagger(\boldsymbol{m})c_\downarrow(\boldsymbol{m})c_\downarrow^\dagger(\boldsymbol{n})c_\downarrow(\boldsymbol{n})\Big] + \\ &\quad -\frac{1}{4}\Big[c_\uparrow^\dagger(\boldsymbol{m})c_\uparrow(\boldsymbol{m})c_\uparrow^\dagger(\boldsymbol{n})c_\uparrow(\boldsymbol{n}) + c_\downarrow^\dagger(\boldsymbol{m})c_\downarrow(\boldsymbol{m})c_\downarrow^\dagger(\boldsymbol{n})c_\downarrow(\boldsymbol{n}) + \\ &\quad +c_\uparrow^\dagger(\boldsymbol{m})c_\uparrow(\boldsymbol{m})c_\downarrow^\dagger(\boldsymbol{n})c_\downarrow(\boldsymbol{n}) + c_\downarrow^\dagger(\boldsymbol{m})c_\downarrow(\boldsymbol{m})c_\uparrow^\dagger(\boldsymbol{n})c_\uparrow(\boldsymbol{n})\Big] \quad \text{(D.28)}\end{aligned}$$

At this point, recalling the standard definition of the number operator: $n(\boldsymbol{i}) \equiv \sum_s c_s^\dagger(\boldsymbol{i})c_s(\boldsymbol{i})$, it is immediate to see that:

$$\overrightarrow{S}_{\boldsymbol{m}} \cdot \overrightarrow{S}_{\boldsymbol{n}} = \frac{1}{2}\sum_{s,s'} c_s^\dagger(\boldsymbol{m})c_{s'}(\boldsymbol{m})c_{s'}^\dagger(\boldsymbol{n})c_s(\boldsymbol{n}) - \frac{1}{4}\hat{n}(\boldsymbol{m})\hat{n}(\boldsymbol{n}) \,, \quad \text{(D.29)}$$

from which we have:

$$\sum_{s,s'} c_s^\dagger(\boldsymbol{m})c_{s'}(\boldsymbol{m})c_{s'}^\dagger(\boldsymbol{n})c_s(\boldsymbol{n}) = 2\left(\overrightarrow{S}_{\boldsymbol{m}} \cdot \overrightarrow{S}_{\boldsymbol{n}} + \frac{1}{4}\hat{n}(\boldsymbol{m})\hat{n}(\boldsymbol{n})\right) \,. \quad \text{(D.30)}$$

Appendix E

Lang-Firsov canonical transformation

This Appendix contains a detailed derivation of the following transformation rules:

$$\begin{cases} \tilde{c}_i = & \exp\left[\sum_{\boldsymbol{q}} \left(u(\boldsymbol{m},\boldsymbol{q})d_q - H.c.\right)\right] \hat{c}_i \equiv X_i \hat{c}_i \\ \tilde{d}_q = & \hat{d}_q - \sum_i \hat{n}_i u^*(\boldsymbol{m},\boldsymbol{q}) \\ \tilde{d}_q^\dagger = & \hat{d}_q^\dagger - \sum_i \hat{n}_i u(\boldsymbol{m},\boldsymbol{q}) \\ \tilde{n}_i = & \hat{n}_i \\ \tilde{n_i d_q} = & \hat{n}_i \hat{d}_q - \hat{n}_i \sum_j \hat{n}_j u^*(\boldsymbol{n},\boldsymbol{q}) \\ \tilde{n_i d_q^\dagger} = & \hat{n}_i \hat{d}_q^\dagger - \hat{n}_i \sum_j \hat{n}_j u(\boldsymbol{n},\boldsymbol{q}) \\ \tilde{d_q^\dagger d_q} = & \hat{d}_q^\dagger \hat{d}_q - \sum_i \left[\hat{d}_q^\dagger \hat{n}_i u^*(\boldsymbol{m},\boldsymbol{q}) + \hat{d}_q \hat{n}_i u(\boldsymbol{m},\boldsymbol{q})\right] \end{cases} . \tag{E.1}$$

as the result of the application of the Lang-Firsov (LF) transformation [10] defined in Eq.(8.5). By means of these relations it will be shown that the microscopic Hamiltonian (8.1) can be written as:

$$\tilde{H} = -\sum_{i,j} \left[\hat{\sigma}_{ij}\delta_{ss'} + \tilde{\mu}\delta_{ij}\right] \hat{c}_i^\dagger \hat{c}_j + \frac{1}{2}\sum_{i\neq j} \frac{e^2}{|\boldsymbol{m}-\boldsymbol{n}|}\left(\frac{1}{\epsilon_\infty} - \frac{1}{\kappa}\right) \hat{n}_i \hat{n}_j + H_{ph} \, . \tag{E.2}$$

E.1 Transformation rules for electronic and phononic operators

Let us consider generic electronic $\hat{O}_i$ and phononic $\hat{O}_p$ operators. According to the notation $i = (\boldsymbol{m}, s)$, i include both site $(\boldsymbol{m})$ and spin (s) degrees of freedom. By applying (8.5) we get:

$$\tilde{O}_{i,p} \equiv e^S O_{i,p} e^{-S} = \exp\left[-\sum_{\boldsymbol{q},j} \hat{n}_j \left[u_j(\boldsymbol{q})\hat{d}_q - H.c.\right]\right] O_{i,p} \exp\left[\sum_{\boldsymbol{q},j} \hat{n}_j \left[u_j(\boldsymbol{q})\hat{d}_q - H.c.\right]\right] . \tag{E.3}$$

In order to simplify this relation it is useful to operate the following scaling: $u(\boldsymbol{n},\boldsymbol{q}) \rightarrow \eta u(\boldsymbol{n},\boldsymbol{q})$ and then differentiate the transformed operator with respect to the scaling parameter η. In this way we get:

$$\begin{aligned}\frac{\partial \tilde{O}_{i,p}}{\partial \eta} &= e^{S}\left\{-\sum_{\boldsymbol{q},j}\hat{n}_j\left[u_j(\boldsymbol{q})\hat{d}_q - u_j^*(\boldsymbol{q})\hat{d}_q^\dagger\right]\hat{O}_{i,p}e^{-S}\right\} \\ &\quad + e^{S}\hat{O}_{i,p}\left\{\sum_{\boldsymbol{q},j}\hat{n}_j\left[u_j(\boldsymbol{q})\hat{d}_q - u_j^*(\boldsymbol{q})\hat{d}_q^\dagger\right]e^{-S}\right\} .\end{aligned}$$

Recalling that $\left[\hat{O}_i,\hat{d}_q\right]=0$ and $\left[\hat{O}_p,\hat{n}_i\right]=0$, we get:

$$\begin{aligned}\frac{\partial \tilde{O}_i}{\partial \eta} &= e^{S}\left\{\sum_{\boldsymbol{q},j}\left[u_j(\boldsymbol{q})\hat{d}_q\left(\hat{O}_i\hat{n}_j - \hat{n}_j\hat{O}_i\right) + u_j^*(\boldsymbol{q})\hat{d}_q^\dagger\left(\hat{n}_j\hat{O}_i - \hat{O}_i\hat{n}_j\right)\right]\right\}e^{-S} = \\ &= \sum_{\boldsymbol{q},j} e^{S}\left[\hat{n}_j,\hat{O}_i\right]e^{-S}\left(u_j^*(\boldsymbol{q})\hat{d}_q^\dagger - u_j(\boldsymbol{q})\hat{d}_q\right) , \qquad \text{(E.4)}\end{aligned}$$

$$\begin{aligned}\frac{\partial \tilde{O}_p}{\partial \eta} &= e^{S}\left\{\sum_{\boldsymbol{q},j}\left[\hat{n}_j u_j(\boldsymbol{q})\left(\hat{O}_p\hat{d}_q - \hat{d}_q\hat{O}_p\right) + \hat{n}_j u_j^*(\boldsymbol{q})\left(\hat{d}_q^\dagger\hat{O}_p - \hat{O}_p\hat{d}_q^\dagger\right)\right]\right\}e^{-S} = \\ &= \sum_{\boldsymbol{q},j}\hat{n}_j\left\{u_j(\boldsymbol{q})\left(e^{S}\left[\hat{O}_p,\hat{d}_q\right]e^{-S}\right) + u_j^*(\boldsymbol{q})\left(e^{S}\left[\hat{d}_q^\dagger,\hat{O}_p\right]e^{-S}\right)\right\} , \qquad \text{(E.5)}\end{aligned}$$

which represents two differential equations that allow us to calculate the transformed operators $\tilde{O}_i$ and $\tilde{O}_p$ with the condition that $\tilde{O}_{i,p} = \hat{O}_{i,p}$ when $\eta = 0$.

E.1.1 Transformation rules for $\hat{c}_i$ and $\hat{d}_q$ operators

Let us now analyze the case in which $\hat{O}_i$ and $\hat{O}_p$ are the electronic and the phononic annihilation operators $\hat{c}_i$ and $\hat{d}_{\boldsymbol{q}}$, respectively. From (E.4) and (E.5) and by means of the condition $\tilde{O}_{i,p} = \hat{O}_{i,p}$ at $\eta = 0$ we get[1]:

$$\begin{cases}\begin{cases}\frac{\partial \tilde{c}_i}{\partial \eta} = -\tilde{c}_i\sum_{\boldsymbol{q}}\left(u_i^*(\boldsymbol{q})\hat{d}_q^\dagger - u_i(\boldsymbol{q})\hat{d}_q\right) \\ \tilde{c}_i = \hat{c}_i \; at \; \eta = 0\end{cases} \\ \begin{cases}\frac{\partial \tilde{d}_q}{\partial \eta} = -\sum_j \hat{n}_j u_j^*(\boldsymbol{q}) \\ \tilde{d}_q = \hat{d}_q \; at \; \eta = 0\end{cases}\end{cases} . \qquad \text{(E.6)}$$

[1]We recall that $\left[\hat{d}_p,\hat{d}_q\right]=0$, $\left[\hat{d}_q^\dagger,\hat{d}_p\right]=-\delta_{p,q}$ and $[\hat{n}_j,\hat{c}_i]=-\delta_{ij}\hat{c}_i$.

The solution of these differential equations with respect to the specified boundary conditions at $\eta = 0$ are:

$$\begin{cases} \tilde{c}_i = & \exp\left[\eta \sum_{\boldsymbol{q}} \left(u(\boldsymbol{m},\boldsymbol{q}) d_q - H.c.\right)\right] c_i \\ \tilde{d}_q = & \hat{d}_q - \eta \sum_i \hat{n}_i u^*(\boldsymbol{m},\boldsymbol{q}) \end{cases} , \tag{E.7}$$

in which, for the sake of simplicity, we can put $\eta = 1$ in order to obtain:

$$\begin{cases} \tilde{c}_i = & \exp\left[\sum_{\boldsymbol{q}} \left(u(\boldsymbol{m},\boldsymbol{q}) d_q - H.c.\right)\right] c_i \equiv X_i c_i \\ \tilde{d}_q = & \hat{d}_q - \sum_i \hat{n}_i u^*(\boldsymbol{m},\boldsymbol{q}) \end{cases} . \tag{E.8}$$

E.1.2 Other important transformation rules

Starting from (E.8), a number of transformation rules for different operators can be obtained. E.g. it is immediate to see that:

$$\tilde{n}_i = e^S \hat{c}_i^\dagger \hat{c}_i e^{-S} = \left(e^S \hat{c}_i^\dagger e^{-S}\right)\left(e^S \hat{c}_i e^{-S}\right) = X_i^\dagger X_i \hat{c}_i^\dagger \hat{c}_i \ ,$$

so, by means of (D.5) (we recall that $\alpha_{m,n}(\boldsymbol{q}) = 0$ when $\boldsymbol{m} = \boldsymbol{n}$) we get $X_i^\dagger X_i = 1$ so:

$$\tilde{n}_i = \hat{n}_i \ . \tag{E.9}$$

Similarly, for $n_i n_j$ operator we get:

$$\hat{n}_i \hat{n}_j \ \rightarrow \ \left(e^S \hat{n}_i e^{-S}\right)\left(e^S \hat{n}_j e^{-S}\right) = \tilde{n}_i \tilde{n}_j = \hat{n}_i \hat{n}_j \ . \tag{E.10}$$

Let us now analyze the transformation of the product of $\hat{n}_i$ with a phononic operator. In this case we get:

$$\hat{n}_i \hat{d}_q \ \rightarrow \ e^S \hat{n}_i \hat{d}_q e^{-S} = \left(e^S \hat{n}_i e^{-S}\right)\left(e^S \hat{d}_q e^{-S}\right) = \tilde{n}_i \tilde{d}_q \ .$$

According to (E.8) and (E.9) we obtain:

$$\begin{cases} \hat{n}_i \hat{d}_q \rightarrow \hat{n}_i \hat{d}_q - \hat{n}_i \sum_j \hat{n}_j u^*(\boldsymbol{n},\boldsymbol{q}) \\ \hat{n}_i \hat{d}_q^\dagger \rightarrow \hat{n}_i \hat{d}_q^\dagger - \hat{n}_i \sum_j \hat{n}_j u(\boldsymbol{n},\boldsymbol{q}) \end{cases} . \tag{E.11}$$

Finally it is immediate to see that $d_q^\dagger d_q$ operator transforms as:

$$\begin{aligned} \tilde{d_q^\dagger d_q} &= e^S \hat{d}_q^\dagger \hat{d}_q e^{-S} = \left(e^S \hat{d}_q^\dagger e^{-S}\right)\left(e^S \hat{d}_q e^{-S}\right) = \tilde{d}_q^\dagger \tilde{d}_q = \\ &= \left(\hat{d}_q^\dagger - \sum_i \hat{n}_i u(\boldsymbol{m},\boldsymbol{q})\right)\left(\hat{d}_q - \sum_i \hat{n}_i u^*(\boldsymbol{m},\boldsymbol{q})\right) = \\ &= \hat{d}_q^\dagger \hat{d}_q - \sum_i \left[\hat{d}_q^\dagger \hat{n}_i u^*(\boldsymbol{m},\boldsymbol{q}) + \hat{d}_q \hat{n}_i u(\boldsymbol{m},\boldsymbol{q})\right] \end{aligned} \tag{E.12}$$

E.2 Transformation rules for the atomic Hamiltonian

In order to obtain the transformation rule for the atomic Hamiltonian (8.1) let us now divide H as follows:

$$H = H_{kin} + H_{el} + H_{el-ph} + H_{ph} \ , \tag{E.13}$$

where:

$$H_{kin} \equiv -\sum_{i,j} \left(T_{ij}\delta_{ss'} + \mu\delta_{ij}\right) \hat{c}_i^\dagger \hat{c}_j \ , \tag{E.14}$$

$$H_{el} \equiv \frac{1}{2}\sum_{i\neq j} \frac{e^2}{\epsilon_\infty |\boldsymbol{m}-\boldsymbol{n}|} \hat{n}_i \hat{n}_j \ , \tag{E.15}$$

$$H_{el-ph} \equiv \sum_{\boldsymbol{q},i} \hbar\omega_0 \hat{n}_i \left[u(\boldsymbol{m},\boldsymbol{q})\hat{d}_q + H.c.\right] \ , \tag{E.16}$$

$$H_{ph} \equiv \sum_{\boldsymbol{q}} \hbar\omega_0 \left(d_{\boldsymbol{q}}^\dagger d_{\boldsymbol{q}} + \frac{1}{2}\right) \ , \tag{E.17}$$

and analyze each term individually. By means of the transformation rules obtained in the previous section, for the kinetic term we have:

$$\begin{aligned} \tilde{H}_{kin} &\equiv -\sum_{i,j} \left(T_{ij}\delta_{ss'} + \mu\delta_{ij}\right) \tilde{c_i^\dagger} \tilde{c_j} = -\sum_{i,j} \left(T_{ij}\delta_{ss'} + \mu\delta_{ij}\right) X_i^\dagger X_j \hat{c}_i^\dagger \hat{c}_j = \\ &\quad -\sum_{i,j} \left[\left(T_{ij} X_i^\dagger X_j\right)\delta_{ss'} + \mu\delta_{ij}\right] \hat{c}_i^\dagger \hat{c}_j = \\ &\equiv -\sum_{i,j} \left[\sigma_{ij}\delta_{ss'} + \mu\delta_{ij}\right] \hat{c}_i^\dagger \hat{c}_j \ , \end{aligned} \tag{E.18}$$

where σ_{ij} is the renormalized hopping integral defined in terms of (8.10) as:

$$\sigma_{ij} \equiv T_{ij} X_i^\dagger X_j \ . \tag{E.19}$$

According to (E.10) instead, for the electronic interaction term we get:

$$\tilde{H}_{LRI} \equiv \frac{1}{2}\sum_{i\neq j} \frac{e^2}{\epsilon_\infty |\boldsymbol{m}-\boldsymbol{n}|} n_i \tilde{n}_j = \frac{1}{2}\sum_{i\neq j} \frac{e^2}{\epsilon_\infty |\boldsymbol{m}-\boldsymbol{n}|} \hat{n}_i \hat{n}_j \ , \tag{E.20}$$

while for the electron-phonon coupling term, according to (E.11),we get[2]:

$$\tilde{H}_{el-ph} \equiv \sum_{\boldsymbol{q},i} \hbar\omega_0 \left[u(\boldsymbol{m},\boldsymbol{q}) n_i \tilde{d}_q + u^*(\boldsymbol{m},\boldsymbol{q}) n_i \tilde{d}_q^\dagger\right] =$$

[2]In the sum over i and j an addition factor $1/2$ has been included in order to avoid double counting.

$$
\begin{aligned}
&= \sum_{\boldsymbol{q},i} \hbar\omega_0 \Bigg[u(\boldsymbol{m},\boldsymbol{q}) \left(\hat{n}_i \hat{d}_q - \hat{n}_i \sum_j \hat{n}_j u^*(\boldsymbol{n},\boldsymbol{q}) \right) \\
&\quad + u^*(\boldsymbol{m},\boldsymbol{q}) \left(\hat{n}_i \hat{d}_q^\dagger - \hat{n}_i \sum_j \hat{n}_j u(\boldsymbol{n},\boldsymbol{q}) \right) \Bigg] = \qquad \text{(E.21)} \\
&= \sum_{\boldsymbol{q},i} \hbar\omega_0 \left[u(\boldsymbol{m},\boldsymbol{q}) \hat{n}_i \hat{d}_q + u^*(\boldsymbol{m},\boldsymbol{q}) \hat{n}_i \hat{d}_q^\dagger \right] + \\
&\quad - \frac{1}{2} \sum_{\boldsymbol{q},i,j} \hbar\omega_0 \left[u^*(\boldsymbol{m},\boldsymbol{q}) u(\boldsymbol{n},\boldsymbol{q}) + u(\boldsymbol{m},\boldsymbol{q}) u^*(\boldsymbol{n},\boldsymbol{q}) \right] \hat{n}_i \hat{n}_j = \\
&= H_{el-ph} - \frac{1}{2} \sum_{\boldsymbol{q},i,j} \hbar\omega_0 \left[u^*(\boldsymbol{m},\boldsymbol{q}) u(\boldsymbol{n},\boldsymbol{q}) + u(\boldsymbol{m},\boldsymbol{q}) u^*(\boldsymbol{n},\boldsymbol{q}) \right] \hat{n}_i \hat{n}_j \qquad \text{(E.22)}
\end{aligned}
$$

By means of (8.2) we can note that:

$$
\begin{aligned}
u^*(\boldsymbol{m},\boldsymbol{q}) u(\boldsymbol{n},\boldsymbol{q}) + u(\boldsymbol{m},\boldsymbol{q}) u^*(\boldsymbol{n},\boldsymbol{q}) &= \frac{|\gamma(\boldsymbol{q})|^2}{2N} \left[e^{-i\boldsymbol{q}\cdot\boldsymbol{m}} e^{i\boldsymbol{q}\cdot\boldsymbol{n}} + e^{i\boldsymbol{q}\cdot\boldsymbol{m}} e^{-i\boldsymbol{q}\cdot\boldsymbol{n}} \right] = \\
&= \frac{|\gamma(\boldsymbol{q})|^2}{N} \left[\frac{1}{2} \left(e^{-i\boldsymbol{q}\cdot(\boldsymbol{m}-\boldsymbol{n})} + e^{i\boldsymbol{q}\cdot(\boldsymbol{m}-\boldsymbol{n})} \right) \right] = \\
&= \frac{|\gamma(\boldsymbol{q})|^2}{N} \cos\left(\boldsymbol{q} \cdot (\boldsymbol{m} - \boldsymbol{n}) \right) \ , \qquad \text{(E.23)}
\end{aligned}
$$

so we obtain:

$$
\tilde{H}_{el-ph} = H_{el-ph} - \frac{1}{2} \sum_{\boldsymbol{q},i,j} \hbar\omega_0 \frac{|\gamma(\boldsymbol{q})|^2}{N} \cos\left(\boldsymbol{q} \cdot (\boldsymbol{m} - \boldsymbol{n}) \right) \hat{n}_i \hat{n}_j \ . \qquad \text{(E.24)}
$$

Finally, by means of (E.12), it is straightforward to see that H_{ph} gives:

$$
\begin{aligned}
\tilde{H}_{ph} &\equiv \sum_{\boldsymbol{q}} \hbar\omega_0 \left(\tilde{d_{\boldsymbol{q}}^\dagger} d_{\boldsymbol{q}} + \frac{1}{2} \right) = \\
&= \sum_{\boldsymbol{q}} \hbar\omega_0 \left[\hat{d}_q^\dagger \hat{d}_q + \frac{1}{2} \right] - \sum_{i,\boldsymbol{q}} \left[\hat{d}_q^\dagger \hat{n}_i u^*(\boldsymbol{m},\boldsymbol{q}) + \hat{d}_q \hat{n}_i u(\boldsymbol{m},\boldsymbol{q}) \right] = \\
&= H_{ph} - \sum_{i,\boldsymbol{q}} \left[u^*(\boldsymbol{m},\boldsymbol{q}) \hat{n}_i \hat{d}_q^\dagger + u(\boldsymbol{m},\boldsymbol{q}) \hat{n}_i \hat{d}_q \right] = H_{ph} - H_{el-ph} \ .
\end{aligned}
$$

Adding together all the contribution, the transformed atomic Hamiltonian reads as:

$$
\begin{aligned}
\tilde{H} &= - \sum_{i,j} \left[\hat{\sigma}_{ij} \delta_{ss'} + \mu \delta_{ij} \right] \hat{c}_i^\dagger \hat{c}_j + \frac{1}{2} \sum_{i \neq j} \frac{e^2}{\epsilon_\infty |\boldsymbol{m} - \boldsymbol{n}|} \hat{n}_i \hat{n}_j \\
&\quad - \frac{1}{2} \sum_{\boldsymbol{q},i,j} \hbar\omega_0 \frac{|\gamma(\boldsymbol{q})|^2}{N} \cos\left(\boldsymbol{q} \cdot (\boldsymbol{m} - \boldsymbol{n}) \right) \hat{n}_i \hat{n}_j + H_{ph} \ . \qquad \text{(E.25)}
\end{aligned}
$$

It is useful to analyze the third term individually:

$$\tilde{H}_{(3)}(i,j) \equiv -\frac{1}{2}\sum_{\boldsymbol{q},i,j}\hbar\omega_0\frac{|\gamma(\boldsymbol{q})|^2}{N}\cos\left(\boldsymbol{q}\cdot(\boldsymbol{m}-\boldsymbol{n})\right)\hat{n}_i\hat{n}_j\ . \tag{E.26}$$

The contribution arising for $i=j$ can be written as:

$$\begin{aligned}
\tilde{H}_{(3)}(i=j) &= -\frac{1}{2}\sum_{\boldsymbol{q},i}\hbar\omega_0\frac{|\gamma(\boldsymbol{q})|^2}{N}\hat{n}_i\hat{n}_i = \\
&= -\frac{1}{2}\sum_{\boldsymbol{q},i}\frac{\hbar\omega_0}{N}\frac{4\pi e^2}{\kappa\Omega\hbar\omega_0 q^2}\hat{n}_i = -\frac{2\pi e^2}{\kappa}\sum_i\left(\frac{1}{N\Omega}\sum_{\boldsymbol{q}}\frac{1}{q^2}\right)\hat{n}_i = \\
&= -\sum_i\left(\frac{2\pi e^2}{\kappa}\int_{BZ}\frac{d^3q}{(2\pi)^3}\frac{1}{q^2}\right)\hat{n}_i \equiv -\sum_i E_p\hat{n}_i\ ,
\end{aligned} \tag{E.27}$$

in which the integration goes over all the Brillouin zone. By including this contribution in the chemical potential, the kinetic part of the transformed Hamiltonian reads as:

$$-\sum_{i,j}\left[\hat{\sigma}_{ij}\delta_{ss'}+\tilde{\mu}\delta_{ij}\right]\hat{c}_i^\dagger\hat{c}_j\ , \tag{E.28}$$

where:

$$\begin{cases}\tilde{\mu}\equiv\mu+E_p\\ E_p\equiv\frac{2\pi e^2}{\kappa}\int_{BZ}\frac{d^3q}{(2\pi)^3}\frac{1}{q^2}\end{cases}\ . \tag{E.29}$$

We are left with the $i\neq j$ contribution that can be written as follows:

$$\begin{aligned}
\tilde{H}_{(3)}(i\neq j) &= -\frac{1}{2}\sum_{\boldsymbol{q},i\neq j}\hbar\omega_0\frac{|\gamma(\boldsymbol{q})|^2}{N}\cos\left(\boldsymbol{q}\cdot(\boldsymbol{m}-\boldsymbol{n})\right)\hat{n}_i\hat{n}_j = \\
&= -\frac{1}{2}\sum_{i\neq j}\sum_{\boldsymbol{q}}\frac{\hbar\omega_0}{N}\frac{4\pi e^2}{\kappa\Omega\hbar\omega_0 q^2}\cos\left(\boldsymbol{q}\cdot(\boldsymbol{m}-\boldsymbol{n})\right)\hat{n}_i\hat{n}_j = \\
&= -\frac{1}{2}\sum_{i\neq j}\frac{1}{N\Omega}\sum_{\boldsymbol{q}}\frac{4\pi e^2}{\kappa q^2}\cos\left(\boldsymbol{q}\cdot(\boldsymbol{m}-\boldsymbol{n})\right)\hat{n}_i\hat{n}_j = \\
&= -\frac{1}{2}\sum_{i\neq j}\frac{1}{N\Omega}\int\frac{d^3q}{(2\pi)^3}\frac{4\pi e^2}{\kappa q^2}\cos\left(\boldsymbol{q}\cdot(\boldsymbol{m}-\boldsymbol{n})\right)\hat{n}_i\hat{n}_j = \\
&= -\frac{1}{2}\sum_{i\neq j}\frac{4\pi e^2}{(2\pi)^3\kappa}\int_0^{2\pi}d\varphi\int_0^{+\infty}dq\int_{-\frac{\pi}{2}}^{\frac{\pi}{2}}d\theta q^2\frac{1}{q^2}\cos\left(q|\boldsymbol{m}-\boldsymbol{n}|\cos\theta\right)\hat{n}_i\hat{n}_j = \\
&= -\frac{1}{2}\sum_{i\neq j}\frac{4\pi e^2}{(2\pi)^3\kappa}(2\pi)\int_0^{+\infty}dq\left[\frac{1}{2}\int_{-\frac{\pi}{2}}^{\frac{\pi}{2}}d\theta e^{iq|\boldsymbol{m}-\boldsymbol{n}|\cos\theta}\right. \\
&\quad \left.+\frac{1}{2}\int_{-\frac{\pi}{2}}^{\frac{\pi}{2}}d\theta e^{-iq|\boldsymbol{m}-\boldsymbol{n}|\cos\theta}\right]\hat{n}_i\hat{n}_j =
\end{aligned}$$

$$
\begin{aligned}
&= -\frac{1}{2}\sum_{i\neq j}\frac{4\pi e^2}{(2\pi)^2\,\kappa}\int_0^{+\infty} dq\pi J_0(q|\boldsymbol{m}-\boldsymbol{n}|)\hat{n}_i\hat{n}_j = \\
&= -\frac{1}{2}\sum_{i\neq j}\frac{e^2}{\kappa}\left[\int_0^{+\infty} J_0(q|\boldsymbol{m}-\boldsymbol{n}|)dq\right]\hat{n}_i\hat{n}_j = -\frac{1}{2}\sum_{i\neq j}\frac{e^2}{\kappa|\boldsymbol{m}-\boldsymbol{n}|}\hat{n}_i\hat{n}_j\ .
\end{aligned}
$$

Finally, the transformed atomic Hamiltonian reads as:

$$
\tilde{H} = -\sum_{i,j}\left[\hat{\sigma}_{ij}\delta_{ss'}+\tilde{\mu}\delta_{ij}\right]\hat{c}_i^{\dagger}\hat{c}_j + \frac{1}{2}\sum_{i\neq j}\frac{e^2}{|\boldsymbol{m}-\boldsymbol{n}|}\left(\frac{1}{\epsilon_\infty}-\frac{1}{\kappa}\right)\hat{n}_i\hat{n}_j + H_{ph}\ . \qquad \text{(E.30)}
$$

Appendix F

Thermodynamic quantities for a Bose-Fermi mixture

Let us consider an ideal gas of n_f fermions and $2n_b$ bosons per volume in the presence of a static and uniform magnetic field h. With the aim of describing the thermodynamic of such a Fermi-Bose mixture at equilibrium , it is useful to introduce the thermodynamic potential $\Omega(n_b, n_p, T, h)$, defined as a function of temperature T, chemical potential μ and magnetic field h for fixed values of entropy S, total particle density $n = 2n_b + n_p$ and total spin-momentum (magnetization) m, as follows:

$$d\Omega = -SdT - nd\mu - mdh \ . \tag{F.1}$$

The above relation allows us to write the following expressions for total particle density $n(T,h)$, entropy $S(T,h)$, specific heat $C(T,h)$, magnetization $m(T,h)$, charge $\chi_c(T,h)$ and spin $\chi_s(T,h)$ susceptibilities:

$$\begin{cases} n(T,h) = -\left.\frac{\partial\Omega}{\partial\mu}(T,h)\right|_{n=const.} \\ S(T,h) = -\left.\frac{\partial\Omega}{\partial T}(T,h)\right|_{\mu=const.} \\ C(T,h) = T\left.\frac{\partial S}{\partial T}(T,h)\right|_{V,n=const.} \\ m(T,h) = -\left.\frac{\partial}{\partial h}\Omega(T,h)\right|_{V,n=const.} \\ \chi_s(T,h) = \left.\frac{\partial}{\partial h}m(T,h)\right|_{V,n=const.} \\ \chi_c(T,h) = T\left.\frac{\partial}{\partial\mu}n(T,h)\right|_{V,n=const.} \end{cases} . \tag{F.2}$$

As shown in detail in Sec.10.3.1, we can use the additivity property of $\Omega(n_b, n_p, T, h)$ to write:

$$\Omega(n_b, n_p, T, h) = \Omega_b(n_b, T, h) + \Omega_p(n_p, T, h) \ , \tag{F.3}$$

where $\Omega_{b,p}(n_{b,p}, T, h)$ is the thermodynamic potential which describes bipolaron/unpaired polaron specie individually:

$$\Omega_{p,b}(n_{p,b}, T, h) = \mp k_B T \sum_s \int_{-\infty}^{+\infty} d\epsilon \mathcal{N}_{p,b}^{(s)}(\epsilon) \ln\left(1 \pm \exp\left[\left(\mu_{p,b} - \epsilon\right)/k_B T\right]\right) \ , \quad \text{(F.4)}$$

which is defined in terms of polaron/bipolaron chemical potential $\mu_{p,b}$, and density of spin-polarized states in the bipolaron/unpaired polaron band $\mathcal{N}_{p,b}^{(s)}(\epsilon, h)$. Here the label s accounts of all the possible spin states. Although bipolaron and unpaired polaron densities, individually, might have two different chemical potentials, there is only one value μ for the chemical potential of the whole mixture which can be unambiguously determined according to the detailed equilibrium principle (10.30) which gives:

$$\mu = \mu_p = \frac{\mu_b}{2} \ . \quad \text{(F.5)}$$

It is worth noting that the chemical potential μ can be calculated self-consistently for a given value of polaron and bipolaron density according to the relation $n = 2n_b + n_p$ where:

$$n_{p,b}(T) \equiv \sum_s \int_{-\infty}^{+\infty} d\epsilon f_{p,b}(\mu_{p,b}, \epsilon, T) \mathcal{N}_{p,b}(\epsilon) \ , \quad \text{(F.6)}$$

hence, for any given energy dispersion in $\mathcal{N}_{p,b}(\epsilon)$, $\Omega_{p,b}(n_{p,b}, T, h)$ can be calculated as a function of temperature, polaron/bipolaron density and intensity of the external magnetic field. We report in the following Sections the expression of entropy, specific heat, magnetization and spin susceptibility for a generic $\epsilon(\boldsymbol{k})$ dispersion. Finally, we report in Sec.(F.3) analytical results obtained in the case of a Heaviside-theta density of state.

F.1 Zero field entropy and specific heat

For the sake of simplicity, let us consider the case with $h = 0$. According to the second law of thermodynamic the specific heat at constant volume can be defined in terms of the entropy of the system as follows:

$$C(T) \equiv T \left.\frac{\partial S}{\partial T}\right|_{V,n=const.} \ , \quad \text{(F.7)}$$

where, from Eq.10.27, we have:

$$S = -\left.\frac{\partial \Omega}{\partial T}\right|_{\mu=const} \ . \quad \text{(F.8)}$$

The entropy enjoys the additivity, therefore:

$$S(T) = S_b(T) + S_b(T) = -\left(\left.\frac{\partial \Omega_b}{\partial T}\right|_{\mu=const} + \left.\frac{\partial \Omega_p}{\partial T}\right|_{\mu=const}\right) \ . \quad \text{(F.9)}$$

Recalling that:

$$\frac{d}{dT}\ln\left(1\pm\exp\left[\left(\mu_{p,b}(T)-\epsilon\right)/k_BT\right]\right)=\pm f_{p,b}(\epsilon,T)\frac{d}{dT}\left(\frac{\mu_{p,b}(T)-\epsilon}{k_BT}\right)\ , \tag{F.10}$$

from Eq.10.29 one can readily obtain:

$$\begin{aligned}\left.\frac{\partial\Omega_{p,b}}{\partial T}\right|_{\mu=const} &= \frac{\Omega_{p,b}}{T}-k_BT\sum_s\int_{-\infty}^{\infty}d\epsilon\mathcal{N}_{p,b}^{(s)}(\epsilon)f_{p,b}(\epsilon,T)\left(\frac{\epsilon-\mu_{p,b}}{k_BT^2}\right)= \\ &= \frac{\Omega_{p,b}}{T}+\frac{\mu_{p,b}}{T}\sum_s\int_{-\infty}^{\infty}d\epsilon\mathcal{N}_{p,b}^{(s)}(\epsilon)f_{p,b}(\epsilon,T) \\ &\quad -\frac{1}{T}\sum_s\int_{-\infty}^{\infty}d\epsilon\mathcal{N}_{p,b}^{(s)}(\epsilon)\epsilon f_{p,b}(\epsilon,T)= \\ &= \frac{1}{T}\left(\Omega_{p,b}(T)+\mu_{p,b}(T)n_{p,b}(T)-\langle E_{p,b}\rangle(T)\right)\ ,\end{aligned} \tag{F.11}$$

where:

$$n_{p,b}(T)\equiv\sum_s\int_{-\infty}^{+\infty}d\epsilon f_{p,b}(\mu_{p,b},\epsilon,T)\mathcal{N}_{p,b}(\epsilon)\ , \tag{F.12}$$

$$\langle E_{p,b}\rangle(T)\equiv\sum_s\int_{-\infty}^{+\infty}d\epsilon\epsilon f_{p,b}(\mu_{p,b},\epsilon,T)\mathcal{N}_{p,b}(\epsilon)\ . \tag{F.13}$$

Therefore bipolaron and unpaired polarons contributions to the entropy read as:

$$\begin{aligned}S_{p,b}(T) &= -\left.\frac{\partial\Omega_{p,b}}{\partial T}\right|_{\mu=const}=\frac{1}{T}\left(\langle E_{p,b}\rangle(T)-\Omega_{p,b}(T)-\mu_{p,b}(T)n_{p,b}(T)\right)= \\ &= \sum_s\int_{-\infty}^{+\infty}d\epsilon\mathcal{N}_{p,b}^{(s)}(\epsilon)\Bigg[\pm k_B\ln\left(1\pm\exp\left[\left(\mu_{p,b}(T)-\epsilon\right)/k_BT\right]\right) \\ &\quad -f_{p,b}(\epsilon,T)\left(\frac{\mu_{p,b}(T)-\epsilon}{T}\right)\Bigg]\ .\end{aligned} \tag{F.14}$$

The knowledge of the entropy allows us to calculate the specific heat at constant volume and particle density as:

$$C(T)|_{V,n}=T\left.\frac{\partial S}{\partial T}\right|_{V,n=const.}=T\left.\frac{\partial S_b}{\partial T}\right|_{V,n=const.}+T\left.\frac{\partial S_p}{\partial T}\right|_{V,n=const.}\ . \tag{F.15}$$

It is worth recalling that, although the total number of particle of the mixture x is constant, bipolaron and unpaired polaron densities depend on temperature ($n_{p,b}\equiv n_{p,b}(T)$) according to Eq.10.36. So that, from the previous equation we get:

$$C_{p,b}(T)|_{V,n} = T\left(-\frac{\langle E_{p,b}\rangle}{T^2}+\frac{\mu_{p,b}(T)n_{p,b}(T)}{T^2}+\frac{\Omega_{p,b}}{T^2}+\frac{1}{T}\left.\frac{d\langle E_{p,b}\rangle}{dT}\right|_{V,n}+=\right.$$

$$
\begin{aligned}
& -\frac{\mu_{p,b}(T)}{T}\left.\frac{dn_{p,b}}{dT}\right|_{V,n}+\frac{n_{p,b}(T)}{T}\left.\frac{d\mu_{p,b}}{dT}\right|_{V,n}-\frac{1}{T}\left.\frac{d\Omega_{p,b}}{dT}\right|_{V,n}\Bigg) = \\
= & \left.\frac{d\langle E_{p,b}\rangle}{dT}\right|_{V,n}-\mu_{p,b}(T)\left.\frac{dn_{p,b}}{dT}\right|_{V,n} = \\
= & \sum_s\int_{-\infty}^{+\infty}d\epsilon\mathcal{N}_{p,b}(\epsilon)\left(\epsilon-\mu_{p,b}(T)\right)\frac{df_{p,b}}{dT}(\epsilon,T)\ . \qquad \text{(F.16)}
\end{aligned}
$$

Summarizing, in the absence of an external magnetic field, entropy and specific heat enjoy the additivity property and can be calculated as the sum of bipolaron and unpaired polarons contributions according to the following relations:

$$
\begin{aligned}
S_{p,b}(T) &= \frac{1}{T}\left(\langle E_{p,b}\rangle(T)-\Omega_{p,b}(T)-\mu_{p,b}(T)n_{p,b}(T)\right)\ , \qquad \text{(F.17)}\\
C_{p,b}(T)|_{V,n} &= \left.\frac{d\langle E_{p,b}\rangle}{dT}\right|_{V,n}-\mu_{p,b}(T)\left.\frac{dn_{p,b}}{dT}\right|_{V,n}\ , \qquad \text{(F.18)}
\end{aligned}
$$

or, alternatively:

$$
\begin{aligned}
S_{p,b}(T) &= \sum_s\int_{-\infty}^{+\infty}d\epsilon\mathcal{N}^{(s)}_{p,b}(\epsilon)\Bigg[\pm k_B\ln\left(1\pm\exp\left[\left(\mu_{p,b}-\epsilon\right)/k_BT\right]\right)\\
&\quad -f_{p,b}(\epsilon,T)\left(\frac{\mu_{p,b}-\epsilon}{T}\right)\Bigg]\ , \qquad \text{(F.19)}\\
C_{p,b}(T)|_{V,n} &= \sum_s\int_{-\infty}^{+\infty}d\epsilon\mathcal{N}_{p,b}(\epsilon)\left(\epsilon-\mu_{p,b}(T)\right)\left.\frac{df_{p,b}}{dT}\right|_{V,n}(\epsilon,T)\ . \qquad \text{(F.20)}
\end{aligned}
$$

It is worth noting that in the case of an ideal Fermi gas and in the low temperature limit, by considering $d\mu/dT\approx 0$, the derivative of the Fermi-Dirac distribution function can be expressed as:

$$
\begin{aligned}
\frac{df_p}{dT}(\epsilon,T) &= \frac{d}{dT}\left(\exp\left(\frac{\epsilon-\mu_{p,b}}{k_BT}\right)+1\right)^{-1} = \\
&= \left(\exp\left(\frac{\epsilon-\mu_{p,b}}{k_BT}\right)+1\right)^{-2}\exp\left(\frac{\epsilon-\mu_{p,b}}{k_BT}\right)\left(\frac{\epsilon-\mu_{p,b}}{k_BT^2}+\frac{1}{k_BT}\frac{d\mu_{p,b}}{dT}\right) = \\
&\approx \left(\exp\left(\frac{\epsilon-\mu_{p,b}}{k_BT}\right)+1\right)^{-2}\exp\left(\frac{\epsilon-\mu_{p,b}}{k_BT}\right)\frac{\epsilon-\mu_{p,b}}{k_BT^2}\ . \qquad \text{(F.21)}
\end{aligned}
$$

Then, recalling that $\mathcal{N}^{(s)}_{p,b}(\epsilon)\approx\mathcal{N}_{p,b}(E_F)$, the polaronic contribution to the specific heat gives:

$$
C(T) = 2\ \ k_B\mathcal{N}_p(E_F)\int_0^{+\infty}d\epsilon\left(\frac{\epsilon-\mu_p}{k_BT}\right)^2\left(\exp\left(\frac{\epsilon-\mu_p}{k_BT}\right)+1\right)^{-2}\exp\left(\frac{\epsilon-\mu_p}{k_BT}\right) =
$$

$$= \quad 2k_BT\mathcal{N}_p(E_F)\int_0^{+\infty} dx \frac{x^2\exp(x)}{(\exp(x)+1)^2} \ . \tag{F.22}$$

where:

$$x \equiv \frac{\epsilon-\mu_{p,b}}{k_BT} \ , \ d\epsilon = k_BTdx \ . \tag{F.23}$$

The resulting integrals can be computed exactly:

$$\int_0^{+\infty} dx \frac{x^2\exp(x)}{(\exp(x)+1)^2} = \frac{\pi^2}{6} \ , \tag{F.24}$$

then, by substituting in the expression of $C(T)$, we obtain the following standard textbook result for an ideal Fermi gas:

$$C(T) = \frac{\pi^2}{3}k_B^2T\mathcal{N}_p(E_F) \ , \tag{F.25}$$

with the well-known Sommerfeld specific heat coefficient $\gamma = \frac{C(T)}{T} = \pi^2k_B^2\mathcal{N}_p(E_F)/3$.

F.2 Magnetic moment and paramagnetic spin susceptibility

The magnetic response function in the presence of a weak magnetic field is given by the sum of a diamagnetic and a paramagnetic contributions. While the former is due to spin magnetic moments, the latter is induced by the coupling of the applied field with the orbital degrees of freedom. In the following treatment we will neglect the diamagnetic response and will restrict our analysis to the paramagnetic case in which the presence of a static and uniform external magnetic field can be described by a simple spin-field coupling $-\sum_{\boldsymbol{i}}\mu_B\boldsymbol{S}(\boldsymbol{i})\cdot\boldsymbol{h}$. Here the sum over $\boldsymbol{i}$ is taken with respect to all the sites of the lattice. Moreover, because of system isotropy, if we label as $\hat{z}$ the axis along which the magnetic field is aligned, the spin field coupling term reads as $-\mu_BS_z^{tot}h$ where S_z^{tot} is the total spin angular momentum of the system along the field direction ($S_z^{tot}=0$ and $S_z^{tot}\pm 1/2$ for bipolarons and unpaired polarons, respectively).

According to this, the statistical distribution of electrons in a magnetic field can be obtained by considering the following shift in the chemical potential $\mu \to \mu - S_z^{tot}\mu_Bh$ that reflects the shift in the energy dispersion: $\epsilon \to \varepsilon + S_z^{tot}\mu_Bh$ induced by the spin-field coupling. Hence, taking the sum over all the possible spin states, bipolaron and unpaired polaron contributions in the thermodynamic potential $\Omega(T,h)$ can be written as follows:

$$\Omega_b(T,h) \quad = \quad \Omega_b(T,\mu_b) \ , \tag{F.26}$$

$$\Omega_p(T,h) \quad = \quad \frac{1}{2}\left[\Omega_p(T,\mu_p+\mu_Bh)+\Omega_p(T,\mu_p-\mu_Bh,)\right] \ , \tag{F.27}$$

where the dependence from h has been taken into account via the polaronic/bosonic chemical potential of the mixture $\mu_{p,b}$. It is immediate to note that bipolarons do

not contribute to the magnetic response functions since they are not affected by the magnetic field h. Therefore, we can focus our analysis on the unpaired polarons contributions only.

According to Eq.10.40, recalling that:

$$\frac{\partial}{\partial h}\ln\left(1+\exp\left[\left(\mu_p \pm \mu_B h-\epsilon\right)/k_BT\right]\right) = \pm\frac{\mu_B}{k_BT}\frac{\exp\left[\left(\mu_p \pm \mu_B h-\epsilon\right)/k_BT\right]}{1+\exp\left[\left(\mu_p \pm \mu_B h-\epsilon\right)/k_BT\right]}\ , \tag{F.28}$$

we can write the magnetization $m(h,T)$ as:

$$\begin{aligned}
m(h,T) &= -\frac{\partial}{\partial h}\Omega(T,h) = -\frac{1}{2}\frac{\partial}{\partial h}\left[\Omega_p(T,\mu_p+\mu_B h)+\Omega_p(T,\mu_p-\mu_B h)\right] = \\
&= \frac{k_BT}{2}\int_{-\infty}^{+\infty} d\epsilon \mathcal{N}_p(\epsilon)\frac{\partial}{\partial h}\left[\ln\left(1+\exp\left[\frac{\mu_p(T)+\mu_B h-\epsilon}{k_BT}\right]\right)\right. \\
&\quad \left.+\ln\left(1+\exp\left[\frac{\mu_p(T)-\mu_B h-\epsilon}{k_BT}\right]\right)\right] = \\
&= \frac{\mu_B}{2}\int_{-\infty}^{+\infty} d\epsilon \mathcal{N}_p(\epsilon)\left[\left(1+\exp\left[\frac{\epsilon-\mu_p(T)-\mu_B h}{k_BT}\right]\right)^{-1}\right. \\
&\quad \left.-\left(1+\exp\left[\frac{\epsilon-\mu_p(T)+\mu_B h}{k_BT}\right]\right)^{-1}\right] = \\
&= \frac{\mu_B}{2}\int_{-\infty}^{+\infty} d\epsilon \mathcal{N}_p(\epsilon)\frac{\sinh\left[\frac{\mu_B h}{k_BT}\right]}{\cosh\left[\frac{\epsilon-\mu_p}{k_BT}\right]+\cosh\left[\frac{\mu_B h}{k_BT}\right]}\ .
\end{aligned} \tag{F.29}$$

Then the spin-susceptibility reads as:

$$\begin{aligned}
\chi_s(h,T) &= \frac{\partial m(h,T)}{\partial h} = \frac{\mu_B}{2}\int_{-\infty}^{+\infty} d\epsilon \mathcal{N}_p(\epsilon)\frac{\partial}{\partial h}\left(\frac{\sinh\left[\frac{\mu_B h}{k_BT}\right]}{\cosh\left[\frac{\epsilon-\mu_p}{k_BT}\right]+\cosh\left[\frac{\mu_B h}{k_BT}\right]}\right) = \\
&= \frac{\mu_B^2}{2k_bT}\int_{-\infty}^{+\infty} d\epsilon \mathcal{N}_p(\epsilon)\frac{1+\cosh\left[\frac{\epsilon-\mu_p}{k_BT}\right]\cosh\left[\frac{\mu_B h}{k_BT}\right]}{\left(\cosh\left[\frac{\epsilon-\mu_p}{k_BT}\right]+\cosh\left[\frac{\mu_B h}{k_BT}\right]\right)^2}\ .
\end{aligned} \tag{F.30}$$

F.3 Theta Approximation for the DOS: analytical results

Let us consider the following approximation for the density of states:

$$\begin{cases}\mathcal{N}_p^{(s)}(\epsilon) = A_p^{(s)}\Theta\left(\epsilon-\Delta\right)\Theta\left(\Delta+2w_p-\epsilon\right) \\ \mathcal{N}_b^{(s)}(\epsilon) = A_b^{(s)}\Theta(\epsilon)\Theta(2w_b-\epsilon)\end{cases}\ , \tag{F.31}$$

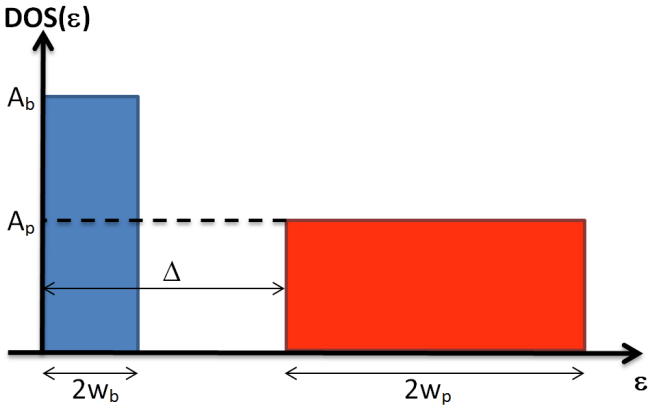

Figure F.1: Schematic representation for bipolaron (blue) and unpaired polarons (red) density of states.

where $A_{p,b}^{(s)}$ and $w_{p,b}$ are intensity and half-bandwidths of polaron and bipolaron contributions, respectively, while Δ is the gap between the bottoms of bipolaron and unpaired polaron bands (see Fig.F.1).

According to this approximation, bipolaron and unpaired polarons densities can be calculated as follows:

$$n_{p,b}(T) = \sum_s \int_{-\infty}^{+\infty} d\epsilon \mathcal{N}_{p,b}^{(s)}(\epsilon) f_{p,b}(\epsilon, T) = \sum_s A_{p,b}^{(s)} \int_{\epsilon_{p,b}^{in}}^{\epsilon_{p,b}^{fin}} d\epsilon \left(\exp\left(\frac{\epsilon - \mu_{p,b}}{k_B T} \right) \pm 1 \right)^{-1} , \tag{F.32}$$

where $\epsilon_{p,b}^{in}$, $\epsilon_{p,b}^{fin}$ represent upper and lower bounds for bipolaron and unpaired polarons DOS:

$$\begin{cases} \epsilon_b^{in} = 0 \\ \epsilon_b^{fin} = 2w_b \end{cases} , \begin{cases} \epsilon_p^{in} = \Delta \\ \epsilon_p^{fin} = \Delta + 2w_p \end{cases} . \tag{F.33}$$

The resulting integral can be easily calculated by means of the following change of variable:

$$\begin{cases} x \equiv \frac{\epsilon - \mu_{p,b}}{k_B T} \\ d\epsilon = k_B T dx \end{cases} , \tag{F.34}$$

that gives:

$$n_{p,b}(T) = \sum_s A_{p,b}^{(s)} k_B T \int_{x_{p,b}^{in}}^{x_{p,b}^{fin}} \frac{dx}{e^x \pm 1} = \pm \sum_s A_{p,b}^{(s)} k_B T \left[x - \log\left(1 \pm e^x\right) \right]_{x_{p,b}^{in}}^{x_{p,b}^{fin}} , \tag{F.35}$$

where, according to (F.33) and (F.34) we have:

$$\begin{cases} x_b^{in} = -\frac{\mu_b}{k_B T} \\ x_b^{fin} = \frac{2w_b - \mu_b}{k_B T} \end{cases} , \begin{cases} x_p^{in} = \frac{\Delta - \mu_p}{k_B T} \\ x_p^{fin} = \frac{\Delta + 2w_p - \mu_p}{k_B T} \end{cases} . \tag{F.36}$$

The final expressions of bipolaron and unpaired polaron densities:

$$n_b(T) = -2A_b w_b + A_b k_B T \log\left[\left(1 - e^{\frac{2w_b - \mu_b}{k_B T}} \right) / \left(1 - e^{-\frac{\mu_b}{k_B T}} \right) \right] , \tag{F.37}$$

$$n_p(T) = 4A_p w_p + 2A_p k_B T \log\left[\left(1+e^{\frac{\Delta-\mu_p}{k_B T}}\right)/\left(1+e^{\frac{\Delta+2w_p-\mu_p}{k_B T}}\right)\right] , \quad \text{(F.38)}$$

allow us to calculate the chemical potential $\mu = \mu_p = \mu_b/2$ according to the conservation of the total number of particles:

$$n = \left(2n_b(T) + n_p(T)\right)_{\mu_p=\mu_b/2=\mu} , \quad \text{(F.39)}$$

as well as the charge susceptibility:

$$\chi_c^p(T) = \frac{2A_p T \sinh\left(w_p/k_B T\right)}{\cosh\left(\frac{\Delta-\mu_p+w_b}{k_B T}\right)+\cosh\left(\frac{w_p}{k_B T}\right)} , \quad \text{(F.40)}$$

$$\chi_c^b(T) = \frac{A_b T \sinh\left(w_b/k_B T\right)}{\cosh\left(\frac{\mu_b-w_b}{k_B T}\right)-\cosh\left(\frac{w_b}{k_B T}\right)} , \quad \text{(F.41)}$$

F.3.1 Zero field entropy and specific heat

The knowledge of bipolaron and unpaired polaron densities allows us to calculate entropy and specific heat. Form Eq.F.17 we can write the entropy as:

$$\begin{aligned} S_{p,b}(T) &= \sum_s \int_{-\infty}^{+\infty} d\epsilon \mathcal{N}_{p,b}^{(s)}(\epsilon)\left[\pm k_B \ln\left(1\pm e^{\frac{\mu_{p,b}-\epsilon}{k_B T}}\right) - f_{p,b}(\epsilon,T)\left(\frac{\mu_{p,b}-\epsilon}{T}\right)\right] = \\ &= \sum_s A_{p,b}^{(s)} \int_{\epsilon_{p,b}^{in}}^{\epsilon_{p,b}^{fin}} d\epsilon \left[\pm k_B \ln\left(1\pm e^{\frac{\mu_{p,b}-\epsilon}{k_B T}}\right) - f_{p,b}(\epsilon,T)\left(\frac{\mu_{p,b}-\epsilon}{T}\right)\right] = \\ &= k_B^2 T \sum_s A_{p,b}^{(s)} \int_{x_{p,b}^{in}}^{x_{p,b}^{fin}} dx \left[\pm \ln\left(1\pm e^{-x}\right) + \frac{x}{e^x \pm 1}\right] . \end{aligned} \quad \text{(F.42)}$$

The resulting integral can be exactly computed in terms of the Poly-log function:

$$\mathcal{P}_n(x) \equiv \sum_{k=1}^{\infty} \frac{x^k}{k^n} . \quad \text{(F.43)}$$

Recalling that:

$$\pm \int dx \log\left(1\pm e^{-x}\right) = \pm\left[\frac{x^2}{2} + x\log\left(\frac{1\pm e^{-x}}{1\pm e^x}\right) - \mathcal{P}_2\left(\mp e^x\right)\right] , \quad \text{(F.44)}$$

$$\int dx \frac{x}{e^x \pm 1} = \pm\left[\frac{x^2}{2} - x\log\left(1\pm e^x\right) - \mathcal{P}_2\left(\mp e^x\right)\right] , \quad \text{(F.45)}$$

we have:

$$\int dx \left[\pm \ln\left(1\pm e^{-x}\right) + \frac{x}{e^x \pm 1}\right] = \pm\left[x^2 + x\log\left(\frac{1\pm e^{-x}}{(1\pm e^x)^2}\right) - 2\mathcal{P}_2\left(\mp e^x\right)\right] , \quad \text{(F.46)}$$

therefore, by substituting in the expression of the entropy we finally obtain:

$$S_{p,b}(T) = \pm \sum_s A_{p,b}^{(s)} k_B^2 T \left[x^2 + x \log\left(\frac{1 \pm e^{-x}}{(1 \pm e^x)^2} \right) - 2\mathcal{P}_2\left(\mp e^x\right) \right]_{x_{p,b}^{in}}^{x_{p,b}^{fin}} , \quad \text{(F.47)}$$

that can be calculated in terms of the DOS parameters $w_{p,b}$, $A_{p,b}$ and Δ according to Eq.F.36.

By following a similar procedure it is also possible to obtain an analytical expression for the specific heat. Starting from Eq.F.18 we have:

$$\begin{aligned} C_{p,b}(T)|_{V,n} &= \sum_s \int_{-\infty}^{+\infty} d\epsilon \mathcal{N}_{p,b}^{(s)}(\epsilon) \left(\epsilon - \mu_{p,b}\right) \frac{df_{p,b}}{dT}(\epsilon, T) = \\ &= k_B T \sum_s A_{p,b}^{(s)} \int_{\epsilon_{p,b}^{in}}^{\epsilon_{p,b}^{fin}} d\epsilon \frac{\left(\epsilon - \mu_{p,b}\right)/k_B T}{\left(\exp\left(\frac{\epsilon - \mu_{p,b}}{k_B T}\right) \pm 1\right)^2} \exp\left(\frac{\epsilon - \mu_{p,b}}{k_B T}\right) \\ &\quad \left(\frac{\epsilon - \mu_{p,b}}{k_B T^2} + \frac{1}{k_B T} \frac{d\mu_{p,b}}{dT} \right) , \end{aligned} \quad \text{(F.48)}$$

that, according to the change of variable defined in Eq.F.34, can be written as:

$$\begin{aligned} C_{p,b}(T)|_{V,n} &= \left(k_B T\right)^2 \sum_s A_{p,b}^{(s)} \int_{x_{p,b}^{in}}^{x_{p,b}^{fin}} dx \frac{x e^x}{\left(e^x \pm 1\right)^2} \left(\frac{x}{T} + \frac{1}{k_B T} \frac{d\mu_{p,b}}{dT} \right) = \\ &= k_B T \sum_s A_{p,b}^{(s)} \left[k_B I_{p,b}^{(2)}(x) + \frac{d\mu_{p,b}}{dT} I_{p,b}^{(1)}(x) \right]_{x_{p,b}^{in}}^{x_{p,b}^{fin}} , \end{aligned} \quad \text{(F.49)}$$

where:

$$I_{p,b}^{(n)}(x) \equiv \int dx \frac{x^n e^x}{\left(e^x \pm 1\right)^2} = \begin{cases} \frac{x e^x}{1 \pm e^x} \mp \log\left(1 \pm e^x\right) & , \; n = 1 \\ x\left(\frac{x e^x}{1 \pm e^x} \mp 2\log\left(1 \pm e^x\right)\right) \mp \mathcal{P}_2\left(\mp e^x\right) & , \; n = 2 \end{cases} . \quad \text{(F.50)}$$

Summarizing, entropy and specific heat of a Fermi-Bose mixture with a rectangular DOS can be written as follows:

$$S_{p,b}(T) = \pm k_B^2 T \sum_s A_{p,b}^{(s)} \left[x^2 + x \log\left(\frac{1 \pm e^{-x}}{(1 \pm e^x)^2} \right) - 2\mathcal{P}_2\left(\mp e^x\right) \right]_{x_{p,b}^{in}}^{x_{p,b}^{fin}} \quad \text{(F.51)}$$

$$C_{p,b}(T)|_{V,n} = k_B T \sum_s A_{p,b}^{(s)} \left[k_B I_{p,b}^{(2)}(x) + \frac{d\mu_{p,b}}{dT} I_{p,b}^{(1)}(x) \right]_{x_{p,b}^{in}}^{x_{p,b}^{fin}} , \quad \text{(F.52)}$$

where $x_{p,b}^{in,fin}$ are expressed in terms of the DOS parameters $w_{p,b}$, $A_{p,b}$ and Δ according to Eq.F.36. From Eq.F.52 it is also possible to calculate the specific heat for a system with constant volume and chemical potential. In this case the thermal

derivative of $\mu_{p,b}$ is zero and we have:

$$C_{p,b}(T)|_{V,\mu} = k_B^2 T \sum_s A_{p,b}^{(s)} \left[x \left(\frac{x e^x}{1 \pm e^x} \mp 2 \log\left(1 \pm e^x\right) \right) \mp \mathcal{P}_2\left(\mp e^x\right) \right]_{x_{p,b}^{in}}^{x_{p,b}^{fin}} . \quad \text{(F.53)}$$

F.3.2 Crossover temperature in the narrow-band limit

Let us consider the narrow-band limit of the rectangular DOS (F.31) which gives $\mathcal{N}_{p,b}(\epsilon) = \delta(\epsilon - \epsilon_{p,b})$. We recall that, by shifting the zero of the energy at the bottom of the bipolaron band, we have $\epsilon_b = 0$, $\epsilon_p = J_p(\tilde{U}) \equiv \Delta$. Let us now calculate the crossover temperature T^* defined as the temperature at which half of the bipolarons are dissociated and the charge is equally distributed between polarons and bipolarons. In this case we have $n_p(T^*) = 2n_b(T^*)$ or, recalling that $n_b(T = 0) = x/2$, $n_p(T = 0) = 0$, $n_b(T^*) = x/4$, $n_p(T^*) = x/2$. Polaron and bipolaron densities can be calculated as:

$$n_{p,b}(T) = A_{p,b} \int_{-\infty}^{+\infty} d\epsilon \mathcal{N}_{p,b}(\epsilon) \frac{1}{e^{\beta\left(\epsilon - \mu_{p,b}\right)} \pm 1} , \quad \text{(F.54)}$$

where, consistently with the narrow-band approximation, $A_{p,b}$ only takes into account the degeneracy of polaron and bipolaron configuration and we consider $\mu_p = \mu_b/2 = \mu$ as follows from the detailed equilibrium. By means of the above relations, at $T = T^*$ we have:

$$n_b(T^*) = \frac{x}{4} = \frac{2}{e^{-2\beta^*\mu} - 1} \Rightarrow e^{-2\beta^*\mu} = 1 + \frac{8}{x} . \quad \text{(F.55)}$$

For the polaronic density we have instead:

$$n_p(T^*) = \frac{x}{2} = \frac{2}{e^{\beta^*(\Delta - \mu)} + 1} \Rightarrow e^{-\beta^*\mu} = e^{-\beta^*\Delta} \left(\frac{4}{x} - 1 \right) . \quad \text{(F.56)}$$

Joining together the last two equations we obtain:

$$e^{-2\beta^*\Delta} \left(\frac{4}{x} - 1 \right)^2 = 1 + \frac{8}{x} , \quad \text{(F.57)}$$

from which we have:

$$e^{-2\beta^*\Delta} = \frac{1 + \frac{8}{x}}{\left(\frac{4}{x} - 1\right)^2} \Rightarrow \beta^* = \frac{1}{2\Delta} \ln \left(\frac{\left(\frac{4}{x} - 1\right)^2}{1 + \frac{8}{x}} \right) , \quad \text{(F.58)}$$

and the following expression for the crossover temperature:

$$k_B T^* = \frac{2\Delta}{\ln \left(\frac{\left(\frac{4}{x} - 1\right)^2}{1 + \frac{8}{x}} \right)} . \quad \text{(F.59)}$$

Index